

VOLUME 80

SEPTEMBER 23, 1976

NUMBER 20

JPCA X

THE JOURNAL OF

PHYSICAL

CHEMISTRY

Michael Kasha Symposium

**ELECTRONIC PROCESSES AND ENERGY
TRANSFER IN ORGANIC, INORGANIC,
AND BIOLOGICAL SYSTEMS**

FLORIDA STATE UNIVERSITY • JANUARY 8-10 1976



PUBLISHED BIWEEKLY BY THE AMERICAN CHEMICAL SOCIETY

WHAT'S HAPPENING IN CHEMISTRY?

Send for This Concise, Information-Packed Summary and Find Out!

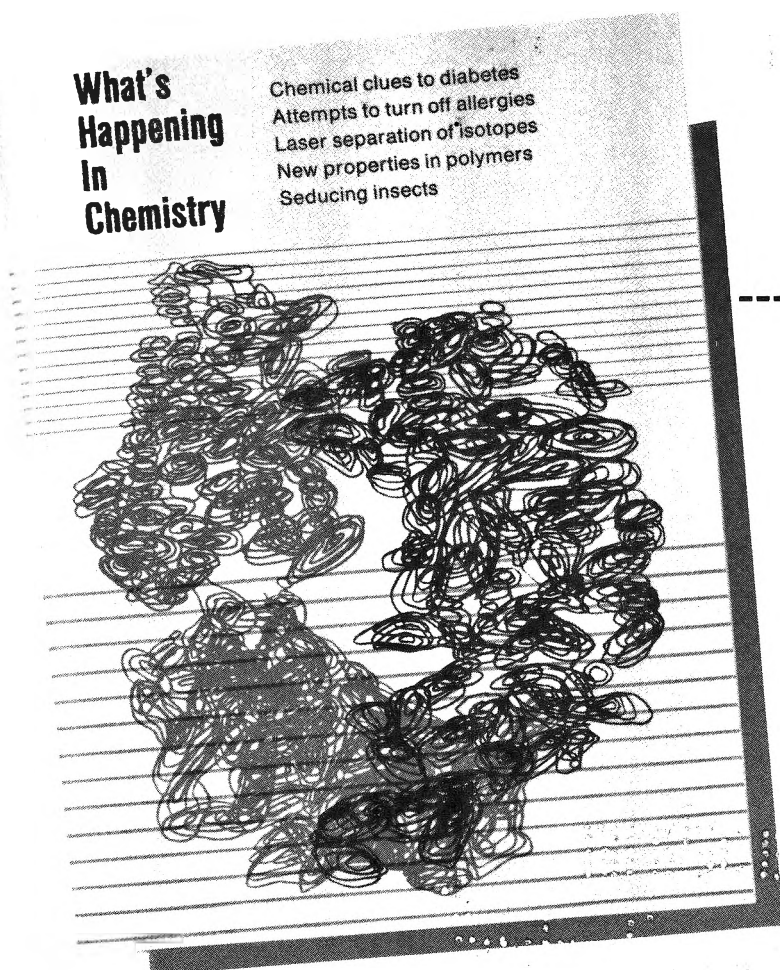
This latest compilation of recent events in chemical research makes absorbing and exciting reading. Every chemist, scientist, instructor, student, and interested layman will find it invaluable as a source of succinct information.

A glance at the contents listed below, will show you the scope of "WHAT'S HAPPENING IN CHEMISTRY?":

- NEW CHEMICAL CLUES TO DIABETES
- ADVANCES IN IMMUNOCHEMISTRY
- CHEMISTRY BY LASER LIGHT
- LEAD POISONING—MORE QUESTIONS AND ANSWERS
- NEW POLYMERS ON THE HORIZON
- A FRESH LOOK AT INSECT CONTROL
- NEW INSIGHTS TO THE DETECTION AND TREATMENT OF CANCER
- FUTURE FOODS
- OLD ENERGY SOURCES, NEW IDEAS
- OZONE—AEROSOL SPRAY . . . FACTS FALL INTO PLACE
- THE 1975 NOBEL PRIZE
- NATIONAL MEDAL OF SCIENCE

Because the book is printed in magazine format, the cost is only \$1.50 per copy. Order 15 copies or more and the cost drops to just \$.75 for each book.

Just fill out the order form below along with your payment and mail it back to us today. Your copy will be in the mail just as soon as we can process your order.



Special Issues Sales

American Chemical Society
1155—16th Street, N.W.
Washington, D.C. 20036

Please send me _____ copies of
"WHAT'S HAPPENING IN CHEMISTRY?"

Name _____

Address _____

City _____

State _____

Zip Code _____

WH 76

THE JOURNAL OF PHYSICAL CHEMISTRY

BRYCE CRAWFORD, Jr., *Editor*
STEPHEN PRAGER, *Associate Editor*
ROBERT W. CARR, Jr., **FREDERIC A. VAN-CATLEDGE,** *Assistant Editors*

EDITORIAL BOARD: C. A. ANGELL (1973-1977), F. C. ANSON (1974-1978), V. A. BLOOMFIELD (1974-1978), J. R. BOLTON (1976-1980), L. M. DORFMAN (1974-1978), H. L. FRIEDMAN (1975-1979), H. L. FRISCH (1976-1980), W. A. GODDARD (1976-1980), E. J. HART (1975-1979), W. J. KAUZMANN (1974-1978), R. L. KAY (1972-1976), D. W. McCLURE (1974-1978), R. M. NOYES (1973-1977), W. B. PERSON (1976-1980), J. C. POLANYI (1976-1980), S. A. RICE (1976-1980), F. S. ROWLAND (1973-1977), R. L. SCOTT (1973-1977), W. A. STEELE (1976-1980), J. B. STOTHERS (1974-1978), W. A. ZISMAN (1972-1976)

Published by the
AMERICAN CHEMICAL SOCIETY
BOOKS AND JOURNALS DIVISION
D. H. Michael Bowen, Director

Editorial Department: Charles R. Bertsch,
Head; Marianne C. Brogan, Associate
Head; Celia B. McFarland, Joseph E.
Yurvati, Assistant Editors

Graphics and Production Department:
Bacil Guiley, Head

Research and Development Department:
Seldon W. Terrant, Head

Advertising Office: Centcom, Ltd., 50 W.
State St., Westport, Conn. 06880.

© Copyright, 1976, by the American
Chemical Society. No part of this publica-
tion may be reproduced in any form with-
out permission in writing from the Ameri-
can Chemical Society.

Published biweekly by the American
Chemical Society at 20th and Northamp-
ton Sts., Easton, Pennsylvania 18042. Sec-
ond class postage paid at Washington, D.C.
and at additional mailing offices.

Editorial Information

Instructions for authors are printed in
the first issue of each volume. Please con-
form to these instructions when submitting
manuscripts.

Manuscripts for publication should be
submitted to *The Journal of Physical*
Chemistry, Department of Chemistry, Uni-
versity of Minnesota, Minneapolis, Minn.
55455. Correspondence regarding **accepted**
papers and proofs should be directed to
the Editorial Department at the ACS East-
on address.

Page charges of \$60.00 per page are as-
sessed for papers published in this journal.
Ability to pay does not affect acceptance or
scheduling of papers.

Bulk reprints or photocopies of indi-
vidual articles are available. For informa-
tion write to Business Operations, Books
and Journals Division at the ACS Wash-
ington address.

Requests for **permission to reprint**
should be directed to Permissions, Books
and Journals Division at the ACS Wash-
ington address. The American Chemical
Society and its Editors assume no responsi-
bility for the statements and opinions ad-
vanced by contributors.

Subscription and Business Information

1976 Subscription rates—including sur-
face postage

	U.S.	PUAS	Canada, Foreign
Member	\$24.00	\$29.75	\$30.25
Nonmember	96.00	101.75	102.25
Supplementary material	15.00	19.00	20.00

Air mail and air freight rates are avail-
able from Membership & Subscription Ser-
vices, at the ACS Columbus address.

New and renewal subscriptions
should be sent with payment to the Office
of the Controller at the ACS Washington
address. **Changes of address** must include
both old and new addresses with ZIP code
and a recent mailing label. Send all address
changes to the ACS Columbus address. Please
allow six weeks for change to become effec-
tive. **Claims** for missing numbers will not
be allowed if loss was due to failure of notice
of change of address to be received in the
time specified; if claim is

dated (a) North America—more than 90
days beyond issue date, (b) all other for-
eign—more than 1 year beyond issue date;
or if the reason given is “missing from
files”. Hard copy claims are handled at the
ACS Columbus address.

Microfiche subscriptions are available
at the same rates but are mailed first class
to U.S. subscribers, air mail to the rest of
the world. Direct all inquiries to Business
Operations, Books and Journals Division,
at the ACS Washington address or call
(202) 872-4444. **Single issues** in hard copy
and/or microfiche are available from Spe-
cial Issues Sales at the ACS Washington
address. Current year \$4.75. Back issue
rates available from Special Issues Sales.
Back volumes are available in hard copy
and/or microform. Write to Special Issues
Sales at the ACS Washington address for
further information. **Microfilm** editions of
ACS periodical publications are available
from volume 1 to the present. For further
information, contact Special Issues Sales at
the ACS Washington address. **Supplemen-
tary material** must be ordered directly
from Business Operations, Books and Jour-
nals Division, at the ACS Washington ad-
dress.

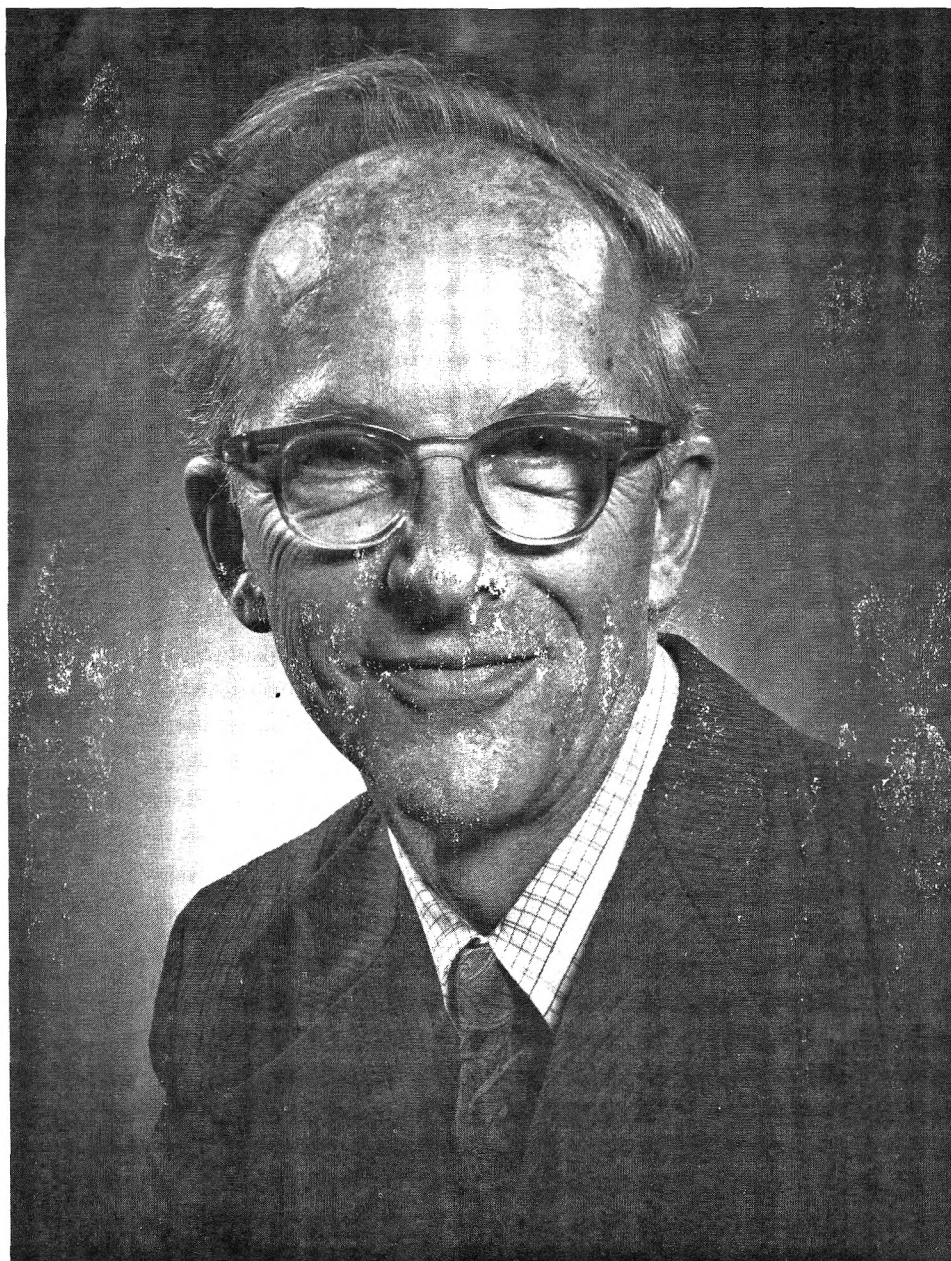
	U.S.	PUAS, Canada	Other Foreign
Microfiche Photocopy	\$2.50	\$3.00	\$3.50
1-7 pages	4.00	5.50	7.00
8-20 pages	5.00	6.50	8.00

Orders over 20 pages are available only on
microfiche, 4 × 6 in., 24X, negative, silver
halide. Orders must state photocopy or mi-
crofiche if both are available. Full bibliog-
raphic citation including names of all au-
thors and prepayment are required. Prices
are subject to change.

American Chemical Society
1155 16th Street, N.W.
Washington, D.C. 20036
(202) 872-4600

Member & Subscription Services
American Chemical Society
P.O. Box 3337
Columbus, Ohio 43210
(614) 421-7230

Editorial Department
American Chemical Society
20th and Northampton Sts.
Easton, Pennsylvania 18042
(215) 258-9111



Michael Kasha

A NOTE OF TRIBUTE

Michael Kasha is widely known for his enduring contributions to the understanding of electronic phenomena in molecular systems. The very mention of the term molecular spectroscopy for many people brings to mind the name of Kasha. It is most fitting, therefore, that at the beginning of his 56th year there be a symposium in his honor, in which his numerous students, friends, and colleagues gather to discuss the areas of endeavor nourished by him.

It is not possible in this brief introduction to describe adequately Kasha's impact on the field of molecular spectroscopy. His early work with G. N. Lewis on the identification of phosphorescence in organic molecules with the triplet state was a landmark. This establishment of the key role of the triplet state has provided a basis for much of the research in photochemistry, photobiology, and molecular spectroscopy. Later, he determined the effect of heavy atoms on singlet-triplet transition rates, which has become known as the Kasha effect and has been a valuable experimental tool.

Kasha introduced many of the terms, such as internal conversion and intersystem crossing, which have become part of the standard terminology of the field. He enunciated the fact that molecules tend to fluoresce from the lowest excited electronic state of the same multiplicity as the ground state; this is now known as Kasha's rule.

Much of the early work on the nature of $n \rightarrow \pi^*$ transitions and ideas concerning the interplay between n , π^* and π , π^* states in heterocyclic aromatic molecules originated in Kasha's laboratory. He is largely responsible for stimulating much of the research on exciton phenomena in molecular aggregates, including biomolecular systems.

As significant as Kasha's specific scientific contributions may be, they represent but a small part of his total impact on the scientific community. For Mike Kasha is a dynamic scientific personality, as anyone who has been in his vicinity is aware. He has a rare ability to inspire, stimulate, and even constructively provoke students, colleagues, and others in

related fields. It has been said that people who interact with him "catch fire" for research, and those of us who know him will certainly agree.

Kasha also has the rare ability to communicate complex and subtle topics to those in other fields. Over the years he has often lectured and has written numerous articles for the biochemist and biologist, with the effect of inspiring old and young alike to explore the role of quantum mechanical phenomena, such as excitons, in biological processes. His interdisciplinary leadership has led to much cross-fertilization and stimulation of research in other areas. It was through his inspiration and vision that the Institute of Molecular Biophysics at Florida State University was established in 1960.

To those who know him well Mike Kasha is not only an outstanding spectroscopist, but a man whose curiosity continually leads him into many other scientific and nonscientific areas. He is known throughout the Tallahassee community for his interests in such diverse activities as architecture, landscaping, sailing, and guitar design. He has a rare gift for quickly absorbing and remembering minute details, as well as for being able to pursue a subject to its origins and to perceive its essential elements. Ask him to give a lecture to any audience and he can come forth with an inspiring, popular lecture on topics ranging from Mendelian genetics to the history and design of stringed musical instruments.

As we proceed into this symposium the influence of Mike Kasha will be felt not only by means of his physical presence but also through the past effects which he has had on each of us both directly and indirectly. Many of the lectures are given by his students and research associates and even those papers that are not will undoubtedly be shaped by his earlier scientific contributions.

William Rhodes
Department of Chemistry
Florida State University

THE JOURNAL OF
PHYSICAL CHEMISTRY

Volume 80, Number 20 September 23, 1976

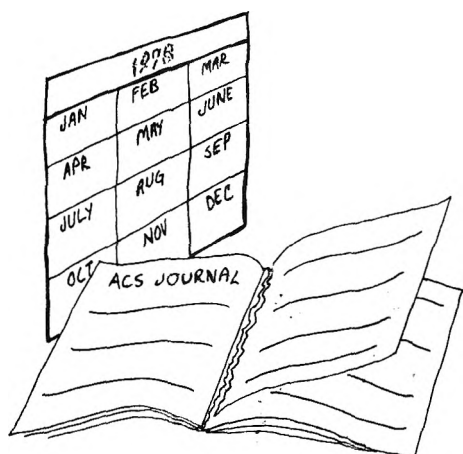
JPCA_x 80(20) 2143-2312 (1976)

ISSN 0022-3654

Michael Kasha Symposium—Electronic Processes and Energy Transfer in Organic, Inorganic, and Biological Systems

Introductory Remarks	G. A. Crosby	2143
Spectroscopic Effects of a Breakdown of the Born–Oppenheimer Approximation	S. J. Strickler	2149
Dynamics of Photodissociation in Solution using Picosecond Spectroscopy	R. W. Anderson, Jr., and R. M. Hochstrasser*	2155
Local Modes and Their Application to the Analysis of Polyatomic Overtone Spectra	Bryan R. Henry	2160
Photoperoxidation of Unsaturated Organic Molecules. 16. Excitation Energy Fission	B. Stevens* and J. A. Ors	2164
Small-Molecule Photochemistry. Theory and Application to Formaldehyde	Gregory D. Gillispie* and E. C. Lim	2166
Relaxation Processes in Photochemical Reactions. An Electron Spin Echo Study of Chemically Induced Spin Orientation	David C. Doetschman	2167
Vibronic Interactions and Environmental Effects on the Phosphorescent State of 9,10-Anthraquinone in Shpol'skii Matrices at 4.2 K	Omar S. Khalil and Lionel Goodman*	2170
Fluorescence Lifetimes and Sensitization Rate Constants for Dyes Adsorbed to Silver Halide Microcrystals	Annabel A. Muentner	2178
Fluorescence, Resonance Raman, and Radiationless Decay in Several Hemoproteins	Fran Adar,* Martin Gouterman, and Sheldon Aronowitz	2184
Exciton Percolation in Mixed Molecular Crystals and Aggregates: From Naphthalene to Photosynthesis	Raoul Kopelman	2191
Triplet Energy Transfer Mechanism in Isotopic Mixed Molecular Crystals	S. D. Colson,* F. B. Tudron, R. E. Turner, and V. Vaida	2196
High-Resolution Optical Spectroscopy of Polyenes Related to the Visual Chromophore	R. L. Christensen* and B. E. Kohler	2197
Pressure Tuning of the Fluorescence Spectra Due to Deep Traps in Anthracene and Naphthalene Crystals	Malcolm F. Nicol	2200
The Mechanism of the $S_1 \rightsquigarrow T_1$ Nonradiative Process in Duraldehyde	Alan Campion and M. A. El-Sayed*	2201
Excited States of Mixed Ligand Chelates of Ruthenium(II) and Rhodium(III)	G. A. Crosby* and W. H. Elfring, Jr.	2206

TIMELY TEARSHEETS



Here's an opportunity to choose any article you wish which has been published during the past 12 months in any one of the American Chemical Society journals.*

The price for this service is very modest—just \$2.50 for the first copy and \$1.25 for each additional copy.

Also, if you wish, you may select articles which have appeared in earlier non-current ACS journal issues, but these will be photocopies rather than tearsheets and an additional 50¢ is required per article.

All you have to do is fill in the order forms below *include your payment*, mail now, and we'll do the rest.

1. Give complete details for each article. Sorry, we cannot provide a search service.
2. **PRINT** or **TYPE** all information, including label.
3. Make check or money order payable to the AMERICAN CHEMICAL SOCIETY, and mail to: ACS, Business Operations, Books and Journals Division, 1155 16th Street, N.W., Washington, D.C. 20036.

Name _____

Address _____

City _____

State/Zip _____

AMERICAN CHEMICAL SOCIETY JOURNALS TIMELY TEARSHEETS Order Form

The following article(s) came to my attention in a recent issue of one of the ACS journals. I would like to order the number of tearsheets of each article indicated in the box(es).

ACS Journal _____

Title _____

Author(s) _____

Issue Date _____ Page(s) _____

ACS Journal _____

Title _____

Author(s) _____

Issue Date _____ Page(s) _____

ACS Journal _____

Title _____

Author(s) _____

Issue Date _____ Page(s) _____

\$2.50 for the first tearsheet.

\$1.25 for each additional tearsheet ordered at the same time.

\$ _____

Total Enclosed

These prices do not apply to articles from Chemical Reviews and Journal of Physical and Chemical Reference Data. For information regarding cost of these copies, contact the Books and Journals Division, ACS.

* Copyright restrictions prevent us from providing copies from other than ACS journals

Photoelectron Spectra of Carbonyls. Propellenes and Propellanones D. Dougherty, J. J. Bloomfield, G. R. Newkome, J. F. Arnett, and S. P. McGlynn*	2212
Singlet Molecular Oxygen. A New Kind of Oxygen Ahsan U. Khan	2219
Magnetic Circularly Polarized Emission from Crystalline $\text{Cs}_2\text{ZrCl}_6\cdot\text{Re}^{4+}$ H. G. Brittain, F. S. Richardson, J. P. Jasinski, W. C. Yeakel, and P. N. Schatz*	2228
Determination of Geometrical Parameters of Excited States. Application to d^6 Transition Metal Complexes of O and D_4 Symmetry K. W. Hipps, G. A. Merrell, and G. A. Crosby*	2232
The Phosphorescence of Phosphorus Richard J. VanZee and Ahsan U. Khan*	2240
Luminescence Studies of Proton Transfer in the Excited Electronic States of Hydrogen Bonded Quinoline and Isoquinoline William R. Moomaw* and Mary F. Anton	2243
Laser Intensity Measurements by Chemical Actinometry. A Photooxygenation Actinometer J. N. Demas,* R. P. McBride, and E. W. Harris	2248 ■
High Resolution Zeeman Experiments on Singlet, Triplet, and Quartet States of Metalloporphines G. W. Canters,* G. Jansen, M. Noort, and J. H. van der Waals	2253
Relaxation Processes in Excited Molecular Systems M. Ashraf El-Bayoumi	2259
Visual Pigments. 4. Comprehensive Consideration of the Spectroscopy and Photochemistry of Model Visual Pigments Ralph S. Becker,* Gordon Hug, P. K. Das, Arnold M. Schaffer, Takeshi Takemura, Naoto Yamamoto, and Walter Waddell	2265
Model Systems for Photosynthetic Energy Conversion Gordon Tollin	2274
Picosecond Flash Photolysis Studies of Dyes, Inorganic Complexes, Biological Pigments, and Photosynthetic Systems Maurice W. Windsor	2278
Excitons, Energy Transfer, and Charge Resonance in Excited Dinucleotides and Polynucleotides. A Photoselection Study Robert W. Wilson and Patrik R. Callis*	2280
In Vitro Energy Transfer in <i>Renilla</i> Bioluminescence William W. Ward* and Milton J. Cormier	2289
Excited State Interactions of α -Tocopherol and Molecular Oxygen Dale E. Brabham* and John Lee	2292
Chemical Production of Excited States. Chemiluminescence of Carcinogenic Hydrocarbons Accompanying Their Metabolic Hydroxylation and a Proposal for Common Active Site Geometries for Hydroxylation H. H. Seliger* and J. P. Hamman	2296
Fluorescence and Multiple Excitation in Photosynthetic Systems D. Mauzerall	2306
Exciton Interactions in the Symmetrical Dimeric Aggregate of Chlorophyll a Monohydrate Vaughn J. Koester and Francis K. Fong*	2310

■ Supplementary material for this paper is available separately (consult the masthead page for ordering information); it will also appear following the paper in the microfilm edition of this journal.

* In papers with more than one author, the asterisk indicates the name of the author to whom inquiries about the paper should be addressed.

COPIES OF THIS ISSUE

Copies of this issue may be purchased for \$4.75 each. Send orders to Business Operations, American Chemical Society, 1155 Sixteenth St., N.W., Washington, D.C. 20036. Payment must be sent with the order.

AUTHOR INDEX

- | | | | |
|---|--|--|--|
| <p>Adar, F., 2184
 Anderson, R. W., Jr., 2155
 Anton, M. F., 2243
 Arnett, J. F., 2212
 Aronowitz, S., 2184</p> <p>Becker, R. S., 2265
 Bloomfield, J. G., 2212
 Brabham, D. E., 2292
 Brittain, H. G., 2228</p> <p>Callis, P. R., 2280
 Champion, A., 2201
 Canters, G. W., 2253
 Christensen, R. L., 2197
 Colson, S. D., 2196
 Cormier, M. J., 2289
 Crosby, G. A., 2143, 2206,
 2232</p> <p>Das, P. K., 2265
 Demas, J. N., 2248
 Doetschman, D. C., 2167</p> | <p>Dougherty, D., 2212</p> <p>El-Bayoumi, M. A., 2259
 Elfring, W. H., Jr., 2206
 El-Sayed, M. A., 2201</p> <p>Fong, F. K., 2310</p> <p>Gillispie, G. D., 2166
 Goodman, L., 2170
 Gouterman, M., 2184</p> <p>Hamman, J. P., 2296
 Harris, E. W., 2248
 Henry, B. R., 2160
 Hipps, K. W., 2232
 Hochstrasser, R. M., 2155
 Hug, G., 2265</p> <p>Jansen, G., 2253
 Jasinski, J. P., 2228</p> <p>Khalil, O. S., 2170</p> | <p>Khan, A. U., 2219, 2240
 Koester, V. J., 2310
 Kohler, B. E., 2197
 Kopelman, R., 2191</p> <p>Lee, J., 2292
 Lim, E. C., 2166</p> <p>Mauzerall, D., 2306
 McBride, R. P., 2248
 McGlynn, S. P., 2212
 Merrell, G. A., 2232
 Moomaw, W. R., 2243
 Muenter, A. A., 2178</p> <p>Newkome, G. R., 2212
 Nicol, M. F., 2200
 Noort, M., 2253</p> <p>Ors, J. A., 2164</p> <p>Richardson, F. S., 2228</p> | <p>Schaffer, A. M., 2265
 Schatz, P. N., 2228
 Seliger, H. H., 2296
 Stevens, B., 2164
 Strickler, S. J., 2149</p> <p>Takemura, T., 2265
 Tollin, G., 2274
 Tudron, F. B., 2196
 Turner, R. E., 2196</p> <p>Vaida, V., 2196
 van der Waals, J. H., 2253
 VanZee, R. J., 2240</p> <p>Waddell, W., 2265
 Ward, W. W., 2289
 Wilson, R. W., 2280
 Windsor, M. W., 2278</p> <p>Yamamoto, N., 2265
 Yeakel, W. C., 2228</p> |
|---|--|--|--|

THE JOURNAL OF PHYSICAL CHEMISTRY

Registered in U. S. Patent Office © Copyright, 1976, by the American Chemical Society

VOLUME 80, NUMBER 20 SEPTEMBER 23, 1976

Michael Kasha Symposium

Electronic Processes and Energy Transfer in Organic, Inorganic, and Biological Systems

FLORIDA STATE UNIVERSITY, TALLAHASSEE, FLORIDA

THURSDAY JANUARY 8—SATURDAY JANUARY 10, 1976

Introductory Remarks

G. A. Crosby

Department of Chemistry, Washington State University, Pullman, Washington 99163

Publication costs assisted by the Department of Chemistry, Washington State University

During the three decades since World War II the expansion of our knowledge about molecular electronic excited states has been rapid and fundamental. Increasingly powerful instrumentation and theoretical formulations pushed the frontiers both deeper and wider, so far, in fact, that investigators in particular areas began to lose the sense of fundamental unity relating their studies to those of others. Thus, a conference emphasizing current research on molecular electronic processes to illuminate their prominent role in organic, inorganic, and biological investigations was deemed desirable.

A primary objective of the meeting was to bring together a group of active scientists, all trained in the field of molecular spectroscopy, who were applying their methods to areas of relevance to molecular energy transfer problems involving organic, inorganic, and biological systems. No attempt was made to cover all the areas related to electronic processes. Indeed, this would have been a futile exercise. A concerted effort was made, however, to underscore the unity of the current research activities in spite of their obvious diversity.

While selecting a tentative roster of participants, the initial organizers recognized the influence of Michael Kasha, both through his own research and especially through the large number of active scientists who have sojourned in his laboratory, either as students, postdoctoral fellows, or visitors. The

recognition of Professor Kasha's influence supplied the underlying harmony sought by the Committee and, incidentally, identified Tallahassee as the obvious location for the meeting. Choice of most of the plenary speakers from former Kasha associates supplied the themes and the emphases of the Conference and, at the same time, guaranteed a rare camaraderie. Contributed papers spanning all the principal areas of the Conference added a rich diversity of ideas and discussion to the meeting.

For partial support of the Kasha Symposium the organizers are grateful to the National Science Foundation, the Energy Research and Development Administration, the Division of Arts and Sciences of Florida State University, the DuPont Science and Engineering Fund of the Florida State University Department of Chemistry, and Control Data Corporation. We are grateful to the Session Chairmen for their help with the program. A special note of thanks is due to Jane Crosby not only for typing the recorded discussion and contributing to its editing but for her constant help throughout the planning and staging of the Conference. A warm note of thanks also goes to Barbara Rhodes for arranging the banquet.

Organizing Committee: G. A. Crosby (Washington State University), M. A. El-Sayed (University of California, Los Angeles), W. C. Rhodes and J. Saltiel (Florida State University).

List of Participants and Affiliation

- Adar, Fran, Department of Biochemistry and Biophysics, University of Pennsylvania, Philadelphia, Pa.
- Akins, Daniel, Department of Chemistry, University of South Florida, Tampa, Fla.
- Barrett, T. W., Department of Physiology and Biophysics, University of Tennessee, Memphis, Tenn.
- Bass, George, Department of Molecular Biology, University of Tennessee, Memphis, Tenn.
- Baum, J. Clayton, Department of Chemistry, Florida State University, Tallahassee, Fla.
- Becker, R. S., Department of Chemistry, University of Houston, Houston, Tex.
- Bernstein, Elliot R., Department of Chemistry, Colorado State University, Fort Collins, Colo.
- Brabham, Dale E., Department of Biochemistry, University of Georgia, Athens, Ga.
- Callis, Patrik R., Department of Chemistry, Montana State University, Bozeman, Mont.
- Campion, Alan, Department of Chemistry, University of California, Los Angeles, Calif.
- Canter, G. W., Department of Chemistry, University of Leiden, The Netherlands.
- Careri, Giorgio, Laboratori Snam-Progetti, University of Rome, Monterotondo, Rome, Italy.
- Christensen, Ronald L., Department of Chemistry, Wesleyan University, Middletown, Conn.
- Clarke, Richard H., Department of Chemistry, Boston University, Boston, Mass.
- Clifford, James, Department of Chemistry, University of Puget Sound, Tacoma, Wash.
- Colson, Steven D., Sterling Chemistry Laboratory, Yale University, New Haven, Conn.
- Cormier, Milton J., Department of Biochemistry, University of Georgia, Athens, Ga.
- Crosby, Glenn, Department of Chemistry, Washington State University, Pullman, Wash.
- Daniels, Malcolm, Department of Chemistry, Oregon State University, Corvallis, Oreg.
- Das, Paritosh Kumar, Department of Chemistry, University of Houston, Houston, Tex.
- Dellinger, Barry, Department of Chemistry, Florida State University, Tallahassee, Fla.
- Demas, James, Department of Chemistry, University of Virginia, Charlottesville, Va.
- Doetschman, David, Department of Chemistry, State University of New York, Binghamton, N.Y.
- El-Bayoumi, Ashraf, Biophysics Department, Michigan State University, East Lansing, Mich.
- El-Sayed, Mostafa, Department of Chemistry, University of California, Los Angeles, Calif.
- Frank, Harry, Department of Chemistry, Boston University, Boston, Mass.
- Freed, Simon, Department of Chemistry, Brookhaven National Laboratory, Upton, Long Island, N.Y.
- Gaffron, Hans, Departments of Biology and Chemistry, Florida State University, Tallahassee, Fla. (Retired).
- Geacintov, Nicholas E., Chemistry Department, New York University, New York, N.Y.
- Giacometti, G., Istituto di Chimica Fisica, Università di Padova, Padova, Italy.
- Gillispie, Gregory D., Department of Chemistry, Wayne State University, Detroit, Mich.
- Goodman, Lionel, School of Chemistry, Rutgers University, New Brunswick, N.J.
- Gouterman, Martin, Department of Chemistry, University of Washington, Seattle, Wash.
- Green, William H., Mahoney, Hadlow, Chambers & Adams, Attorneys, Tallahassee, Fla.
- Hameka, H. F., Department of Chemistry, University of Pennsylvania, Philadelphia, Pa.
- Hempel, Judith C., Department of Chemistry, Wake Forest University, Winston-Salem, N.C.
- Henry, Bryan R., Department of Chemistry, University of Manitoba, Winnipeg, Manitoba, Canada.
- Hipps, K. W., Department of Chemistry, University of Michigan, Ann Arbor, Mich.
- Hochstrasser, Robin M., Department of Chemistry, University of Pennsylvania, Philadelphia, Pa.
- Hug, Gordon, Department of Chemistry, University of Houston, Houston, Tex.
- Kasha, Michael, Department of Chemistry and Institute of Molecular Biophysics, Florida State University, Tallahassee, Fla.
- Kawaoka, Kenji, Chemistry Division, Eastman Kodak Company, Rochester, N.Y.
- Khalil, Omar, School of Chemistry, Rutgers University, New Brunswick, N.J.
- Khan, Ahsan U., Department of Chemistry, Michigan State University, East Lansing, Mich.
- Koester, Vaughn, Department of Chemistry, Purdue University, West Lafayette, Ind.
- Kopelman, Raoul, Department of Chemistry, University of Michigan, Ann Arbor, Mich.
- Lim, Edward C., Department of Chemistry, Wayne State University, Detroit, Mich.
- Linder, Bruno, Department of Chemistry, Florida State University, Tallahassee, Fla.
- Longworth, J. W., Biology Division, Oak Ridge National Laboratory, Oak Ridge, Tenn.
- Mauzerall, David, Rockefeller University, New York, N.Y.
- McClure, D. S., Department of Chemistry, Princeton University, Princeton, N.J.
- McGlynn, Sean, Department of Chemistry, Louisiana State University, Baton Rouge, La.
- Moomaw, William R., Department of Chemistry, Williams College, Williamstown, Mass.
- Morgan, James, Chemistry Department, Oregon State University, Corvallis, Oreg.
- Muenter, Annabel A., Emulsion Research Laboratory, Eastman Kodak Company, Rochester, N.Y.
- Mulliken, Robert S., Department of Chemistry, University of Chicago, Chicago, Ill.
- Nicol, Malcolm F., Department of Chemistry, University of California, Los Angeles, Calif.
- Noyes, W. Albert, Department of Chemistry, The University of Texas at Austin, Austin, Tex.
- Parmenter, Charles, Department of Chemistry, Indiana University, Bloomington, Ind.
- Quagliano, James V., Department of Chemistry, Auburn University, Auburn, Ala.
- Rahn, Ronald, Biology Division, Oak Ridge National Laboratory, Oak Ridge, Tenn.
- Rawls, H. Ralph, Gulf South Research Institute, New Orleans, La.

Rhodes, William, Department of Chemistry, Florida State University, Tallahassee, Fla.

Ross, Ian G., Department of Chemistry, Australian National University, Canberra, Australia.

Sager, W. F., Chemistry Department, University of Illinois at Chicago Circle, Chicago, Ill.

Saltiel, Jack, Department of Chemistry, Florida State University, Tallahassee, Fla.

Schatz, Paul N., Department of Chemistry, University of Virginia, Charlottesville, Va.

Seliger, Howard, McCollum-Pratt Institute and Department of Biology, Johns Hopkins University, Baltimore, Md.

Seybold, Paul, Chemistry Department, Wright State University, Dayton, Ohio.

Simpson, W. T., Department of Chemistry, University of Oregon, Eugene, Oreg.

Stevens, Brian, Department of Chemistry, University of South Florida, Tampa, Fla.

Strickler, Stewart, Department of Chemistry, University of Colorado, Boulder, Colo.

Stwalley, William C., Chemistry Division, National Science Foundation, Washington, D.C.

Takemura, Takeshi, Department of Chemistry, University of Houston, Houston, Tex.

Tollin, Gordon, Department of Chemistry, University of Arizona, Tucson, Ariz.

Vala, Martin T., Jr., Department of Chemistry, University of Florida, Gainesville, Fla.

VanZee, Richard J., Department of Chemistry, Michigan State University, East Lansing, Mich.

Walborsky, Harry M., Department of Chemistry, Florida State University, Tallahassee, Fla.

Ward, William W., Department of Biochemistry, University of Georgia, Athens, Ga.

Watson, Brian, Department of Chemistry, University of Miami, Coral Gables, Fla.

Williams, Theodore P., Department of Biological Science, Florida State University, Tallahassee, Fla.

Wilson, Robert W., Institute of Molecular Biology, University of Oregon, Eugene, Oreg.

Windsor, Maurice, Department of Chemistry, Washington State University, Pullman, Wash.

Yang, N. C., Department of Chemistry, University of Chicago, Chicago, Ill.

Participating FSU Graduate Students

Katherine Bisset
Craig Brown
Ron Cable
Scott Chambers

David Chang
Dennis Cravens
Steve Finson
Gamal Khalil

David Lorenz
Claude Needham
Steve Redmann

Pradeep Sengupta
William Smothers
Joseph Zupancic

**MICHAEL KASHA SYMPOSIUM ON ENERGY TRANSFER IN
ORGANIC, INORGANIC, AND BIOLOGICAL SYSTEMS**

(Papers as presented at the sessions.)

SESSION I: Plenary Lectures

Session Chairman: Ian Ross, Australian National University

Stewart Strickler, University of Colorado

Use of True Born–Oppenheimer Wavefunctions in the Treatment of Vibronic Effects and Born–Oppenheimer Breakdown

Robin Hochstrasser, University of Pennsylvania

Studies of Fast Processes in the Condensed Phase

Bryan Henry, University of Manitoba

A General Local Mode Theory for the Description of Highly Vibrationally Excited Molecules with Applications to the Description of Polyatomic Overtone Spectra

* *Lionel Goodman*, Rutgers University

Vibrational Electronic Interactions between Aromatic Carbonyl Triplet States

SESSION II: Contributed Lectures

Session Chairman: C. Parmenter, Indiana University

B. Stevens and J. A. Ors, University of South Florida

Excitation Energy Fission in Solution

* *Gregory D. Gillispie and E. C. Lim*, Wayne State University

Small Molecule Photochemistry. I. Theory and Application to Formaldehyde

David C. Doetschman, State University of New York at Binghamton

Relaxation Processes in Photochemical Reactions: An Electron Spin Echo Study of Chemically Induced Spin Orientation

Omar S. Khalil and Lionel Goodman, Rutgers University

Vibronic Interactions in the Lowest Triplet State of 9,10-Anthraquinone

* *G. Hug and R. S. Becker*, University of Houston

Solvent and Temperature Effects on Natural Radiative Lifetimes of Some Substituted Polyenes

Session Chairman: E. Bernstein, Colorado State University

Annabel A. Muentzer, Eastman Kodak Research Laboratories

Fluorescence Lifetimes and Sensitization Rate Constants for Dyes Adsorbed to Silver Halide Microcrystals

Fran Adar, University of Pennsylvania, **and** *Martin Gouterman*, University of Washington

Fluorescence, Resonance Raman, and Radiationless Decay in Several Hemoproteins

Raoul Kopelman, University of Michigan

Exciton Percolation in Mixed Molecular Crystals and Aggregates: From Naphthalene to Photosynthesis

* *S. D. Colson, F. B. Tudron, R. E. Turner, and V. Vaida*, Yale University

On the Triplet Energy Transfer Mechanism in Isotopic Mixed Molecular Crystals

Ronald L. Christensen and Bryan E. Kohler, Wesleyan University

High Resolution Optical Spectroscopy of Polyenes Related to the Visual Chromophore

Malcolm F. Nicol, University of California–Los Angeles

Pressure Tuning of Fluorescence Spectra Due to Deep Traps in Anthracene and Naphthalene Crystals

SESSION III: Plenary Lectures

Session Chairman: D. S. McClure, Princeton University

- * *Mostafa El-Sayed*, University of California—Los Angeles
Triplet Spin Labels and Molecular Dynamics

Glenn Crosby, Washington State University

Excited States of Mixed Ligand Chelates of Ruthenium(II) and Rhodium(III)

- * *Sean McGlynn*, Louisiana State University

The Color of Inorganic Ions

Ahsan Khan, Michigan State University

Singlet Molecular Oxygen: A New Kind of Oxygen

SESSION IV: Contributed Lectures

Session Chairman: M Gouterman, University of Washington

- * *A. Campion and M. A. El-Sayed*, University of California—Los Angeles

The Mechanism of the $S_1 \rightsquigarrow T_1$ Intersystem Crossing in Duraldehyde by Zeeman-PMDR Techniques

- * *E. R. Bernstein, G. R. Meredith, and J. D. Webb*, Colorado State University

Jahn-Teller Effect and Vibronic Coupling in Octahedral Molecules— ReF_6 and IrF_6

Harry G. Brittain, F. S. Richardson, J. P. Jasinski, and P. N. Schatz, University of Virginia

Magnetic Circularly Polarized Emission from Crystalline $Cs_2ZrCl_6:Re^{4+}$

K. W. Hipps, G. A. Merrell, and G. A. Crosby, Washington State University

Geometrical Distortion of the Excited States of d^6 Transition Metal Complexes: Systems of O and D_4 Symmetry

Richard J. VanZee and Ahsan U. Khan, Michigan State University

The Phosphorescence of Phosphorus

Session Chairman: H. F. Hameka, University of Pennsylvania

William R. Moomaw, Williams College

Luminescence Studies of Proton Transfer in the Excited Electronic States of Hydrogen Bonded Quinoline and Isoquinoline

- * *D. L. Akins*, University of South Florida

Energy Transfer and Electron Transfer Rate Constants in Electrochemiluminescent (ECL) Systems

D. G. Taylor, R. P. McBride, E. W. Harris, and J. N. Demas, University of Virginia

New Tools in Photochemistry and Photophysics

- * *T. W. Barrett*, University of Tennessee

Parametric Excitation as the Means of Energy Transfer in Quantal Systems With Reference to Carcinogens

G. W. Canters, G. Jansen, M. Noort, Gorlaeus Laboratories, and *J. H. van der Waals*, Huygens Laboratory, Rijksuniversiteit

High Resolution Zeeman Experiments on Singlet, Triplet, and Quartet States of Metalloporphines

SESSION V: Plenary Lectures

Session Chairman: W. Simpson, University of Oregon

Ashraf El-Bayoumi, Michigan State University

Relaxation Processes in Excited Molecular Systems. Some Biological Applications

Ralph Becker, University of Houston

The Spectroscopy and Photochemistry of Model Visual Pigments

Gordon Tollin, University of Arizona

Model Systems for Photosynthetic Energy Conversion

- * *Maurice Windsor*, Washington State University

Picosecond Flash Photolysis Studies of Dyes, Biological Pigments, and Photosynthetic Systems

SESSION VI: Contributed Lectures

Session Chairman: Simon Freed, Brookhaven National Laboratory

* **Robert W. Wilson**, University of Oregon, **J. P. Morgan**, Oregon State University, and *Patrik R. Callis*, Montana State University

Anomalous Fluorescence Excitation Spectra in the DNA Bases: Are We Asking Too Much of Vavilov's Law?

James Morgan and **Malcolm Daniels**, Oregon State University

Polarization Studies of the Excited States of the Nucleic Acid Bases at Room Temperature

Robert W. Wilson, University of Oregon, and **Patrik R. Callis**, Montana State University

Polarized Fluorescence of the Dinucleotides

William W. Ward and **Milton J. Cormier**, University of Georgia

In Vitro Energy Transfer in *Renilla* Bioluminescence

Dale E. Brabham and **John Lee**, University of Georgia

Excited State Interactions of α -Tocopherol and Molecular Oxygen

Howard Seliger, Johns Hopkins University

Chemiluminescence from Liver Microsomes During Hydroxylation of Carcinogens

D. Mauzerall, Rockefeller University

Multiple Excitations in Photosynthetic Systems

Vaughn Koester and **Francis K. Fong**, Purdue University

Physicochemical Properties of the 700 nm Absorbing Chlorophyll a -H₂O Dimer

* Papers marked with an asterisk were presented at the Symposium but, for various reasons, are not included in this symposium issue, or are included in abstract or modified form.

Spectroscopic Effects of a Breakdown of the Born–Oppenheimer Approximation

S. J. Strickler

Department of Chemistry, University of Colorado, Boulder, Colorado 80309 (Received February 17, 1976)

Publication costs assisted by the National Science Foundation

Some effects of a breakdown of the Born–Oppenheimer approximation on vibronic intensities in electronic spectra are discussed. The treatment starts from “true Born–Oppenheimer” electronic wave functions which follow the nuclei in their motion. A simple conceptual picture is derived relating the displacement of the electron distribution to that of the nuclei during a vibration. This picture is used to predict qualitative spectroscopic consequences. A calculation based on CNDO/S wave functions is presented for the lowest singlet–singlet transition of naphthalene. The results are in at least qualitative agreement with experiment.

Introduction

The Schroedinger equation for a molecule may be written:

$$\mathcal{H}\Psi(x, X) = \left\{ -\sum_{j=1}^{3n} \frac{\hbar^2}{2m} \frac{\partial^2}{\partial x_j^2} - \sum_{\alpha=1}^{3N} \frac{\hbar^2}{2M_\alpha} \frac{\partial^2}{\partial X_\alpha^2} + V(x, X) \right\} \Psi(x, X) = E\Psi(x, X) \quad (1)$$

Here x_j represents a Cartesian coordinate of one of the n electrons and X_α a Cartesian coordinate for one of the N nuclei, having mass M_α . Born and Oppenheimer¹ (BO) showed that it is often possible to write a wave function

$$\Psi(x, X) = \psi(x, X)\phi(X) \quad (2)$$

a product of an electronic wave function ψ and a nuclear wave function ϕ , which is a good approximation to the true wave function. They gave a prescription for finding this wave function; it involves solving the electronic part of the problem for nuclei fixed at each geometry, X , thus obtaining $\psi(x, X)$ and an energy $V(X)$, and then solving for the motion of the nuclei in the potential $V(X)$ to get $\phi(X)$.

The coordinates X cover vibrational, rotational, and translational motions of the molecule. This paper will be concerned only with vibrational motions. It is possible to transform from the Cartesian coordinates to vibrational normal coordinates, Q (including rotational and translational coordinates for completeness), by the methods of normal coordinate analysis.² The result is to make the replacement in the nuclear kinetic energy part of the Hamiltonian operator:

$$\sum_{\alpha} \frac{\hbar^2}{2M_\alpha} \frac{\partial^2}{\partial X_\alpha^2} = \sum_i \frac{\hbar^2}{2} \frac{\partial^2}{\partial Q_i^2} \quad (3)$$

We will write the wave functions as $\psi(x, Q)$ and $\phi(Q)$, thinking of them in this paper as functions of vibrational normal coordinates.

When the nuclear kinetic energy terms (3) in the Hamiltonian operate on a product function (2) the result is three types of terms: second derivatives of ϕ , second derivatives of ψ , and products of first derivatives of ϕ and ψ . The essence of the BO approximation is to neglect the latter two terms since the electronic wave function varies only slowly with Q . It is these two types of terms which make (2) only an approximate solution to the Schroedinger equation and which must be considered in dealing with a breakdown of the Born–Oppenheimer approximation.

In their pioneering work on vibronic effects in the spectra of polyatomic molecules, Herzberg and Teller³ made use of a so-called “crude Born–Oppenheimer” basis, starting from electronic wave functions at the equilibrium position and expanding the wave functions at other configurations in terms of them:

$$\psi_i(x, Q) = \sum_j C_{ij}(Q)\psi_j(x, O) \quad (4)$$

The coefficients $C_{ij}(Q)$ are generally obtained by perturbation theory. Herzberg and Teller showed that, unless the electronic states are close in energy, mixing coefficients due to BO breakdown are much smaller than those due to ordinary vibronic mixing. The ratio is of the order of the vibration frequency divided by the electronic energy separation. Most subsequent treatments of vibronic effects and BO breakdown have been based on expansions such as (4).

However, these expansions are often slow to converge because it takes many terms to express an electron distribution about an atom in one position in terms of orbitals centered about another position. The use of an expansion truncated after a few terms can lead to serious difficulties. Recently it has become feasible to do electronic wave function calculations in some suitable approximations at a series of nuclear configurations. Although the results are approximate and at only a finite set of configurations, they may be called “true Born–Oppenheimer” wave functions in the sense that they allow direct calculation of vibrational–electronic interactions without requiring expansion (4). Extensive calculations of vibronic intensities in naphthalene⁴ and other molecules⁵ have been carried out by Robey et al. using a CNDO/S calculation.⁶

The purpose of this paper is to point out some advantages of starting with true BO electronic wave functions in considering breakdown of the BO approximation. The emphasis will be on the effects on vibronic intensities in electronic spectra. Some simple conceptual pictures will be presented relating the displacement of the electron cloud to the nuclear displacements when BO breakdown mixes a vibrational level of one electronic state with higher electronic states. This is the usual situation where vibronic intensities can be studied in detail. The pictures help to visualize the spectroscopic consequences expected. Calculation of BO breakdown may be carried out quite readily starting from the true BO wave functions in the CNDO approximation. Some calculations on the mixing of the first and second excited singlet states of

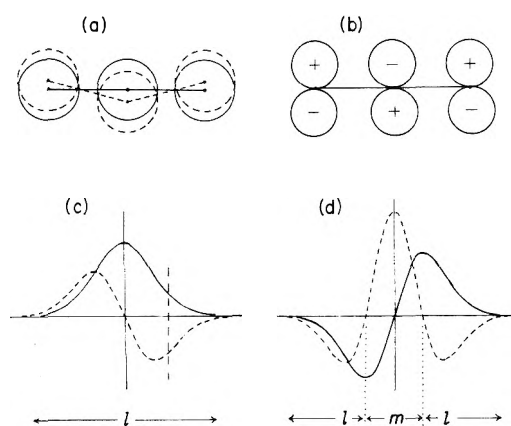


Figure 1. Wave functions for visualizing the Born-Oppenheimer breakdown: (a) $\psi(x, O)$ solid lines and $\psi(x, Q)$ dashed lines; (b) $\partial\psi/\partial Q$ or π^* wave functions; (c) ϕ_0 and $\partial\phi_0/\partial Q$; (d) ϕ_1 and $\partial\phi_1/\partial Q$. l and m indicate regions where the electron cloud is displaced less or more than expected from nuclear displacements.

naphthalene and the spectroscopic consequences are presented as an example.

A Picture of Born-Oppenheimer Breakdown

Let us consider a particular vibrational level a of a particular electronic state, 1. The BO approximation to its wave function is $\psi_1(x, Q)\phi_{1a}(Q)$. If we go beyond the BO approximation we must consider that other vibronic wave functions may be mixed with this one. Perturbation theory gives the result that, to first order, the corrected wave function is

$$\Psi_{1a} = \psi_1\phi_{1a} - \sum_{k,l} \frac{\langle \phi_{kl} | \mathcal{H} | \psi_1\phi_{1a} \rangle}{E_{kl}^0 - E_{1a}^0} \psi_k\phi_{kl} \quad (5)$$

where the sum is over all other BO wave functions. To evaluate the changes in Ψ_{1a} we must examine the matrix element of the Hamiltonian \mathcal{H} between BO wave functions. For the purposes of this paper we shall be interested in matrix elements involving different electronic states.

Consider the matrix element between state 1a and another particular state 2b belonging to another electronic state, and for simplicity consider only one vibration Q as mixing the two levels. The results are easily generalized to several vibrations. There are two sorts of terms in the Hamiltonian matrix elements:

$$\frac{-\hbar^2}{2} \left\langle \phi_{2b}(Q) \left| \left\langle \psi_2(x, Q) \left| \frac{\partial^2}{\partial Q^2} \right| \psi_1(x, Q) \right\rangle_x \right| \phi_{1a}(Q) \right\rangle_Q \quad (6)$$

and

$$-\hbar^2 \left\langle \phi_{2b}(Q) \left| \left\langle \psi_2(x, Q) \left| \frac{\partial}{\partial Q} \right| \psi_1(x, Q) \right\rangle_x \frac{\partial}{\partial Q} \right| \phi_{1a}(Q) \right\rangle_Q \quad (7)$$

arising from the two terms neglected in the BO approximation. Here the subscripts on the brackets indicate the integration coordinates in the matrix element. The electronic matrix elements are still functions of Q , and should properly be inside the vibrational brackets as written. However, it should frequently be satisfactory to remove them from the vibrational brackets; this amounts to neglecting higher order vibronic effects. We can rewrite the two terms as

$$-\frac{\hbar^2}{2} \left\langle \psi_2(x, Q) \left| \frac{\partial^2}{\partial Q^2} \right| \psi_1(x, Q) \right\rangle_x \left\langle \phi_{2b}(Q) \left| \phi_{1a}(Q) \right\rangle_Q \quad (8)$$

and

$$-\hbar^2 \left\langle \psi_2(x, Q) \left| \frac{\partial}{\partial Q} \right| \psi_1(x, Q) \right\rangle_x \left\langle \phi_{2b}(Q) \left| \frac{\partial}{\partial Q} \right| \phi_{1a}(Q) \right\rangle_Q \quad (9)$$

Now the electronic matrix element in (8) vanishes unless the two electronic states are of the same symmetry. It is generally considered to be small for mixing of different electronic states. The term in (9) can mix states of the same or different symmetry (depending on the symmetry of Q), and we shall examine it in more detail.

Use of a simple example is helpful in visualizing the effects of BO breakdown. The following discussion refers to Figure 1. Let ψ_1 be a simple one-electron wave function in a linear triatomic molecule, represented as a linear combination of 1s orbitals on each nucleus, schematically indicated by the circles in Figure 1a. The solid circles represent $\psi_1(x, O)$, the orbitals in the equilibrium configuration, the dashed circles represent $\psi_1(x, Q)$, the orbitals when the molecule is distorted along the bending normal coordinate Q . That particular distortion will be taken as a positive Q . The major effect in distortion is that *the orbitals follow the nuclei*. It is easily seen that $\partial\psi_1/\partial Q \approx [\psi(x, Q) - \psi(x, O)]/Q$ will be a function resembling a p orbital on each atom (although the radial dependence is not identical with a p orbital). This function is schematically shown in Figure 1b. It bears a resemblance to a molecular orbital which we would call a π^* orbital, and Figure 1b could also be taken to represent that π^* orbital. We would then expect a positive and nonzero overlap between π^* and $\partial\psi_1/\partial Q$. In other words, if we let ψ_2 be the π^* electronic state, the matrix element

$$\left\langle \psi_2 \left| \frac{\partial}{\partial Q} \right| \psi_1 \right\rangle_x > 0 \quad (10)$$

Now consider what happens to state 1a when we mix all the vibrational levels of ψ_2 with it according to eq 5 with matrix elements as in eq 9.

$$\Psi_{1a} = \psi_1(x, Q)\phi_{1a}(Q)$$

$$+ \sum_b \hbar^2 \frac{\left\langle \psi_2 \left| \frac{\partial}{\partial Q} \right| \psi_1 \right\rangle_x \left\langle \phi_{2b} \left| \frac{\partial}{\partial Q} \right| \phi_{1a} \right\rangle_Q}{E_{2b}^0 - E_{1a}^0} \times \psi_2(x, Q)\phi_{2b}(Q) \quad (11)$$

This equation can be simplified if we make the approximation that the individual denominators $E_{2b}^0 - E_{1a}^0$ can all be replaced by an average or effective separation between the electronic states, $E_2 - E_1$. We can then make use of a sum rule that

$$\sum_b \left\langle \phi_{2b} \left| \frac{\partial}{\partial Q} \right| \phi_{1a} \right\rangle_Q \phi_{2b} = \frac{\partial\phi_{1a}}{\partial Q} \quad (12)$$

which holds because the $\phi_{2b}(Q)$ form a complete set of functions. Then eq 11 becomes

$$\Psi_{1a} = \psi_1(x, Q)\phi_{1a}(Q) + \hbar^2 \frac{\left\langle \psi_2 \left| \frac{\partial}{\partial Q} \right| \psi_1 \right\rangle_x}{E_2 - E_1} \psi_2(x, Q) \frac{\partial\phi_{1a}(Q)}{\partial Q} \quad (13)$$

We are now in a position to translate this mathematical expression into a conceptual picture of what should happen to the electron distribution because of BO breakdown. Let us suppose that state 2 lies above state 1, so the level of interest is interacting with higher levels; this will be the usual case of

interest. Then $E_2 - E_1 > 0$ and the entire mixing coefficient in eq 13 is positive. We can write

$$\Psi_{1a} = \psi_1(x, Q)\phi_{1a}(Q) + c\psi_2(x, Q) \frac{\partial\phi_{1a}(Q)}{\partial Q} \quad (14)$$

where c is a small positive coefficient. If a is the $v = 0$ level of state 1, the result may be visualized with reference to Figure 1c, where the solid line represents ϕ_{1a} and the dashed line $\partial\phi_{1a}/\partial Q$. Now pick a particular positive Q such as that indicated by the dashed vertical line. Here ϕ_{1a} and $\partial\phi_{1a}/\partial Q$ have opposite signs. Inspection of eq 14 then shows that, at this *instantaneous configuration*, the electronic wave function is $\psi_1(x, Q)$ with a small amount of $\psi_2(x, Q)$ mixed in with *negative sign* (i.e., with coefficient $c \partial\phi/\partial Q < 0$). The mixing of a bit of $2p$ character into the $1s$ orbital on each atom gives a hybrid orbital which has the electron density predominantly on one side of the nucleus. Reference to Figures 1a and 1b, with careful attention to the signs of all terms, will show that the electron density is higher on the side closer to the equilibrium position. Similar considerations when Q is negative will show that the electron density is again on the side toward the equilibrium position. The conclusion is that *for the $v = 0$ level the electrons are distorted from the equilibrium position less than expected from the nuclear positions.*

Similar considerations can be applied to the $v = 1$ level shown in Figure 1d. It is found that in the region labeled m near the equilibrium position the electrons will be displaced more than expected, while for the regions labeled l toward the classical turning points the electrons will be displaced less than expected for the BO wave functions. Higher vibrational levels will show alternating regions where the electrons are displaced more or less than expected; as above the outermost regions will always have the electrons displaced less than expected.

It would be noted that this whole treatment was based on a BO state interacting with higher electronic states. If a level were interacting primarily with a lower state, the sign of $E_2 - E_1$ would be negative and the conclusions would be just the opposite—regions l and m would be interchanged. Furthermore, the picture cannot be applied at all to radiationless transitions where the initial level interacts with nearly isoenergetic levels of a lower electronic state. In that case an average energy and the sum of eq 12 cannot be used and the vibrational levels must be considered individually. Nevertheless, the case discussed above is one of frequent interest.

The conceptual pictures presented above can be used to aid in understanding the effects of BO breakdown on vibronic intensities in electronic spectra. For example, a lack of mirror image symmetry between absorption and emission can be caused by BO breakdown. This has been discussed by Geldof, Rettschnik, and Hoytink⁷ and by Orlandi and Siebrand.⁸ Another example in the spectrum of naphthalene will be considered below. This will illustrate the qualitative behavior expected from the conceptual pictures.

Application to Naphthalene

The lowest excited singlet state of naphthalene has symmetry B_{2u} , and the second state B_{1u} . The transition from the ground state to S_1 is allowed for light polarized along the long axis, and to S_2 allowed polarized along the short (in-plane) axis. However, the transition to S_1 is extremely weak due to nearly exact cancellation of transition moments coupling the ground state to the two major configurations making up S_1 . In fact, most of the intensity of the S_1 band is short-axis polarized, made allowed vibronically by B_{3g} vibrations. A good spectrum of this transition is given by Knight, Selinger, and

Ross.⁹ The dominant band in the spectrum is the band having one quantum of vibration $8B_{3g}$ excited in the upper state. When the molecule is distorted along a B_{3g} coordinate its symmetry is reduced from D_{2h} to C_{2h} , and S_1 and S_2 belong to the same irreducible representation in that group. Therefore B_{3g} vibrations can mix S_1 and S_2 . Since mode $8B_{3g}$ (the lowest frequency of the eight vibrations of that symmetry) induces the most intensity, it is likely to mix the states most strongly. We first qualitatively consider what the effect of BO breakdown should be.

For a symmetry forbidden transition like the short-axis polarized component of S_1 , the transition moment is zero at the equilibrium position but becomes nonzero when the molecule is distorted, in this case along $8B_{3g}$. Of course, the important thing is how far the electron cloud is distorted rather than how far the nuclei are distorted. Thus we see that BO breakdown may affect intensities. Mixing of S_1 with S_2 due to BO breakdown will affect the extent to which the electron cloud is distorted from the equilibrium distribution during the $8B_{3g}$ vibration.

One way this could show up is in a lack of mirror image relationship between absorption and emission.^{8,9} A related quantity which could be checked experimentally is the relative intensities of the dominant $(8B_{3g})_0^0$ band and the $(8B_{3g})_1^0$ hot band in the absorption spectrum. In this notation the right superscript and subscript are the quantum numbers of this vibration in the upper and lower states, respectively. In the absence of BO breakdown the relative intensities can be calculated readily if the vibrations are assumed harmonic and the transition moment assumed to vary linearly with displacement. Both assumptions are probably good. It is also assumed that there is no rotation of normal coordinates between the two states, i.e., no Duschinsky effect.¹⁰ Now BO breakdown involving S_1 should have the following effects. In the $v = 0$ level the electrons are always distorted less than expected from the nuclear displacements, and this results in a lower intensity for $(8B_{3g})_0^0$. On the other hand, in the $v = 1$ level the electrons are distorted more than the nuclei in the region near equilibrium (region m in Figure 1d), and it is just this region which overlaps well with the $v = 0$ level of the ground state, so the $(8B_{3g})_0^1$ band should be increased in intensity by BO breakdown. Qualitatively then, the ratio of intensities of $(8B_{3g})_1^0$ to $(8B_{3g})_0^0$ should be decreased relative to that calculated from the vibrational wave functions and Boltzmann factors.

Another observable effect should be the following: if the $(8B_{3g})_0^1$ band is excited by a narrow band of exciting light in a low pressure gas, a single vibronic level (SVL) emission can be observed from the $v = 1$ level. The emission should go primarily to the $v = 2$ and $v = 0$ levels of the ground state, i.e., the $(8B_{3g})_2^0$ and $(8B_{3g})_0^0$ bands should be predominant in the SVL emission spectrum. The ratio of the intensities of these two bands should be about 2 to 1 on the same assumptions as above. The exact ratio can be calculated from vibrational wave functions and frequencies. However, BO breakdown should make the $(8B_{3g})_0^1$ stronger for the reasons mentioned above. On the other hand, the $v = 2$ level of the ground state will overlap most with the regions called l in Figure 1d, where the electrons are distorted less than expected from the nuclear displacements, and this will result in a lower intensity for $(8B_{3g})_2^0$. BO breakdown will then lower the intensity ratio of $(8B_{3g})_2^0$ to $(8B_{3g})_0^0$ from the expected value near 2 to 1 to some smaller value.

These two qualitative effects are predicted on the basis of the simple conceptual pictures presented above. The next

section describes a calculation of the expected magnitude of the effects based on CNDO/S wave functions. Mixing of S_1 with S_2 due to BO breakdown caused by the $8B_{3g}$ vibration will be considered. The results will then be compared with some experiments already in the literature.

CNDO Calculations

The calculations described here are based on wave functions for the ground and excited singlet states of naphthalene obtained by Robey et al.⁴ These are done in the CNDO/S approximation.⁶ In this method all valence electrons are treated, and in the ground state these completely fill the molecular orbitals up to number 24. The excited states are described by fairly extensive configuration interaction (CI) between singly excited configurations $\Theta_{st}(x, Q)$:

$$\psi_i(x, Q) = \sum_{st} C_{ist}(Q) \Theta_{st}(x, Q) \quad (15)$$

Each Θ_{st} is a sum of two antisymmetrized products of MO wave functions θ with an electron promoted from orbital s to an originally unfilled orbital t . Each MO θ_j is in turn given by a linear combination of atomic orbitals χ :

$$\theta_j(x, Q) = \sum_{\mu} a_{j\mu}(Q) \chi_{\mu}(x, Q) \quad (16)$$

At the equilibrium geometry, the first excited singlet state $\psi_1(x, 0)$ is a linear combination of configurations (24,26), (23,25), (24,29), and (22,28) while the second state $\psi_2(x, 0)$ is a combination of (24,25), (23,26), (22,27), and (23,29). All of these promotions involve only π orbitals. When the molecule is distorted along the $8B_{3g}$ coordinate, three things happen within the BO approximation: (a) First and most importantly, the orbitals follow the nuclei. (b) The coefficients $a_{j\mu}$ change, so that the MO's have a slightly different form as expressed in eq 16. (c) The CI coefficients C_{ist} defining the states by eq 15 change. In particular, there is a mixing of the configurations of ψ_2 into ψ_1 and vice versa.

The distorted molecule has lower symmetry, and one would expect a nonzero short-axis transition moment for the ground state to S_1 transition. In fact, each of the three effects contribute to this transition moment. It happens that the first effect contributes very little in this case; most of the short-axis transition moment comes from the changes of coefficients. Effects (b) and (c) produce transition moments which partially cancel, with the predominant contribution being (c), the change in CI coefficients.⁴

We wish to consider the mixing of S_1 with S_2 due to BO breakdown, so we must look at the matrix element $\langle \psi_2 | H | \psi_1 \rangle_x$, which will reduce to terms such as eq 8 and 9. The terms of eq 8 will vanish in first order because the two states have different symmetry. We will consider the term from eq 9 which will involve the derivative of ψ_1 with respect to $Q(8B_{3g})$. We must take account of each of the three types of changes described above. Consider first changes of type (a). Because all of the configurations in S_1 and S_2 are π, π^* , we need only consider the $2p\pi$ type atomic orbitals. The derivative of such an orbital when the nucleus moves in the molecular plane will resemble a d orbital on the atom. This will have zero overlap with the original p orbital on the same center. It may overlap with p orbitals on other centers, but such terms are neglected in the CNDO approximation. Thus matrix elements between S_1 and S_2 involving the motions of the orbitals in following the nuclei will be taken to be zero.

Terms of types (b) and (c) will both contribute to the electronic matrix element. Some straightforward algebra, making

use of the orthogonality of wave functions and neglecting overlap between orbitals on different atoms shows that the whole matrix element reduces to a simple expression involving coefficients and their derivatives:

$$\left\langle \psi_2 \left| \frac{\partial}{\partial Q} \right| \psi_1 \right\rangle = \sum_{st} C_{2st} \frac{\partial C_{1st}}{\partial Q} + \sum_{r,s,t} C_{2st} C_{1rt} \sum_{\mu} a_{s\mu} \frac{\partial a_{r\mu}}{\partial Q} + \sum_{s,t,u} C_{2st} C_{1su} \sum_{\nu} a_{t\nu} \frac{\partial a_{u\nu}}{\partial Q} \quad (17)$$

Here the first sum involves terms of type (c) and the other two sums terms of type (b). The second sum involves configurations where in the two states electrons are promoted from different filled orbitals r and s to the same empty orbital t , while the third sum involves promotions from the same filled orbitals s to different empty orbitals t and u .

All these coefficients and derivatives can be evaluated from the CNDO wave functions obtained by Robey⁴ at $Q = 0$ and at the zero point rms value of Q , $Q^* = (\overline{Q^2})^{1/2} = (\hbar/8\pi^2 c \bar{\nu})^{1/2}$, where $\bar{\nu}$ is the frequency of the vibration, taken to be 509 cm^{-1} for $8B_{3g}$. One must be careful to use a consistent set of phases for all wave functions, since these phases are arbitrary and the CNDO program often chooses them differently at $Q = Q^*$ and at $Q = 0$. The derivative of a coefficient is taken to be $\partial C/\partial Q = [C(Q^*) - C(0)]/Q^*$. The calculation does give good linearity over the small displacements used.^{4,5} The value of the matrix element is found to be

$$\left\langle \psi_2 \left| \frac{\partial}{\partial Q} \right| \psi_1 \right\rangle_x = +1.354 \times 10^{19} \text{ g}^{-1/2} \text{ cm}^{-1} \quad (18)$$

We now wish to make use of this value in eq 12 to get corrected vibronic wave functions for the $(8B_{3g})^0$ and $(8B_{3g})^1$ levels of S_1 . To do so, we must pick a suitable electronic energy separation. It is probably best to use the separation of the absorption band maxima which is about 4850 cm^{-1} . It also simplifies the equation to make use of the harmonic oscillator relationship

$$\partial \phi_v / \partial Q = (\pi c \bar{\nu} / \hbar)^{1/2} \{ \sqrt{v} \phi_{v-1} - \sqrt{v+1} \phi_{v+1} \} \quad (19)$$

where $\bar{\nu}$ is the vibration frequency, 438 cm^{-1} for $8B_{3g}$ in state S_1 .

The results for the wave functions are

$$\Psi[S_1, (8B_{3g})^0] = \psi_1 \phi_{(8B_{3g})^0} - 3.092 \times 10^{-3} \psi_2 \phi_{(8B_{3g})^1} \quad (20)$$

$$\Psi[S_1, (8B_{3g})^1] = \psi_1 \phi_{(8B_{3g})^1} + 3.092 \times 10^{-3} \psi_2 \{ \phi_{(8B_{3g})^0} - \sqrt{2} \phi_{(8B_{3g})^2} \} \quad (21)$$

The vibrational wave functions ϕ in these expressions all refer to states of S_1 with 0, 1, or 2 quanta of the $8B_{3g}$ vibration excited.

The wave functions (20) and (21) can be used to compute transition moments between various vibrational levels of the ground state and these two levels of the S_1 state. In each case, one can calculate a transition moment in the absence of BO breakdown from the first term in the wave function. Inclusion of the second term then gives important interference effects which may increase or decrease the transition moment.

Even the small component of S_2 can have a large effect because the electronic transition moment to S_2 is much larger than that to S_1 . The absolute value of the transition moment is given only approximately by the CNDO calculation,⁴ but the relative values produced by vibronic effects and BO breakdown should be reasonable. It is necessary to take account of the difference in vibration frequencies in the two states, as this plays a role in the relative intensities of bands.

In absorption, the integrated intensity, $\int \epsilon d\nu$, is proportional to the frequency multiplied by the square of the transition moment. For bands of similar shape and width, the relative peak height would be proportional to the relative values of $\bar{\nu}M^2$. If transitions originate in different vibrational levels, the relative populations must also be taken into account. In emission, the integrated intensity of a band, measured in photons per unit time, is proportional to $\bar{\nu}^3M^2$.

Calculated transition moments for three vibronic bands are shown in Table I. The column headed M^0 gives the calculation in the absence of BO breakdown, while column M gives the value including the latter. Actually, these values correspond to the sum of all transitions with these particular changes in $8B_{3g}$ and all possible changes in A_g modes. However, the relative values should apply to the particular bands where no other vibrations change.

As indicated above, the ratio of the $(8B_{3g})_1^0$ to $(8B_{3g})_0^0$ bands in absorption is one place where BO breakdown should show up. Table I shows clearly that M for the first band is decreased while that for the second is increased by BO breakdown. The Boltzmann factor for $(8B_{3g})_1^0$ at 296 K is 0.084 24. We then obtain a ratio of intensities of 0.0950 in the absence of BO breakdown and 0.0810 including BO breakdown. This is not a large change and is on the borderline of detectability. The prediction can be compared with the spectrum of Knight et al.⁹ The ratio of band intensities (measured from the large spectrum in a preprint of their paper) is about 0.07 ± 0.01 , in reasonable agreement with the present estimate.

Another test for BO breakdown is the ratio of intensities of $(8B_{3g})_2^1$ to $(8B_{3g})_0^1$ in the fluorescence spectrum. Table I shows that the transition moment for the former decreases while that for the latter increases due to BO breakdown, in accord with the earlier qualitative picture. Use of the moments and frequencies in Table I gives a ratio of intensities of 2.25 in the absence of BO breakdown and 1.93 when it is taken into account. Again the predicted effect (a 14% decrease in ratio) is significant but not large. A single-vibronic-level fluorescence spectrum from level $(8B_{3g})_1^1$ has been published recently by Stockburger, Gattermann, and Klusman.¹¹ There are experimental difficulties because the $(8B_{3g})_0^1$ band is subject to self-absorption and to interference by scattered exciting light. However, their reported ratio, corrected for these effects, is 1.16, which is a great deal smaller than calculated. They recognize that this is lower than expected, but mistakenly conclude that this cannot be due to BO breakdown, so they attribute it to anharmonicity in the ground state.

Both of the above experiments suggest that our calculation has underestimated the BO breakdown. In particular, the second experiment would require that the BO breakdown matrix element be larger by a factor of 4.34. If that were the case, the ratio of $(8B_{3g})_1^0$ to $(8B_{3g})_0^0$ in absorption should be about 0.0476 which seems too low to be consistent with the absorption experiment. It seems possible that there are still scattered light problems in the emission spectrum.

A few possible sources of error in the calculation should be mentioned. Of course, the wave functions are only approximate. The neglect of overlap between the derivative of an atomic orbital and another orbital could be a problem. However, it would be quite inappropriate to include such terms when the wave functions were obtained by neglecting overlap. Improvement of this approximation would require a different sort of wave function. We have also neglected any rotation of normal coordinates between the ground and excited state. This would affect vibronic intensities without the BO breakdown. We have assumed the vibrations to be harmonic, in-

TABLE I: Frequencies and Transition Moments Calculated for Vibronic Bands in the Ground to S_1 Transition of Naphthalene

Transition	$\bar{\nu}$, cm ⁻¹	M^0 , eÅ	M , eÅ
$(8B_{3g})_1^0$	31 500	0.049 69	0.047 86
$(8B_{3g})_0^1$	32 470	0.046 10	0.048 07
$(8B_{3g})_2^1$	31 450	0.072 52	0.070 04

cluding no Fermi resonance or mixing of different normal modes. Parmenter et al. have shown that the latter effect plays a significant role in vibronic intensities in benzene,¹² but it probably has less influence in naphthalene where most of the oscillator strength is in the bands with no change in totally symmetric vibrations. The average energy separation of 4850 cm⁻¹ was chosen fairly arbitrarily. Use of the separation of the origins of S_1 and S_2 would about double the effect calculated, but this would surely be too small a value to use for the average separation. Any of these approximations may affect the accuracy of the calculations, although all seem unlikely to produce a very large effect. In any case, the absorption experiment suggests that the calculations are not too far off.

In summary, we have reviewed a method of treating breakdown of the BO approximation, starting from a true BO basis. We have shown how the treatment can lead to a simple conceptual picture of the effects in certain cases. This picture was based on the terms we have called type (a), emphasizing the importance of the orbitals following the nuclei. But terms of types (b) and (c) work in analogous ways. If a wave function varies with Q by changes of coefficients, i.e., changes of electron distribution among atoms, then BO breakdown will make the changes greater or smaller in different regions of the vibration just as it can make the electron displacements greater or smaller. (It should be mentioned that it is possible to imagine a situation where the effects on transition moment are in the opposite direction from that predicted. This could happen if say the major transition moment came from terms of type (a), while a nearby mixing state affected only terms of type (b) or (c) and these were in the opposite direction.) The conceptual picture was used to help understand the expected spectral effects of BO breakdown. A method of calculation of these spectral effects using CNDO wave functions was summarized, and applied to the first singlet transition of naphthalene. Finally the results were compared with experiment and found to be in at least qualitative agreement.

Acknowledgments. This work was supported in part by the National Science Foundation. The author also wishes to thank the Council on Research and Creative Work of the University of Colorado for the grant of a Faculty Fellowship during which this work began, and to thank the Australian National University for their hospitality during that time. Special thanks are due to Dr. M. J. Robey and Professor I. G. Ross for many discussions and for providing the CNDO calculations used in this study.

References and Notes

- (1) M. Born and R. Oppenheimer, *Ann. Phys.*, **84**, 457 (1927).
- (2) E. B. Wilson, Jr., J. C. Decius, and P. C. Cross, "Molecular Vibrations", McGraw-Hill, New York, N.Y., 1955.
- (3) G. Herzberg and E. Teller, *Z. Phys. Chem. (Leipzig)*, **B21**, 410 (1933).
- (4) M. J. Robey, I. G. Ross, R. Southwood-Jones, and S. J. Strickler, to be submitted for publication.
- (5) M. J. Robey, Ph.D. Thesis, The Australian National University, Canberra, A.C.T., 1974.
- (6) J. Del Bene and H. H. Jaffe, *J. Chem. Phys.*, **48**, 1807 (1968).
- (7) P. A. Geldof, R. P. H. Rettschnik, and G. J. Hoytink, *Chem. Phys. Lett.*, **10**,

- 549 (1971).
 (8) G. Orlandi and W. Siebrand, *Chem. Phys. Lett.*, **15**, 465 (1972).
 (9) A. E. W. Knight, B. K. Selinger, and I. G. Ross, *Aust. J. Chem.*, **26**, 1159 (1973).
 (10) F. Duschinsky, *Acta Physicochim. URSS*, **7**, 551 (1937).
 (11) M. Stockburger, H. Gattermann, and W. Klusman, *J. Chem. Phys.*, **63**, 4519 (1975).
 (12) C. S. Parmenter, private communications.

Discussion

R. M. HOCHSTRASSER. How does this work compare with the recent work done by Metz?

S. J. STRICKLER. I believe that most of his calculations—in fact, most of the calculations that have been done—have been based on the crude Born–Oppenheimer basis set, where one starts with wave functions only at the equilibrium geometry and expands the wave functions for distorted geometry in terms of them. Then a perturbation treatment is used to obtain the distorted wave functions followed by a perturbation treatment to get the Born–Oppenheimer breakdown. There are cases where that sort of expansion is very slow to converge. In some of the cases that you are looking at, naphthalene really is an example, the particular coupling between S_1 and S_2 does not really contribute to making those orbitals follow the nuclei, and so one may be able to get by with it. If the particular coupling that you are interested in does contribute to making the orbitals follow the nuclei, then the expansion is slow to converge. One gets by with it if the terms that he is looking at are very small anyway. This, of course, certainly can give trouble, although one can probably reasonably calculate this particular case because the S_2, S_1 mixing doesn't contribute to making the orbitals follow the nuclei.

W. R. MOOMAW. If I understood you correctly, you calculate the changes in the intensity based upon the root mean square displacement rather than by integrating over the actual displacements (which might include anharmonicity effects). How does the error due to this approximation compare in magnitude with the other approximations in your formalism and the use of CNDO wave functions?

S. J. STRICKLER. The calculations that Ross and Robey^{4,5} did were based only on the value at the root mean square displacement; however, they did in various cases check to see that the variation appeared to be linear, and it does. As long as it's linear, then that's good.

W. R. MOOMAW. I was wondering how much of that might account for discrepancies compared to using inaccurate wave functions or some of the other approximations which you discussed on the first slide.

S. J. STRICKLER. The linearity looks pretty good in this case. The errors must be due to other factors.

R. KOPELMAN. What is the precise nature of your zero-order wavefunctions? What are the exact nuclear configurations for these?

S. J. STRICKLER. This is a CNDO calculation which just starts from atomic orbitals, 2s and 2p on the carbon atoms plus the 1s orbitals on the hydrogens, but being a CNDO calculation it's semiempirical and doesn't really use the forms of the atomic orbitals on the nuclei in the calculation. It uses semiempirical sorts of electronic repulsion integrals, and so on, in doing the SCF and CI calculations.

R. KOPELMAN. But for what nuclear configuration?

S. J. STRICKLER. The equilibrium position, I guess, is an x-ray structure, and the normal coordinate analysis was actually done with two different force constant sets which led to somewhat different normal coordinates. The best results are from a potential function derived by Kydd. (R. A. Kydd, Ph.D. Thesis, University of British Columbia, Vancouver, B.C. 1969). They look quite good in terms of the normal coordinate analysis.

L. GOODMAN. Rotation of the normal modes on going from the ground to the excited state could by itself cause a change in the coupling mode transition probability in absorption compared to emission. Would you comment on how you distinguish between this effect and corrections to the Born–Oppenheimer approximation, especially for a case like naphthalene where the observed intensity change is only a few percent?

S. J. STRICKLER. I have not worried about a rotation of normal coordinates. In other words, I have assumed in everything I have said here that the normal coordinate in the ground state was parallel to that in the excited state, but I have corrected for the difference in frequencies.

Well, the rotation is something that one has to worry about. I'm not sure that I can prove this, but I believe that looking at that ratio of the two things in the single vibronic level emission is probably less sensitive to rotation than looking at the mirror image relationship between absorption and emission. That's one reason I think that's probably a better check.

C. PARMENTER. The exploration of the $8(b_{1g})_2^2/8g_0^1$ fluorescence intensity ratios in naphthalene to test the proposition concerning non-BO behavior is reminiscent of a study recently completed by Dr. K. Tang at Indiana on a similar question in benzene. He found that analogous intensity ratios involving the inducing mode in benzene depart from the BO expected values, but he was able to show that the effect was dominantly (if not entirely) due to Fermi resonances involving levels more than 100 cm^{-1} apart. His results were consistent with the discussion of these effects by Fischer, Scharf, and Parmenter in *Molecular Physics*, 1975. I wonder if such effects could occur also in naphthalene to complicate the search for non-BO behavior?

S. J. STRICKLER. Yes, I think that that's the thing that's most likely to affect it—the Fermi resonance interaction between the levels.

S. P. MCGLYNN. It appears to me that you have analyzed CNDO results at a root mean square geometry in terms of zero-order results (defined at the ground state geometry and, also, by the CNDO algorithm). This may or may not have relevance to *fact* (i.e., experiment). I would believe such relevance if the f number at the root mean square geometry obtained by CNDO/CI was in good correspondence with respect to polarization? How good is the numerical agreement?

S. J. STRICKLER. I am analyzing the effect relative to calculated short axis polarized intensity induced by the vibrations. In other words, at the equilibrium position there is a calculated long-axis polarized intensity but no calculated short-axis polarized intensity. As one distorts the molecule along that mode, one obtains some short axis intensity. One also gets a calculated Born–Oppenheimer breakdown, which does things to the intensity which I have taken relative to the calculated intensity because they are calculated from the same wave function. So I think that even if the wave functions are some what inadequate, probably the ratios that I calculate are what the Born–Oppenheimer breakdown does compared to the intensity that is induced by that distortion. The ratio is probably reasonable.

S. P. MCGLYNN. In other words, what you are doing, is that you are partitioning the calculated root mean square geometric f value into contributions added to the zero-order or ground state conformational oscillator strength. Now my question simply is how does the root mean square calculated oscillator strength compare with the actual known oscillator strength for this (transitions). In other words, are you partitioning yourself way off relative to experiment or something that's right on.

S. J. STRICKLER. The calculated short-axis polarized intensity is somewhat low in the calculation—maybe a factor of 2 or something of that order. It comes from a very interesting mix of the orbitals following the nuclei, changes in AO coefficients in the MO's, and the changes in coefficients in the CI, and it turns out for this particular mode the CI is the dominant thing. For other modes which are calculated to be much weaker, the CI is not always the dominant thing.

Dynamics of Photodissociation in Solution using Picosecond Spectroscopy¹

R. W. Anderson, Jr.,² and R. M. Hochstrasser*

Department of Chemistry and Laboratory for Research on the Structure of Matter, University of Pennsylvania, Philadelphia, Pennsylvania 19174 (Received March 22, 1976)

Publication costs assisted by the National Science Foundation

Measurements of the photolysis of tetraphenylhydrazine in fluid solution at 300 K on the picosecond time scale are described in this work. These measurements include both spectral and kinetic studies which were conducted through the use of a mode-locked Nd³⁺/glass laser spectroscopic apparatus. Tetraphenylhydrazine is shown to dissociate into radicals with a well-characterized spectrum in a time less than ~ 2 ps while during times from ca. 0 up to 2 ns cage recombination of the radicals does not appear to occur.

1. Introduction

In 1941 Lewis and Lipkin^{3a} reported on the production of free radicals from tetraphenylhydrazine^{3b} (TPH) in a rigid glass at 77 K. The glass containing colorless TPH was irradiated with uv light and became strongly colored because of the development of a product having absorption maxima at ~ 470 and ~ 800 nm. At 77 K these radicals did not recombine appreciably, although on softening the glass the color disappeared. A simple model for this process is that the light causes photodissociation of the N-N bond and that the two radicals formed thereby are frozen into configurations unsuitable for thermally unassisted recombination. Wiersma and Kommandeur⁴ studied the EPR and optical spectra of the radicals in glasses and in crystals at low temperatures. These authors exposed a residual weak interaction between the pairs of radicals in the glass and crystal, such that at 77 K the radical pairs were found to consist of a thermal mixture of singlet and triplet states, rather than the noninteracting doublets expected from two essentially isolated radicals. The exchange energies estimated by Wiersma and Kommandeur^{4a} are in the range $30\text{--}100\text{ cm}^{-1}$ indicating that the nitrogen atoms of the radicals in the pairs are ca. $3\text{--}4\text{ \AA}$ apart. Attempts were also made to understand the electronic spectrum of the radical and of the radical pair and although in the earlier work^{4a} the 800-nm band was attributed to a charge-separated state exclusive to the radical pair, more recent studies of the kinetic spectroscopy of the TPH photodissociation⁵ have shown convincingly that both of the photoinduced bands correspond to transitions in the radical itself as originally assumed by Lewis and Lipkin.^{3a}

In the present study we have devised experiments to obtain a more detailed analysis of the dynamics of the photodissociation and the cage recombination of the radicals in fluid solution at 300 K. As part of this study we have developed a reliable picosecond laser system that will be described in some detail. The essence of this experimental approach is that it is relatively cheap and reliable, although the data analysis is significantly more time consuming than if automatic data handling methods were employed.

2. Experimental Section

2.1 Materials. Tetraphenylhydrazine, hereafter referred to as TPH, from Frinton Laboratories was purified by repeated recrystallization from a 1:1 mixture of chloroform and toluene.^{4a} The purity of the final product was ascertained by chromatography, melting point determination, and compar-

ison with previously reported uv absorption spectra.^{4a} Purified TPH was kept under refrigeration and in darkness prior to its use. The solvents benzene and CCl₄ were Baker spectrophotometric grade; the 1-methylnaphthalene and octoil were from Kodak and Consolidated Vacuum Corp., respectively. None of the solvents used in this work exhibited measurable absorption at the excitation frequency used in the laser photolysis experiments and so were used without further purification. All TPH solutions were made to concentrations of 10^{-3} M and used in 1-mm path length cells such that the optical density at 353 nm was ca. 2. This arrangement minimized uncertainties in the measurement of time.

2.2 The Laser Photolysis Apparatus. The mode-locked neodymium/glass laser utilized in this apparatus as well as the determination of its output optical pulse characteristics has been described in more detail elsewhere.⁶ Briefly, the mode-locked laser produces a train of picosecond pulses from which a single pulse is extracted by a fast optical switch. The extracted pulse, taken from the beginning of the train, is amplified by a second flash lamp pumped Nd³⁺/glass rod to yield a single optical pulse at 1060 nm with an energy content of ca. 50 mJ. The second and third harmonics of 1060 nm, at 530 and 353 nm, are produced using KDP crystals with the conversion to 530 nm being ca. 10% and that from 530 to 353 nm being ca. 25%. The natures of the pulses at the three wavelengths were determined by a number of techniques^{6,7} and in this work are well characterized by gaussians having a width (fwhm) of 8 ps.

In this apparatus the system being studied is excited with the single 353-nm pulse and the excited states or photoproducts are detected spectrally and kinetically with a second pulse which is a spectroscopic continuum. We have used the four-wave mixing continuum⁸ first brought out as a practical tool by Alfano and Shapiro⁹ and subsequently used by many other workers to detect transient absorption.¹⁰⁻¹² The temporal, spectral, and spatial characteristics of these laser-produced continua are particularly suited for determining transient spectra as well as for kinetic studies of the spectral features. Continua produced by high-intensity 1060-nm pulses focused into CCl₄ are spectrally broad and structureless as well as being spatially coherent with the driving pulse. The intensity of a single 8-ps continuum pulse is sufficient to substantially blacken photographic plates from ca. 1000 to 430 nm after it has been dispersed in a spectrograph. The temporal characteristics of these continua are generally equivalent to the pulse profile of the driving radiation; however, within its envelope the frequencies are distributed such that longer wavelengths

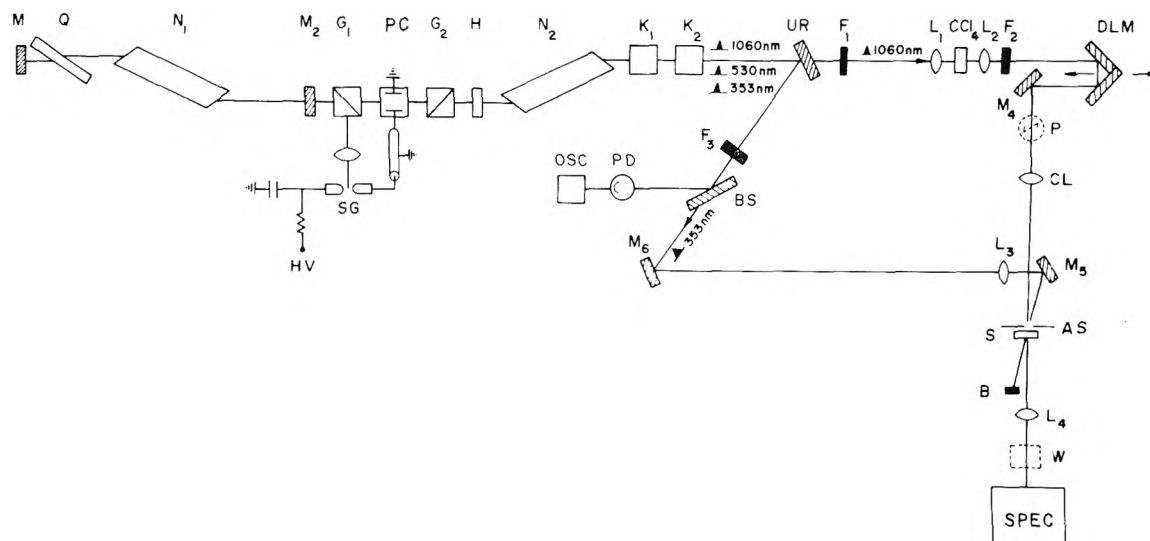


Figure 1. Experimental apparatus: M, mirror; Q, q-switch cell; N, neodymium rod; G, Glan laser prism; PC, Pockels cell; SG, spark gap; HV, high voltage; H, half-wave plate; K, KDP crystal; UR, ultraviolet reflecting dielectric mirror; F, filter; L, lens; CCl₄, 2-cm carbon tetrachloride cell; DLM, variable-delay mirrors; P, Polaroid polarizer; CL, cylindrical lens; BS, 8% beam splitter; PD, photodiode; OSC, oscilloscope; AS, adjustable slit; S, sample; B, optical stop; W, Wollaston prism; SPEC, spectrograph.

shift toward the front of the pulse while the short wavelengths are shifted to the tail of the continuum pulse. This effect can be minimized by using as few dispersive elements, such as lenses and prisms, as possible and by keeping the extra length of the CCl₄ cell, itself a dispersive element, as short as possible.

Referring to Figure 1, the continuum is collimated from the CCl₄ cell and directed to the sample via a movable delay line so that the sample can be probed either before, during, or after excitation by the 353-nm pulse. As before⁶ the $t = 0$ position on the delay line, where the continuum pulse and excitation pulse optical lengths are balanced and the pulses reach the sample simultaneously, is determined by using a sample such as 1-methylphenanthrene, in which a transient is assumed to be produced instantaneously.

It is important to emphasize that with this apparatus a spectrum covering a large spectral region is obtained with a single laser shot. Also, this spectrum can be recorded at various delay times ranging from picoseconds to a few nanoseconds—one shot being required at each setting. As a result a variety of both spectral and kinetic information can be obtained quickly.

In this apparatus we use a cylindrical lens to focus the continuum onto an adjustable slit behind which lies the thin sample. The ultraviolet pulse is focused to a small spot at the sample in the center of the region probed by the continuum. By use of an adjustable slit set to a width no greater than the 353-nm spot diameter the sample can be masked such that the continuum only probes a narrow strip of the sample containing regions either excited or unexcited. Special care must be taken so that the crossing angle, of the continuum beam with the excitation beam, will allow substantial overlap of the two beams in the thin sample. Finally, the image of this strip was transferred to a $\frac{3}{4}$ -m Spex grating spectrograph and recorded with photographic plates. We have shown that a low-aperture Hilger Littrow spectrograph can be used for these spectra if a wider wavelength range needs to be covered in one shot.

As mentioned earlier a complete spectrum can be recorded over many hundred angstroms with a single laser firing, but in addition, by using a Wollaston prism after the sample, this same spectrum can be divided into two similar spectra differing only in their polarizations. To complete this arrange-

ment, we have determined that the continuum generated in CCl₄ is polarized mainly parallel to the electric vector of the 1060-nm driving pulse. Consequently, for the Wollaston to see both parallel and perpendicular polarizations, the continuum was transformed by these components by inserting a polarizer before the sample as shown in Figure 1. The placement or orientation of this polarizer is such that its polarization axis and that of the continuum form an angle of 45°.

2.3 Treatment of the Data. The successful recording and analysis of our experimental results depends to a large extent on the proper use of photographic techniques. Three prerequisites must be met when using photographic plates in conjunction with a picosecond laser-produced continuum: (i) all exposures should fall within the linear range of the emulsion characteristic curve; (ii) the reciprocity relation must be obeyed for plates exposed by laser continua; (iii) the emulsion γ , which is the slope of the linear range on the characteristic curve, must be used when two or more emulsion types are needed to cover a given spectral range.

In this work two emulsions, types 1-F and 1-N, were used and each one was calibrated using the picosecond continuum such that the above three prerequisites were satisfied. The calibration consisted of measuring a range of plate densities and corresponding continuum intensities over a range of wavelengths. A semilog plot of these data revealed a normal emulsion characteristic curve with a linear region defined by

$$D = \gamma \log I \quad (1)$$

Plate densities were measured on a Joyce-Lobel microdensitometer and the intensities were recorded with a 1P28 photomultiplier/oscilloscope detection system.

The determination of a transient spectrum from an exposed plate consisted of taking densitometer traces of the profile of the spectral image at appropriate intervals corresponding to different wavelengths. Each profile measurement included a range of 50 Å, for averaging purposes, and a typical profile is shown in Figure 2. The optical density of the transient at a particular wavelength is computed by

$$OD = \frac{1}{\gamma} (D_0 - D) \quad (2)$$

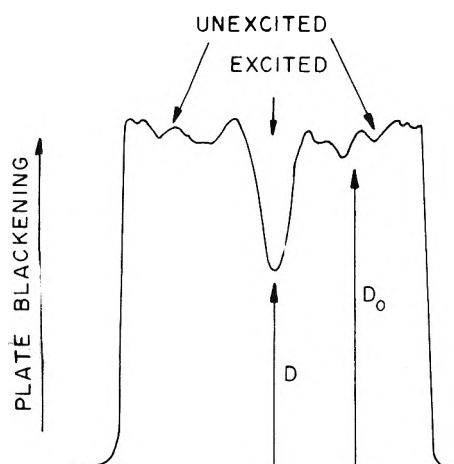


Figure 2. Microdensitometer tracing (see text) taken from a plate corresponding to a specific wavelength. The central, less exposed region (density D) is the image of the continuum, at the selected wavelength, transmitted through the sample region excited by 353-nm radiation. The exposed-plate regions on either side (density D_0) represent exposures from the continuum transmitted through unexcited regions of the sample. The scale is linear in density.

where γ is the slope of the linear portion of the emulsion characteristic curve and D_0 and D are the plate densities resulting from exposure by the continuum transmitted through unexcited and excited regions of the sample, respectively.

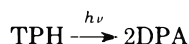
In cases where the spectrum extends over a wide spectral range, more than one photographic emulsion is required. In such a situation the spectrum over this full range obviously needs more than one laser shot and the OD calculated by eq 2 must be normalized to the 353-nm excitation intensity. Also, care must be taken to ensure that the sample is not optically saturated by the 353-nm pulse. To guard against this we determined that the sample OD is linear with 353-nm intensity and that the intercept of this response is zero. The 353-nm intensity is monitored, as shown in Figure 1, by taking a small reference portion of the excitation intensity with a beam splitter and monitoring this with an oscilloscope.

Kinetic measurements are recorded in much the same manner as the spectra except that only a few selected wavelengths were studied in detail and normalized transient optical densities were determined with several laser firings at each delay time. The smooth curves drawn through the kinetic data, as shown in Figure 4, are calculated curves which incorporate eight picosecond gaussian excitation and probe pulses into a first-order rate process.⁶

3. Results

The results of experiments with TPH in benzene solution at 300 K are shown in Figures 3 and 4. Figure 3 shows the transient absorption spectra taken near $t = 0$ and at $t = 1$ ns. At both times the spectra are in reasonable agreement with the microsecond transients previously observed⁵ and characterized as due to the diphenylamine free radical. These spectra also appear the same as the steady-state spectra seen previously in rigid glasses^{3a,4a} and crystals.^{4b}

The kinetic data are shown in Figure 4 which contains the plots of transient optical density at wavelengths corresponding to the 470- and 800-nm absorption peaks. In both cases the calculated curves refer to the process



considering that pumping and probing pulses are 8 ps and

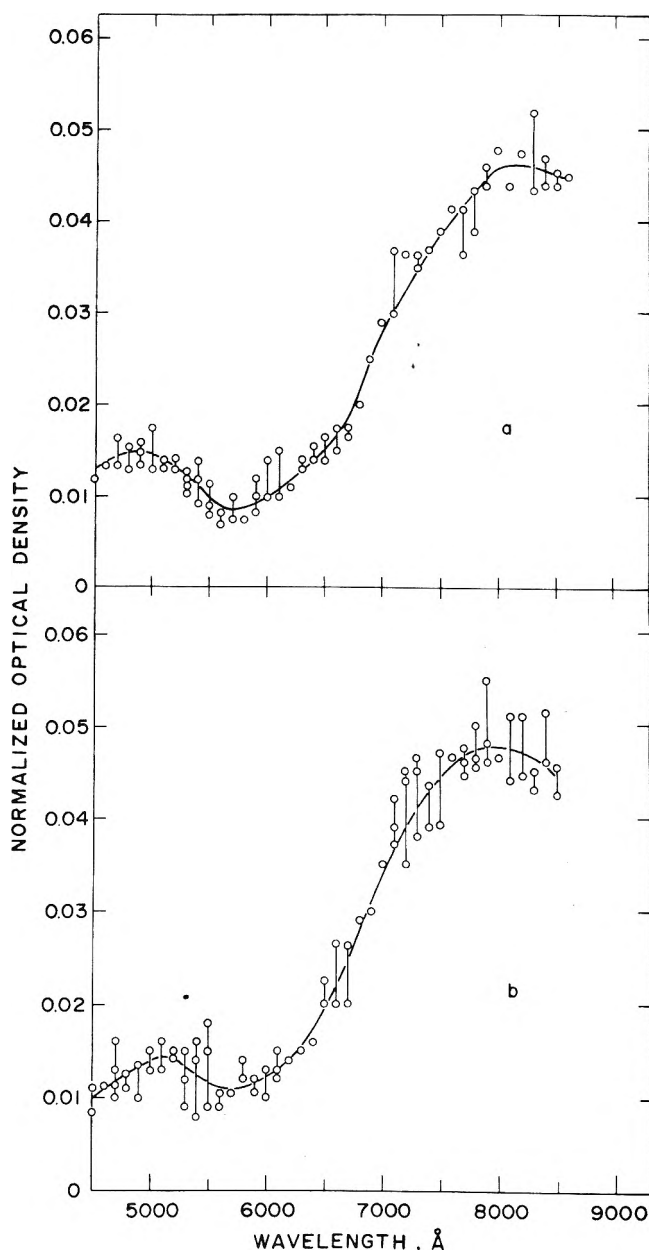


Figure 3. Spectrum of TPH (a) 6 ps after excitation with 353 nm and (b) 1000 ps after excitation. The optical density scale shown here is arbitrary and the two spectra are normalized to each other at the peak of the near-ir band. Actual sample optical densities at the maximum of the near-ir band in one particular case were 0.12 and 0.15 for cases a and b, respectively. Each spectrum shown here is a composite which includes the data from four separate determinations.

gaussian and that the radicals are produced instantaneously. We have searched without success for transient absorption near $t = 0$ corresponding to the absorption of the TPH excited state produced by the 353-nm excitation. Thus either the TPH photoexcited state does not have a detectable spectrum between 400 and 850 nm or the photodissociation occurs in less than ca. 2 ps. On the basis of our experience that every large molecule we have studied whose ground state absorbs at 353 nm has an excited state absorption in the range of the 1060-nm pumped CCl_4 continuum, we favor the latter interpretation. This generalization includes aromatics, substituted aromatics, ketones, nitrogen heterocyclics, and porphyrins. The main point of this discussion is that our failure to detect a transient fixes the timing of the radical formation more accurately than the fitting of a theoretical curve (as in Figure 4) to the kinetic

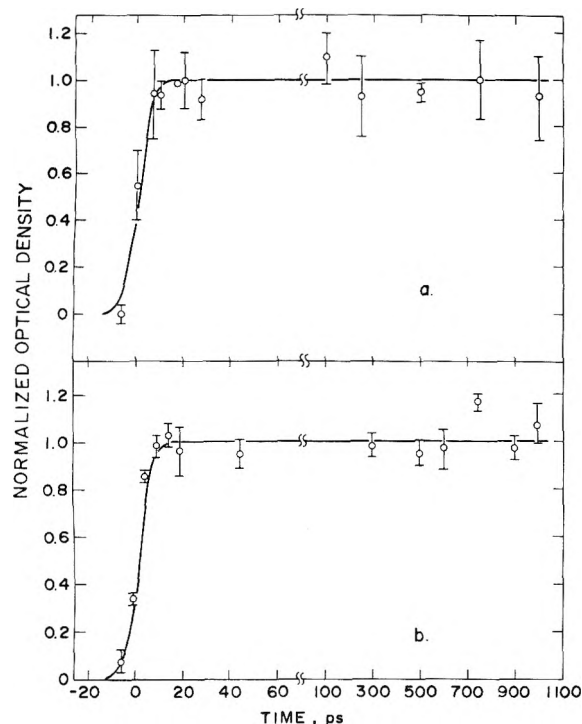


Figure 4. Optical densities at 500 and 730 nm, respectively, for parts a and b as a function of delay following excitation of TPH and a 353-nm laser pulse of duration 8 ps. The Φ 's are normalized optical densities representing an average of at least four data values. The optical density scale is arbitrary and the asymptotic values are related to the sample optical densities as discussed in the caption of Figure 3.

data. The curve fitting provides firm evidence that the radical formation is not taking more time than the pulse width (6–8 ps). We would observe a normally intense transient if its lifetime were longer than ca. 2 ps.

Within experimental error the bands at 470 and 800 nm grow in at the same rate and both maintain a constant intensity after a few picoseconds up to 2 ns. The suggestion^{4a} that the 800-nm peak is due exclusively to the radical pair therefore appears to be unacceptable. We have obtained essentially the same kinetic results as shown in Figure 4 for the additional solvents 1-methylnaphthalene and octoil.

Polarization measurements were obtained in benzene and octoil solutions at 300 K with the picosecond apparatus. The result of these experiments was that the bands at 470 and 800 nm are unpolarized (with polarization ratios of 1.0 ± 0.2) in both solvents. This result was obtained in experiments where the spectra were observed at the earliest possible times, commensurate with obtaining signals, such that loss of polarization through rotational relaxation was minimized. For a given solute the rotational relaxation time in the Debye formulation is dependent only on the solvent viscosity and the temperature. Since the viscosity of octoil is ca. 10^2 times larger than that of benzene at 300 K, rotational relaxation should not play a significant part in this polarization result in the more viscous solvent. As a further check on the polarization of the TPH photoproducts we conducted a photoselection experiment on TPH in EPA glass at 77 K. In this experiment the frozen-glass sample was irradiated with a polarized beam centered at 353 nm (5-nm band pass) obtained from a 1000-W xenon lamp with a $\frac{1}{4}$ -m Bausch and Lomb monochromator and a Glan-Thompson polarizer. Particular care was taken to minimize the depletion of TPH molecules which absorb the polarized excitation. Irradiation periods up to 30 min limited

the depletion of ground-state TPH molecules to ca. 10%. Polarization measurements taken on this frozen sample of photoproducts demonstrated that the characteristic spectrum of DPH radicals is unpolarized with a polarization ratio of 1.0 ± 0.1 . This experiment was repeated with other excitation wavelengths and the result remained unchanged.

4. Discussion

There are four definitive new pieces of information resulting from this work. (a) The radical formation occurs in less than the pulsewidth and therefore it is unlikely that any electronic relaxation is occurring in bound states prior to dissociation. (b) The visible and near-infrared spectrum of radicals does not change substantially in the range $2 \text{ ps} \leq t \leq 2 \text{ ns}$. (c) The initial buildup of radicals is not followed by a decrease in radical concentration during the time $6 \text{ ps} \leq t < 2 \text{ ns}$. This result implies that there is no recombination of the radicals during this time regime. (d) The distribution of radical transition moments produced is effectively random.

There have been measurements of photophysical processes in numerous phenylamines¹³ and the fluorescence and the intersystem crossing times are known thereby to be longer than nanoseconds. For example, for diphenylamine the ratio of phosphorescence to fluorescence yields in rigid solution at 77 K is 3.26, and the fluorescence lifetime¹⁴ is 1.4 ns. It therefore seems most unlikely that TPH can undergo a non-radiative process such as intersystem crossing or internal conversion on the time scale of a few picoseconds. The photodissociation is therefore expected to occur by predissociation of the singlet excited state reached by 353 nm excitation. It also seems reasonable to conclude that the dissociation must produce a singlet state of the radical pair during dissociation, since there is insufficient time for the formation of a triplet state by means of a spin-orbit coupling induced process.

Our spectra (Figure 3a and b) at $t \approx 0$ and $t = 1 \text{ ns}$ are quite similar to both the rigid-glass spectra^{3a,4a} and the transients previously measured on the microsecond time scale.⁵ In glasses^{4a} and crystals^{4b} the main species are radical pairs whereas the microsecond transients are free radicals. It appears as if the radicals and radical pairs have essentially the same spectra. It is therefore not possible from our results to study the cage dissociation. Our data suggest a small shift of the 470-nm band with time (red shifts with increasing time) but the data are not quite good enough to provide an accurate assessment of this effect.

The depolarization of the spectra even at times very short compared with the rotational relaxation is not unexpected. TPH presumably occupies a range of ground-state configurations, but even if there were a unique configuration for the molecule the spectra might still be unpolarized. The incident light forms a distribution of molecules described by $\cos^2 \theta$, where θ is the angle between the electric vector of the light and the transition moment direction in the TPH. On the basis of previous characterizations of the spectral bands of phenylamines^{13,15} and some photoselected EPR experiments,¹⁶ the lowest energy transition in these molecules is likely to be polarized along a C–N axis of the molecule. The transition moment is therefore in one of the CNC planes of the molecule. However when the dissociation occurs, two radicals are produced and they do not have parallel transition moments in the laboratory frame. The visible transitions of the NH_2 radical are known¹⁷ to be polarized perpendicular to the molecular plane. If this is also the case in diphenylamine (CNC plane) the polarization ratio expected in a normal photoselection experiment would be 2:1 in favor of perpendicular. However

in this case two fragments are produced having different orientations to the electric vector of the light. Thus even if there is no movement of the TPH nuclei following excitation, the optical polarization can be expected to be small both because of the photofragmentation into differently oriented radicals and because of the distribution of TPH configurations expected.

The observation that the radicals do not recombine can be rationalized on a simple argument. If the $(C_6H_5)_2N$ radicals are assumed to have structure similar to that of NH_2 , the two nonbonding electrons are essentially sp^2 whereas the odd electron is mainly of nitrogen $2p$ type. In TPH on the other hand the lone pairs are mainly sp^3 as are the N-N bonding electrons. Thus a substantial electronic rearrangement should occur on dissociation. A simple orbital correlation indicates that re-formation of the N-N σ bond could require one of the radicals to be in an excited state. This may account for the absence of fast recombination at 300 K and also for the observation that TPH formation is brought about by irradiation of the radical pair by red light.^{4b}

Acknowledgment. We express our gratitude to the Frankford Arsenal and its Chemistry Research Division for its support and encouragement of R.W.A. through a generous training program.

References and Notes

- (1) This research was supported by a grant from the National Science Foundation and by the M.R.L. program at the University of Pennsylvania.
- (2) Permanent affiliation and supporting institution: Pitman-Dunn Laboratories, Frankford Arsenal, Philadelphia, Pa.

- (3) (a) G. N. Lewis and D. Lipkin, *J. Am. Chem. Soc.*, **64**, 2801 (1942); (b) H. Wieland, *Justus Liebigs Ann. Chem.*, **381**, 200 (1911).
- (4) (a) D. A. Wiersma and J. Kommandeur, *Mol. Phys.*, **13**, 241 (1967). (b) D. A. Wiersma, J. H. Lichtenhelt, and J. Kommandeur, *J. Chem. Phys.*, **50**, 2794 (1969).
- (5) T. Shida and A. Kira, *J. Phys. Chem.*, **73**, 4315 (1969).
- (6) R. W. Anderson, Jr., R. M. Hochstrasser, H. Lutz, and G. W. Scott, *J. Chem. Phys.*, **61**, 2500 (1974).
- (7) J. A. Giordmaine, P. M. Rentzepis, S. L. Shapiro, and K. W. Wecht, *Appl. Phys. Lett.*, **11**, 216 (1967); P. M. Rentzepis and M. A. Duguay, *ibid.*, **11**, 218 (1967).
- (8) A. Penzkofer, A. Laubereau, and W. Kaiser, *Phys. Rev. Lett.*, **31**, 863 (1973).
- (9) R. Alfano and S. L. Shapiro, *Chem. Phys. Lett.*, **8**, 631 (1971).
- (10) G. E. Busch, R. P. Jones, and P. M. Rentzepis, *Chem. Phys. Lett.*, **18**, 178 (1973).
- (11) D. Magde and M. W. Windsor, *Chem. Phys. Lett.*, **27**, 31 (1974).
- (12) R. M. Hochstrasser and A. C. Nelson in "Lasers in Chemistry and Biophysics", Elsevier, Amsterdam, 1975, p 305.
- (13) M. Kasha, H. R. Rawls, and M. A. El-Bayoumi, *Pure Appl. Chem.*, **11**, 371 (1965).
- (14) V. L. Ermolaev, *Opt. Spectrosc. (USSR)*, **11**, 266 (1961).
- (15) M. Kasha and H. R. Rawls, *Photochem. Photobiol.*, **7**, 561 (1968).
- (16) Y. O. Grinberg, A. A. Dubinsku, and S. Y. Lebedev, *Dokl. Akad. Nauk SSSR*, **193**, 848 (1970).
- (17) G. Herzberg, "Molecular Spectra and Molecular Structure". Vol. III, Van Nostrand-Reinhold, Princeton, N.J., 1966.

Discussion

M. A. EL-SAYED. Have you studied the transient absorption as a function of solvent or temperature? Would there be any effect?

R. M. HOCHSTRASSER. The photoproperties of TPH have been studied as a function of solvent polarity and negative ions are often formed. In practice at room temperature the nitroxide radical is found instead of DPA. We have studied the dissociation in benzene, methylnaphthalene, and octoil in order to test the effects of viscosity, but none was observed.

Local Modes and Their Application to the Analysis of Polyatomic Overtone Spectra

Bryan R. Henry

Department of Chemistry, University of Manitoba, Winnipeg, Manitoba, Canada R3T 2N2 (Received February 4, 1976)

Publication costs assisted by the National Research Council of Canada

Because of an interest in the terminal state of a radiationless transition, an attempt is made to find an adequate description for highly vibrationally excited molecules through an understanding of molecular overtone spectra. In particular, it is shown that the positions of the overtone band maxima for XH-stretching motions can be understood on the basis of the assumption that the XH oscillators of a molecule vibrate anharmonically but essentially independently. This local-mode analysis leads to a description of the spectrum in terms of the components of highly coupled anharmonic normal modes. The successful application of this approach to an analysis of the overtone spectra of benzene, ammonia, and methane establishes the paramount importance of off-diagonal normal-mode coupling and indicates the limitations of a normal-mode representation for higher overtones. The approach, however, although able to account for average energies, is unable to account for the unexpected simplicity of the spectra and for the narrowness of the observed overtone bands. Moreover the normal-mode coupling effects are so large that it seems unreasonable to think of overtone bands as arising from transitions from the ground state to a set of symmetry allowed, anharmonic, normal-oscillator states. Through a detailed analysis of the overtone spectra of ammonia and dichloromethane, it is shown that the XH-stretching contributions to these spectra can be accounted for through the assumption that, with increasing vibrational energy, local-oscillator excitation becomes a more probable type of transition. In other words, in higher energy XH-overtone bands, the radiation field appears to selectively drive states of local excitation. Additional experimental data are presented and interpreted to support this contention. The combination regions of the overtone spectra of dichloromethane and chloroform are interpreted in terms of coupling between local CH-stretching modes and lower frequency normal modes. High pressure gas phase spectra for the overtones of methane and ethane are also interpreted from this local-mode point of view. Finally, the overtone spectra of toluene and the xylenes are presented. The resolution between the two inequivalent local CH-stretching motions in the higher overtones of these molecules is explained and correlated to primary aspects of molecular structure.

Introduction

Although there has been a great deal of interest in the correct theoretical description of the initial state in a radiationless transition,^{1,2} relatively little attention has been given to the properties of the terminal states. In particular for some radiationless transitions, and, in fact, for those that have been most extensively studied, the final state is one of high vibrational excitation. Thus if one wishes to obtain a correct theoretical description of a radiationless transition, one must be able to adequately account for the vibrational properties of this terminal state. We have felt that an appropriate vibrational model for these states should not be obtained solely by analogy to the description used to explain the fundamental regions of the ir spectrum but rather that the parallel should be drawn with higher energy overtone spectra. In this paper, we will attempt to show how information from the overtone spectra of several different molecules leads finally to a description of highly excited vibrational states that is significantly different than the conventionally accepted normal-mode interpretation.

Local-Mode Derivation of Normal-Mode Coupling

Initially an attempt was made to understand the CH-stretching overtone spectrum of benzene.^{3,4} The CH-stretching contributions to the vibrational energy were expressed in terms of normal modes

$$E = E_0 + \sum_K v_K \hbar \omega_K + \sum_{K \geq L} v_K v_L X_{KL} \quad (1)$$

and in terms of local modes

$$E = E_0 + \sum_i v_i \hbar \omega_i + \sum_{i > j} C_{ij} \omega_{ij} + \sum_{i \geq j} v_i v_j X_{ij} \quad (2)$$

where local modes were taken as corresponding to the stretching of individual CH bonds. The terms ω_{ij} correspond to harmonic coupling and the rest of the terms in eq 1 and 2 have their usual significance. Transformation equations were obtained between anharmonicity constants expressed in terms of the normal-mode basis (X_{KL}) and the local-mode basis (X_{ij}). The single diagonal local-mode anharmonicity (X_{11}) was obtained by analogy to the Morse relation for diatomic molecules.⁵ Thus we can write⁴

$$X_{11} = (\omega_1/\omega_{CH})^2 (D_{CH}/D_1) X_{CH} \quad (3)$$

which yielded $X_{11} = -57.5 \text{ cm}^{-1}$ when the relevant experimental data were inserted.^{3,4} ω_{CH} , D_{CH} , and X_{CH} are the stretching frequency, dissociation energy, and anharmonicity of the CH molecule in its electronic ground state, whereas ω_1 and D_1 refer to the corresponding quantities for CH in benzene. Through the assumption that off-diagonal local-mode coupling was negligible, numerical values for the normal-mode anharmonicities could be obtained.

These calculated normal-mode anharmonicities were then used to reproduce the spectrum, in the following way. From these anharmonicities and the observed fundamental frequencies, the energy of each of the symmetry allowed normal-mode components of a given overtone band could be calculated. The relative intensity of a normal-mode component within a given overtone was assessed on the basis of its

statistical degeneracy and its anharmonicity. The anharmonicity must contribute to the intensity since it is the departure from harmonicity that allows overtones to occur at all. Thus it is reasonable to expect that, in the normal-mode description, the more anharmonic components will contribute more to the intensity. With the energy of a component as an abscissa and its calculated intensity as an ordinate, a Lorentzian band was generated for each component. The Lorentzians were summed, and an overall band maximum for each CH-stretching overtone out to $\Delta\nu_{\text{CH}} = 8$ was obtained.^{3,4}

The analysis could successfully account for the experimental frequencies, in the spectrum measured by Ellis,⁶ of the overtones corresponding to $\Delta\nu_{\text{CH}} \geq 4$. The set of normal-mode anharmonicities generated in this procedure showed small values for the diagonal constants (-9 and -18 cm^{-1}), but very large values for the off-diagonal constants (-55 , -82 , and -184 cm^{-1}). It is these latter anharmonicities that serve to couple the normal modes. Because of these large off-diagonal anharmonicities, as the vibrational quantum numbers increase, the energy becomes increasingly more nondiagonal in a normal-mode representation. In summary then, what we had accomplished was a successful explanation of the CH-stretching overtone spectrum of benzene on the basis of the assumption that the six local CH bonds vibrated anharmonically but essentially independently.

We applied a similar analysis to the NH- and CH-stretching overtone spectra of methane and ammonia and we obtained the same kind of results.⁷ The overtone frequencies in the spectra could be accounted for in the same manner although, for these smaller molecules, there was some evidence for non-zero off-diagonal local-mode couplings. As in the case of benzene, the predominant anharmonic terms in a normal-mode representation were the large off-diagonal normal-mode couplings.

In summary then, it appears that this procedure can successfully account for the average energies of transitions in overtone spectra with a local-mode analysis which leads to a description of the spectrum in terms of the components of highly coupled anharmonic normal modes. However, a closer examination reveals two difficulties. In general, the observed spectral width of the overtone bands is much smaller than expected on the basis of the calculated energies of the anharmonic normal-mode components. Moreover the spectra seem simpler than expected and any traces of structure due to the different symmetry allowed normal-mode components seems to rapidly disappear. It is as if the description of the excited state in terms of normal modes is breaking down and the presumption that all of the symmetry allowed normal-mode combinations will be excited is invalid. It appears that the radiation field only sees a specific group of the symmetry allowed components. In fact later results show^{8,9} that the peaks of the overtone spectra correspond, in normal-mode language, to the most anharmonic combination modes. This result could be rationalized in local-mode language by saying that for high vibrational excitations, one does not expect the large number of "allowed" states which a normal-mode analysis predicts, but instead, the relatively small number corresponding to multiple excitation of local modes.

However the analysis given above, which was capable of providing accurate numerical predictions for band maxima, did describe the spectrum in terms of anharmonic normal-mode components. In order to understand its success, given the apparent unsuitability of a normal-mode representation, one must examine in some detail the experimental band shapes and band widths in the overtone regions. In the next

section, we will demonstrate how the XH-stretching contributions to these overtone spectra can be understood solely in terms of local-mode concepts without any recourse to normal-mode components.

Local-Mode Description of XH-Stretching Overtones

A. *Ammonia*. The model⁸ will be introduced through an examination of the general structure of the entire overtone spectrum of ammonia on the basis of experimental gas-phase data obtained some time ago.¹⁰⁻¹⁴ The procedure involves the use of a state counting algorithm developed by Beyer and Swinehart and by Stein and Rabinovitch¹⁵ to generate a kind of occupation number map (ONM) that shows the overall degeneracy of any particular vibrational state. In other words the ONM, given the modes put into it, describes all possible overtone or combination states of these modes. For ammonia, an ONM is constructed from the following modes. The NH-stretching modes are taken to be three degenerate local NH modes with a frequency between the two normal-mode frequencies (3363 cm^{-1}) and an anharmonicity of -70 cm^{-1} calculated from the Morse relation (eq 3). The remaining three modes are taken to be harmonic bending modes with frequencies taken from Herzberg¹⁶ (1628 cm^{-1} , doubly degenerate, and 950 cm^{-1}). In order to compare the calculated states with the overall structure of the experimental spectrum, it is helpful to select three kinds of states out of the complete ONM. The first, and it turns out the most important kind of states, are pure local-mode overtones where all of the energy is localized in *one* of the three NH oscillators. The other two types of states correspond to a pure local-mode overtone and one quantum of one of the two bending frequencies. Comparison with the observed spectra shows a remarkable correspondence between the energy levels of this selected group of overtone and combination bands and the measured spectral features.⁸ In fact the high frequency regions of the spectrum ($>12\,000 \text{ cm}^{-1}$) correspond almost exactly, on an energy basis, simply to pure local-mode overtone states. In a normal-mode description, these are the very regions where we would expect the spectrum to be more complex.

The region of the spectrum between 6300 cm^{-1} ($\Delta\nu_{\text{NH}} = 2$) and 9500 cm^{-1} ($\Delta\nu_{\text{NH}} = 3$) corresponds to combinations of the high frequency stretching modes and the lower frequency bending modes. For this region, the same ONM can be used to obtain a very simple zeroth order description of the spectrum. Here however no selection of contributing combinations is made from the ONM. There are 24 different states in this energy range. By weighting them solely on the basis of their degeneracy and assigning each component a Lorentzian function, and then summing the curves, one can obtain a calculated band shape for this region. Comparison with a graphical representation of Unger's data¹⁰ shows a considerable correspondence between the two curves especially given the very simple nature of the calculation.⁸

B. *Dichloromethane*. We will now consider the molecule dichloromethane since its molecular simplicity makes it suitable for the development of a general local-mode theory. We have obtained the overtone spectrum of this liquid out to $\Delta\nu_{\text{CH}} = 6$.⁸ The spectrum consists of a series of CH-stretching overtone bands which, in general, are relatively narrow and lack structure. There is also combination activity between $\Delta\nu_{\text{CH}} = 3$ and $\Delta\nu_{\text{CH}} = 4$ as well as between $\Delta\nu_{\text{CH}} = 4$ and $\Delta\nu_{\text{CH}} = 5$. It is very straightforward to treat this molecule by the techniques discussed earlier for benzene. There are only two normal CH-stretching modes. They are nondegenerate and we can immediately write down the equivalence relations for

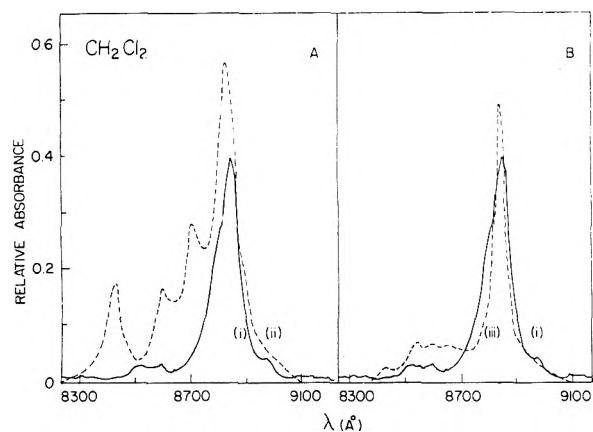


Figure 1. Taken from Figure 5 of ref 8. Calculated and observed CH-stretching overtone band of dichloromethane corresponding to $\Delta\nu_{\text{CH}} = 4$: A, (---) the calculated curve based on anharmonic normal-mode components; (—) the low resolution experimental spectrum; B, (---) the computed spectrum of overtones and combinations of the modes with frequency and anharmonicity 2991 (–55), 2991 (–55), and 1429 (0) cm^{-1} with a weighting of the fundamental local-mode overtone 50 times that of a combination band of the same degeneracy. All computed components were assigned a band width of 80 cm^{-1} .

the diagonal and the single off-diagonal normal-mode anharmonicity constants. Thus we have

$$\begin{aligned} X_{A_1A_1} &= X_{B_1B_1} = (2X_{11} + X_{12})/4 \\ X_{A_1B_1} &= (6X_{11} - X_{12})/2 \end{aligned} \quad (4)$$

If we take the diagonal local-mode constant X_{11} from methane¹⁷ and set $X_{12} = 0$, we can obtain numerical values for the normal-mode anharmonicities and thus calculate the energies of the normal-mode components of any overtone band. If these components are weighted according to their anharmonicity and the total overtone band constructed as in the case of benzene, one obtains the results shown on the left of Figure 1 for the $\Delta\nu_{\text{CH}} = 4$ transition. The solid curve represents the experimental spectrum at slightly lower resolution than is optimally possible under our experimental conditions,⁸ and the dotted curve corresponds to anharmonic normal-mode components. It is obvious from this figure why the earlier method was successful. Because the components are weighted by their anharmonicity, it is the lower frequency components that are given the most weight. Therefore the maximum of the overtone band can be relatively accurately predicted but not its width since the peaks at about 8400 and 8600 Å, which correspond in normal-mode language to pure normal-mode overtones (four quanta of B_1 and four quanta of A_1 , respectively), seem to contribute very little to the total band intensity. In fact the whole series of experimental overtone peaks out to $\Delta\nu_{\text{CH}} = 6$ appears to be much like the series of the most anharmonic normal-mode components,⁸ that is those components where normal-mode coupling is greatest. The superposition of these two normal CH-stretching modes corresponds to a local CH-stretching mode. Thus, here again there is evidence that the molecule and radiation field are interacting in such a way that the molecule effectively selects those photons which will lead to states of localized excitation.

It is possible to use the concept of a local mode to reproduce the observed band shape. The dotted curve on the right of Figure 1 is constructed from an ONM generated from two degenerate local CH oscillators with a frequency between the two normal-mode frequencies and an anharmonicity the same

as for methane, and a single normal harmonic CH-bending mode (1429 cm^{-1} ¹⁶). A local-mode overtone with all the energy localized in a single local CH oscillator is arbitrarily weighted 50 times compared to other combination modes and a Lorentzian is assigned to each component and the resultant curves summed. The weighting is a parameter and actually a value of 80 gives the best fit but the curves of Figure 1 illustrate the nature of the result. The agreement of the fitted and experimental curves is very good and suggests the following selection rules:⁸

1. *Local-mode overtones involving high frequency oscillators are the most intense but decrease rapidly in intensity with increasing $\Delta\nu$.*

2. *Combination bands involving degenerate oscillators of high frequency and combination bands involving modes of high and low frequency appear with much less intensity "pure local-mode overtones".*

A similar pattern is observed for higher overtone bands. For the $\Delta\nu_{\text{CH}} = 5$ band, again the normal-mode components span a far wider energy range than the experimental band.⁸ However it is possible to account for the band shape and width on the basis of the same ONM used for $\Delta\nu_{\text{CH}} = 4$ except that here the "pure local-mode overtone" is assigned a weight 200 times that of a combination band of the same degeneracy. Lower ratios than this gave wings to the spectrum that are not observed experimentally. The successful description of this band suggests a third selection rule:⁸

3. *Combination bands fall off more quickly in intensity than the local-mode overtone bands.*

In other words, the effective weighting of pure local-mode overtones compared to combinations increases with increasing $\Delta\nu$. This result is heartening in the sense that as we go to lower overtones the intensity of these combination bands will increase, and this is what is required at lower $\Delta\nu$ for convergence to the more traditional normal-mode overtone combination pattern, which generally does fit the data in the first and second overtone regions of many molecules. A similar analysis for $\Delta\nu_{\text{CH}} = 6$ shows that the structural aspects of this band correspond to just those expected for single oscillator excitation without any discernible combination component.⁸

We have also investigated, at somewhat higher resolution, the regions between the CH overtones for both dichloromethane and chloroform.⁹ These transitions are, in general, weaker than the pure overtone transitions, and they vanish for higher overtones. The two spectra show marked similarities. In the region between $\Delta\nu_{\text{CH}} = 4$ and $\Delta\nu_{\text{CH}} = 5$, the extra CH oscillator in dichloromethane gives rise to a local-mode combination band just to the high energy side of the $\Delta\nu_{\text{CH}} = 4$ overtone. This provides direct experimental evidence for some coupling of the local modes.

The other combination peaks in this region can be understood in terms of coupling as well. We interpret them as corresponding to multiple excitation of a local CH oscillator plus one quantum of a lower frequency normal mode.⁹ Thus for chloroform the major combination peaks at 1155 and 747 cm^{-1} to the high energy side of $\Delta\nu_{\text{CH}} = 4$ correspond to coupling of the local mode with the normal CH bend (1205 cm^{-1} ¹⁶) and CCl stretch (760 cm^{-1} ¹⁶). The spectrum is somewhat more congested in dichloromethane due to the presence of the local-mode combination band but the observed peaks at 726, 886, and 1095 cm^{-1} ⁹ most probably correspond to coupling of the local mode with the normal modes¹⁶ CCl stretch (737 cm^{-1}), the rocking mode (899 cm^{-1}), and the torsional mode (1155 cm^{-1}). It is clear that the off-diagonal couplings between the local modes and these lower frequency modes are not zero,

however, the magnitude of the coupling appears relatively small in comparison to the diagonal CH local-mode anharmonicities.

C. Methane and Ethane. We have also measured the overtone spectra of methane and ethane in a relatively high pressure gas cell.⁹ Once again the band shapes of the higher CH overtones are much simpler than predicted by any normal-mode model. There is also a striking similarity between the two spectra especially in the higher energy regions. In fact there are marked similarities of these spectra and the spectra of benzene, dichloromethane, and chloroform. Moreover the common features among the spectra are not entirely limited to the pure CH overtones. The relative number and symmetries of the normal-mode fundamentals in methane and ethane might lead one to expect more complicated band structures for ethane than methane, if a normal-mode approach is appropriate, and this is not the case. The structure in the $\Delta\nu_{\text{CH}} = 4$ band of methane is very similar to the rotational structure that is seen for similar bands in simpler molecules such as acetylene;⁹ in other words this appears to be like the rotational structure for a single vibrational transition.

D. Inequivalent CH Groups. There is an evident frequency shift of the ethane CH overtones as compared to the methane peaks. In trying to understand the reasons for this shift, we considered a parameter, $\omega^{\text{D}}_{\text{CH}}$. $\omega^{\text{D}}_{\text{CH}}$ is defined⁹ as the fundamental CH-stretching frequency in a molecule where all the H's but one are replaced by deuterium. This deuterium decoupled CH-stretching frequency should reflect the nature of the individual CH bond in the undeuterated molecule. A plot of $\omega^{\text{D}}_{\text{CH}}$ vs. the frequency of the band maximum for the $\Delta\nu_{\text{CH}} = 5$ peak for a series of seven molecules shows a very strong, in fact almost a linear, correlation.⁹ A true linear correlation is not expected here, even in a local-mode description, but the observed correlation between this local CH property and overtone frequency is far stronger than would be expected in a normal-mode description. Thus a difference in the deuterium decoupled CH-stretching frequency in the CH_4 type environment of methane and the CH_3 type environment of ethane manifests itself in the observed frequency shift in the band maxima of the overtone spectra.

The question then arises would one expect these frequency shifts to be resolved as separate bands in the overtone spectra of a molecule with two different kinds of CH oscillators. The greatest disparity observed in $\omega^{\text{D}}_{\text{CH}}$ for the molecules studied⁹ was a difference of about 100 cm^{-1} for CH stretching in an aryl environment such as benzene and in an alkyl environment such as ethane. Toluene and the xylenes are molecules which contain both of these groups, and we have investigated the liquid phase overtone spectra of these molecules.⁹ Figure 2 shows the spectra for $\Delta\nu_{\text{CH}} = 5$ and 6 for benzene, toluene, and the three xylenes. In toluene the higher wavelength peak in the $\Delta\nu_{\text{CH}} = 5$ region occurs at the same energy as the corresponding CH overtone in ethane. Thus this peak corresponds to the alkyl CH transition, and the other, because of its correspondence to the benzene peak, to the aryl CH transition. There is even a correlation between the ratios of the peak areas and the number of alkyl and aryl hydrogens. In toluene the ratio of aryl area to alkyl area is 2:1 whereas in the xylenes the corresponding ratio is about 5:7. "Doublet" structure can also be seen for the $\Delta\nu_{\text{CH}} = 6$ peak although the lower intensity becomes a problem. Similar patterns are observed for the other overtones corresponding to $\Delta\nu_{\text{CH}} = 4$ and 3, although, as expected, the frequency separation between the alkyl and the aryl peaks decreases from $\Delta\nu_{\text{CH}} = 5$ to 4 to 3 (e.g., for *p*-

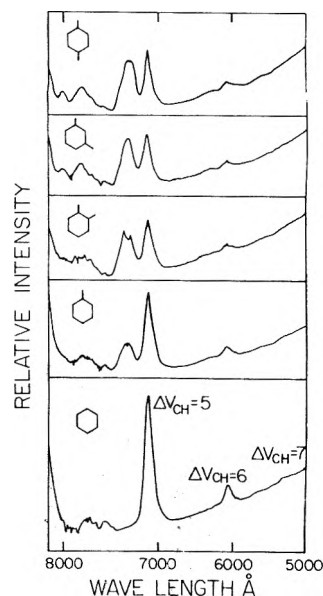


Figure 2. Taken from Figure 4 of ref 9. Experimental overtone spectra of liquid benzene, toluene, *o*-xylene, *m*-xylene, and *p*-xylene at room temperature (296 K) in the region from 5000 to 8000 Å.

o-xylene, $\omega(\text{aryl}) - \omega(\text{alkyl})$ goes from 495 to 395 to 297 cm^{-1} , respectively).⁹

Thus the predictions based on the deuterium decoupled CH frequencies are born out. The aryl - alkyl difference in $\omega^{\text{D}}_{\text{CH}}$ of about 100 cm^{-1} is magnified about five times for $\Delta\nu_{\text{CH}} = 5$, and since the band widths are much less than 500 cm^{-1} , the two groups appear in the spectrum as two distinct local-mode type bands. This type of simplicity would be very difficult to predict using normal modes as a basis. The magnification of $\Delta\omega^{\text{D}}_{\text{CH}}$ by about 5, 4, and 3 for the splittings between the corresponding overtones is only expected in a local-mode model if off-diagonal local-mode couplings are small compared to diagonal anharmonicities, which provides even further support for the suitability of such a model.

Acknowledgment. I gratefully acknowledge the collaboration of Dr. R. J. Hayward whose Ph.D. Thesis involved much of the work discussed here.

References and Notes

- (1) B. R. Henry and W. Siebrand, "Organic Molecular Photophysics", Vol. 1, J. B. Birks, Ed., Wiley, New York, N.Y., 1973, p 153.
- (2) B. R. Henry and W. Siebrand, "Organic Molecular Photophysics", Vol. 2, J. B. Birks, Ed., Wiley, New York, N.Y., 1975, p 303.
- (3) B. R. Henry and W. Siebrand, *J. Chem. Phys.*, **49**, 5369 (1968).
- (4) R. J. Hayward, B. R. Henry, and W. Siebrand, *J. Mol. Spectrosc.*, **46**, 207 (1973).
- (5) G. Herzberg, "Spectra of Diatomic Molecules", Van Nostrand, Princeton, N.J., 1945.
- (6) J. W. Ellis, *Trans. Faraday Soc.*, **25**, 888 (1928).
- (7) R. J. Hayward and B. R. Henry, *J. Mol. Spectrosc.*, **50**, 58 (1974).
- (8) R. J. Hayward and B. R. Henry, *J. Mol. Spectrosc.*, **57**, 221 (1975).
- (9) R. J. Hayward and B. R. Henry, *Chem. Phys.*, **12**, 387 (1976).
- (10) H. J. Unger, *Phys. Rev.*, **43**, 123 (1933).
- (11) R. Robertson and J. J. Fox, *Proc. R. Soc. London, Ser. A*, **120**, 161 (1928).
- (12) R. M. Badger, *Phys. Rev.*, **35**, 1038 (1930).
- (13) V. P. Leug and K. Hedfield, *Z. Phys.*, **75**, 599 (1932).
- (14) G. Jung and H. Gude, *Z. Phys. Chem. B*, **18**, 308 (1932).
- (15) S. E. Stein and B. S. Rabinovitch, *J. Chem. Phys.*, **58**, 2438 (1973).
- (16) G. Herzberg, "Infrared and Raman Spectra", Van Nostrand, Princeton, N.J., 1945.
- (17) The experimental dissociation energy for $\text{CH}_2\text{Cl}_2 \rightarrow \text{CHCl}_2 + \text{H}$ is not known and so the Morse relation cannot be used.

Discussion

D. S. MCCLURE. Is the intensity of the high overtones you see caused by the electrical anharmonicity of the bonds being stretched?

B. R. HENRY. We have actually looked on the problem more from the point of view of mechanical anharmonicity than of electrical anharmonicity, but in this region of the spectrum it may be impossible to disentangle one from the other. The detailed intensity problem in normal mode language is one that I think we haven't solved, and to my knowledge, neither has anyone else.

S. J. STRICKLER. I do not believe you can say the results are all due to electrical anharmonicity. The local mode states are just those for which the mechanical anharmonicity is a maximum. One can think of anharmonicity in terms of a sort of Morse potential—the lower the dissociation energy, the greater the anharmonicity. For a CH_2 group, for example, the Morse curve for a symmetric CH stretch would level off at the energy of breaking two CH bonds. But a localized mode levels off at breaking one bond, so would be much more anharmonic. In terms of normal modes this is a combination of symmetric and antisymmetric modes. The mechanical anharmonicity would therefore favor appearance of the local modes discussed by Dr. Henry.

B. R. HENRY. I think the whole analysis in terms of local modes, as a matter of fact, follow the kind of argument that Dr. Strickler has just described. When energy is pumped into a benzene molecule, and in particular, into the C–H stretching modes, six C–H bonds would not break off simultaneously. What would happen, I think, is that one bond is going to break off because that's a much lower energy process. That's why eventually, on physical grounds, the vibrational pattern must change to a local mode pattern. And that shows up, I think, in the very large value of the normal mode coupling anharmonicity constants. Because the anharmonic contribution to the energy goes up (quadratically) with vibrational quantum number, it tells us that, as the energy increases, the normal modes are more and more highly coupled. In our language, really what we are producing are local modes.

M. KASHA. In these local mode states is it possible to follow the anharmonic combinations out into the visible and uv? Your experiments and theory offer the interesting possibility for studying in-

tramolecular perturbations by comparing the progressions for vapor and for condensed systems (liquid solutions and solid matrices).

B. R. HENRY. I agree

R. KOPELMAN. I would like to go back to the previous problem. How do the spectral-density-of-states and the energy-density-of-states compare? If they differ, does not this imply electrical anharmonicity considerations in addition to mechanical anharmonicity?

B. R. HENRY. I really don't think that what we have done is that sophisticated. All we are doing is saying that from the evidence of the ir spectrum it appears that selection rules are operating so that the radiation field interacts with the molecule in such a way as to select certain states. Now the interesting question is: Are these states that the radiation field appears to see the same states that we should be using when we calculate photophysical processes, such as radiationless transitions, for instance, or unimolecular reactions? Now it is not necessarily true that they are the same states. Intuitively, one would feel, strictly because of the large values of the off-diagonal terms in a normal mode representation, that local modes might be a better starting point for the calculation of Franck–Condon factors for radiationless transitions or for insertion into the theory of unimolecular reactions, if you are trying to think about energy flow in a unimolecular process.

W. T. SIMPSON. I'd like to make a comment. I think what the radiation field sees, in this case, are stationary states. I think, however, that the stationary states are not the normal modes. They involve what you might call configuration interaction among modes that have the same symmetry.

B. R. HENRY. I don't think that these can be true stationary states in the sense that as we saw in one of those last spectra I presented there are couplings between the local modes. My physical picture of what does go on is that if we think of the benzene molecule and consider something like $\Delta\nu_{\text{CH}} = 6$ excitations, then what's happening is that the energy is moving around the benzene ring in a kind of a way that one C–H bond is stretching, then the next one, then the next one, and the next one. Then, at any one time the chances are that the energy is localized in a single C–H oscillator. Do you agree with that?

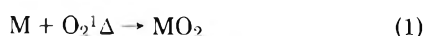
W. T. SIMPSON. No, this represents a difference in your point of view and mine.

Photoperoxidation of Unsaturated Organic Molecules. 16. Excitation Energy Fission

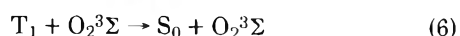
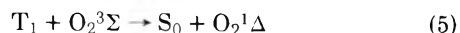
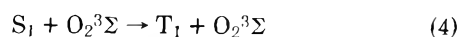
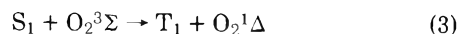
B. Stevens* and J. A. Ors

Department of Chemistry, University of South Florida, Tampa, Florida 33620 (Received February 12, 1976)

The quantum yield γ_{MO_2} of photosensitized addition of molecular oxygen to an organic acceptor M is the product of the quantum yield γ_{Δ} of $\text{O}_2^1\Delta$ formation and the efficiency ϕ_{MO_2} of $\text{O}_2^1\Delta$ addition to the acceptor (process 1) where



$\phi_{\text{MO}_2} = k_1[\text{M}]/(k_1[\text{M}] + k_2)$. Measurements of γ_{MO_2} as a function of dissolved oxygen concentration have been analyzed¹ to identify the operative oxygen quenching process of singlet (S_1) and triplet (T_1) states of the sensitizer of which the processes



are spin-allowed and exothermic if both the singlet–triplet splitting ΔE_{ST} (process 3) and triplet energies E_{T} (process 5) exceed the excitation energy of $\text{O}_2^1\Delta$ at 8000 cm^{-1} . In terms of the parameters $\alpha = k_3/(k_3 + k_4)$ and $\epsilon = k_5/(k_5 + k_6)$ the overall reaction quantum yield is given by

$$\gamma_{\text{MO}_2} = \phi_{\text{MO}_2} \{ \epsilon \gamma_{\text{IS}} + P_{\text{O}_2} [\alpha + \epsilon(1 - \gamma_{\text{IS}})] \} \quad (I)$$

TABLE I: Photoperoxidation Parameters^a

Sensitizer/acceptor	Tetracene	DMBA ^b	Rubrene	DMA ^c
γ_F	0.19 ± 0.02	0.36 ± 0.03	0.98 ± 0.02	0.90 ± 0.04
γ_{IS}	0.68 ^d	≤0.64 ± 0.03	≤0.02 ± 0.02	≤0.10 ± 0.06
$\gamma_{MO_2}(P_{O_2} = 0)$	0.10	0.066	0.02 ± 0.02	0.02 ± 0.03
$\gamma_{MO_2}(P_{O_2} = 1)$	0.16	0.10	0.55	0.50
$\epsilon\gamma_{IS}/(\alpha + \epsilon)^e$	0.61 ± 0.07	0.66 ± 0.06	0.04 ± 0.04	0.04 ± 0.10
$[M], M$	4.0(-4)	1.7(-4)	4.0(-4)	4.0(-4)
β, M^{-1}	2.4(-3)	1.6(-3)	1.0(-3)	1.2(-3)
ϕ_{MO_2}	0.14 ± 0.01	0.096 ± 0.01	0.29 ± 0.03	0.25 ± 0.03
$\alpha + \epsilon$	1.2 ± 0.2	1.0 ± 0.2	1.9 ± 0.4	2.0 ± 0.4
k_{IS}, s^{-1}	1.2(8)	2.7(7)	3.0(6)	1.5(6)
$\Delta E_{ST}, cm^{-1}$	10 400	~11 000	~9 000	~11 000

^a Solvent benzene at 25 °C. ^b 9,10-Dimethyl-1,2-benzanthracene. ^c 9,10-Dimethylanthracene. ^d Reference 2. ^e From eq II.

where γ_{IS} is the sensitizer intersystem crossing yield and the probability that S_1 is quenched by $O_2^3\Sigma$, $P_{O_2} = K[O_2]/(1 + K[O_2])$ is available from independent measurements of the Stern–Volmer fluorescence quenching constant K .

Linear plots of the data $\gamma_{MO_2}(P_{O_2})$ provide the quotients (Table I)

$$\gamma_{MO_2}(P_{O_2} = 0)/\gamma_{MO_2}(P_{O_2} = 1) = \epsilon\gamma_{IS}/(\alpha + \epsilon) \quad (II)$$

which are close to independent measurements of γ_{IS} (tetracene²) or to values estimated as $1 - \gamma_F$ (DMBA) indicating that $\alpha \ll \epsilon$ for these compounds or that (4) and (5) are the dominant quenching processes. However, this conclusion is not unambiguous for those sensitizers with high fluorescence quantum yield (rubrene and DMA) where the estimate of γ_{IS} as $1 - \gamma_F$ is exceeded by the uncertainty in measurement of γ_F .

We have recently used a dynamic competition technique³ to determine values for $\beta = k_2/k_1$ for the compounds listed in Table I. The corresponding values for ϕ_{MO_2} at the prevailing acceptor concentrations permit the direct evaluation of γ_{Δ} as $\gamma_{MO_2}/\phi_{MO_2}$ and of $\alpha + \epsilon$ as $\gamma_{MO_2}(P_{O_2} = 1)/\phi_{MO_2}$ (eq I). Since ϵ as defined cannot exceed unity the values of $\alpha + \epsilon \sim 2$ found for rubrene and DMA indicate that $\alpha \sim \epsilon \sim 1$ for these sensitizers or that $O_2^1\Delta$ is produced by the energy fission process 3 in addition to the energy transfer process 5. This is contrary to the behavior of tetracene and DMBA, for which $\alpha + \epsilon \sim 1$ or $\alpha \sim 0$ since $\epsilon \sim 1$ (eq II), and (4) and (5) are the dominant quenching processes.

These findings confirm an earlier report by Bowen and Williams⁴ that the sum of the fluorescence and photoperoxidation quantum yields of rubrene exceed unity at higher concentrations, and support the conclusion of Livingston and Rao⁵ to the effect that “interaction of the fluorescent state with O_2 is the principal step (in photoperoxidation) in strongly fluorescent solutions (whereas) for weakly fluorescent solutions the triplet state plays the dominant role”. It is also of interest to note that Kenner and Khan⁶ have shown that the energy pooling process represented by the reverse of process

3 leads to oxygen enhancement of fluorescence under conditions where triplet state relaxation is relatively slow.

Since ΔE_{ST} exceeds 8000 cm^{-1} for the sensitizers examined here, the nature of the singlet quenching process is essentially determined by the relative rates of nonradiative transitions from the complex formed initially $^3\Gamma_i(S_1^3\Sigma)$ to lower energy complex states $^3\Gamma_f(T_1^1\Delta)$ and $^3\Gamma_g(T_n^3\Sigma)$. If processes 3 and 4 operate by an exchange mechanism these rates will largely depend on the relative energies of these states, viz.

$$^3\Gamma_g(T_n^3\Sigma) > ^3\Gamma_i(S_1^3\Sigma) > ^3\Gamma_f(T_1^1\Delta) \quad k_3 \gg k_4$$

$$^3\Gamma_i(S_1^3\Sigma) > ^3\Gamma_g(T_n^3\Sigma) > ^3\Gamma_f(T_1^1\Delta) \quad k_3 \ll k_4$$

which reflect the ordering of molecular states

$$T_n \gtrsim S_1 > T_1 \quad \gamma_{IS} \sim 0$$

$$S_1 > T_n > T_1 \quad \gamma_{IS} \gg 0$$

expected for sensitizers of high and low fluorescence yields and intersystem crossing rate constants k_{IS} which differ by an order of magnitude (Table I). The quenching processes 3 and 4 should not therefore be mutually exclusive particularly for sensitizers where $\Delta E_{gf} \sim 0$.

NOTE ADDED IN PROOF: As pointed out by a referee, it is assumed that the acceptors listed do not also quench $O_2^1\Delta$ in the physical sense. Significant physical quenching would lead to upward revision of γ_{Δ} computed here from chemical reaction, in which case $\epsilon\gamma_{IS}/(\alpha + \epsilon)$ will exceed γ_{IS} (tetracene) or $1 - \gamma_F$ (DMBA) while $(\alpha + \epsilon)$ will be greater than 2.0 for rubrene and DMA.

References and Notes

- (1) B. Stevens and B. E. Algar, *Ann. N.Y. Acad. Sci.*, **171**, 50 (1970).
- (2) A. Kearvell and F. Wilkinson, *Chem. Phys. Lett.*, **11**, 472 (1972).
- (3) B. Stevens, S. R. Perez, and J. A. Ors, *J. Am. Chem. Soc.*, **96**, 6846 (1974).
- (4) E. J. Bowen and A. H. Williams, *Trans. Faraday Soc.*, **35**, 765 (1939).
- (5) R. Livingston and V. S. Rao, *J. Phys. Chem.*, **63**, 794 (1959).
- (6) R. D. Kenner and A. U. Khan, *Chem. Phys. Lett.*, **36**, 643 (1975).

Small-Molecule Photochemistry. Theory and Application to Formaldehyde¹

Gregory D. Gillispie*² and E. C. Lim

Department of Chemistry, Wayne State University, Detroit, Michigan 48202 (Received January 8, 1976)

Publication costs assisted by the National Science Foundation

Intramolecular energy transfer plays a crucial role in many photochemical reactions as evidenced by the fact that the molecular bonds which break are often not those in which vibrational energy is initially localized by the optical absorption process. For example, absorption to the S_1 state of aliphatic carbonyl compounds under collision-free conditions usually leads to rupture of a C-H bond or CO elimination even though a progression in the C-O stretching vibration is the predominant spectral feature. Moreover, the total vibrational energy content in the S_1 state is often far too small to allow the decomposition to occur on the S_1 potential hypersurface. In such cases it must be concluded that a radiationless transition has first taken place to a lower electronic state (e.g., T_1 or S_0) in which the vibrational energy content is in excess of the bond strength. This paper develops the theory necessary to treat photochemistry via interelectronic intramolecular energy transfer.

A formal solution is presented for the time evolution of a molecular system in which an initially populated single vibronic level of an excited electronic state is indirectly coupled to a dissociative continuum via an intermediate manifold of vibrational levels of a lower electronic state. In particular, the results are applicable to systems in which the intermediate manifold is insufficiently dense in the absence of coupling to the dissociative continuum to function as an effective continuum for a radiationless transition from the initially prepared level. Variable-coupling matrix elements and manifold level spacings are accommodated within the theory; it is also not necessary to assume that the widths of the manifold levels arising from coupling to the dissociative continuum exceed the manifold level spacings.

Recent experimental data on the photodecomposition and

radiationless decay of formaldehyde are used to qualitatively illustrate the principal features of this work. We shall also briefly discuss an application of the theory to intersystem crossing in aromatic molecules.

References and Notes

- (1) Work supported by a grant from the National Science Foundation.
- (2) National Science Foundation Energy Related Postdoctoral Fellow, 1975-1977; Junior Fellow of the University of Michigan Society of Fellows, 1975-1978.

Discussion

B. STEVENS. Does dissociation take place from S_1 or from hot S_0 ?

G. D. GILLISPIE. From hot S_0 .

B. STEVENS. Have you done an orbital correlation or a state correlation diagram?

G. D. GILLISPIE. Yes, the adiabatic correlation diagram shows that the photochemistry must be occurring from the vibrationally hot ground state.

E. C. LIM. Can you comment on the observed isotope effects on fluorescence and phosphorescence lifetimes of formaldehyde?

G. D. GILLISPIE. The lifetimes are primarily determined by the nonradiative decay rates, which are essentially directly proportional to the unimolecular decay rates of the vibrationally hot S_0 levels. There is likely an order of magnitude difference in these unimolecular rates between H_2CO and D_2CO . This is most probably the source of the very large observed isotope effect.

Relaxation Processes in Photochemical Reactions. An Electron Spin Echo Study of Chemically Induced Spin Orientation¹

David C. Doetschman

Department of Chemistry, State University of New York at Binghamton, Binghamton, New York 13901 (Received February 2, 1976)

Following a short historical introduction which traces the paper's subject back to early work of Kasha and others, electron spin echo experiments on the photochemically induced spin orientation in triplet diphenylmethylene are reviewed. The remainder is an interpretation of the highly preferential photochemical population of one of the triplet sublevels, an interpretation in which the photochemically excited reaction product relaxes via an intersystem crossing.

1. Introduction

This work, like so much else, has its origin in Lewis and Kasha's early work on the phosphorescence of organic molecules² which established the triplet character of the emitting state. Lewis, Calvin, and Kasha's subsequent photomagnetism experiments³ together with other efforts eventually led to the successful application of EPR to photoexcited triplet molecules.⁴

Since then interest has turned to the dynamic photophysical processes which are set in motion by photoexcitation. Kasha recognized that there are prominent pathways of molecular excitation which seem to stand out from the many processes imaginable.⁵ The spin-orbit coupling selection rules were identified which govern intersystem crossing as well as the triplet decay to the ground state.⁶⁻⁸ The triplet spin substate preferences of these pathways often generate remarkable nonthermal population distributions in the triplet sublevels when the temperature is low enough to retard thermal equilibration.⁷ Moreover, the spin substate selectivity may be predicted with spin-orbit coupling theory in which only one center atomic integrals are retained.⁶⁻⁸ The presence of large nonthermal population differences among the triplet sublevels, which are often called spin polarizations or orientations, have led to the use of new magnetic resonance techniques. Two examples are the microwave induced phosphorescence effects^{9,10} and the spin echo methods.^{11,12} A by-product of these techniques is the ability to easily monitor moderately fast changes in the triplet sublevel populations. For example, with spin echoes a time resolution of a few microseconds in solids at low temperatures is possible.¹²

First to be described will be some recent experiments¹ on a *photochemical* reaction for which electron spin echo techniques were borrowed from earlier photophysical work. Then an interpretation of the photochemistry results will be presented, also in terms of what has been learned about photoexcitation and decay processes.

2. Photochemically Induced Triplet Electron Spin Orientation Experiments

Recent electron spin echo experiments¹ reveal an orientation of the electron spin in the ground triplet state of diphenylmethylene (DPM) which is induced by the photolysis of diphenyldiazomethane (DPDAM). See Figure 1. The DPDAM is the dopant in an appropriate single crystal host^{13,14} which is in an X-band microwave cavity in a magnetic field and at $T \sim 1.2$ K. The crystal is photolyzed with a pulsed

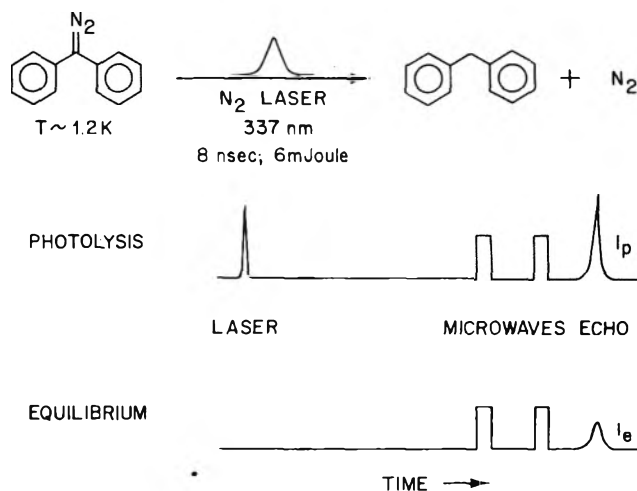


Figure 1. Experimental sequence in the two pulse spin echo detection of the triplet spin orientation in diphenylmethylene which is induced by photolyzing diphenyldiazomethane with a N_2 laser pulse.

N_2 laser. A somewhat idealized experimental sequence, shown in Figure 1, is the laser flash, followed by a pair of resonant microwave pulses and the subsequent spin echo. The echo intensity is a measure of the population difference between two of the DPM triplet sublevels. The time scale must, of course, be less than the spin-lattice relaxation times, which are all found to be greater than 3 ms.¹ After the DPM spins have reached thermal equilibrium, a reference experiment is done without the laser flash. In practice it is necessary to use several laser flashes, to make minor spin-lattice relaxation corrections, and to subtract the echo intensity of the residual DPM which is inevitably left behind from previous experiments.

The echo intensity I_p in the photolysis experiment is proportional to the difference Δp in the relative populating rates of the two triplet sublevels connected by the microwaves. The reference intensity I_e at thermal equilibrium is proportional to the relative Boltzmann population difference Δb , a quantity which is readily calculated. Here relative means to all *three* triplet sublevels. So Δp may be determined from the experiment through

$$\Delta p = (I_p/I_e)\Delta b \quad (1)$$

Δp may as well be expressed in terms of the populating rates p_x, p_y, p_z of the sublevels in zero field, as in

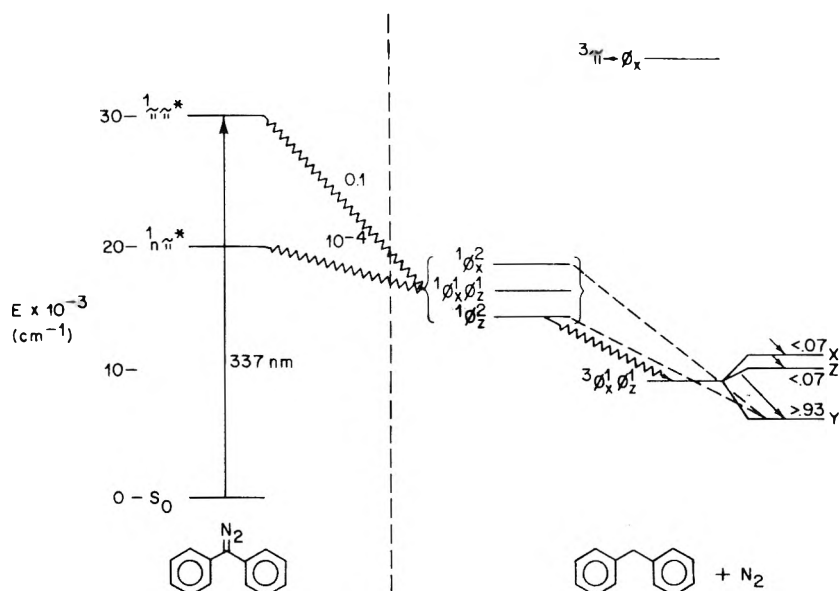


Figure 2. Diphenyldiazomethane and diphenylmethylene energy level diagrams which are juxtaposed according to a lower limit for the endothermicity of the diphenyldiazomethane photodissociation (see text) when zero N_2 excitation is assumed. The wavy lines indicate the proposed relaxation scheme in the reaction and the numbers adjacent are quantum yields. The dotted lines connect the states which may be strongly coupled by spin-orbit interaction. The relative populating rates of the diphenylmethylene ground triplet sublevels are indicated numerically and with arrows of proportionate length.

$$\Delta p = \Delta C_x^2 p_x + \Delta C_y^2 p_y + \Delta C_z^2 p_z \quad (2)$$

The numbers denoted by the ΔC^2 's depend on the transformation between the DPM spin functions in the magnetic field of the experiment and in zero field. Thus the p_x , p_y , p_z may be determined from three or more Δp measurements at distinct fields. In DPM there are altogether four different $\Delta m = \pm 1$ X-band transitions for fields along the principal axes. Experiments on the four lines show that p_y is at least 0.93. Only upper limits are established for p_x and p_z . The relative rates are indicated in Figure 2 on the "blow up" of the DPM triplet level. Insofar as the echo experiments could determine, the appearance of the spin oriented triplet after the laser flash is instantaneous.

3. Interpretation

The photochemical processes to be examined are displayed in the adapted Jablonski diagram, Figure 2. The laser excites the DPDAM to a singlet state from which dissociation occurs with the relatively high quantum yield indicated.¹³ When the lower singlet is excited, the quantum yield is much smaller,¹³ a fact which suggests that intersystem crossing from $^1\pi\pi^*$ DPDAM before dissociation is not appreciable. The reaction is endothermic but the dissociation energy is not known and the difference shown in Figure 2 is a reasonable lower limit.¹⁵ Also, no direct spectroscopic information exists for the bracketed DPM singlet states. These low lying states derive from single and double occupancy of the two nearly degenerate methylene-like orbitals which are singly occupied in the ground triplet state. The events which take place may be cast in familiar photophysical terms. There is a photo(chemical) excitation step followed eventually by an intersystem crossing to a (chemically) metastable triplet. Return to the reactant ground state presumably is inhibited by diffusion of the "hot" N_2 away from the DPM in the crystal.

There are two interrelated questions about these processes which can be partially answered, namely, why there is so great a spin preference for the Y substate of triplet DPM and what the pathway is by which excitation goes from $^1\pi\pi^*$ DPDAM

to the DPM triplet? In the slightly bent prototype methylene CH_2 the two nearly degenerate triplet orbitals are essentially the carbon p_x and the sp_2 hybrid. Herzberg's diazomethane photolysis experiments¹⁶ and theoretical calculations of the CH_2 electronic states¹⁷ suggest that the doubly occupied sp_2 methylene singlet is first formed and then converts to the ground triplet. One center spin-orbit coupling between these two states clearly involves matrix elements of the y orbital angular momentum component. Consequently the Y spin sublevel of the triplet is singlet contaminated⁷ and is expected to be the recipient in intersystem crossing.

It is no surprise to find the strong Y selectivity reflected in DPM. However, the 93% preference seems too good because it is known^{14b} that approximately 40% of the DPM triplet electron spin does not even reside on the central carbon atom! So any explanation of the high preference must also take into account the delocalization of the DPM wave functions onto the phenyl rings.

The DPM bend angle θ about the central carbon atom is only 16° ^{14b} so the molecule has approximately D_2 symmetry. Reasonable methylene-like DPM orbitals ϕ_x and ϕ_z will belong to the representations B_3 and B_1 of the D_2 group. The representations of the four two electron configurations in these orbitals are given in Table I. Only spin-orbit coupling between the Y sublevel of the triplet B_2 and the singlet A_1 states is symmetry allowed and the matrix elements are the same to both A_1 states. So in the D_2 approximation symmetry fully accounts for the spin selectivity.

Symmetry, however, does not reveal the relative contributions of coupling on the rings and on the central carbon atom nor how the coupling varies with the angle ϕ of phenyl ring twist from coplanarity. See Figure 3. It is clear from magnetic resonance studies of the DPM triplet state that electron delocalization into the σ system of the phenyl rings is very small.^{14b} In a π approximation for the phenyl rings, the molecular orbitals ϕ_x , ϕ_z contain only the ring carbon p orbitals directed normal to the ring planes. All one center integrals of orbital angular momentum on the ring carbons, which appear in the spin-orbit coupling matrix element between ϕ_x and ϕ_z ,

TABLE I: Representations to Which the Two-Electron Configuration in the ϕ_x and ϕ_z Diphenylmethylene Orbitals Belong for Molecular Symmetries D_2 and C_2

Configuration		Representation	
		D_2	C_2
$\left\{ \begin{array}{l} \phi_x^2 \\ \phi_x^1 \phi_z^1 \end{array} \right\}$	Singlet	A_1	A
		B_2	B
		A_1	A
$\left\{ \begin{array}{l} \phi_z^2 \\ \phi_x^1 \phi_z^1 \end{array} \right\}$	Triplet	B_2	B
		A_1	A

will therefore vanish. In other words, no appreciable spin-orbit coupling contribution from the rings is expected. Higuchi's simple orbitals¹⁸ in

$$\phi_x = \frac{1}{\sqrt{4 + 6 \sin^2 \phi}} [2p_{1x} - \sin \phi (p_{\pi 3} - p_{\pi 3'} - p_{\pi 5} + p_{\pi 5'} + p_{\pi 7} - p_{\pi 7'})] \quad (3)$$

and

$$\phi_z = \frac{1}{\sqrt{4 + 6 \cos^2 \phi}} [2p_{1z} - \cos \phi (p_{\pi 3} + p_{\pi 3'} - p_{\pi 5} - p_{\pi 5'} + p_{\pi 7} + p_{\pi 7'})] \quad (4)$$

conform to this approximation and lead to the twist angular dependence of the central carbon spin-orbit coupling matrix element given in

$$\frac{4}{\sqrt{40 + 9 \sin^2 2\phi}} \quad (5)$$

where unity represents the element between two orthogonal p orbitals. The actual DPM twist angle $\phi = 54^\circ$ is close to the angle for which the element is minimum.

DPM actually has C_2 symmetry and ϕ_x and ϕ_z can be modified for the bend θ and for sp_2 hybridization on the central carbon atom. The orbitals now belong to representations B and A of C_2 . The representations of the two electron configurations in C_2 are also given in Table I. Spin-orbit mixing of the singlets A is now formally symmetry forbidden only with the Z spin state of triplet B. However, within the π approximation for the rings there can still be no ring contribution to mixing with the X substate. Moreover, sp_2 hybridization on the central carbon atom can lead to no X mixing either. The angular dependence of the central carbon spin-orbit coupling on both θ and ϕ is given in

$$\frac{4 \cos^{1/2} 2\theta}{\sqrt{(4 + 6 \sin^2 \phi)[2(1 + \cos 2\theta) + 6 \cos^2 \phi \cos 2\theta]}} \quad (6)$$

again relative to the element between two orthogonal p orbitals. One concludes that very high Y substate selectivity is a result of the nearly complete dominance of spin-orbit coupling by the central C atom, a dominance which arises because the σ delocalization in the ring system is small. One also predicts the selectivity to be quite insensitive to molecular geometry so long as σ delocalization remains negligible.

The experiments are consistent with triplet coupling to one or both of the singlets indicated by the dotted lines in Figure 2 and with intersystem crossing from among the bracketed singlets. It is unlikely that other π -type DPM singlets lie lower than the observed $^3\pi \leftarrow \phi_x^{14a}$ which is well above the excitation of the reactant. Herzberg's experiments and evidence from the chemical reactivity of methylene derivatives in general both point to the transient existence of singlet methylenes before crossing to the triplet.

The pathway for relaxation in the photochemical reaction in Figure 2 is a scheme which is consistent with the experi-

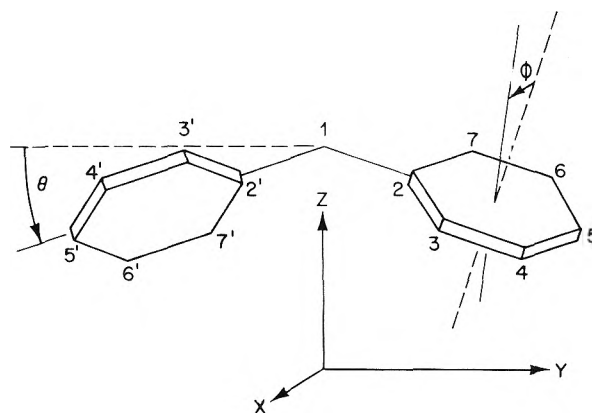


Figure 3. The diphenylmethylene molecule. The axis system, the carbon atom numbering scheme, and the bend (θ) and twist (ϕ) angles are illustrated.

mental information currently available. Time-resolved optical absorption experiments on DPDAM and DPM could provide a crucial test of the scheme. Similar spin echo experiments on methylenes with different geometries are planned to test the spin-orbit coupling mode, in particular, the predicted insensitivity to molecular geometry.

References and Notes

- (1) The experiments reviewed here were performed in collaboration with B. J. Botter, J. Schmidt, and J. H. van der Waals at the Center for the Study of Excited States of Molecules, Huygens Laboratories, The University of Leiden, Leiden, The Netherlands. The detailed description of the experiments will be published elsewhere.
- (2) G. N. Lewis and M. Kasha, *J. Am. Chem. Soc.*, **66**, 2100 (1944); **67**, 994 (1945).
- (3) G. N. Lewis, M. Calvin, and M. Kasha, *J. Chem. Phys.*, **17**, 804 (1949).
- (4) C. A. Hutchison, Jr., and B. W. Mangum, *J. Chem. Phys.*, **34**, 908 (1961).
- (5) M. Kasha, *Radiat. Res.*, Suppl. 2, 243 (1960).
- (6) D. S. McClure, *J. Chem. Phys.*, **17**, 665 (1949); **20**, 682 (1952).
- (7) J. H. van der Waals and M. S. deGroot in "The Triplet State", A. B. Zahlan, Ed., Cambridge University Press, London, 1967, p. 101.
- (8) W. S. Veeman and J. H. van der Waals, *Mol. Phys.*, **18**, 63 (1970).
- (9) M. Sharnoff, *J. Chem. Phys.*, **46**, 3263 (1967).
- (10) J. Schmidt, D. A. Antheunis, and J. H. van der Waals, *Mol. Phys.*, **22**, 1 (1971).
- (11) J. Schmidt, *Chem. Phys. Lett.*, **14**, 411 (1972).
- (12) B. J. Botter, D. C. Doetschman, J. Schmidt, and J. H. van der Waals, *Mol. Phys.*, **30**, 609 (1975).
- (13) D. C. Doetschman and C. A. Hutchison, Jr., *J. Chem. Phys.*, **56**, 3964 (1972).
- (14) (a) G. Closs, C. A. Hutchison, Jr., and B. E. Kohler, *J. Chem. Phys.*, **44**, 413 (1966); (b) C. A. Hutchison, Jr., and B. E. Kohler, *ibid.*, **51**, 3327 (1969).
- (15) That DPM may be formed by excitation to $^1n\pi^*$ DPDAM¹³ indicates that $^3\phi_x^1\phi_z^1$ DPM lies to lower energy. The DPM ground state has been placed 2000 cm^{-1} lower than the activation energy for CH_2N_2 pyrolysis, to the authors knowledge the lowest conceivable indicator of the reaction endothermicity. More reliable indicators such as bond energy estimates and methylene excess energy measurements in CH_2N_2 photolysis all point to a considerably higher endothermicity.
- (16) G. Herzberg, *Proc. R. Soc. London, Ser. A*, **262**, 291 (1961); *Can. J. Phys.*, **39**, 1511 (1961); "Molecular Spectra and Molecular Structure, III, Electronic Spectra and Electronic Structure of Polyatomic Molecules", Van Nostrand, New York, N.Y., 1966, p. 492; G. Herzberg and J. W. C. Johns, *J. Chem. Phys.*, **54**, 2276 (1971).
- (17) J. F. Harrison and L. C. Allen, *J. Am. Chem. Soc.*, **91**, 807 (1969).
- (18) J. Higuchi, *J. Chem. Phys.*, **38**, 1237 (1963).

Discussion

M. W. WINDSOR. What is the energy of the optical transition (from lowest triplet ground state to higher triplet) in diphenylmethylene?

D. C. DOETSCHMAN. The difference between that ground triplet and the excited triplet is the lowest optical absorption band which lies at 4500 \AA , I believe. The absorption spectrum of diphenylmethylene has been observed by Hutchison and Kohler. With our lower limits that places that level well above the energy that we put into the system in the first place.

Vibronic Interactions and Environmental Effects on the Phosphorescent State of 9,10-Anthraquinone in Shpol'skii Matrices at 4.2 K¹

Omar S. Khalil and Lionel Goodman*

Wright and Riemann Chemistry Laboratories, Rutgers, The State University of New Jersey, New Brunswick, New Jersey 08903 (Received April 16, 1976)

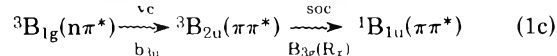
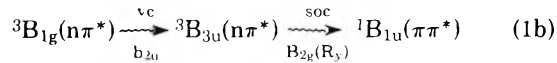
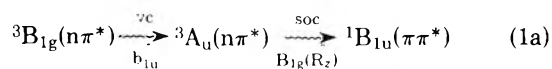
Highly resolved phosphorescence spectra arising from the ${}^3B_{1g}(n\pi^*) \rightarrow {}^1A_g$ electric dipole forbidden transition in 9,10-anthraquinone (AQ) and in AQ- d_8 are recorded and analyzed at 4.2 K in n -alkanes. The vibrational structure of the phosphorescence is found to be sensitive to the n -alkane's unit cell characteristics. In n -hexane and n -heptane the vibrational analysis shows that the molecule retains its inversion center and the transition is vibronically induced by b_u type vibrations. The unobserved origin is estimated from the phonon spectrum to lie at $21\,783\text{ cm}^{-1}$ in AQ. Analysis of the weak bands allows assignment of an odd quantum progression in ν_{32} , a b_{1u} skeletal deformation. This is interpreted as evidence for potential surface distortion of the ${}^3B_{1g}$ state arising from ${}^3A_u(n\pi^*)$ - ${}^3B_{1g}(n\pi^*)$ vibrational-electronic interaction. The similarity in spectra and energy spacings in anthraquinone and p -benzoquinone suggests that similar evidence might be found in the p -benzoquinone phosphorescence spectrum.

I. Introduction

A feature of the D_{2h} symmetric quinones, p -benzoquinone (BQ) and 9,10-anthraquinone (AQ), is their very similar electronic spectra.² Spectroscopic data on BQ³⁻¹⁴ and AQ¹⁵⁻²⁰ indicate that the symmetry and orbital nature of the two lowest-energy triplet states are identical in the two molecules: ${}^3B_{1g}(n\pi^*)$ and ${}^3A_u(n\pi^*)$. The estimated ${}^3A_u(n\pi^*)$ - ${}^3B_{1g}(n\pi^*)$ energy gap in their respective isotopically mixed crystals are quite comparable: 340 cm^{-1} for BQ and 410 cm^{-1} for AQ. The energy level diagrams of the two molecules are shown in Figure 1. The phosphorescence spectra of the two molecules have electric dipole forbidden origins and are induced by b_u type vibrations, the most prominent of which being the b_{1u} , $\nu(\text{C}=\text{O})$ asymmetric stretching mode.

The ${}^3B_{1g}(n\pi^*) \rightarrow {}^1A_g$ transition is parity and spin forbidden. Vibronic coupling in the triplet manifold with those odd parity states that possess singlet character, as a result of spin-orbit coupling, is a source of electric dipole character.

The following vibronic-spin-orbit coupling routes are probable sources of the intensity:



Route 1a, which has been discussed before for BQ,²¹ is of particular interest because of the small spacing between ${}^3B_{1g}(n\pi^*)$ and ${}^3A_u(n\pi^*)$. At this energy separation strong vibronic interactions, of the *pseudo*-Jahn-Teller type, are expected to occur as has been postulated for azines and aromatic carbonyls.²²⁻²⁶ These interactions can lead to potential surface distortions and ultimately to a double minimum potential well along the coupling coordinate.^{22,23} Such a double minimum potential has also been postulated for the ${}^3B_{1g}(n\pi^*)$ state of BQ^{6,8,10,12} along a b_{1u} vibrational coordinate.

In order to obtain an expression for the $T_e \rightarrow S_0$ transition moment, we write the ground state wave function Ψ_g and a non-Born-Oppenheimer emitting state wave function Ψ_e in

terms of adiabatic Born-Oppenheimer products (θ , electronic; χ , vibrational) as follows:

$$\Psi_g(q, Q) = \theta_0(q, Q)\chi_0(Q) \quad (2)$$

$$\Psi_e(q, Q) = \theta_1(q, Q)\chi_1(Q) + \theta_2(q, Q)\chi_2(Q) \quad (3)$$

The $T_e \rightarrow S_0$ transition moment can be expressed as

$$\langle \Psi_g | \sum \mathbf{r}_i e | \Psi_e \rangle = \mathbf{M}_{01} \langle \chi_0 | \chi_1 \rangle + \mathbf{M}_{02} \langle \chi_0 | \chi_2 \rangle \quad (4)$$

The labels 1 and 2 refer to the zero-order wave functions of the ${}^3B_{1g}(n\pi^*)$ and the vibronically coupled state, respectively. For the case of AQ (or BQ), \mathbf{M}_{02} will have the z polarization of the ${}^1B_{1u}(\pi\pi^*) \leftarrow {}^1A_g$ transition, in agreement with experiment,^{15,20} because of the ${}^1B_{1u}(\pi\pi^*) \xrightarrow{\text{soc}} {}^3A_u(n\pi^*)$ interaction in (1a). M_{01} is identically zero. Since M_{02} is the ${}^3A_u(n\pi^*) \leftrightarrow {}^1A_g$ transition moment and $\chi_1(-Q) = \chi_1(Q)$ for a g state and $\chi_2(-Q) = -\chi_2(Q)$, for a u state, odd quanta only of the coupling vibration should appear in the phosphorescence.

Modulated Stark effect experiments,^{6,8,12} and ENDOR measurements on the lowest triplet state of BQ,¹³ suggest strong vibronic perturbations. However, in their vibrational analysis of the phosphorescence of single and mixed crystals of BQ,^{8,10,13} Wiersma et al. do not report any odd quanta progression in the coupling vibrations. The $T \leftarrow S$ absorption spectrum of AQ showed strong vibronic interactions.²⁰ This makes the lack of odd quanta progressions in the phosphorescence quite puzzling.

In this paper we examine the highly resolved phosphorescence spectra of AQ in Shpol'skii matrices. The only previously reported high resolution study of AQ is in isotopically mixed crystals.²⁰ Our purpose is twofold: (1) to search for odd quanta progressions in the coupling mode, and (2) to examine environmental perturbations on the vibrational structure of the phosphorescence spectra.

II. Experimental Section

Zone refined AQ- h_8 was obtained from Materials Limited (Fairfield, N.J.). AQ- d_8 was obtained from Professor D. A. Wiersma, University of Gronigen, The Netherlands. Both compounds were used as received. Spectroquality solvents (MCB) were dried over molecular sieves and chromato-

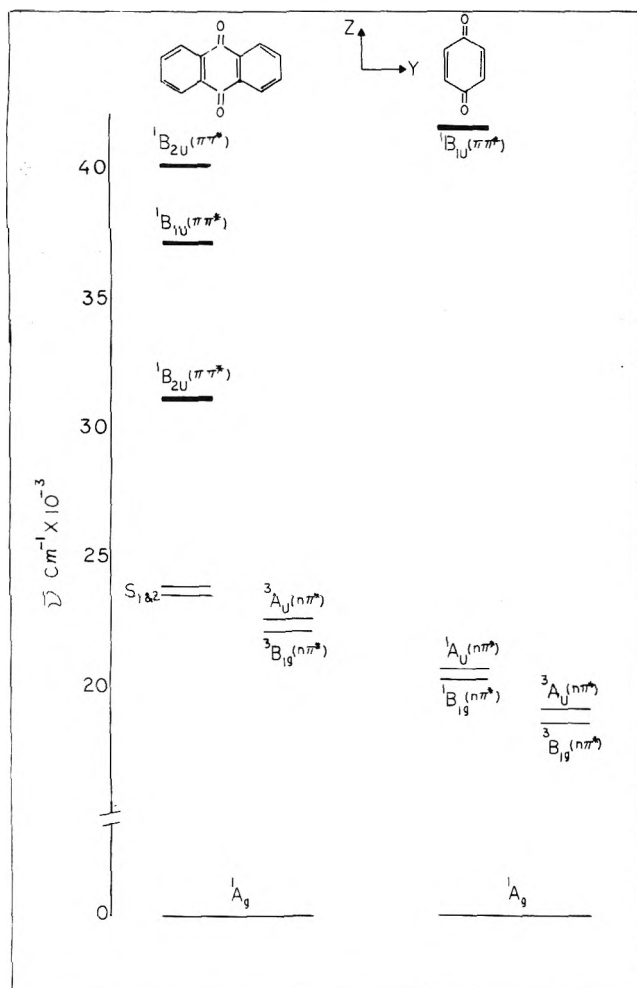


Figure 1. Energy level diagram of AQ and BQ. The data on BQ are taken from ref 3. The ${}^1n\pi^*$ states of AQ are from ref 1, the ${}^1\pi\pi^*$ states are taken from ref 15, and the ${}^3n\pi^*$ states are from ref 20.

graphed over activated alumina. Deuterated solvents were supplied by Merck Sharp and Dohm of Canada and were chromatographed over activated alumina.

The polycrystalline samples were excited by a Hanovia 500-W xenon arc lamp, and a 0.25-m Spex monochromator. Phosphorescence was analyzed in the first order by a Spex 1702-0.75 m Czerny-Turner monochromator (grating 1200 groves/mm blazed at 5000 Å). The recording system utilized a 6256S EMI photomultiplier with a Kiethly 414S picoammeter. Calibration was affected by mercury lines. Cooling was achieved by direct immersion of the samples in liquid helium under atmospheric pressure.

III. General Features of the Spectra

Phosphorescence spectra of AQ in *n*-alkanes at 4.2 K appear as sharp (half-band width 5 cm^{-1}) two-site emissions in *n*-pentane, *n*-heptane, and *n*-octane, as a sharp one-site emission in *n*-hexane, and is broadened (half-band width $\sim 300\text{ cm}^{-1}$) in *n*-nonane and higher homologues. Sample spectra are displayed in Figure 2A-D.

At 77 K, phosphorescence spectra in all *n*-alkane matrices are broad and resemble the spectrum displayed in Figure 2D. The origin region acquires considerable intensity indicating that the 0-0 is phonon assisted.

Quickly frozen and slowly frozen samples gave identical spectra. Prolonged annealing lead to appearance of broad

structure underlying the sharp spectra. This broad structure resembles that obtained from quickly frozen concentrated solutions and is probably due to molecular aggregates. The invariance of the sharp structure to the rate of cooling indicates that the multiplets^{27,28} are not due to "frozen-in liquid structures".^{29,31} Polymorphism in the crystal lattice is eliminated as a source of the multiplet structure by variation of the cooling rate and by matrix deuteration experiments. For polymorphic crystals, deuteration will favor one crystalline modification over the other due to differences in zero point energies.^{32,33} This phenomenon was observed for *p*-dichlorobenzene crystals³² and methylcyclohexane polycrystalline matrix.³³ Phosphorescence of AQ in *n*-hexane and *n*-hexane-*d*₁₄ are identical except for a $\sim 10\text{-cm}^{-1}$ blue shift in the latter case. In *n*-heptane-*d*₁₆ there are also blue shifts, slightly different from one site to the other. No change in the vibrational structure of the phosphorescence is observed upon host deuteration or variation of cooling rate in the perprotonated or the perdeuterated matrices. Since these changes are observed in polymorphic polycrystalline matrices,^{32,33} we conclude that the AQ molecules are occupying substitutional sites in the polycrystalline lattice of *n*-alkanes. Studies on polycyclic aromatic hydrocarbons embedded in single and polycrystals of *n*-heptane indicate that solute molecules are trapped in similar substitutional sites in both instances.^{30,31} It is not unreasonable then to adopt this conclusion in the case of AQ in *n*-alkanes.

The origin region, with one exception, has negligible intensity. Only broad phonon side bands could be recognized, indicating a forbidden origin for the transition. Thus the emitting entity seems to retain its inversion center, i.e., the site symmetry is at least C_i , similar to the phosphorescence emission in the crystal. In *n*-pentane, one of the two sites has a moderately intense origin band indicating lack of inversion center.

IV. Phosphorescence Vibrational Analysis in *n*-Hexane

The one site nature of phosphorescence facilitates vibrational assignments. Vibrational analysis of the $T_1 \rightarrow S_0$ emissions of AQ-*h*₈ and AQ-*d*₈ in *n*-hexane at 4.2 K are presented in Tables I and II. The spectrum of AQ-*h*₈ is displayed in Figure 3. The ground state vibrational frequencies were taken from the literature^{34,35} with the Raman frequencies checked by us. Since there are some discrepancies between the literature Raman data³⁵ and ours,⁴⁴ we will utilize our frequencies, although assignments of the *g*-type vibrations are still incomplete. A resolved phosphorescence of AQ in *n*-hexane at 77 K has been reported,¹⁷ but the lack of agreement with ground state vibrational frequencies³⁴⁻³⁶ suggests that it is erroneous.

The 0-0 band is missing and its position was located by determining the average frequency difference for the lowest energy phonon side band built on intense vibronic bands in the spectrum. This average frequency was then added to the highest energy broad phonon band observed in the origin region under high sensitivity conditions. This procedure introduces a possibility of error in locating the origin, but may not cause discrepancy in vibrational assignments because of the simplicity of the spectrum. A similar situation was encountered with BQ where mistaken origin locations were reported.^{7,14}

The unobserved origin band located by this described procedure lies at $21\,783\text{ cm}^{-1}$ for AQ-*h*₈ and $21\,802\text{ cm}^{-1}$ for

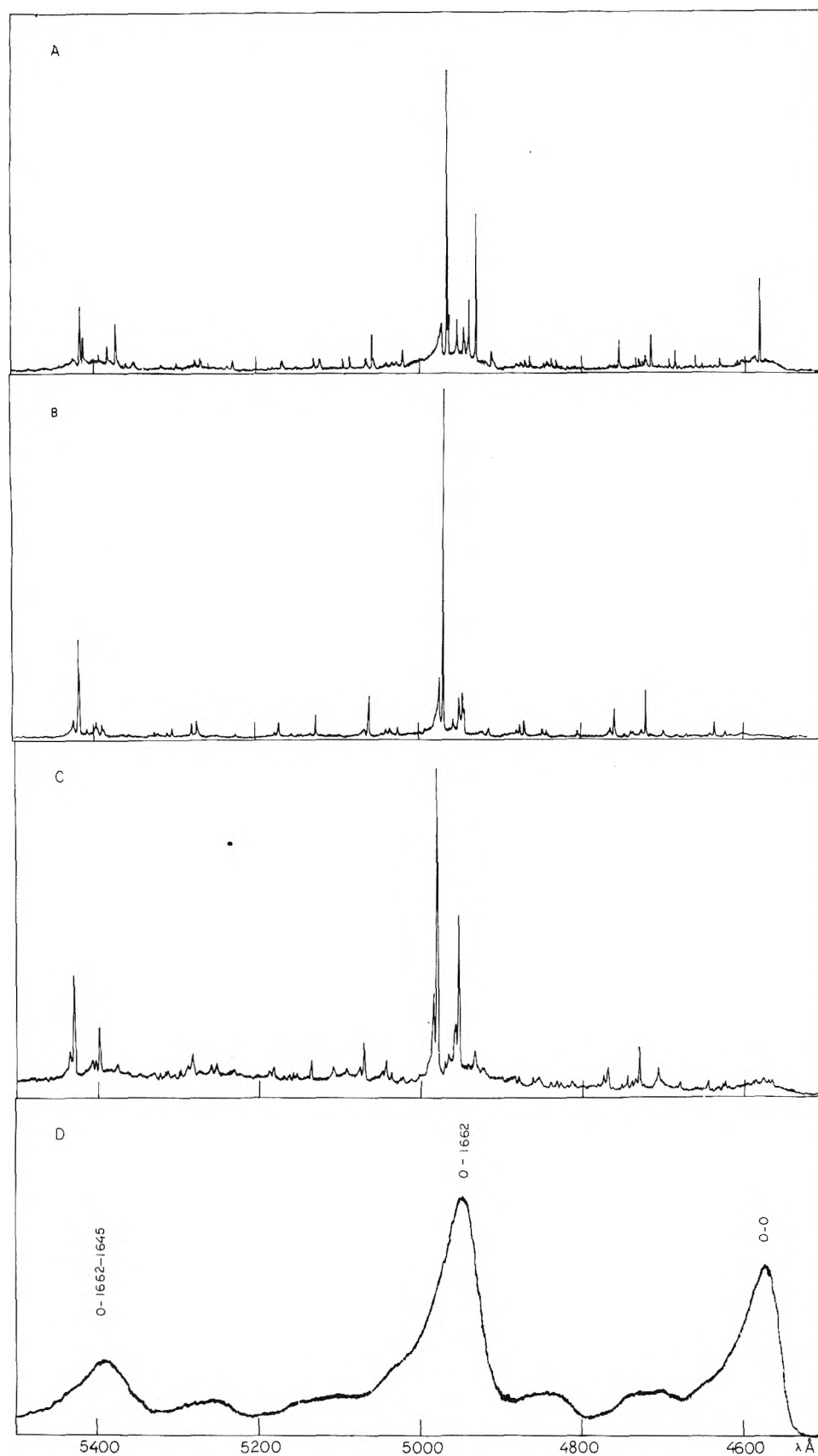


Figure 2. General features of the phosphorescence spectra of AQ in *n*-alkanes at 4.2 K: (A) in *n*-pentane; (B) in *n*-hexane; (C) in *n*-heptane; (D) in *n*-nonane.

AQ- d_8 , both are red shifted compared to their energies in the crystal spectra.

Seven out of eleven possible b_{1u} fundamentals can be recognized in the spectrum, namely, ν_{32} , ν_{31} , ν_{28} , ν_{27} , ν_{26} , ν_{25} , and

ν_{24} vibrations, in Mulliken's notation.³⁴ All either involve skeletal deformation, ring stretch, or C=O asymmetric stretching according to the approximate description of Pecile and Lunelli.³⁴ The most intense vibration in the phospho-

TABLE I: Vibrational Analysis of the Phosphorescence Spectrum of 9,10-Anthraquinone- h_8 in n -Hexane at 4.2 K

ν , cm^{-1}	$\Delta\nu$, cm^{-1}	Intensity ^b	Assignment ^c	Ground state vibration ^e	
				ν , cm^{-1}	Symmetry
21 783	0	Unobsd	0-0		
21 763	20	VVW	0-lattice		
21 743	40	VW	0-lattice		
21 724	59	VW	0-lattice		
21 707	76	VW	0-lattice		
21 616	167	W	0- ν_{66} , op skeletal deformation	167	b_{3u}
21 555	228	M	0- ν_{32} , ip skeletal deformation	237	b_{1u}
21 529	254	W	0- ν_{32} -lattice		
21 371	412	W	0- ν_{66} -240 Raman		
21 266	517	W	} 0-3 \times ν_{66} and/or ν_{32} + 301 Raman		
21 259	524	W			
21 185	598	W	0- ν_{32} -360 Raman		
21 163	620	S	0- ν_{31}	626	b_{1u}
21 140	643	M	0- ν_{31} -lattice		
21 096	687	W	} 0-3 \times ν_{32}		
21 089	694	W			
21 078	705	W	0- ν_{63}	705	b_{3u}
21 058	725	VW	0- ν_{63} -lattice		
20 992	791	S	0- ν_{62} , skeletal deformation	816	b_{3u}
20 970	813	W	0- ν_{62} -lattice		
20 838	945	W	0- ν_{47} , skeletal deformation or 0- ν_{63} -240 Raman	939	b_{2u}
20 796	987	M	0- ν_{31} -360 Raman		
20 628	1155	W	0- ν_{46} , CH bend	1150	b_{2u}
20 613	1170	W	0- ν_{28} , ring stretch	1173	b_{1u}
20 520	1263	M	0-combination ^d		
20 490	1293	M	0-combination ^d		
20 476	1307	W	0- ν_{47} -360 Raman		
20 463	1320	W	0- ν_{61} -360 Raman		
20 444	1339	W	0- ν_{44} , ring stretch	1335	b_{2u}
20 432	1351	VW	0-combination ^d		
20 421	1362	VW	0-combination ^d		
20 327	1456	M	or 0- ν_{43} , ring stretch	1373	b_{2u}
20 301	1482	W	0- ν_{26} , ring stretch	1454	b_{1u}
20 288	1495	W	0- ν_{26} -lattice		
20 204	1576	S	0- ν_{63} -790 Raman		
20 198	1585	S	0- ν_{41} , ring stretch	1335	b_{2u}
20 180	1603	MS	0- ν_{25} , ring stretch	1593	b_{1u}
20 152	1631	MW	0- ν_{25} -lattice		
20 101	1682	VVS	0- ν_{64} -1141 Raman		
20 077	1706	S	0- ν_{24} , asymmetric C=O stretch	1676	b_{1u}
19 873	1910	M	0- ν_{24} -lattice		
19 836	1947	W	0- ν_{24} -240 Raman		
19 818	1965	W	0-combination ^d		
19 738	2045	MS	0-combination ^d		
19 714	2069	M	0- ν_{24} -360 Raman		
19 486	2297	M	0- ν_{24} -360 Raman-lattice		
19 307	2476	M	0- ν_{31} -1666 Raman		
19 292	2491	W	0- ν_{24} -790 Raman		
18 945	2838	M	0- ν_{24} -790 Raman-lattice		
18 922	2861	W	0- ν_{24} -1144 Raman		
18 836	2947	W	0- ν_{24} -1144 Raman-lattice		
18 644	3139	W	0- ν_{27} -1666 Raman		
18 544	3239	W	0- ν_{42} -1666 Raman		
18 537	3246	W	0-combination ^d		
18 517	3266	M	0-combination ^d		
18 510	3273	W	0- ν_{25} -1666 Raman		
18 505	3278	W	} 0- ν_{24} -1595 Raman		
18 472	3311	W			
18 438	3345	VS	0- ν_{43} -790 Raman-1144 Raman		
18 414	3369	M	0- ν_{24} -1666 Raman		
18 072	3711	W	0- ν_{24} -1666 Raman-lattice		
17 824	3959	W	0- ν_{24} -1666 Raman-360 Raman		
17 713	4070	W	0- ν_{31} -2 \times 1666 Raman		
17 286	4497	W	0- ν_{25} -1666 Raman-790 Raman		
			0- ν_{24} -1666 Raman-1144 Raman		

^a Corrected to vacuum. ^b Uncorrected for phototube response. ^c Assignments are based on ground state vibration of ref 34 with Mulliken's numbering. ^d Unassigned combination bands. ^e Single crystal infrared vibrational frequencies determined at room temperature.³⁴

TABLE II: Vibrational Analysis of the Phosphorescence Spectrum of 9,10-Anthraquinone- d_8 in n -Hexane at 4.2 K^a

$\bar{\nu}$, cm ⁻¹	N ν , cm ⁻¹	Intensity	Assignment	Ground state vibration	
				ν , cm ⁻¹	Symmetry
21 802	0	Unobsd	0-0		
21 780	22	VW	0-lattice		
21 651	51	VW	0-lattice		
21 646	156	W	0- ν_{66} , op skeletal deformation	161	b _{3u}
21 595	207	MW	0- ν_{32} , skeletal deformation	222	b _{1u}
21 419	383	MW	0- ν_{64} , carbonyl op bend	398	b _{3u}
21 325	477	W	3 \times ν_{66} and/or ν_{32} + 292 Raman		
21 316	486	W			
21 248	554	W	0- ν_{69} , C-D op bend	570	b _{3u}
21 217	585	S	0- ν_{31} , skeletal deformation	605	b _{1u}
21 195	607	W	0- ν_{31} -lattice		
21 174	628	W broad	} 3 \times ν_{32}		
21 165	637	W broad			
21 066	736	MS	0- ν_{62} , op skeletal deformation	744	b _{3u}
21 044	758	W	0- ν_{62} -lattice		
20 989	801	W	0- ν_{30} , skeletal deformation	815	b _{1u}
20 864	938	W	0- ν_{45} , C-D bend	965	b _{2u}
20 788	1014	W	0- ν_{27} , C-D bend	1020	b _{1u}
20 715	1097	W	0- ν_{29} , ring stretch	1120	b _{1u}
20 564	1238	MW	0- ν_{44} , ring stretch	1246	b _{2u}
20 541	1261	W	0- ν_{44} -lattice		
20 453	1349	W	0-combination		
20 436	1366	W	0-combination		
20 415	1387	W	0- ν_{26} , ring stretch	1395	b _{1u}
20 407	1395	W	0- ν_{42} , ring stretch	1403	b _{2u}
20 340	1462	W	0- ν_{63} -736 Raman		
20 278	1524	W	0- ν_{41} , ring stretch	1530	b _{2u}
20 241	1561	S	0- ν_{25} , ring stretch	1565	b _{2u}
20 219	1593	M	0- ν_{25} -lattice		
20 133	1669	VVS	0- ν_{24} , C=O assymmetric stretch	1676	b _{1u}
20 117	1785	S	0- ν_{24} -lattice		
19 923	1879	VW	0- ν_{24} -220 Raman		
19 887	1915	VW	0- ν_{30} -1097 Raman		
19 781	2021	W	0- ν_{24} -355 Raman		
19 545	2257	MW	0- ν_{37} -1661 Raman		
19 393	2409	MW	0- ν_{24} -736 Raman		
19 309	2493	VW	0- ν_{42} -1097 Raman		
19 144	2658	VW	0- ν_{27} -1661 Raman		
19 035	2767	VW	0- ν_{24} -1097 Raman		
18 809	2993	VW	0- ν_{24} -1097 Raman-220 Raman		
18 742	3060	VW	0- ν_{42} -1661 Raman		
18 575	3227	W	} 0- ν_{25} -1661 Raman		
18 568	3234	W			
18 476	3326	S	0- ν_{24} -1661 Raman		
18 455	3347	W	0- ν_{24} -1661 Raman-lattice		
18 124	3678	VW	0- ν_{24} -1661 Raman-358 Raman		

^a See footnotes of Table I.

rescence spectrum of AQ in n -hexane is ν_{24} (1682 cm⁻¹) and its combinations with Raman lines of frequencies 240, 360, 790, 1149, 1595, 1666, 1666 + 360, and 1666 + 1149 cm⁻¹.

Three out of eleven possible b_{2u} fundamentals appear weakly in the spectrum, these are ν_{46} , ν_{44} , and ν_{43} . The vibration ν_{46} does not appear in the ir crystal absorptions,³⁴ but a band at 1150, 1152, and 1153 cm⁻¹ appeared in the ir absorption of the polycrystalline solid, AQ in dioxane solution, and AQ in nujol mull, respectively.³⁵ This frequency may correspond to the b_{2u} fundamental appearing in the phosphorescence at 1155 cm⁻¹. The ν_{46} vibration has been assigned to a C-H bending vibration, while ν_{44} and ν_{43} are ring stretching vibrations. Another b_{2u} vibration, ν_{47} , appears as a combination with the 360-cm⁻¹ Raman line. A weak band in the phosphorescence at 945 cm⁻¹ can be either assigned as ν_{47} or a combination of ν_{63} and the 240-cm⁻¹ Raman line.

Three of six possible b_{3u} fundamentals are observed in the phosphorescence spectrum of AQ in n -hexane, namely, ν_{66} , ν_{63} , and ν_{62} . ν_{61} appears as a combination band with the 360-cm⁻¹ Raman line and ν_{64} combines with the 1141-cm⁻¹ Raman line. Only ν_{62} at 791 cm⁻¹, assigned as C-H out-of-plane bending,³⁴ is strong. There is a possibility of a fourth b_{3u} fundamental. The weak doublet at 517 and 524 cm⁻¹ might be attributed to ν_{64} which lies at 491 cm⁻¹ in the infrared crystal absorption and 485 cm⁻¹ in the infrared absorption of a nujol mull^{34,35} split by crystal field. However, the AQ- d_8 phosphorescence shows the pair at 477 and 486 cm⁻¹ eliminating this possibility since ν_{64} is observed to shift to 398 cm⁻¹ in the single crystal ir spectrum of AQ- d_8 .³⁴ Thus the pair must be assigned as due to combinations or multiple quanta.

We now examine the possibility of odd quanta progressions

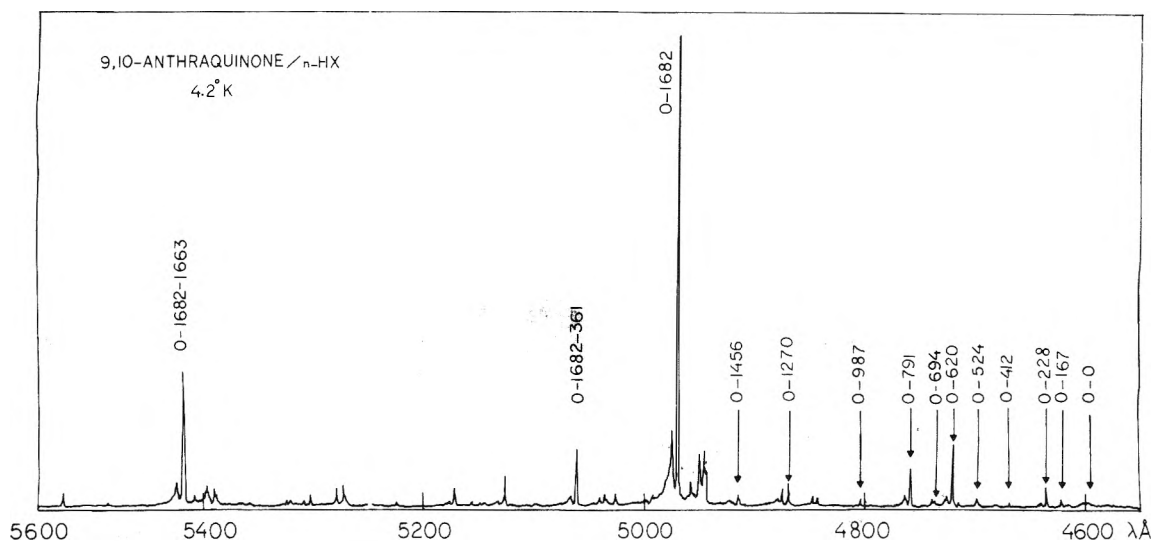


Figure 3. Vibrational analysis of the phosphorescence spectrum of AQ in *n*-hexane at 4.2 K.

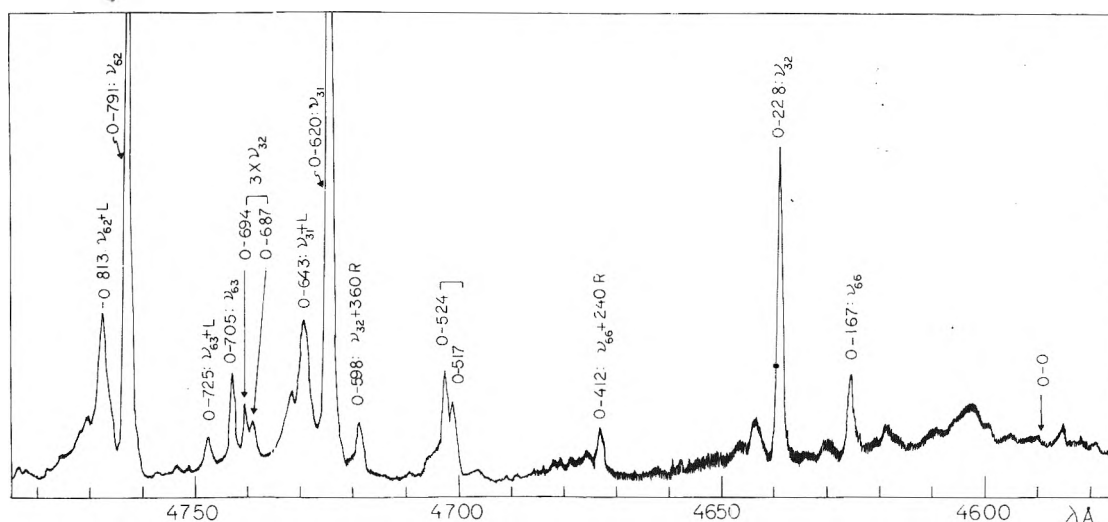


Figure 4. The high energy region of the phosphorescence spectrum of AQ in *n*-hexane at 4.2 K, recorded under 30X higher sensitivity conditions than in Figure 3.

in the AQ phosphorescence. Figure 4 shows the first region of the spectrum recorded under high sensitivity conditions. Possible assignments for the weak bands at 517 and 524 cm^{-1} are $3 \times \nu_{66}$ (167) = 501 cm^{-1} , and a combination of ν_{32} (227) and weak Raman line observed at 301 cm^{-1} in AQ powder (somewhat shifted by the *n*-hexane environment). The former assignment has the disadvantage of an unaccounted large discrepancy between calculated and observed frequency even for the lower frequency band. A difficulty with the $\nu_{32} + 301$ assignment is the absence of *any* combination bands involving the 301-cm^{-1} Raman line with other phosphorescence active b_u vibrations. In AQ- d_8 $3 \times \nu_{66}$ (156) = 468 cm^{-1} , and the Raman line shifts to 292 cm^{-1} giving for the predicted combination band frequency ν_{32} (207) + $292 = 497 \text{ cm}^{-1}$. Although the phosphorescence deuteration shifts marginally favors assignment of the 517-cm^{-1} band to $3 \times \nu_{66}$ and 524 to $\nu_{32} + 301$, it only inconclusively does so, and we prefer to leave assignment of the $517, 524 \text{ cm}^{-1}$ pair an open question.

A second possibility of multiple quanta assignment is the weak pair at 687 and 694 cm^{-1} in the AQ phosphorescence. It cannot be assigned as a fundamental. It might, however, be assigned as a combination band of the b_{2u} mode ν_{46} (387) and

the 301-cm^{-1} Raman line, or $3 \times \nu_{32}$ (228) = 684 cm^{-1} , involving a b_{1u} skeletal deformation. A major difficulty with the former assignment is that ν_{46} , while ir active, does not appear in the phosphorescence spectrum. The calculated combination band frequency in AQ- d_8 is $381 + 292 = 673 \text{ cm}^{-1}$, whereas the observed phosphorescence bands are at 628 and 637 cm^{-1} . Since the calculated $3 \times \nu_{32}$ frequency in AQ- d_8 is 621 cm^{-1} , the deuteration shift leads to $3 \times \nu_{32}$ as the preferred assignment. The 7-cm^{-1} splitting may be due to an asymmetric *n*-hexane crystal field interaction with AQ along the high amplitude $3 \times \nu_{32}$ coordinate.

Three quanta of the most intense, fundamental, ν_{24} will be at 5000 cm^{-1} from the origin, i.e., in the 6000-Å range where the photomultiplier tube used has low sensitivity, and the second order of the scattered exciting light begins to interfere.

The experimental observations can be summarized as: (1) Only b_u type vibrations are observed to be active in the phosphorescence spectrum of AQ in *n*-hexane. With very few exceptions, these are observed in the phosphorescence of the isotopically mixed crystal.²⁰ In all environments the most prominent mode is the b_{1u} $\nu(\text{C}=\text{O})$ asymmetric stretching

TABLE III: Space Groups and Unit Cell Dimensions of *n*-Alkanes^a

<i>n</i> -Alkane	Crystal system	Space group	Molecules in unit cell	Vol of unit cell, Å ³	Unit cell dimensions					
					<i>a</i> , Å	<i>b</i> , Å	<i>c</i> , Å	α ⁰	β ⁰	γ ⁰
<i>n</i> -C ₅ H ₁₂	Orthorhombic	<i>Pbc</i> ₂₁	4	545	4.1	9.04	14.70	90	90	90
<i>n</i> -C ₆ H ₁₄	Triclinic	<i>P</i> $\bar{1}$	1	165	4.19	4.75	8.62	97.0	85.6	105.0
<i>n</i> -C ₇ H ₁₆	Triclinic	<i>P</i> 1	2	382	4.18	4.75	20.16	93.1	94.9	106.2
<i>n</i> -C ₈ H ₁₈	Triclinic	<i>P</i> $\bar{1}$	1	208.5	4.16	4.75	11.00	94.8	84.5	105.1

^a Reference 37.

TABLE IV: Environmental Effects on the Origin of T₁ → S₀ Emission of AQ

Environment	High energy site $\bar{\nu}$, cm ⁻¹	Low energy site ν , cm ⁻¹
Single crystal	22 156 ^a	
<i>n</i> -Pentane	21 914 ^b	21 789 ^b
<i>n</i> -Hexane		21 783 ^c
<i>n</i> -Heptane	21 866 ^c	21 761 ^c

^a Estimated origin at 1.8 K, ref 20. ^b Observed origin at 4.2 K. ^c Estimated origins at 4.2 K, see text.

vibration. (2) It is possible to make a quite firm assignment of a weak band attributed to three quanta of ν_{32} , a b_{1u} skeletal deformation. (3) There is a possibility that three quanta of ν_{66} , a b_{3u} out-of-plane deformation, are also active in the phosphorescence. However this assignment is inconclusive.

V. Environmental Perturbations on the Lowest Triplet State of AQ

Appearance of one or two sharp structured emissions for AQ in the C₅–C₈ alkane matrices indicate unique orientations of AQ molecules in the unit cell of the polycrystalline lattice. X-ray structural data³⁷ on these alkanes are collected in Table III. *n*-Hexane, *n*-heptane, and *n*-octane have triclinic lattices; *n*-hexane has the smallest unit cell volume. The crystal structure of *n*-pentane is quite different. It has an orthorhombic lattice; the volume of the unit cell is much larger than those of other alkanes and has four molecules per unit cell. Based on x-ray structural data, the crystal packing in *n*-pentane is different from the C₆–C₈ alkanes.

These structural data allow an explanation of the multiplet structure in the Shpol'skii-type spectra of AQ in the lower alkanes. In the three triclinic lattices C₆–C₈, AQ retains the free molecule's inversion center indicating at least a C_i site symmetry as is the case in the crystal.²⁰ In *n*-hexane, with the smallest unit cell volume, only one site emission was observed. In the larger unit cells of *n*-heptane and *n*-octane, two substitutional sites are possible, explaining the two sharp emissions.

The phosphorescence spectrum in the orthorhombic *n*-pentane is quite different. One of the two sites has a strong origin band and the spectrum can be analyzed in terms of both infrared and Raman active vibrations. The second strong origin band, 125 cm⁻¹ to the red of the first site origin, cannot be attributed to molecules in a different lowest energy triplet state, e.g., ³A_u($n\pi^*$). The estimated origin energy of ³B_{1g}($n\pi^*$) → S₀ is not sensitive to variation of the *n*-alkane matrix as shown in Table IV. The two electronic states have similar electronic structure and preferential ~400-cm⁻¹ stabilization

of one $n\pi^*$ state relative to the other (only differing in inversion phase) due to the crystal field cannot be visualized. The most feasible interpretation is that the latter spectrum originates from molecules distorted in their ground and/or excited states, i.e., the emitting species no longer retain an inversion center. Both site spectra exhibit multiple quanta of several infrared and Raman active vibrations indicating distortion of the molecule. The extent of distortion varies from one site to the other.

The band that we have interpreted as three quanta of ν_{32} is retained for both two site emissions of AQ in *n*-heptane. In *n*-pentane the spectrum is complicated by the different distortions in each site. The origin band and even and odd quanta of many nontotally symmetric and totally symmetric vibrations appear in the spectrum. It is difficult to follow the progressions, and assignment of combination bands becomes tentative.

A basis for an active three quantum band of ν_{32} is given by the theory developed in the Introduction based on route 1a involving strong vibronic interactions between the closely spaced ³A_u($n\pi^*$) and ³B_{1g}($n\pi^*$) states. The absence of this progression in the single crystal spectrum suggests a concerted vibronic perturbation. Concerted matrix and vibronic perturbations have been discussed for several molecular systems.^{38–42}

If an active three quantum progression in ν_{66} , out-of-plane deformation is indeed present, it must arise from a different mechanism involving route 1c.

VI. Conclusions

Detailed analysis of the vibrational structure of the highly resolved ³B_{1g}($n\pi^*$) → ¹A_g phosphorescence spectra of AQ in *n*-alkanes shows an odd quanta progression in ν_{32} , a b_{1u} skeletal deformation mode. In *n*-hexane and *n*-heptane this is attributed to potential surface distortion of the ³B_{1g} state due to vibrational–electronic interaction between closely spaced ³A_u($n\pi^*$) and ³B_{1g}($n\pi^*$).

In *n*-pentane matrix the spectrum shows multiple quanta of totally and nontotally symmetric modes built on allowed origins. Crystal-packing-induced molecular distortions in the ground state of AQ in *n*-pentane probably overwhelm excited state distortions induced by vibronic or valence distortive effects.

The conclusions of our study on AQ suggest that vibrational–electronic induced potential surface distortion is also present in BQ. Thus, careful examination of weak combination bands for odd quanta progressions in the BQ spectrum might be fruitful.

Acknowledgments. We thank Mr. Ilker Ozkan and Professor R. M. Hochstrasser (University of Pennsylvania) for fruitful discussions. Professor D. A. Wiersma (University of

Groningen, The Netherlands) for the gift of AQ- d_6 and Ms. Sandra Hankin for technical assistance. The critical comments of a referee were very valuable.

References and Notes

- (1) (a) Supported by National Science Foundation Grant No. MPS 71-03359 A04. (b) Presented at the Michael Kasha Symposium, Jan 8-10, 1976, Tallahassee, Fla.
- (2) (a) J. W. Sidman, *J. Am. Chem. Soc.*, **78**, 2363 (1956); (b) H. Hartman and Z. Lorenz, *Z. Naturforsch. A*, **7**, 360 (1952).
- (3) H. P. Trommsdorff, *J. Chem. Phys.*, **56**, 5358 (1972).
- (4) T. M. Dunn and A. H. Francis, *J. Mol. Spectrosc.*, **50**, 1 (1974).
- (5) T. M. Dunn and A. H. Francis, *J. Mol. Spectrosc.*, **50**, 14 (1974).
- (6) R. M. Hochstrasser, L. W. Johnson, and H. P. Trommsdorff, *Chem. Phys. Lett.*, **21**, 251 (1973).
- (7) A. I. Attia, B. H. Loo, and A. H. Francis, *Chem. Phys. Lett.*, **22**, 537 (1973).
- (8) H. Veenvliet and D. A. Wiersma, *Chem. Phys. Lett.*, **22**, 87 (1973).
- (9) H. Veenvliet and D. A. Wiersma, *J. Chem. Phys.*, **60**, 704 (1974).
- (10) H. Veenvliet and D. A. Wiersma, *Chem. Phys.*, **8**, 432 (1975).
- (11) H. Veenvliet and D. A. Wiersma, *Chem. Phys. Lett.*, **33**, 305 (1975).
- (12) H. Veenvliet and D. A. Wiersma, *Chem. Phys.*, **2**, 69 (1973).
- (13) J. H. Lichtenbelt, J. G. F. M. Fremeyer, H. Veenvliet, and D. A. Wiersma, *Chem. Phys.*, **10**, 107 (1975).
- (14) M. Koyanagi, Y. Kogo, and Y. Kanda, *J. Mol. Spectrosc.*, **34**, 450 (1970).
- (15) H. R. Drott and H. H. Dearman, *J. Chem. Phys.*, **47**, 1896 (1967).
- (16) M. Kasha, *Radiat. Res.*, Suppl. **2**, 243 (1960).
- (17) R. N. Nurmukhametov and D. N. Shigorin, *Russ. J. Phys. Chem.*, **35**, 34 (1961).
- (18) A. Kuboyama and S. Yabe, *Bull. Chem. Soc. Jpn.*, **40**, 2475 (1967).
- (19) H. H. Dearman, N. Sundarachari, and D. Ulku, *J. Chem. Phys.*, **45**, 4363 (1966).
- (20) K. E. Drabe, H. Veenvliet, and D. A. Wiersma, *Chem. Phys. Lett.*, **35**, 469 (1975).
- (21) J. M. Hollas and L. Goodman, *J. Chem. Phys.*, **43**, 760 (1965).
- (22) R. M. Hochstrasser and C. A. Marzocco in "Molecular Luminescence", E. C. Lim, Ed., W. A. Benjamin, New York, N.Y., 1969, p 631.
- (23) A. Duben, L. Goodman, and M. Koyanagi in "Excited States", Vol. I, E. C. Lim, Ed., Academic Press, New York, N.Y., 1974, p 295.
- (24) I. Suzuka, N. Mikami, and M. Ito, *J. Mol. Spectrosc.*, **52**, 21 (1974).
- (25) E. F. Zalewski, D. S. McClure, and D. L. Narva, *J. Chem. Phys.*, **61**, 2964 (1974).
- (26) D. L. Narva and D. S. McClure, *Chem. Phys.*, **11**, 151 (1975).
- (27) E. V. Shpol'skii, *Sov. Phys. USP*, **5**, 522 (1962).
- (28) E. V. Shpol'skii and T. N. Bolotinkova, *Pure Appl. Chem.*, **37**, 183 (1974).
- (29) C. Pfister, *Chem. Phys.*, **2**, 171 (1973).
- (30) M. Lamotte and J. Jousset-Dubien, *J. Chem. Phys.*, **61**, 1892 (1974).
- (31) M. Lamotte, A. M. Merle, J. Jousset-Dubien, and F. Dupuy, *Chem. Phys. Lett.*, **35**, 410 (1975).
- (32) S. D. Colson and G. L. Wheeler, *J. Chem. Phys.*, **60**, 4634 (1974).
- (33) O. S. Khalil and L. Goodman, *J. Chem. Phys.*, in press.
- (34) C. Pecile and B. Lunelli, *J. Chem. Phys.*, **46**, 2109 (1967).
- (35) (a) S. N. Singh and R. S. Singh, *Spectrochim. Acta, Part A*, **24**, 1591 (1968); (b) F. Stenman, *J. Chem. Phys.*, **51**, 3413 (1969).
- (36) Unpublished results, this Laboratory.
- (37) N. Norman and H. Mathisen, "The Structure of Linear Polymers: Lower n-Hydrocarbons", Government Research Report PB 171181, U.S. Department of Commerce, Washington, D.C., 1960.
- (38) R. M. Hochstrasser and D. A. Wiersma, *Isr. J. Chem.*, **10**, 517 (1972).
- (39) O. S. Khalil, L. Goodman, and S. W. Hankin, *Chem. Phys. Lett.*, **39**, 221 (1976).
- (40) P. J. Vergragt and J. H. van der Waals, *Chem. Phys. Lett.*, **36**, 283 (1975).
- (41) J. M. Van Prussen and S. D. Colson, *Chem. Phys.*, **6**, 382 (1974).
- (42) M. A. El-Sayed, W. R. Moomaw, and J. B. Chodak, *J. Chem. Phys.*, **57**, 4061 (1972).
- (43) M. Koyanagi and L. Goodman, *Chem. Phys. Lett.*, **21**, 1 (1973).
- (44) E.g., the weak 288-cm^{-1} band reported in ref 35b is not found in carefully purified AQ and in fact is at the same frequency as a strong anthracene line.

Discussion

G. W. CANTERS. Was any effect observed on the width of the zero-phonon lines of anthraquinone that depended upon whether normal or perfluorooheptane was used as a host?

O. S. KHALIL. We have not looked into this yet.

S. P. MCGLYNN. How well established is it that benzoquinone possesses two different *electronic* states of ${}^1\Gamma_{n\pi^*}$ character within 300 cm^{-1} of each other? In other words, is it possible that our desire to find two such almost degenerate ${}^1\Gamma_{n\pi^*}$ (and ${}^3\Gamma_{n\pi^*}$) states is an historic remnant, a coloring of our thinking from the time when the two populated ground state n-MO's, n_+ and n_- , were thought to be degenerate?

O. S. KHALIL. It is well established that there are two electronic states, and that they have approximately a 300-cm^{-1} separation. We are indeed looking at electronic states. No, this has nothing to do with the old history of *p*-benzoquinone.

Fluorescence Lifetimes and Sensitization Rate Constants for Dyes Adsorbed to Silver Halide Microcrystals

Annabel A. Muentzer

Research Laboratories, Eastman Kodak Company, Rochester, New York 14650 (Received February 17, 1976)

Publication costs assisted by Eastman Kodak Company

Using a mode-locked argon-ion laser and a time-correlated single-photon-counting detection system, fluorescence lifetimes were measured for two carbocyanine sensitizing dyes in gelatin and adsorbed to AgCl and AgBr microcrystals. Fluorescence quantum yields for these samples were also determined. The dyes studied, 3,3'-diethyloxthiacarbocyanine (OC-THC) and 3,3'-diethylthiacarbocyanine (THC), both showed large decreases in fluorescence lifetimes and quantum yields as they went from a gelatin environment to the surface of either silver halide, with the decreases being most pronounced on silver bromide. From these data, rate constants k_s for sensitization of the silver halide photographic response by the lowest excited singlet states of the dyes were calculated. These rate constants are in the range of 10^9 – 10^{10} s⁻¹ and, for a given dye, are larger on AgBr than AgCl. On the same silver halide, k_s is larger for OC-THC than for THC.

Introduction

Dye sensitization of silver halide photographic response, a process which makes the silver halide sensitive to light of wavelengths longer than its intrinsic blue absorption, is a subject which has long been of interest to both spectroscopists and photographic scientists.¹ Absorption of light by the singlet manifold of a good sensitizing dye is known to result in free electrons in the silver halide conduction band,²⁻⁴ just as absorption of light by the silver halide itself creates free electrons in the conduction band and free holes in the valence band. The free electrons subsequently interact with interstitial silver ions, beginning the process of photographic latent image formation. The dominant mechanism for this dye sensitization is currently thought to be electron transfer from the lowest excited singlet state of the dye to the conduction band of the silver halide. Support for such a mechanism is based on observed correlations relating polarographic reduction potentials of dyes,⁵ measurements⁶ and molecular orbital calculations^{7,8} of the ionization potential of the dyes' ground and excited states, and the dyes' spectral sensitizing ability. Measurement of the rate constant for this sensitization step on various silver halides and study of its dependence on dye structure and reduction potential are needed to gain a more detailed understanding of the sensitization process.

One approach to the determination of these sensitization rate constants is measurement of the fluorescence lifetimes τ_f for dyes adsorbed to silver halide and comparison of these lifetimes to those obtained for the same dyes in a photographically inert medium such as gelatin. In this approach, the standard equation for the fluorescence lifetime is written

$$\tau_f = \frac{1}{k_f + k_{ic} + k_{isc} + k_s}$$

where k_f is the natural radiative rate constant, k_{ic} and k_{isc} are the rate constants for the intramolecular radiationless processes of internal conversion and intersystem crossing, and k_s is the rate constant for sensitization of the silver halide.

Since k_s is necessarily zero for dyes in gelatin, the fluorescence lifetime of an efficient sensitizing dye should be markedly shortened as the dye's environment is changed from

gelatin to a silver halide surface. With appropriate evaluation of the changes in k_f , k_{ic} , and k_{isc} that occur under such conditions, this lifetime shortening can be used to calculate k_s for the dye on that silver halide. The experiments to be described are the initial results of a program using such an approach to measure k_s .

Experimental Section

The fluorescence lifetime measuring apparatus, schematically illustrated in Figure 1, consists of a mode-locked argon-ion laser and a time-correlated single-photon-counting detection system. The laser output is a train of 514.5-nm pulses with a FWHM of ~ 0.3 ns and a period of 7.1 ns (140.8-MHz repetition rate). The detection system used is similar to that described by Ware and coworkers⁹ but several modifications have been made to accommodate the laser and the high repetition rate of its pulse output. The signal having a constant time relationship to the exciting light pulses is derived from the 70.4-MHz signal which drives the mode-locking crystal. This signal is used as the stop input to the time to amplitude converter (TAC) and the pulses derived from the sample fluorescence photons are used as start signals. This reversal of the conventional procedure is employed because the TAC stop input can handle higher repetition rates than the start input. Nevertheless, for the TAC to function optimally, it is also necessary that the fast discriminator (A), which converts a portion of the 70.4-MHz driver signal into stop pulses, be held normally off. It is gated on, allowing stop pulses to reach the TAC, only when a start pulse has arrived at the constant fraction discriminator (B). With this experimental arrangement, there is a stop pulse for every start pulse and the practical limitation on the rate of detection of fluorescent photons is determined by the conversion time of the multi-channel analyzer (MCPHA). In a normal experiment, the laser intensity is attenuated such that this detection rate is 10–50 kHz, allowing a reasonable fluorescence decay curve to be collected in ~ 5 min. Since the sample is being excited at a rate of 140.8 MHz, this detection rate represents a 10^{-3} – 10^{-4} ratio of detected fluorescent events to excitation pulses and is more than sufficient to ensure operation in the single-photon regime. To produce this detection rate, the 200-mW average

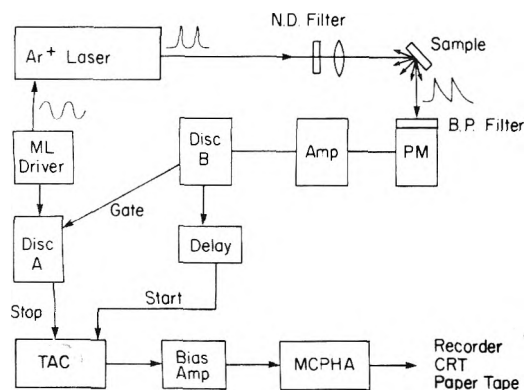


Figure 1. Schematic diagram of fluorescence lifetime measuring apparatus: Ar⁺ laser and ML driver, Spectra Physics 165-00 with 361 acousto-optic mode locker; PM, Amperex 56 TVP photomultiplier with voltage divider circuit based on ref 9; Amp, Ortex 454 timing filter amplifier; Disc B, Ortex 463 constant fraction discriminator; Disc A, EG + G T/200N fast trigger; TAC, Ortex 437A time-to-pulse height converter; Bias amp, Ortex 408A biased amplifier; MCPHA, Nicolet 1074 signal averager with SW-75 pulse height analyzer. Not shown in the figure is a gating signal from the MCPHA to the TAC to hold the TAC off while the MCPHA is busy.

power of the laser is typically attenuated by a factor of 10^5 – 10^6 . Such low light levels are particularly useful for samples, such as the dyed silver halides, which are sensitive to photolysis.

In measuring fluorescence lifetimes with this system, both a fluorescence decay curve and an exciting light pulse shape are collected for each sample. For solution samples, a suspension of Ludox is used as the inert scatterer for obtaining the excitation pulse shape; for film samples, a thick coating of powdered BaSO₄ is used as this scatterer. The curve shapes collected in the multichannel analyzer are punched out on paper tape and subsequent data manipulation is handled by an IBM 360 computer. Lifetime calculations are carried out with a slightly modified version of a convolution program obtained from Rice.¹⁰ The program uses Bevington's nonlinear least-squares program CURFIT¹¹ to find a fluorescence decay function whose convolution with the observed excitation pulse gives the best fit to the observed fluorescence decay curve. The decay function is assumed to be exponential or a sum of exponentials.

Time calibration of the system can be accomplished by two methods—the standard technique using calibrated delay lines or a measurement of the laser pulse period, which is very accurately known from measurement of the rf mode-locker driving frequency. The two procedures give time/channel calibrations agreeing within 2%. The 7.1-ns pulse period of the laser, while useful in this type of time calibration, does complicate the choice of a standard compound for checking the system performance, since many of the compounds normally used have lifetimes which are too long to be accurately measured in this time period. However, measurement of the lifetime of a 3.3×10^{-6} M solution of 3,3'-diethyloxadicarbocyanine iodide in a 90:5:5 mixture of ethyl, methyl, and isopropyl alcohol gave 1.11 ns, in good agreement with several other determinations.^{12,13} A conservative estimate of the accuracy of this measurement, as well as others in the time range from 1 to 4 ns, is $\pm 5\%$. Although the instrumental FWHM obtained for the exciting light pulses is just under 800 ps, use of the convolution procedure allows measurement of lifetimes as short as 100 ps. Accuracy of lifetimes in the range from 100 ps up to 1 ns is estimated to be $\pm 10\%$.

The silver halide samples studied were films containing cubic AgCl or AgBr microcrystals, 0.2 μm in edge length, dis-

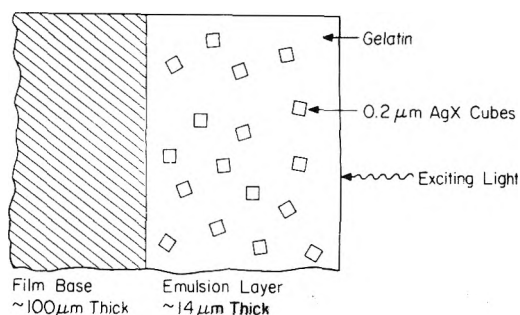


Figure 2. Schematic diagram of coated sample format. The silver halide was coated at 5.4 g of Ag/m² and the gelatin at 10.8 g of gelatin/m².

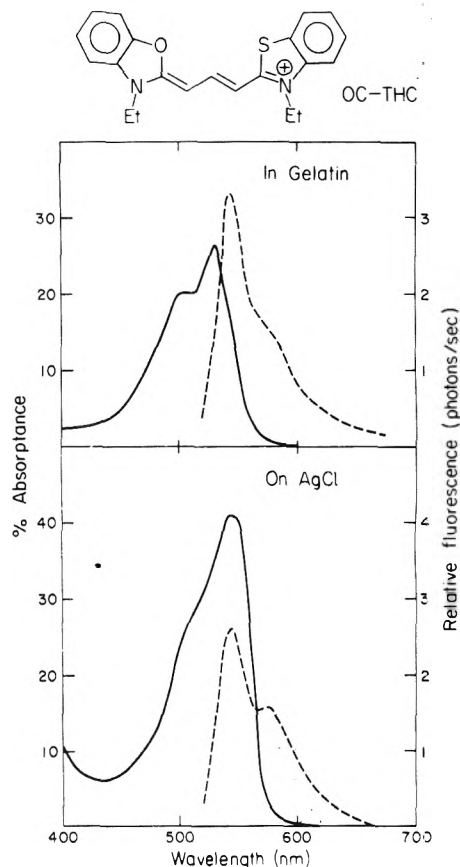


Figure 3. Absorbance (—) and laser-excited fluorescence (---) for the OC-THC dye in gelatin and adsorbed to AgCl microcrystals.

persed in a gelatin matrix. This format, which is also suitable for photographic measurements, is illustrated in Figure 2. Dyes were adsorbed to the microcrystals by adding dye solution to the liquid dispersion and allowing the mixture to equilibrate before coating it onto film base. Under the conditions used in these experiments, 95–99% of the added dye was adsorbed to the microcrystals. The dyes examined were two carbocyanines, 3,3'-diethyloxathiacarbocyanine iodide (OC-THC) and 3,3'-diethylthiacarbocyanine paratoluenesulfonate (THC).¹⁴ The structure of OC-THC is illustrated in Figure 3. The THC dye is very similar; its structure can be obtained by replacing the oxygen in the OC-THC with a sulfur. Adsorption isotherm studies indicate that the dye concentration used, 0.93 – 1.0×10^{-4} mol/mol of AgX, is approximately 4% of full monolayer coverage on the surface of the silver halide microcrystals. With the coating conditions employed, this dye concentration gives 4.2 – 4.5×10^{-6} mol of

dye/m² of coated sample. Samples containing the dyes and gelatin only were prepared at three times this dye concentration, $1.3\text{--}1.4 \times 10^{-5}$ mol of dye/m². Bromide ion, added as 1.5×10^{-6} mol/m² of KBr, was also present in these gelatin samples. All measurements on these samples were performed at room temperature, except for the determinations of dye phosphorescence lifetimes and intensities, done at 77 K.

Absorbance spectra¹⁵ for the samples studied were measured by the Spectrophotometry Laboratory of the Analytical Sciences Division of these laboratories. Fluorescence spectra were obtained with the argon-ion laser 514.5-nm line as an excitation source and the same right angle geometry illustrated in Figure 1. In this experimental arrangement, the fluorescence is detected by a double monochromator and photomultiplier tube combination calibrated for wavelength and polarization sensitivity with a standard lamp. This setup was also used in initial determinations of fluorescence quantum yields. Dye phosphorescence at 77 K was studied using a conventional spectrofluorometer¹⁶ equipped with a rotating can phosphoroscope for steady state measurements and a shutter system for lifetime measurements.

Fluorescence quantum yields for the film samples were measured relative to a coating of rhodamine 6G (R6G) in gelatin (1.4×10^{-5} mol of dye/m², 1.5×10^{-6} mol of KBr/m², 10.8 g of gelatin/m²). Quantum yield determinations on this sample by Mr. Costa of these laboratories, using a technique employing a coating of powdered BaSO₄ as a standard scatterer,¹⁷ gave $\phi_f = 0.65$. Combination of this value with the sample's measured lifetime, 3.82 ns, gives 1.71×10^8 s⁻¹ for k_f , the natural radiative rate constant of R6G. This value is in reasonable agreement with the $1.5\text{--}1.8 \times 10^8$ s⁻¹ rate constant calculated from literature values for ϕ_f and τ_f of R6G in ethanol ($\phi_f = 0.83\text{--}0.85$, $\tau_f = 4.8\text{--}5.5$ ns).¹⁸⁻²⁰ Thus, the gelatin matrix apparently causes only small perturbations in the dye's lowest singlet transition and the sample of R6G in gelatin can be considered an acceptable standard for the quantum yield measurements.

The quantum yield determinations were carried out using the fluorescence lifetime apparatus, the necessary intensity data being obtained by counting fluorescent photons/second during the actual lifetime measurements. For measurements on the adsorbed cyanine dyes, subsequent analysis of the concurrently collected lifetime data allowed the observed fluorescent intensity to be easily separated into a fraction associated with a short-lived component (the adsorbed dye) and a fraction belonging to a long-lived component (residual dye in gelatin). Appropriate corrections were made for the transmittance of the interference filters and the wavelength dependence of photomultiplier tube sensitivity. Time dependent variations in instrument sensitivity were corrected by using the intensity of the laser light scattered by the BaSO₄ coating as a reference. Only the fluorescence intensity at the wavelength maximum of the emission was measured. This intensity reading was taken within 1–2 s after a shutter in the laser beam path opened to excite the sample. The fluorescence spectrum was assumed to have the same shape as the R6G standard. This assumption was necessary for the coatings of the cyanine dyes adsorbed to silver halide, since determination of accurate spectra is severely complicated by the rapid fatigue of their fluorescence on illumination and the interfering fluorescence from residual dye in gelatin (see Figure 3 and associated discussion in Results section). For the cyanine dyes in gelatin, where good spectra can be obtained and compared to the R6G standard, the assumption produced at most a 5% error in the measured value for ϕ_f . Similar errors are anti-

ciated for the cases of the adsorbed dyes. Quantum yield measurements for the adsorbed dyes have the additional complication that the silver halide microcrystals strongly scatter the fluorescent radiation, causing an apparent fluorescence intensity enhancement which is dependent on microcrystal size and halide content, coating thickness, and fluorescence wavelength. An approximate correction for this effect was derived by measuring the apparent enhancement at 560 nm which occurred for control coatings containing the silver halide dispersions studied and R6G. The R6G was determined to be poorly adsorbed to the silver halide microcrystals and the true ϕ_f of this dye in gelatin should be minimally affected by the presence of the silver halide. The enhancement factors at 560 nm were measured to be 2.9 for the coatings containing the AgCl microcrystals and 3.7 for those containing the AgBr microcrystals. The ratio between these two factors is identical with the ratio between the diffuse reflectance at 560 nm of the undyed AgCl and AgBr coatings. Consequently, the wavelength dependence of each enhancement factor was assumed to be proportional to the wavelength dependence of the diffuse reflectance for the appropriate undyed coating, giving a range of 3.0–2.8 for the AgCl factors and 3.9–3.4 for the AgBr factors over the wavelength region 540–620 nm.

The overall accuracy of the quantum yield determinations is estimated to be $\pm 25\%$, taking into account measurement reproducibility, band shape approximations, error in the standard yield, and uncertainty in the fluorescence enhancement factors. The accuracy of yields for dyes in gelatin with no silver halide present is estimated to be somewhat better, $\pm 15\%$, since no enhancement factors were required.

Results and Discussion

Representative spectra obtained for the samples studied are illustrated in Figure 3, using the OC-THC dye as an example. Absorbance and laser-excited fluorescence spectra for this dye in gelatin, shown in the upper half of the figure, are typical of a monomeric cyanine dye.²¹⁻²³ Both spectra have a partially resolved vibronic band structure indicating a 1200–1300-cm⁻¹ progression, commonly attributed to symmetrical C=C and C=N stretching vibrations in the dye chromophore. The absorbance spectrum for the dyed silver chloride sample, given in the lower half of Figure 3, shows that the dye remains monomeric on adsorption to the AgCl microcrystals. The ~ 15 -nm red shift observed between this dye spectrum and the spectrum of the dye in gelatin is predominantly due to the larger refractive index of the AgCl substrate.²⁴ The fluorescence of the adsorbed dye has a maximum at ~ 575 nm but, as shown in Figure 3, the laser-excited fluorescence spectrum for this species is complicated by the overlap of the spectrum of residual dye in gelatin. Although the actual quantity of dye remaining in the gelatin is small, its fluorescence is strong enough to interfere with that of the adsorbed dye for two reasons: the adsorbed dye fluorescence is strongly quenched by the silver chloride and this fluorescence fatigues rapidly on illumination, causing the apparent intensity obtained during a spectral scan to be low. The spectra obtained for the sample containing OC-THC and silver bromide microcrystals are very similar to those illustrated for the dye and silver chloride. For the THC dye, the first singlet absorption band is at lower energy than the OC-THC case, giving an absorbance maximum at 560 nm for the monomeric dye in gelatin. The absorbance spectrum of THC in gelatin shows some presence of dimeric dye aggregates,²⁵ but these aggregates do not fluoresce and are not apparent for

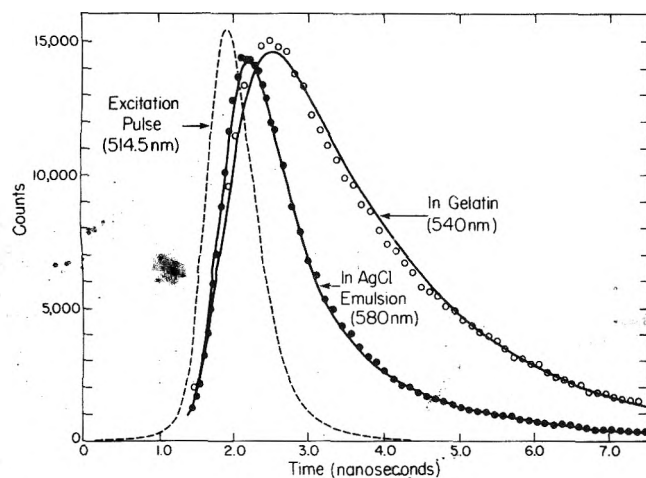


Figure 4. Fluorescence decay curves for the OC-THC dye in gelatin and adsorbed to AgCl microcrystals. Circles are data points and solid lines are computer fits to these data.

the dye adsorbed to silver chloride or silver bromide. Except for the longer wavelength of the dye transitions, the absorbance and fluorescence spectra obtained for the coatings of THC with the silver halide microcrystals are analogous to those obtained for OC-THC under the same conditions.

The results of fluorescence lifetime measurements for OC-THC are illustrated in Figure 4. The fluorescence decay curve for the dye in gelatin, with no silver halide present, was measured at an emission wavelength of 540 nm and indicates a reasonably long lifetime, 1.88 ns. For the coating containing the dyed silver chloride, the fluorescence decay measured at an emission wavelength of 580 nm has an obvious component with a much shorter lifetime. A component with a lifetime similar to that for the dye alone in gelatin is also noticeable. Computer analysis of this decay curve gives a lifetime of 0.31 ns for the short-lived component, which is assumed to be due to the adsorbed dye. The lifetime obtained for the longer-lived component is 1.73 ns, agreeing within error with the measured lifetime for the dye in gelatin. Lifetime measurements at 540 nm for the dyed silver chloride coating also give a value (1.83 ns) corresponding to dye in gelatin. Consequently, the lifetime data support the assignment of the 540-nm fluorescence peak in this sample as residual dye in gelatin and the identification of the 580-nm peak as fluorescence of the adsorbed dye. All of the coated samples containing dyed silver halide microcrystals show similar two-component fluorescence decay curves at the fluorescence peak assigned to adsorbed dye.

Table I summarizes the fluorescence lifetimes and quantum yields obtained for the two dyes studied. Both dyes in gelatin have relatively long lifetimes. These lifetimes are considerably shortened when the dyes are adsorbed to silver chloride and are shorter still for the dyes on silver bromide. Comparing the two dyes on the same silver halide indicates that the lifetime for OC-THC is consistently shorter than that for THC. The fluorescence quantum yields follow the same qualitative trends.

Calculation of the natural radiative rate constant k_f from the data given in Table I and the relationship $k_f = \phi_f/\tau_f$ gives values in the range $1.9\text{--}2.8 \times 10^8 \text{ s}^{-1}$ for the dyes in gelatin or adsorbed to silver chloride. Such numbers are in reasonable agreement with the $1\text{--}3 \times 10^8 \text{ s}^{-1}$ values derived from O'Brien, Kelly, and Costa's²⁶ measurements of ϕ_f and τ_f for several oxo- and thiocarbocyanine dyes in methanol. This agreement indicates that the lifetimes obtained for the dyes adsorbed to silver chloride are characteristic of the majority of the ad-

TABLE I: Fluorescence Lifetimes and Quantum Yields for Dyes in Gelatin and Adsorbed to Silver Halide

Dye	Substrate	λ_{em} , nm	τ_f , ^a ns	ϕ_f ^b
OC-THC	In gelatin	540	1.88	0.43
	1.4×10^{-5} mol/m ²			
	On AgCl	580	0.31	0.059
	1.0×10^{-4} mol/mol of Ag			
	On AgBr	580	0.12	0.011
	1.0×10^{-4} mol/mol of Ag			
THC	In gelatin	580	2.06	>0.11 ^c
	1.3×10^{-5} mol/m ²			
	On AgCl	620	0.58	0.17
	0.93×10^{-4} mol/mol of Ag			
	On AgBr	620	0.30	0.027
	0.93×10^{-4} mol/mol of Ag			

^a Accuracy is $\pm 5\%$ for lifetimes greater than 1 ns and $\pm 10\%$ for lifetimes less than 1 ns. ^b Accuracy is $\pm 15\%$ for dyes in gelatin and $\pm 25\%$ for dyes on silver halide. ^c Dye absorption at excitation wavelength used (514.5 nm) is known to contain a substantial fraction of nonfluorescent dimer, causing the measured ϕ_f to be too low.

sorbed dye molecules. For the dyes adsorbed to silver bromide, the values calculated for k_f are somewhat low ($0.8\text{--}0.9 \times 10^8 \text{ s}^{-1}$), a factor of 2 to 3 times less than k_f for the same dye on silver chloride. This discrepancy could be explained by postulating the existence of two populations of dye molecules adsorbed to silver bromide—one population with the measured fluorescence lifetime and another with a lifetime much shorter than the time resolution of the apparatus. Under these conditions, the fluorescence quantum yield measurement would be a weighted average of the ϕ_f of the longer-lived population and the much lower ϕ_f of the shorter-lived population. Since the lifetime measurement would measure only the longer τ_f , the calculated k_f would be low. Further experiments on a larger variety of dyes are needed to test the validity of this proposed explanation. However, at this point, it seems reasonable to assume that the lifetimes measured for the two dyes studied on silver bromide represent the lifetimes of at least a sizeable fraction of the adsorbed dye molecules.

Before using the lifetime shortening observed for the adsorbed dyes to determine values for the sensitization rate constant k_s , other possible causes of decreases in the dyes' fluorescence lifetimes must be considered. An obvious possibility is the external heavy atom effect, which is expected to increase k_{isc} , the intersystem crossing rate from the adsorbed dye's excited singlet state to its triplet manifold. Table II summarizes some relevant data on low temperature triplet lifetimes and phosphorescence intensities for the dyed samples studied. The triplet lifetimes measured do indicate an external heavy atom effect for the dyes adsorbed to both silver halides. However, data of Buettner²⁷ and of O'Brien et al.²⁶ indicate that for cyanine dyes, ϕ_{isc} , the yield for intersystem crossing is never larger than 3% in the absence of a heavy atom effect. The changes in triplet lifetimes observed for the dyes studied here indicate a heavy-atom induced increase in spin-orbit coupling of roughly a factor of 10, enough to increase this maximum ϕ_{isc} to about 25% for the case of the dyes on silver bromide. However, a change in ϕ_{isc} from 3 to 25% will

TABLE II: Phosphorescence Lifetimes and Intensities at 77 K for Dyes in Gelatin and Adsorbed to Silver Halide

Dye	Substrate ^a	τ_p , ^b ms	I_p/I_f ^c
OC-THC	In gelatin	76	3.1×10^{-2}
	On AgCl	23	1.1×10^{-2}
	On AgBr	11	1.4×10^{-1}
THC	In gelatin	29	2.8×10^{-2}
	On AgCl	15	1.2×10^{-2}
	On AgBr	7.1	1.4×10^{-1}

^a Concentrations same as given in Table I. ^b Time for emission to decay to $1/e$ of initial value. Lifetimes for OC-THC on silver halide have nonexponential component, indicating some of phosphorescence comes from recombination. Accuracy estimated as $\pm 10\%$. ^c Corrected for wavelength dependence of spectrofluorometer detection system.

only cause a 20% decrease in τ_f , while the observed decrease for the dyes on silver bromide is a factor of 7–15. In addition, the data in Table II on the intensity ratios of dye phosphorescence to fluorescence as the dyes go from gelatin to silver chloride to silver bromide can be used to derive an alternate estimate for ϕ_{isc} . These intensity ratios can be written

$$\frac{I_p}{I_f} = \frac{\phi_p}{\phi_f} = \frac{\phi_{isc} Q_p}{\phi_f}$$

where ϕ_p is the overall quantum yield for phosphorescence and Q_p is the quantum efficiency of phosphorescence from molecules that have crossed into the triplet manifold. Taking Q_p to be fairly close to unity (or at least similar to ϕ_f), an assumption which is reasonable for these 77 K measurements, the I_p/I_f ratios give an estimate for ϕ_{isc} . For the dyes on silver bromide, this value is even smaller than the 25% maximum derived from the previous argument. Consequently, the assumption that the external heavy atom effect plays only a minor role in the observed fluorescence lifetime shortening seems well justified. Such an assumption is also in accord with the visual observations of West²⁸ and the more quantitative experiments of Tani^{29,30} showing that the fluorescence of cyanine dyes is strongly quenched on adsorption to silver halides but at most slightly diminished on adsorption to nonphotosensitive heavy atom substrates.

Another hypothesis which must be examined is that adsorption of the dyes to the surface of the silver halide microcrystals is changing the rate of internal conversion from the excited singlet to ground singlet states. However, available data on the cyanine dyes indicates that internal conversion rates tend to decrease as the dyes' structure or environment becomes more rigid.^{26,27} Since a dye adsorbed to a crystalline surface can reasonably be considered to be more rigidly constrained than a dye in a gelatin matrix, the expected effect of dye adsorption on the internal conversion rate should lead to longer, not shorter, fluorescence lifetimes. Finally, the possibility that adsorption to the silver halide is affecting the dyes' natural radiative rate constants k_f must be considered. Drexhage^{31,32} has calculated the effect of placing a dye, modeled as a radiating dipole, at a dielectric interface such as that formed by the silver halide and gelatin. For the case of the dye transition dipole parallel to the interface, his results indicate that, compared to the value for dye in gelatin, k_f should increase by a factor of 1.26 for gelatin–silver chloride and 1.35 for gelatin–silver bromide interfaces. Such changes, while leading to decreases in τ_f , are quite small compared to the observed shortening of the fluorescence lifetimes.

TABLE III: Sensitization Rate Constants and Quantum Yields from Lifetime Data

Dye	Substrate	k_s , s ⁻¹	ϕ_s	ϕ_f ^a
OC-THC	On AgCl	2.8×10^9	0.84	0.95
	On AgBr	7.6×10^9	0.93	0.57
THC	On AgCl	1.2×10^9	0.72	0.59
	On AgBr	2.8×10^9	0.85	0.60

^a A photographically determined quantum yield for spectral sensitization at the absorbance maximum of the dye measured relative to the blue (400 nm for AgBr, 380 nm for AgCl) sensitivity of the same dyed coating. Exposures used were 1-s duration and coatings were processed for 20 min in Metol and ascorbic acid developer. Accuracy is estimated to be $\pm 10\%$.

Since the estimated changes in k_f , k_{isc} , and k_{ic} for the adsorbed dyes can account for at best minor differences in the fluorescence lifetimes, it is reasonable to attribute the major part of the observed lifetime shortening to sensitization of the silver halide by the dyes' excited singlet states. Sensitization rate constants can then be approximately calculated from the equation

$$k_s = \frac{1}{\tau_{AgX}} - \frac{1}{\tau_{gel}}$$

Values of these rate constants for the dyes and silver halides studied are listed in Table III. For both dyes, k_s is larger on silver bromide than on silver chloride. For a given silver halide, the rate of sensitization by the OC-THC dye is larger than that for THC. Table III also gives quantum yields ϕ_s for the sensitization by the dyes calculated from

$$\phi_s = k_s \tau_{AgX}$$

These values represent the yield for the initial step in spectral sensitization, presumably electron transfer from the dye's excited singlet state. Listed for comparison are values of the photographically measured relative quantum yield for spectral sensitization ϕ_r , a computation comparing the quantum efficiency of photographic latent image formation by light absorbed in the dye to that by light absorbed in the silver halide.¹ The two quantum yield values are in moderately good agreement for the dyes on silver chloride and illustrate the fact that OC-THC is a more efficient sensitizing dye than THC. The agreement for the dyes on silver bromide is not as good, with the ϕ_r values significantly lower than the calculated values of ϕ_s . This discrepancy could be related to the population of extremely short-lived dye molecules postulated to explain the low values of ϕ_f obtained for the dyes on AgBr. If the process causing this very short lifetime interferes with efficient sensitization by this dye population, the resulting photographic ϕ_r values would be expected to be lower than ϕ_s , since ϕ_s is calculated solely from τ_f for the longer-lived adsorbed dye population. An equally valid explanation for the difference between ϕ_s and ϕ_r can be made in terms of the secondary processes in formation of the photographic latent image. The value for ϕ_r includes the relative efficiency of these secondary processes; the value for ϕ_s does not.

Summary

The results obtained for the two carbocyanine dyes studied show that fluorescence lifetimes for sensitizing dyes adsorbed to silver halide can be measured and these lifetimes used to determine rate constants k_s for the dyes' sensitization of the silver halide photographic response. The fact that k_s for a given dye is found to be larger on silver bromide than silver

chloride is qualitatively consistent with a spectral sensitization mechanism involving electron transfer from the dyes' excited singlet state to the silver halide conduction band, since the silver chloride conduction band is estimated to lie ~ 0.2 eV above the conduction band for silver bromide.³³ Similarly, the larger values for k_s found for the OC-THC dye as compared to the THC dye on the same silver halide are consistent with this electron transfer model. The polarographic reduction potentials³⁴ measured for OC-THC (-1.09 eV) and THC (-1.00 eV) indicate that OC-THC's lowest excited singlet state should have a smaller ionization potential than the lowest excited singlet of THC. To extend and quantify these relationships, further fluorescence lifetime measurements are planned on a variety of sensitizing dyes adsorbed to different silver halides.

Acknowledgments. The continuing interest and support of Dr. T. H. James and Dr. Walter Cooper throughout the course of this experimental program is gratefully acknowledged. The advice of Dr. Karl Drexhage during the initial phases of the lifetime measurements and discussions with Mr. L. Costa concerning quantum yield determinations in turbid media have been most helpful. The technical assistance of Mrs. Rebecca Ott and Mrs. Joan Kittle in the spectrofluorometer measurements is also much appreciated.

References and Notes

- W. West and B. H. Carroll in "The Theory of the Photographic Process", 3d ed, C. E. K. Mees and T. H. James, Ed., Macmillan, New York, N.Y., 1966, Chapter 12 and references cited therein.
- W. West and B. H. Carroll, *J. Chem. Phys.*, **15**, 529 (1947).
- V. I. Saunders, R. W. Tyler, and W. West, *J. Chem. Phys.*, **46**, 199 (1967).
- L. M. Kellogg, N. B. Liebert, and T. H. James, *Photogr. Sci. Eng.*, **16**, 115 (1972).
- P. B. Gilman, Jr., *Photogr. Sci. Eng.*, **18**, 475 (1974).
- R. C. Nelson, *J. Mol. Spectrosc.*, **23**, 213 (1967).
- D. M. Sturmer, W. S. Gaugh, and B. J. Bruschi, *Photogr. Sci. Eng.*, **18**, 49, 56 (1974).
- R. C. Nelson and R. G. Selsby, *Photogr. Sci. Eng.*, **14**, 342 (1970).
- C. Lewis, W. R. Ware, L. J. Doemeny, and T. L. Nemzek, *Rev. Sci. Instrum.*, **44**, 107 (1973).
- K. G. Spears and S. A. Rice, *J. Chem. Phys.*, **55**, 5561 (1971).
- P. R. Bevington, "Data Reduction and Error Analysis for the Physical Sciences", McGraw-Hill, New York, N.Y., 1969, Chapter 11.
- D. Magde and M. W. Windsor, *Chem. Phys. Lett.*, **27**, 31 (1974).
- C. V. Shank and E. P. Ippen, *Appl. Phys. Lett.*, **26**, 62 (1974).
- Dyes were obtained from Mr. D. W. Heseltine, of these Laboratories.
- Measurement of absorbance, given by $1 - (\text{total reflectance} + \text{total transmittance})$, allows determination of the actual amount of light absorbed by turbid samples such as the coatings studied here. See F. Grum in "Physical Methods of Chemistry", Part III B, A. Weissberger and B. W. Rossiter, Ed., Wiley-Interscience, New York, N.Y., 1972, Chapter III, pp 248-273, for a detailed discussion.
- W. Cooper, S. P. Lovell, and W. West, *Photogr. Sci. Eng.*, **14**, 184 (1970).
- L. Costa, F. Grum, and D. J. Paine, *Appl. Opt.*, **8**, 1149 (1969).
- J. P. Webb, W. C. McColgin, O. G. Peterson, D. L. Stockman, and J. H. Eberly, *J. Chem. Phys.*, **53**, 4227 (1970).
- A. K. Chibisov, H. A. Kezle, L. V. Levshin, and T. D. Slavnova, *J. Chem. Soc., Chem. Commun.*, 1292 (1972).
- H. E. Lessing, E. Lippert, and W. Rapp, *Chem. Phys. Lett.*, **7**, 247 (1970).
- J. Pouradier, *J. Chim. Phys.*, **61**, 1107 (1964).
- S. F. Mason, *J. Soc. Dyers Colour.*, **84**, 604 (1968).
- W. West, S. P. Lovell, and W. Cooper, *Photogr. Sci. Eng.*, **14**, 52 (1970).
- W. West and A. L. Geddes, *J. Phys. Chem.*, **68**, 837 (1964).
- W. West and S. Pearce, *J. Phys. Chem.*, **69**, 1894 (1965).
- D. F. O'Brien, T. M. Kelly, and L. F. Costa, *Photogr. Sci. Eng.*, **18**, 76 (1974).
- A. V. Buettner, *J. Chem. Phys.*, **46**, 1398 (1967).
- W. West in "Scientific Photography", H. Souvenier, Ed., Pergamon Press, Oxford, 1962, pp 557-568.
- T. Tani, S. Kikuchi, and T. Sekiguchi, *Kogyo Kagaku Zasshi*, **71**, 631 (1968).
- T. Tani and S. Kikuchi, *Photogr. Korresp.*, 104 (1968).
- K. H. Drexhage, *J. Lumin.*, **1,2**, 693 (1970).
- K. H. Drexhage in "Progress in Optics", E. Wolf, Ed., North-Holland Publishing Co., Amsterdam, 1974, Chapter 4.
- C. R. Berry, *Photogr. Sci. Eng.*, **19**, 93 (1975).
- Reduction potentials measured with a dropping mercury electrode vs. an aqueous silver-silver chloride reference electrode at 20 °C ($E_s = +0.22$ V). Measurements made by Dr. R. F. Large, of these Laboratories. See R. F. Large in "Proceedings of the Symposium on Photographic Sensitivity", R. J. Cox, Ed., Academic Press, New York, N.Y., 1972, pp 241-263, for a discussion of polarographic measurements on cyanine dyes.

Discussion

M. KASHA. There's a paper in by E. Clementi and M. Kasha [*J. Chem. Phys.*, **26**, 956 (1957)], and I think that gives you an index on the spin-orbital coupling constants. It does give a nonsensitized surface which would allow for spin-orbit coupling.

A. A. MUENTER. It is difficult to make good emulsions out of lead bromide and to make the comparison I would need to make the sample in the same way. Also lead bromide can be spectrally sensitized. I'm a little concerned about using that as an inert heavy-atom substrate.

M. KASHA. Isn't it possible that there is something, in addition to the conduction band, which may be activated by dye sensitization? Isn't it possible that a metastable band between the conduction band and the valence band of the photosensitive crystal could offer a limited frequency sensitization?

A. A. MUENTER. I feel that that is unlikely because there have been a number of experiments [V. I. Saunders, *Photogr. Sci. Eng.*, **19**, 71 (1975)] now that have been done on silver halide single crystals, looking for a long wavelength optical absorption that would be much, much weaker than in the blue region. And there is no evidence of another stable band of the type we are talking about down to four or five orders of magnitude below the absorption of the silver halide itself.

W. T. SIMPSON. Have you measured the lifetime of any J-aggregated dyes?

A. A. MUENTER. Yes, one. It is quite short.

W. T. SIMPSON. Don't the dyes aggregate on the silver halide surface?

A. A. MUENTER. These are not aggregated. There is sufficiently low coverage such that they are not prone to aggregate.

R. KOPELMAN. Is there any relationship between your sensitization mechanism and the experiments and mechanisms in the work of Kuhn et al.?

A. A. MUENTER. Kuhn and his group [H. Bucher, H. Kuhn, B. Mann, D. Möbius, L. v. Szentpaly, and P. Tillmann, *Photogr. Sci. Eng.*, **11**, 233 (1967); L. v. Szentpaly, D. Möbius, and H. Kuhn, *J. Chem. Phys.*, **52**, 4618 (1970)] have done a number of monolayer experiments, some of them using silver halides, to try and demonstrate Förster type energy transfer as a mechanism for spectral sensitization of silver halides. There does not seem to be a concentration of acceptor centers at the longer wavelengths in the silver halides that would explain the kind of sensitization efficiencies that we were able to obtain with the dyes. Also one gets a much better correlation between the reduction potentials of the dyes and their abilities to sensitize. So, for those two reasons, I think energy transfer is not the dominant mechanism.

R. HOCHSTRASSER. If you had long-range transfer, your decays would be nonexponential ($\exp[-t/\tau]^{1/2}$); and they are not.

A. A. MUENTER. I do not want to state unequivocally that it's an exponential decay, because when you are doing a convolution in a lifetime of 0.3 ns with an instrumental function 0.8 ns wide, you could have a somewhat nonexponential decay and still obtain a reasonably decent fit. It's exponential within my error limits, but I wouldn't want to say that it is strictly exponential.

Fluorescence, Resonance Raman, and Radiationless Decay in Several Hemoproteins

Fran Adar,*

Department of Biochemistry and Biophysics, University of Pennsylvania, Philadelphia, Pennsylvania 19174

Martin Gouterman, and Sheldon Aronowitz

Department of Chemistry, University of Washington, Seattle, Washington 98195 (Received December 18, 1975)

Resonance Raman (RR) spectra are reported for five hemoproteins: (a) ferrocycytochrome b_5 ; (b) oxyhemoglobin; (c) ferricytochrome b_5 ; (d) deoxyhemoglobin; and (e) methemoglobin. Compound a shows background fluorescence bands which give evidence for incomplete vibrational relaxation. Relative fluorescence yields for (a):palladium mesoporphyrin:zinc mesoporphyrin are $1:2.5 \times 10^2:10^4$. Compounds (b) through (e) show no fluorescence but decreasing RR intensity. The presence of fluorescence in (a) and the decreasing RR intensity of (a) through (e) are attributed to decreasing electronic radiationless decay times, τ_e , from 100 to 3 fs across the series (a) > (b) > (c) ~ (d) > (e). The times τ_e are estimated from the resolution of the visible absorption bands. Iterative extended Hückel calculations are used to rationalize τ_e : Thus for (a) the visible band is $^1Q(\pi, \pi^*)$ and at lower energy the only state of the same spin is $^1(d, d)$; for (b) at lower energy than $^1Q(\pi, \pi^*)$ there is not only a possible $^1(d, d)$ state but singlets involving transitions on the O_2 ligand and charge transfer singlets ring \rightarrow oxygen; for (c) the visible excited state is $^2Q(\pi, \pi^*)$ and there are $^2(d, d)$, $^2(\pi, d)$, and $^2T(\pi, \pi^*)$ excited states at lower energy; similarly for (d) there are $^5(d, d)$ and $^5T(\pi, \pi^*)$ at lower energy than the visible state $^5Q(\pi, \pi^*)$; finally (e) has both $^6Q(\pi, \pi^*)$ and $^6(\pi, d)$ electronic states in the visible energy region with heavy vibronic mixing between them. The roles of photon coherence time, τ_p , and vibrational relaxation, τ_v , in determining the nature of the scattering process are explored.

Introduction

Recently there has been considerable interest in the resonance Raman spectra of many hemoproteins¹⁻³ as well as resonance Raman spectra of porphyrins coordinated to metals other than iron.⁴⁻⁷ In addition there has been theoretical consideration of the relation between resonance Raman and resonance fluorescence.⁸⁻¹⁰ These phenomena reflect two aspects of the same physical process, whose differentiation depends on the relative lengths of the photon coherence time, τ_p , and the lifetime of the resonant excited state, τ_i . The metalloporphyrins provide an ideal set of systems in which to study these phenomena because of the very strong dependence of excited state lifetime on the central metal.¹¹⁻¹³ In this paper we shall report on the observed relationship of resonance Raman spectra (RR), resonance fluorescence (RF), and relaxed fluorescence (f) among several hemoproteins and metalloporphyrins with very short excited state lifetimes and relate these observations to the time durations of the various processes.

Background

For most metalloporphyrins the visible spectrum is assigned as a $Q(\pi, \pi^*)$ excited state.¹² The natural radiative lifetime is determined from the absorption coefficient and for a wide variety of metals has a value¹⁴

$$\tau_f \sim 60 \text{ ns} \quad (1)$$

Metalloporphyrins with closed atomic shells (e.g., d^0 or d^{10}) show fluorescence yields, ϕ_f , in the range $0.2 > \phi_f > 10^{-3}$.^{15,16} Excited electronic state lifetimes τ_e in these cases can be determined from the relation

$$\phi_f = \tau_e / \tau_f \quad (2)$$

Hence they vary from about 12 ns to 60 ps. In the case of metalloporphyrins with partly filled shells [e.g., d^n , $1 < n < 9$, or

p^2 main group metals such as Pb(II)] fluorescence yields are below 10^{-3} and in some cases no fluorescence has been observed using conventional fluorimetric systems.¹¹⁻¹⁹ However, with laser Raman apparatus detection of fluorescence yields can be pushed to lower levels, perhaps 10^{-6} . Thus we can explore the emission properties of systems with excited state lifetimes in the range 60 ps to 60 fs.

With such short lived systems it becomes important to distinguish the processes that contribute to τ_i , the lifetime of the initial excited state. There is of course radiative emission, with a lifetime given by eq 1. In addition there is the electronic state relaxation time, τ_e . This is the process generally described as "radiationless decay", which is presumed to be intramolecular and isoenergetic, from one electronic state to another.²⁰⁻²² Also there is vibrational relaxation, occurring with time τ_v , in which the vibrational state decays through anharmonic coupling and through dissipation of its energy to the solvent environment. Thus the overall decay process is written

$$\tau_i^{-1} = \tau_f^{-1} + \tau_e^{-1} + \tau_v^{-1} \quad (3)$$

Finally, it has been noted that, in deciding which emission processes occur, the coherence time of the exciting photon, τ_p , must also be considered.⁸⁻¹⁰

The processes just defined have been related to the line width of various types of photons through the uncertainty relation

$$\Delta\bar{\nu}\tau \sim (2\pi c)^{-1} \quad (4)$$

where $\Delta\bar{\nu}$ is the line width at half maximum (cm^{-1}) and τ is the process decay time. For convenience these values have been listed in Table I. Equation 4 can be applied to the incident photon, which has a line width of $\sim 1 \text{ cm}^{-1}$ to get a value

$$\tau_p \sim 5 \text{ ps} \quad (5)$$

TABLE I: Line Width, Lifetime, and Fluorescence Yields for Metalloporphyrins

$\Delta\bar{\nu}$, cm^{-1} ^a	τ^a	ϕ_f^a	τ_e	
			3 fs	Hb(III)
			6 fs	Hb(II)
530	10 fs	1.7×10^{-7}		
			15 fs	HbO ₂
53	100 fs	1.7×10^{-6}	100 fs	cyt <i>b</i> ₅ (II)
				$\tau_v(300 \text{ K}) \sim 500 \text{ fs}^b$
5.3	1 ps	1.7×10^{-5}	1 ps	PtP
				$\tau_v(15 \text{ K}) \sim 3 \text{ ps}^c$
				$\tau_p(\text{laser}) \sim 5 \text{ ps}^b$
5.3×10^{-1}	10 ps	1.7×10^{-4}	12 ps	PdP
5.3×10^{-2}	100 ps	1.7×10^{-3}		
5.3×10^{-3}	1 ns	1.7×10^{-2}	1.2 ns	ZnP
5.3×10^{-4}	10 ns	1.7×10^{-1}		

^a $\tau\Delta\bar{\nu} = (2\pi c)^{-1}$; $\phi_f = \tau/60 \text{ ns}$. ^b See text for basis of estimates. ^c This value is poorest known; we only know $1.3 \text{ ps} < \tau_v < 12 \text{ ps}$. See text.

The line width of resonance Raman photons observed at room temperature is $\sim 10 \text{ cm}^{-1}$, giving a vibrational relaxation time in the ground state of

$$\tau_v \sim 500 \text{ fs} \quad (6)$$

We shall be concerned with the nature of fluorescence as τ_e becomes shorter than τ_v . Over the series of metal complexes zinc porphyrin (ZnP), palladium porphyrin (PdP), and platinum etioporphyrin (PtEtio) quantum yields, ϕ_f , have value 2×10^{-2} , 2×10^{-4} , and $\leq 2 \times 10^{-5}$.^{13,18b} From Table I we see that τ_e is 1.2 ns, 12 ps, and $\leq 1.2 \text{ ps}$, respectively; the uncertainty line widths would be 4.5×10^{-3} , 4.5×10^{-1} , and $\sim 4.5 \text{ cm}^{-1}$. The smallest line widths are observed in Shpol'skii matrices¹⁸ where a minimal line width at 4.2 K appears to be $\sim 3.2 \text{ cm}^{-1}$.²³ Under these conditions it is necessary to write

$$\Delta\bar{\nu}_{\text{shp}} = \Delta\bar{\nu}_i + \Delta\bar{\nu}_{\text{min}} \quad (7)$$

where $\Delta\bar{\nu}_{\text{shp}}$ is the observed Shpol'skii line width, $\Delta\bar{\nu}_i$ the uncertainty broadening due to the excited state lifetime τ_i given by (3) and (4), and $\Delta\bar{\nu}_{\text{min}}$ is a minimal line width due to other factors that are slightly temperature dependent. A minimal line width of 4 cm^{-1} has been observed for ZnP and PdP^{18c} under similar low temperature conditions to those showing significantly broader Shpol'skii line width for PtP.^{18c} Since conditions for these experiments are otherwise identical we assume that broader $\Delta\bar{\nu}_{\text{shp}}$ observed for PtP is due to a shorter τ_e , in agreement with the estimate from τ_f . The $\Delta\bar{\nu}_{\text{shp}} \sim 4 \text{ cm}^{-1}$ observed for ZnP and PdP at 15 K implies $\tau_v > 1.2 \text{ ps}$ in these low temperature matrices, a limit that probably holds for Pt complexes. Moreover, if τ_v were this short one might expect the vibrational bands Q(1,0) of the visible Shpol'skii absorption spectrum to be broader than the Q(0,0) band. Since this is not observed,^{18c} it is reasonable to presume that under these low temperature conditions τ_v is rather longer than 1.2 ps. On the other hand, τ_v is probably shorter than the electronic relaxation time of 12 ps. Thus we can say that $12 \text{ ps} > \tau_v > 1.2 \text{ ps}$ and estimate $\tau_v \sim 3 \text{ ps}$ at low temperatures.

(An interesting point can be made concerning palladium porphyrin fluorescence. At room temperature, where $\tau_v \ll \tau_e$, a clear relaxed fluorescence is observed,^{18a} but no Shpol'skii fluorescence has been seen. It may be that because τ_v approaches τ_e at low temperature, the fluorescence in a Shpol'skii matrix is not vibrationally relaxed and hence is broad. More study of palladium porphyrin fluorescence is needed to clarify this situation.)

For convenience we have listed these various time estimates in Table I. The line widths for NiP and CuP in absorption are

substantially broader than those of PtP^{18c} and the fluorescence yields are vanishing. Thus as τ_e drops through the range 10^{-3} to 10^{-6} in porphyrin complexes we move from a case where $\tau_e \gg \tau_v$ to one where $\tau_e \ll \tau_v$. Emission from porphyrins satisfying the former condition will be referred to as relaxed fluorescence (f) while the latter type of emission will be referred to as resonance fluorescence (RF). (This empirical definition of RF may not coincide with the theoretical definition based on photon coherence time τ_p .⁸⁻¹⁰ This difference will be discussed more fully in the last section of this paper.)

The observation of RF was earlier reported for metallophthalocyanines.²⁴ Under these conditions eq 2 needs to be modified. If it is assumed that τ_v represents the time for a single decay process to produce a vibrationally relaxed excited state, then simple kinetic arguments establish that the relaxed fluorescence yield is

$$\phi_f = \tau_i \tau_e / \tau_v \tau_f \quad (2')$$

where (2') reduces to (2) if $\tau_f^{-1} + \tau_e^{-1} \gg \tau_v^{-1}$. The resonance fluorescence yield is

$$\phi_{\text{RF}} = \tau_i / \tau_f \quad (8)$$

so that

$$\phi_{\text{RF}} / \phi_f = \tau_v / \tau_e \quad (9)$$

Equations 2', 8, and 9 would, of course, have to be modified if several vibrational relaxations are needed to produce relaxed fluorescence.^{24b} Equations 1-9 make it clear that, for metalloporphyrins, as observed fluorescence yield decreases below 10^{-4} resonance fluorescence (RF) tends to dominate over relaxed fluorescence (f).

The above kinetic arguments implicitly assume that the exciting photon is shorter lived than the molecular state, so that the interaction between the photon field and the molecule is complete before the molecule has a chance to rearrange itself. In fact for all cases reported here, since the emission studies were done at room temperature, eq 5 and 6 show that $\tau_v \ll \tau_p$. The implications of this will be taken up in the Discussion section.

Methods

Emission spectra were excited by photons from an Ar⁺-Kr⁺ mixed gas ion laser. Spectra were analyzed on a Spex Ramalog 4 equipped with a cooled GaAs photomultiplier. The monochromator was run at a spectral resolution of about 12 cm^{-1} . (Previous runs established that at room temperature little

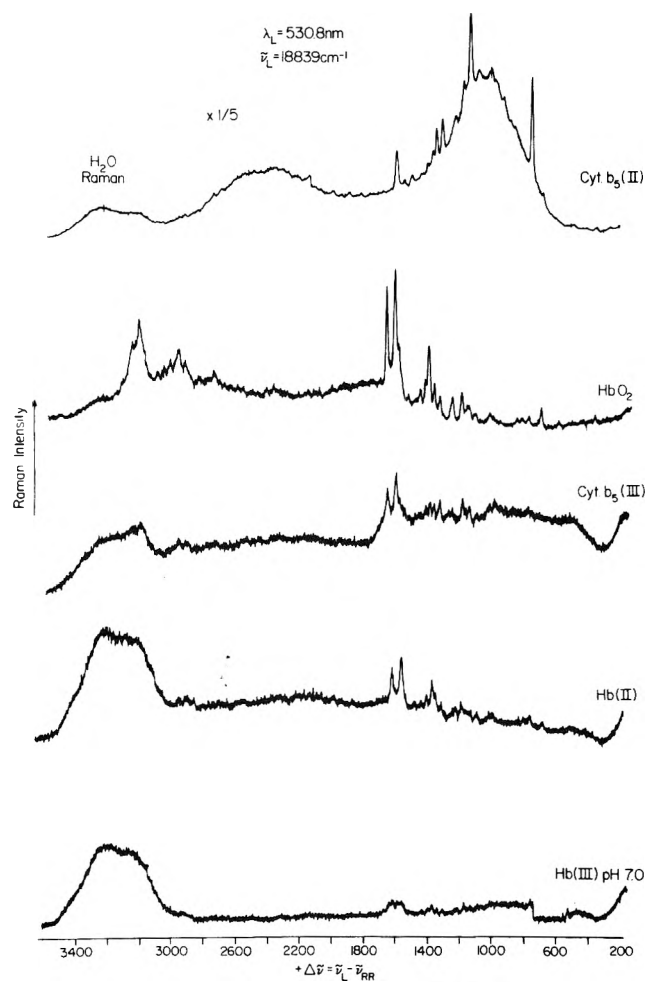


Figure 1. Resonance Raman spectra in room temperature aqueous solution of (a) ferrocyanochrome b_5 [shows fluorescence]; (b) oxyhemoglobin; (c) ferricytochrome b_5 ; (d) deoxyhemoglobin; (e) methemoglobin. $\lambda_{ex} = 530.8$ nm.

resolution was lost with such slit widths.) The line width of the laser is determined by the Doppler profile and measures a little less than 1 cm^{-1} .

Samples were contained in 1-mm i.d. melting point capillaries. A polarization scrambler was introduced to eliminate the possibility of intensity artifact due to the dichroism of the gratings. Samples were prepared at concentrations such that all had equivalent optical density at 530.8 nm ($OD = 0.45 \pm 0.03$ in a 2-mm cuvette). The following hemoproteins were studied: ferrocyanochrome b_5 , oxyhemoglobin, ferricytochrome b_5 , deoxyhemoglobin, and methemoglobin. Deoxyhemoglobin was prepared with a minimum of dithionite and sealed in the melting point capillary.

The fluorescence quantum yield of ferrocyanochrome b_5 was measured relative to the fluorescence of zinc and palladium mesoporphyrin dimethyl ester in samples prepared with the same optical density at 530.8 nm. Neutral density filters were introduced in the exciting beam to reduce the intensity of emission from the Zn and Pd samples; the laser power incident on the sample was then measured with a power meter. The relative quantum yields were measured by weighing the spectra and calculating the appropriate ratios.

The hemoproteins' absorption spectra at 77 K were measured on a split beam spectrophotometer specially adapted for work on diffuse scatterers. All spectra were recorded at the same slit conditions so that the differences in line widths would be intrinsic to the samples.

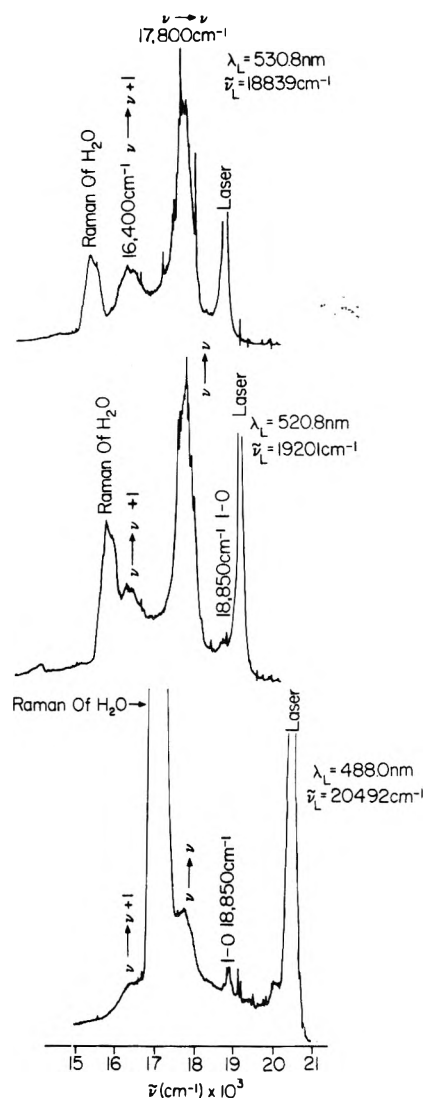


Figure 2. Resonance Raman and fluorescence of ferrocyanochrome b_5 excited at (a) 530.8 nm; (b) 520.8 nm; (c) 488.0 nm. [Spectra are in absolute wave numbers to emphasize the fluorescence.]

Results

Hemoprotein emission and Raman spectra excited by the 530.8-nm laser line are shown in Figure 1a–e, with the Raman spectrum of water included for comparison. The sharp peaks evident in the traces of ferrocyanochrome b_5 [cyt b_5 (II)], ferricytochrome b_5 [cyt b_5 (III)], and oxy- and deoxyhemoglobin [HbO₂ and Hb(II)] are Raman lines corresponding to in-plane porphyrin vibrations.¹ The Raman spectrum of methemoglobin [Hb(III)] is almost nondetectable under these conditions. In addition to the sharp Raman peaks, the spectrum of cyt b_5 (II) exhibits two pronounced broad background bands: a main peak centered at 562 nm and a weaker emission at 611 nm. These correspond in wavelength to the expected appearance of Q(0,0) and Q(0,1) fluorescence.

Figure 2a–c shows emission spectra of cyt b_5 (II) excited at 530.8, 520.8, and 488.0 nm. In order to emphasize the fluorescence emission, they are illustrated on an absolute wave number scale. When excited with the 530.8-nm laser line an emission appears at about 18850 cm^{-1} (530 nm) with about 3% of the intensity of the main 561-nm emission. When excited by the 488.0-nm laser line the intensity of this 530-nm emission relative to that at 561 nm rises to about 30%. Table

TABLE II: Peak Absorption and Emission Lines of Ferrocytochrome b_5

	Assignment	λ , nm	$\bar{\nu}(\text{cm}^{-1}) = \lambda^{-1}$
Absorption	Q(1,0)	530	18 800
	Q(0,0)	561	17 800
Fluorescence	Q(1,0)	530	18 850
	Q(v,v) ^a	561	17 800
	Q($v,v+1$) ^a	610	16 400

^a The broadness of these bands, whose wavelength corresponds with the relaxed fluorescence bands Q(0,0), Q(0,1), suggests that they come from various unrelaxed vibrational levels v . See text.

II lists the wavelengths and wave numbers of these emission bands with the 530-nm band identified as the nontotally relaxed fluorescence Q(1,0) from the upper vibrational levels of the electron excited state. The 561- and 610-nm bands are identified as Q(v,v) and Q($v,v+1$) rather than Q(0,0) and Q(0,1) for reasons to be given in the next section.

In order to determine the relative fluorescence yield of cyt b_5 (II) with respect to known metalloporphyrins, its fluorescence intensity was measured under similar conditions together with zinc and palladium mesoporphyrin (Meso). The resulting fluorescence yields are listed in Table III. The samples were partly degassed, so the emission of the Pd complex probably includes some delayed fluorescence as suggested by comparison with earlier measurements.^{18a}

In order to compare the absorption line widths of the five hemoproteins, absorption spectra were recorded under identical conditions at 77 K in Figure 3. With the exception of cyt b_5 (II), none of the spectra indicate any resolution within the vibronic peaks. The resolution shown for cyt b_5 (II) should be intrinsic to the species rather than the instrument, since the resolution was similar when studied on a higher resolution instrument with better signal-to-noise ratio.²⁶

Table III summarizes the results of the experiments. We list the compounds studied, the spin, the narrowest line width observed in absorption, and estimates of the relative strength of RR and of total fluorescence.

Discussion

A. Empirical Characterization. There are four distinct types of fluorescence/resonance Raman behavior shown by the hemoproteins of Figures 1–3 and Tables II and III.

Cyt b_5 (II). Experimentally we see clear indications of fluorescence. While earlier workers believed iron porphyrins would show no fluorescence, the rather sharp resolution of $\Delta\bar{\nu} \sim 60 \text{ cm}^{-1}$ observed by Estabrook et al.²⁵ at 77 K in ferrocytochrome c suggests (Table I) some minimal fluorescence yield. Using the data of Hagihara²⁵ on cytochrome b_5 we can estimate $\tau_i \sim 0.5 \text{ ps}$. More recently fluorescence background in the RR spectra of ferrous low spin cytochromes has been noted.^{3,8} Taking the fluorescence yield of ZnMeso as $\phi_f = 0.04$, the data of Table III suggest a fluorescence yield for cyt b_5 (II) of $\sim 4 \times 10^{-6}$. From Table I we see that this is roughly consistent with the observed $\Delta\bar{\nu}$ and a lifetime $\tau_e \sim 100 \text{ fs}$. Thus we see from eq 6 that $\tau_e \sim \tau_v/5$ so that the observed fluorescence should be largely unrelaxed. Consistent with this view is the appearance in emission of the Q(1,0) band. Also the great broadness of the background bands at 561 and 610 nm, where the relaxed fluorescence bands Q(0,0) and Q(0,1) are expected, suggests that the bands are a superposition of emissions from various unrelaxed vibrational states v of the Q electron state.

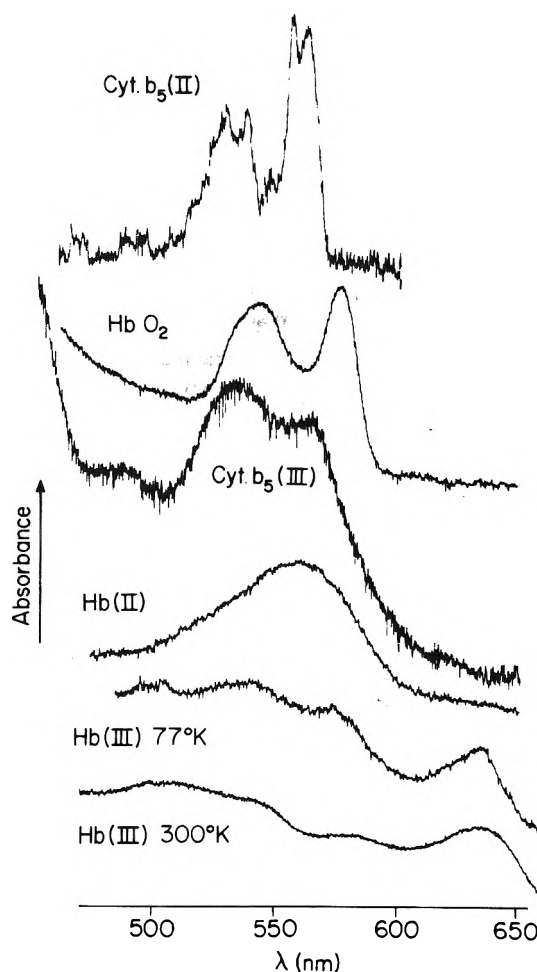


Figure 3. Absorption spectra at 77 K taken in water of hemoproteins: (a) ferrocytochrome b_5 ; (b) oxyhemoglobin; (c) ferricytochrome b_5 ; (d) deoxyhemoglobin; (e) methemoglobin.

Thus we have denoted these bands Q(v,v) and Q($v,v+1$).

HbO₂. While this compound resembles cyt b_5 (II) in having a singlet ground state and showing clear α and β bands [i.e., $^1Q(0,0)$ and $^1Q(1,0)$ in absorption], its spectroscopic behavior differs in two ways: (i) At low temperature there is no evidence of sharpening in the absorption spectra of Figure 3; (ii) the RR spectrum of Figure 1 shows no evidence for background emission. Using the absorption line width as a guide, we deduce from Tables I and III that $\tau_e \sim 15 \text{ fs}$, a number consistent with the lack of any background emission. In addition, this reduction of τ_i in HbO₂ compared to cyt b_5 (II) has the effect of reducing the amplitude of the resonant state, in turn reducing the intensity of RR. The reduction of τ_e is roughly comparable to the reduction of I_{rel} (RR) given in Table II.

Cyt b_5 (III) and Hb(II). These compounds (Figure 1 and Table III) show comparable RR spectra and both lack any emission. While cyt b_5 (III) shows visible α and β bands, only one broad band is shown in Hb(II). The reduction in intensity of the RR spectra of these compounds is consistent with reduction of the resonant state lifetime, τ_i , through the reduction of τ_e .

Hb(III). The spin state of methemoglobin is known to be temperature dependent.²⁷ Figure 3 shows the spectrum at pH 7.0 at room temperature and 77 K. At room temperature the compound is mostly $S = 5/2$; at 77 K some hint of the $S = 1/2$ spectrum can be seen. In neither case is there pronounced sharpening of the absorption spectrum. At room temperature,

TABLE III: Spin, Absorption Line Width, Resonance Raman Intensity, and Fluorescence Intensity

Compound	Solvent	Spin	$\Delta\bar{\nu}(77\text{ K})$	$I_{\text{rel}}(\text{RR})^a$	$I_{\text{rel}}(\text{F})^c$
Zn meso	Benzene	0	$(4\text{ cm}^{-1})^b$		10^4
Pd meso	Benzene	0	$(4\text{ cm}^{-1})^b$		2.5×10^2
(PtP) ^b	(n-Octane) ^b	0	$(12\text{--}15\text{ cm}^{-1})^b$		
Cyt b ₅ (II)	Water	0	60 cm^{-1}	25	1
HbO ₂	Water	0	350 cm^{-1}	5	
Cyt b ₅ (III)	Water	1/2	500 cm^{-1}	2	
Hb(II)	Water	2	2000 cm^{-1}	2	
Hb(III)	Water	5/2	$>2000\text{ cm}^{-1d}$	≤1	

^a Estimated from RR peak above background. ^b For ZnP, PdP, and PtP in low temperature Shpol'skii matrices.^{18b} ^c Since the sample was partly deoxygenated, this figure includes some delayed fluorescence. See ref 18a. ^d Hb(III) is so diffuse, this number is hard to define.

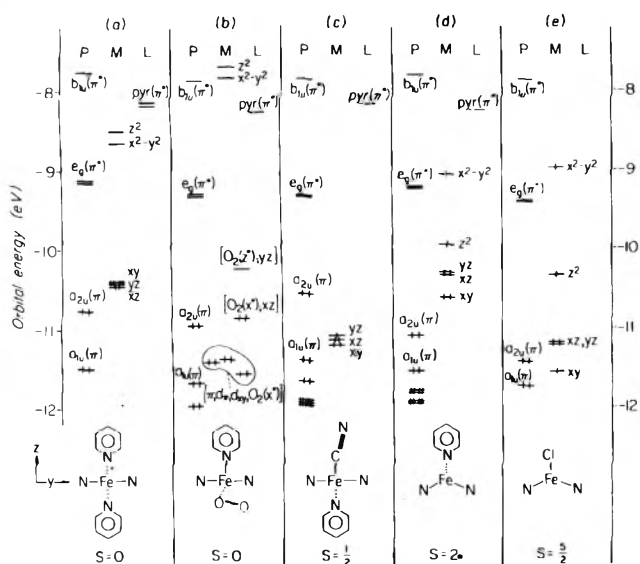


Figure 4. MO energy levels by IEH method for model compounds resembling: (a) ferrocyclochrome b₅; (b) oxyhemoglobin; (c) ferricytochrome b₅; (d) deoxyhemoglobin; (e) methemoglobin. P, M, and L refer to orbitals primarily porphin, metal (d), and ligand in character. Diagrams show structure around iron in yz plane. See text.

where the RR spectrum of Figure 1 was studied, the absorption is particularly diffuse. This is consistent with the shortest τ_e of the compounds studied and the weakest RR spectrum.

B. Explanation of τ_e by IEH Calculations. The emission data just discussed suggest considerable variation of τ_e for the hemoprotein visible transitions. In order to account for this we look to iterative extended Hückel (IEH) calculations, which provide estimates for the molecular orbital (MO) energies and hence allow cataloging of the low-energy excited states. The method has been used for metalloporphyrins^{28a} and hemes in particular.^{28b} Calculations on systems not previously reported were done using an updated symmetry adapted program.²⁹

Figure 4 shows IEH-MO energies for a series of model compounds whose HOMO (highest occupied) and LEMO (lowest empty) energy pattern is expected to resemble that of the hemoproteins studied. Three columns for each compound contain orbitals primarily porphin, metal and ligand, respectively; mixed orbitals lie between columns. The ligand structure around the iron atom is indicated below the energy level diagram. Diagram e was previously published^{28b} and diagram a is taken from work in progress on Fe, Ru, and Os complexes.^{30a} Calculations b, c, and e are from a larger IEH study of heme complexes with oxygen^{30b} and various diatomic

ligands.^{30c} In cases d and e, the iron was out of plane by 0.75 and 0.455 Å, respectively. In case c the CN axis was tilted by 15° from the porphyrin symmetry axis. The use of pyridine for imidazole only weakly affects the HOMO and LEMO energy levels.^{30b} Also they are only weakly affected by rotation of the pyridine plane from parallel to the N-N porphyrin axis to parallel to the methine axis, by small changes in bond lengths, and by slight tilting of a closed shell ligand like CN⁻ or CO.^{30c} We now discuss each calculation with respect to the insight it gives on τ_e .

(a) Cytochrome b₅(II) is represented by porphinatobispyridineiron(II). While the diagram appears to suggest that (d, π^*) charge transfer transitions are at lower energy than the porphyrin (π, π^*) transition, arguments given elsewhere³¹ show that IEH calculations systematically underestimate charge transfer transition energies. Hence, for this hemoprotein the only possible excited singlet with lower energy than ¹Q(π, π^*) is a ¹(d,d). In fact two ¹(d,d) transitions were identified by Eaton and Charney in ferrocyclochrome c at 816 and either 730 or 631 nm.³² Presumably then the radiationless decay ¹Q(π, π^*) \rightarrow ¹(d,d) is responsible for $\tau_e \sim 100$ fs in cytochrome b₅(II). Recently Watts et al.³³ have shown that for d⁶ transition metal complexes there are some selection rules for radiationless decay. In particular, there is some slowness to decay involving change in orbital parentage. Thus radiationless decay ¹Q(π, π^*) \rightarrow ¹(d,d) might be a bit slower than ¹B(π, π^*) \rightarrow ¹Q(π, π^*) or some of the radiationless decays to be discussed in the other hemoproteins below. The existence of a ¹(d,d) at lower energy than ¹Q(π, π^*) may explain why τ_e is much shorter in cytochrome b₅(II) than in PdP (Table III), and the selection rule on radiationless decay may account for why τ_e is as "slow" as 100 fs.

(b) HbO₂ is represented by porphinatodioxyporphyrineiron(II). In calculations on this species a number of geometries for O₂ were tried.^{30b} The most stable structure of HOMO/LEMO energies, i.e., the one which has the largest gap between filled and empty orbitals, is the "Griffith structure"; i.e., the O₂ is symmetrically situated with the O₂ axis parallel to the porphyrin plane. Results of an IEH calculation with this structure for porphinatodioxyporphyrineiron(II) were reported sometime ago,^{28b} with pyridine in place of water the Griffith structure seems even more stable.^{30b} On the other hand, with iron attached to oxygen in a "Pauling structure" (currently favored for oxyhemoglobin) and the Fe-O-O angle bent 100° or more, the two O₂ π^* orbitals are so nearly degenerate that the molecule would be expected to have S = 1.^{30b} Figure 4b shows the energy levels for an asymmetric geometry between "Griffith" and "Pauling" structures: The O₂ axis is tilted 5° from the porphyrin plane and the nearer O atom is 0.37 Å from the porphyrin symmetry axis. This asymmetric structure is

among a group of related structures, between "Griffith" and "Pauling", that IEH calculations show to be stable and diamagnetic.^{30b}

Whatever the actual geometry of oxyhemoglobin, Figure 4b makes clear the electron bookkeeping that necessarily holds for any diamagnetic HbO₂ complex. There is a structure of filled orbitals rather like in Figure 4a. Thus the α, β absorption band structure in Figure 3b is not surprising. In addition, one O₂(π^*) orbital is filled and one is empty. Thus in addition to porphyrin (π, π^*) transitions, oxyhemoglobin should have low-energy transitions from the filled O₂(π_x^*) to the empty O₂(π_z^*) and possibly a charge transfer transition from $a_{2u}(\pi)$ to the empty O₂(π^*). In fact weak near-ir absorption is apparent in HbO₂ which has been assigned as a transition $a_{1u}(\pi), a_{2u}(\pi) \rightarrow O_2(\pi_z^*)$, on the basis of crystal polarized absorption.^{34a} Thus it is fairly clear that there are several other singlets at lower energy than ${}^1Q(\pi, \pi^*)$ in HbO₂. Hence a τ_e substantially shorter than for cyt $b_5(II)$ is expected.

(c) Cyt $b_5(III)$ is represented by cyanoporphinatopyridineiron(III). In this case the ground state is a doublet, and the visible spectrum is due to an excited ${}^2Q(\pi, \pi^*)$ state. Below this are other doublets, in particular a ${}^2(\pi, d_\pi)$ charge transfer state identified in the near-ir at 8000 cm⁻¹.^{34b} There is also the possibility of low-energy ${}^2(d, d)$ states resulting from reshuffling the hole among d_{xy}, d_{xz}, d_{yz} . Also there are low-energy "tripdoublets" arising from the coupling of the metal $S = 1/2$ with the $S = 1$ of the T(π, π^*) states.³⁵ Work on copper(II) porphyrins with d^9 metal configuration shows fairly strong exchange coupling between ${}^2Q(\pi, \pi^*)$ and similar tripdoublet states ${}^2T(\pi, \pi^*)$.³⁵ Thus there are several excited doublets at lower energy than ${}^2Q(\pi, \pi^*)$, and a τ_e lower than for HbO₂ is not surprising.

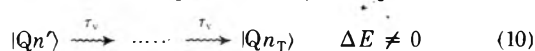
(d) Hb(II) is represented by porphinatopyridineiron(II), with the iron out-of-plane. In this case the ground state is a quintet and the visible spectrum is due to an excited ${}^5Q(\pi, \pi^*)$. Below this state are low-energy ${}^5(d, d)$ levels as well as "tripquintets" arising from the coupling of the metal $S = 2$ with the $S = 1$ of the T(π, π^*) states. It is not clear whether ${}^5(\pi, d)$ charge transfer transitions also occur at lower energies than ${}^5Q(\pi, \pi^*)$. In any event there are several excited quintet states below ${}^5Q(\pi, \pi^*)$ of a type that could explain the similarity of τ_e deduced for Hb(II) with that of cyt $b_5(III)$.

(e) Hb(III) is represented by chloroporphinatoiron(III), whose energy levels were presented earlier as an example of high-spin ferriheme.^{28b} In this case the ground state is a sextet, and there are "tripsextets" at lower energy than the states responsible for the visible absorption, in this respect e resembles d and c. However the data (Table I) suggest τ_e is even shorter in e. The four-banded visible spectrum of Hb(III) is strikingly different from that of the other hemoproteins, and it is believed that there are allowed ring-to-metal charge transfer transitions in the visible absorption region.^{36,37} The presence of more than one allowed electronic state in the visible region suggests very strong vibronic coupling among the vibrational levels of the different electronic states. This could explain the fact that this complex has the shortest τ_e among the hemoproteins.

The IEH diagrams of Figure 4 provide fairly good qualitative reasons for the observed radiationless decay rates of the hemoproteins as expressed in the various τ_e of Table I. Our experience with the IEH model suggests that fairly similar patterns would be obtained if more realistic geometries around the iron were used. The most sensitive level of Figure 4 is the empty O₂(π_z^*) level of Figure 4b. Recent spectroscopic^{34a} and theoretical^{30b} studies suggest that the location of O₂(π_z^*) in

Figure 4b is roughly correct, even if the exact structure is not.

C. Emission Types and Photon Coherence Time, τ_p . We have spoken of three types of spectra involving photons leaving the system: resonance Raman (RR), resonance fluorescence (RF), and relaxed fluorescence (f). We here wish to discuss these in more detail. To do so we introduce the notation $|Jn\rangle$ to describe the molecular state, where J refers to the electronic state and n is a set of $3N - 6$ integers which specify the vibrational quantum numbers for each normal mode of the N atom system. The $|Jn\rangle$ are not necessarily steady states due to vibronic coupling and anharmonicities. The ground state $|0n_T\rangle$ consists of a set of n_T determined by Boltzmann factors. The radiation field couples states $\langle Qn' | r | 0n_T \rangle$, where $(n' - n_T)$ in general will be 0 or will contain one or two modes that are active in absorption. This matrix element determines interaction with the radiation field and hence is responsible for the various photons leaving the system as RR, RF, or f. In addition to these matrix elements, the system has an internal dynamics that we have expressed as τ_v and τ_e :



The dots for eq 10 represent several relaxation steps leading to thermal relaxation. All the emission spectra at room temperature have $\tau_v \ll \tau_p$, where τ_p is the photon coherence time. The parameter that varies is τ_e . The following spectral types are observed:

(A) $\tau_v \ll \tau_p \ll \tau_e$: ZnMeso and PdMeso: Emission occurs from excited states $|Qn_T\rangle$ and is relaxed fluorescence. This process is so strong as to swamp any resonance Raman.

(B) $\tau_e \ll \tau_p \sim \tau_e$: PtP or PtEtio: this case should be particularly interesting as an intermediate between (A) and (C). We plan to undertake study of its fluorescence and RR in the near future.

(C) $\tau_e < \tau_v \ll \tau_p$: cyt $b_5(II)$: In this case a strong resonance Raman is observed with a line width determined by τ_v . An extremely broad fluorescence is also observed. Presumably this is occurring from states $|Qn''\rangle \neq |Qn_T\rangle$ containing a nonthermal set of n'' . There will be a far bigger spread in energies of allowed transitions from $|Qn''\rangle$ than from $|Qn_T\rangle$, thus accounting for the broad emission $Q(\nu, \nu)$ (Figure 2). This type of broadening is also observed in fluorescence from metallophthalocyanine vapors at low pressures, where thermal relaxation is not possible.³⁸ The observation of $Q(1,0)$ in emission suggests states $|Qn'\rangle$ containing nonthermal population of the optically allowed modes are populated during the time period before τ_e sweeps away the electronic state Q.

(D) $\tau_e \ll \tau_v \ll \tau_p$: This case applies to the other hemoproteins studied. With decreasing τ_e we first see the loss of any fluorescence; decreasing τ_e also decreases the RR intensity. Presumably this arises because the RR matrix element contains τ_i^{-1} in the denominator,⁸⁻¹⁰ i.e., the RR transition $|00\rangle \rightarrow |0n_T\rangle$ depends on:

$$\sum_i \frac{\langle 00 | r | Qn \rangle \langle Qn | r | 0n_T \rangle}{(E_{Qn} - E_{00} - h\nu_{exc} - i\hbar\tau_{Qn}^{-1})}$$

Clearly as τ_{Qn} (i.e., τ_i for $|Qn\rangle$) decreases, the RR scattering will become smaller. Moreover, as τ_{Qn} decreases, the dependence of RR on ν_{exc} will also decrease, as the resonance with the individual vibronic levels $|Qn\rangle$ becomes poorer. The variation of the RR spectrum of cytochrome c with ν_{exc} has been elegantly analyzed³⁹ and utilized in separating the RR

spectra of the b and c type cytochromes in the mitochondrial preparation known as succinate cytochrome c reductase.³ In contrast to this is the case of HbO₂, where τ_e^{-1} is so large that the dependence of RR on ν_{exc} is expected to be small.

Finally we would like to relate the cases reported here to the two cases distinguished in the earlier paper which reported fluorescence from ferrocytochrome c:⁸ (a) $\tau_p \ll \tau_i$ should give resonance fluorescence (RF) while (b) $\tau_i \ll \tau_p$ should give resonance Raman (RR). Because of the intervention of $\tau_v \ll \tau_p$ our own case (A) shows relaxed fluorescence (f) rather than RF. Cases (D) may indeed correspond to (b), showing RR only. In between, case (C) shows emission that appears unrelaxed. It is not altogether clear if this emission is the same as RF envisaged in ref 8 since τ_p of the emitted photon is unknown.

The results reported in this paper suggest experiments to better explore cases (a) and (b). From our analysis it would seem that a porphyrin complexed to a metal such as Pd or Pt can be found so that at low temperature $\tau_e \sim \tau_v \sim 3$ ps. With pulsed lasers τ_p can be shortened to below 1 ps. Thus the case $\tau_p < \tau_i$ can be realized in a situation where relaxed fluorescence f does not swamp RR and RF processes. The RF process envisaged in ref 8 as case (a) can then be explored as a function of $h\nu_{exc}$. Alternatively the same system can be studied with an ion laser fitted with an intracavity etalon. This produces laser emissions with line widths ~ 10 MHz and $\tau_p \sim 100$ ns. Thus case (b) can be realized and studied as a function of $h\nu_{exc}$. The empirical realization of these two cases would greatly help to clarify the relation of τ_p and τ_i in radiationless decay processes.

Summary

The metalloporphyrins and the hemoproteins form a series with variable electronic radiationless decay times, τ_e . For metalloporphyrins with zinc and palladium, $\tau_e > 12$ ps and relaxed fluorescence is observed. For ferrocytochrome b₅, $\tau_e \sim 100$ fs; unrelaxed fluorescence and strong resonance Raman is observed. The relatively long τ_e is also manifested experimentally in relatively sharp absorption line widths $\Delta\bar{\nu} \sim 60$ cm⁻¹. The other hemoproteins fall in a series with successively shorter τ_e ; no fluorescence is seen, the resonance Raman spectrum gets progressively less intense, and the absorption spectrum shows decreasing resolution. The τ_e can be rationalized by IEH calculations: For ferrocytochrome b₅, between the ¹Q(π, π^*) excited state responsible for the visible absorption bands and the ground state there is only ¹(d,d), and ¹Q(π, π^*) \rightsquigarrow ¹(d,d) takes 100 fs. In the other cases various other excited states of the same multiplicity as the Q(π, π^*) visible excited state intervene between it and the ground state, enhancing τ_e . Methemoglobin has the shortest $\tau_e \sim 3$ fs as manifested in lack of fluorescence, a very weak resonance Raman, and a very diffuse absorption spectrum. Its very short τ_e is explained by the presence of charge transfer excited states ⁶(π, d_π) together with ⁶Q(π, π^*) in the visible region.

Acknowledgments. The work at the University of Pennsylvania was supported by Public Health Services Grants No. HL 14508 and 05060, and National Science Foundation Grant No. BMS 75-07355. The work at the University of Washington was supported by Public Health Service Grant No. AM 16508. F.A. wishes to express appreciation to Professor Takashi Yonetani for encouraging studies on the Raman effect of purified hemoproteins and for use of his low temperature spectrophotometer.

References and Notes

- (1) T. G. Spiro and T. C. Streckas, *Proc. Natl. Acad. Sci. U.S.A.*, **69**, 2622 (1972).
- (2) T. Yamamoto, G. Palmer, D. Gill, I. T. Salmeen, and L. Rimai, *J. Biol. Chem.*, **248**, 5211 (1973).
- (3) F. Adar and M. Erecinska, *Arch. Biochem. Biophys.*, **165**, 570 (1974).
- (4) A. L. Verma, R. Mendelsohn, and H. J. Bernstein, *J. Chem. Phys.*, **61**, 383 (1974).
- (5) R. Mendelsohn, S. Sunder, A. L. Verma, and H. J. Bernstein, *J. Chem. Phys.*, **62**, 37 (1975).
- (6) L. D. Spaulding, C. C. Chang, N.-T. Yu, and R. H. Felton, *J. Am. Chem. Soc.*, **97**, 2517 (1975).
- (7) W. H. Woodruff, D. H. Adams, T. G. Spiro, and T. Yonetani, *J. Am. Chem. Soc.*, **97**, 1695 (1975).
- (8) J. M. Friedman and R. M. Hochstrasser, *Chem. Phys.*, **6**, 155 (1974).
- (9) J. O. Berg, A. Langoff, and G. W. Robinson, *Chem. Phys. Lett.*, **29**, 305 (1974).
- (10) S. Mukamel and J. Jortner, *J. Chem. Phys.*, **62**, 3609 (1975).
- (11) R. Becker and J. Allison, *J. Phys. Chem.*, **67**, 2662, 2669 (1963).
- (12) (a) M. Gouterman, *J. Mol. Spectrosc.*, **6**, 138 (1961); (b) M. Gouterman, "Excited States of Matter", Vol. 2, C. W. Shoppee, Ed., Graduate Studies of Texas Tech University, 1973, pp 63-100; (c) M. Gouterman, review in preparation.
- (13) A. T. Gradyushko and M. P. Tsvirko, *Opt. Spectrosc.*, **31**, 548 (1971). [*Opt. Spectrosc. (USSR)*, **31**, 291 (1971).]
- (14) P. G. Seybold and M. Gouterman, *J. Mol. Spectrosc.*, **31**, 1 (1969).
- (15) M. Gouterman, F. P. Schwartz, P. D. Smith, and D. Dolphin, *J. Chem. Phys.*, **59**, 676 (1973).
- (16) M. Gouterman, L. K. Hanson, G. E. Khalil, J. W. Buchler, K. Rohbock, and D. Dolphin, *J. Am. Chem. Soc.*, **97**, 3142 (1975).
- (17) D. Eastwood and M. Gouterman, *J. Mol. Spectrosc.*, **30**, 437 (1969); **35**, 359 (1970).
- (18) (a) J. B. Callis, J. M. Knowles, and M. Gouterman, *J. Phys. Chem.*, **77**, 154 (1973); (b) J. B. Callis, M. Gouterman, Y. M. Jones, and B. H. Henderson, *J. Mol. Spectrosc.*, **39**, 410 (1971); (c) M. Gouterman and Y. M. Jones-Aronowitz, *ibid.*, submitted for publication.
- (19) L. K. Hanson, M. Gouterman, and J. C. Hanson, *J. Am. Chem. Soc.*, **95**, 4822 (1973).
- (20) J. I. Steinfeld, "Molecules and Radiation", Harper and Row, New York, N.Y., 1974, pp 217-225.
- (21) J. Jortner and S. Mukamel, "Preparation and Decay of Excited States", in Proceedings of the First International Conference on Quantum Chemistry, R. Dandel and B. Pullman, Ed., Reidef, Amsterdam, 1974, pp 145-209.
- (22) G. W. Robinson, "Molecular Electronic Radiationless Transitions in Excited States", Vol. 1, E. C. Lim, Ed., Academic Press, New York, N.Y., 1975, pp 1-34.
- (23) G. W. Canters, M. Noort, and J. H. van der Waals, *Chem. Phys. Lett.*, **30**, 1 (1975).
- (24) (a) K. E. Rieckhoff, E. R. Menzel, and E. M. Voigt, *Phys. Rev. Lett.*, **28**, 261 (1972); (b) E. R. Menzel, K. E. Rieckhoff, and E. M. Voigt, *Chem. Phys. Lett.*, **13**, 604 (1972).
- (25) R. W. Estabrook in "Haematin Enzymes", Vol. 2, J. Falk, R. Lemberg, and R. K. Morton, Ed., Pergamon Press, Oxford, 1961, pp 436-460.
- (26) B. Hagihara and T. Iizuka, *J. Biochem.*, **69**, 355 (1971).
- (27) T. Iizuka and M. Kotani, *Biochem. Biophys. Acta*, **194**, 351 (1969).
- (28) (a) M. Zerner and M. Gouterman, *Theor. Chim. Acta (Berl.)*, **4**, 44 (1966); (b) M. Zerner, M. Gouterman, and H. Kobayashi, *ibid.*, **6**, 363 (1966).
- (29) A. M. Schaffer, M. Gouterman, and E. R. Davidson, *Theor. Chim. Acta (Berl.)*, **30**, 9 (1973).
- (30) (a) A. Antipas, J. W. Buchler, M. Gouterman, and P. D. Smith, work in progress; (b) S. Aronowitz, M. Gouterman, and J. C. W. Chien, *Theor. Chim. Acta (Berl.)*, submitted for publication; (c) S. Aronowitz and M. Gouterman, unpublished.
- (31) M. Gouterman, L. K. Hanson, G. E. Khalil, W. R. Leenstra, and J. W. Buchler, *J. Chem. Phys.*, **62**, 2343 (1975).
- (32) W. A. Eaton and E. Charney, *J. Chem. Phys.*, **51**, 4502 (1969).
- (33) (a) R. J. Watts, M. J. Brown, B. G. Griffith, and J. S. Harington, *J. Am. Chem. Soc.*, in press; (b) R. J. Watts, T. P. White, and B. G. Griffith, submitted for publication.
- (34) (a) W. A. Eaton, J. Hofrichter, L. K. Hanson, and M. W. Makinen, Proceedings of the Taniguchi International Symposium in Biophysics, "Metalloprotein Studies Utilizing Paramagnetic Effects of the Metal Ions as Probes", Lake Biwa, Japan, Nov 1975, to be published; (b) J. C. Cheng, G. A. Osbourne, P. J. Stephens, and W. A. Eaton, *Nature (London)*, **241**, 193 (1973).
- (35) R. L. Ake and M. Gouterman, *Theor. Chim. Acta (Berl.)*, **15**, 20 (1969).
- (36) D. Day, D. W. Smith, and R. J. P. Williams, *Biochemistry*, **6**, 1563 (1967).
- (37) W. A. Eaton and R. M. Hochstrasser, *J. Chem. Phys.*, **49**, 985 (1968).
- (38) D. Eastwood, L. Edwards, M. Gouterman, and J. Steinfeld, *J. Mol. Spectrosc.*, **20**, 381 (1966).
- (39) J. M. Friedman and R. M. Hochstrasser, *Chem. Phys.*, **1**, 457 (1973).

Discussion

G. W. CANTERS. You mentioned that in some of your compounds the crystal field lost the degeneracy. Is this through the action of the ligands?

F. ADAR. Yes.

G. W. CANTERS. Did you calculate the magnitude of this splitting or was it found from the experiment?

F. ADAR. You know that the splitting is possible because the crystal field has lower symmetry than that of free space. You know that the 5d orbitals split into two levels with two- and threefold degeneracies. Then you can calculate which set is low in energy.

G. W. CANTERS. But you mentioned that the splitting would be

large. What do you mean by large?

F. ADAR. Large enough to observe a diamagnetic species.

E. R. BERNSTEIN. Do you have any other information besides line width on the lifetimes of the states you observe?

F. ADAR. We ran the absorption spectra at liquid nitrogen temperature from which we estimated the line widths. We found that the emission was consistent with quantum yields that the line widths would predict.

Exciton Percolation in Mixed Molecular Crystals and Aggregates: From Naphthalene to Photosynthesis

Raoul Kopelman

Department of Chemistry, The University of Michigan, Ann Arbor, Michigan 48109 (Received February 2, 1976)

Dynamic exciton percolation in a ternary solid is formulated in terms of the static percolation theory of a binary solid for the simple, but common, limit where it is independent of the excitation lifetime, jump time, coherence time, and trapping time. Experiments on the S_1 exciton in the naphthalene- d_8 /naphthalene- h_8 / β -methyl-naphthalene system are interpreted within this limit. This limit is also appropriate for the description of the exciton transfer in the photosystems of higher plants. It predicts correctly the range of chlorophyll a:chlorophyll b concentration ratios. The energy transport in the ternary naphthalene system appears to mimic the natural process. The general case, where the coherence time is an important factor, can also be utilized to experimentally determine coherence times and lengths as a function of temperature. Preliminary results on naphthalene are reported (for 2 K).

Introduction

The traditional approach to the *long-range* energy transport problem has been molded by the examples of the resonance energy transport (exciton motion) in ordered molecular solids (nearly perfect crystals, usually at low temperature). The traditional ideas are summarized as follows. Perfect resonance transfer can only occur among molecules that are not only chemically identical but also in physically indistinguishable sites. These conditions are guaranteed by the translational¹ and interchange² symmetry of the crystal, i.e., its perfect order. While energy can be transferred between two different molecules (or chromophores)^{3,4} in a nonresonance process, this usually leads to fast degradation of the energy, and generally this process is also irreversible in its direction. Thus, for a multistep process, the majority of the energy-transfer steps have to occur inside highly ordered domains, arranged like perfect crystals. Any significant portion of defects or impurities, i.e., disorder, will either trap or block the energy transport.

This traditional picture given above hampered the investigation of energy (exciton) transport in biological aggregates in two ways. First, it lowered the expectations concerning the occurrence of exciton transfer because of the low probability for "perfect" crystallinity in biomolecular aggregates. Second, even in the case where exciton energy transfer is fairly well established,^{4,5} it led to some confusion as well as to the belief

that the appropriate molecular aggregates have to be organized with a very high degree of order, leaving little room for "sloppiness" or damage and thus highly constraining one's models of reality.

A very similar situation existed a few years ago in solid-state physics concerning the electrical conduction of semiconductors. A crystal of germanium or silicon had to be extremely pure and perfect before it could serve as a "solid-state device". Also, a little radiation damage would affect it badly. Theoretically it was hard to believe in the mere existence of *amorphous* (glassy, disordered) semiconductor devices. The fact is that they do exist⁶ and that the new theoretical concepts advanced to explain these facts turned out to be useful in additional situations, such as dense gaseous metals and metal-ammonia solutions.^{7,8} The key concept is charge "percolation".⁶

Our studies of excitations in mixed molecular crystals⁹ have led us to the concept of *exciton percolation*.⁹⁻¹² This approach allows a significant amount of lattice disorder to exist in a molecular condensate without the elimination of long-range exciton transport. It also defines new kinds of constraints for the persistence of such energy transport. While it is still true that complete order is required for *strictly one-dimensional systems*, this is not so for other topologies, not even for a linear but "stranded" system. One can define a "phase transition" in a molecular condensate, where the change is from an "exciton conductor" to an "exciton insulator", this change oc-

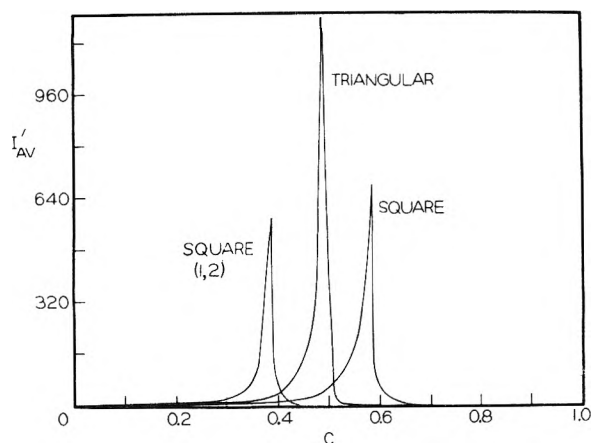


Figure 1. Reduced average cluster size I'_{av} (see eq 2) vs. the A component concentration C , for square, triangular, and square (1,2) lattices. The square (1,2) topology is a square lattice with both nearest and next nearest ("diagonal") interactions⁹ while the other two topologies include only nearest-neighbor interactions. The locations of the sharp maxima give the critical (percolation) concentrations for the A component while the peak height has no meaning (due to statistical fluctuations). Each computer lattice had 200×200 sites.

curing as a function of an order parameter (i.e., concentration).

We have been able to put together a simple three-component mixed molecular crystal system (substitutionally disordered) which is amenable to experimental investigations under the most controlled conditions. This system mimics the essential features of the primary process of photosynthesis. Moreover, the "mimicking" fails completely¹³ for the very values of the disorder parameter that do not appear in natural systems (aggregates with such parameters have presumably been eliminated in the evolutionary process). We also give here a theoretical synopsis of exciton percolation and a model of "percolation through a semirandom lattice" for the energy transport in the primary process of photosynthesis.

Synopsis of Theory

Exciton percolation—the migration of excitons in disordered materials—is based on the availability of a disordered exciton conducting quasi-lattice (A). Simultaneously there exists a (disordered) exciton insulating quasi-lattice (B). The condition of exciton percolation, i.e., efficient migration of the excitation, requires an effectively connected A quasi-lattice. The simplest case of exciton percolation is found in a binary mixed crystal with random substitutional disorder and where the B quasi-lattice is energetically inaccessible to the A excitons.

Dynamic percolation, i.e., the migration of excitons throughout a quasi-lattice, is described, formally, in terms of the static percolation of this quasi-lattice. The static percolation, in turn, is a well-defined mathematical concept. In the simple case of a binary, substitutionally random lattice the essence of the site percolation problem is the question: What is the probability for any site A to belong to the "infinite A cluster" (maxicluster)? This probability (\bar{P}) is zero when the fraction of A is zero and unity when the fraction of A is unity. However, the significant fact is that this probability (\bar{P}) is zero over a wide range of concentration. For instance, in a square lattice it is zero for concentrations⁹ up to 0.59. The critical concentration (C_c) is here 0.59 (0.50 for a triangular lattice, 0.31 for a simple cubic lattice etc.). Above C_c the probability \bar{P} rises sharply and approaches unity at concentrations quite lower than unity.

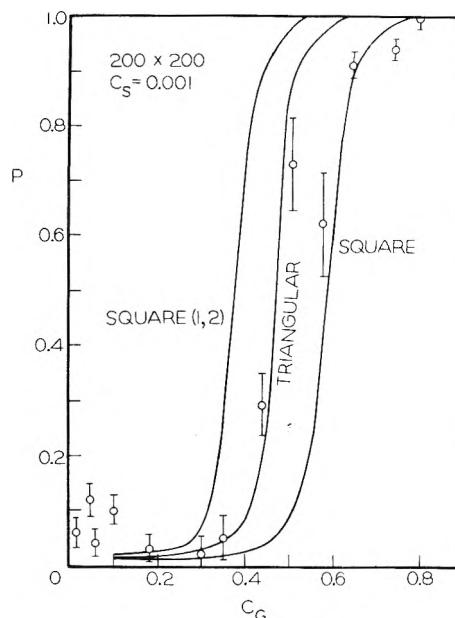


Figure 2. Experimental and theoretical dynamical exciton percolation: first singlet excitation of naphthalene. The experimental points are integrated fluorescence intensity ratios I_S/I_{total} where I_S is the sensor (β -methyl-naphthalene) emission intensity and $I_{total} = I_S + I_A$ the combined sensor and exciton conductor (naphthalene- h_8) emission intensity (see eq 5 and 6). Here $C_S \approx 10^{-3}$ (mole fraction) so that $C \approx C_A$. The low concentration data ($C < 0.1$) actually include contributions from a "dark current" (see text) and are therefore excluded from a comparison to theory. The theoretical curves give the dynamical percolation P according to eq 3 (using the more precise eq 14 for the C_c regions) for the three topologies described in the Figure 1 caption.

The above statements are strictly correct for an "infinite lattice". In order to preserve the concept of static percolation we defined C_c as the concentration at which the "average cluster size" diverges. The definition we use¹⁴ for the "average cluster size" is

$$I_{av} = G^{-1} \sum_m i_m m^2 \quad (1)$$

where m is the size of the cluster, i_m the frequency of finding an A cluster of size m (the number of times an m cluster appears), and G the total number of A sites. A more convenient definition^{14,15} is the "reduced average cluster size"

$$I'_{av} = G^{-1} \sum_{m \neq m'} i_m m^2 \quad (2)$$

By excluding the maxicluster (m') we achieve a λ -type function, similar to the heat capacity function near a " λ point" phase transition (see Figure 1). Obviously this function is a functional of topology.

The dynamic exciton percolation can be derived theoretically from the static percolation data. We have formulated the problem for a number of situations, depending on the method of exciton sensing. We discuss here the case where the sensors are randomly distributed throughout the lattice (i.e., impurity quenching, defect quenching, exciton fusion, photosynthetic active centers). In the limit of very efficient exciton transport and trapping, the probability of the exciton registering at the sensor is¹⁴

$$P = \bar{P} + (Z/G)I'_{av} \quad (1 \ll Z \ll G, C < C_c \text{ or } C > C_c) \quad (3)$$

where Z is the number of sensor sites. Note that both P and \bar{P} as well as I'_{av} are functions of the concentration C and that C_c is considered to designate the range of fluctuations, where

large miniclusters ($m \geq G/Z$) appear. This probability of exciton registration (P), which is now the *operational* definition of the *dynamic exciton percolation*, changes drastically at the percolation (critical) concentration C_c , as do \bar{P} and I'_{av} . All of these are functionals of topology (see Figures 1 and 2). The “midpoint” of the dynamic exciton percolation P can be defined as a “titration point” (see Figure 2).

For the case where the exciton transport is not “very efficient” eq 3 has to be modified,¹⁴ i.e.

$$P = \bar{P}[1 - (1 - n_m/G)^2] + (Z/G)I'_{av} \quad (4)$$

$$(C < C_c \text{ or } C_c > C)$$

Here n_m is the average number of distinct sites visited by an exciton, within its lifetime, if confined to the maxicluster, *in the absence of sensors*. Thus n_m is a function not only of concentration but also of the exciton lifetime τ , the pure crystal coherence time t_c (i.e., average exciton–phonon scattering time), and the exciton jump times. The exciton jump time T_j depends on the pairwise interaction (M_{ij}) between site i and site j and is therefore a tensorlike property, depending on the direction of the exciton jump in the lattice. We note that all three kinds of “times” involved have statistical distributions. This is particularly important in the case of the coherence time. We notice that while the computation of \bar{P} and I'_{av} involves only the topology of the lattice (i.e., the *topology* of the exciton interactions), n_m involves a number of specific parameters, characteristic of a specific kind of exciton. Experimentally, by choosing a high or low concentration of sensor (C_S), one determines whether eq 3 or eq 4 should be used, thus providing for a limiting case where the physical properties of the exciton are unimportant or for a case where they are. It appears that Nature (see below) prefers the limiting case of eq 3. However, for a study of coherence time we obviously prefer the case of low C_S (sensor concentration). We notice also that the case of eq 3 involves *no* computer simulation of exciton migration, only a computation of the cluster distribution. While the case of eq 4 does require a computer simulation of the exciton migration, this simulation is for a binary, not a ternary, lattice.

The Naphthalene Singlet Exciton

We have operationally defined (above) the dynamic exciton percolation as the probability (P) of the exciton registering on a sensor (eq 3, 4). We now describe a method of monitoring it experimentally. If excitons are introduced into the A quasi-lattice, they migrate until one of two events takes place: (a) they decay (radiatively or nonradiatively) inside the quasi-lattice; (b) they are registered by the sensor (trap), i.e., decay in it. We assume that no direct excitation of the sensors occurs and that no exciton can return from the sensor (“supertrap”) back to the A quasi-lattice. Furthermore, we assume that the internal radiationless decay is relatively inefficient and that it is about the same for an isolated A species and for the isolated sensor (S). We also assume that the radiative decay is about even for A and S. Finally, we assume that the trapping efficiency (γ) is about the same. Thus we expect, in an excitation experiment, to have the relation

$$P \approx I_S/I_{total} \quad (5)$$

where I_S is the sensor emission intensity, and I_{total} the total emission intensity (assuming no emission from the B species)

$$I_{total} = I_S + I_A \quad (6)$$

TABLE I: Schematic Comparison of Exciton Parameters in Plant Photosystems and Mixed Crystal Analogue

	Chlorophyll a	Naphthalene
M , cm ⁻¹	~300	~20
T_j , ps	~0.03	~0.5
τ , ns	~5	~75
τ/T_j	~2 × 10 ⁵	~2 × 10 ⁵
γ (S)	~1	~1
S phonons	Amalgamated	Amalgamated
$E_B - E_A$	> kT , $T = 300$ K	> kT , $T = 2$ K
$E_A - E_S$	> kT , $T = 300$ K	> kT , $T = 2$ K

Experimentally, we used the ternary system perdeuterionaphthalene (B)–naphthalene (A)– β -methyl-naphthalene (S). The experimental details have been given.^{12,14} The results compare very well with the theoretically derived percolation probability P (see Figure 2), provided that the exciton interaction topology is roughly between triangular and square. While the nearest neighbor interactions^{9,15} create a square-lattice topology, the next nearest neighbors (in the ab plane, at least) give a triangular-like topology.^{14,15} We notice that our actual experimental setup introduced some complications, such as direct excitation into the sensor (bypassing the A lattice). At low A concentration ($C < 0.1$), that would create¹⁴ an effective “dark current” (i.e., emission from the sensor). Thus we ignore the very low C region points (Figure 2). Also, the *intrinsic* intensity and trapping efficiency ratios (A:S) appear to be small and opposing and thus roughly cancel.¹²

We have seen therefore both an experimental and a theoretical verification of the concept of exciton percolation, or at least its existence above the critical concentration (C_c). Next, we look at some of its uses and applications.

The exciton percolation experiments give us a way of determining the degree of the exciton motional coherence *in the pure crystal*. This is the first method we are aware of for measuring the coherence properties of any singlet excitons (we discuss triplet excitons elsewhere).^{11,14} Our method is to compare experiments at low C_S with theoretical predictions based on eq 4, with the coherence time as a parameter. Agreement is achieved^{14,16} for a value of about 10 ps, at 1.8 K. This agrees well with the highest available *lower limit* of about 5 ps, based on spectral line width measurements.^{16,17}

An important general conclusion, based on our computations,¹⁶ is the unexpected effect of exciton coherence on exciton transport in disordered aggregates. For perfect lattices it is well-known that the longer the coherence time, the more efficient the energy transport. It turns out that quite the opposite is true for exciton percolation over a wide concentration domain above the percolation point.¹⁶ Thus for an increase in temperature, which increases exciton phonon coupling, the concomitant decrease in coherence time t_c actually improves the exciton transport! This may have interesting biological implications (see below).

Simulation of Photosynthesis?

There is an amazing similarity between our “synthetic” experimental ternary system discussed above and the photosynthetic systems of the higher plants. This similarity is shown, in part, in Table I. We list for both chlorophyll a⁵ and naphthalene^{9,12} a number of important parameters: the nearest-neighbor exciton pairwise interaction (M); the exciton jump time, $T_j = (4cM)^{-1}$, where c is the speed of light; the exciton lifetime τ ; the important ratio τ/T_j , equivalent to the average number of exciton steps; the exciton trapping effi-

ciency γ (at the sensor S, i.e., P700 or β -methylnaphthalene); the nature of the sensor-based phonons;^{13,14} and the energy denominators between the exciton "conductor" A and the exciton "insulator" B (chlorophyll b or C₁₀D₈), as well as between the exciton conductor A and the exciton sensor S.

In the primary process of photosynthesis, the transfer of excitation from the "antenna" pigment to the reactive centers is of major importance, especially in the green plants. In our *quasi-random* model, most of the light-absorbing pigments are distributed in a substitutionally nearly random fashion. The light absorbed by the higher energy pigments (B) quickly cascades down to the nearby lowest energy pigment (A), and then this A excitation migrates in the A *quasi-lattice*, until it reaches a reactive center (S). The same migration occurs for light absorbed directly by A.

The topology of the chromophore aggregates in the photosystems is not known but is probably made of a few layers, with a trigonal, square, or triangular topology of nearest-neighbor interactions.⁵ This puts the critical concentration (roughly, compare Figures 1 and 2 and Figures 6 and 7 of ref 14) at

$$0.35 < P_c < 0.6 \quad (7)$$

or the *ratio* of exciton "insulator" (B) to "conductor" (A) chromophore concentrations is

$$[B]/[A] < 1 \pm 0.5 \quad (8)$$

This prediction of the *quasi-random model* is certainly amenable to experimental test. We note that the traditional *funnel model* (i.e., adjacent layers of B and A), involves no such restrictions on the ratio $[B]/[A]$. We also notice that the present experimental information^{5,18} gives the region of ratios

$$0.1 \leq [B]/[A] \leq 1.0 \quad (9)$$

Actually there may exist much lower ratios than 0.1, but there is a difficulty in measuring such low ratios.¹⁸

We note that the above considerations apply mainly to the "higher" (green) plants, containing large numbers of chromophores, with a nonzero B/A ratio as discussed, for instance, in ref 18, i.e., where both chl-a and chl-b are represented. However, in a way our considerations could apply even to cases where only one chromophore (i.e., chl-a) is present, but with different enough energies,^{19,20} due to different environments of the chromophore sites (i.e., state of aggregation, see below). On the other hand, once there is a large enough number of such species (i.e., chl-a), differing in excitation energy by less than kT , then such species should all be treated practically as one (see Table I). We have treated this problem in much more detail elsewhere.^{13,14} It suffices to stress here that in order for our approach to be meaningful it is required that

$$E_B - E_A \gtrsim kT \quad (10)$$

and

$$E_A - E_S \gtrsim kT \quad (11)$$

as well as a demand for a large number of (statistically meaningful) chromophores. Needless to say, we tried here to present the simplest model which still retains the essential characteristics of exciton percolation. One problem under active consideration is a "cooperative" percolation-thermalization model, related to both mixed crystals and photosynthesis systems for which the constraints of eq 10 and 11 apply only marginally.²¹

Finally, we note that in our "simulation experiments" involving naphthalene, the sensor S is kept at a small concentration ($<10^{-2}$) so as to avoid sensor clusters and other complications. The analogous low sensor (i.e., P700) concentration in the photosystems^{5,18} may be related to the same reason or may just be dictated by spatial access considerations. Even so, the analogy between our synthetic ternary system and the photosynthetic systems seems to go beyond coincidence. . . . We also notice that a sensor of 10^{-2} or 10^{-3} definitely falls within the limit of very efficient transport¹⁴ and therefore the limit of validity of eq 3. Actually, at sensor concentrations below 10^{-3} , the efficiency of the exciton transport (to the sensor) suffers significantly,²² whether this transport is coherent or incoherent.¹⁴ We thus should not be surprised that the ratio of antenna-to-sensor chromophores in photosynthetic systems has not exceeded 10^{-3} . However, our conclusion about the predicted ratios (see (8)) is independent of this consideration. Actually, with eq 4 the ratios $[B]/[A]$ tend to be slightly lower than the given limit (unity) of (8), but this might be compensated for by some partial ordering, such as a preference for A-A aggregation (or, alternatively, A-B aggregation).⁵ In conclusion, we demonstrated that exciton percolation may play an important role in biomolecular aggregates, since it relaxes the hitherto assumed requirement of a highly ordered aggregate so as to permit efficient, long-range exciton transport.

Acknowledgment. The help of my collaborators, Dr. J. Hoshen and E. M. Monberg, with the computation and graphical representation is gratefully acknowledged. As pointed out in the text, the experimental data were taken from work with P. Argyrakis, E. M. Monberg, and F. W. Ochs. This research was supported by NSF Grant GH-32578X and NIH Grant NS08116.

References and Notes

- (1) A. S. Davydov, "Theory of Molecular Excitons", Plenum Press, New York, N.Y., 1971.
- (2) R. Kopelman, *J. Chem. Phys.*, **47**, 2631 (1967).
- (3) Th. W. Foerster, *Ann. Phys. (Leipzig)*, **2**, 55 (1948).
- (4) R. S. Knox in "Bioenergetics of Photosynthesis", Govindjee, Ed., Academic Press, New York, N.Y., 1975.
- (5) K. Sauer, ref 4.
- (6) S. Kirkpatrick, *Rev. Mod. Phys.*, **45**, 574 (1973), and references therein.
- (7) T. P. Eggarter and M. H. Cohen, *Phys. Rev. Lett.*, **25**, 807 (1970).
- (8) J. Jortner and M. H. Cohen, *J. Chem. Phys.*, **58**, 5170 (1973).
- (9) R. Kopelman, "Excited States", Vol. II, E. C. Lim, Ed., Academic Press, New York, N.Y., 1975.
- (10) H.-K. Hong and R. Kopelman, *J. Chem. Phys.*, **55**, 5380 (1971).
- (11) R. Kopelman, E. M. Monberg, F. W. Ochs, and P. N. Prasad, *J. Chem. Phys.*, **62**, 292 (1975).
- (12) R. Kopelman, E. M. Monberg, F. W. Ochs, and P. N. Prasad, *Phys. Rev. Lett.*, **34**, 1506 (1975).
- (13) R. Kopelman, *J. Lumin.*, **12**, 775 (1976).
- (14) R. Kopelman in "Non-Radiative Relaxation Processes in Molecules, Solids and Photosynthesis", Vol. 15 of Applied Physics Series, F. K. Fong, Ed., Springer-Verlag, Berlin, in press.
- (15) D. M. Hanson, *J. Chem. Phys.*, **52**, 3409 (1970).
- (16) P. Argyrakis and R. Kopelman, unpublished work.
- (17) F. W. Ochs, P. N. Prasad, and R. Kopelman, *Chem. Phys.*, **6**, 253 (1974); J. Small, private communication, Sept 1975.
- (18) C. Arntzen, private communication, July 1975; C. J. Arntzen and J.-M. Briantis in ref 4.
- (19) C. S. French, *Proc. Natl. Acad. Sci. U.S.A.*, **68**, 289 (1971).
- (20) Govindjee, "Bioenergetics of Photosynthesis", Govindjee, Ed., Academic Press, New York, N.Y., 1975.
- (21) F. W. Ochs, E. M. Monberg, and R. Kopelman, unpublished results.
- (22) J. Hoshen and R. Kopelman, *J. Chem. Phys.*, in press.

Discussion

M. W. WINDSOR. If it is the chlorophyll a quasi lattice that initiates exciton migration in green plant photosynthesis, then why has Nature provided so much chlorophyll b? What is the role of the chlorophyll b? Does it, in your opinion, function solely as an accessory pigment?

R. KOPELMAN. First of all, the question should really be asked the other way around. Why hasn't Nature provided us with about 10 pigments to cover the spectrum very efficiently? And the only answer I know is that you wouldn't be able to have excess of one pigment, if you divided yourself between 10 different pigments.

M. W. WINDSOR. But it does provide many accessory pigments.

R. KOPELMAN. Yes, but accessory does not mean substitutional in the same kind of lattice. With addition of the (b), one can reduce the concentration of (a) down to about 60% almost without losing any efficiency of exciton transfer. The bottleneck doesn't start until about 50-50. So why not have another pigment to absorb about twice as much light?

R. M. HOCHSTRASSER. What assumptions are being made in regard to long-range vs. short-range energy transfer in your models? Won't chlorophylls exhibit long-range transfer?

R. KOPELMAN. Basically I have assumed short-range interactions. Now this does not mean the nearest neighbor only. Like in naphthalene we talk about nearest neighbor, next nearest, next, next, and so on. Even if one has dipole-dipole interactions it is limited to a plane and that is not very long range. As long as the interactions are not terribly long, then this model is going to work.

D. MAUZERALL. For red and brown algae, which do cover the whole absorption spectrum, Nature seems to have chosen the funnel model. The accessory pigments are in the form of clusters (called phycobilisomes) which plug into the photosynthetic membranes. There is even some evidence that the phycoerythrin and phycocyanin may be arranged in layers with the phycocyanin closer to the chlorophyll.

R. KOPELMAN. In certain algae Nature has built a completely different situation where a lot of pigments cover the spectrum much more efficiently. My model is not made for those algae because there is a whole photosynthetic unit; it is very small, and the whole statistical approach would break down anyhow. I am not saying that our

model will work for those algae. Probably for the most developed systems, which have the largest antenna, our kind of mechanism can work. It certainly does not work for all classes of systems.

M. KASHA. Why work with 40 000 if you have only say 400 in a photosynthetic natural system?

R. KOPELMAN. The answer is, we wanted to check ourselves, so we overkilled the problem by going to large systems. However, one of my slides showed that qualitatively there is very little difference between 300 or 500 units and an infinite number of them. There is really little quantitative difference between 400 units and 40 000 or even up to 400 000 units. We were pushing the problem from the solid state point of view and wanted to make sure that in the limit the computer gave us the analytical solution. Obviously, we also imply *ensembles* of the 400 size systems.

H. SELIGER. What is the applicability of the model for the random formation of chlorophyll aggregates to facilitate energy percolation in the natural photosynthetic system? In the latter there is a formal structure to the lamelles of the chloroplasts where there are special places for the electron transport sensitizer chlorophyll and some regular spacing in the membrane phospholipids for the inclusion of antenna chlorophyll. In fact the chlorophyll appears to be necessary to the formation of the lamellae themselves.

R. KOPELMAN. There is some question as to the validity of the structure of the lamellar system which has been assumed. I was at the Gordon Photosynthesis Conference last summer—and I am obviously not prepared to quote a lot of information—but my overall impression was that for large harvesting systems in green plants it really isn't that obvious how much structure one has. And my own feeling is that people invented a lot of structure because they were stuck with a model that demanded structure. Now I'm not saying that the system has to be perfectly random, in fact calculations on partially random systems produce different numbers, but qualitatively the situation is the same. One has to have very good order, and nearly perfect structure, before this model breaks down completely.

Triplet Energy Transfer Mechanism in Isotopic Mixed Molecular Crystals

S. D. Colson,* F. B. Tudron, R. E. Turner, and V. Vaida

Department of Chemistry, Yale University, New Haven, Connecticut 06520 (Received January 8, 1976)

Publication costs assisted by Yale University

The transfer of triplet excitation energy between isotopic traps in benzene isotopic mixed crystals has been investigated using both steady-state and pulsed excitation sources. It has been demonstrated for the first time that the excitation-tunneling transfer mechanism¹ predicts the correct dependence of the transfer rate on trap depth. This theory is shown to predict that the coupling between two different isotopic traps separated by N host molecules is given by

$$\beta_N = L(\epsilon)[f\beta_0]^{N+1}/\Delta E$$

where f and $L(\epsilon)$ are molecular and "lattice" phonon Franck-Condon factors, β_0 is the pure crystal electronic excitation exchange interaction, ΔE is the depth of the shallow trap, and ϵ is the difference between the trap energies. The efficiency of energy transfer is studied as a function of ΔE with fixed ϵ and as a function of ϵ with fixed ΔE .

It is shown that the Perrin approximation, which grossly simplifies the treatment of the experimental data, is a reasonable albeit not perfect approximation for this system. At least 90% of the energy transfer is completed during times much shorter than the benzene triplet-state lifetime. This is consistent with the strong distance dependence of the transfer rate constant predicted by a tunneling mechanism. Using the Perrin approximation, it has been shown that the use of a linear-chain tunneling mechanism predicts the excitation exchange integral to be of the correct magnitude, a conclusion that is also consistent with a strong distance dependence of the transfer rate constant. (Energy can be transferred through two or three intervening host molecules.) There is no evidence for the existence in this system of the intermolecular triplet energy relaxation mechanism recently shown to be operative in chemically mixed crystals.² Likewise, we find no evidence for trap-trap energy transfer via thermal population of host triplet excitons, a mechanism found to be important for isotopic traps in tetrachlorobenzene.³ The difference is interpreted in terms of the different energetics in the two systems.

References and Notes

- (1) (a) G. C. Nieman and G. W. Robinson, *J. Chem. Phys.*, **37**, 2150 (1962); (b) G. W. Robinson and R. P. Frosch, *ibid.*, **38**, 1187 (1963); (c) H. Sternlicht, G. C. Nieman, and G. W. Robinson, *ibid.*, **38**, 1326 (1963); (d) S. D. Colson and G. W. Robinson, *ibid.*, **48**, 2550 (1968).
- (2) H. C. Brenner and C. A. Hutchison, *J. Chem. Phys.*, **58**, 1328 (1973).
- (3) M. T. Lewellyn, A. H. Zewail, and C. B. Harris, *J. Chem. Phys.*, **63**, 3687 (1975).

Discussion

M. GOUTERMAN. What is the triplet exciton bandwidth?

S. D. COLSON. We have been able to relate the rates that we get to the bandwidth. The nearest neighbor coupling is on the order of a wavenumber, and that is the same number we get from an approxi-

mate application of the theory. We do get a value between 1 and say 7 cm^{-1} for nearest neighbor coupling that would be predicted by these data.

W. T. SIMPSON. What's the radius of the sphere of interaction?

S. D. COLSON. Well, you'd have to presume it was a sphere, but it's not really a sphere . . .

W. T. SIMPSON. What's the characteristic length?

S. D. COLSON. It's about 15 \AA .

R. KOPELMAN. I agree with you on the mechanism of tunneling for excitation transfer in your system. We, too, get the same result for isotopic mixed crystals of naphthalene. I would like, however, a clarification on the role of the longer lived excited species in cw excitation vs. pulsed excitation.

S. D. COLSON. The question is: In the case of pulsed vs. continuous excitation do we expect a change in the phosphorescence intensity ratio if there is a variation in the lifetime of trapped molecules due to energy transfer? I think that you can see that Perrin and non-Perrin models would give rise to different lifetimes since the longer-lived species would definitely build up in time compared to those that were short-lived in the case of non-Perrin transfer. The effect of this difference on the transfer efficiency has been demonstrated for specific non-Perrin transfer mechanisms. [M. Inokuti and F. Hirayama, *J. Chem. Phys.*, **43**, 1978 (1965).] Whether or not this would cause a large change in the intensity ratio would depend upon whether or not those species that built up were then somehow affecting the trapping rate.

R. KOPELMAN. Is a high concentration produced?

S. D. COLSON. For a pulsed excitation you do have a very high instantaneous radiation. In any case, it is quite easy to produce concentrations where annihilation is going on and that would effect the intensity due to the long-lived species.

R. M. HOCHSTRASSER. Aren't the variations with trap-supertrap separation entirely consistent with Förster behavior as well as with a tunnelling mechanism?

S. D. COLSON. That variation in ϵ , the difference between the trap and the supertrap, is anticipated in order to get the proper matching of the emission and the absorption for a Förster mechanism. But the dependence upon trap depth is not expected by a Förster mechanism. It shouldn't matter where the host energy levels are. The coupling should be independent of how deep the traps are, if they are coupled by direct interaction either by radiation field or by Dexter coupling. The trap depth dependence eliminates the Förster mechanism.

E. R. BERSTEIN. Shouldn't you use pulses faster than $1\text{ }\mu\text{s}$ to study the kinetic and time dependence of energy transfer?

S. D. COLSON. Certainly there is a distribution of transfer times. The nearest neighbor transfer time is much shorter than the pulse time, but the pulse time is much shorter than the lifetime.

High-Resolution Optical Spectroscopy of Polyenes Related to the Visual Chromophore

R. L. Christensen* and B. E. Kohler

Department of Chemistry, Wesleyan University, Middletown, Connecticut 06457 (Received February 23, 1976)

Publication costs assisted by the National Institutes of Health

High-resolution optical spectroscopy has been used to elucidate several features of polyene excited states. Spectra at 4.2 K of 2,10-dimethylundecapentaene in *n*-nonane and 2,12-dimethylundecapentaene in *n*-undecane are presented. Vibrational analyses of these spectra support the 1A_g assignment for the lowest excited singlet states in these and other linear polyenes. The energy gap between the 1A_g and the higher lying 1B_u state increases from 3000 cm^{-1} in the pentaene to almost 4000 cm^{-1} in the hexaene. The tridecahexaene can be produced in several distinct *n*-undecane crystal sites. Differences in the spectra of these sites provide indications of the extreme sensitivity of polyene electronic structure to the details of local environments. The extension of these findings toward an understanding of the spectra of polyenes related to the visual chromophore is discussed.

1. Introduction

We previously have reported studies in which high-resolution optical spectroscopy has been used to gain a more detailed description of linear polyene electronic states.^{1,2} Our initial work has concentrated on simple linear polyenes which are taken as models for the more complicated isoprenoid structures used in visual systems (Figure 1).³ So far, the optical spectra of the model compounds have been more susceptible to unambiguous interpretation than have the corresponding spectra of the retinals. This can be illustrated by comparing the absorption and fluorescence spectra of *all-trans*-retinal and 2,10-dimethylundecapentaene (Figure 2) in 77-K glass. Even under such low-resolution conditions, the vibronic features in the undecapentaene spectra prove sufficiently distinct to allow the location of the origin of a forbidden electronic state (1A_g) approximately 3000 cm^{-1} below the origin of the strongly allowed 1B_u state.⁴ An even more significant advantage of the model compounds is seen in the 4.2-K spectra of the undecapentaene substitutionally dispersed into an *n*-nonane host crystal (Figure 3a). These spectra are rich in vibrational structure with line widths of only a few reciprocal centimeters. Analysis of the vibronic details showed that for the undecapentaene the transitions between the ground and first excited states are induced by low-frequency, nontotally symmetric vibrations.² This provided direct proof that these transitions are electronically forbidden (${}^1A_g \leftarrow {}^1A_g$) and are made allowed through vibronic mixing.

In addition to their relevance to retinal's electronic structure, the simple model compounds discussed here are interesting from a theoretical point of view. Thus the diphenyl and the dimethyl polyenes provide smoothly varying molecular systems with symmetries that are sufficient to test various theoretical predictions. One of the important milestones in the development of π -electron theories was the ability of the simple Hückel and free-electron treatments to account for the excitation energies of the strongly allowed ${}^1B_u \leftarrow {}^1A_g$ transitions.⁵ The recent discoveries of low-lying forbidden ${}^1A_g \leftarrow {}^1A_g$ transitions in the linear polyenes^{1,2,4,6} present new theoretical challenges. For example, the ${}^1B_u \leftarrow {}^1A_g$ transition converges to a constant excitation energy, but the dependence of the 1A_g energy on polyene length is not yet clear. This problem is particularly intriguing with regard to the infinitely

long polyenes which might serve as models for one-dimensional superconductors.

In this paper, we present preliminary high-resolution spectra of 2,12-dimethyltridecahexaene in polycrystalline matrices of *n*-undecane. Preliminary analysis of the highly detailed vibronic structure is consistent with the 1A_g assignment for the lowest excited singlet state. By varying experimental conditions we have been able to place the hexaene in different sites in the *n*-undecane host. Comparison of the spectra from these sites provides some indication of the influence which the environment has on polyene electronic structure. Insights into the problems encountered in the low-resolution spectroscopy of the retinyl polyenes as well as impetus for future high-resolution efforts follow from these observations.

2. Experimental Section

a. Samples. Both the 2,10-dimethylundecapentaene and the 2,12-dimethyltridecahexaene were gifts from Professor T. S. Sorenson.⁷ The pentaene had a melting point in agreement with that previously reported⁷ and was used without further purification. The hexaene was at most 25% pure and was, therefore, subjected to chromatography on Woelm alumina (activity grade I). The hexaene was eluted with petroleum ether, benzene, and diethyl ether. The predominant and as yet unidentified impurity came off the column first, giving a clean separation from the desired hexaene. The absorption spectra taken of the hexaene from the leading and tailing fractions off the column gave no evidence that our preparation was not homogeneous. After chromatography, the solvents were vacuum-evaporated and the hexaene was dissolved in small amounts of alkanes. The alkanes were used as obtained from Eastman. The alkane solutions when stored at -15°C appear to be quite stable over a time period of several weeks. Sample solutions for spectroscopy were degassed by repeated freeze-pump-thaw cycles before being sealed off under vacuum.

For the pentaene, highly resolved optical spectra were obtained by freezing as quickly as possible concentrated *n*-nonane solutions. This was best accomplished by quickly lowering room-temperature solutions into a liquid helium cryostat. A similar technique also worked for obtaining spectra

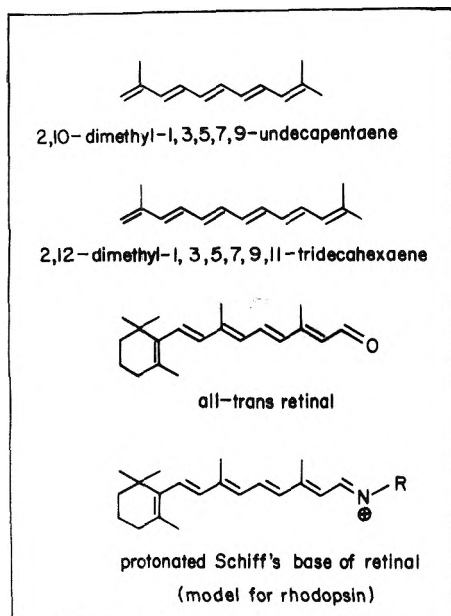


Figure 1. Polyenes related to the visual pigment.

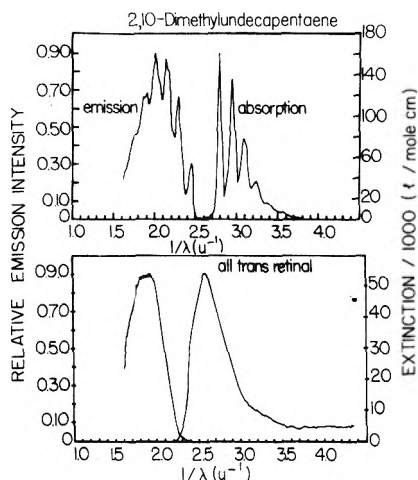


Figure 2. The 77-K absorption and emission of *all-trans-retinal* and 2,10-dimethylundecapentaene in EPA (ether-isopentane-ethanol, 5:5:2 by volume). The emissions are corrected for the spectral sensitivities of the monochromator and photomultiplier. ($1 \mu^{-1} = 10\,000 \text{ cm}^{-1}$).

of the hexaene. For the hexaene-undecane system, however, well-resolved spectra also could be obtained by slow cooling of room-temperature samples. This was done in most instances by placing the sample in the liquid helium cryostat before liquid nitrogen was placed in the outer jacket for pre-cooling. The sample was thus cooled from room temperature to 77 K in about 2-3 h.

Emission spectra of both the slowly grown and quickly grown samples consist of sharp (minimum line widths $\sim 4 \text{ cm}^{-1}$) peaks on top of a broad continuous background. The background emission could be reduced, but never completely eliminated, by adjusting the rate of cooling and the concentration of the samples. The background is presumably due to aggregation of solute molecules into microcrystallites and/or individual solute molecules which find themselves in a broad distribution of solvent environments. The spectra of those molecules which do end up in well-defined environments indicate that, unlike many other such Shpol'skii systems,⁸ only a few predominant sites are occupied. This had been noted before in the undecapentaene-nonane system and, of course,

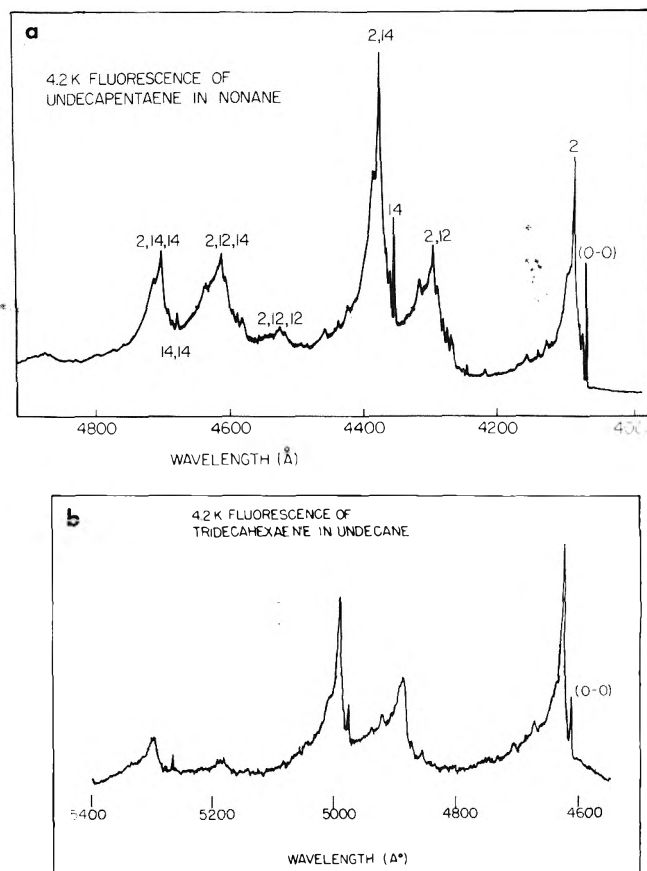


Figure 3. The 4.2-K fluorescence of 2,10-dimethylundecapentaene in *n*-nonane and 2,12-dimethyltridecahexaene in *n*-undecane. Note difference in wavelength scales.

greatly facilitates analyses of the spectra.

b. Spectral Measurements. The emission spectra were recorded using a Jarrell-Ash 1-m Czerny-Turner monochromator which was operated in second order with typical instrumental resolution of $2-3 \text{ cm}^{-1}$. The fluorescence was induced by $\sim 1-2 \text{ mW}$ of uv light (λ 364, 351 nm) from a Spectra Physics Model 171-05 argon ion laser. Background light from the laser was filtered by a Corning 9863 glass filter. The resulting fluorescence passed through a Corning 3389 filter before being focused on the entrance slit of the monochromator. The light was detected with an EMI 6256 B photomultiplier operating in a photon-counting configuration. The high-resolution fluorescence spectra reported here are not corrected for the sensitivities of the monochromator and photomultiplier but these are relatively flat over the wavelength region studied.

3. Results and Discussion

a. Comparison of the Fluorescence of 2,10-Dimethylundecapentaene with that of 2,12-Dimethyltridecahexaene. The fluorescence from a quickly frozen sample of the undecapentaene in *n*-nonane is compared with the fluorescence from a slowly grown sample of the tridecahexaene in *n*-undecane in Figure 3. The assignments indicated in the pentaene spectrum have been discussed in detail in an earlier paper.² The overlap between the absorption and emission spectra enabled features due to different crystal sites to be distinguished from those due to true vibrations of the undecapentaene. These studies showed that the bulk of the fluorescence was built not on the origin but on a quantum of a low-frequency, nontotally symmetric promoting mode (mode 2 in

Figure 3a). The undecapentaene fluorescence spectrum thus was seen to agree with Herzberg-Teller expectations for a forbidden transition and furnished strong proof for the 1A_g assignment of the lowest excited singlet state.

Figure 3 shows that there is a remarkable similarity between the vibronic details seen in the emissions from the undecapentaene and the tridecahexaene. Preliminary absorption measurements indicate the tentative assignment of the electronic origin shown in Figure 3b. We again see evidence of Herzberg-Teller vibronic coupling with most of the intensity being built not on the sharp, forbidden origin but on a low-frequency inducing vibration. The tridecahexaene spectra thus provide further support for the A_g assignment for the lowest excited singlet state in these and other linear polyenes.^{1,2,6}

The difference in energy between the origin of the 1A_g state and the origin of the strongly allowed 1B_u state seen in room-temperature absorption spectra is for the hexaene about 4000 cm^{-1} . The corresponding energy gap in the undecapentaene is closer to 3000 cm^{-1} . It appears, therefore, that the 1B_u state converges more rapidly to its long ("infinite") polyene energy limit than the 1A_g state. This is in accord with previous observations.⁶ It is, of course, of theoretical interest to consider the 1A_g energy of an infinitely long polyene. Because the longer polyenes (e.g., β -carotene) are not fluorescent, the weakly absorbing, low-lying states in these systems have not yet been located. A related problem for which experimental data are available is to account for the energy trends in the shorter molecules. We presently are studying the high-resolution spectra of 2,8-dimethylnonatetraene. The data gained from this molecule along with those from the undecapentaene and tridecahexaene should provide a reasonable calibration for various theoretical treatments.

The increased separation between the lowest lying 1A_g and 1B_u states in the longer polyenes has one other important consequence. We previously had found from the absorption work on the undecapentaene that the predominant C=C double-bond stretching frequency increases from a ground-state value of 1598 cm^{-1} to 1737 cm^{-1} in the lowest excited 1A_g state.² This was quite unexpected in view of the overall decreases in carbon-carbon double-bond orders predicted by molecular orbital calculations.⁹ This discrepancy could be rationalized by postulating substantial mixings of excited-state vibrations. However, such effects have not been noted before in polyene spectroscopy. Unambiguous assignments for such large molecules are quite difficult to obtain. This is especially true for the undecapentaene where the 3000-cm^{-1} gap between the 1A_g and 1B_u states prevents the observation of overtones of the interesting peak 1737 cm^{-1} above the origin. This shortcoming is absent in the longer tridecahexaene. The 4000-cm^{-1} separation provides a wider window for observing the 1A_g vibronic states and thus for confirming the unusual frequency changes observed for the undecapentaene. These experiments are in progress and will be reported in a subsequent paper.

b. Comparison of the Fluorescence of 2,12-Dimethyltridecahexaene in Different n-Undecane Crystal Sites. The fluorescences from the quickly grown and slowly grown undecane samples are compared in Figure 4. Assignments of the electronic origins are based on their overlap with corresponding peaks in the absorptior. spectrum. In the quickly grown site, the emission intensity is built on the origin rather than on a Herzberg-Teller promoting vibration. This implies that the tridecahexaene is distorted significantly along the coordinates of the promoting mode such that the π -electron

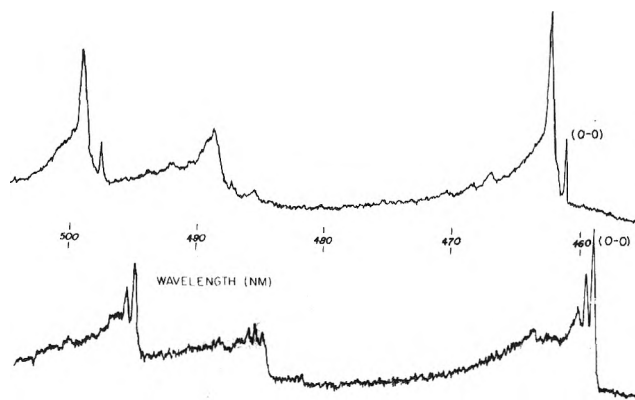


Figure 4. The 4.2-K fluorescence of 2,12-dimethyltridecahexaene in *n*-undecane. The upper spectrum is of a sample which was slowly cooled; the lower spectrum is of a quickly frozen sample.

system no longer contains even an approximate center of symmetry. This emphasizes the point that, unlike aromatic and cyclic polyene systems, the linear polyenes are quite flexible and are particularly sensitive to nonbonded interactions with the local solvent environment.

Experiments on polyenes for which the solvent environment is not well defined, therefore, may be extremely difficult to interpret. In low-resolution spectra such as those seen in Figure 2, the molecules are in a random distribution of environments. This gives rise not only to nonhomogeneous spectral shifts but also, as we have seen for electronically forbidden transitions, to a *nonhomogeneous distribution of vibronic coupling*. In a solution or glass, one must deal with a complex superposition of spectra of which those indicated in Figure 4 represent a very small sample.

These complications are magnified in retinal. This is illustrated in the comparison between the low-resolution optical spectra of retinal and the undecapentaene (Figure 2). The sources of retinal's broad spectra have been considered before.⁴ Nonbonded intramolecular repulsions arising from the isoprenoid structure of retinal's ring and side chain are relieved by rotations about single polyene bonds. As a consequence, there may be multiple closely lying minima in a plot of energy vs. conformation. The interaction between conformational and solvent effects means that many different conformers are populated in a solution or glass. Furthermore, the equilibrium torsional angles will be different in each electronic state. These effects not only lead to broad optical spectra but also must result in a nonhomogeneous distributions of other excited-state properties such as fluorescent lifetimes and fluorescent and photochemical quantum yields.

In conclusion, we wish to stress the importance of high-resolution techniques in studying the electronic properties of the linear polyenes. Restricting our experimental attention to a finite number of molecular sites is essential in order to untangle effects due to the local solvent environments from those due to intramolecular properties. Further details gained from these high-resolution systems will be reported later.

Acknowledgments. This work was supported in part by the National Institutes of Health (Grant RO1 00062-01 BBCA).

References and Notes

- (1) B. Hudson and B. Kohler, *J. Chem. Phys.*, **59**, 4984 (1973).
- (2) R. Christensen and B. Kohler, *J. Chem. Phys.*, **63**, 1837 (1975).
- (3) (a) E. W. Abrahamson and S. E. Ostroy, *Prog. Biophys. Mol. Biol.*, **17**, 179 (1967); (b) G. Wald, *Science*, **162**, 230 (1968).

- (4) R. Christensen and B. Kohler, *Photochem. Photobiol.*, **18**, 293 (1973).
 (5) J. N. Murrell, "The Theory of the Electronic Spectra of Organic Molecules", Wiley, New York, N.Y., 1963.
 (6) B. Hudson and B. Kohler, *Annu. Rev. Phys. Chem.*, **25**, 437 (1974).
 (7) T. S. Sorenson, *J. Am. Chem. Soc.*, **87**, 5057 (1965).
 (8) (a) E. V. Shpol'skii, *Usp. Fiz. Nauk*, **77**, 321 (1962) [*Sov. Phys.—Usp. (Engl. Transl.)* **5**, 522 (1962)]; (b) *Usp. Fiz. Nauk*, **80**, 255 (1963) [*Sov. Phys.—Usp. (Engl. Transl.)*, **6**, 411 (1963)].
 (9) K. Schulten and M. Karplus, *Chem. Phys. Lett.*, **14**, 305 (1972).

Discussion

G. A. CROSBY. What is the experimental evidence supporting the assignment of the lowest singlet state?

R. L. CHRISTENSEN. The most direct evidence is that in the optical spectra of both the pentaene and the hexaene there are weak absorptions with origins coincident with the origins of fluorescence. In neither of these molecules are there emissions coincident with the origin of the higher energy 1B_u state. Thus, by Kasha's rule, the lowest excited singlet state is not the 1B_u state.

A. EL-BAYOUMI. What is the experimental evidence that the weak long wavelength bands are due to an electronically forbidden transition to a 1A_g state rather than due to highly Franck-Condon forbiddenness or conformers of different geometries?

R. L. CHRISTENSEN. The high resolution spectra provide us with a very detailed picture of the vibronic states. The analyses of these

spectra lend no support to the idea that the weak absorptions are due to Franck-Condon forbiddenness (ref 2). That the spectra are not due to different conformers is seen in the insensitivity of the fluorescence spectra to the wavelength of excitation. Thus, excitation into the strongly allowed 1B_u state results in the same emission as excitation into the weak, long wavelength absorption.

R. M. HOCHSTRASSER. I suggest that your 1700-cm⁻¹ mode frequency increase may be due to the fact that the total vibronic "symmetry" of that level may be the same as that of the ground state of a noncentrosymmetric molecule. In the two-photon spectra of benzene and naphthalene the strongest bands (all having the same symmetry as the ground state and not allowed in one-photon absorption) go up in frequency on excitation. Vibronic mixing with the ground state is a reasonable interpretation of this. Why don't you study the two-photon spectrum of these polyenes? You would thereby get all the odd vibrations of the "g" state.

R. L. CHRISTENSEN. Two-photon spectra certainly would be very interesting, particularly if done under high resolution conditions such as those I have described here. Both one photon and two photon spectra of low resolution systems suffer from the inability to distinguish different cases of vibronic coupling, e.g., vibronically allowed components of electronically forbidden transitions vs. purely electronically allowed transitions.

Pressure Tuning of the Fluorescence Spectra Due to Deep Traps in Anthracene and Naphthalene Crystals^{1a}

Malcolm F. Nicol^{1b}

Department of Chemistry,^{1c} University of California, Los Angeles, California 90024 (Received February 9, 1976)

Publication costs assisted by the Energy Research and Development Administration

At low pressures and room temperature, excitation of relatively pure melt-grown anthracene crystals by the 458-nm line of an argon-ion laser yields a relatively weak structured fluorescence which has about the same intensity as the Raman spectrum of the crystal.²⁻⁵ This emission is assigned to anthracene deep traps which are thought to be located near defects and can be directly excited by absorption of a single 458-nm photon. Compression of anthracene crystals at either room (nominally 20 °C) or liquid helium temperatures, however, drastically change the nature and intensity of this fluorescence.⁶ At pressures as low as 2 kbars, the spectrum broadens to an excimer-like emission, the fluorescence intensity increases dramatically for fixed excitation wavelength, and the excitation spectrum dramatically shifts to lower wave numbers (by ~ 160 cm⁻¹ kbar⁻¹). Thus, when a crystal at 15 kbars is excited at 514.5 nm, the broad fluorescence swamps the Raman spectrum; and 632.8-nm excitation at 30 kbars yields a broad fluorescence extending beyond 700 nm. At room temperature, the broad fluorescence extends to higher wave numbers of the excitation by several hundred cm⁻¹, but this hot-band emission is quenched upon cooling. Similarly broad fluorescence can be observed for naphthalene crystals at 30 kbars with 458-nm excitation. These spectral effects are completely reversible to compression.

Support for this assignment of the emission is obtained by observation of the appearance of a similar broad emission background in Raman spectra of powdered crystals of dian-

thracene compressed to 10 kbars and excited at 458, 488, 514.5, or 632.8 nm.⁷ This fluorescence is believed to arise from pairs of anthracene molecules occluded in the crystal during the growth of the photodimer crystals, since the intensity of this fluorescence is sensitive to the degree of purification of the dianthracene.

References and Notes

- (1) (a) Supported by ERDA Contract No. E(04-3)34, PA 88 and the Alfred P. Sloan Foundation. (b) Alfred P. Sloan Foundation Fellow, 1973-1977. (c) Contribution No. 3592.
- (2) H. H. Perkampus and L. Pohl, *Z. Phys. Chem.*, **39**, 397 (1963).
- (3) W. Helfrich and F. R. Lipsett, *J. Chem. Phys.*, **43**, 4368 (1965).
- (4) P. E. Fielding and R. C. Jarnagin, *J. Chem. Phys.*, **47**, 247 (1967).
- (5) D. Goode et al., *Chem. Phys. Lett.*, **25**, 308 (1974).
- (6) M. Nicol, M. Vernon, and J. T. Woo, *J. Chem. Phys.*, **63**, 1992 (1975).
- (7) Y. Ebisuzaki, T. J. Taylor, J. T. Woo, and M. Nicol, unpublished work.

Discussion

R. KOPELMAN. What is the pressure effect on the vibrational exciton bands (factor group splitting) in your crystals?

M. NICOL. We see no changes in the Raman spectra that would indicate a change of crystal structure. There obviously is compression of the crystal; the lattice phonon frequencies increase by large amounts and some factor group splittings of the internal phonons increase. We have not been able to model the pressure dependence of the internal phonons; we are able to model that of the lattice phonons [*J. Chem. Phys.*, **61**, 1380 (1974); **63**, 1992 (1975)]. When we begin

to detect this emission at a particular excitation wavelength, we change the exciting wavelength and find only a pure Raman spectrum of the bulk crystal. Indications of a second phase are described in the literature by Bridgman, but we have not been able to transform the crystals at temperatures up to 150 °C.

M. GOUTERMAN. Is there any evidence that these signals are photoinduced?

M. NICOL. No, these come immediately. The earlier work with mercury excitation indicated that those were photoinduced, and irreversible. These have been shown to be reversible and do not seem to be photoinduced. We have irradiated the crystals for as long as 24 h up to 100–200 mW in one of the green or blue bands and have seen no change in their fluorescence intensity normalized by the Raman spectrum of the same sample as an internal standard.

B. STEVENS. Have you compressed crystals of the anthracene photodimer, with a view to possibly forming crystalline anthracene with a "pair" structure?

M. NICOL. The powdery photodimer crystals that precipitate from solution have enough anthracene impurity in them already to have a similar background at these pressures. We are now recrystallizing some dianthracene powder and we have grown large crystals, up to 0.5-mm in dimension, that we will harvest and compress to see whether we have removed enough of the anthracene from the original preparation. And then we intend to cleave some dianthracene photochemically to prepare pairs of anthracene molecules within the crystal.

R. M. HOCHSTRASSER. Are they linear?

M. NICOL. The defect luminescence is linear with excitation intensity as far as we can measure, but again we can measure the intensity going into the cell but we cannot measure it inside the cell.

E. R. BERNSTEIN. Do you know that some of the light coming from the sample is not a triboluminescence? The crystals don't emit?

M. NICOL. We have not studied the triboluminescence in the high pressure cell, but under other conditions we have seen triboluminescence from anthracene. However triboluminescence stops shortly after a constant pressure is applied. This emission continues.

B. STEVENS. If you take the photodimer and compress it, do you think it will dissociate?

M. NICOL. No, but there are conflicting reports. About 1955 Pitts had a student who ground dianthracene with sodium chloride and claimed the dianthracene entirely disappeared. We have compressed the photodimer for up to 48 h at comparable pressures and have seen no loss of Raman intensity due to the photodimer and no growth of Raman bands associated with the monomer. To date, we have not photolyzed the dianthracene under pressure. In the experiments that we have done so far, the dianthracene has been stable to compression.

O. S. KHALIL. Are these broad emissions excimer type emissions?

M. NICOL. Yes, I think so.

O. S. KHALIL. Do you mean you are exciting directly into an excimer state?

M. NICOL. Our interpretation of the fact that we can change the emission spectrum with the excitation wavelength is that we are exciting directly to something like an excimer state.

The Mechanism of the $S_1 \xrightarrow{h\nu} T_1$ Nonradiative Process in Duraldehyde

Alan Campion^{1a} and M. A. El-Sayed*

Department of Chemistry,^{1b} University of California, Los Angeles, California 90024 (Received February 9, 1976)

Publication costs assisted by the Energy Research and Development Administration

The use of double resonance techniques and the low-field Zeeman PMDR method in elucidating the mechanism of the $S_1 \xrightarrow{h\nu} T_1$ nonradiative process are discussed and contrasted. The method of low-field Zeeman PMDR is then applied to understand the mechanism of this process in duraldehyde in durene at 1.6 K. The results could be explained by assuming that most of the molecules undergo a direct $S_1(n, \pi^*) \xrightarrow{h\nu} T_1(\pi, \pi^*)$ mechanism, but 10–30% of the molecules undergo an $S_1(n, \pi^*) \xrightarrow{h\nu} T_2(n, \pi^*) \xrightarrow{h\nu} T_1(\pi, \pi^*)$ indirect mechanism. We propose that this latter mechanism is a result of pseudo-Jahn-Teller forces that mix the $T_2(n, \pi^*)$ and $T_1(\pi, \pi^*)$ states which are believed to be separated by only 0.05 eV in this molecule.

Introduction

Recently, the new technique of Zeeman PMDR²⁻⁴ has been successfully applied to the elucidation of the mechanism by which molecules initially excited to the lowest singlet state (S_1) intersystem cross (ISC) to the lowest triplet (T_1). The experiments use phosphorescence-microwave double resonance⁵ (PMDR) techniques to monitor changes in the steady-state populations of the three magnetic sublevels of the T_1 state, as they are mixed by a weak (<1 kG) external

magnetic field. The results of the experiments to date have confirmed the importance of a selection rule⁶ which predicts that ISC between states arising from different types of electronic promotion (e.g., $n, \pi^* \xrightarrow{h\nu} \pi, \pi^*$) should be at least an order of magnitude more important than ISC between states of the same type of electronic promotion (e.g., $n, \pi^* \xrightarrow{h\nu} n, \pi^*$ or $\pi, \pi^* \xrightarrow{h\nu} \pi, \pi^*$). This has been convincingly demonstrated for the nitrogen heterocyclics where it was shown^{3,4} that intermediate triplet states play an important role in the

ISC process if they are of different orbital configuration than S_1 . In addition, these experiments reveal previously hidden information about the sublevel order and zero-field splittings (ZFS) of the intermediate triplets.

We now wish to apply this technique to answer similar questions in another important class of molecules, the aromatic carbonyls. In addition to the intrinsic interest in the order, ZFS, and interactions of these triplet states, this information would be valuable in understanding the photochemistry of these widely studied molecules. The arguments that led to the $n, \pi^* \leftarrow \rightleftharpoons \pi, \pi^*$ selection rule in the nitrogen compounds result in precisely the same prediction in the aromatic carbonyls, provided that the carbonyl moiety is coplanar with the aromatic ring. We intend to experimentally assess the validity of this rule as applied to these carbonyls.

In the only aromatic carbonyl studied so far (benzophenone), ISC was shown^{2b} to occur between S_1 and T_1 directly, states which are both n, π^* . However, the existence of a $^3\pi, \pi^*$ state lower in energy than S_1 has never been proven in benzophenone, and furthermore it is known that the phenyl rings are not coplanar. A better choice to test this selection rule would be a molecule in which the triplet states that lie below S_1 have been identified.

We have chosen duraldehyde (2,4,5-trimethylbenzaldehyde) to study since it fulfills the above requirement. The lowest singlet state⁷ is $^1n, \pi^*$, T_1 is $^3\pi, \pi^*$, and T_2 , which lies⁸ ca. 400 cm^{-1} higher in energy than T_1 , is an $^3n, \pi^*$ state. In addition, the principal axes of the zero field tensor of the T_1 state have been found⁹ for this molecule in a durene host single crystal and the dynamic parameters that characterize the T_1 state in this host at 1.5 K have been reported.¹⁰

The use of double resonance techniques and the low-field Zeeman PMDR method in determining the mechanism of the $S_1 \rightleftharpoons T_1$ nonradiative process is first discussed in the next two sections. This is then followed by the results and discussion of the low-field Zeeman method as applied to duraldehyde. One interesting proposal that came out of this work is the role that pseudo-Jahn-Teller forces play in the mechanism of this nonradiative process.

The Mechanism of the ISC from Double Resonance¹¹

The intersystem crossing process between a singlet and a triplet electronic state involves the creation of a unit of angular momentum in the spin motion. This must come from the change in the electronic orbital motion in the nuclear configuration upon going from the singlet to the triplet state involved in the ISC process. To conserve angular momentum, the change in the orbital motion creates the spin angular momentum in a certain direction in the molecule, thus leading to the population of a certain spin level(s) of the triplet state produced. If the triplet state produced is not the lowest one, further T-T relaxation would take place. In this process, the spin direction is conserved and if the magnetic system is the same for the two states, the same spin levels will be populated in T_1 as they are first produced in the higher triplet state. Since the electronic motion in T_1 is different from T_2 , then the created spin angular momentum would have a different direction if crossing from S_1 takes place to T_2 from that when crossing involves only T_1 . One should then ask: Can we determine the mechanism of the ISC (i.e., $S_1 \rightleftharpoons T_2 \rightleftharpoons T_1$ vs. $S_1 \rightleftharpoons T_1$) from the observed direction of the spin angular momentum? The answer is yes if the following conditions are satisfied.

(1) If we know the symmetry of S_1 and all the triplet states below S_1 .

(2) If the triplet states of lower energy than S_1 all have different symmetries.

(3) If the geometry of the molecule is known and known to remain of high enough symmetry (of C_{2v} or higher symmetry) during the ISC process, i.e., no change of geometry (e.g., via vibronic coupling or static distortion) is allowed or if it takes place, the type of distortion must be known. This latter condition sets up great limitations upon PMDR methods in determining ISC mechanisms. Our lack of knowledge of the involvement of vibronic or static distortion during the ISC process makes any conclusion using PMDR a mere proposal. Furthermore, the type of lower triplet states in many molecules is not known. However, in the few cases when these are reasonably known, PMDR could and has suggested possible mechanisms. In aromatic hydrocarbons, it is known and assumed that all the low-energy triplets are of the (π, π^*) type. From this knowledge and the produced spin direction in the $S_1 \rightleftharpoons T_1$ ISC process, it was concluded¹² that out-of-plane distortion must take place during the ISC process. In nitrogen heterocyclics,¹¹ if one assumes the absence of molecular distortion, the determined spin direction in T_1 can distinguish between an $S_1(n, \pi^*) \rightleftharpoons T(n, \pi^*)$ mechanism and an $S_1(n, \pi^*) \rightleftharpoons T(\pi, \pi^*)$ mechanism. The assumption of retaining a high symmetry molecular geometry during the ISC process might not be a good one, in particular for the one ring N heterocyclics, e.g., pyrazine and pyrimidine, for which the double resonance results on the phosphorescence mechanisms in the former¹³ and the nonradiative mechanisms of the latter¹⁴ strongly suggest a molecular geometry lower than that in the free molecule. It is thus clear that a new method must be sought that can be used to determine the mechanism of the ISC process involved. A step forward toward accomplishing this goal is described below and is known as the Zeeman PMDR technique.

Zeeman PMDR Method

Basic Idea. As was mentioned before, the net spin direction produced (i.e., the relative population of the different zero field levels) in T_1 reflects the manner in which the spin angular momentum is created in the system as a result of crossing from S_1 to the triplet manifold. Suppose now that all the molecules cross from S_1 directly to T_1 . The observed net spin direction can be changed by the application of a magnetic field in a manner that depends on the field strength and direction as well as the energy required to tilt the spin moment from one direction to the other (i.e., the zero field pattern) in the triplet state involved in the ISC. Since we know all these quantities, we can calculate the effect of the magnetic field on the spin direction in T_1 along different crystal directions and at different field strengths. The equation required for this calculation is given below. A comparison with the experimental results should then be made. If excellent agreement is obtained, then the $S_1 \rightleftharpoons T_1$ is most likely the dominant ISC mechanism. If no agreement is obtained, a computer fit of the observed results could in some cases give the zero field parameters and the relative probability of crossing to T' to that for crossing to T_1 can be obtained. This is in cases where the nature of T' is known so the range of D and E values can be given to the computer to make the fit close to being unique.

Equations. Detailed descriptions of the Zeeman PMDR technique may be found elsewhere^{2b} so only an outline will be presented here. In zero field, the spin functions of a triplet state may be chosen to satisfy the eigenvalue equation

$$S_i |\tau_i\rangle = 0 \quad (1)$$

where the subscript labels a principal axis of the zero field tensor. These spin functions are mixed by a magnetic field and the new eigenfunctions in the field may be expressed in the zero field basis as

$$|\tau_i^H\rangle = \sum_j C_{ij} |\tau_j\rangle \quad (2)$$

where the mixing coefficients C_{ij} are determined by diagonalization of the Hamiltonian that now contains the Zeeman term.

If all of the rate constants K and k that characterize the populating (from S_1) and decay (to S_0) processes, respectively, of the individual component of T_1 (e.g., T_{1i}) may be described by a Fermi golden rule expression as

$$K_{S_x \rightsquigarrow T_{1i}} \propto |\langle S_x | H | T_{1i} \rangle|^2 \quad (3)$$

where H contains the perturbation terms leading to the ISC process, then the new rates in the field will be given by

$$K_i^H = \sum_j |C_{ij}|^2 K_j^0 \quad (4)$$

for an $S_1 \rightsquigarrow T_1$ direct ISC process,^{2b} where K^0 's are the zero field rates. If some higher triplet state T' is involved, then in addition we take the scalar product of the resulting spin function of T' with T_1 to project the spins in the $T' \rightsquigarrow T_1$ internal conversion, a process in which the spin angular momentum is conserved. This yields^{2b}

$$K_i^H = \sum_{j,m} \left| \sum_k C_{ik}^* C_{jk}' \right|^2 |C_{jm}'|^2 K_m^0 \quad (5)$$

for the ISC rate. The summation over k describes this projection and the primed coefficients refer to the mixing of the intermediate triplet state spin functions.

There are several assumptions built into the above treatment, which we will mention now:

(1) Field induced spin-lattice relaxation (SLR) is assumed absent although it is known¹⁵ that SLR increases as a function of the field. We measured the total decay rates of all sublevels of duraldehyde, in fields of 1 kG, and found no increase in the decay rates other than that due to the mixing of the spin states of T_1 , so apparently SLR is not a problem in the present experiment.

(2) The simple projection of the T' spin function onto those of T_1 requires that the internal conversion process in this molecule is electrostatic in nature and thus the corresponding operator is spin free, i.e., T_1 - T' spin-orbit coupling must be small. Spin-orbit coupling between the lowest triplet states of duraldehyde is estimated^{16,17} to be about 3%.

(3) The principal axes of the zero field tensors in both states are assumed to coincide. This implies that the structure of the molecule as well as the electron density in the two states are similar.

The preceding equations are used to calculate the change in the PMDR signal as a function of field. Agreement between predictions based upon $S_1 \rightsquigarrow T_1$ direct ISC and experiment indicate negligible involvement of higher triplets. Radical departure from the predicted behavior could indicate significant involvement of higher triplet state(s) and the experimental results may be used to model the zero field splittings of the T' state. However, due to the assumptions discussed above and the fact that the fit in many cases is not unique, the conclusions concerning the zero field parameters obtained by this method should be taken lightly. The most important use of this method is to answer the question: Is the ISC process direct or not? If the observed results agree with those calcu-

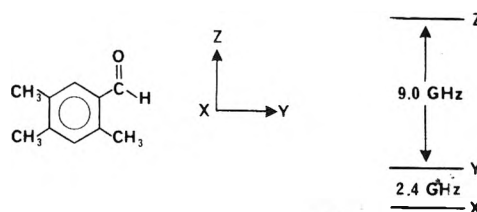


Figure 1. Magnetic axis system, zero field splittings, and absolute sublevel order for the T_1 state of duraldehyde in durene.

lated for an $S_1 \rightsquigarrow T_1$ process, then the ISC process is direct. It should be pointed out, however, that disagreement with calculation for a direct process does not necessarily rule out a direct ISC mechanism. The reason for this is the fact that in the calculation we use the zero field parameters of T_1 in the zero-point level of this state. The $S_1 \rightsquigarrow T_1$ process occurs to an excited vibronic level of T_1 almost degenerate with the zero-point level of S_1 . Only if the potential energy surface of T_1 remains harmonic and the zero field parameters do not change with changing the vibration quantum number in T_1 would the calculated and observed behavior coincide exactly.

Results

The principal axes of the zero field tensor for the lowest triplet state of duraldehyde in durene have been located⁹ in a high-field EPR experiment and are nearly parallel ($\pm 4^\circ$) to the symmetry axes of the parent durene molecule. Figure 1 shows the axis system adopted from this work. The molecular z axis is parallel to the carbonyl bond, x is the out-of-plane direction and y completes the right-handed Cartesian frame. Before determining the relative ISC rates in the field, we measured the energies of the microwave transitions as a function of field and compared them with the eigenvalues calculated from diagonalization of the Zeeman Hamiltonian. In this manner we were able to determine that the precision of the crystal orientation was within $\pm 5^\circ$.

The dynamic parameters of the T_1 state of duraldehyde have been measured by Cheng and Hirota,¹⁰ and are tabulated in Table I. We have remeasured these and found our results to be in good agreement. Therefore, these parameters were used as input to the computer program^{2b} which calculated the expected behavior of the PMDR signal in weak magnetic fields assuming a direct ISC process. The results of this calculation for the 9.0-GHz zero field transition are shown in Figure 2 as the solid curve. The PMDR signal obtained under continuous wave optical excitation and rapid microwave passage is given by:

$$\frac{\Delta J_{yz}}{I} = \frac{f(n_z^0 - n_y^0)(k_y^r - k_z^r)}{n_x^0 k_x^r + n_y^0 k_y^r + n_z^0 k_z^r} \quad (6)$$

where f is the fraction of the population difference transferred by the pulse, n_i^0 is the steady-state population of level i and k_i^r the effective radiative rate constant for that level. As may be seen from Table I and Figure 2, the signal is negative in zero field for this transition and would become smaller in magnitude for a direct mechanism as the applied field (along the durene a axis) approaches 1 kG. The experimental points are the vertical bars which represent a typical uncertainty of $\pm 10\%$. Clearly they do not follow the calculated curve and in fact the signal changes sign at ca. 400 G, strongly suggesting a T' involvement in the ISC.

A reasonable fit to the observed data can be achieved by several sets of parameters for the T' state. The major source

TABLE I: Zero Field Parameters for the T_1 State of Duraldehyde in Durene at 1.5 K

Sublevel	$K(\text{rel})$	$k^r(\text{rel})$	k, s^{-1}	$N_0(\text{rel})$
z	1.0	1.0	105.0	1.0
y	0.014	0.064	2.12	0.69
x	0.10	0.093	8.20	1.28

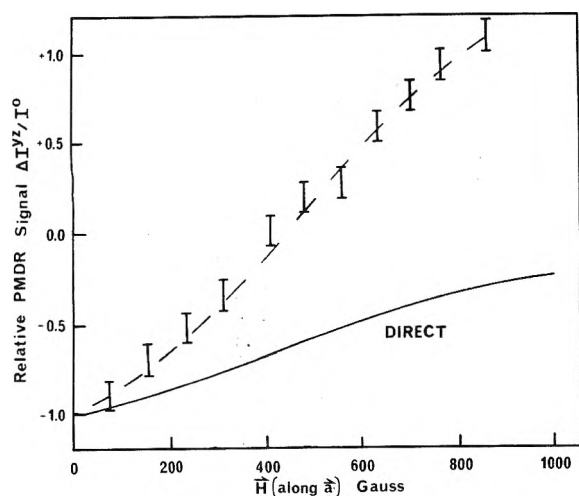


Figure 2. Normalized change in the y - z PMDR signal as a function of magnetic field along the durene a crystal axis. Solid line is the calculated behavior based upon direct $S_1 \xrightarrow{\text{ISC}} T_1$ ISC. Vertical bars are experimental points and the dotted line was calculated for an 80% direct and 20% indirect (to T_2) intersystem crossing to the z -magnetic spin levels; an x - z splitting in T_2 of 18 GHz and a y - z splitting of 11 GHz are assumed in this calculation.

of uncertainty in fitting lies in the difficulty of determining the relative probability of $S_1 \xrightarrow{\text{ISC}} T'$ ISC to $S_1 \xrightarrow{\text{ISC}} T_1$ ISC in zero field. If this were known, then a unique set of T' energies could be found; alternatively, if the T' splittings were known, this factor could be extracted. The approach we will take is to model T' with several sets of splittings and attempt to bracket the allowed range of the relative probability. In addition to the measurements reflected in Figure 1, we have measured the change in the PMDR signals for both the 11.4- and 9.0-GHz transitions with fields parallel to the crystal a and c' axis. The sets of parameters arrived at were then chosen to give simultaneous best fits to these four separate experiments.

We assume that T' in duraldehyde is the $T_2(n, \pi^*)$ state for which we used the zero field splittings and the absolute order of formaldehyde¹⁹ as a start. For this molecule, it is known that the order is $E_x > E_y > E_z$ with splittings $D = +0.42 \text{ cm}^{-1}$, $E = +0.04 \text{ cm}^{-1}$. Comparison of the experimental results with calculations for duraldehyde based on this model indicated that the order of the levels in T' is exactly inverted with respect to T_1 , that is $E_x > E_y > E_z$ for T' . No other T' order could reasonably fit the observations. Once the order was established, we varied the magnitude of the T' splittings. A decrease in the splittings could result if the n, π^* state is more delocalized than that of formaldehyde so we allowed the $|D + E|$ splitting in T_2 to decrease to 12 GHz and found that a satisfactory agreement with experiment could be obtained with a T'/T_1 z level relative ISC rate of 0.1. We feel that the splitting represents a reasonable lower limit to the upper state splitting since spin-orbit coupling with T_1 would tend to offset the effects of delocalization.

TABLE II: Possible Values of the ZFS of T_2 in Duraldehyde Deduced from Trial Fits of the Observed Effect of Low Magnetic Field on Its $S_1 \xrightarrow{\text{ISC}} T_1$ Nonradiative Process

Relative T_2/T_1 z level ISC	0.1	0.2	0.3
x - z splitting, GHz	12	18	20
x - y splitting, GHz	5	7	7
y - z splitting, GHz	7	11	13

To estimate the maximum T_2 splitting, we have used the results of Hayashi and Nagakura¹⁶ who have empirically determined a spin-orbit coupling matrix element of ca. 9 cm^{-1} for ${}^3n, \pi^* \text{--} {}^3\pi, \pi^*$ mixing in substituted benzaldehydes. This mixing makes an additional contribution of ca. 6 GHz to the zero field splittings of both triplet states. Consequently, if the (pure) $n, \pi^* |D + E|$ value were as large as 14 GHz, the spin-orbit coupling would increase this to 20 GHz. Based upon this value the relative z level T'/T_1 ISC ratio is 0.3.

Table II lists three sets of parameters that equally well fit the data. The dotted curve shown in Figure 1 was generated by the middle set of values but similar curves result from the other sets.

Discussion

The conclusion of this work is that the observed magnetic field effects on the T_1 population in duraldehyde cannot be explained by having all the molecules directly intersystem cross to T_1 . Some molecules must cross via a T' state. Since there must be an n, π^* triplet lower in energy than S_1 and since the small S_1 - T_1 splitting makes it unlikely that there is a third triplet below S_1 , we infer that the $T_2(n, \pi^*)$ state is the state involved. On the basis of our calculations, we also suggest that the order of the zero field levels of T_2 is inverted with respect to that for T_1 , a model that is consistent with the absolute order of the energy levels in the formaldehyde n, π^* triplet. By assigning limits to the possible T_2 splittings we can estimate the relative probability of T_2/T_1 ISC to be 0.1 to 0.3.

That most of the ISC is direct ${}^1n, \pi^* \text{ to } {}^3\pi, \pi^*$ is consistent with several other observations^{3,4} which have suggested that the ISC between states of different configurations should be faster than that between states of the same configuration. These observations are in agreement with a selection rule that had been predicted earlier.⁶ The present observation of ${}^1n, \pi^* \text{ to } {}^3n, \pi^*$ ISC need not represent an apparent violation of this rule but could occur as a result of vibronic mixing of the close-lying⁸ T_1 and T_2 states. Suppose that (pure) $n, \pi^* \text{ to } n, \pi^*$ ISC is negligibly slow compared to $n, \pi^* \text{ to } \pi, \pi^*$ ISC. Then the observed ratio of relative ISC rates may be used to estimate the degree of vibronic mixing. Let the vibronically mixed states be represented as

$$\begin{aligned} {}^3\phi_{T_1} &= a^3\phi_{\pi, \pi^*} + b^3\phi_{n, \pi^*} \\ {}^3\phi_{T_2} &= b^3\phi_{\pi, \pi^*} - a^3\phi_{n, \pi^*} \end{aligned}$$

and the relative ISC rates be given by experiment as

$$\frac{|\langle S_1 | H_{\text{s.o.}} | T_2 \rangle|^2}{|\langle S_1 | H_{\text{s.o.}} | T_1 \rangle|^2} = 0.1\text{--}0.3$$

Then by substitution one finds that

$$b^2/a^2 = 0.1\text{--}0.3$$

That is, the T_2 state has from 10–30% π, π^* character mixed in vibronically. This is a very reasonable amount, considering the proximity of the states involved. If T_2 and T_1 are separated by $\sim 500 \text{ cm}^{-1}$ and the mode mixing the two states is of 200

cm^{-1} , the mixing of the two states would be $\sim(200/500)^2 \approx 0.16$, i.e., 10–20% contamination of one state with the other.

We have presented a picture of the duraldehyde ISC where the involvement of T_2 cannot be neglected. We have also made the suggestion that the indirect path $S_1(n, \pi^*) \rightsquigarrow T_2(n, \pi^*) \rightsquigarrow T_1(\pi, \pi^*)$ arises as a consequence of the extensive vibronic mixing between T_1 and T_2 and is not due to breakdown of the $n, \pi^* \leftarrow \rightsquigarrow \pi, \pi^*$ selection rule. These conclusions are entirely consistent with other observations that have confirmed the importance of the $n, \pi^* \leftarrow \rightsquigarrow \pi, \pi^*$ ISC selection rule in planar heteroaromatics.

Experimental Section

Samples. Duraldehyde was a gift from Dr. S. J. Sheng, who synthesized it according to the method described by Fischer.⁷ Durene was repeatedly recrystallized from ethanol and chromatographed over alumina. Solid solutions of ca. 10^{-3} M duraldehyde were prepared and single crystals were grown by the Bridgman method.

Apparatus. Durene crystals were cleaved and polished, then oriented conoscopically so that the magnetic field was parallel to either the a or c' durene crystal axes. The field was provided by a 1-in. diameter superconducting Helmholtz coil, which could generate fields up to 1 kG with the available power supply.

The PMDR apparatus used in these experiments has been previously described.¹⁸ The 313-nm Hg line from a filtered 100-W arc illuminated the sample, whose phosphorescence was detected by a 1-m Jarrell-Ash monochromator equipped with an EMI 9502B photomultiplier. The resolution of the monochromator was 0.04 nm, sufficient to resolve the emission from the two sites that are separated by 23 cm^{-1} . All of the present experiments were performed monitoring the more intense high energy emission.

The geometry of the experiment was arranged so that the magnetic field, the optical axis of the monochromator, and the propagation direction of the microwaves were all coaxial. This arrangement ensured that both molecules in the unit cell experience the same magnetic field and also eliminated any polarization effects of either the viewing monochromator or the incident polarized microwave radiation.

Microwaves in the 7–12.4-GHz region were generated by an HP 8960B sweep generator amplified to ca. 10 W with a Hughes 117H TWT amplifier and transmitted to the sample by a Systron Donner linearly polarized horn antenna. An NS-560 signal averager is used in the detection system.

Acknowledgment. The authors wish to acknowledge the financial support of the Energy Research and Development Administration. A.C. wishes to acknowledge IBM for a predoctoral research fellowship. Computing time was made available by the UCLA Campus Computing Network, to whom we are grateful.

References and Notes

- (1) (a) IBM Predoctoral Fellow. (b) Contribution No. 3587.
- (2) (a) R. W. Leyerle, Ph.D. Dissertation, University of California, Los Angeles, Calif., 1974; (b) M. A. El-Sayed and R. W. Leyerle, *J. Chem. Phys.*, **62**, 1579 (1975).
- (3) P. E. Zinsli and M. A. El-Sayed, *Chem. Phys. Lett.*, **34**, 304 (1975).
- (4) P. E. Zinsli and M. A. El-Sayed, *Chem. Phys. Lett.*, **36**, 290 (1975).
- (5) M. A. El-Sayed, *Annu. Rev. Phys. Chem.*, **26**, 235 (1975).
- (6) M. A. El-Sayed, *J. Chem. Phys.*, **38**, 2834 (1963).
- (7) G. Fischer, *Mol. Cryst. Liq. Cryst.*, **11**, 85 (1970).
- (8) E. Migirdicyan, *Chem. Phys. Lett.*, **12**, 473 (1972).
- (9) M. Sharnoff, *Mol. Cryst.*, **5**, 297 (1969).
- (10) T. H. Cheng and N. Hirota, *Mol. Phys.*, **27**, 281 (1974).
- (11) M. A. El-Sayed, W. R. Moomaw, and J. B. Chodak, *J. Chem. Phys.*, **57**, 4061 (1972).
- (12) M. A. El-Sayed, *Acc. Chem. Res.*, **4**, 23 (1971).

- (13) A. A. Gwaiz and M. A. El-Sayed, *Chem. Phys. Lett.*, **19**, 11 (1973).
- (14) D. M. Burland and J. Schmidt, *Mol. Phys.*, **22**, 19 (1971).
- (15) L. H. Hall and M. A. El-Sayed, *Mol. Phys.*, **22**, 361 (1971).
- (16) H. Hayashi and S. Nagakura, *Mol. Phys.*, **24**, 801 (1972).
- (17) M. Batley and R. Brambley, *Chem. Phys. Lett.*, **15**, 337 (1972).
- (18) M. A. El-Sayed, E. Gossett, and M. Leung, *Chem. Phys. Lett.*, **21**, 20 (1973).
- (19) W. T. Raynes, *J. Chem. Phys.*, **41**, 3020 (1964).

Discussion

G. W. CANTERS. Applying your techniques on individual vibronic bands, would you be able to say something about the symmetry of the vibrations involved?

M. A. EL-SAYED. The question is: Can you do this experiment on different vibronic bands and therefore determine the symmetry of the vibration involved in the radiative process? This is quite correct; you can also just simply determine which spin level it comes from—one of two things, either you know the symmetry of the spin level and therefore once you use microwave induced delayed phosphorescence, such as discussed previously, you can immediately deduce the symmetry of the vibration, or, by knowing the polarization of the emission through optical experiments, one can tell what the symmetry is.

M. KASHA. I want to ask this question simultaneously of the speaker and the chairman. I admire the fine detail of this deduction on the paths of excitation. Last summer we heard Professor Ed Schlag (Munich) speaking on the mechanisms of spin-orbital coupling via promoting vibrations. He seems to be maintaining that there are no direct electronic spin-orbital paths, as they are all vibronically determined. Do you include vibronic spin-orbital coupling mechanisms?

M. A. EL-SAYED. Let us differentiate two terms. In my talk, when I said direct mechanism, I meant an $S_1 \rightsquigarrow T_1$ mechanism. This mechanism can involve direct spin-orbit coupling or higher order vibronic-spin-orbit coupling interaction. I take it you mean that Schlag indicated that you need nuclear (as well as electronic) displacement in radiationless transitions, i.e., an involvement of a promoting mode is indicated. However, the promoting mode could be a totally symmetric vibration. In the basis set I am using in my discussion, this would correspond to direct spin-orbit coupling, e.g., in N-heterocyclics. If the promoting mode is nontotally symmetric, then vibronic in addition to spin-orbit interaction are involved (aromatic hydrocarbons could be an example of this mechanism).

L. GOODMAN. Is it possible to distinguish between emission from an upper state triplet (i.e., exciting from a single ground state molecular ensemble) and emissions from rotomers and conformers in different environmental sites by these techniques?

M. A. EL-SAYED. Not unless you know the zero field parameters of each. Furthermore, if the higher triplet state relaxes to T_1 at a faster rate than the spin frequency, i.e., the line width of each spin level of T_2 is larger than its zero field splitting, this technique becomes inapplicable to T_2 .

R. M. HOCHSTRASSER. Does it matter to your interpretative method what the detailed structure in the quasi-continuum involved in the radiationless transition is? Won't it be that levels having the same *spin* will be all mixed together regardless of the electronic or vibrational symmetries?

M. A. EL-SAYED. What we do is we put the magnetic axis that we have for the lowest triplet state and keep it there in the magnetic field. We are saying that somewhere there the fine structure is preserved. That is our principal assumption.

H. A. FRANK. What solvent was used in the benzophenone experiment and would not a dramatic effect on the ISC rate occur upon changing the solvent if the molecule were sufficiently distorted in its solvent?

M. A. EL-SAYED. The solvent was a crystal of 4,4'-dibromodiphenyl ether. Hochstrasser and his group determined the magnetic axis of benzophenone in this host, which is very important to know when a magnetic field is applied to it. The answer to the second part of your question is yes. Solvents that change the configuration should change the ISC rate. It is interesting to point out that as long as the C_2 symmetry axis is preserved, the top spin level would be the preferred spin level in the pumping process both in the $S_1(n, \pi^*) \rightsquigarrow T_2(\pi, \pi^*) \rightsquigarrow T_1(n, \pi^*)$ mechanism in the planar configuration and in the $S_1(n', \pi'^*) \rightsquigarrow T_1(n', \pi'^*)$ mechanism in the nonplanar configuration.

E. C. LIM. When two electronic states of different orbital character ($n\pi^*$ vs. $\pi\pi^*$) are very close in energy, it would be difficult to distinguish a direct process from an indirect one, since the two electronic states are most probably of mixed character.

M. A. EL-SAYED. This is correct. The paper by Campion and myself discusses the effect of vibronic mixing between the triplet states on the results of the mechanism of the ISC process.

L. GOODMAN. If the direct intersystem crossing proceeds because of vibrational-electronic coupling between T_1 and T_2 , it should be revealed by selective deuteration experiments. Deuteration of the aldehyde hydrogen should increase the ${}^3n,\pi^* - {}^3\pi,\pi^*$ spacing; perdeuteration of the ring (and methyls) should decrease it significantly.

M. VALA. This remark pertains to the assignment and origin of the second triplet state of duraldehyde. In our laboratory we have recently completed a study of the temperature dependence (10–160 K) of the phosphorescence spectra and lifetimes of duraldehyde in crystalline durene. Our results show that there are two environmentally different duraldehydes (i.e., two sites) in the durene lattice and that the previously-assigned upper ${}^3n,\pi^*$ state ($\Delta E = 400 \text{ cm}^{-1}$) emission of the *E* conformer (transoid form) originates instead from the lowest ${}^3n,\pi^*$ state of the *Z* conformer (cisoid form) which is formed by the excited

state rotation of the aldehyde group. A similar, though lower energy ($\Delta E = 160 \text{ cm}^{-1}$), emission was also detected above the low temperature 0-0 band and assigned to the ${}^3n,\pi^*$ emission from the *Z*-like conformer in the second site.

R. KOPELMAN. How did you excite your sample? A change in excitation wavelength might possibly affect your results, in terms of T_2 vs. T_1 intersystem crossing.

A. CAMPION. The samples were excited with Hg 3130-Å light, whose energy is greater than the S_1 origin but does not excite the S_2 state.

O. KHALIL. Are you exciting directly into the $S_1(n,\pi^*)$ or into a higher singlet state? Does this affect your results, i.e., exciting in $S_2(n,\pi^*)$ or into the π,π^* as far as intersystem crossing is concerned?

A. CAMPION. We are exciting vibronic levels of the duraldehyde S_1 state directly. Since the experiments are done in the condensed phase, I wouldn't expect to observe any differences if we were to excite S_2 , but we haven't done this experiment.

E. C. LIM. As long as intersystem crossing takes place from the lowest excited singlet state, the wavelength of excitation should not affect their conclusion.

Excited States of Mixed Ligand Chelates of Ruthenium(II) and Rhodium(III)¹

G. A. Crosby* and W. H. Elfring, Jr.

Department of Chemistry, Washington State University, Pullman, Washington 99163 (Received March 3, 1976)

Publication costs assisted by the Air Force Office of Scientific Research, Directorate of Chemical Sciences

Photoluminescence and proton magnetic resonance measurements on complexes of the type $[M(\text{bpy})_m(\text{phen})_n]\text{Cl}_x$ [$M = \text{Rh(III)}$, $x = 3$; $M = \text{Ru(II)}$, $x = 2$; $m = 3 - n$, $n = 0, 1, 2, 3$] lead to the conclusion that the lowest excited term of the rhodium(III) species is ${}^3\pi\pi^*$ in nature and that interligand interaction is small both in the ground and lowest excited states of the complexes. For the ruthenium(II) systems the lowest excited states are charge-transfer-to-metal in nature, and strong ligand-ligand interaction is manifested both in the excited and the ground electronic states. The data on the mixed-ligand ruthenium(II) complexes are rationalized on the basis of a model previously developed for tris (trigonal) species. Within the accuracy of current experimental information the model adequately accounts for both the optical and proton magnetic resonance data. A semiquantitative approach to $d\pi$ back-bonding through the configurational mixing of charge-transfer excited states into the ground state is proposed.

Luminescence measurements on d^6 complexes have yielded detailed information about the electronic excited states. By judicious choices of metal ions, oxidation states, and the nature of the coordinated ligands, the lowest excited configurations have been varied systematically, thus leading to a coherent picture of metal complex excited states.^{2,3} The $(nd)^6$ ($n = 3, 4, 5$) configuration has played a key role in these investigations, since complexes with metal ions of this structure often have diamagnetic ground states and electronic excitation can only be achieved through a one-electron orbital promotion. For complexes of elements of the second- and third-transition series containing strong ligands, this promotional requirement for excitation places the lowest excited states in the visible or near-infrared region of the spectrum. The large energy gap between the lowest excited states and the ground state allows radiative processes (emission) to compete with nonradiative ones (quenching). Thus, the powerful tools of emission spectroscopy (such as decay time and quantum yield

measurements) can be used to elucidate the electronic structures in spite of the general diffuseness of the observed spectra.

Studies have shown that emission spectral parameters at 77 K can be used as criteria for assigning orbital and spin labels to excited states and, when their temperature dependencies can be analyzed, for extracting detailed information on the splittings and radiative and radiationless rate constants of manifolds of excited states.³⁻⁵ If this information is coupled with appropriate theoretical models, insight into the disposition and characteristics of higher excited states (not seen in emission) can be gained.⁶

To date, the most comprehensive luminescence studies have been carried out on ruthenium(II) complexes containing π -conjugated ligands whose lowest excited states are charge-transfer-to-metal (CTTM) in nature and whose symmetry (D_3) is the highest possible for a trigonal complex with equivalent bidentate ligands. From these investigations a

model of CTTM excited states has been generated that focuses on the key role that spin-orbit coupling plays in dictating their properties and on the failure of S as a good quantum number.⁶ In contrast, emission measurements on d⁶ complexes of rhodium(III) that contain π -conjugated ligands have led to a $^3\pi\pi^*$ assignment for the emitting term^{7,8} and to the conclusion that spin-orbit coupling plays a minor role in dictating the state properties. For d⁶ complex ions, such as [Co(CN)₆]³⁻ whose emissions arise from a ³dd term, spin-orbit coupling plays an intermediate role.⁹

In the present article we address the question of the degree of ligand-ligand interaction in d⁶ complexes of ruthenium(II) and rhodium(III) containing π -conjugated ligands and report the results of a systematic investigation of the emission spectra of complexes of the type [M(bpy)_m(phen)_n]^{x+} ($m = 3 - n$, $n = 0, 1, 2, 3$; M is either Ru(II) with $x = 2$ or Rh(III) with $x = 3$).

Experimental Section

Syntheses, Purifications, and Analyses. All syntheses were carried out using reagent grade materials. [Ru(bpy)₃]Cl₂·6H₂O was purchased from G. Frederick Smith Chemical Co. and used directly. The starting materials, *cis*-[RhCl₂(NN)₂]Cl¹⁰ and *cis*-[RuCl₂(NN)₂]¹¹ [NN = 2,2'-bipyridine (bpy) or 1,10-phenanthroline (phen)], were prepared by literature methods or by appropriately modified procedures. Confirmation of the stoichiometry of all the synthesized complex ions was obtained by preparing additional species containing methyl- and phenyl-substituted ligands. Their compositions were verified by ¹H NMR measurements and elemental analyses.

Preparation of [Rh(bpy)₃](PF₆)₃. *cis*-[RhCl₂(bpy)₂]Cl·2H₂O (0.557 g, 1 mmol) and bpy (0.187 g, 1.2 mmol) in 50 ml of 75% ethanol (aqueous) were refluxed for about 17 h. The solution turned from a straw-yellow to a pale-yellow color. It was then filtered and evaporated to dryness on a rotoevaporator. The residue was dissolved in 10–15 ml of 0.1 N NaCl in 0.01 M PO₄³⁻ buffer, and the solution was filtered. The sample was loaded on a Bio-Gel column (vide infra) and eluted for about 2.5 h with 0.1 N NaCl (0.01 M PO₄³⁻) to remove a neutral colorless, a charged yellow, and a charged red band. Elution was continued with 0.5 N NaCl (0.01 M PO₄³⁻) to remove the colorless [Rh(bpy)₃]³⁺ fraction. The PF₆⁻ salt was obtained by slowly adding an aqueous, filtered, neutralized solution of NaPF₆ (0.5 g/10 ml) to the stirring solution of [Rh(bpy)₃]³⁺. The microcrystalline, white precipitate was collected, rinsed several times with cold water, and air dried. This salt was finally dried overnight at 100 °C, in vacuo, over P₄O₁₀; 70% yield. *Anal.* Calcd for [Rh(C₁₀H₈N₂)₃](PF₆)₃: C, 35.80; H, 2.41; N, 8.35. Found: C, 35.71; H, 2.31; N, 8.26.

Preparation of [Rh(bpy)₂(phen)](PF₆)₃, [Rh(bpy)(phen)₂](PF₆)₃, and [Rh(phen)₃](PF₆)₃. These complexes were prepared by substituting the appropriate starting materials and ligands and following the above procedure. *Anal.* Calcd for [Rh(C₁₀H₈N₂)₂(C₁₂H₈N₂)](PF₆)₃: C, 37.30; H, 2.35; N, 8.15. Found: C, 37.12; H, 2.24; N, 8.17. Calcd for [Rh(C₁₀H₈N₂)(C₁₂H₈N₂)₂](PF₆)₃: C, 38.73; H, 2.29; N, 7.96. Found: C, 38.34; H, 2.52; N, 8.07. Calcd for [Rh(C₁₂H₈N₂)₃](PF₆)₃: C, 40.09; H, 2.25; N, 7.79. Found: C, 40.06; H, 2.20; N, 7.72.

Preparation of [Rh(bpy)₃]Cl₃, [Rh(bpy)₂(phen)]Cl₃, [Rh(bpy)(phen)₂]Cl₃, and [Rh(phen)₃]Cl₃. [Rh(bpy)₃](PF₆)₃ (0.5 g) was dissolved in 50 ml of acetone. To this stirring solution was slowly added dropwise acetone, saturated with

LiCl, until the precipitation stopped. The white precipitate was collected, rinsed with acetone and then ether, and redissolved in 2 ml of methanol, and the solution was filtered. To this stirring, filtered methanol solution ether (9 ml) was slowly added, dropwise. After cooling to -10 °C the microcrystalline white precipitate was collected, rinsed with ether, and dried overnight at room temperature, in vacuo, over P₄O₁₀; 69% yield. *Anal.* Calcd for [Rh(C₁₀H₈N₂)₃]Cl₃·5H₂O: C, 46.92; H, 4.47; Cl, 13.85; N, 10.95. Found: C, 46.91; H, 4.14; Cl, 14.11; N, 10.94. Essentially the same procedure was used to prepare the other complexes. *Anal.* Calcd for [Rh(C₁₀H₈N₂)₂(C₁₂H₈N₂)]Cl₃·5H₂O: C, 48.53; H, 4.34; Cl, 13.43; N, 10.61. Found: C, 48.60; H, 3.99; Cl, 13.71; N, 10.56. Calcd for [Rh(C₁₀H₈N₂)(C₁₂H₈N₂)₂]Cl₃·6H₂O: C, 48.96; H, 4.36; Cl, 12.75; N, 10.08. Found: C, 48.93; H, 3.98; Cl, 13.43; N, 10.21. Calcd for [Rh(C₁₂H₈N₂)₃]Cl₃·5H₂O: C, 51.47; H, 4.08; Cl, 12.66; N, 10.01. Found: C, 51.35; H, 3.58; Cl, 13.18; N, 9.98.

Preparation of [Ru(bpy)₂(phen)]Cl₂, [Ru(bpy)(phen)₂]Cl₂, and [Ru(phen)₃]Cl₂. [RuCl₂(bpy)₂]·2H₂O (0.52 g, 1 mmol) and phen (0.23 g, 1.2 mmol) were dissolved in 75 ml 75% ethanol (aqueous). The solution was filtered and then refluxed overnight. The resultant cherry-red solution was cooled and evaporated to dryness, and the solid extracted three times with benzene or ether. The solid residue was then dissolved and filtered in 10–15 ml of methanol and passed down a Sephadex LH-20 column (vide infra). The middle portion of the cherry-red band was collected and evaporated to dryness. The dark crystalline solid was further dried at room temperature, in vacuo, over P₄O₁₀; 0.25 g yield. *Anal.* Calcd for [Ru(C₁₀H₈N₂)₂(C₁₂H₈N₂)]Cl₂·H₂O: C, 56.39; H, 3.70; Cl, 10.40; N, 12.33. Found: C, 56.84; H, 4.26; Cl, 10.14; N, 12.28. The other complexes were prepared by substituting the appropriate starting materials and following the above procedure. *Anal.* Calcd for [Ru(C₁₀H₈N₂)(C₁₂H₈N₂)₂]Cl₂· $\frac{9}{2}$ H₂O: C, 53.05; H, 4.33; Cl, 9.21; N, 10.92. Found: C, 53.09; H, 3.55; Cl, 9.39; N, 11.06. [Ru(C₁₂H₈N₂)₃]Cl₂·xH₂O was not analyzed. Analysis of the PF₆⁻ salt is given below.

Preparation of [Ru(bpy)₂(phen)](PF₆)₂, [Ru(bpy)₃](PF₆)₂, [Ru(bpy)(phen)₂](PF₆)₂, and [Ru(phen)₃](PF₆)₂. Ru(bpy)₂(phen)]Cl₂·H₂O (0.1 g) was dissolved in 30 ml of water. To this filtered stirring solution was added slowly a filtered, neutral solution of aqueous NaPF₆ (0.3 g in 15 ml). The precipitate was collected, rinsed several times with water, then with ethanol, and finally with ether. The microcrystalline, red-orange solid was dried overnight at 100 °C, in vacuo, over P₄O₁₀. *Anal.* Calcd for [Ru(C₁₀H₈N₂)₂(C₁₂H₈N₂)](PF₆)₂: C, 43.49; H, 2.74; N, 9.51. Found: C, 43.79; H, 2.70; N, 9.62. Essentially the same procedure was used to prepare the other complexes. *Anal.* Calcd for [Ru(C₁₀H₈N₂)₃](PF₆)₂: C, 41.91; H, 2.82; N, 9.78. Found: C, 41.90; H, 2.75; N, 9.78. Calcd for [Ru(C₁₀H₈N₂)(C₁₂H₈N₂)₂](PF₆)₂: C, 44.98; H, 2.67; N, 9.26. Found: C, 44.87; H, 2.37; N, 9.17. Calcd for [Ru(C₁₂H₈N₂)₃](PF₆)₂: C, 45.50; H, 2.80; N, 8.80. Found: C, 45.92; H, 2.55; N, 8.80.

Preparation of the Bio-Gel¹² and Sephadex¹³ Columns. Bio-Gel CM-2 (Bio-Rad 100–200 mesh, 20 g) was stirred for 14 h in 500 ml of 0.1 N NaCl in 0.01 M PO₄³⁻ buffer. The gel was poured into a column (2.5 i.d. × 46 cm) and yielded a bed volume of 110 ml with a flow rate of about 3.5 ml/min. About 1.5 l. of starting buffer was eluted through the column before adding the sample. The column effluent was monitored with a uv absorbance monitor. A 0.01 M PO₄³⁻ buffer was prepared by dissolving NaH₂PO₄·H₂O (0.9 g), Na₂HPO₄ (3.2 g), and NaN₃ (0.6 g) in 3 l. of water. The resultant pH was about 7.3. The Sephadex LH-20 column was prepared by stirring 115 g

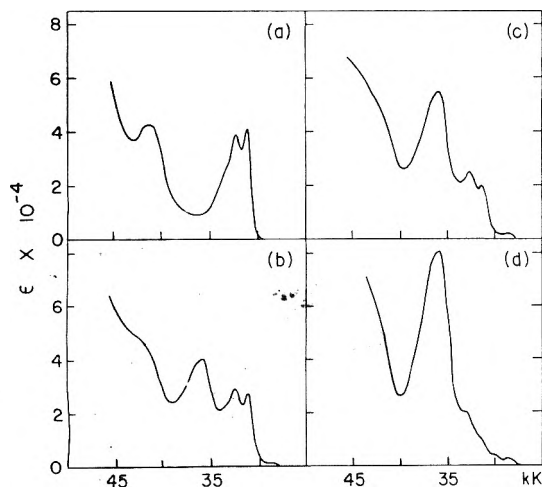


Figure 1. Absorption spectra of rhodium(III) chelates in ethanol-methanol (4:1, v/v) at room temperature: (a) $[\text{Rh}(\text{bpy})_3]\text{Cl}_3$, (b) $[\text{Rh}(\text{bpy})_2(\text{phen})]\text{Cl}_3$, (c) $[\text{Rh}(\text{bpy})(\text{phen})_2]\text{Cl}_3$, (d) $[\text{Rh}(\text{phen})_3]\text{Cl}_3$.

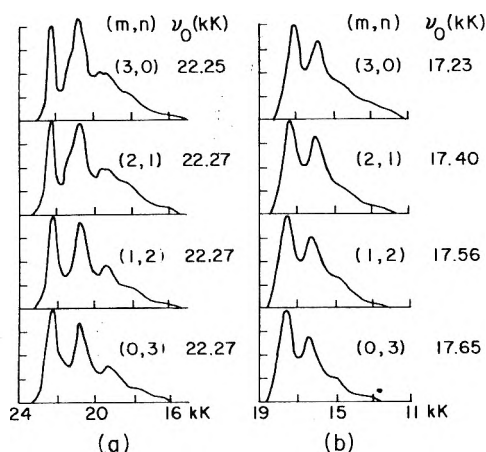


Figure 2. Emission spectra of rhodium(III) and ruthenium(II) chelates in clear ethanol-methanol (4:1, v/v) glasses at 77 K: (a) $[\text{Rh}(\text{bpy})_m(\text{phen})_n]\text{Cl}_3$, (b) $[\text{Ru}(\text{bpy})_m(\text{phen})_n]\text{Cl}_2$; $m = 3 - n$, $n = 0, 1, 2, 3$.

of dry Sephadex LH-20 in 500 ml of methanol for 2 h. This slurry was poured into a large column (2.5 i.d. \times 120 cm) and eluted with about 600 ml of methanol before addition of the first sample. The flow rate was about 2.6 ml/min, and the sample size, about 0.5 g.

Elution rates of inorganic complexes on these columns are exceedingly sensitive to both size and structure. Mixed chelates separate clearly into identifiable bands that are not coincident with bands arising from the trigonal parent species.

Spectroscopic Measurements. All absorption spectra were measured at room temperature on a Cary Model 14 spectrophotometer. The emission spectra were measured on samples dissolved in a glass at 77 K (4:1, v/v ethanol-methanol) and have been corrected for wavelength dependence of the instrument.¹⁴ Emission spectra of the rhodium complexes were measured on a Hitachi Perkin-Elmer Model MPF-2A spectrofluorimeter, and those of the ruthenium complexes were measured with a near-infrared spectrophotometer constructed in the laboratory.⁷ Quantum efficiencies¹⁴ and temperature-dependent lifetimes⁴ were measured as previously described, with the exception that in place of a plastic matrix, a glass (4:1, v/v ethanol-methanol) contained in a specially constructed copper sample holder was employed. Each reported measured

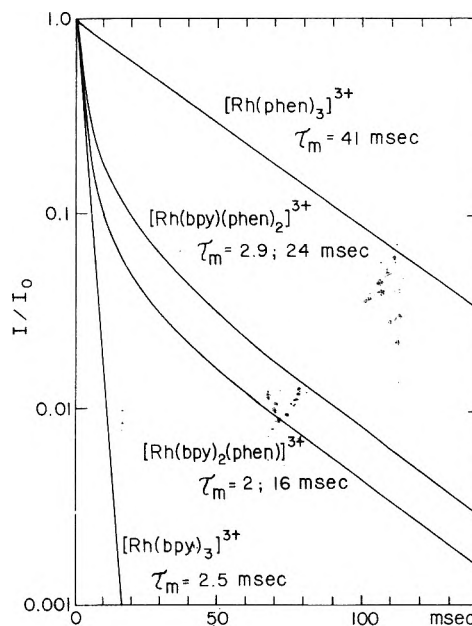


Figure 3. Phosphorescence decay of rhodium(III) complexes. Semi-logarithmic plots of normalized intensity vs. time for $[\text{Rh}(\text{bpy})_m(\text{phen})_n]\text{Cl}_3$ at 77 K in ethanol-methanol (4:1, v/v) glasses. Excitation at 337 nm by pulsed nitrogen laser. For mixed chelates, the decays were analyzed into two exponentials whose τ_m are given on the figure.

lifetime, τ_m , is the average of at least five measurements. At both 77 and 4.2 K the luminescence decays for the ruthenium(II) complexes were exponential over at least three mean lives. For the rhodium(III) complexes containing three identical ligands strict exponentiality was observed. For the mixed-ligand complexes of rhodium(III) only nonexponential decays were obtained.

The ^1H NMR spectra were obtained on a Varian Model HA-60 using sodium 3-trimethylsilylpropanesulfonate (DSS) as an internal standard. The chemical shifts were all estimated in Hz downfield from DSS.

Results

Optical Properties of Rhodium(III) Complexes. Absorption spectra for the four complexes of rhodium(III) are displayed in Figure 1. It is apparent that the two prominent peaks lying in the region 30–35 kK that are characteristic of the bipyridine ligands are progressively replaced by the intense band at approximately 36 kK that is characteristic of the 1,10-phenanthroline moiety as the series becomes richer in phen ligand. In Figure 2 the emission spectra show a similar trend, but the differences are subtle. In fact, both the frequency of the luminescence origin and the band structure remain essentially the same for the series.

The measured decay time of the observed phosphorescence for a rhodium(III) complex is a sensitive index of the molecular structure. As shown in Figure 3, the exponential decay of 2.5 ms for $[\text{Rh}(\text{bpy})_3]^{3+}$ is replaced by nonexponential decays for $[\text{Rh}(\text{bpy})_2(\text{phen})]^{3+}$ and $[\text{Rh}(\text{bpy})(\text{phen})_2]^{3+}$ but becomes exponential once more for $[\text{Rh}(\text{phen})_3]^{3+}$, albeit with a much longer lifetime (41 ms).

Optical Properties of Ruthenium(II) Complexes. The emission spectra (77 K) of the series of four ruthenium(II) complexes are also displayed in Figure 2. Unlike the analogous rhodium(III) spectra, those for the ruthenium(II) species show a progressive shift of origin as phen replaces bpy in the coord-

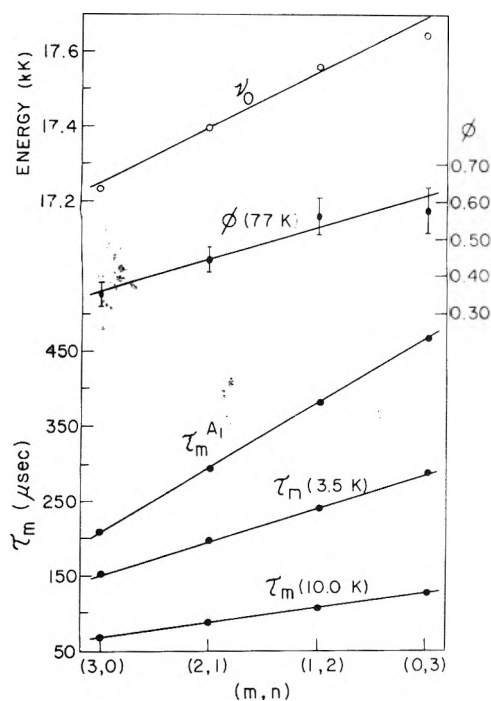


Figure 4. Optical parameters of ruthenium(II) chelates. All measurements were performed on $[\text{Ru}(\text{bpy})_m(\text{phen})_n]\text{Cl}_2$ ($m = 3 - n$, $n = 0, 1, 2, 3$) dissolved in ethanol-methanol (4:1, v/v) glasses: ν_0 = frequency of highest energy vibrational peak (top left-hand scale); ϕ = absolute quantum efficiency (right-hand scale); $\tau_m^{A_1}$ = limiting measured decay time at 0 K, $\tau_m(3.5 \text{ K})$ and $\tau_m(10.0 \text{ K})$ = measured decay times at 3.5 and 10.0 K, respectively (lower left-hand scale).

dination sphere. The structure of the emission, however, remains invariant.

Several indices relevant to the properties of the lowest excited states of the four chelates of ruthenium(II) are plotted on Figure 4 as a function of ligand composition. They are (a) the frequency of the band origin, (b) the measured quantum yield, ϕ , at 77 K, (c) the measured decay time extrapolated to 0 K (vide infra), (d) the measured mean decay time at 3.5 K, and (e) the measured mean decay time at 10 K. For the fixed point of 77 K the measured decay times of $[\text{Ru}(\text{bpy})_m(\text{phen})_n]^{2+}$ in ethanol-methanol (4:1, v/v) are 5.2, 6.6, 9.1, and 9.8 μs for $(m, n) = (3, 0), (2, 1), (1, 2),$ and $(0, 3)$, respectively.

^1H NMR Spectra. A final index of the chemical composition of each series of complexes is given in Figure 5 where the chemical shifts in D_2O of selected ligand protons relative to the internal standard (DSS) are displayed. To quantify the trends in chemical shifts the protons H_3 and H_3' of bpy and H_4 and H_7 of phen were selected. Both of these protons appear in the downfield portion and as apparent doublets in their respective spectra based on the full analyses of $[\text{Fe}(\text{bpy})_3]^{2+}$ and $[\text{Ru}(\text{phen})_3]^{2+}$.^{15,16} In the spectra of the complexes containing both types of ligands, these resonances appear as a broad doublet since the absorptions of H_3 and H_3' fall approximately at the same frequency as those of H_4 and H_7 . As one can perceive instantly from Figure 5, the chemical shift of these ring protons of the ruthenium(II) complexes changes dramatically with ligand composition, whereas for the rhodium(III) species, the change is slight.

Discussion

Rhodium(III) Complexes. The long lifetimes ($> \text{ms}$) of the emissions observed for all complexes of the type $[\text{Rh}(\text{bpy})_m(\text{phen})_n]^{3+}$ clearly label them as phosphorescences, i.e., spin-forbidden transitions. The frequencies and the structures of the emission bands also clearly identify them as essentially ligand-localized transitions of $\pi\pi^*$ type. Thus, we assign the emitting level(s) of all four rhodium complexes to be $^3\pi\pi^*$. These assignments are in concert with previous work.^{7,8} Because all the decay times are in the millisecond range, we also infer that the amount of singlet character mixed into the lowest triplet term is also exceedingly small.

A distinguishing feature of the two mixed chelates is the incidence of nonexponential decay of the phosphorescence. This behavior, first reported by Halper and DeArmond,¹⁷ strongly suggests that the coordinated ligands are virtually isolated from each other and are effectively decaying independently. We have chosen to deconvolute our decay data into two exponentials, although three have been used.¹⁷ As shown in Figure 3, the curve resolutions of the mixed chelates produce a short decay time component comparable in magnitude to that of the $[\text{Rh}(\text{bpy})_3]^{3+}$ species coupled with a longer component that begins to approach the single decay time of $[\text{Rh}(\text{phen})_3]^{3+}$. Since the observed emission spectra are superposable, one is led to the proposition that the excitation energy residence time on an individual ligand is not short compared to the intrinsic ligand decay time, a conclusion reached by Halper and DeArmond.

Another indicator, but a less sensitive one, of the relative isolation of the chelated ligands is the preservation of the integrity of the characteristic uv absorption bands of the bpy and phen ligands as the ligand composition changes (Figure 1). In fact, it is exceedingly difficult to distinguish the absorption spectrum of a $[\text{Rh}(\text{bpy})_m(\text{phen})_n]^{3+}$ ion from that of an $m[\text{Rh}(\text{bpy})_3]^{3+}/n[\text{Rh}(\text{phen})_3]^{3+}$ mixture.

The ^1H NMR data (Figure 5) show that the magnetic screening of the proton nuclei by the ring electrons is affected by the presence of the other ligands to a slight extent. The ligand coupling, both in the ground state and the $^3\pi\pi^*$ excited term, is weak.

Ruthenium(II) Complexes. In contrast to the long-lived ($> \text{ms}$) blue-green emissions displayed by the rhodium(III) complexes, those arising from $[\text{Ru}(\text{bpy})_m(\text{phen})_n]^{2+}$ are short lived ($\sim 5 \mu\text{s}$ at 77 K), lie in the orange region of the spectrum, and display the $\sim 1300\text{-cm}^{-1}$ prominent vibrational structure characteristic of $d\pi^* \rightarrow ^1A_1$ transitions involving these ligands

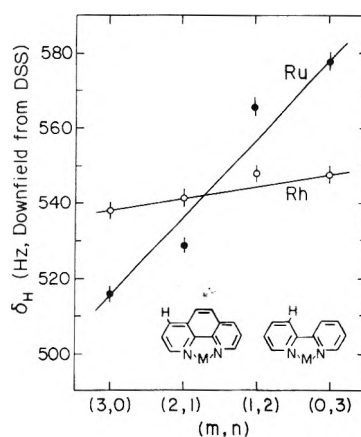


Figure 5. Chemical shifts of selected protons in rhodium(III) and ruthenium(II) chelates of type $[\text{M}(\text{bpy})_m(\text{phen})_n]\text{X}$ ($\text{M} = \text{Rh}$, $\text{X} = \text{Cl}_3$; $\text{M} = \text{Ru}$, $\text{X} = \text{Cl}_2$; $m = n - 3$; $n = 0, 1, 2, 3$). Proton magnetic resonance frequencies are plotted for a broad doublet that is composed of the H_3 and H_3' signal from the bpy ligands and the H_4 and H_7 signal from the phen ligands. All shifts were measured downfield from sodium 3-trimethylsilylpropanesulfonate (DSS).

(Figure 2). In fact, the $[\text{Ru}(\text{bpy})_3]^{2+}$ complex ion is the prototype of a charge-transfer emitter. Both $[\text{Ru}(\text{bpy})_3]^{2+}$ and $[\text{Ru}(\text{phen})_3]^{2+}$ have been studied extensively, and the charge-transfer assignment is no longer in doubt.⁴ For the mixed-ligand species we make the same assignment.

Whereas the rhodium(III) mixed ligand chelates exhibit optical properties indicative of vanishingly small ligand–ligand interaction in the $^3\pi\pi^*$ state, the $[\text{Ru}(\text{bpy})_m(\text{phen})_n]^{2+}$ complexes display behavior that points to strong ligand–ligand interaction in the lowest $d\pi^*$ excited configuration. In fact, as seen in Figure 4, virtually every measurable optical property of the mixed ligand molecules that can be traced to the lowest $d\pi^*$ excited configuration can be obtained from a simple interpolation between the tris chelate end points. This remarkable consistency leads us to the conclusion that the electronic structure of a mixed-ligand ruthenium(II) ion is best viewed as an inherent property of the entire complex and not as a consequence of weakly coupled ligand electronic systems.

With the exception of $\tau_m^{A_1}$, all the quantities plotted on Figure 4 are derived directly from experimental measurements without any concatenation of intervening logic. The quantity $\tau_m^{A_1}$ requires, however, some explanation. Extensive studies of the temperature dependence of the decay times of the charge-transfer luminescence emanating from a series of ruthenium(II) chelates led to the development of a multiple-state phenomenological model to rationalize the results.¹⁸ Briefly, the emission is viewed as arising from a manifold of several states that remain in Boltzmann equilibrium throughout the decay process. Such a view is quantified in the expression

$$\tau_m(T) = \frac{1 + 2e^{-\Delta\epsilon_1/kT} + e^{-\Delta\epsilon_2/kT}}{(1/\tau_1) + (2/\tau_2)e^{-\Delta\epsilon_1/kT} + (1/\tau_3)e^{-\Delta\epsilon_2/kT}}$$

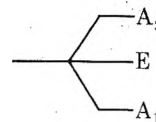
Here $\tau_m(T)$ is the measured decay time of a three-level ensemble, whose second level is degenerate, after an excitation flash. The equation was derived for a trigonal (D_3) complex¹⁸ but would be applicable to any three-level system obeying the assumptions built into it, if the factors of 2 were deleted from the second terms. The important point is that a computer fit of $\tau_m(T)$ over a temperature range of ~ 2 –100 K leads to a unique value for τ_1 . For trigonal molecules displaying charge-transfer luminescence a theoretical model assigns the label A_1 to the lowest level,⁶ and thus $\tau_m^{A_1} = 1/k_1$ can be identified as the limiting measured decay time at 0 K.

The data from extensive experimental studies of trigonal (D_3) complexes of ruthenium(II) have been analyzed using the above equation, and all yield reasonable values for both τ_i and ϵ_i .^{4,5} Surprisingly, however, analogous data for the mixed-ligand chelates $[\text{Ru}(\text{bpy})_2(\text{phen})]^{2+}$ and $[\text{Ru}(\text{bpy})(\text{phen})_2]^{2+}$ can also be fit to the equation over large temperature ranges. This brings us to the question: Is the low (C_2) symmetry of a mixed-ligand complex reflected in the excited state levels and thus the molecules are really emitting from a four-level manifold with one level too high to be thermally populated, or does a mixed-ligand complex essentially retain a D_3 electronic symmetry in charge-transfer excited states? A third alternative is that our data on trigonal (D_3) complexes have been misinterpreted. Irrespective of what model one uses, however, $\tau_m^{A_1}$ represents the limiting decay time for a given complex ion at 0 K. From our data on mixed-ligand chelates this quantity appears to be a weighted average of the values found for the parent tris complexes. Thus, we are led to the conclusion that even the single lowest state of a $d\pi^*$ emitting manifold in a mixed-ligand complex possesses

properties that are weighted averages of the analogous states of the two tris parents.

If one accepts our view that the luminescence arising from all the ruthenium(II) complexes discussed here really emanates from a manifold of levels whose populations are temperature dependent, the data in Figure 4 lead one to the further conclusion that *all* the emitting levels possess properties that are weighted averages of the corresponding levels of the parent tris complexes. Furthermore, the temperature dependent τ and ϕ curves of the mixed-ligand complexes allow them to be fit to a three-level scheme. From an analysis of all the data we came to the conclusion that within the accuracy of our current measurements the mixed-ligand chelates are exhibiting a higher electronic symmetry (D_3) than the molecular geometry.

Once we adopt the view that the excited $d\pi^*$ states of all four complexes of the formula $[\text{Ru}(\text{bpy})_m(\text{phen})_n]^{2+}$ reflect trigonal symmetry, the mathematical model previously proposed for the tris species can be applied quantitatively. The model leads to a description of the lowest $d\pi^*$ configuration as a set of three levels (four states) whose splittings are small and are a consequence of weak exchange interactions between the excited (optical) electron that resides in an a_2 (D_3 symmetry) orbital encompassing all three ligands and the electrons remaining in the d^5 core. The derived energy-level scheme is depicted below. For infinite separation of the optical electron from the metal ion core these levels would collapse into a fourfold degenerate set.



The quantitative descriptions of each of these states are given in ref 6, eq 17a, b, c. The feature pertinent to the current discussion is that the wave function for each state given above contains the ligand a_2 orbital. The expression is

$$\psi(a_2) = \frac{1}{\sqrt{3}} \{\chi_1 + \chi_2 + \chi_3\}$$

where χ_i is the lowest antibonding π orbital on the i th ligand, and ligand–ligand overlap is ignored. For trigonal complexes with D_3 symmetry this expression is correctly symmetry adapted. For mixed-ligand chelates of the type discussed here we assume the equality of the coefficients to remain. From this point of view each single state and thus the entire $d\pi_{a_2}^*$ excited manifold should reflect properties that are averages of those exhibited by the parent tris complexes, in concert with the data. Thus, the excited charge-transfer states are really best described as true molecular states in which the optical electron resides on all three ligands.

Finally, we turn to the ground state electronic structure of the ruthenium(II) chelates as reflected in the ^1H NMR data. As seen in Figure 5 there is a strong correlation between the ring proton chemical shifts and the composition of the ligand sphere. It is apparent that the magnetic screening of the proton nuclei by the ring electrons is affected through the metal in the case of ruthenium(II) complexes. There is electronic communication among the ligands. If one assumes some charge-transfer excited configurational mixing in the ground state, i.e.

$$|\psi_{gs}\rangle = a|d^6\rangle + b|d^5\pi^*\rangle$$

then a mechanism for electronic interaction is available if the

π^* orbital is viewed as extending over all three ligands, exactly what the luminescence measurements demand. From this point of view $d\pi$ back-bonding could be placed on a semi-quantitative foundation.

References and Notes

- (1) (a) Research supported by AFOSR(NC)-OAR, Grants No. AFOSR-72-2207 and 76-2932. (b) Plenary address presented at the Michael Kasha Symposium on Energy Transfer in Organic, Inorganic, and Biological Systems, Florida State University, Jan 8-10, 1976.
- (2) M. K. DeArmond, *Acc. Chem. Res.*, **7**, 309 (1974).
- (3) G. A. Crosby, *Acc. Chem. Res.*, **8**, 231 (1975).
- (4) G. D. Hager and G. A. Crosby, *J. Am. Chem. Soc.*, **97**, 7031 (1975).
- (5) G. D. Hager, R. J. Watts, and G. A. Crosby, *J. Am. Chem. Soc.*, **97**, 7037 (1975).
- (6) K. W. Hipps and G. A. Crosby, *J. Am. Chem. Soc.*, **97**, 7042 (1975).
- (7) D. H. W. Carstens and G. A. Crosby, *J. Mol. Spectrosc.*, **34**, 113 (1970).
- (8) M. K. DeArmond and J. E. Hillis, *J. Chem. Phys.*, **54**, 2247 (1971).
- (9) G. A. Crosby, K. W. Hipps, and W. H. Elfring, Jr., *J. Am. Chem. Soc.*, **96**, 629 (1974).
- (10) P. M. Gidney, R. D. Gillard, and B. T. Heaton, *J. Chem. Soc., Dalton Trans.*, 2621 (1972).
- (11) B. Bosnich and F. P. Dwyer, *Aust. J. Chem.*, **19**, 2229 (1966).
- (12) Registered trademark, Bio-Rad Laboratories.
- (13) Registered trademark, Pharmacia Fine Chemicals.
- (14) J. N. Demas and G. A. Crosby, *J. Am. Chem. Soc.*, **92**, 7262 (1970).
- (15) S. Castelano, H. Gunther, and S. Ebersole, *J. Phys. Chem.*, **69**, 4166 (1965).
- (16) J. D. Miller and R. H. Prince, *J. Chem. Soc.*, 3185 (1965).
- (17) W. Halper and M. K. DeArmond, *J. Lumin.*, **5**, 225 (1972).
- (18) R. W. Harrigan and G. A. Crosby, *J. Chem. Phys.*, **59**, 3468 (1973); R. W. Harrigan, G. D. Hager, and G. A. Crosby, *Chem. Phys. Lett.*, **21**, 487 (1973).

Discussion

M. GOUTERMAN. Do you see the charge-transfer transition in the rhodium complexes?

G. A. CROSBY. Yes, in these molecules, we have somewhat unconvincing evidence that we see a charge-transfer band. It's located among the $\pi\pi^*$ s. We definitely see a charge-transfer band in tris(acetylacetonato)rhodium(III). If one makes tris(acetylacetonates) of, say, the rare earths, such as gadolinium or lanthanum, then one sees, just as he sees in most closed shell ions, a beautiful carbonyl band right around 2900 Å. When one makes the corresponding rhodium complex, that band is gone. Two new bands appear, however, shifted symmetrically from the original one. We think we are getting a near coincidence of charge transfer and $\pi\pi^*$ levels. It's a very convincing demonstration. It happens both for iridium and for rhodium, so I do think in the acetylacetonates we do see some charge transfer. That may be charge transfer into the metal and not charge transfer out to the ligands, however. I don't know what it is.

D. S. McCLURE. Have you done enough examples to obtain correlations between ionization potentials or electron affinities of donors and acceptors and the energies of the charge-transfer bands?

G. A. CROSBY. I think we can do that. I haven't shown it today, but there's a great deal of data lying around in my laboratory not yet published that demonstrates some correlation. For instance, when one oxidizes Ru(II) to Ru(III), that is very easy to do. In fact it is so easy to do it often happens on the columns and things. The charge-transfer bands are correspondingly low in energy. If you think of charge transfer as an incipient oxidation, then this correlation is easy to understand. Oxidation of Ir(III) to Ir(IV) would be the analogous process. That's much tougher to do; it is difficult to pull the electron off. It is significant that we see charge-transfer spectra for these iridium(III) complexes, but they are moved up into the high-energy region of the spectrum. In fact, they begin to crowd into the $\pi\pi^*$ transitions, and one sees interesting mixing between charge-transfer and $\pi\pi^*$ states. So, from the standpoint of ease of oxidation of the metal ions, the charge-transfer bands do march around the way one would expect. I haven't attempted to carry out any systematic correlations, however.

M. KASHA. I have a question relative to the last slide and especially in terms of distinguishing between the charge transfer and $\pi\pi^*$ states, which by now are qualitatively rather similar spectroscopically except for lifetime. And the question is: Have you thought of using $MgCl_2 \cdot 6H_2O$ as a medium?

G. A. CROSBY. Yes. Professor Kasha is mentioning to me one of his old discoveries, using magnesium chloride as a glass. We have attempted to do that. Unfortunately, these are cations, and so with high concentrations of chloride, they all precipitate out. Even for a molecular species one has trouble with that glass. Of course, I have looked for years for hosts to put these substances in, and the only host I have found (I have not discussed the crystal work today) is tris(2,2'-bipyridine)zinc sulfate heptahydrate that forms an orthorhombic crystal. We have doped into that lattice both osmium(II) and ruthenium(II) complexes. We have studied the latter in this host in many, many ways; for instance, emission from surfaces, polarization, circularly polarized emission, etc.

W. R. MOOMAW. With the large difference in the lifetimes of the dual luminescences you observed for the mixed ligand chelates, it should be possible to do time-resolved spectroscopy. Have you had an opportunity to do this, and thereby obtain the luminescence from each state separately?

G. A. CROSBY. A very good question. Professor K. DeArmond at North Carolina State, working with simple apparatus, the best he had, began to try to look for that. When I first read his work, I thought it was impurity emission. It's not; I don't think so now. Recently, we have built a nitrogen-pulsed laser, and we are procuring a box-car integrator. With this equipment we want to do these very experiments; we wish to scan through the emission and see if we can see it change as a function of observation wavelength. Professor Richard Watts at the University of California, Santa Barbara, who spent several years in my laboratory, is doing this sort of thing on iridium complexes. He is detecting, as he scans through certain emission bands, resolvable multiple lifetimes of the emission. He interprets this as the incidence of emission from closely-lying states that are not thermally equilibrating.

Photoelectron Spectra of Carbonyls, Propellenes and Propellanones¹

D. Dougherty, J. J. Bloomfield,[†] G. R. Newkome, J. F. Arnett,[‡] and S. P. McGlynn*

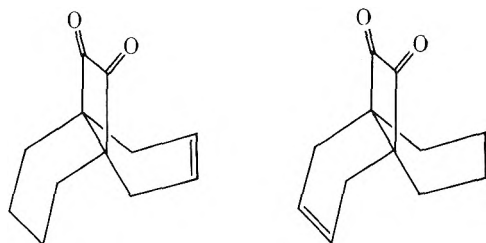
The Coates Chemical Laboratories, The Louisiana State University, Baton Rouge, Louisiana 70803 (Received February 9, 1976)

The He I photoelectron spectra (UPS) of a number of unsaturated [4.4.2]propellanes and [4.4.2]propellane-dione derivatives are presented. The interpretation of the UPS data is based on through-space and through-bond interaction models and on CNDO/s computations. An analysis of the photoelectron spectra of [4.4.2]propella-3,8-diene-11,12-dione (1), [4.4.2]propell-3-ene-11,12-dione (2), [4.4.2]propellane-11,12-dione (3), [4.4.2]propella-3,8-dien-11-one (4), and [4.4.2]propella-3,8-diene (5) involves the assignment of n_+ , n_- , π_+ , π_- , and σ_{\square} (i.e., cyclobutane σ) ionization events. The analysis of the data for 5, [4.4.2]propella-3,8,11-triene (6), [4.4.2]propella-3,11-diene (7), and [4.4.2]propell-11-ene (8) leads us to the conclusion that the photoelectron spectrum of 6 should be reassigned. The ${}^1\Gamma_{n\pi^*} \leftarrow {}^1\Gamma_1$ absorption spectra of 1, 2, and 3 have been investigated as a function of temperature. The low energy of this transition in 1 is attributed to a high degree of CO/CO coplanarity, the high energy of this transition in 3 is attributed to CO/CO noncoplanarity, and the isomerism evident in 2 is attributed to multiple minima of the potential energy along the CO/CO dihedral angle coordinate of the ground state.

Introduction

Considerable recent work has been invested in the [4.4.2]-propellanes. Gleiter et al.² have investigated the photoelectron spectra (UPS) of the polyunsaturated [4.4.2]propellanes. In specific, they have made a quite tentative assignment of the UPS of compounds 6, 7, and 8 of Figure 1. These assignments were based on a model which was described as "interaction of semi-localized π -orbitals". This model, while intuitively appealing, is very difficult to parametrize. Hence, the assignments of Gleiter et al.² are vested in three types of parametric inputs: (a) The zero-order energies of the semilocalized π orbital for substituted cyclohexene and cyclobutene entities; (b) The magnitudes of the two types of "through-space" interactions (i.e., cyclohexene-cyclohexene and cyclohexene-cyclobutene); and (c) The extent of the various "through-bond" interactions of the π and σ orbitals. The net result of these considerations was the provision of a "working hypothesis" on which the tentative UPS assignments were based.²

The uv-vis and ir spectra of the diones, compounds 1, 2, and 3 of Figure 1, have been investigated by Bloomfield and Moser.^{3a} They suggested that 2 exists in two isomeric forms in solution. These two forms were thought to be



They also found that the ${}^1\Gamma_{n\pi^*} \leftarrow {}^1\Gamma_1$ transition of 1 occurred at rather long wavelengths, $\lambda_{\max} = 537.5 \text{ m}\mu$ and $\epsilon = 71.7$. This latter observation, which implies a low-energy ${}^1\Gamma_{n\pi^*}$ state of 1, was attributed to "resonance stabilization of the excited state involving a double bond and the dione system". This

conclusion was later revised by Neely et al.^{3b} and the dominance of "through-bond" interactions with the σ orbitals was asserted. In particular, these latter authors seem to be of the opinion that the major effect, and the one presumed to be capable of interpreting the low-energy ${}^1\Gamma_{n\pi^*} \leftarrow {}^1\Gamma_1$ transition of 1, is the interaction of the higher-energy, non-bonding, filled orbital of the dicarbonyl grouping with both σ and π orbitals of the remainder of the molecule.

In this paper, we present and interpret the photoelectron spectra of 1, 2, 3, 4a, and 5 of Figure 1. This work was undertaken for a number of reasons. These are: (i) To ascertain the presence or absence of isomerism of 2 in the gas phase. (ii) To determine whether the filled MO sequence of the ground state of 1 provides any clues to the origin of the low-energy ${}^1\Gamma_{n\pi^*} \leftarrow {}^1\Gamma_1$ transition. (iii) To determine the effects of ethylenic π insertions on the n -MO energies in the series 3:2:1. (iv) To investigate the effects of carbonyl group insertions on the π -MO energies in the series 5:4a:1. (v) To elicit and classify the subset of weakly bound σ MO's on the cyclobutane ring. Two of these are expected to lie in the 10–11-eV range and to be sensitive to ethylenic and, especially, carbonyl bond insertions. (vi) To correlate the UPS data obtained for 5 with that published² for 6, 7, and 8. Heilbronner⁴ has recently proposed a rather simple scheme for the assignment of the lower-energy electronic states of unsaturated hydrocarbon radical cations. With reference to Figure 1, this method implies that a knowledge of the photoelectron spectrum of 6 should lead to an assignment of that of 5. It was of interest to determine whether or not this was the case.

The photoelectron spectra of 6, 7, and 8 were determined previously.² Professor Heilbronner² has been gracious enough to provide us with copies of the original photoelectron spectra for these compounds.

This work also reports CNDO/s MO calculations⁵ for 1, 4a, 5, 6, and 7, and utilizes these computational results, in conjunction with the experimental data, to attempt answer to queries (i)–(vi) posed above. Finally, the absorption spectra of 1, 2, and 3 were investigated as a function of temperature in order to arrive at some consensus concerning queries (i) and (ii) above.

[†] Monsanto Co., St. Louis, Mo. 63188.

[‡] Dow Chemical Co., Wayland, Mass.

Experimental Section

The He I photoelectron spectra (UPS) of **1**, **2**, **3**, **4a**, and **5** were obtained on a Perkin-Elmer PS-18 photoelectron spectrometer, using Xe and Ar for calibration. All experimental details concerning apparatus, techniques, and measurements are available elsewhere.⁶

Absorption studies of **1**, **2**, and **3** in the visible region were performed on a Cary 14 instrument. The absorption spectra of glassy and liquid solutions, range 400–77 K, were obtained using the apparatus of Freeman and Lewis.⁷ The glassy matrix was EPA, which is a 5/5/2 by volume mixture of ether/isopentane/ethanol, respectively.

All melting points were obtained in capillary tubes with a Thomas-Hoover Uni-Melt and are uncorrected. Infrared spectra (ir) were recorded with a Perkin-Elmer Model 621 spectrophotometer. Nuclear magnetic resonance (NMR) spectra were recorded on a Varian Associates H-60A spectrometer, tetramethylsilane being used as an internal standard. The carbon-13 magnetic resonance (¹³C NMR) data were obtained on a Bruker HFX spectrometer equipped with Fourier transform.

[4.4.2]Propella-3,8-diene-11,12-dione (**1**) was prepared from 9,10-dimethyl- $\Delta^{2,6}$ -hexalindicarboxylate by previously described procedures: mp 119–120 °C (lit.⁸ mp 119.6–120.8 °C); ¹³C NMR (CDCl₃-TMS) δ 62.9 (C-1, 6), 30.5 (C-2, 5, 7, 10), 127.2 (C-3, 4, 8, 9); $\lambda_{\text{max}}^{\text{C}_6\text{H}_{12}} = 537.5 \text{ m}\mu$ ($\epsilon = 71.7$).

[4.4.2]Propell-3-ene-11,12-dione (**2**) was prepared from 9,10-dimethyl- Δ^2 -octalindicarboxylate by previously described procedures:⁸ mp 45–46 °C (lit.⁸ mp 46.7–48.3 °C); ¹³C NMR (CDCl₃-TMS) δ 60.7, 57.3 (C-1, 6) 28.8, 27.5 (C-2, 5 and C-7, 10), 19.5 (C-8, 9), 125.4 (C-3, 4); $\lambda_{\text{max}}^{\text{C}_6\text{H}_{12}} = 460\text{--}464 \text{ m}\mu$ ($\epsilon = 38.8$), 532–535 m μ ($\epsilon = 32$).

[4.4.2]Propella-11,12-dione (**3**) was prepared from 9,10-dimethyldecalindicarboxylate by previously described procedures:⁸ mp 44–45 °C (lit.⁸ mp 42.5–43.4 °C); ¹³C NMR (CDCl₃-TMS) 56.1 (C-1, 6), 26.5 (C-2, 5, 7, 10), 20.9 (C-3, 4, 8, 9); $\lambda_{\text{max}}^{\text{C}_6\text{H}_{12}} = 461 \text{ m}\mu$ ($\epsilon = 73$).

[4.4.2]Propella-3,8-dien-11-one (**4**). To zinc amalgam, prepared from zinc granules (50 g), water (100 ml), mercuric chloride (5 g), and concentrated hydrochloric acid (10 ml), was added 6 N hydrochloric acid (100 ml), pentane (150 ml), and 12-hydroxy[4.4.2]propella-3,8-dien-11-one (**9**) (mp 88–89 °C, 10 g, 5.3 mol). The mixture was vigorously stirred for 5 h at 26 °C and then for 11 h at 35 °C. After cooling, the pentane layer was decanted, washed with water and a sodium bicarbonate solution, dried over anhydrous magnesium sulfate, and evaporated to provide a pale-yellow solid. Recrystallization from hexane gave (40%) of the pure ketone **4**: mp 78–80 °C; NMR (CDCl₃) δ 2.63 (CH₂CO, s, 2 H), 1.7–2.6 (allylic H, m, 8 H), 5.6–6.0 (vinylic H, m, 4 H); ir (CCl₄) 1773 cm⁻¹ (C=O). Anal. Calcd for (C₁₂H₁₄O): C, 82.7; H, 8.1. Found: C, 82.6; H, 8.0.

From the mother liquor, upon concentration, the white crystalline 12-chloro-[4.4.2]propella-3,8-dien-11-one (**4b**) was isolated: mp 83–84 °C (cyclohexane); 15%; NMR (CDCl₃) δ 4.51 (CHClCO, s, 1 H), 1.7–2.7 (allylic H, m, 8 H); 5.7–5.95 (vinylic H, m, 4 H). Anal. Calcd for (C₁₂H₁₃OCl): C, 69.1; H, 6.3. Found: C, 69.0; H, 6.4.

The unreacted starting acyloin (40%) and several traces (<5%) of unidentified compounds were also isolated.

[4.4.2]Propella-3,8-diene (**5**). A mixture of **4** (1 g, 5.7 mmol), diethylene glycol (20 ml), hydrazine (4 ml), and potassium hydroxide (5 g) was refluxed for 1 h under nitrogen. Then the mixture was distilled slowly until the temperature reached 210 °C. After cooling, the apparatus was washed with pentane and

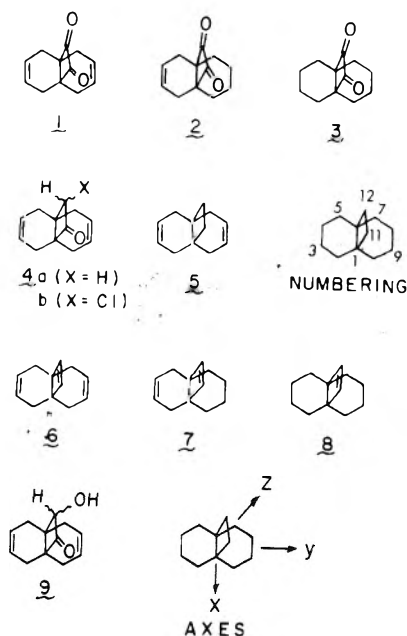


Figure 1. The molecules of interest in this work. Atom numbering and axes conventions are also shown: **1**, [4.4.2]propella-3,8-diene-11,12-dione; **2**, [4.4.2]propell-3-ene-11,12-dione; **3**, [4.4.2]propella-11,12-dione; **4a**, [4.4.2]propella-3,8-dien-11-one; **4b**, 12-chloro[4.4.2]propella-3,8-dien-11-one; **5**, [4.4.2]propella-3,8-diene; **6**, [4.4.2]propella-3,8,11-triene; **7**, [4.4.2]propella-3,11-diene; **8**, [4.4.2]propell-11-ene; **9**, 12-hydroxy[4.4.2]propella-3,8-dien-11-one.

the residue was extracted with pentane. The combined pentane solution was washed with water, aqueous (10%) hydrochloric acid, sodium bicarbonate solution, and water, then dried and concentrated to yield 600 mg of a pale yellow liquid which upon preparative thick-layer chromatography (Brinkmann silica gel PF; 2 mm; hexane) afforded 66% of the pure diene: bp 65–70 °C (5 mm) [microdistillation]; NMR (CCl₄) δ 1.43 (¹¹CH₂, ¹²CH₂, s, 4 H), ~1.9 (allylic H, bd, $J = 4$ Hz), 5.9 (vinylic H, bd, $J = 4$ Hz); ir (neat) 3030, 1640 cm⁻¹. Anal. Calcd for (C₁₂H₁₆): C, 89.94; H, 10.06. Found: C, 89.98; H, 10.02.

CNDO/s calculations⁵ were performed for **1**, **4a**, **5**, **6**, and **7**. The crystal structure⁹ of **1** is known, and is very nearly C_{2v} . The geometrical parameters used for **1** in the CNDO/s calculation were "symmetrized" crystal coordinates (i.e., whenever symmetry-related bond lengths or angles were different, their average value was used to get an exact C_{2v} molecular geometry). The geometrical parameters used for **4a**, **5**, **6**, and **7** were related to the basic skeleton of **1** by means of appropriate atomic "substitutions" and/or "deletions". The basic conformation of **1** (i.e., that in which both of the cyclohexane rings bend up and toward the cyclobutane ring) was assumed to be general because of the absence of any contrary evidence. The bond length changes required were obtained by varying the dihedral angle about carbon centers 1 and 6 (see Figure 1), and any intervening carbon centers, equally. For example, to saturate the bond between carbons 3 and 4, the angles centered on carbons 1, 2, 5, and 6 were increased equally to get the longer bond length required between carbons 3 and 4. Standard bond length changes were imposed on the known structure of **1** in order to obtain those for any of the other compounds.

Results

The Series 1, 2 and 3. The UPS of **1**, **2**, and **3** are shown in

TABLE I: Ionization Energies (eV) and Assignments^a

Compd	<i>I</i> (1)	<i>I</i> (2)	<i>I</i> (3)	<i>I</i> (4)	<i>I</i> (5)	<i>I</i> (6)	<i>I</i> (σ onset)
1	8.70	9.35	10.00	10.7 \pm 0.2	10.7 \pm 0.2	11.1 \pm 0.2	12.1
MO $\gamma(C_{2v})$	n_+ a_1	π_- b_2	π_+ a_1	n_- b_1	σ_{\square} a_1	σ_{\square} a_2	
2	8.60	9.50	10.5	10.8	10.95		11.7
MO $\gamma(C_s)$	n_+ a'	π a'	n_- a'	σ_{\square} a''	σ_{\square} a'		
3	8.65	10.4	10.7	10.7			11.4
MO $\gamma(C_{2v})$	n_+ a_1	n_- b_1	σ_{\square} a_1	σ_{\square} a_2			
4a	8.85	9.15	9.65	10.3	10.6 \pm 0.2	11.2	11.7
MO $\gamma(C_s)$	n a'	π_- a''	π_+ a'	σ_{\square} a'	σ_{\square} a''	σ_{\square} a'	
5	9.00	9.30	10.0 \pm 0.2	10.0 \pm 0.2	11.2		11.2
MO $\gamma(C_{2v})$	π_- b_2	π_+ a_1	σ_{\square} a_1	σ_{\square} a_2	σ		

^a Vertical ionization energies for the molecule pictured in Figure 1. All values are good to ± 0.05 eV, unless otherwise indicated. The MO designations n_+ , π_- , etc., are empirical; the symmetry designations, a_1 , a' , etc., are taken from the CNDO/s results for the molecular point group indicated.

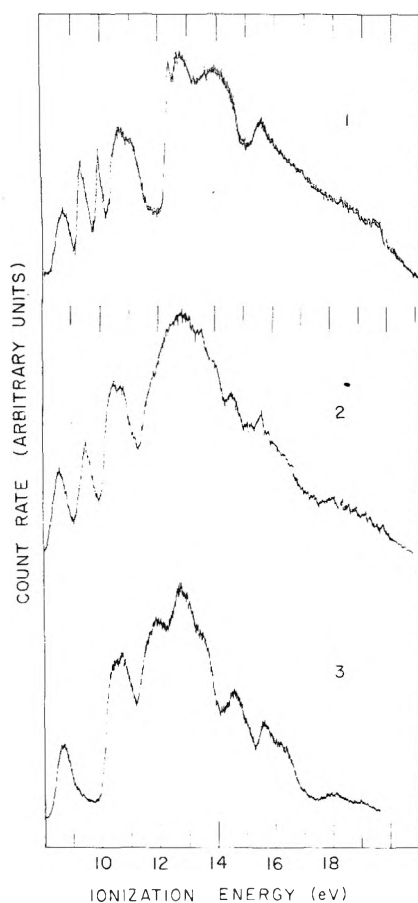


Figure 2. The He I photoelectron spectra of 1, 2, and 3.

Figure 2. If, using Koopmans' theorem,¹⁰ we make a one-to-one association of ionization energies with MO energies, the interpretation of these spectra is straightforward. The UPS energies and assignments are given in Table I.

The expected set of low-energy MO's for 1 consists of the n_+ , n_- , π_+ , and π_- orbitals. The primitive n MO of a single carbonyl unit consists of a $2p$ AO on the oxygen atom, an AO which lies perpendicular to the C=O bond direction and in the plane of the cyclobutane ring. The symmetry-adapted, linear combination of these two AO's in the dicarbonyl, which

we label¹¹ n_+ and n_- , are often termed n_s and n_a and transform as a_1 and b_1 , respectively, in the C_{2v} point group of molecule 1. The π_+ and π_- MO's consist of linear combinations of the two ethylenic π orbitals and transform as a_1 and b_2 , respectively, in C_{2v} .

The cyclobutane ring also introduces a low-energy set of σ MO's which, collectively, we denote σ_{\square} . In the case of 5, for example, these three σ_{\square} MO's are computed to occur at -10.33 , -10.42 , and -11.35 eV and to consist of 55% $2p_x$, 40% $2p_y$, and 55% $2p_z$ carbon AO amplitudes, respectively, on the cyclobutane ring. While the energies of these three σ_{\square} MO's do vary from compound to compound, they nonetheless retain their cyclobutane character and two of them are invariably predicted to be at considerably lower ionization energy than the remainder of the σ subset of MO's.

A considerable body of previous work indicates that the n_+/n_- splitting in α -dicarbonyls is ~ 2 eV, almost all of it attributable to through-bond interactions.¹¹ The π_+/π_- splitting, on the other hand, is expected² to be quite small. For example, it would not be unreasonable to expect this splitting to be less than the 0.85-eV splitting found in norbornadiene.

The spectrum of 3 shows an unambiguous n_+ band at 8.15 eV, and, some 2 eV to higher energy, two weakly defined structures on a band which, on the basis of intensity, contains three ionization events. This band is thought to contain the n_- and two of the σ_{\square} ionization events. The onset of deeper σ ionization events begins at ~ 11.4 eV, a value in keeping with computation and prior experience with six-membered rings.

The integrity of the first and second UPS bands of 3 is maintained through the progression from 2 to 1; hence these bands are similarly identified. The major effect of insertion of the ethylenic double bond(s) is the appearance of one unmistakably new band in 2 at 9.50 eV, and two new bands in 1 at 9.35 and 10.00 eV. These new bands are immediately identifiable as π in 2, and π_-/π_+ in 1.

The order of the π_+ and π_- events in 1 may be deduced using Figure 3. Through-space interaction of the cyclohexene π MO's with each other is thought to be insignificant because of the physical separation of the two ethylenic systems. Through-space interactions with the carbonyl π MO's are thought to be small for reasons of energy-denominator magnitudes and spatial geometry. The most probable interaction

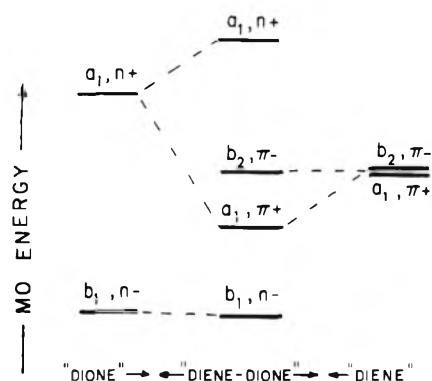


Figure 3. The interaction of the n and π orbitals of the diene dione **1** as represented by a zero-order "dione" set in which the n_+/n_- splitting is taken to be ~ 2 eV and a zero-order "diene" set in which the π_+/π_- splitting is supposed to be very small.

is that between the n_+ and π_+ orbitals, both of which are a_1 . This interaction rationalizes both the asymmetry of the π_+/π_- splitting (relative to **2**) and the rather large split of 0.65 eV (relative to extrapolation from the case of norbornadiene where the splitting is 0.85 eV but the two ethylenic bonds are much closer). This argument could be made considerably more complicated by invoking interactions with the deeper σ MO's and by including inductive and other effects caused by introduction of a new ethylenic bond. Such arguments will not change the conclusion that the order should be "natural" (i.e., π_+ more tightly bound than π_-) although the reasons for the occurrence of this ordering may have altered.

Some other features of interest are the following:

The value $I(n_+)$ changes very little in the series **1**, **2**, **3**. Hence, any interpretation of ${}^1\Gamma_{n\pi^+} \leftarrow {}^1\Gamma_1$ transition energies which invokes alteration of n_+ MO energies within this series must be incorrect.

The asymmetry of the π_+/π_- splitting of **1** relative to **2** is quite obvious in Figure 4. This asymmetry has been rationalized above on the supposition that n_+/π_+ interactions were large, n_-/π_- interactions were absent, and through-space π_-/π_+ splitting was small. These conclusions are in full accord with the form of the MO eigenvectors obtained by the same CNDO/s methods as were used in generating Figure 5.

The 11-eV band is stabilized (i.e., moves to higher binding energy) by ~ 0.1 – 0.2 eV per added ethylenic double bond. This stabilization is attributed to a decreased shielding of the cyclobutanedione electrons by the unsaturation, or π , electrons of the ethylenic groups.

The deeper σ onset is stabilized by ~ 0.2 – 0.3 eV per added ethylenic unsaturation.

The Series 2, 4a, and 5. The members of this series are related by sequential removal of carbonyl groups. The UPS of these molecules are shown in Figure 6. The spectra of **4a** and **5** are more crowded in the low-energy ionization region than are those of the previous section. Hence, they present a more severe interpretive problem.

Assuming that the UPS assignment of **1** is correct, the expected low-energy ionization events of **4a** and **5** consist of the sets [n , π_- , π_+ , and two σ_{\square} 's], and [π_- , π_+ , and two σ_{\square} 's], respectively.

The UPS of **4a**, as detailed in Table I, contains five ionization events in the 8.75–10.6-eV region, with a sixth evident at 11.2 eV. Since only five low-energy events are expected, the occurrence of the 11.2-eV peak requires the introduction of at least one new assignment. In addition, the complexity of the spectrum of **4a** introduces a greater uncertainty in as-

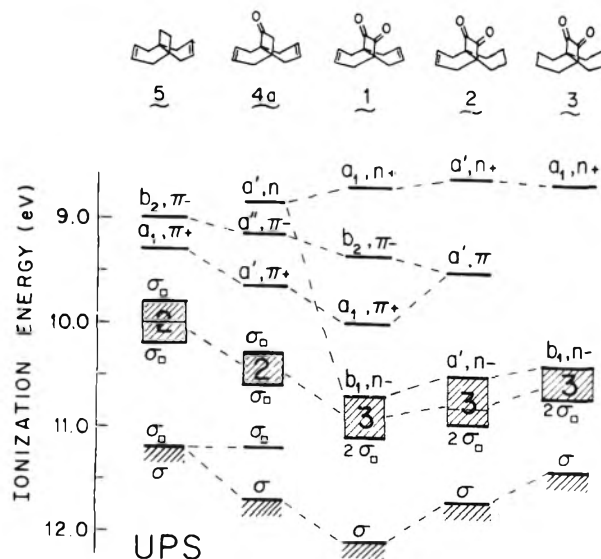


Figure 4. A correlation diagram of empirical origins for the photoelectron spectra of molecules **1**, **2**, **3**, **4a**, and **5**. The σ MO's which are largely localized on the cyclobutane ring are denoted σ_{\square} . The onset of more or less continuous ($\kappa\sigma$) ionization events is denoted σ . The number of ionization events in an unresolved band structure is denoted by an insert arabic numeral.

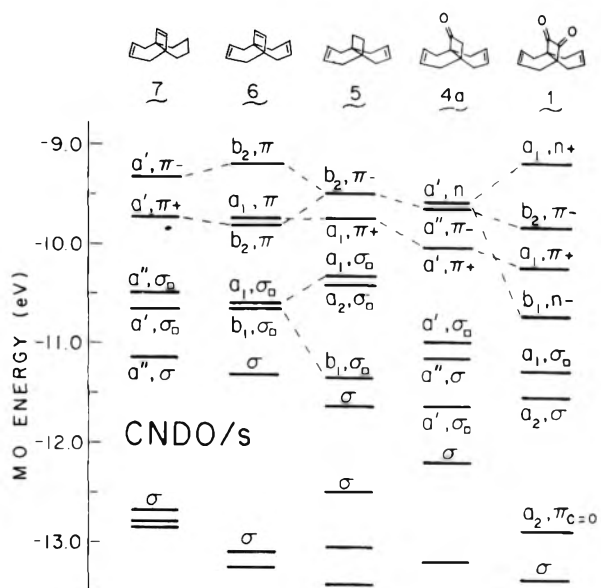


Figure 5. MO energy correlation diagram obtained by CNDO/s procedures for **1**, **4a**, **5**, **6**, and **7**.

segment than was present in the very straightforward UPS data of **1**, **2**, and **3**.

The removal of a carbonyl unit in passing from **1** to **4a** cannot be expected to increase the π_-/π_+ splitting found in **1**. Thus, $I(\pi_-)/I(\pi_+)$ must be associated with either $I(1)/I(2)$, with a 0.3-eV splitting, or $I(2)/I(3)$, with a 0.5-eV splitting. The $I(2)/I(3)$ assignment is preferred for several reasons: First, the band shapes resemble those of $I(\pi_-)/I(\pi_+)$ as assigned in **1**. Secondly, the inductive destabilization of the π orbitals caused by the removal of a carbonyl group should be minimal: After all, three bonds do intervene between the carbonyl and ethylenic groups. Thirdly, any assignment for the $I(\pi)$ events other than $I(2)/I(3)$ would be inconsistent with any reasonable UPS assignment for **5**. Consistency would dictate a large de-

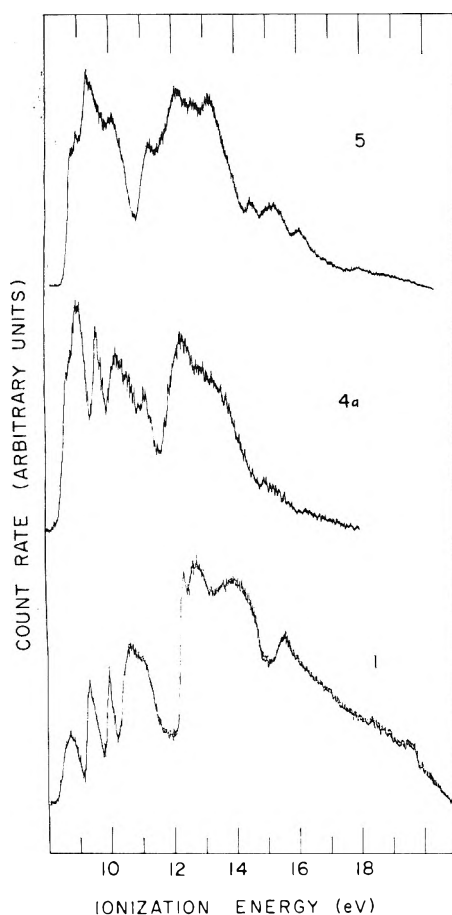


Figure 6. The He I photoelectron spectra of the molecules 1, 4a, and 5.

crease of $I(\pi)$ upon removing the first carbonyl group and virtually none upon removing the second! Finally, the assignments, as given in Table I, are in accord with the CNDO/s results of Figure 5.

The removal of one carbonyl group from 1 destabilizes all weakly bound MO's. This statement refers also to the n MO's because the n MO of 4a must be compared to the n_+/n_- barycenter of 1. This destabilization is the expected result of replacing a strongly electron-withdrawing carbonyl group with an electron-donating methylene group, and also evolves from CNDO/s computations. As another consequence of this destabilization, the 11.2-eV event is most conveniently assigned as the third $I(\sigma_{\square})$ event, which was previously mentioned.

The UPS of 5 should exhibit four low-energy events. This expectation appears to agree with experiment. The low-energy UPS region of 5 is shown in expanded scale in Figure 7. The three features at ~ 8.8 , 9.0, and 9.2 eV probably represent vibrational structure of ~ 1600 cm^{-1} associated with the $I(\pi_-)$ event, the vertical transition lying at 9.00 eV. The $I(\pi_+)$ event is assigned to the 9.3-eV peak, leaving an $I(\pi_-)/I(\pi_+)$ splitting of 0.3 eV. This decrease from the 0.5-eV splitting in 4a and the 0.65-eV splitting in 1 is in accord with our contention that the dominant part of the π_-/π_+ MO splitting is attributable to interactions of π_+ with the n and n_+ MO's.

The vibrational progression associated with $I(1)$ of 5 probably consists of quanta of the ethylenic stretching frequency. This, $\nu_2(a_g)$ occurs at 1623 cm^{-1} in the ground state of ethylene,¹² at 1450 cm^{-1} in the $I(\pi)$ event of ethylene,¹³ and at 1420 cm^{-1} in the $I(\pi)$ event of cyclohexene.¹⁴

Intensity considerations seem to indicate the presence of

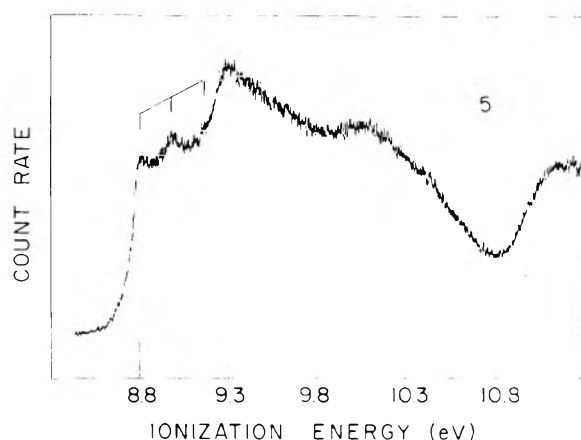


Figure 7. The high-resolution He I photoelectron spectrum of the low-energy region of molecule 5.

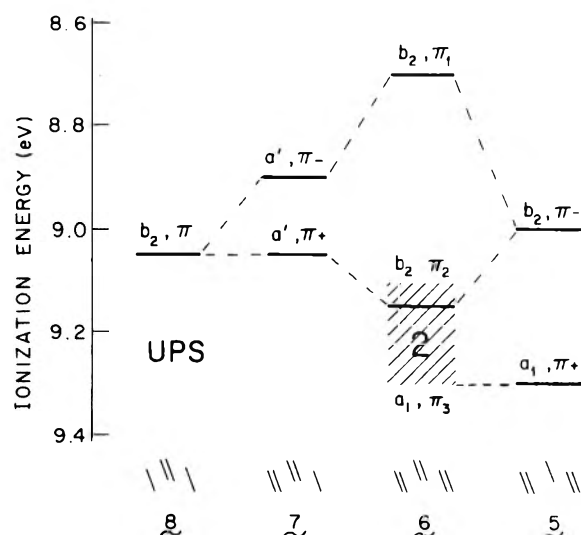


Figure 8. Experimental photoelectron energies and empirical assignments for molecules 5, 6, 7, and 8. The data and assignments for 7 and 8 are taken from Gleiter et al.² The data for 6 are also abstracted from Gleiter et al.;² however, the assignments for 6 have been altered to accord with arguments advanced in the text.

two transitions under the band centered at 10.0 eV. These, almost certainly, are the two $I(\sigma_{\square})$ events that have appeared regularly throughout these molecules. They are both arbitrarily placed at 10.0 ± 0.2 eV, the maximum of the band as quoted in Table I. The isolated event at 11.2 eV is probably associated with a third cyclobutane σ orbital, and is prelude to the deeper σ structure.

The CNDO/s calculational results in Figure 5 reproduce the experimental correlations of Figure 4 quite faithfully. All major experimental trends are identical between the two correlation diagrams; indeed, the primary difference between the two diagrams is that the CNDO/s energies are too deep by ~ 0.75 eV.

The Series 5, 6, 7, and 8. The UPS of 6, 7, and 8 have been analyzed by Gleiter et al.;² that of 5 was determined in this work (see Figures 6 and 7). The analysis of this spectrum, considered as a member of the series 1, 4a, 5, appears to be quite trustworthy. However, the observation of coupled vibrational structure in what appears to be an ethylenic stretching frequency, while nicely confirmatory of the $I(\pi_-)$ event in 5, raises some doubt concerning the location of the vertical event of $I(\pi_-)$ in 5. The vibrational nature of this

structure is also supported by comparison of the UPS of 5 with those of 6, 7, and 8. No structure is visible in the $I(\pi)$ event of 8, whereas the lowest energy $I(\pi)$ events of 7, 5, and 6 all exhibit $\sim 1600\text{-cm}^{-1}$ intervals of increasing intensity.

The UPS data for 5 suggest strongly that the previous assignment of 6 was incorrect in placing origins at both 8.7 and 8.9 eV; and that, in fact, there is one origin at 8.7 eV with a vibrational member at 8.9 eV. The second $I(\pi)$ event is displaced, therefore, to higher ionization energy, as is also the third $I(\pi)$ event from which it is not resolved. The resulting data for 5, 6, 7, and 8 are presented in Figure 8. The implication of Figure 8, that the MO ordering is $(\pi_2 b_2) > (\pi_3 a_1)$, is arbitrary: These two transitions are not resolved in the spectrum. We justify the order of Figure 8 simply because we can see no particular reason why the a_1 MO should be destabilized on proceeding from 5 to 6.

The CNDO/s results of Figure 9 mimic the experimental pattern quite well. One interesting anomaly occurs on comparing the π_-/π_+ splitting in 5 and 7: Computationally, $\Delta I(\pi_-/\pi_+)$ is greater in 7 than in 5, whereas the reverse is true experimentally. The energetic ordering of the π MO's of 5, 6, and 7 is the "natural" order⁴ (i.e., π_+ below π_-). Thus, the insertion of a b_2 ethylenic bond in the cyclobutane ring in passing from 5 to 6 is seen, from Figure 9, to correspond to "Case B(2) antisymmetric" of Heilbronner.⁴ Hence, theoretically, in terms of "Case B(2) antisymmetric", we must again conclude that the previous UPS assignment² of 6 was erroneous.

Discussion

The purposes of this work, as outlined in the Introduction under items (i)–(vi), have already been realized to a considerable degree. In order to be specific, we will now itemize our conclusions under the same numbering system as was used in the Introduction.

(i) No evidence of any isomerism was found in the dione monoene 2. This result discords with both electronic and vibrational absorption studies where such isomerism is readily detected. The UPS studies differ from the others in that the UPS data refer to the gas phase whereas the vis and ir data refer to liquid solution phases. Thus, it may be that isomerism is confined to the condensed phase or that the UPS studies are insufficiently sensitive to discriminate between the various isomeric forms.

(ii) The ${}^1\Gamma_{n\pi^*} \leftarrow {}^1\Gamma_1$ absorption bands of 1, 2, and 3 are found to be quite different.^{3a} There is no facet of the UPS data which can explain such energy differences. Inspection of Figure 4 leads one to expect, perhaps naively, that the ${}^1\Gamma_{n\pi^*} \leftarrow {}^1\Gamma_1$ transition of 3 should occur at lower energy than that of 1 whereas the opposite is the case experimentally. Indeed, the UPS data suggest that the variability of the ${}^1\Gamma_{n\pi^*} \leftarrow {}^1\Gamma_1$ energies must be a function of virtual $\pi^*(\text{CO})$ MO characteristics.

The energies of ${}^1\Gamma_{n\pi^*} \leftarrow {}^1\Gamma_1$ transitions in α -dicarbonyls are quite variable. This variability is usually attributed to changes in the CO/CO dihedral angle.^{15,16} It has been shown that the energy of the n_+ MO, as well as the n_+/n_- splitting, is reasonably insensitive to dihedral angle variations whereas those of the π_{\pm}^* carbonyl antibonding MO's are exceedingly sensitive to variations of this same angle.¹⁶ Thus, when the CO/CO dihedral angle is 90° , the π_+^* and π_-^* MO's are more or less degenerate. As the dihedral angle varies from 90° , the π_+^* and π_-^* MO's exhibit an increase and decrease, respectively, of binding energy, so that at 0° (or 180°), the π_+^* MO possesses its maximum binding energy.¹⁶ As a result, the ${}^1\Gamma_{n+\pi_+^*} \leftarrow {}^1\Gamma_1$ transition is expected, on a simple MO basis,

TABLE II: Vibronic Structure of the ${}^1\Gamma_{n\pi^*} \leftarrow {}^1\Gamma_1$ Transition of the Dione Dione 1 at 77 K in an EPA Glassy Matrix

\AA	$\Delta\nu, \text{cm}^{-1}$	Interpretation
5500		0,0
5340	545	ν_1
5280	757	ν_2
5050	1560	ν_3
4920	2083	$\nu_3 + \nu_1^*$
4850	2377	$\nu_3 + \nu_2$

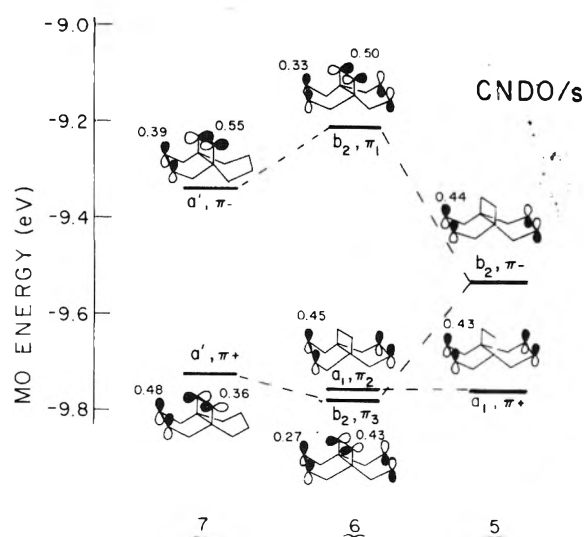


Figure 9. CNDO/s MO calculations for molecules 5, 6, and 7. MO diagrams are also provided.

to be of lowest energy in the coplanar (cis or trans) conformation of the dicarbonyl system.

On the experimental side, it is known that when coplanarity of two α -carbonyl groups is sterically enforced the ${}^1\Gamma_{n+\pi_+^*} \leftarrow {}^1\Gamma_1$ transition may occur at $\lambda \geq 500 \text{ m}\mu$.¹⁷ In cases in which the CO/CO dihedral angle is $\sim 90^\circ$, it is known¹⁶ that the ${}^1\Gamma_{n+\pi_+^*} \leftarrow {}^1\Gamma_1$ transition may lie at $\lambda \leq 400 \text{ m}\mu$. Finally, when noncoplanar α -dicarbonyls are excited in the ${}^1\Gamma_{n+\pi_+^*} \leftarrow {}^1\Gamma_1$ absorption, they will normally²⁰ emit a weak fluorescence of ${}^1\Gamma_{n+\pi_+^*} \rightarrow {}^1\Gamma$ type only when the ${}^1\Gamma_{n+\pi_+^*}$ state can achieve minimum energy (i.e., twist into a conformation in which CO/CO coplanarity is achieved). In sum, if the carbonyl groups are coplanar, or nearly coplanar, the ${}^1\Gamma_{n+\pi_+^*} \leftarrow {}^1\Gamma_1$ absorption band will exhibit coincidence of vertical and adiabatic events and, if the ${}^1\Gamma_{n+\pi_+^*} \rightarrow {}^1\Gamma_1$ emission be observed, it will exhibit little or no Stokes shift relative to the vertical event in absorption and will be a good mirror image of the absorption band. If the carbonyl groups are noncoplanar, the ${}^1\Gamma_{n+\pi_+^*} \leftarrow {}^1\Gamma_1$ event will exhibit a large separation of vertical and adiabatic events (i.e., the adiabatic event may be so weak as to be unobservable and the band shape may be nearly Gaussian) and, if the ${}^1\Gamma_{n+\pi_+^*} \rightarrow {}^1\Gamma_1$ emission be observed, it will exhibit a large Stokes shift relative to the vertical event in absorption and it need not be a good mirror image of the absorption band. Thus, having outlined some simple experimental criteria, it is now pertinent to enquire whether any of the absorption spectroscopic differences between 1, 2, and 3 might be attributable to a variable CO/CO dihedral angle.

The ${}^1\Gamma_{n+\pi_+^*} \leftarrow {}^1\Gamma_1$ absorption spectra of 1, 2, and 3 in liquid solution at $\sim 300 \text{ K}$ are already available;^{3a} they will not be repeated here. These compounds do not emit detectable flu-

TABLE III: Calculated and Observed Shifts, $\Delta\pi_{\pm}$ and Δn_{\pm} , for Molecules Investigated in This Work

Splittings	5		4a		1		2		3	
	Calcd	Obsd	Calcd	Obsd	Calcd	Obsd	Calcd	Obsd	Calcd	Obsd
$\Delta\pi_{\pm}$	0.22	0.3	0.38	0.5	0.41	0.65				
Δn_{\pm}					1.51	2.0		1.9		1.85

orescence at the sensitivities available to us. Hence, the present studies consist only of absorption studies at various temperatures $77 \leq T \leq 400$ K.

The pertinent compounds are **1** and **3** (i.e., those where no obvious isomerism occurs). Inspection of the published ${}^1\Gamma_{n+\pi+}$ \leftarrow ${}^1\Gamma_1$ absorption spectra of these two compounds^{3a} indicates a considerable difference of band shapes. The ${}^1\Gamma_{n+\pi+}$ \leftarrow ${}^1\Gamma_1$ absorption band of **1** has a rather sharp onset and appears to exhibit weak vibrational structure. This latter suspicion is verified by the absorption spectra obtained in glassy matrices at 77 K where the 0,0 band is the most intense feature and a readily analyzed vibrational structure is evident. This analysis is detailed in Table II. One may conclude from the Franck-Condon absorption-band shape of **1** that the CO/CO dihedral angle is identical in both the ${}^1\Gamma_1$ and ${}^1\Gamma_{n+\pi+}$ states. In addition, since the ${}^1\Gamma_{n+\pi+}$ state is most stable when the dihedral angle is zero,²⁰ one may conclude that the two carbonyl groups of **1** are closely coplanar in the ${}^1\Gamma_1$ state also. This conclusion, of course, is in agreement with the x-ray data⁹ for the ${}^1\Gamma_1$ state. Compound **3**, on the other hand, exhibits a Gaussian band shape for the ${}^1\Gamma_{n+\pi+}$ \leftarrow ${}^1\Gamma_1$ transition; the band maximum lies now at 4630 Å and the half-width is ~50% greater than that of **1**. Apart from a red shift to 4710 Å, which is associated with increased solvent-solute dispersive interactions, the band shape neither alters in any significant way nor is any vibronic structure resolved at 77 K. In view of the Franck-Condon absorption-band shape, we must conclude that the geometries in the ${}^1\Gamma_{n+\pi+}$ and ${}^1\Gamma_1$ states are quite different. Whether this difference is associated with change of the CO/CO dihedral angle—from noncoplanar in the ${}^1\Gamma_1$ state to planar in the ${}^1\Gamma_{n+\pi+}$ state—we cannot say with certainty. It is, however, a supposition which provides a reasonably neat interpretation for the absorption spectroscopic differences between compounds **1** and **3**.

The ${}^1\Gamma_{n+\pi+}$ \leftarrow ${}^1\Gamma_1$ transition of **2** is interesting in that it appears, at 300 K, to be a 50/50 composite of the spectra of **1** and **3**. As the temperature of the solution of **2** is decreased, the 1-like absorption component disappears and, at 77 K, the ${}^1\Gamma_{n+\pi+}$ \leftarrow ${}^1\Gamma_1$ absorption band of **2** is essentially identical with that of **3**. These changes are totally reversible and the presence of an equilibrium is fully established. The interpretation of these effects is quite another matter. The previous interpretation^{3a} implied a folding up (i.e., folding toward the carbonyls) or a folding down (i.e., folding away from the carbonyls) of the ethylenic bond of **2**. This may well be the case. However, if it is, it seems pertinent to insist that the major effects which such folding induces is probably the creation of multiple potential minima along the CO/CO dihedral angle coordinate (i.e., at least two in the range $0^\circ < \text{CO/CO} < 180^\circ$). It also seems safe to insist that luminescence techniques which are adequate to the detection of weak ${}^1\Gamma_{n\pi^*}$ \leftarrow ${}^1\Gamma_1$ luminescences should lead to complete resolution of the problem.

(iii) and (iv). These purposes have been fully achieved in the discussions of the three previous sections. However, a slight summary of splitting effects is in order.

The \pm MO's, denoted $\Delta\pi_{\pm}$ and Δn_{\pm} , are collected in Table

III where they are compared with computation. The agreement is good. The decrease of $\Delta\pi_{\pm}$ in the series $1 > 4a > 5$ implies a considerable through-bond interaction of π_+ and n_+ MO's, as previously discussed. The rough constancy of $\Delta n_{\pm} \approx 2$ eV is in accord with a considerable body of previous work for α -dicarbonyls.¹¹ The small decrease of Δn_{\pm} in the series $1 > 2 > 3$, insofar as it is real, is probably attributable to an increase of interactions of n_- with the σ -MO system. These σ MO's, as previously noted, are progressively destabilized by removal of the ethylenic π unsaturation and probably exert a relatively larger perturbative effect on the n_- than on the n_+ MO energies.

(v) The σ_{\square} subset of MO's has been discussed in some detail. One further comment should be made: The insertion of ethylenic bonds leads to progressive stabilization of the σ_{\square} subset, as is evident in the series $8 < 7 < 6, 5 < 6$, and $3 < 2 < 1$. The primary effect operative in these instances appears to be a simple deshielding of the system by the progressive conversion of σ electrons into loosely bound π electrons.

(vi) As outlined in the previous section, the Heilbronner model,⁴ as used in conjunction with the UPS data for **5**, indicates that the assignment of the UPS of **6** by Gleiter et al.² is probably incorrect. All in all, however, the present work constitutes a remarkable vindication of the argument of Gleiter et al.²

Acknowledgment. The authors wish to express their thanks to D. A. Bude for the ¹³C NMR investigations; to J. J. Freeman for all the absorption spectroscopic work; and to E. Heilbronner for copies of the photoelectron spectra of **6**, **7**, and **8** and much helpful discussion on virtually every aspect of this work.

References and Notes

- (1) This work was supported by contract between the United States Energy Research and Development Administration and The Louisiana State University.
- (2) R. Gleiter, E. Heilbronner, L. A. Paquette, G. L. Thompson, and R. E. Wingard, Jr., *Helv. Chim. Acta*, **29**, 565 (1973).
- (3) (a) J. J. Bloomfield and R. E. Moser, *J. Am. Chem. Soc.*, **90**, 5625 (1968); (b) S. C. Neely, R. Fink, D. van der Helm, and J. J. Bloomfield, *ibid.*, **93**, 4903 (1971).
- (4) E. Heilbronner, *Isr. J. Chem.*, **10**, 143 (1972). See also M. J. Goldstein, S. Natowsky, E. Heilbronner, and V. Horning, *Helv. Chim. Acta*, **56**, 294 (1973).
- (5) The program used was QCPE: CNDO 174. See also J. Del Bene and H. H. Jaffe, *J. Chem. Phys.*, **50**, 1126 (1969).
- (6) D. Dougherty, K. Wittel, J. Meeks, and S. P. McGlynn, *J. Am. Chem. Soc.*, **98**, 3815 (1976).
- (7) R. G. Lewis and J. J. Freeman, *J. Mol. Spectrosc.*, **32**, 24 (1969).
- (8) J. J. Bloomfield, J. R. S. Irelan, and A. P. Marchand, *Tetrahedron Lett.*, 5647 (1968).
- (9) F. Fink, D. van der Helm, and S. C. Neely, Abstracts, American Crystallographic Association Meeting, March, 1969, p 34.
- (10) T. Koopmans, *Physica*, **1**, 104 (1934).
- (11) J. L. Meeks, H. J. Maria, P. Brint, and S. P. McGlynn, *Chem. Rev.*, **75**, 603 (1975); J. L. Meeks and S. P. McGlynn, *J. Am. Chem. Soc.*, **97**, 5079 (1975); J. L. Meeks, J. F. Arnett, D. B. Larson, and S. P. McGlynn, *ibid.*, **97**, 3095 (1975).
- (12) G. Herzberg, "Infrared and Raman Spectra of Polyatomic Molecules", Van Nostrand, New York, N.Y., 1945, p 326.
- (13) C. R. Brundle and D. D. Brown, *Spectrochim. Acta, Part A*, **27**, 2491 (1971); G. R. Branton, D. C. Frost, T. Makita, C. A. McDowell, and I. A. Stenhouse, *Phil. Trans. R. Soc. London*, **268**, 77 (1970).

- (14) P. Bischof and E. Heilbronner, *Helv. Chem. Acta*, **53**, 1677 (1970).
 (15) N. J. Leonard and P. M. Mader, *J. Am. Chem. Soc.*, **72**, 5388 (1950).
 (16) J. F. Arnett, G. Newkome, W. L. Mattice, and S. P. McGlynn, *J. Am. Chem. Soc.*, **96**, 4385 (1974).
 (17) C. Sandris and G. Ourisson, *Bull. Soc. Chim. Fr.*, **23**, 958 (1956), report $\lambda_{\text{max}} = 495$ and $508 \text{ m}\mu$, $\epsilon = 38$; $530 \text{ m}\mu$, $\epsilon = 31$ for 3,3,5,5-tetramethyl-1,2-cyclopentanedione. $\lambda_{\text{max}} = 562 \text{ m}\mu$, $\epsilon = 40$ for 3,3,5,5-tetramethyl-4-oxa-1,2-cyclopentanedione.
 (18) The tetrafluoro-1,2-cyclobutanedione is reported to be blue [D. C. England, *J. Am. Chem. Soc.*, **83**, 2205 (1961); British Patent 873 222; *Chem. Abstr.*, **56**, 1363 C (1962)]. Although no absorption spectrum is available, it may be inferred that the ${}^1\Gamma_{\pi\pi^*} \leftrightarrow {}^1\Gamma_1$ transition in this compound occurs at $\lambda \geq 530 \text{ m}\mu$.
 (19) 3,3-Dimethyl-1,2-indanedione has a 0,0 band at $18\,900 \text{ cm}^{-1}$: See ref 20.
 (20) J. F. Arnett and S. P. McGlynn, *J. Am. Chem. Soc.*, **79**, 626 (1975).

Singlet Molecular Oxygen. A New Kind of Oxygen¹

Ahsan U. Khan

Departments of Chemistry and Biophysics, Michigan State University, East Lansing, Michigan 48824 (Received February 9, 1976)

The discovery by Khan and Kasha in 1963 that the singlet states of molecular oxygen exist in chemical systems created a new and rapidly expanding field of research. A general class of photochemical reactions, the sensitized photooxidations of organic molecules, has been shown to proceed by singlet oxygen. Theoretical and experimental studies have shown that singlet oxygen is readily generated by energy transfer from the triplet excited states of organic molecules and from the decomposition of organic peroxides, so that singlet oxygen has become an important new chemical entity. The long lifetimes of the singlet oxygen states and the availability of double molecule singlet oxygen states offer a versatility of energy transfer and energy pooling options as is illustrated by oxygen dependent chemiluminescence and oxygen enhanced fluorescence studies. This paper presents a theoretical analysis of the generation and quenching of singlet oxygen in electron-transfer reactions of the superoxide anion. A critical dependence on the precise number of water molecules present was found in the generation of excited states of molecular oxygen from the dismutation reaction of ion clusters of O_2^- with H_2O . At high concentration of H_2O , singlet oxygen was found to be the major product of the reaction. Quenching of singlet oxygen by O_2^- was found to be very efficient approaching diffusion controlled rates. Recently reported experimental evidence is cited to support the optical residue-singlet oxygen theory of photocarcinogenicity. Finally a new analytical technique for the detection of singlet oxygen (${}^1\Delta_g$) in aqueous solutions which has the advantage of extended time integration has been developed. This technique has enabled the unambiguous identification of singlet oxygen in the xanthine-xanthine oxidase system.

The initial shock presented by the discovery of molecular oxygen was the fact that this substance was found to be intimately involved in all living processes. Each advance in the physical description of the oxygen molecule revived the question of why this molecule was essential to such a wide variety of chemical reactions. With the recognition of paramagnetism and its subsequent interpretation by molecular orbital theory,² it was thought that the uniqueness of the oxygen molecule arose from the very unusual fact that molecular oxygen has a paramagnetic ground triplet state, ${}^3\Sigma_g^-$. However, it is becoming increasingly apparent that to a great extent the special nature of oxygen chemistry depends upon the existence of two low lying excited singlet states, ${}^1\Delta_g$ and ${}^1\Sigma_g^+$. The long lifetimes and favorable energy dispositions (${}^1\Delta_g \rightarrow {}^3\Sigma_g^-, \tau = 45 \text{ min}, \nu_{00} = 7882.39 \text{ cm}^{-1}$; ${}^1\Sigma_g^+ \rightarrow {}^3\Sigma_g^-, \tau = 7.1 \text{ s}, \nu_{00} = 13\,120.9080 \text{ cm}^{-1}$) of these two states give molecular oxygen a unique versatility; so that singlet oxygen is better described as a new chemical entity with its own special properties and reactivities. In this paper we will present a perspective of singlet oxygen research starting with its discovery in a chemical system by Khan and Kasha.^{4,5} The results of two new investigations are reported: (1) a theoretical investigation using electron transfer theory for the generation and quenching of singlet oxygen in electron transfer reactions of the superoxide anion and (2) a new analytical technique for the detection of singlet oxygen in aqueous solutions.

Discovery of Singlet Oxygen in a Chemical System

The discovery of singlet oxygen in a chemical system began with a brief red flash seen when hydrogen peroxide is mixed with sodium hypochlorite. The flash had been discovered independently by a number of workers as an ultraweak emission accompanying the use of these reagents to trigger the chemiluminescence of organic molecules.⁶⁻⁹ In 1960 Seliger published a narrow band spectrum of the emission at approximately 6330 \AA .¹⁰ Based on a wavelength coincidence of this narrow band emission with liquid oxygen spectra, Stauff and Schmidkunz in 1962 suggested that the emission was a double molecule, $[({}^1\Delta_g)({}^1\Delta_g)] \rightarrow [({}^3\Sigma_g^-)({}^3\Sigma_g^-)]$, transition involving molecular oxygen.¹¹

Khan and Kasha in 1963 reported a spectrum of the hydrogen peroxide-hypochlorite reaction, ($\text{H}_2\text{O}_2/\text{OCl}^-$), containing a band at 6334 \AA and an additional band of stronger intensity at 7032 \AA (see Figure 1A, third spectrum).⁴ Based on the fact that the band separation, 1567 cm^{-1} , correlated with the ground state vibrational frequency of molecular oxygen and the fact that the isotope studies of Cahill and Taube showed that the oxygen-oxygen bond of H_2O_2 remained intact in the molecular oxygen generated in the reaction,¹² Khan and Kasha identified the red chemiluminescence as emission from the singlet excited states of molecular oxygen. Because of the energetics of the emission, the spectral

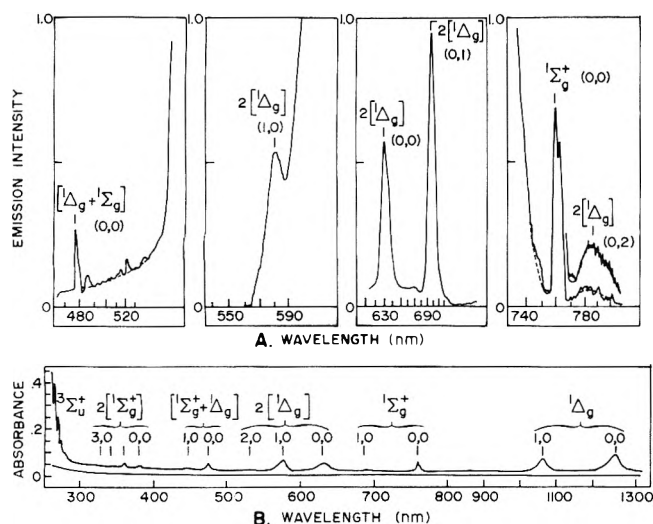


Figure 1. The spectra in Figure 1A are chemiluminescence bands for the aqueous reaction at 20 °C of $\text{H}_2\text{O}_2/\text{OCl}^-$. B is the complete absorption spectrum from 260 to 1340 nm of gaseous molecular oxygen at 150 atm in a 6.5-cm cell at 20 °C. Bands labeled according to upper electronic state by energy convention with vibronic components. Adapted from Khan and Kasha.⁵

diffuseness, and the aqueous environment, two alternative interpretations for the detailed assignment were considered: (1) Stauff and Schmidkunz's suggestion of double molecule ${}^1\Delta_g$ emission and (2) a hydrated O_2 molecule with solvent shifted ${}^1\Sigma_g^+ \rightarrow {}^3\Sigma_g^-$ emission. Arnold, Ogryzlo, and Witzke, working with a microwave discharge in the gas phase, obtained the same emission, thus giving evidence that the bands originated from double molecule states.¹³ A medium resolution spectrum of the chemiluminescence by Khan and Kasha revealed rotational structure of the (0,0) ${}^1\Sigma_g^+ \rightarrow {}^3\Sigma_g^-$ transition, demonstrating that the emission originates inside bubbles in the reaction; i.e., despite the aqueous matrix, the emission is from gaseous oxygen.¹⁴ Because of the emission from the $[({}^1\Delta_g)({}^1\Delta_g)]$ state in the microwave discharge in the gas phase and the ${}^1\Sigma_g^+ \rightarrow {}^3\Sigma_g^-$ emission from inside bubbles in the chemiluminescence reaction, Khan and Kasha predicted and subsequently identified a band at 4780 Å corresponding to the (0,0) transition of the double molecule $[({}^1\Sigma_g^+)({}^1\Delta_g)] \rightarrow [({}^3\Sigma_g^-)({}^3\Sigma_g^-)]$ emission in the $\text{H}_2\text{O}_2/\text{OCl}^-$ reaction¹⁵ (see Figure 1A). This conclusively established the detailed correspondence between the chemiluminescence spectrum of the $\text{H}_2\text{O}_2/\text{OCl}^-$ reaction with the high pressure absorption spectrum (Figure 1B) of molecular oxygen.

The mechanism of oxygen production in the reaction, $\text{H}_2\text{O}_2 + \text{OCl}^- \rightarrow \text{O}_2 + \text{Cl}^- + \text{H}_2\text{O}$, was studied by Cahill and Taube who showed that the oxygen is generated from the chloroperoxy (OClO^-) ion.¹² An electron pairing analysis of the reaction necessitates the production of electron paired or singlet oxygen. From the adiabatic spin-state correlation diagram in Figure 2, it is evident that both the ground and first excited singlet states of the OClO^- ion correlate to the doubly degenerate ${}^1\Delta_g$ state of molecular oxygen. Production of either ${}^1\Sigma_g^+$ or the ${}^3\Sigma_g^-$ states of molecular oxygen are excluded by this adiabatic correlation diagram. Emissions from the ${}^1\Sigma_g^+$ state and the double molecule $[({}^1\Sigma_g^+)({}^1\Delta_g)]$ state have been detected in the $\text{H}_2\text{O}_2/\text{OCl}^-$ chemiluminescence. The ${}^1\Sigma_g^+$ oxygen could be generated from the reaction ${}^1[({}^1\Delta_g)({}^1\Delta_g)] \rightarrow {}^3[({}^1\Sigma_g^+)({}^3\Sigma_g^-)]$ via a spin forbidden process. The concentration ratio $[{}^1\Sigma_g^+]/[{}^1\Delta_g]$ in the reaction is small, less than $10^{-6.5}$.

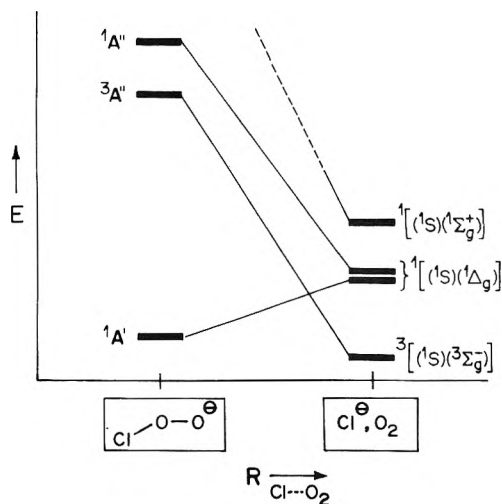


Figure 2. Adiabatic spin state correlation diagram for the dissociation of the chloroperoxy ion $\text{ClO}_2^- \rightarrow \text{Cl}^- + \text{O}_2$. Adapted from Khan and Kasha.⁵

Singlet Oxygen Chemistry

After the spectral identification of the singlet species of molecular oxygen in the $\text{H}_2\text{O}_2/\text{OCl}^-$ reaction, singlet oxygen was quickly recognized as the common intermediate in a general class of chemical reactions, the dye sensitized photooxygenation reactions of organic molecules. Kautsky postulated in 1939 a general mechanism for these reactions involving the generation of singlet oxygen via energy transfer from the triplet state of the dye sensitizer molecule, and the subsequent reaction of singlet oxygen with the organic acceptor to form the final oxygenation product.¹⁶ In 1964 two groups, Corey and Taylor,¹⁷ and Foote and Wexler,¹⁸ revived and substantially verified Kautsky's mechanism. Foote and Wexler showed that the $\text{H}_2\text{O}_2/\text{OCl}^-$ reagent could be used to produce the same product distribution with the organic acceptor as the dye sensitized photooxygenation reaction. Corey and Taylor obtained similar results using singlet oxygen generated in a gas discharge. Later experiments have shown that, regardless of the method of singlet oxygen generation, the product distribution and stereochemistry (cis-trans isomerism and optical activity) of the reaction is identical.¹⁹ As a note of caution, although the majority of dye sensitized photooxygenation reactions proceed by singlet oxygen, exceptions exist. Kearns has compiled a recommended list of tests which should be applied when considering a new reaction.²⁰

As a result of this new understanding of the reaction mechanism, research in the field of photooxygenation reactions has blossomed spectacularly over the last 12 years. There are now three generally recognized types of singlet oxygen addition reactions with unsaturated organic molecules: (1) A 1,4 transannular cycloaddition of singlet oxygen to cis dienes or aromatic hydrocarbons to form cyclic peroxides. With aromatic hydrocarbons this reaction is a unique singlet oxygen reaction; no other reagent produces the 1,4 transannular oxygenation product. (2) A 1,2 cycloaddition of singlet oxygen with certain olefins to form an unstable dioxetane intermediate which readily cleaves to form carbonyl fragments. The existence of unstable dioxetane intermediates has been established by the recent discovery of synthetic routes to stable dioxetanes and the isolation of a stable dioxetane from the sensitized photooxidation of *cis*-diethoxyethylene. (3) An "ene" reaction of singlet oxygen with olefins to form allylic

hydroperoxides. The most common form of singlet oxygen addition, the "ene" reaction is thought to proceed by either a concerted "ene" mechanism or by formation of a peroxirane intermediate.²⁰

Kinetic and Lifetime Studies of Singlet Oxygen

Because of the rapid quenching of the $^1\Sigma_g^+$ singlet oxygen species in aqueous solution ($k \approx 10^9 \text{ M}^{-1} \text{ s}^{-1}$ by H_2O and D_2O , gas phase²⁰), the singlet oxygen addition reactions with unsaturated organic molecules (reactions 1–3 above) are essentially reactions of the $^1\Delta_g$ species. The lifetime of the $^1\Delta_g$ species in solution has been extensively studied and there are several bimolecular processes which may affect the $^1\Delta_g$ lifetime in a given solution.²¹ Kearns and Merkel, with laser pulse techniques, have extrapolated lifetimes for $^1\Delta_g$ in H_2O ($\tau = 2 \mu\text{s}$), D_2O ($\tau = 20 \mu\text{s}$), and various organic solvents (the longest solution lifetime recorded was in CCl_4 , $\tau = 700 \mu\text{s}$) from the rate of photobleaching of an $^1\Delta_g$ acceptor.²² In addition to the lifetime studies of singlet oxygen, extensive investigations are being carried out on the rates of reaction of singlet oxygen with organic molecules both in the gas and solution phase. Recently a surprising result arose from a kinetic analysis by Stevens and Ors of rubrene and 9,10-dimethylantracene sensitization in benzene: that two molecules of excited oxygen ($^1\Delta_g$) can be generated from one electronically excited singlet state of the organic molecule, giving a quantum yield of two for singlet oxygen production.²³

Theoretical Investigations

A. Generation of Singlet Oxygen ($^1\Delta_g$ and $^1\Sigma_g^+$) by Energy Transfer. Kautsky's photooxygenation mechanism assumes the efficient generation of singlet oxygen by the quenching of organic triplet states. However, prior to the discovery of singlet oxygen in chemical systems, the quenching of the phosphorescence of organic molecules by molecular oxygen was thought to proceed principally by enhanced intersystem crossing with paramagnetic molecular oxygen acting as a catalyst for the degradation of the organic triplet into vibrational energy of the ground singlet state of the organic molecule. Kawaoka, Khan, and Kearns²⁴ compared theoretically calculated quenching rate constants for two phosphorescence quenching mechanisms, (1) energy transfer to generate singlet oxygen ($^1\Sigma_g^+$ and $^1\Delta_g$) and (2) enhanced intersystem crossing to the vibrationally excited ground state organic molecule. A quantum mechanical description of a weak $\text{M}\cdots\text{O}_2$ complex between the organic molecule, M, and molecular oxygen, O_2 , was constructed. At infinite distance M and O_2 are in their stationary states described by $H_{\text{O}_2}\psi_{\text{O}_2} = E_{\text{O}_2}\psi_{\text{O}_2}$, and $H_{\text{M}}\psi_{\text{M}} = E_{\text{M}}\psi_{\text{M}}$. As M and O_2 begin to interact, these states are no longer stationary with respect to the new Hamiltonian, $H = H_{\text{M}} + H_{\text{O}_2} + H'_{\text{int}}$. Under the influence of the perturbation term H'_{int} , radiationless transitions occur between the states of the complex. To determine the quenching rate constants, the radiationless transition theory of Robinson and Frosch²⁵ was used where $k = (2\pi\rho/\hbar N)\beta_{ei}^2 F_{if}$ and k is the rate of radiationless transition; ρ , the density of the final states which are nearly degenerate with the initial state; N , Avogadro's number; β_{ei} , the electronic matrix element between the initial state i and the final state f ; and F_{if} , the Franck-Condon factor between i and f . The electronic matrix elements β_{ei} for both energy transfer to generate $^1\Sigma_g^+$ or $^1\Delta_g$ and to the ground state $^3\Sigma_g^-$ are similar ($\approx 20 \text{ cm}^{-1}$) and ρ is also approximately constant for each case, so that the Franck-Condon factors essentially determine whether singlet oxygen is produced in the quenching process. For an organic triplet state energy of

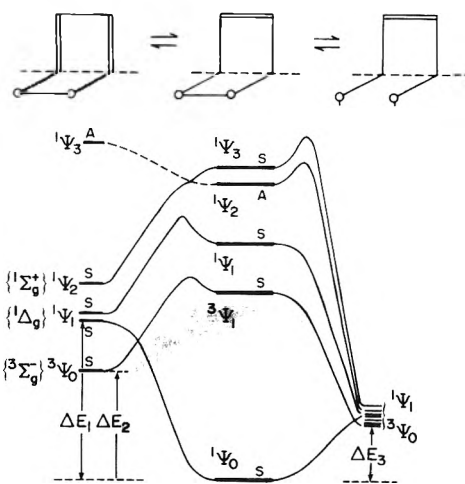


Figure 3. Schematic of the state correlation diagram for the (diene + O_2) \rightleftharpoons peroxide \rightleftharpoons diradical interconversions. States of the diene- O_2 complex are on the left [state of molecular oxygen is specifically noted for each state]. States of the peroxide are depicted in the middle. The nearly degenerate set of low lying singlet and triplet states of the diradical are shown on the right. The states are arranged in order of increasing energy. Adapted from Khan and Kearns.³⁸

72 kcal with all the vibrational energy going to the aromatic hydrocarbon (Franck-Condon factors determined by the empirical relationship of Siebrand²⁶), the quenching rate constants are: to generate $^1\Sigma_g^+$, 10^{11} ; to generate $^1\Delta_g$, 10^{10} ; to generate $^3\Sigma_g^-$, $10^8 \text{ (M}^{-1} \text{ s}^{-1})$. The results predict that, with organic triplet states of sufficient energy, quenching proceeds essentially by the generation of singlet oxygen.

The results of this theoretical investigation have been substantially confirmed by experimental evidence of the generation of singlet oxygen in the quenching of organic triplet states in a number of systems.^{27–31} The quenching of the electronic excited states of inorganic molecules can also generate singlet oxygen.^{32,33} In an isotopic labeling experiment, Jones and Bayes have found evidence for efficient electronic energy transfer between oxygen molecules.³⁴ The interpretation of Jones and Bayes' experiment has recently been disputed;³⁵ however, if confirmed, their results indicate that the energy transfer radius for singlet oxygen reactions can be significantly extended.

This theoretical investigation also predicted a deuterium substitution effect on the rate of generation of singlet oxygen via the involvement of the Franck-Condon factors. Benson and Geacintov have demonstrated this effect on the triplet quenching rate for deuterium substituted aromatic hydrocarbons.³⁶ A variation in the ratio of [$^1\Sigma_g^+$]/[$^1\Delta_g$] production with the energy of the triplet state is also predicted by the theory; however, a clear experimental verification of this aspect is still lacking.

B. Adiabatic State Correlation Diagrams. Another approach which is widely applied to singlet oxygen reactions is the construction of adiabatic state correlation diagrams with varying degrees of theoretical sophistication.³⁷ One approach developed by Khan and Kearns³⁸ uses (1) available thermodynamic information on the total energy of the initial and the final states, (2) available spectroscopic information for the electronic excited states, and (3) adiabatic orbital correlations to correlate the initial and the final states, to follow the adiabatic transformation of the states from the reactants to the products. Figure 3 shows an adiabatic state correlation diagram for the reaction of molecular oxygen with a cis diene giving a 1,4 endoperoxide and the subsequent dissociation of

the peroxide to give either the reactants back or, by cleavage of the O–O bond, a diradical species. In the initial reaction of molecular oxygen with the diene, the ${}^1\Delta_g$ state correlates smoothly to the ground state of the peroxide. In contrast the ground state ${}^3\Sigma_g^-$ of molecular oxygen correlates with the first triplet state of the peroxide in an endothermic fashion. Starting from the ground state of the peroxide, thermal excitation would lead to the production of the diradical species as long as ΔE_3 is much smaller than ΔE_1 . Since this relative energy difference varies with the resonance energy of the organic molecule, the relative energies of ΔE_1 and ΔE_3 can be reversed, and thermal dissociation of the peroxide could follow the reverse reaction and produce singlet oxygen. For example, anthracene peroxide is expected to dissociate into diradicals. In contrast rubrene peroxide and 9,10-diphenylanthracene peroxide thermally dissociate to yield singlet oxygen and the parent hydrocarbon.^{39,40}

Methods of Generation and Detection

In addition to the energy transfer reactions, microwave discharge reactions, and thermal dissociations of endoperoxides already discussed, singlet oxygen can be generated by thermal dissociation of ozone phosphite,⁴¹ basic hydrolysis of PAN (peroxyacetyl nitrates which are the major irritants of photochemical smog),⁴² enzymatic reactions,^{43–45} and electron transfer reactions involving the superoxide anion, O_2^- .^{46–48}

The methods of detection of singlet oxygen have been extensively reviewed; see, for example, the excellent review by Wayne.⁴⁹ A word of caution here is appropriate. In systems generating singlet oxygen in small quantities or in environments in which singlet oxygen is strongly quenched as in single phase aqueous media where the intrinsic lifetime of the ${}^1\Delta_g$ species is reduced from 45 min to 2 μ s, the detection of singlet oxygen by its emission is almost impossible. Experimentally in medium or low resolution spectra, the emission from a singlet oxygen state has an identical frequency whether originating in the low pressure gas phase or in an aqueous matrix. Because of the Franck–Condon factors of the oxygen molecule, only the (0,0) transitions from single molecule states and (0,0) and (0,1) transitions from double molecule states are to be expected. These are ${}^1\Sigma_g^+ \rightarrow {}^3\Sigma_g^-$, (0,0) λ 7620 Å; ${}^1\Delta_g \rightarrow {}^3\Sigma_g^-$, (0,0) λ 12 687 Å; $[({}^1\Delta_g)({}^1\Delta_g)] \rightarrow [({}^3\Sigma_g^-)({}^3\Sigma_g^-)]$, (0,0) λ 6334 Å, (0,1) λ 7032 Å. Identification based on only $[({}^1\Sigma_g^+)({}^1\Delta_g)] \rightarrow [({}^3\Sigma_g^-)({}^3\Sigma_g^-)]$, (0,0) λ 4780 Å without other supporting spectral evidence is not a critical test for the presence of singlet oxygen. Considering the chemical methods of detection, only the formation of transannular peroxides with aromatic hydrocarbons is specific for singlet oxygen. Other chemical methods should be subject to the warnings of Kearns.²⁰ Kinetic effects such as the quenching by β -carotene and lifetime variations introduced by substituting deuterated solvents²² are not unequivocal tests of the presence of singlet oxygen and should be considered with caution.

Chemiluminescence

The discovery of singlet oxygen in the H_2O_2/OCl^- reaction has had a large impact on the field of chemiluminescence reactions because the H_2O_2/OCl^- system is often used as a luminescence charger in the chemiluminescence reactions of organic molecules. Generally in vitro chemiluminescence reactions are characterized by (1) a requirement for molecular oxygen or peroxide, (2) an apparent square dependence of the light intensity on the peroxide decomposition, and (3) a luminescence which usually corresponds to the fluorescence of

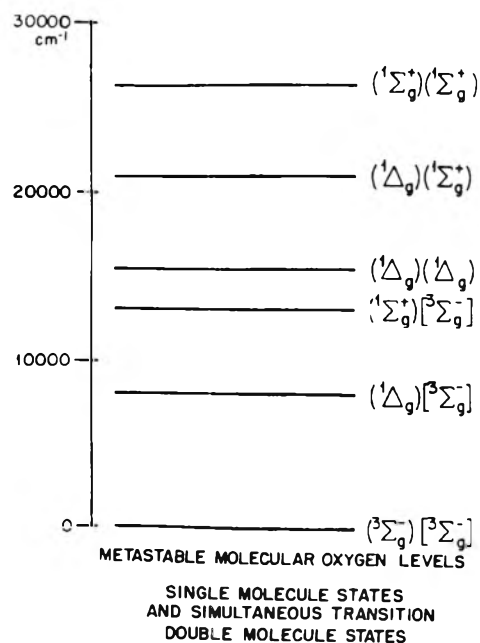


Figure 4. Complete experimental energy level diagram of molecular oxygen up to the near-uv observed for single molecule states and simultaneous transition molecular pair states. Adapted from Khan and Kasha.⁵

the organic molecule.^{5,15} The difficulty in understanding these chemiluminescence reactions involves the energetics of the reaction; a blue photon, for example, has about 70–80 kcal mol⁻¹ of energy, but the H_2O_2/OCl^- reaction produces only about 32 kcal mol⁻¹.

Khan and Kasha suggested that the rich variety of double molecule states of molecular oxygen observed in the H_2O_2/OCl^- chemiluminescence (Figure 4) could be used as a quantum ladder for sensitizing the luminescence of organic molecules. This mechanism satisfies the known characteristics of these chemiluminescence reactions and the energy requirements.^{5,15}

A somewhat different mechanism involving the stepwise energy transfer from two singlet oxygen molecules to the organic fluorescer was suggested by Ogryzlo and Pearson.⁵⁰ The first energy transfer collision excites the organic molecule to its triplet state and the second to its singlet excited state. Rubrene chemiluminescence seems to proceed by energy transfer from double molecule states of singlet oxygen,⁵¹ while vilanthrone chemiluminescence has been attributed to stepwise excitation by singlet oxygen.⁵² However, the exact location of the triplet state is not known for either molecule. The results of Nilsson and Kearns from an investigation of the sensitized fluorescence of fluorescein by H_2O_2/OCl^- seem to support a double molecule sensitization by singlet oxygen.⁵³

Recently Brabham and Kasha have studied an unusual infrared chemiluminescence from thiazine dyes sensitized by H_2O_2/OCl^- .⁵⁴ The luminescence does not correspond to the fluorescence of the dye molecules, and Brabham and Kasha have suggested the direct sensitization of the triplet state of the dye molecule by energy transfer from ${}^1\Sigma_g^+$ without the involvement of double molecule states.

A group of chemiluminescence reactions which do not suffer from the energy deficiency described above involve the thermal decomposition of dioxetanes. Participation of singlet oxygen in this mechanism comes in the initial 1,2 cycloaddition reaction with dienes to generate the dioxetane. Figure 5

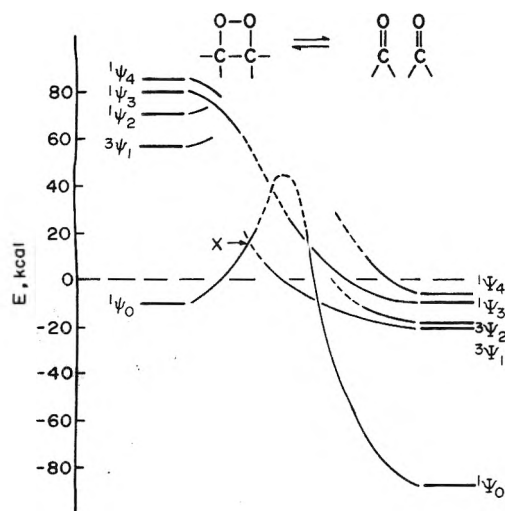


Figure 5. Generalized adiabatic state correlation diagram for the decomposition of a dioxetane generated by 1,2 cycloaddition of singlet oxygen to an olefin. Thermochemical and spectroscopic data and information from orbital correlations between the reactants and the products were used to construct the diagram. Adapted from Kearns and Khan.⁵⁵

is an adiabatic state correlation diagram of the decomposition reaction constructed by Kearns and Khan.⁵⁵ Energetic considerations predict a singlet-triplet intersystem crossing in the transition state leading to the generation of one of the two carbonyl fragments in the electronically excited triplet state and the other in the ground singlet state. Recent work by Turro and Devaquet on the photochemical fragmentation of tetramethyl-1,2-dioxetane⁵⁶ and by Wilson and Schaap on the thermal decomposition of *cis*-diethoxy-1,2-dioxetane support this suggestion.⁵⁷

Although no one general mechanism for chemiluminescence reactions sensitized by singlet oxygen has yet emerged, research in this field has been greatly stimulated by the discovery of singlet oxygen in chemical systems.

Molecular Oxygen Enhanced Fluorescence

Singlet Oxygen-Triplet Organic Molecule Annihilation Fluorescence. Geacintov, Oster, and Cassen, in studying the fluorescence of organic molecules in polymer matrices, found that for 1,2:5,6-dibenzanthracene in polystyrene matrix the fluorescence intensity of the evacuated sample is less than that of the sample equilibrated in air,⁵⁸ a very unusual observation in view of the well-known oxygen quenching effect on luminescence. In an investigation of this effect Bolton, Kenner, and Khan suggested a singlet oxygen feedback mechanism: $T_1 + {}^1O_2 ({}^1\Sigma_g^+ \text{ or } {}^1\Delta_g) \rightarrow S_1 + {}^3O_2 ({}^3\Sigma_g^-)$ where T_1 and S_1 are the first excited triplet and the first excited singlet states, respectively, of the organic molecule.⁵⁹ This interpretation was disputed by Jones and Nesbitt who suggested that in reality the phenomenon was a trivial ground state depletion effect; i.e., depletion of the ground state singlet concentration of the organic molecule in the evacuated sample produced an apparent enhancement on exposure of the sample to air when the ground state population was replenished by quenching of T_1 by oxygen.⁶⁰ The Jones and Nesbitt mechanism clearly predicts that the maximum fluorescence enhancement is equal to the steady state triplet population of the organic molecule in the evacuated sample. To examine this possibility, Kenner and Khan performed a cross beam experiment directly monitoring the steady state triplet population of the organic molecule immediately before admitting air to the system and

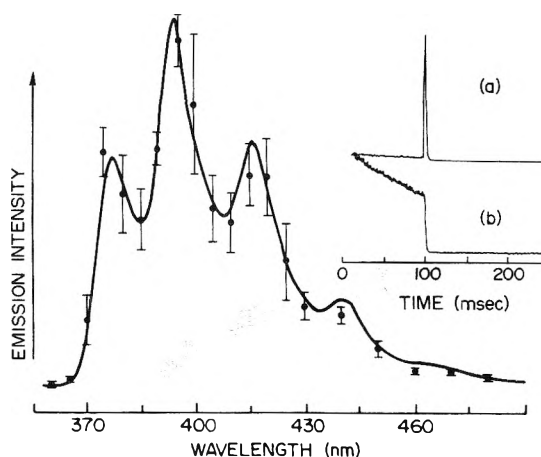


Figure 6. Representative oscillogram of the fluorescence burst on the admission of air in the dark to chrysenes ($\sim 10^{-2}$ M) in a polystyrene fluff. (a) is the oxygen induced fluorescence burst, (b) the accompanying phosphorescence quenching. The solid line in the spectrum is the normal fluorescence spectrum of the sample. The points are the average relative intensity of the oxygen induced fluorescence. Adapted from Kenner and Khan.⁶¹

measuring the enhancement.⁶¹ The results show that the magnitude of the enhancement is far larger than could be expected from a ground state depletion effect; for example, a 71% enhancement is found for 1,2:5,6-dibenzanthracene in polystyrene matrix for a 9.3% steady state triplet population.

To remove any remaining ambiguity, a further experiment was designed using organic fluorophores embedded in polymer fluffs. The fluff containing the chromophore was placed in an evacuated system and excited with a 1000-W xenon lamp. After the exciting radiation was cutoff, the sample continued to phosphoresce strongly, and on exposure to air, a sharp burst of light accompanied the quenching of the phosphorescence. In the absence of any exciting radiation, this fluorescence burst could only have originated from a singlet oxygen feedback mechanism. Figure 6 shows a representative oscillogram of the flash and a spectral analysis indicating that the emission corresponds to the fluorescence of the organic molecule.⁶¹

In high resolution gas phase experiments Ishiwata et al. have found a triplet HNO-singlet oxygen annihilation fluorescence from the reaction $\text{HNO} ({}^3A'') + O_2 ({}^1\Delta_g) \rightarrow \text{HNO} ({}^1A') + O_2 ({}^3\Sigma_g^-)$.⁶² Giachardi et al., reacting electronically excited states of NO_2 with molecular oxygen, have found evidence for the enrichment of the $O_2 ({}^1\Sigma_g^+)$ population from the reaction $\text{NO}_2^* + O_2 ({}^1\Delta_g) \rightarrow \text{NO}_2 + O_2 ({}^1\Sigma_g^+)$ in discharge experiments.⁶³ These experiments illustrate the energy pooling options available by energy transfer to ground and excited molecular oxygen.

Theory of Electron Transfer Generation and Quenching of Singlet Oxygen (${}^1\Sigma_g^+$ and ${}^1\Delta_g$) by Superoxide Anion

A. Generation of Singlet Oxygen (${}^1\Sigma_g^+$ and ${}^1\Delta_g$) from Superoxide Anion. One of the startling recent advances in enzyme chemistry was the suggestion of⁶⁴ and the direct identification of the presence of the superoxide anion, O_2^- , by EPR measurements in the xanthine-xanthine oxidase system.⁶⁵ Recently a controversy has arisen over whether or not singlet oxygen can be generated in electron transfer reactions of the O_2^- ion. A weak luminescence of organic chromophores can be sensitized in dimethyl sulfoxide (Me_2SO) solutions of O_2^- when a small amount of moisture is added to

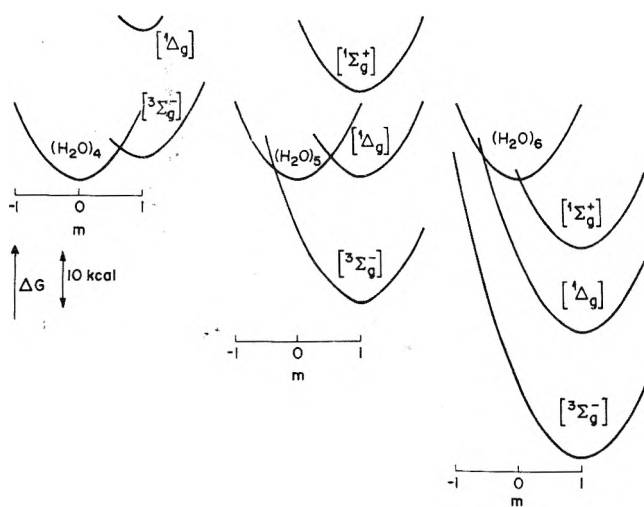


Figure 7. Potential energy diagrams for the dismutation reactions: (A) $\text{O}_2^{\cdot-}(\text{H}_2\text{O})_4 + \text{O}_2^{\cdot-}(\text{H}_2\text{O})_4 \rightarrow \text{O}_2^{2-}(\text{H}_2\text{O})_4 + \text{O}_2(\text{H}_2\text{O})_4$; (B) $\text{O}_2^{\cdot-}(\text{H}_2\text{O})_5 + \text{O}_2^{\cdot-}(\text{H}_2\text{O})_5 \rightarrow \text{O}_2^{2-}(\text{H}_2\text{O})_5 + \text{O}_2(\text{H}_2\text{O})_5$; and (C) $\text{O}_2^{\cdot-}(\text{H}_2\text{O})_6 + \text{O}_2^{\cdot-}(\text{H}_2\text{O})_6 \rightarrow \text{O}_2^{2-}(\text{H}_2\text{O})_6 + \text{O}_2(\text{H}_2\text{O})_6$. The potential well for the combined reactants is labeled $(\text{H}_2\text{O})_n$ and the wells for the combined products are labeled explicitly by the molecular oxygen state. m is the fraction of charge transferred, $-1 \leq m \leq +1$.

the solution.^{46,53} Trace amounts of peroxides can be detected by the iodide test using 2,5-dimethylfuran as the singlet oxygen scavenger in a moist Me_2SO solution of the superoxide anion.⁴⁶ In a similar experiment Nilsson and Kearns failed to obtain sufficient singlet oxygen addition products with chemical scavengers to isolate by chromatographic techniques.⁵³ However, Mayeda and Bard have obtained products characteristic of singlet oxygen in the reaction of 1,3-diphenylisobenzofuran in the electrochemical generation of $\text{O}_2^{\cdot-}$.⁴⁷ Pederson and Aust have isolated the singlet oxygen addition product of the scavenger 1,3-diphenylisobenzofuran by paper chromatographic techniques from the lipid peroxidation reaction of xanthine oxidase.⁴³ Because of the potential importance of the generation of singlet oxygen from $\text{O}_2^{\cdot-}$ in enzymatic systems, we have investigated theoretically the generation of excited oxygen from the dismutation reaction of $\text{O}_2^{\cdot-}$ using the electron transfer theory of Marcus.

Since the presence of moisture has been found to be critical in experimental studies involving $\text{O}_2^{\cdot-}$ in solution^{46,53} and gas phase,⁴⁸ we have examined theoretically the consequences of the presence of varying amounts of H_2O molecules on the dismutation reaction of the superoxide anion. Hydration energies for the $\text{O}_2^{\cdot-}$ ion can be obtained from gas phase dissociation energies D_0 for ion clusters $\text{O}_2^{\cdot-}(\text{H}_2\text{O})_n$, D_0 , $\text{O}_2^{\cdot-}(\text{H}_2\text{O})_n \rightarrow \text{O}_2^{\cdot-} + n(\text{H}_2\text{O})$, available from mass spectroscopic studies of thermal electron attachment to O_2 .^{66,67} These are: $n = 1$, 18.4; $n = 2$, 35.6; $n = 3$, 51; and $n = 5$, 76 (kcal mol⁻¹). We have estimated values for $n = 4$ and 6 from a plot of D_0 vs n . Since hydration energy is directly proportional to the square of the ionic charge, D_0 for $\text{O}_2^{2-}(\text{H}_2\text{O})_n$ can be approximated as four times that of D_0 $\text{O}_2^{\cdot-}(\text{H}_2\text{O})_n$ for a given n . The oxygen molecule has relatively little solvent interaction; therefore the hydration energy of O_2 is approximately zero. Then, equating entropic terms for the initial and final states, the free energy of the reaction $\text{O}_2^{\cdot-}(\text{H}_2\text{O})_n + \text{O}_2^{\cdot-}(\text{H}_2\text{O})_n \rightarrow \text{O}_2^{2-}(\text{H}_2\text{O})_n + \text{O}_2(\text{H}_2\text{O})_n$ can be estimated using the electron affinity of O_2 (10 kcal mol⁻¹) and ΔH_f (110 kcal mol⁻¹) for the reaction $\text{O}_2 + 2e^- \rightarrow \text{O}_2^{2-}$ available from Born-Haber cycle calculations.⁶⁸ The ion clusters $\text{O}_2^{\cdot-}(\text{H}_2\text{O})_n$ were considered embedded in a dielectric continuum (Me_2SO)

where $(\text{H}_2\text{O})_n$ represents the inner coordination shell of the $\text{O}_2^{\cdot-}$ ion. The free energy change resulting from the solvation of reactant and product cluster in the aprotic solvent Me_2SO was assumed negligible since the inner coordination sphere about the ion is considered fixed at a given n . Subsequent chemical reaction of $\text{O}_2^{2-}(\text{H}_2\text{O})_n$ was not considered.

In the initial state of the electron transfer reaction each cluster is surrounded by a shell of oriented solvent dipoles. From the theory of Marcus on adiabatic electron transfer reactions,⁶⁹⁻⁷¹ on proceeding from the initial state of the reaction a crossing point is reached where the spatial configurations of the nuclei, including the solvent orientation, are the same for both the reactants and products. This intersection point represents the activation barrier ΔG_d^* of the reaction. Marcus has developed an empirical formula $G_d = m^2\lambda$ where $-1 \leq m \leq +1$ is the fraction of charge transferred and therefore $m = 0$ is the initial state of the reaction, and λ is a constant depending upon the polarizability of the solvent, the size of the ions, and the interionic separation distance. To estimate λ , we have used the theoretically derived expression, $\lambda = (\Delta e^2/2)(\frac{1}{2}a_1 + \frac{1}{2}a_2 - 1/R)(1/\epsilon_{\text{op}} - 1/\epsilon_s)$; where Δe is the total electronic charge transferred; a_1 and a_2 the ionic radii; R the interionic separation, and ϵ_{op} and ϵ_s the optical and static dielectric constants, respectively.⁶⁹ The distance R of closest approach between two hydrated $\text{O}_2^{\cdot-}$ ions in Me_2SO solution will be limited by the Coulombic repulsion and by the increasingly massive reorientation of the solvent dipoles by the approach of the second ion. An $R = 10 \text{ \AA}$, approximately corresponding to the separation of the ions by two solvent layers, is expected to be a reasonable limiting distance.⁷¹

Figure 7 shows the resulting potential energy surfaces, $G_d = m^2\lambda$, for the dismutation reaction with $n = 4, 5$, and 6 H_2O molecules. The bottoms of the wells represent ΔG going from the initial (left-hand side) state to the final (right-hand side) states. The intersections of the wells correspond to ΔG_d^* the activation barrier imposed by the reorientation of the nuclear configurations from the initial state at $m = 0$.⁷⁰ Interactions between electronic states of the same multiplicity will cause splitting at the intersection point, i.e., the lowering of the activation barrier. At $R = 10 \text{ \AA}$ this effect will be small and is not considered in the present discussion. A comparison of the wells for $n = 4, 5$, and 6 is a striking illustration of the critical effect of water on the energetics of the dismutation reaction. Moreover, as the free energy change of the dismutation reaction becomes increasingly large and negative, the intersection point where the potential surface of the ground state products crosses the potential surface of the reactants becomes increasingly inaccessible.⁷⁰ For $n = 4$, $\text{O}_2(^3\Sigma_g^-)$ is the only energetically accessible product. For $n = 5$, the route to the excited product $\text{O}_2(^1\Delta_g)$ is also accessible. For $n = 6$, $\text{O}_2(^3\Sigma_g^-)$ is inaccessible and only excited oxygen is produced with $\text{O}_2(^1\Sigma_g^+)$ predominating.

Marcus gives an expression to estimate the reaction rate $k = Z\kappa\rho \exp(-\Delta G_d^*/kT)$ where Z , the number of collisions occurring between two neutral species in a unit volume of solution in a unit time interval for $R = 10 \text{ \AA}$, is $10^{11} \text{ mol}^{-1} \text{ s}^{-1}$ and κ and ρ are approximately unity.⁶⁹ Adding a statistical factor g of $3/4$ for crossing to the triplet ground state of O_2 and $1/4$ for crossing to the singlet excited states, the estimated rates for the dismutation reaction at room temperature are given in Table I.

The rates in Table I are expected to be accurate insofar as they illustrate the general trend of excited oxygen production as H_2O is added to the solution. Increasing the estimated ionic radii has no appreciable effect on the results. Decreasing the

ionic radius down to 2.4 Å changes the relative ratios of the O₂ species produced. However, at $n = 6$, singlet oxygen is clearly the dominant product. This theoretical analysis emphasizes the critical nature of H₂O concentration on the generation of excited oxygen in the dismutation reaction predicting narrow concentration region over which O₂(¹Δ_g) can be efficiently generated. At higher H₂O concentration the dismutation reaction generates O₂(¹Σ_g⁺).

B. Quenching of Singlet Oxygen (¹Σ_g⁺ and ¹Δ_g) by Superoxide Anion. The possibility that singlet oxygen (¹Σ_g⁺ or ¹Δ_g) could be efficiently quenched by an electron transfer reaction with the ground state O₂⁻(²π) ion has been explored for O₂⁻ + O₂(¹Δ_g) → O₂(³Σ_g⁻) + O₂⁻ and O₂⁻ + O₂(¹Σ_g⁺) → O₂(³Σ_g⁻) + O₂⁻. The quenching rates obtained for O₂(¹Δ_g) and O₂(¹Σ_g⁺) quenching by O₂⁻ in dry Me₂SO can be estimated using the electron transfer theory.⁶⁷⁻⁶⁹ The magnitude of the quenching rate depends on the singlet oxygen species and varies with the effective ionic and molecular radii in solution. Quenching of ¹Σ_g⁺ is predicted to be very rapid (10¹⁰-10¹¹ M⁻¹ s⁻¹). Quenching of ¹Δ_g varies with the axial orientation of the oxygen molecule and the O₂⁻ ion (minor to minor 5 × 10⁸, minor to major 5 × 10⁹ for either possibility, and major to major 3 × 10¹⁰), but quenching in all cases is expected to be efficient.

This clearly predicts that it will be difficult to detect singlet oxygen in Me₂SO solutions having high O₂⁻ concentration. There is a self-limiting quenching effect under our earlier experimental conditions⁴⁶ and improving the singlet oxygen yield from O₂⁻ solutions in nonaqueous solvents is not straightforward. Enzymatic generation of the superoxide ion occurs in the hydrophobic environment surrounding the active site. Enzymatic control of water and O₂⁻ concentration could yield appreciable singlet oxygen production; on the other hand, generation of singlet oxygen in other enzymatic systems could indicate the presence of a few aberrant H₂O molecules.

Optical Residue Singlet Oxygen Theory of Photocarcinogenicity

In 1970 Khan and Kasha suggested a mechanism for the photocarcinogenic activity of the polycyclic hydrocarbons (PCH) involving the intermediacy of singlet oxygen.⁷² The PCHs have two active sites for electrophilic addition: the K region that results in addition to two adjacent carbons and an L region that results in addition to para carbons across the ring. The Pullmans have performed extensive theoretical calculations on the charge density distribution of the PCHs and have related the carcinogenic activity of the molecule to a limiting charge density value for the K region of the PCH.⁷³

Khan and Kasha suggested that, in order to initiate photocarcinogenesis, the optical properties of the bound PCH must be such that the residual bound molecule continues to absorb natural light (visible or near ultraviolet). Optical excitation of the residual molecule to a singlet excited state is followed by intersystem crossing to a long-lived triplet state and oxygen quenching of the triplet state generates singlet oxygen by energy transfer. The singlet oxygen then reacts with cellular material such as DNA to initiate the carcinogenic process. This mechanism accounts for the observation that a chemically active K region tends to increase the carcinogenicity of a PCH while an active L region decreases it; addition at a K region to adjacent carbon atoms on the PCH leaves a residual molecule more likely to absorb natural light than transannular addition to the carbon atoms of an L region

TABLE I

O ₂ species	g	$k = g\rho\kappa Z$ exp $(-\Delta G_d^*/kT)$, ^a M ⁻¹ s ⁻¹
O ₂ ⁻ (H ₂ O) ₄	³ Σ _g ⁻	3/4
	¹ Δ _g	1/4
	¹ Σ _g ⁺	1/4
O ₂ ⁻ (H ₂ O) ₅	³ Σ _g ⁻	3/4
	¹ Δ _g	1/4
	¹ Σ _g ⁺	1/4
O ₂ ⁻ (H ₂ O) ₆	³ Σ _g ⁻	3/4
	¹ Δ _g	1/4
	¹ Σ _g ⁺	1/4

^a References 69 and 70.

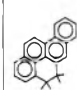
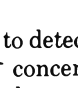
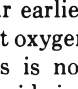
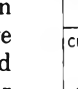
PRECURSOR HYDROCARBON	ABSORPTION ONSET (Room temp) λ _A	OPTICAL RESIDUE	HYDROCARBON ANALOG OPTICAL RESIDUE	ABSORPTION ONSET (Room temp) λ _A	PHOTOCARCINOGENIC ACTIVITY EXCITING AT λ = 3660	
					FROM THEORY	EXPERIMENTAL OBSERVATION*
Benzo[<i>a</i>]pyrene	4166		Chrysene	3703	YES	YES
Benzo[<i>b</i>]pyrene	3846		Triphenylene	3490	NO	NO
Pyrene	3802		Phenanthrene	3500	NO	NO
Chrysene	3703		Naphthalene	3190	NO	NO

Figure 8. A schematic representation of the optical residues and their optical analogues for four polycyclic hydrocarbons. Optical absorption onset is shown. Predicted photocarcinogenic activity from the optical residue theory and experimental observation from Cavalieri and Calvin⁷⁷ are presented.

which may remove more than one ring from the conjugated system.⁷²

There is a strong synergistic light effect on the carcinogenicity of the PCHs. Santamaria et al.⁷⁴ and Khan and Lipner⁷⁵ have shown that in a collection of mice painted with benz(*a*)-pyrene the incidence of carcinogenesis increases for the group kept in natural light as compared to those maintained in the dark. Moreover, chemical evidence indicates that the PCH is metabolized in vivo by preferential binding at the K region as predicted by the Pullmans.⁷⁶ Recently Cavalieri and Calvin have suggested that binding of the carcinogen benz(*a*)pyrene to cellular constituent, especially the DNA bases, occurs at the 6 position rather than at the (4, 5) K region of the PCH.⁷⁷ They have isolated and identified a 6-position adduct of benz(*a*)pyrene with 1-methylcytosine from photochemical reaction in a deoxygenated system (a continuous stream of N₂ was bubbled through the solution). However, isotopic labeling studies have shown that the metabolism of the PCHs in vivo incorporates atmospheric oxygen,⁷⁶ and the photoadducts isolated by Cavalieri and Calvin probably do not duplicate the metabolic products of benz(*a*)pyrene. Cavalieri and Calvin also investigated the photoenhanced carcinogenicity of chrysene, pyrene, benz(*e*)pyrene, and benz(*a*)pyrene by comparing the tumor incidence of four groups of mice each painted with one of the PCHs and kept in natural light to four

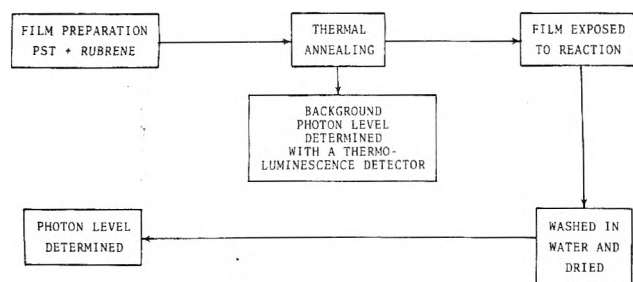


Figure 9. Flow chart for the singlet oxygen photon storage technique showing the major steps.

similarly painted groups kept in natural light and also irradiated at regular intervals with 3660-Å light from an Hg lamp.⁷⁷ Of the PCHs chosen only benz(a)pyrene is known experimentally to be carcinogenic; however, the K values of each are very similar. The structural and bond order similarities between benz(a)pyrene and benz(e)pyrene make this a particularly interesting experiment. Irradiation with 3660-Å light failed to induce carcinogenesis in the groups painted with chrysene, pyrene, or with benz(e)pyrene, but the incidence of tumors was doubled in the irradiated group painted with benz(a)pyrene as compared to the benz(a)pyrene group kept in natural light.⁷⁷ Since the absorption spectra of the 6-position adduct is perturbed only slightly from that of the precursor hydrocarbon and all of the parent compounds strongly absorb 3660-Å light, and longer, these results are difficult to reconcile with cellular binding at the 6 position. However, the optical residue model predicts exactly these results since, after binding at the K region, only the bound residue of benz(a)pyrene could absorb 3660-Å light (see Figure 8). Furthermore, these results strongly suggest that cellular binding is of the type indicated in Figure 8.

Polymer Supported Singlet Oxygen Photon Storage (with H. C. Pant, to be published)

Now that singlet oxygen is well established as a chemical reagent and circumstantial evidence has accumulated for singlet oxygen activity in biological systems, a sensitive analytical technique for the detection of singlet oxygen is needed which has the potential of incorporating the specificity of a chemical scavenger and the sensitivity of photon detection, but does not interfere with ongoing reactions. We have designed such a system, suitable for the detection of $O_2(^1\Delta_g)$ in aqueous solutions, using the reaction of singlet oxygen with rubrene to form the transannular peroxide. The transannular peroxide is produced exclusively by singlet oxygen ($^1\Delta_g$) addition.³⁹ On thermal decomposition of the peroxide, the rubrene molecule is regenerated with an accompanying chemiluminescence characteristic of rubrene fluorescence. The regenerated singlet oxygen is involved in the chemiluminescence; however, the mechanism of the chemiluminescence, although fairly well characterized, is not at present germane to this technique.

The flow chart of the photon storage technique is given in Figure 9. Thin films (approximately 100 μ) are made by evaporating a solution of rubrene and polystyrene in benzene. After evacuation in a vacuum chamber for 7 days, the film is cut into small sections approximately 2 \times 3 cm. All subsequent steps take place in the dark. The film is annealed by slowly raising the temperature of the oven to 130 °C and maintaining it at that temperature for 20 min. The sample is removed from the oven and allowed to cool to room temperature overnight.

TABLE II: Polymer Supported Singlet Oxygen Photon Storage Technique

Experimental conditions	Integrated photon counts	Comment
1. Room light	25 000	Involves the bulk of the polymer film.
2. Background (after annealing)	106	
3. H ₂ O ₂ (~30% aq soln)	200	
4. NaOCl (~7% aq soln)	500	
5. H ₂ O ₂ (~30%) + NaOCl (~7%)	1 528	Involves mainly the surface of the film.
6. Xanthine solution ^a	105	
7. Xanthine oxidase ^a	107	
8. Xanthine-xanthine oxidase ^a	1 073	Involves mainly the surface of the film.
9. Recheck background	105	

^a The xanthine-xanthine oxidase system contained xanthine and 50 μ g/ml of xanthine oxidase (50 μ g/ml of xanthine oxidase (Sigma type 1) was dissolved in 0.05 M Tris-HCl (pH 7.5) and the solution was passed through a Sephadex G-50 column immediately prior to use), 0.25 M Tris-HCl (pH 6.8 at 37 °C), 0.25 M NaCl, 0.1 mM FeCl₃, and 0.1 mM EDTA-Fe. The reaction of the air saturated solution was initiated by the addition of xanthine oxidase. The reaction ran for 30 min.

Next the background photon count is made with a Teledyne isotope thermoluminescence detector Model 7300. The four cycle operation of the instrument was modified to operate in two cycles. In the first part of the cycle the film is heated at the rate of 30 °C/s to a temperature of 140 °C by passing a current through an infrared heater. The temperature is held at 140 °C for approximately 8 s via a feedback mechanism, the total time of this cycle being 18 s. The total number of photons emitted during this interval is counted by a photomultiplier (RCA 9750A) and displayed as a digital number. An infrared cutoff filter and a CS 2-59 filter to cutoff the blue end of the spectrum isolates the rubrene fluorescence. The second part of the cycle consists of cooling the sample. The stability of the electronics was calibrated against a C-14 radioactive source embedded in a polymer matrix containing blue phosphors. The overall reproducibility of the data was better than $\pm 1\%$. If the background count is high, further annealing is done; or, if it is reasonably low, three or four flash heating cycles are repeated until the count is small and constant.

Once the film is characterized (note: All steps are in the dark), the same film is placed in the reacting matrix for an appropriate time period. The sample is then removed and thoroughly washed in flowing distilled water for several hours and dried by evacuation in a dark chamber for at least 2 days. Thorough washing and subsequent drying are necessary, since, apart from direct optical excitation, all reactions take place on the surface of the film. Then the film is placed in the TLD and photon counted, and the photon count is compared against the initial background value. The film is again flash heated several times to return it to a stable background count which constitutes the final check on the film, and the film is ready for reuse. Table II is a typical run for a single film. Since the formation of rubrene peroxide is a specific singlet oxygen reaction, this is an unambiguous demonstration of the generation of singlet oxygen in the xanthine-xanthine oxidase system. The pure OCl⁻ (7% solution) system gives a consistently high photon count. The reason for this is not yet clear and is under investigation. Various modifications of the films

and the singlet oxygen acceptor are currently under investigation.

Conclusion

The discovery of singlet oxygen in chemical systems has helped to explain many puzzling oxygen dependent luminescent and chemical phenomena. Interest is currently being directed toward the biological activity of singlet oxygen. Recent developments include research on the photodynamic effect,⁷⁸ therapeutic treatment of neonatal jaundice by the photooxygenation of bilirubin,⁷⁹ and the biosynthesis of prostaglandin.⁸⁰ 8-Methoxypsoralen, a known carcinogen, has been shown to generate singlet oxygen by energy transfer.⁸¹ β -Carotene efficiently quenches singlet oxygen apparently by a physical method and has been postulated to be involved in protecting photosynthetic units from singlet oxygen.⁸² Vitamin E has one of the highest chemical reactivities toward singlet oxygen.⁸³⁻⁸⁵ Singlet oxygen has also been suggested to be involved in the photochemical generation of smog.^{86,87}

References and Notes

- Presented at the Michael Kasha Symposium on Energy Transfer in Organic, Inorganic, and Biological Systems, held at Florida State University at Tallahassee, Fla., Jan 8-10, 1976.
- (a) R. S. Mulliken, *Phys. Rev.*, **32**, 880 (1932); (b) *Rev. Mod. Phys.*, **4**, 1 (1932).
- G. Herzberg, "Spectra of Diatomic Molecules", Van Nostrand, Princeton, N.J., 1950.
- A. U. Khan and M. Kasha, *J. Chem. Phys.*, **39**, 2105 (1963); **40**, 605 (1964).
- A. U. Khan and M. Kasha, *J. Am. Chem. Soc.*, **92**, 3293 (1970).
- L. Mallet, *Compt. Rend.*, **185**, 352 (1927).
- P. Groh, *Bull. Soc. Chim. Fr.*, **5**, 12 (1938).
- P. Groh and K. A. Kirrman, *C. R. Acad. Sci., Paris*, **215**, 275 (1942).
- G. Gattow and A. Schneider, *Naturwissenschaften*, **41**, 116 (1954).
- H. H. Seliger, *Anal. Biochem.*, **1**, 60 (1960).
- J. Stauff and H. Schmidkunz, *Z. Phys. Chem. (Frankfurt am Main)*, **35**, 295 (1962).
- A. E. Cahill and H. Taube, *J. Am. Chem. Soc.*, **74**, 2312 (1952).
- S. J. Arnold, E. A. Ogryzlo, and H. Witzke, *J. Chem. Phys.*, **40**, 1769 (1964); R. J. Browne and E. A. Ogryzlo, *Proc. Chem. Soc.*, 117 (1964).
- A. U. Khan and M. Kasha, *Nature (London)*, **204**, 241 (1964).
- A. U. Khan and M. Kasha, *J. Am. Chem. Soc.*, **88**, 1574 (1966).
- H. Kautsky, *Trans. Faraday Soc.*, **35**, 216 (1939).
- E. J. Corey and W. C. Taylor, *J. Am. Chem. Soc.*, **86**, 3881 (1964).
- C. S. Foote and S. Wexler, *J. Am. Chem. Soc.*, **86**, 3879, 3880 (1964).
- C. S. Foote, *Acc. Chem. Res.*, **1**, 104 (1968).
- D. R. Kearns, *Chem. Rev.*, **71**, 395 (1971), and references therein.
- I. B. C. Matheson and J. Lee, *Chem. Phys. Lett.*, **14**, 350 (1972).
- P. B. Merkel and D. R. Kearns, *J. Am. Chem. Soc.*, **94**, 7244 (1972).
- B. Stevens and J. A. Ors, Michael Kasha Symposium on Energy Transfer, Florida State University, Tallahassee, Fla., Jan 8-10, 1976, Abstract p 10.
- K. Kawaoka, A. U. Khan, and D. R. Kearns, *J. Chem. Phys.*, **46**, 1842 (1967), and references therein.
- G. W. Robinson and R. P. Frosch, *J. Chem. Phys.*, **37**, 1962 (1962); **38**, 1187 (1963).
- W. Siebrand, *J. Chem. Phys.*, **44**, 4055 (1966).
- D. R. Snelling, *Chem. Phys. Lett.*, **2**, 345 (1968).
- D. R. Kearns, A. U. Khan, C. K. Duncan, and A. H. Maki, *J. Am. Chem. Soc.*, **91**, 1039 (1969).
- E. Wasserman, V. J. Kuck, W. H. Delman, and W. A. Yager, *J. Am. Chem. Soc.*, **91**, 1040 (1969).
- C. K. Duncan and D. R. Kearns, *J. Chem. Phys.*, **55**, 5822 (1971).
- L. J. Andrews and E. W. Abrahamson, *Chem. Phys. Lett.*, **10**, 113 (1971).
- I. T. N. Jones and K. D. Bayes, *Chem. Phys. Lett.*, **11**, 163 (1971).
- T. Frankiewicz and R. S. Berry, *Environ. Sci. Technol.*, **6**, 365 (1972).
- I. T. N. Jones and K. D. Bayes, *J. Chem. Phys.*, **57**, 1003 (1972).
- G. Parker, *J. Chem. Phys.*, **62**, 2235 (1975).
- R. Benson and N. Geacintov, *J. Chem. Phys.*, **60**, 3251 (1974).
- K. Yamaguchi, T. Fueno, and H. Fukutome, *Chem. Phys. Lett.*, **22**, 466 (1973); M. J. S. Dewar and W. Thiel, *J. Am. Chem. Soc.*, **97**, 3978 (1975).
- A. U. Khan and D. R. Kearns, *Adv. Chem. Ser.*, **No. 77**, 143 (1969).
- T. Wilson, *J. Am. Chem. Soc.*, **88**, 2989 (1966).
- H. H. Wasserman, J. R. Scheffer, and J. L. Cooper, *J. Am. Chem. Soc.*, **94**, 4991 (1972).
- R. W. Murray and M. L. Kaplan, *J. Am. Chem. Soc.*, **90**, 4161 (1968).
- R. P. Steer, K. R. Darnall, and J. N. Pitts, *Tetrahedron Lett.*, 3765 (1969).
- T. C. Pederson and S. D. Aust, *Biochem. Biophys. Res. Commun.*, **52**, 1071 (1973).
- K. Goda, J. Chu, T. Kemura, and A. Paul Schaap, *Biochem. Biophys. Res. Commun.*, **52**, 1300 (1973).
- O. F. Oliveira, D. L. Sanioto, and C. Cilento, *Biochem. Biophys. Res. Commun.*, **58**, 391 (1974).
- A. U. Khan, *Science*, **168**, 476 (1970).
- E. A. Mayeda and A. J. Bard, *J. Am. Chem. Soc.*, **95**, 6223 (1973).
- J. Stauff, V. Sander, and W. Jaeschke in "Chemiluminescence and Bioluminescence", M. J. Cormier, D. M. Hercules, and J. Lee, Ed., Plenum Press, New York, N.Y., 1973, p 131.
- R. P. Wayne, *Adv. Photochem.*, **7**, 311 (1969).
- E. A. Ogryzlo and A. E. Pearson, *J. Phys. Chem.*, **72**, 2913 (1968).
- T. Wilson, *J. Am. Chem. Soc.*, **91**, 2387 (1969).
- S. R. Abbott, S. Ness, and D. M. Hercules, *J. Am. Chem. Soc.*, **92**, 1128 (1970).
- R. Nilsson and D. R. Kearns, *J. Phys. Chem.*, **78**, 1681 (1974).
- D. E. Brabham and M. Kasha, *Chem. Phys. Lett.*, **29**, 159 (1974).
- D. R. Kearns and A. U. Khan, *Photochem. Photobiol.*, **10**, 193 (1969).
- N. J. Turro and A. Devaquet, *J. Am. Chem. Soc.*, **97**, 3859 (1975).
- T. Wilson and A. P. Schaap, *J. Am. Chem. Soc.*, **93**, 4126 (1971).
- N. Geacintov, G. Oster, and T. Cassen, *J. Opt. Soc., Am.*, **58**, 1217 (1968).
- P. H. Bolton, R. D. Kenner, and A. U. Khan, *J. Chem. Phys.*, **57**, 5604 (1972).
- P. F. Jones and R. S. Nesbitt, *J. Chem. Phys.*, **59**, 6185 (1973).
- R. D. Kenner and A. U. Khan, *J. Chem. Phys.*, in press; *Chem. Phys. Lett.*, **36**, 643 (1975).
- T. Ishiwata, H. Akimoto, and I. Tanaka, VIII International Conference on Photochemistry, Edmonton, Canada, Aug. 1975, Abstracts, p V-11.
- P. J. Giachardi, G. W. Harris, and R. P. Wayne, VIII International Conference on Photochemistry, Edmonton, Canada, Aug. 1975, Abstracts, p F-11.
- I. Fridovich and P. Handler, *J. Biol. Chem.*, **233**, 1578, 1581 (1958); **236**, 1836 (1961); **237**, 916 (1962).
- V. Massey, S. Strickland, S. G. Mayhew, L. G. Howell, P. C. Engel, R. G. Matthews, M. Schuman, and P. A. Sullivan, *Biochem. Biophys. Res. Commun.*, **36**, 891 (1969); D. Ballou, G. Palmer, and V. Massey, *ibid.*, 898 (1969); W. H. Orme-Johnson and H. Beinert, *ibid.*, 905 (1969).
- A. V. Phelps, preprint No. 795, Joint Institute for Laboratory Astrophysics, University of Colorado, Boulder, Colo., 1974.
- M. Arshadi and P. Kebarle, *J. Phys. Chem.*, **74**, 1483 (1970).
- M. G. Evans and N. Urey, *Trans. Faraday Soc.*, **45**, 244 (1949).
- R. A. Marcus, *Annu. Rev. Phys. Chem.*, **155** (1964), and references therein.
- R. A. Marcus, *J. Chem. Phys.*, **43**, 2654 (1965).
- G. J. Hoytink in "Chemiluminescence and Bioluminescence", M. J. Cormier, D. M. Hercules, and J. Lee, Ed., Plenum Press, New York, N.Y., 1973, p 147.
- A. U. Khan and M. Kasha, *Ann. N.Y. Acad. Sci.*, **171**, 5 (1970).
- A. Pullman and B. Pullman, "Cancerization par les Substances Chimiques et Structure Moleculaire", Masson, Paris, France, 1955.
- L. Santamaria, C. G. Giordano, M. Alfisi, and F. Cacione, *Nature (London)*, **210**, 824 (1966).
- A. U. Khan and H. J. Lipner, Bulletin No. 38, Institute of Molecular Biophysics, Florida State University, Tallahassee, Fla., 1970.
- E. Boyland, Jerusalem Symposia on Quantum Chemistry and Biochemistry Vol. 1, E. D. Bergmann and B. Pullman, Ed., Israel Academy of Sciences and Humanities, Jerusalem, Israel, 1969, p 25.
- E. Cavalieri and M. Calvin, *Photochem. Photobiol.*, **14**, 641 (1971).
- L. I. Grossweiner, *Curr. Top. Radiat. Res.*, **11** (1975).
- R. Bonnett and J. C. M. Stewart, *Biochem. J.*, **130**, 895 (1972).
- R. V. Panganamala, N. R. Brownlee, H. Sprecher, and D. G. Cornwell, *Prostaglandins*, **7**, 21 (1974).
- W. Pappé and L. I. Grossweiner, *Photochem. Photobiol.*, **22**, 217 (1975).
- C. S. Foote, R. W. Denny, L. Weaner, Y. Chang, and J. Peters, *Ann. N.Y. Acad. Sci.*, **171**, 130 (1970).
- G. W. Grams, *Tetrahedron Lett.*, **No. 50**, 4823 (1971).
- G. W. Grams, K. Eskins, and G. E. Inglett, *J. Am. Chem. Soc.*, **94**, 866 (1972).
- G. W. Grams and K. Eskins, *Biochemistry*, **11**, 606 (1972).
- A. U. Khan, J. N. Pitts, Jr., and E. B. Smith, *Environ. Sci. Technol.*, **1**, 656 (1967).
- J. N. Pitts, Jr., A. U. Khan, E. B. Smith, and R. P. Wayne, *Environ. Sci. Technol.*, **3**, 249 (1969).

Discussion

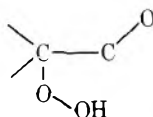
B. STEVENS. Is the oxygen enhanced fluorescence intensity effect restricted to polymer-supported systems where the triplet state is not subject to "solvent" quenching or would you expect it to be observed in liquid solutions?

A. KHAN. I think it would be very difficult, but I think it is possible. I think one can see it in some chemiluminescent reactions, in the decomposition of some dioxetanes, for instance.

R. RAHN. Is there evidence that singlet oxygen will react with the bases in native DNA?

A. KHAN. Yes, there has been extensive work on that, particularly guanine is sensitive to reaction with singlet oxygen.

H. SELIGER. In the bioluminescent systems in biological organisms nature appears to have chosen an oxygenation mechanism which initially adds oxygen as



Then possibly by dioxetane or hydroxyl attack the C-C bond is split, and an excited state product molecule *different* from the parent substrate emits fluorescence or sensitizes the fluorescence of a suitable acceptor. There are many methods of achieving excited states and some of the $^1\text{O}_2$ mechanism you have shown are possible. However, for biological chemiluminescence, singlet oxygen does not appear to be a necessary constituent. In the delayed luminescence of chloroplasts there are several experimental lines of evidence which imply

a *chemical* origin of the excited state emitter, i.e., pH or ion gradient effects. This, of course, does not eliminate the necessity for initial excitation by light. The lifetimes observed are not exponential but appear to follow a log-log relation. Again singlet oxygen requirement would not be a unique pathway.

A. KHAN. Only the basic physical process, the occurrence of a triplet state, for instance, of chlorophyll and the occurrence of a singlet state of oxygen would be necessary. They could annihilate and elect to produce an excited state. Now, the source of singlet oxygen; we know, for instance, dioxetane decomposition could stimulate an excited state, which could generate by sensitization singlet oxygen. There are a large number of ways whereby one can generate singlet oxygen.

B. WATSON. I would like to comment on the supposed involvement of singlet oxygen in various chemiluminescent reactions in biological systems, as observed by several groups using scintillation counters operated in out-of-coincidence mode. Contrary to the assertions of these authors, direct singlet oxygen contribution to the observed luminescence is quite unlikely and could be proved or disproved using a simple monochromator setup with photon counting.

Magnetic Circularly Polarized Emission from Crystalline $\text{Cs}_2\text{ZrCl}_6:\text{Re}^{4+}$

H. G. Brittain, F. S. Richardson, J. P. Jasinski, W. C. Yeakel, and P. N. Schatz*

Department of Chemistry, University of Virginia, Charlottesville, Virginia 22901 (Received January 29, 1976)

Publication costs assisted by the Petroleum Research Fund

High resolution, low temperature magnetic circularly polarized emission (MCPE) and total emission spectra are reported for $\text{Re}^{4+}(5d^3)$ doped into single crystals of Cs_2ZrCl_6 . With $\lambda_{\text{ex}} < 367.0$ nm, sharp-line emission is observed in the 700–740-nm region which is assigned to vibronic components of the single ion $\Gamma_7(^2T_{2g}) \rightarrow \Gamma_8(^4A_{2g})$ transition. As λ_{ex} is varied from 367 to 458 nm, emission in the 700–740-nm region gradually diminishes to zero but emission in the 740–770-nm region appears and gradually increases in intensity. At $\lambda_{\text{ex}} > 458$ nm, only emission in the 740–770-nm region is observed. Both concentration dependence data and excitation dependence studies suggest that the 740–770-nm emission originates with Re pairs, whereas the 700–740-nm emission features arise entirely from single ion transitions. The energy difference between single ion and pair emission (~ 350 cm^{-1}) is much too great to be accounted for by exchange coupling. It is suggested that the pair species involves a rhenium dimer.

I. Introduction

The differential emission of left and right circularly polarized light by luminescent samples placed in a longitudinal magnetic field has recently been reported for a number of systems.^{1–5} This phenomenon is the emission analogue of magnetic circular dichroism (MCD) and holds significant promise as a sensitive probe of molecular electronic structure. We refer to this phenomenon as magnetic circularly polarized emission (MCPE) and to its zero field counterpart (which is exhibited only by naturally optically active systems) as circularly polarized emission (CPE).

In the present study we report total emission and MCPE spectra of Re^{4+} ions doped into the cubic host Cs_2ZrCl_6 . Re^{4+} is a $5d^3$ system and in a strong, cubic crystalline field its t_{2g}^3 ground configuration splits into the following terms: $^4A_{2g}$, 2E_g , $^2T_{1g}$, and $^2T_{2g}$. Under the influence of spin-orbit coupling, further splittings of these states occur giving: $\Gamma_8(^4A_{2g})$,

$\Gamma_8(^2T_{1g})$, $\Gamma_6(^2T_{1g})$, $\Gamma_8(^2E_g)$, $\Gamma_7(^2T_{2g})$, and $\Gamma_8(^2T_{2g})$. Luminescence from crystalline $\text{Cs}_2\text{ZrCl}_6:\text{Re}^{4+}$ in the region 700–740 nm has previously been reported by Reinberg and Parker.⁶ Using the energy-level scheme of Dorain and Wheeler⁷ for Re^{4+} , these workers assigned this luminescence to intracongfigurational t_{2g}^3 d-d transitions originating from the $\Gamma_7(^2T_{2g})$ excited state and terminating in the ground state, $\Gamma_8(^4A_{2g})$. Based on both theoretical considerations and the emission spectra of Re^{4+} in similar systems,^{8,9} this assignment appears to be secure.

We have measured both the total emission (TE) and the MCPE spectra of the $\text{Cs}_2\text{ZrCl}_6:\text{Re}^{4+}$ system in the region 700–770 nm using excitation wavelengths 520 nm $> \lambda_{\text{ex}} > 365$ nm. With $\lambda_{\text{ex}} < 367$ nm, we observe a TE spectrum very similar to that reported by Reinberg and Parker.⁶ However, with $\lambda_{\text{ex}} > 458$ nm, emission in the 700–740-nm region disappears and emission is observed only in the 740–770-nm region. Upon going from $\lambda_{\text{ex}} 367$ nm to $\lambda_{\text{ex}} 458$ nm, 700–740-nm emission

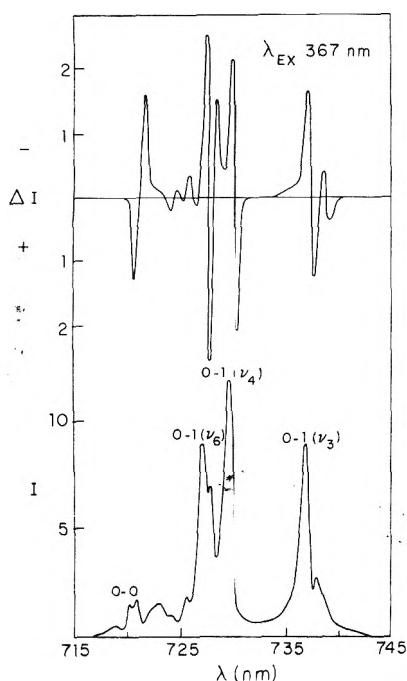


Figure 1. Total emission (I) and MCPE (ΔI) spectra excited with λ_{ex} 367.0 nm and spectral slit width ~ 0.5 Å. I and ΔI are expressed in the same relative units. $\Delta I = (I_L - I_R)$ is positive downward to facilitate comparison with the MCD of Figure 1, ref 11, which is plotted on an energy scale. A positive A term will thus first go down and then up from left to right both in ref 11 and in the present figures. The converse applies for a negative A term. Magnetic field strength was 5.2 T and sample temperature was 10–15 K. The Zeeman splitting of the 0–0 line is partially resolved in total emission. The partially resolved shoulder on the high energy side of 0–0 is an emission hot band.

intensity steadily decreases while the 740–770-nm emission intensity steadily increases. MCPE intensities exhibit a similar variation with excitation wavelength. With Reinberg and Parker,⁶ we assign the 700–740-nm emission features to vibronic components of the single ion transition, $\Gamma_7(^2T_{2g}) \rightarrow \Gamma_8(^4A_{2g})$. In this report, we suggest that the 740–770-nm emission lines may be associated with a rhenium dimer species formed in low concentration during the growth of the crystal from the melt.

II. Experimental Section

Crystals of Cs₂ZrCl₆:Re⁴⁺ were prepared by methods described elsewhere.¹⁰ Crystals of two different Re⁴⁺ concentrations were examined in the present study. Relative Re⁴⁺ concentrations were calculated by measuring the thickness of the two crystals and comparing corresponding sharp absorption lines at liquid helium temperature in the 725–745-nm region. Absolute concentrations were estimated from previously published¹¹ approximate molar extinction coefficients. The Re⁴⁺ concentrations were ~ 1.1 and 0.7% in the two crystals hereafter referred to respectively as crystals 1 and 2. Whereas the absolute concentrations are very rough ($\pm 50\%$), the ratio of concentrations should be reliable to $\pm 10\%$. All measurements were obtained on crystals oriented so that the light (excitation and emission) traveled along the [111] crystallographic direction. The crystals did not significantly depolarize circularly polarized light.

The emission measurements were carried out using a high-sensitivity, high-resolution emission spectrophotometer in which emission is detected “head-on” (that is, 0° to the direction of excitation). This instrument was designed and

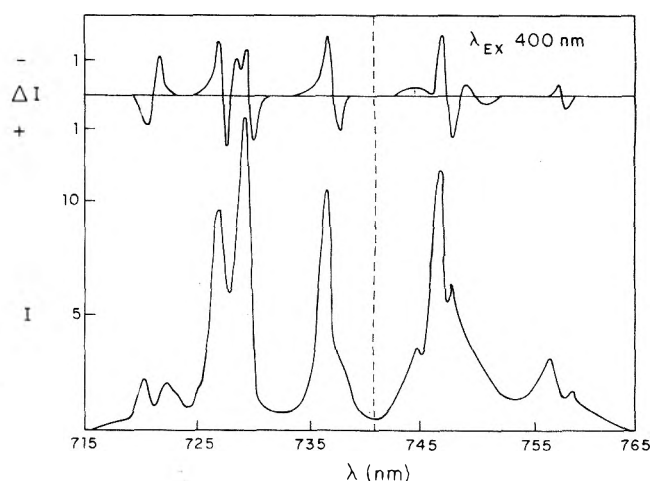


Figure 2. Total emission (I) and MCPE (ΔI) spectra excited with λ_{ex} 400.0 nm and spectral slit width ~ 1 Å. Other conditions are as in Figure 1.

constructed in our laboratory and has previously been described in conjunction with the study of the luminescence and CPE spectra of naturally optically active systems.^{12,13} With this instrument, intensities of the circularly polarized components of the emitted radiation may be determined with a precision of a few percent even when present in a 10^4 – 10^5 excess of unpolarized background radiation.

For the low temperature emission experiments reported here, the sample was mounted in the bore of a superconducting magnet; the crystal was under vacuum and the bore was surrounded by liquid helium. Excitation light was provided either by a Coherent Radiation Model CR-5 argon ion laser (458- and 488-nm lines) or by a 1000-W Xe–Hg arc lamp using a Spex minimize, and a Corning black glass filter (for the 250–400-nm range). The circularly analyzed emission beam was focussed onto the slits of a Spex Model 1800-11 $\frac{3}{4}$ m, single grating monochromator, and the TE and MCPE spectra were recorded simultaneously by a two-pen recorder. The two quantities measured directly in our emission experiments are: total emission ($I = I_L + I_R$) and the differential emission of left and right circularly polarized light ($\Delta I = I_L - I_R$). Both I (TE) and ΔI (MCPE) are reported in the same relative quantal units so that their ratio is an absolute value.

III. Results

The TE and MCPE spectra obtained for crystal 1 (1.1% Re⁴⁺) at low temperature are shown in Figures 1 and 2 with abscissas linear in wavelength. Figure 1 shows spectra observed with λ_{ex} 367 nm in the region 715–745 nm. No emission is observed in the 745–765-nm region.

At λ_{ex} 400 nm, TE and MCPE are observed throughout the 715–765-nm region as shown in Figure 2. At λ_{ex} 458 nm, no emission is observed in the 715–740-nm region, but the TE and MCPE in the 745–765-nm region, which have continued to grow in intensity, remain identical in appearance with that in Figure 2.

The concentration dependence of TE in the 715–765-nm region differs significantly from that observed in the 740–765-nm region. This is demonstrated by the spectra displayed in Figure 3. These spectra were recorded with instrumentation sensitivity parameters set so that the intensity of the band max at ~ 727 nm was the same for both crystal 1 ($\sim 1.1\%$ Re⁴⁺) and crystal 2 ($\sim 0.7\%$ Re⁴⁺). Assuming that the spectra observed in the 705–745-nm region are predominantly from

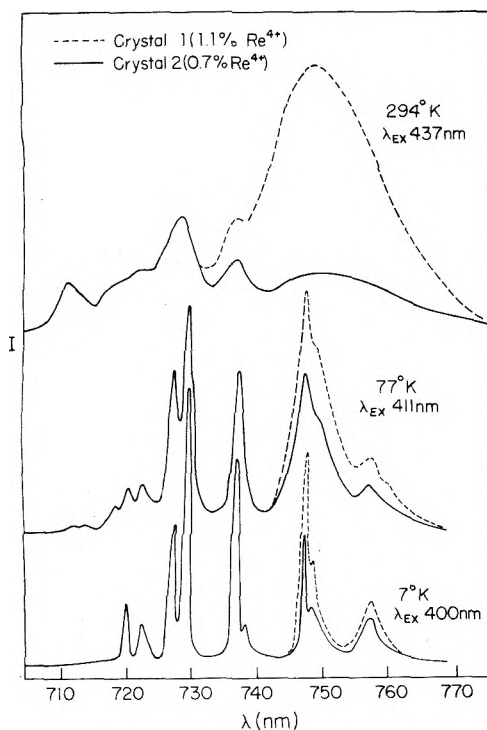


Figure 3. Total emission spectra recorded for crystals 1 (1.1% Re^{4+}) and 2 (0.7% Re^{4+}) in zero field. For these spectra, instrumentation parameters were set so that the intensity of the band max at ~ 727 nm was the same for both crystal 1 and crystal 2.

single ion emission and that the intensity of this type of emission has a linear dependence on ion concentration, then the intensity differences between the emission from crystals 1 and 2 as shown in Figure 3 can be attributed to a nonlinear concentration dependence which is indicative of pair effects. The excitation wavelengths used in Figure 3 were chosen to give observable emission throughout the 705–765-nm region.

IV. Discussion

With Reinberg and Parker⁶ we assign the emission line centered at ~ 720.5 nm ($13\,879\text{ cm}^{-1}$) to the no-phonon ($0 \rightarrow 0$) line of the magnetic-dipole-allowed transition, $\Gamma_7(^2T_{2g}) \rightarrow \Gamma_8(^4A_{2g})$. In the MCPE spectrum, this transition yields a simple A term very similar to that observed in the MCD of the no-phonon line of the $\Gamma_8(^4A_{2g}) \rightarrow \Gamma_7(^2T_{2g})$ transition.¹¹ The strong emission lines centered at 727.3 ($13\,749\text{ cm}^{-1}$), 729.7 ($13\,704\text{ cm}^{-1}$), and 737.1 nm ($13\,567\text{ cm}^{-1}$) are nominally assigned, assuming that the octahedral ReCl_6^{2-} moiety is the absorbing center, to the $0 \rightarrow \nu_6(t_{2u})$, $0 \rightarrow \nu_4(t_{1u})$, and $0 \rightarrow \nu_3(t_{1u})$ one-phonon components of $\Gamma_7(^2T_{2g}) \rightarrow \Gamma_8(^4A_{2g})$. These transitions gain their intensities via a vibronically induced electric-dipole mechanism. The weaker emission features between the $0 \rightarrow 0$ origin and $0 \rightarrow 1(\nu_6)$ probably arise primarily from lattice phonons built on the origin. Two very weak lines (not shown in Figures 1 and 2) are observed respectively 341 cm^{-1} to lower energy of $0 \rightarrow I(\nu_4)$ and $0 \rightarrow I(\nu_3)$. This interval is undoubtedly the ground state value of $\nu_1(a_{1g})$ which may be compared with 346 cm^{-1} in pure Cs_2ReCl_6 .⁷

If we consider an isolated molecular moiety (such as ReCl_6^{2-}) and compare the vibronic transitions $A_\lambda \rightarrow J_\mu + \nu_i^j$ (absorption) and $A_\lambda + \nu_i^j \leftarrow J_\mu$ (emission) where A and J are electronic states, λ and μ distinguish degenerate electronic components, and $A_\lambda + \nu_i^j$ and $J_\mu + \nu_i^j$ signify vibronic states

activated by vibrational mode ν_i , then one finds¹⁴ in the harmonic approximation that

$$\nu_i^A \sum_\alpha |\langle A_\lambda | m_\beta | J_\mu + \nu_i^j \rangle|^2 = \nu_i^j \sum_\alpha |\langle A_\lambda + \nu_i^A | m_\beta | J_\mu \rangle|^2$$

where α designates the component of a degenerate vibration of frequency ν_i and β designates an arbitrary polarization component (e.g., linear or circular) of the electric dipole operator, m . One therefore expects an A term of the same sign for an absorption line and its emission counterpart.

A detailed examination of the vibronic structure in the one-phonon ν_6 , ν_4 region discloses significant differences in MCD¹¹ and MCPE (Figure 1). In MCD, the ν_6 vibronic line at 133 cm^{-1} (above the origin) shows a positive A term¹¹ (sigmoid dispersion going first negative and then positive to higher energy). The ν_4 line is split into two components at energies of 159 and 175 cm^{-1} (perhaps due to a splitting of the transverse and longitudinal optical branches), and both components show negative A terms.¹¹ In the MCPE, it is seen in Figure 1 that the ν_6 , ν_4 region still shows one positive and two negative A terms, but the energy and intensity pattern is quite different. The lowest energy component at 130 cm^{-1} , nominally assigned as ν_6 in Figure 1, corresponds to a negative A term followed by a partially superimposed positive A term which goes with the smaller shoulder at 139 cm^{-1} . Then finally another negative A term at 175 cm^{-1} is associated with $0 \rightarrow \nu_4$, as in the MCD. There is thus the suggestion that the ν_6 and ν_4 vibronic components are scrambled (mixed) in the MCPE spectrum relative to the MCD. As has been emphasized recently by Durocher and Dorain,¹⁵ mixing of vibronic transitions of differing symmetry occurs if one abandons the $k = 0$ approximation and therefore assumes coupling with phonons throughout the Brillouin zone. If such a mechanism is responsible for the difference we observe in the MCD and MCPE patterns, it implies significantly different phonon coupling in the ground ($\Gamma_8(^4A_{2g})$) and excited ($\Gamma_7(^2T_{2g})$) electronic states since the TE and MCPE probe vibrations in the former and the absorption and MCD probe vibrations in the latter. This point is under further investigation. The ν_3 region which is well separated to higher energy shows negative A terms both in MCD¹¹ and MCPE.

We attribute essentially all emission observed in the 715–740-nm region to single ion (Re^{4+}) transitions and tentatively associate the emission lines appearing between 740 and 760 nm with Re “pairs”. In fact, the spectra of exchanged coupled Re^{4+} pairs have been previously observed¹⁶ in the closely related host of the same structure, K_2PtCl_6 , and these perhaps make some contributions in the region of the unresolved lattice structure near $0 \rightarrow 0$, Figure 1. However, these pair lines are observed within $20\text{--}30\text{ cm}^{-1}$ of the corresponding single ion lines¹⁶ and hence can bear no relation to our “pair” spectra whose lines are $\sim 350\text{ cm}^{-1}$ from the single ion lines.

Figure 4 displays excitation spectra for both the single ion and “pair” emission regions. It is evident that these emissions are excited at distinctly different energies with a small amount of energy transfer from single ion to “pair” implied by the small maxima in the pair excitation spectrum at the single ion excitation maxima. The larger single ion excitation maximum at 354 nm is approximately at the energy predicted¹⁷ for the lowest energy parity-forbidden ligand-to-metal Re^{4+} charge-transfer transition, and the 300-nm excitation maximum is in the region of the corresponding first allowed charge-transfer transition. Much weaker interconfigurational d–d transitions are also predicted⁷ throughout the region of both single ion excitation maxima.

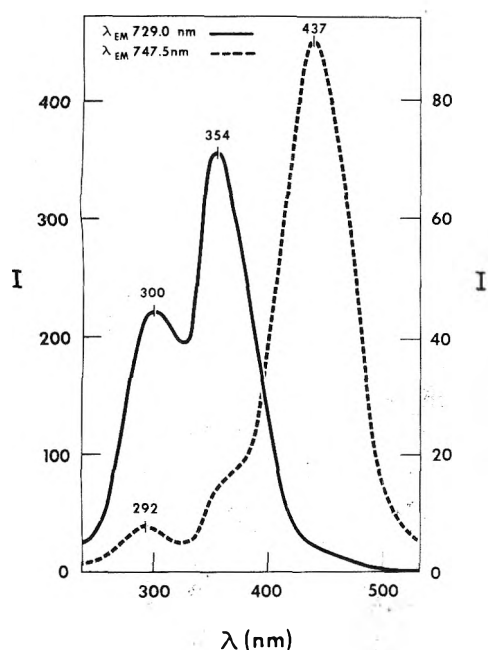


Figure 4. Excitation spectra of $\text{Cs}_2\text{ZrCl}_6:\text{Re}^{4+}$ at liquid nitrogen temperature. The solid and dashed lines respectively were recorded monitoring single ion emission at 729.0 nm and "pair" emission at 747.5 nm with ~ 50 Å resolution in zero magnetic field. The spectra have been corrected for source intensity variation, and the single ion and pair intensities are in the same relative units (left and right band ordinate scales, respectively).

The "pair" excitation maximum, at 437 nm, is at an energy several thousand cm^{-1} away from any predicted Re^{4+} single ion charge-transfer¹⁷ or d-d¹⁸ transitions, and we associate this excitation with a transition of the "pair" species. We are able only to speculate on the nature of this species at present. However, binuclear species containing Re^{4+} are well known, e.g., Re_2Cl_9^- and $\text{Re}_2\text{Cl}_9^{2-}$,¹⁹ and one could conceive of the former, for example, substituting into the lattice for a ZrCl_6^{2-} and adjacent Cs^+ ion. However, this is unsupported speculation, and the Re_2Cl_9^- solution spectrum¹⁹ does not appear a priori to predict an excitation maximum just at 437 nm.

Kopelman²⁰ has suggested that a lattice defect may account for the substantial energy shift (~ 350 cm^{-1}) from the single ion transitions. This certainly seems possible and in fact would not be inconsistent with the formation of a dimeric Re species which would certainly perturb the lattice structure. The comparable sharpness of the "pair" and single ion features (Figure 2) does seem to suggest a single, specific geometrical structure for the pair entity rather than a range of configurations which would be expected to produce a broad, less structured spectrum.

Support for the idea that the pair species is associated with the high temperature growth of the crystal (~ 760 °C) is provided by an examination of aqueous solution-grown crystals of $\text{Cs}_2\text{SnCl}_6:\text{Re}^{4+}$ and $\text{K}_2\text{PtCl}_6:\text{Re}^{4+}$. In both cases, TE spectra were obtained which were very similar to those in Figure 1. However, no emission in the "pair" region was observed even for crystals containing much higher concentrations of Re^{4+} than crystals 1 and 2. The excitation spectrum of $\text{Cs}_2\text{SnCl}_6:\text{Re}^{4+}$ (Figure 5) shows (approximately) the same two single ion excitation maxima (though with substantially different relative intensities) as $\text{Cs}_2\text{ZrCl}_6:\text{Re}^{4+}$.

V. Conclusions

The principal results of this study may be summarized as

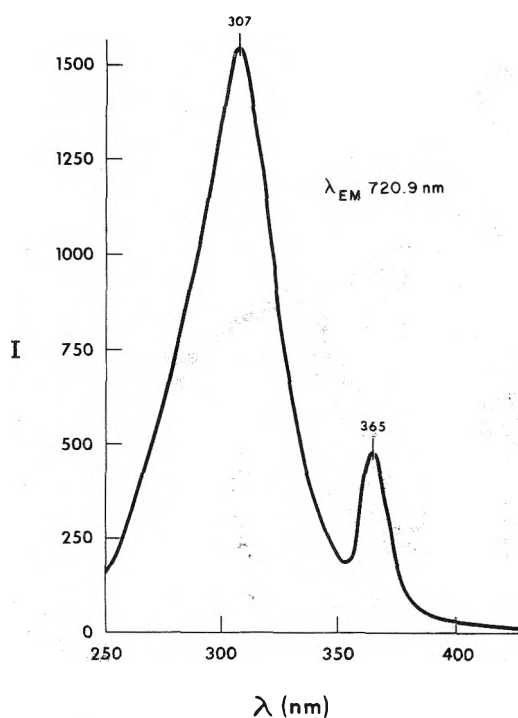


Figure 5. Excitation spectrum of $\text{K}_2\text{SnCl}_6:\text{Re}^{4+}$ at liquid nitrogen temperature, ~ 50 Å resolution and zero field, recorded monitoring single ion emission at 720.9 nm (the same line monitored in Figure 4, which is displaced 8.8 nm to the red in the tin host). No emission is observed in the "pair" region. The intensity scale is arbitrary but has been corrected for source intensity variation.

follows. *First*, luminescence from $\text{Cs}_2\text{ZrCl}_6:\text{Re}^{4+}$ in the 700–740-nm region can be assigned to vibronic components of the intraconfigurational (t_g^3) $\Gamma_7(^2T_{2g}) \rightarrow \Gamma_8(^4A_{2g})$ transition of single Re^{4+} ions occupying sites of O_h symmetry. *Second*, differences between the MCPE and MCD observed in specific vibronic components of this electronic transition suggest differences in the vibronic mechanisms and phonon coupling in the ground and excited states. These observations emphasize that the MCPE gives information about the states involved in an electronic transition not obtained from the corresponding MCD. *Third*, concentration dependence studies, excitation spectra, and theoretical considerations suggest that the emission observed in the 740–760-nm region is associated with a rhenium pair entity formed in low concentrations under the high temperature conditions employed in growing $\text{Cs}_2\text{ZrCl}_6:\text{Re}^{4+}$.

Acknowledgments. This work was supported by the National Science Foundation, the Petroleum Research Fund, administered by the American Chemical Society, and the Camille and Henry Dreyfus Foundation (through a Teacher-Scholar Grant to F.R.). We wish to acknowledge a number of very informative discussions with Dr. J. N. Demas.

References and Notes

- (1) M. Marrone and M. N. Kabler, *Phys. Rev. Lett.*, **27**, 1283 (1971).
- (2) (a) R. A. Shatwell and A. J. McCaffery, *Chem. Commun.*, 546 (1973); (b) A. J. McCaffery, P. Brint, R. Gale, and R. A. Shatwell, *Chem. Phys. Lett.*, **22**, 600 (1973).
- (3) (a) R. A. Shatwell, R. Gale, A. J. McCaffery, and K. Sichel, *J. Am. Chem. Soc.*, **97**, 7015 (1975); (b) R. A. Shatwell and A. J. McCaffery, *Mol. Phys.*, **30**, 1489 (1975).
- (4) N. Moreau, A. C. Boccara, and J. Badoz, *Phys. Rev. B*, **10**, 64 (1974).
- (5) C. K. Luk, W. C. Yeakel, F. S. Richardson, and P. N. Schatz, *Chem. Phys. Lett.*, **34**, 147 (1975).

- (6) A. R. Reinberg and S. G. Parker, *Phys. Rev. B*, **1**, 2085 (1970).
 (7) P. B. Dorain and R. G. Wheeler, *J. Chem. Phys.*, **45**, 1172 (1966).
 (8) (a) H. H. Patterson, J. L. Nims, and C. M. Valencia, *J. Mol. Spectrosc.*, **42**, 567 (1972); (b) A. M. Black and C. D. Flint, *J. Chem. Soc., Faraday Trans. 2*, **71**, 1871 (1975).
 (9) P. B. Dorain in "Transition Metal Chemistry", Vol. 4, R. L. Carlin, Ed., Marcel-Dekker, New York, N.Y., 1968, Chapter 4.
 (10) (a) J. R. Dickinson, S. B. Piepho, J. A. Spencer, and P. N. Schatz, *J. Chem. Phys.*, **56**, 2668 (1972); (b) S. B. Piepho, J. R. Dickinson, J. A. Spencer, and P. N. Schatz, *ibid.*, **57**, 982 (1972); (c) R. W. Schwartz and P. N. Schatz, *Phys. Rev. B*, **8**, 3229 (1973).
 (11) J. C. Collingwood, S. B. Piepho, R. W. Schwartz, P. A. Dobosh, J. R. Dickinson, and P. N. Schatz, *Mol. Phys.*, **29**, 793 (1975), particularly Figure 1.
 (12) C. K. Luk and F. S. Richardson, *Chem. Phys. Lett.*, **25**, 215 (1974).
 (13) C. K. Luk and F. S. Richardson, *J. Am. Chem. Soc.*, **96**, 2006 (1974).
 (14) W. C. Yeakel, et al., submitted for publication.
 (15) D. Durocher and P. B. Dorain, *J. Chem. Phys.*, **61**, 1361 (1974).
 (16) P. B. Dorain and R. G. Wheeler, *Phys. Rev. Lett.*, **15**, 968 (1965).
 (17) Reference 11, Figure 10.
 (18) Reference 7, Table III.
 (19) F. Bonati and F. A. Cotton, *Inorg. Chem.*, **6**, 1353 (1967).
 (20) See discussion comment following this paper.

Discussion

R. KOPELMAN. Could your "cluster" state be a "defect" state where the "defect" (generalized term) is induced by the higher concentration and thus is behaving superlinear with concentration?

P. N. SCHATZ. This would be a possibility, but I am not convinced it would account for the observed concentration dependence of the emission.

Determination of Geometrical Parameters of Excited States. Application to d^6 Transition Metal Complexes of O and D_4 Symmetry^{1a}

K. W. Hippis,^{1b} G. A. Merrell, and G. A. Crosby*

Department of Chemistry and Chemical Physics Program, Washington State University, Pullman, Washington 99163
 (Received May 10, 1976)

Publication costs assisted by the Air Force Office of Scientific Research, Directorate of Chemical Sciences

Analyses of luminescence emission band envelopes arising from ligand field transitions of transition metal complexes are discussed from both theoretical and practical points of view. Equations are developed that allow geometrical parameters of electronic excited states to be obtained from a full Franck-Condon analysis, direct numerical integration of the band envelopes, or Gaussian curve-fitting techniques. The usefulness, inherent complications, limitations, and accuracy of the several methods are pointed out. Emission spectra for potassium hexacyanocobaltate(III), *trans*-dibromotetrakis(4-methylpyridine)rhodium(III) bromide, *trans*-dichlorotetrakis(pyridine)rhodium(III) chloride, and *trans*-dibromotetrakis(pyridine)rhodium(III) bromide at 2 K are given and analyzed. Symmetry-preserving expansions occur in all cases.

Franck-Condon analysis (FCA) of vibrational structure on electronic spectra to obtain information about excited state geometries of diatomic molecules was pioneered by Hutchison in 1930.² Coon et al.³ have applied the method to triatomics, and Craig⁴ determined the ¹B_{2u} excited-state C-C distance of benzene by FCA. More recently, many conjugated organics have been subjected to FCA.⁵⁻⁷ In contrast, FCA of electronic spectra of inorganic materials is just beginning to yield information (excited-state geometries, excited-state force constants, and ground-state anharmonicities)⁸⁻¹⁰ of importance to those concerned with radiationless transitions,^{11,12} photochemistry,¹³ and the redistribution of charge during an electronic transition.^{14,15} Excited-state parameters derived from FCA of inorganic molecules are a desideratum of modern chemistry.

The lack of Franck-Condon investigations of inorganic complexes is due to the fact that most of the reported spectra have been either so sharp that they were essentially atomic and FCA was unnecessary or so broad and diffuse that detailed analyses were precluded. In this study we address the analysis of complexes of the second type. First, we consider the origins of the diffuse emission spectra of inorganic complexes. Then we present a detailed mathematical machinery

for FCA and restrict its application to complexes of O and D_4 microsymmetry. For spectra that are too diffuse for FCA, we propose two methods for determining excited-state parameters. Finally, we present the results of applying FCA and the approximate methods to several complexes of the d^6 type that are of photochemical interest.

Experimental Section

All complexes were prepared in our laboratory by methods given elsewhere.^{16,17} Each substance was recrystallized several times and thoroughly dried. Distillation of the pyridine (py) and 4-methylpyridine (4-Mepy) was required or the resultant compounds did not produce well-structured spectra.

All emission spectra were obtained from exciting the pure solids. The samples were mounted in the bore of an Andonian Associates helium cryostat; ~2 K temperatures were obtained by pumping directly on the helium liquid in which the sample was totally immersed. Excitation was accomplished by directing the output of a 1000-W Hg-Xe lamp through 5 cm of aqueous CuSO₄ solution (100 g/l.) and a Corning 7-60 glass filter. Scattering exciting light was blocked by two 500-nm cutoff filters located before the entrance slit of a 0.5-m Jarrell-Ash monochromator equipped with curved bilateral slits

for the $K_3[Co(CN)_6]$ measurements. For the others only a 550-nm cutoff filter was placed directly before the exit slit. Resolution was sample limited. The signal from a dry ice-methanol cooled RCA 7102 photomultiplier was amplified by a Keithley microammeter and displayed on an X-Y recorder.

Recorded signals were corrected to give the relative photon intensity $\text{sec}^{-1} \text{cm}^{-2}$ per cm^{-1} bandwidth by comparison with a calibrated NBS standard lamp.¹⁸ *Photon intensities (quantum yields) per unit area per kK (or cm^{-1}) bandwidth are reported here rather than the true intensity.* The FCA, moments calculation, and least-squares Gaussian fits were all performed on the same data set for a given molecule.

Theoretical Development

Origin of Broad Luminescence Bands of Complexes. As first pointed out by Orgel,¹⁵ the expected width of a dd transition is related to the relative slopes of the energy vs. Dq plots of the terms involved in the transition. Since Kasha's rule¹⁹ as modified by Demas and Crosby²⁰ is usually satisfied for inorganic complexes, perusal of the Tanabe and Sugano diagrams²¹ leads to the conclusion that only broad emission will be seen from all hexacoordinate dd emitters with a d^s configuration, provided that $s = 5, 6, \text{ or } 7$. Additionally, it could occur for suitable ranges of Δ/B from metal complexes with d^k configurations where $k = 2, 3, 4, \text{ or } 8$. For many complexes, however, no emission may occur at all.

Emission bandwidths are a clear indication of a difference between ground- and excited-state geometry and binding. This can be easily visualized provided one posits that most of the bond strength in a complex does not derive from d electrons. In this vein, the t_{2g} orbitals are nonbonding or weakly antibonding, whereas the e_g set is antibonding. Changes in the electron populations of the e_g and t_{2g} orbitals would then lead to a geometrical rearrangement. This argument, first given by Orgel,¹⁵ may be stated in an alternate way. The slopes of the term energies represent the first derivative of the crystal field potential (d electrons only) with respect to the totally symmetric breathing mode. Two terms having different slopes are therefore required to have different geometries but the same symmetry. Information concerning symmetry changes is not contained in these diagrams.

For complexes of D_4 symmetry, the lines of the octahedral Tanabe-Sugano diagrams become surfaces. Two totally symmetric coordinates (Q_a , axial; Q_{eq} , equatorial) are required to specify the energy. We may relate the amount of extension in direction i ($i = a \text{ or } eq$) to

$$T_i \approx (1/M_i \omega_i^2) [(\partial E'/\partial Q_i)_{\bar{Q}=\bar{Q}_M} - (\partial E/\partial Q_i)_{\bar{Q}=\bar{Q}_M}] \quad (1)$$

where E' is the energy of the initial term, E is the energy of the final term, and \bar{Q}_M is the mean of the equilibrium nuclear positions of the two terms. This relation is a simple generalization of Orgel's treatment. As for the octahedral case, the Tanabe-Sugano surfaces provide no direct information about possible symmetry changes for transitions between terms.

Besides the band structure generated by a difference in geometry, there are other factors that can, and often do, affect the band shape. Since virtually every emission that is predicted to be diffuse has either a degenerate ground or excited term, the influence of spin-orbit coupling cannot be ignored. For first-row transition metals such as Co^{3+} , a term really represents a set of levels spread over as much as 500 cm^{-1} , or perhaps more.²² Further, second-order and higher order spin-orbit coupling will cause the equilibrium position and potential surface of each state arising from the same term to

be different. At temperatures above about 20 K, the observed spectrum usually becomes a superposition of different electronic transitions.^{9,10,22} Furthermore, each of the consequent bands may have one or more origins.¹⁰

If, after spin-orbit coupling is accounted for, degeneracies still remain, then electronic-nuclear coupling must be considered. The symmetry changes associated with the Jahn-Teller effect will reveal themselves as progressions in nontotally symmetric vibrational frequencies. In addition, interaction between potential surfaces can lead to multiple minima of complex forms. It is only for the lowest excited state (electronic and vibrational) that a harmonic oscillator type potential seems reasonable. In all that follows, we assume that the Born-Oppenheimer approximation (BOA) is valid for the lowest excited level. At a sufficiently low temperature (~ 0 K), only the lowest excited level will be populated; we then have only to contend with the emission spectrum from a single excited level.

Having circumvented the bulk of the excited-state contributions to the diffuseness of a spectrum, we must now consider the ground-term contribution. An appealing simplification is to consider only those systems in which the ground term is nondegenerate, for which the ~ 0 K spectrum should be relatively uncomplicated. This condition obtains for all of the complexes studied here. Therefore we limit our discussion to transitions from a single electronic excited state in its lowest ($n' = 0'$) vibrational state to a single vibrational level of a nondegenerate electronic state. The terminal vibrational state is determined by the selection rules. Unfortunately, even from systems obeying these tight restrictions, sharply resolved spectra may not necessarily arise.

In condensed phases, molecules are not isolated, but for dd transitions we may often treat a complex as a nearly independent entity. Nevertheless the total specification of the molecular state must include the quasi-continuum of the phonon bath. States having the same electronic and vibrational quantum numbers can have different phonon quantum numbers, and transitions will therefore be "blurred." Factor group splittings and nonuniformity of sites in the crystal can also lead to further reductions in the resolution of vibrational components of a band. Quantitative treatment of these factors is beyond our capability at this time, and with a posteriori justification we assume that lattice contributions to band structure are identical for every vibronic transition. We therefore introduce the same shape function, $h(\omega)$, for each intrinsic band (vide infra).

Franck-Condon Analysis. We now turn our attention to the predicted band pattern and FCA when the special situation of ~ 0 K and a nondegenerate ground state apply. Consider a molecule having p degrees of vibrational freedom. Adopt the BOA²³ and assume only two electronic states to be involved in the transition. The excited state is then specified by

$$|E\rangle = |e\rangle |\bar{0}'\rangle \quad (2)$$

where the excited electronic function $|e\rangle$ is a function both of the electronic coordinates, \bar{q} , and, parametrically, of the nuclear coordinates, \bar{x} . $|\bar{0}'\rangle$ is taken as the p -factored product of $n' = 0$ harmonic oscillator functions of the excited normal displacement coordinates, \bar{Q}' . The possible terminal states, $|F\rangle$, are given as

$$|F\rangle = |f\rangle |\bar{n}\rangle \quad (3)$$

where we again use the harmonic approximation to specify $|\bar{n}\rangle$ as a p -factored product of harmonic oscillator functions of the

ground ($|f\rangle$) state normal coordinates, \bar{Q} . The p -fold collection of n values specifies a single terminal level.

In order to investigate the overall band shape for the $|e\rangle \rightarrow |f\rangle$ transition, we first evaluate the intensity and energy of the individual $|E\rangle \rightarrow |F\rangle$ transitions and then superpose the results for all $|F\rangle$. If m_k is the k th component of an electronic transition moment operator, the transition probability between states $|E\rangle$ and $|F\rangle$ for k polarization depends on the square of the integral

$$\langle E|m_k|F\rangle = \langle \bar{0}'|e|m_k|f\rangle|\bar{n}\rangle \quad (4)$$

where the central integral is over electronic coordinates only. Because of the parametric dependence of the electronic functions on \bar{Q} , the electronic integral is a function of \bar{Q} . Calling it $M_k(\bar{Q} + \bar{X}_0)$, where \bar{X}_0 is the ground-state nuclear geometry, we have

$$\langle E|m_k|F\rangle = \langle \bar{0}'|M_k(\bar{Q} + \bar{X}_0)|\bar{n}\rangle \quad (5)$$

The usual procedure at this point is to expand M_k in a power series of \bar{Q} about \bar{X}_0 . Terms higher than linear are neglected,²³ i.e.

$$\langle E|m_k|F\rangle = M_k(\bar{X}_0)\langle \bar{0}'|\bar{n}\rangle + \sum_j M_k^j\langle \bar{0}'|Q_j|\bar{n}\rangle \quad (6)$$

where $M_k^j = (\partial M_k/\partial Q_j)_{\bar{Q}=\bar{X}_0}$ and the sum is over all p values of j . If $M_k(\bar{X}_0)$ is nonvanishing, it usually dominates, and the transition is said to be equilibrium geometry allowed (EGA). If $M_k(\bar{X}_0)$ vanishes, the transition is said to be vibrationally allowed (VA).

A transition is usually VA only if $M_k(\bar{X}_0)$ vanishes by symmetry; in this case, M_k^j also vanishes if j labels a totally symmetric mode. For t totally symmetric modes, we choose to label their occupation numbers consecutively as n_1, n_2, \dots, n_t .

$$\langle E|m_k|F\rangle = M_k(\bar{X}_0)\langle \bar{0}'|\bar{n}\rangle + \sum_{j=t+1}^p M_k^j\langle \bar{0}'|Q_j|\bar{n}\rangle \quad (7)$$

For the EGA case the terms in the summation can be neglected. For the VA case only the terms in the summation contribute to the matrix element. For an intermediate case [$M_k(\bar{X}_0) \approx M_k^j$], eq 7 requires modification, since the set of M_k^j ($j \leq t$) does not vanish by symmetry. We consider this interesting case no further in what follows, and we assume the validity of eq 7 henceforth.

In the general case of a symmetry change during the transition, the vibrational overlap calculation is very complicated. For example, if an octahedral molecule is tetragonally distorted in the excited state, we would expect progressions in both a_1 and e_g ground-state modes, both of these appearing totally symmetric to the excited state. If the excited-state symmetry is subgroup related to the ground-state symmetry, partial factorization of the overlap integral is possible. Here, coordinates transforming as the irreducible representations of the lowest symmetry group are independent. Fortunately, it appears that most broad dd luminescence is principally due to a symmetry-conserving expansion. Certainly the data presented here demand a vanishingly small symmetry change. Because of the localized nature of a dd transition, we expect that the internal ligand vibrations should be unaffected by the transition. We therefore restrict the analysis to the case where the ligands behave as point masses and symmetry is preserved.

The above restriction allows us to place $t = 1$ for O symmetry and $t = 2$ for D_4 symmetry. We may now simplify eq 7 considerably by setting $\langle 0'_j|n_k\rangle = \delta(j,k)\delta(n,0)$ provided $j >$

t . Substitution into eq 7 provides us with the result

$$\langle E|m_k|F\rangle = \prod_{s=1}^t \langle 0'_s|n_s\rangle \left[M_k(\bar{X}_0) \prod_{r=t+1}^p \delta(0,n_r) + \sum_{j=t+1}^p M_k^j \langle 0'_j|Q_j|n_j\rangle \prod_{\substack{r=t+1 \\ r \neq j}}^p \delta(0,n_r) \right] \quad (8)$$

The probability of a transition depends on the square of eq 8 times the cube of the energy difference between states $|E\rangle$ and $|F\rangle$. Assuming

$$M_k^j \langle 0'_j|Q_j|n_j\rangle = M_k^j \delta(n_j, 1) \quad (9)$$

we have

$$P_{\bar{0}' \rightarrow \bar{n}} = \gamma \prod_{s=1}^t |\langle 0'_s|n_s\rangle|^2 |M_k(\bar{X}_0)|^2 \times \prod_{r=t+1}^p \delta(0,n_r) (\alpha - \sum_{s=1}^t n_s \omega_s)^3 \quad (10a)$$

for the EGA case and

$$P_{\bar{0}' \rightarrow \bar{n}} = \gamma \prod_{s=1}^t |\langle 0'_s|n_s\rangle|^2 \left\{ \sum_{j=t+1}^p |M_k^j|^2 \delta(n_j, 1) \times \prod_{\substack{r=t+1 \\ r \neq j}}^p \delta(0,n_r) (\alpha - \sum_{s=1}^t n_s \omega_s - \omega_j)^3 \right\} \quad (10b)$$

in the VA case. ω_m is the ground-state oscillator frequency of the m th mode, and γ is a collection of constants. The quantities $|\langle 0'_s|n_s\rangle|^2$ are the totally symmetric vibration (a_1) FC factors. The modes j , for which M_k^j is nonzero, are called allowing modes. α is the $\bar{0}' \rightarrow \bar{0}$ transition energy.

For a VA transition with a single allowing mode, eq 10a and 10b are formally identical. The only distinction is that the predicted intensity distribution for a VA transition begins at $\alpha^* = \alpha - \omega_j$ rather than α . For either case, the 0 K emission spectrum is therefore

$$I(\omega) = A \sum_{\{n_t\}} |\langle 0'_1|n_1\rangle|^2 |\langle 0'_2|n_2\rangle|^2 \dots |\langle 0'_t|n_t\rangle|^2 \times h\left(\omega - \alpha^* + \sum_{s=1}^t n_s \omega_s\right) \omega^3 \quad (11)$$

where $h(\omega)$ is the shape function for a single vibronic line and α^* is the effective origin for the transition. $h(\omega - \delta)$ maximizes at $\omega = \delta$ and has unit area. If more than one allowing mode contributes to the band, $I(\omega)$ will be a sum of terms like eq 11, one term for each allowing mode.

For a single a_1 progression, eq 11 may be simplified to

$$I(\omega) = A \sum_n |\langle 0'|n\rangle|^2 h(\omega - \alpha^* + n\omega_0) \omega^3 \quad (12)$$

The FC factors can be calculated. In Appendix A we generate their values for a harmonic oscillator model where excited-state geometry ($Q' = Q - a$) and frequency ($\omega'/\omega_0 = k^2$) differ from those of the ground state. By comparing the calculated $I(\omega)$ to that observed, we may use "best fit" criteria to arrive at values of a and k^2 . The difficulty, of course, is in the choice of $h(\omega)$. As discussed earlier, it has been introduced in an ad hoc manner. A normalized Gaussian form was chosen for convenience. For cases where more than one progression is observed, eq 10b is consistent with a superposition of equations of the form of eq 12.

Moments Analysis. Although eq 12 can be used effectively for well-resolved spectra by the utilization of numerical analysis, it leaves much to be desired as a qualitative or semiquantitative formulation. It is essentially useless for bands

with unresolved vibrational structure. In an attempt to circumvent these difficulties, we resort to the method of moments.^{24,25} We define the s th moment of the (photon) emission spectrum as

$$[I]_{\nu}^s = \int_{\text{band}} I(\omega)[(\omega - \nu)^{3+s}/\omega^3] d\omega \quad (13)$$

In Appendix B, we show that (consistent with eq 12)

$$[I]_{\nu} n 0^{-2}/[I]_0^{-3} \cong \bar{\omega} = \alpha^* - \bar{n}\omega_0 \quad (14)$$

$$[I]_{\bar{\omega}}^{-1}/[I]_0^{-3} = \omega_0^2[\bar{n} + \Delta(2\bar{n} + 1)] \quad (15)$$

$$[I]_{\bar{\omega}}^0/[I]_0^{-3} = -\omega_0^3[\bar{n}(8\Delta^2 + 8\Delta + 1) + \Delta(3 + 4\Delta)] \quad (16)$$

where

$$\begin{aligned} \bar{n} &= \Delta + b^2/2 \\ \Delta &= (k^2 - 1)^2/4k^2 \quad b^2 = M\omega_0 a^2/\hbar \end{aligned} \quad (17)$$

For comparison, a "Gaussian" band with intensity distribution $G(\omega) = A\omega^3 \exp[-c(\omega - \bar{\omega})^2]$ has moments

$$\begin{aligned} [G]_0^{-2}/[G]_0^{-3} &= \bar{\omega} \\ [G]_{\bar{\omega}}^{-1}/[G]_0^{-3} &= 1/2c \\ [G]_{\bar{\omega}}^0 &= 0 \end{aligned} \quad (18)$$

Several qualitative features become immediately apparent. Both the Stokes shift ($\sim 2\bar{n}\omega_0$) and the $1/e$ width depend on the displacement, a , and the difference in ground and excited oscillator frequencies. The $1/e$ width varies linearly with the displacement and therefore is proportional to T_i , while the Stokes shift goes as T_i^2 . Moreover, a Gaussian shape function is too symmetrical. The actual intensity distribution has more intensity at lower frequencies than does $G(\omega)$.

In principle, all of the information contained in eq 12 is available from algebraic manipulation of the moments, $m + 1$ moments being required to determine m parameters, if, as usual, only relative rather than absolute intensities are available. Unfortunately, the imprecision in our measurements of relative intensities renders this procedure impractical for more than two parameters. Furthermore, for just those cases where moments fitting procedures are required, ω_0 is also an unknown. In order to extract information under these circumstances, further approximations are required. For the systems under consideration, b^2 is usually ~ 20 . On the other hand, Δ is seldom larger than 0.1 ($k^2 \approx 0.5$). To a good approximation we may take $\bar{n} = b^2/2$. With less certainty, the terms in Δ for the $[I]_{\bar{\omega}}^{-1}$ moment can also be neglected to give

$$[I]_{\bar{\omega}}^{-1}/[I]_0^{-3}(\alpha^* - \bar{\omega}) \cong \omega_0 \quad (19a)$$

$$\sqrt{2[I]_{\bar{\omega}}^{-1}/([I]_0^{-3}\omega_0^2)} \cong b \quad (19b)$$

Or, if we fit a Gaussian to the data, we obtain

$$[2c(\alpha^* - \bar{\omega})]^{-1} \cong \omega_0 \quad (20a)$$

$$(\omega_0^2 c)^{-1/2} \cong b \quad (20b)$$

These approximate equations have significance only when a single progression is responsible for the observed spectrum.

Estimation of α^* , made reasonable by the relative sharpness of the high-energy side of the band, allows estimation of b and ω_0 from either the calculated moments (eq 19a, 19b) or the Gaussian parameters (eq 20a, 20b). Both the moments and the Gaussian procedures for estimating b are expected to function best when a reliable estimate of ω_0 is available without recourse to eq 19a or 20a. This is possible when the emission is

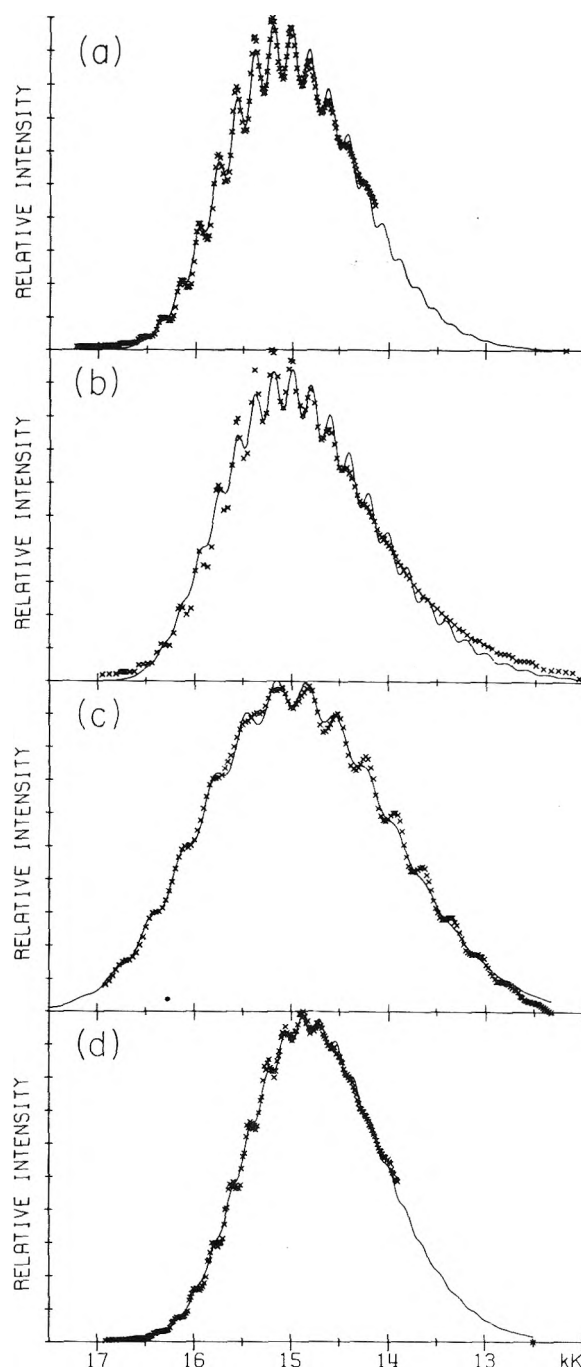


Figure 1. Solid-state emission spectra of D_4 complexes at 2 K: $\times\times\times$, experimental data points; —, computer-generated "best fit" Franck-Condon envelope as defined by least squares (see eq 12 and 22); (a) *trans*-[RhBr₂(4-Mepy)₄]Br, "best fit" of truncated data set; (b) *trans*-[RhBr₂(4-Mepy)₄]Br; (c) *trans*-[RhCl₂(py)₄]Cl; (d) *trans*-[RhBr₂(py)₄]Br.

sufficiently structured to allow direct observation of ω_0 or, less accurately, when the estimate from eq 19a or 20a identifies a particular known vibrational frequency.

Results

Figures 1 and 2 represent the results of a least-squares comparison of eq 12 to the emission spectra of four complexes at 2 K. The physical quantities determined from the computer-generated fits are presented in Table I. Seven parameters were adjusted to give the minimum square deviation between eq 12 and the observed spectra (vide infra). The an-

TABLE I: Geometrical Parameters of O and D_4 Complexes Derived from Franck-Condon Analyses

Complex	k^2 ^a	b ^b	α^*, c kK	ω_0, d kK	χ, d kK
<i>trans</i> -[RhBr ₂ (4-Mepy) ₄]Br (Figure 1a)	0.70	4.43	16.753	0.200	0.0001
<i>trans</i> -[RhBr ₂ (4-Mepy) ₄]Br (Figure 1b)	0.57	4.57	16.676	0.180	0.0007
<i>trans</i> -[RhCl ₂ (py) ₄]Cl (Figure 1c)	0.95	4.36	17.809	0.350	0.0021
<i>trans</i> -[RhBr ₂ (py) ₄]Br (Figure 1d)	0.73	4.84	16.700	0.184	0.0002
K ₃ [Co(CN) ₆] (Figure 2)	0.65	4.49	17.071	0.423	0.0026

^a $k^2 = \omega'/\omega_0$. ^b See eq 17. ^c α^* is the effective origin of the transition. ^d See eq 21; $\omega_0 = \omega_i + \chi$; see eq 22.

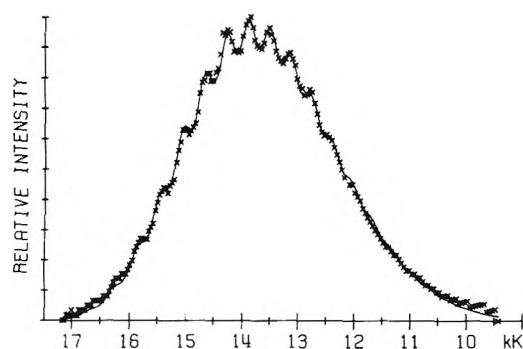


Figure 2. Solid-state emission spectrum of K₃[Co(CN)₆] at 2 K: XXX, experimental data points; —, computer-generated "best fit" Franck-Condon envelope as defined by least squares (see eq 12 and 22).

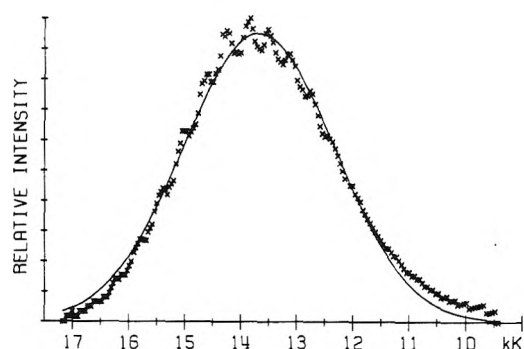


Figure 4. Gaussian representation of electronic emission spectrum of K₃[Co(CN)₆]: XXX, experimental data points; —, computer-generated "best fit" of data to $G(\omega) = A \exp[-c(\omega - \bar{\omega})^2]$. $A = 0.38667 \times 10^{-3}$, $\bar{\omega} = 13.290$, and $c = 0.27196$.

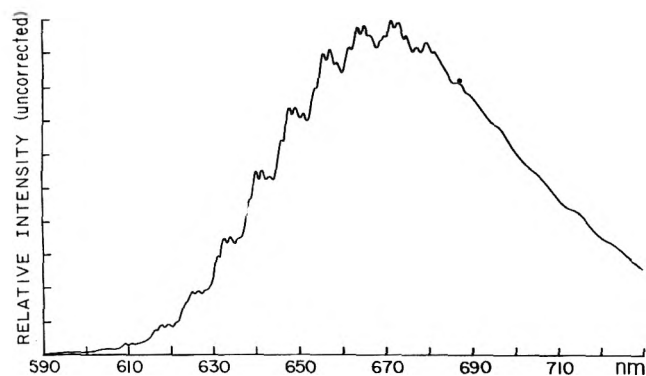


Figure 3. Emission spectrum of solid *trans*-[RhBr₂(py)₄]Br at 2 K. Phonon structure is superposed on a single totally symmetric progression. Compare Figure 1d.

harmonicity term for the ground state was introduced to account for the location of each vibrational peak, but no corresponding corrections were made to the overlaps. ω_0 and χ satisfy the ground vibrational energy relation

$$\omega_n = (n + \frac{1}{2})\omega_0 - (n + \frac{1}{2})^2\chi \quad (21)$$

For K₃[Co(CN)₆] and [RhBr₂(py)₄]Br, the fitting procedure converged rapidly and uniquely to give the rather good predicted curves shown. For [RhBr₂(4-Mepy)₄]Br, however, slightly different results were obtained from very closely spaced data taken only from the structured part of the band (Figure 1a), as opposed to the same number of points spread over the entire spectrum (Figure 1b). In the latter case the predicted curve falls significantly below the observed spectrum on the low-energy tail. We believe that the parameters associated with Figure 1a are the more accurate ones. Our

reasons for this conjecture are as follows: (a) for high n the calculation of overlaps via harmonic oscillator functions becomes questionable; (b) for large local distortions of the lattice, i.e., large n , the assumption that every line should have the same shape, $h(\omega)$, becomes less reasonable; (c) with our detector, uncertainty in the relative intensity is largest at long wavelengths.

Figure 3 shows the unusually well-resolved phonon structure that was recorded for [RhBr₂(py)₄]Br. The spectrum has been reproduced without correction in order to show its unique features. For the subsequent analyses the phonon structure was ignored by manually smoothing the curve. The smoothed experimental curve supplied the data points in Figure 5c.

Figures 4 and 5 depict the best Gaussians [$G(\omega)$], as defined by least squares, to represent the emission spectra of K₃[Co(CN)₆], [RhBr₂(4-Mepy)₄]Br, [RhCl₂(py)₄]Cl, and [RhBr₂(py)₄]Br, respectively. We note that, in general, the observed intensity is higher at low frequencies than that predicted by $G(\omega)$. Values of A , $\bar{\omega}$, and c are given in the figure captions. Rather than report numerical values for the integrated moments, we report certain extracted parameters in Table II.

Discussion

The most obvious result is that a single vibrational progression can account for the observed bands in Figures 1 and 2. For K₃[Co(CN)₆], the 420-cm⁻¹ vibration is the totally symmetric one, just as predicted by the Tanabe-Sugano diagram. The values recorded in Table I allow us to assign the progressions in the D_4 cases to metal-halogen (M-X) stretches rather than to the M-N stretching frequency. In Appendix

TABLE II: Comparison of Geometrical Parameters Derived from Franck-Condon, Direct-Integration, and Gaussian Analyses

Complex	Parameter	FCA ^a	Integration ^b	Gaussian ^c
<i>trans</i> -[RhBr ₂ (4-Mepy) ₄]Br	ω_0 , kK	0.200	0.258	0.295
	Δr_{M-Br} , Å	0.156	0.097	0.093
<i>trans</i> -[RhCl ₂ (py) ₄]Cl	ω_0 , kK	0.350	0.281	0.311
	Δr_{M-Cl} , Å	0.161	0.192	0.173
<i>trans</i> -[RhBr ₂ (py) ₄]Br	ω_0 , kK	0.184	0.242	0.249
	Δr_{M-Br} , Å	0.164	0.124	0.119
K ₃ [Co(CN) ₆]	ω_0 , kK	0.423	0.518	0.467
	Δr_{M-CN} , Å	0.100	0.079	0.088

^a Obtained from Figures 1 and 2 and eq 12. ^b Obtained from Figures 4 and 5 and eq 19. ^c Obtained from Figures 4 and 5 and eq 20.

C we show that this domination by M-X stretching is predicted from the crystal field theory by eq 1.

In order to compare the relative merits of the direct integration and Gaussian fitting procedures for estimating the degree of geometrical distortion and the energy of the vibration responsible for the progression, we have prepared Table II. The values determined by FCA (eq 12) are the best values. Although both approximate methods give poor estimates of ω_0 , the Gaussian approximation gives surprisingly good results relative to the more tedious direct integration. The inferior quality of the results from direct integration is probably due to the experimental uncertainty of the relative photon intensity at low energies. Also, any deviations from the model implicit in eq 12, such as anharmonicity, would tend to appear at lower energies. Any extra low-energy intensity would greatly affect the calculated moments.

Either of the methods associated with eq 19 and 20 should be used with extreme caution when insufficient structure is available to ascertain the existence, and spacing, of a single progression. Arguments based on analogies with similar complexes are not satisfactory. For example, [RhCl₂(4-Mepy)₄]Cl shows *two* origins for the M-X stretching progression.²⁶ Only when structure is observed and understood, may these methods be applied to give estimates of b and k^2 without resorting to FCA.

One last point relates to the practical assessment of the time when the system is at an effective 0 K temperature in its excited state. For complexes of the type reported here, monitoring the emission lifetime as a function of temperature allows one to define an effective 0 K temperature. Some of the details of this procedure have been reported.^{22,27}

Computational Details

Substitution of the equation for $|\langle u_0 | u_n \rangle|^2$ derived in Appendix A into eq 12 and insertion of the shape function $h(\omega)$ produce the working expression

$$I(\omega) = S \frac{\sqrt{k^2}}{1+k^2} e^{-k^2 b^2 / (1+k^2)} \omega^3 \sum_{n=0}^{30} [h(\omega) / 2^{n-1} n!] \times \left[\sum_{m=0}^n |C_m^n| (k^2 b)^m (1 - k^2)^{(n-m)/2} / (1+k^2)^{(n+m)/2} \right]^2 \quad (22)$$

where $h(\omega) = e^{-[\omega + n\omega_0 - n^2 \alpha^*]^2 / (\omega^2 / 4)}$, $\omega_i = \omega_0 - \chi$, and w is the full width at $1/e$ height of a single vibrational peak. S is a scaling factor. Since no progressions extending beyond $n \approx 20$ have been observed, the series was truncated at $n = 30$.

To obtain a realistic fit of this equation to the experimental curves (and save money) good initial guesses of all seven pa-

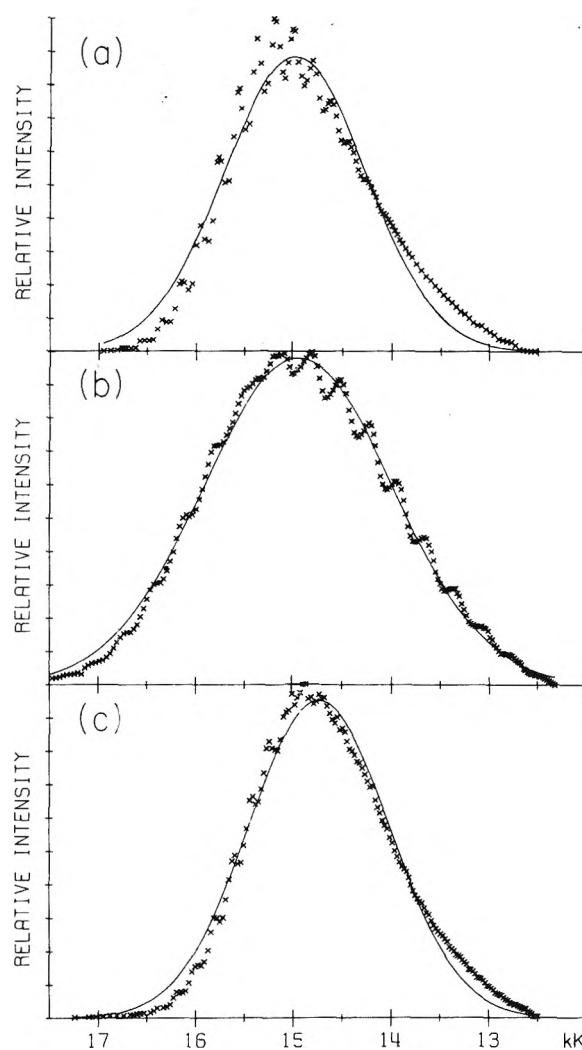


Figure 5. Gaussian representations of electronic emission spectra of D_4 complexes: $\times \times \times$, experimental data points; —, computer-generated "best fit" of data to $G(\omega) = A \exp[-c(\omega - \bar{\omega})^2]$; (a) *trans*-[RhBr₂(4-Mepy)₄]Br, $A = 0.41831 \times 10^{-2}$, $\bar{\omega} = 14.887$, $c = 0.94621$; (b) *trans*-[RhCl₂(py)₄]Cl, $A = 0.43434 \times 10^{-2}$, $\bar{\omega} = 14.760$, $c = 0.52768$; (c) *trans*-[RhBr₂(py)₄]Br, $A = 0.41739 \times 10^{-2}$, $\bar{\omega} = 14.629$, $c = 0.97051$.

rameters should be made. Our procedure was as follows: k^2 was assigned a value of 0.8, a physically reasonable number; b was chosen as 4.3, a value first determined for K₃[Co(CN)₆] (in general, an initial value for b can be best extracted from a Gaussian type fit of the intensity distribution); α^* was chosen as the frequency of the first perceptible peak appearing in the

spectrum on the high-energy side of the band; S was assigned the value of the maximum experimental photon intensity; w was chosen to be the $1/e$ width of a typical vibrational peak. First estimates for ω_i and χ were obtained from a rough fit of eq 21 to the observed vibrational progression on the band. All seven parameters were varied to minimize the least-squares deviation of the computed curve from the experimental intensities corrected for instrumental response. Typically, the total spectrum was divided into about 200 segments for data analysis. Moments were calculated using Simpson's rule.

Appendix A. Calculation of Franck-Condon Factors

Throughout this appendix we drop the prime on Q' . First, we write

$$\langle u_0 | u_n \rangle \equiv \int_{-\infty}^{+\infty} N_0 N_n e^{-\alpha'^2 Q^2/2} H_n[\alpha(Q+a)] e^{-\alpha^2(Q+a)^2/2} dQ \quad (\text{A1})$$

where $H_n(x)$ is the n th Hermite polynomial of argument x . Let $x = Q + a$; then

$$\langle u_0 | u_n \rangle \equiv N_0 N_n \int_{-\infty}^{+\infty} e^{-\alpha'^2(x-a)^2/2} H_n \alpha x e^{-\alpha^2 x^2/2} dx$$

Let $b = \alpha a$, $\beta = \alpha x$, and $k = \alpha'/\alpha$; then

$$\langle u_0 | u_n \rangle = \frac{N_0 N_n}{\alpha} e^{-k^2 b^2/2} \times \int_{-\infty}^{+\infty} H_n(\beta) e^{-(1+k^2)(\beta^2/2) + k^2 b \beta} d\beta \quad (\text{A2})$$

Using the generating function for $H_n(\beta)$

$$\sum_{n=0}^{\infty} H_n(\beta) \frac{s^n}{n!} = e^{-s^2 + 2s\beta}$$

we have

$$\begin{aligned} \sum_{n=0}^{\infty} \langle u_0 | u_n \rangle \frac{s^n}{n!} &= \frac{N_0 N_n}{\alpha} e^{-(k^2 b^2/2) - s^2} \\ &\times \int_{-\infty}^{+\infty} e^{-[(1+k^2)(\beta^2/2) - \beta(2s + k^2 b)]} d\beta \\ &\times \sum_{n=0}^{\infty} \langle u_0 | u_n \rangle \frac{s^n}{n!} = \frac{N_0 N_n}{\alpha} e^{-k^2 b^2/2} \\ &\times \sqrt{2\pi/(1+k^2)} e^{k^4 b^2/2(1+k^2)} \\ &\times e^{[s^2(1-k^2)/(1+k^2) + 2k^2 b s/(1+k^2)]} \quad (\text{A3}) \end{aligned}$$

Define

$$\begin{aligned} s' &= i\sqrt{(1-k^2)/(1+k^2)}s \\ \gamma &= -ik^2 b \sqrt{(1+k^2)(1-k^2)} \\ \sum_{n=0}^{\infty} \langle u_0 | u_n \rangle \frac{s^n}{n!} &= \frac{N_0 N_n}{\alpha} e^{-k^2 b^2/2(1+k^2)} \\ &\times \sqrt{2\pi/(1+k^2)} e^{-s'^2 + 2\gamma s'} \\ &= \frac{N_0 N_n}{\alpha} e^{-k^2 b^2/2(1+k^2)} \sqrt{2\pi/(1+k^2)} \sum_{n=0}^{\infty} H_n(\gamma) \\ &\times [i\sqrt{(1-k^2)/(1+k^2)}]^n \frac{s^n}{n!} \end{aligned}$$

Equating powers of s , we obtain

$$\begin{aligned} \langle u_0 | u_n \rangle &= \frac{N_0 N_n}{\alpha} e^{-k^2 b^2/2(1+k^2)} \sqrt{2\pi/(1+k^2)} H_n(\gamma) \\ &\times [i\sqrt{(1-k^2)/(1+k^2)}]^n \end{aligned}$$

where

$$\begin{aligned} N_n &= (\alpha/\sqrt{\pi} 2^n n!)^{1/2} \\ \langle u_0 | u_n \rangle &= \sqrt{k/(1+k^2)} 2^{n-1} n! e^{-k^2 b^2/2(1+k^2)} \\ &\times H_n(\gamma) [i\sqrt{(1-k^2)/(1+k^2)}]^n \\ H_n(x) &= \sum_m C_m^n X^m \\ H_0(x) &= 1 \end{aligned}$$

Then, we have

$$|\langle u_0 | u_n \rangle|^2 = [k/(1+k^2)] [e^{-k^2 b^2/(1+k^2)}/2^{n-1} n!] \times [(1-k^2)/(1+k^2)]^n |H_n(\gamma)|^2 \quad (\text{A4})$$

Let $\gamma = -iu$. If $k^2 \leq 1$, γ is purely imaginary and

$$|H_n(-iu)|^2 = \left\{ \sum_{m=0}^n |C_m^n| (k^2 b)^m / [(1+k^2)(1-k^2)]^{m/2} \right\}^2$$

and

$$\begin{aligned} |\langle u_0 | u_n \rangle|^2 &= k e^{-k^2 b^2/(1+k^2)} / (1+k^2) 2^{n-1} n! \\ &\times \left[\sum_{m=0}^n |C_m^n| (k^2 b)^m (1 - k^2)^{(n-m)/2} / (1+k^2)^{(n+m)/2} \right]^2 \quad (\text{A5}) \end{aligned}$$

If $k^2 \geq 1$, γ is real and

$$\begin{aligned} |\langle u_0 | u_n \rangle|^2 &= k e^{-k^2 b^2/(1+k^2)} / (1+k^2) 2^{n-1} n! \\ &\times \left[\sum_{m=0}^n C_m^n (k^2 b)^m (k^2 - 1)^{(n-m)/2} / (1+k^2)^{(n+m)/2} \right]^2 \quad (\text{A6}) \end{aligned}$$

Note that $(-1)^k 2^{n-2k} n! / k!(n-2k)! = C_{n-2k}^n$.

Appendix B

If in eq 12 we assume $h(\omega)$ to be a δ function, then

$$[I]_v^s = A \sum_n |\langle 0' | n \rangle|^2 (\alpha^* - n\omega_0 - v)^{3+s} \quad (\text{B1})$$

By carrying out the summation we find

$$[I]_0^{-3} = A \sum_n |\langle 0' | n \rangle|^2 = A \quad (\text{B2})$$

$$[I]_0^{-2}/A = \alpha^* - \bar{n}\omega_0 \equiv \bar{\omega} \quad (\text{B3})$$

$$[I]_{\omega}^{-1}/A = \omega_0^2(\bar{n}^2 - \bar{n}^2) \quad (\text{B4})$$

$$[I]_{\omega}^0/A = \omega_0^3(-\bar{n}^3 + 3\bar{n}\bar{n}^2 - 2\bar{n}^3) \quad (\text{B5})$$

Our problem is to evaluate \bar{n}^s in terms of displacement and potential parameters. This is most easily done by finding a recurrence relation via the step-up (b_+ , a_+) and step-down (b_- , a_-) operators for the excited and ground-state vibrational functions, respectively.²⁸ Using

$$\langle 0' | b_+ = 0 \quad (\text{B6})$$

$$b_+ = \alpha_+ a_+ + \alpha_- a_- + \alpha_0 \quad (\text{B7})$$

where $\alpha_{\pm} = (k/2)(1 \pm k^{-2})$ and $\alpha_0 = kb/2$ (k and b are as previously defined in the text), we have

$$\begin{aligned} \langle 0' | b_+ | n \rangle &= \alpha_+ \sqrt{n+1} \langle 0' | n+1 \rangle \\ &+ \alpha_- \sqrt{n} \langle 0' | n-1 \rangle + \alpha_0 \langle 0' | n \rangle \quad (\text{B8}) \end{aligned}$$

ADDITIONS AND CORRECTIONS

1976, Volume 80

K. W. Hipps, G. A. Merrell, and G. A. Crosby:
 Determination of Geometrical Parameters of Excited States. Application to d^6 Transition Metal Complexes of O and D_4 Symmetry.

Page 2239. Equations B9, B10, B12, and B13 are wrong, as are their reproductions in the text (eq 15 and 16). In the limit where $k^2 = 1$, the equations are correct, as are the table entries which were computed in this approximation. The correct expressions are as follows:

$$\alpha_+^3(n+1)|\langle O'|n+1\rangle|^2 = \alpha_- \Delta(n-1)|\langle O'|n-2\rangle|^2 + [\alpha_+ \Delta n - \alpha_- \alpha_0^2] |\langle O'|n-1\rangle|^2 + [\alpha_+ \alpha_0^2 - \alpha_- \alpha_+^2 n] |\langle O'|n\rangle|^2 \quad (B9)$$

$$\alpha_+(1+\Delta)n|\langle O'|n\rangle|^2 = \alpha_- \Delta(n-2)|\langle O'|n-3\rangle|^2 + [\alpha_+ \Delta(n-1) - \alpha_- \alpha_0^2] |\langle O'|n-2\rangle|^2 + [\alpha_+ \alpha_0^2 - \alpha_- \alpha_+^2(n-1)] |\langle O'|n-1\rangle|^2 \quad (B10)$$

$$\overline{n^2} = \bar{n}^2 + 2\Delta(\Delta+1) + \frac{b^2}{2k^2} \quad (B12)$$

$$\overline{n^3} = \bar{n}^2[\bar{n} + (1 - 2/k^2)(k^2 - 1)] + 2\bar{n}^2 + \bar{n} \left\{ \frac{7}{2} - (b^2/2)(k^2 - 1) + \left(\frac{1}{k^2} \right) \left[\frac{1}{2} + 3\Delta(3k^2 - 1) \right] \right\} + \frac{5(k^2 - 1)^3}{8k^4} - \frac{3b^2(3k^2 - 1)}{4k^2} \quad (B13)$$

$$\alpha_0 = kb/\sqrt{2}$$

—G. A. Crosby

V.Ph. 3 Jan. 1979

When this equation is squared in two ways and the $\langle 0'|n \pm 1\rangle\langle 0'|n\rangle$ terms are eliminated, we find

$$\begin{aligned} \alpha_+(\alpha_+ + \alpha_-)(n+1)|\langle 0'|n+1\rangle|^2 \\ = \alpha_-^2[1 + (\alpha_-/\alpha_+)]n|\langle 0'|n-1\rangle|^2 \\ + (k^2b^2/2)[1 - (\alpha_-/\alpha_+)]|\langle 0'|n\rangle|^2 \end{aligned} \quad (\text{B9})$$

which can be algebraically manipulated to give

$$\begin{aligned} n|\langle 0'|n\rangle|^2 = [4k^2/(1+k^2)^2][\Delta(n-1)|\langle 0'|n-2\rangle|^2 \\ + (b^2/8)|\langle 0'|n-1\rangle|^2] \end{aligned} \quad (\text{B10})$$

Summation of eq B10 gives

$$\bar{n} = \Delta + b^2/2 \quad (\text{B11})$$

Multiplication of eq B10 by n followed by summation gives

$$\bar{n}^2 = \bar{n}(\bar{n} + 1) + \Delta(2\bar{n} + 1) \quad (\text{B12})$$

Multiplication of eq B10 by n^2 followed by summation yields

$$\begin{aligned} \bar{n}^3 = \bar{n}(\bar{n}^2 + 3\bar{n} + 1) + \Delta(6\bar{n}^2 + 11\bar{n} + 3) \\ + 4\Delta^2(2\bar{n} + 1) \end{aligned} \quad (\text{B13})$$

Substitution of eq B11, B12, and B13 into B3, B4, and B5 produces the results given earlier.

Appendix C

In ref 29 it is shown that the d-orbital energies for a D_4 symmetry complex with axial (a) and equatorial (eq) ligands are

$$\begin{aligned} E(b_1) &= 6Dq(\text{eq}) + 2Ds - Dt \\ E(a_1) &= 6Dq(\text{eq}) - 2Ds - 6Dt \\ E(b_2) &= -4Dq(\text{eq}) + 2Ds - Dt \\ E(e) &= -4Dq(\text{eq}) - Ds + 4Dt \end{aligned} \quad (\text{C1})$$

and $Dt \approx (4/7)[Dq(\text{eq}) - Dq(\text{a})]$. Assuming $Ds \approx 3Dt$,³⁰ we have

$$\begin{aligned} E(b_1) &\approx 8.86Dq(\text{eq}) - 2.86Dq(\text{a}) \\ E(a_1) &\approx -0.86Dq(\text{eq}) + 6.86Dq(\text{a}) \\ E(b_2) &\approx -1.14Dq(\text{eq}) - 2.86Dq(\text{a}) \\ E(e) &\approx -3.43Dq(\text{eq}) - 0.57Dq(\text{a}) \end{aligned} \quad (\text{C2})$$

where the ordering is as expected if $Dq(\text{a}) < Dq(\text{eq})$.

If one assumes that the emitting level is predominantly represented by the configuration $e^4b_2a_1$, while the ground level is predominantly $e^4b_2^2$, the change in crystal field energy on transition, ΔV_{cf} , is

$$\Delta V_{cf} \approx 0.28Dq(\text{eq}) + 9.72Dq(\text{a}) \quad (\text{C3})$$

This suggests that

$$(\partial\Delta V_{cf}/\partial Q_a) \approx 35(\partial\Delta V_{cf}/\partial Q_{\text{eq}}) \quad (\text{C4})$$

We predict (eq 1 of text) that excitation of a D_4 complex will produce a very large expansion of the M-X distance but a tiny

increase in the M-4-Mepy distance whenever $Dq(\text{a}) < Dq(\text{eq})$.

For the case where $Dq(\text{a}) > Dq(\text{eq})$, the weaker ligand is still maximally displaced but now only by a factor of ~ 5 . This procedure may be used for any other configurational transition. It is more proper to use the actual energies; these are linear combinations of configurational energies.

References and Notes

- (1) (a) Research supported by AFOSR(NG)-OAR USAF Grant AFOSR-76-2932. (b) Presented at the Michael Kasha Symposium on Energy Transfer in Organic, Inorganic, and Biological Systems, Florida State University, Jan 8-10, 1976, by K.W.H. during tenure of a National Science Foundation post-doctoral fellowship at the University of Michigan.
- (2) E. Hutchison, *Phys. Rev.*, **36**, 410 (1930).
- (3) J. B. Coon, R. E. DeWames, and C. M. Loyd, *J. Mol. Spectrosc.*, **8**, 285 (1962).
- (4) D. P. Craig, *J. Chem. Soc.*, 2146 (1950).
- (5) G. R. Hunt, E. F. McCoy, and I. G. Ross, *Aust. J. Chem.*, **18**, 591 (1962).
- (6) K. Miller and J. N. Murrell, *Theor. Chim. Acta*, **3**, 231 (1965).
- (7) Y. Fujimura, M. Onda, and T. Nakajima, *Bull. Chem. Soc. Jpn.*, **46**, 2034 (1974).
- (8) H. H. Patterson, J. J. Godfrey, and S. M. Khan, *Inorg. Chem.*, **11**, 2872 (1972).
- (9) (a) K. W. Hipps and G. A. Crosby, *Inorg. Chem.*, **13**, 1543 (1974); (b) G. A. Crosby, G. D. Hager, K. W. Hipps, and M. L. Stone, *Chem. Phys. Lett.*, **28**, 497 (1974).
- (10) P. Hochmann, H. T. Wang, and S. P. McGlynn, Abstracts, 29th Southwest Regional Meeting of the American Chemical Society, El Paso, Tex., Dec 1973, No. 83.
- (11) G. Blasse and A. Brill, *Philips Tech. Rev.*, **31**, 304 (1970).
- (12) Y. Haas and G. Stein, *Chem. Phys. Lett.*, **15**, 12 (1972).
- (13) M. S. Wrighton, L. Pdungsap, and D. L. Morse, *J. Phys. Chem.*, **79**, 66 (1975).
- (14) T. M. Dunn in "Modern Coordination Chemistry", J. Lewis and R. G. Wilkins, Ed., Interscience, New York, N.Y., 1960, Chapter 4.
- (15) L. E. Orgel, *J. Chem. Phys.*, **23**, 1824 (1955).
- (16) *Inorg. Synth.*, **2**, 225 (1946).
- (17) R. W. Gillard and R. Ugo, *J. Chem. Soc.*, 549 (1963).
- (18) R. Stair, N. Schneider, and J. Jackson, *Appl. Opt.*, **2**, 1151 (1963).
- (19) M. Kasha, *Discuss. Faraday Soc.*, No. **9**, 14 (1950).
- (20) J. N. Demas and G. A. Crosby, *J. Am. Chem. Soc.*, **92**, 7262 (1970).
- (21) For example, F. A. Cotton, "Chemical Applications of Group Theory", 2d ed, Wiley-Interscience, New York, N.Y., 1971, pp 266-267.
- (22) G. D. Hager and G. A. Crosby, *J. Am. Chem. Soc.*, **97**, 7031 (1975); G. D. Hager, R. J. Watts, and G. A. Crosby, *ibid.*, **97**, 7037 (1975); K. W. Hipps and G. A. Crosby, *ibid.*, **97**, 7042 (1975).
- (23) H. Sponer and E. Teller, *Rev. Mod. Phys.*, **13**, 75 (1941).
- (24) M. Lax, *J. Chem. Phys.*, **20**, 1752 (1952).
- (25) S. E. Schnatterly, C. H. Henry, and C. P. Slickter, *Phys. Rev. [Sect.] A*, **137**, 583 (1965).
- (26) Unpublished work, this laboratory.
- (27) R. W. Harrigan and G. A. Crosby, *J. Chem. Phys.*, **59**, 3468 (1973).
- (28) While this paper was in preparation, a general treatment of the overlap problem appeared: E. E. Bergman, *Nuovo Cimento Soc. Ital. Fis. B*, **22b**, 249 (1974).
- (29) M. Gerloch and R. C. Slade, "Ligand Field Parameters", Cambridge University Press, London, 1973.
- (30) H. J. Clifford, Ph.D. Thesis, University of New Mexico, Albuquerque, N.M., 1970.

Discussion

M. GOUTERMAN What is the origin of these bands? Singlet-triplet? How intense are they?

K. W. HIPPS. The question is very well chosen. We are going to address it in another publication. For a discussion relative to $K_3Co(CN)_6$, see K. W. Hipps and G. A. Crosby, *Inorg. Chem.*, **13**, 1543 (1974). For an analogous situation in ruthenocene, see G. A. Crosby, G. D. Hager, K. W. Hipps, and M. L. Stone, *Chem. Phys. Lett.*, **28**, 497 (1974). We believe we are picking out a single electronic level derived from a ligand field term of triplet parentage.

The Phosphorescence of Phosphorus¹

Richard J. VanZee[†] and Ahsan U. Khan*

Departments of Chemistry and Biophysics, Michigan State University, East Lansing, Michigan 48824 (Received March 3, 1976)

The electronically excited species in the chemiluminescence associated with the oxidation of P₄ vapor under reduced pressure and oxygen deficient conditions are markedly different from those of the oxygen sufficient, atmospheric pressure system. P₂(C¹Σ_u⁺ → X¹Σ_g⁺ and A¹Π_g → X¹Σ_g⁺) transitions are the dominant emission in the near-ultraviolet region, replacing the PO emission found under atmospheric pressure. A comparison of the spectra shows that the visible continuum is red shifted by ~2000 cm⁻¹ in the reduced pressure, oxygen deficient system compared to atmospheric pressure conditions. Two alternative suggestions are offered to explain the origin of the visible continuum in the reduced pressure system: (i) as in the atmospheric pressure system, the emitting species is the (PO)₂* excimer, with different vibrational distribution; (ii) an exciplex of P₂ and PO is responsible for the emission. The existing mechanism for phosphorus chemiluminescence suggested by Semenov and Dainton fails to interpret these experimental observations.

Introduction

The phosphorescence of phosphorus is the oldest known chemiluminescing system.² The major fine band systems in the visible and near-ultraviolet portion of the chemiluminescence under atmospheric conditions are due to the PO γ system, the PO β system, and HPO.^{3a} The broad continuum emission which is responsible for most of the visible intensity has been identified as an excimer of PO, (PO)₂*.^{3b,4} In addition the reaction under ambient conditions produces infrared emission corresponding to transitions between vacuum ultraviolet and ultraviolet states of PO, identifying part at least of the previously unidentified vacuum ultraviolet emission from the reaction.⁵ In this paper we report the effect of reduced pressure, oxygen deficient conditions on the chemiluminescence reaction. These conditions drastically alter the nature of the emitting species; the PO emission disappears and is replaced by P₂ emission in the ultraviolet region of the chemiluminescence, and the continuum emission in the visible region also changes. The existing chemiluminescence model for phosphorus oxidation is inadequate in interpreting these observations.⁶

Experimental Section

White phosphorus (Baker) was placed in a 50-ml round-bottom glass flask connected directly to the quartz reaction chamber. Air was used as the source of molecular oxygen and was regulated into a glass tube by a fine needle valve. The tube serving as the air inlet was led into the 50-ml flask containing the phosphorus and terminated at the entrance to the quartz (22 mm o.d. and 20 cm long) reaction chamber. A vacuum pump, separated by a liquid nitrogen trap, maintained 0.1 Torr total pressure inside the quartz tube. A dim chemiluminescence glow filled the entire length of the tube and hose to the trap. A Heath Model EU-700, 0.5 m monochromator, with a grating of 1200 lines/mm and blazed at 250 nm, connected to a Heath Model EU-701-30 photomultiplier module containing a RCA 1P28 photomultiplier was used to monitor the spectra which were recorded with a Heath Model EU-703-31 photometric readout unit with a typical sensitivity of 10⁻⁸ A.

[†] Present address: Department of Chemistry, University of Florida, Gainesville, Florida.

Atmospheric Pressure, Oxygen Sufficient

Figure 1 is the visible and ultraviolet chemiluminescence spectrum of the reaction of water saturated P₄ vapor with air at atmospheric pressure and room temperature. The discrete band structure in the 228–272-nm region is the PO γ system, PO(A²Σ⁺) → PO(X²Π). The weak bands at 450–650 nm superimposed on the broad continuum were identified, by substitution of D₂O for H₂O in the reaction, as the HPO transition $\bar{A}(^1A'') \rightarrow \bar{X}(^1A')$.^{3a} The broad visible continuum is due to an excimer of PO, (PO)₂*^{3b}, involving the lowest excited state of PO, the ⁴Π state. Because radiative transition from the ⁴Π state to the ground X²Π state is spin forbidden, and since the ⁴Π state is close enough energetically for thermal population of the B²Σ⁺ state of the PO β system to occur, the excimer has the following equilibrium: (PO)₂* ⇌ PO(X²Π) + PO(⁴Π) ⇌ PO(X²Π) + PO(B²Σ⁺). Increasing the temperature of the reaction or dilution of the P₄ vapor stream at higher temperatures with inert gas results in the appearance of PO β system transitions, PO(B²Σ⁺) → PO(X²Π), in the spectrum at 325–337 nm.^{3b} Reduced pressure and oxygen sufficient conditions also produce PO β system emission in the chemiluminescence. These results are analyzed in detail elsewhere.⁴

The chemiluminescence spectrum of the oxidation of P₄ vapor by moist air at atmospheric pressure also contains infrared emissions, some of which correspond to transitions between vacuum ultraviolet and ultraviolet states of PO.⁵ Transitions from the vacuum ultraviolet states, G²Σ⁺ and F²Σ⁺, PO(G²Σ⁺) → PO(A²Σ⁺), PO(F²Σ⁺) → PO(A²Σ⁺), and PO(F²Σ⁺) → PO(B²Σ⁺); and between the ultraviolet states PO(A²Σ⁺) → PO(B²Σ⁺) have been identified in the spectrum.⁵ The presence of the G²Σ⁺ and F²Σ⁺ states of PO in the phosphorus flame can partially account for the unidentified vacuum ultraviolet emission from the reaction, first observed by Downey in 1924.⁷ A summary of the PO transitions so far identified in phosphorus chemiluminescence is given in Figure 2.

Reduced Pressure, Oxygen Deficient

Figure 3 is the visible and ultraviolet chemiluminescence spectrum of the reaction of P₄ vapor with air at approximately 0.1 Torr total pressure and room temperature. When compared to the ambient chemiluminescence spectrum, there are three striking differences in the spectrum of the reduced

TABLE I: Wavelengths of Band Heads of P_2 $C^1\Sigma_u^+ - X^1\Sigma_g^+$ and $A^1\Pi_g - X^1\Sigma_g^+$ Emission

Literature Values					Present Work	
Intensity	(v',v'')	Transition	λ_{air} , nm	Ref	λ_{air} , nm	Intensity
4	7,15	C-X	256.56	14	257.0	5
5	11,18	C-X	258.66	14	259.5	8
5	5,15	C-X	262.55	14	262.5	10
5	9,18	C-X	264.52	14	265.5	8
4	6,16	C-X	264.21	14	266.5	8
	3,0	A-X	275.82	15	275.0	9
6	4,17	C-X	275.71	14		
	5,19	C-X	283.0	14	283.5	7
	0,1	A-X	296.984	16	296.0	2
4	7,24	C-X	302.87	14	302.5	8
	0,2	A-X	303.929	16	304.0	8
	8,25	C-X	304.64	14		
	1,3	A-X	305.37	15	305.5	8
4	9,26	C-X	306.42	14		
5	10,27	C-X	308.20	14	308.5	7
	0,3	A-X	311.243	16	310.5	6
	8,26	C-X	310.54	14		
4	10,29	C-X	320.19	14	320.0	2

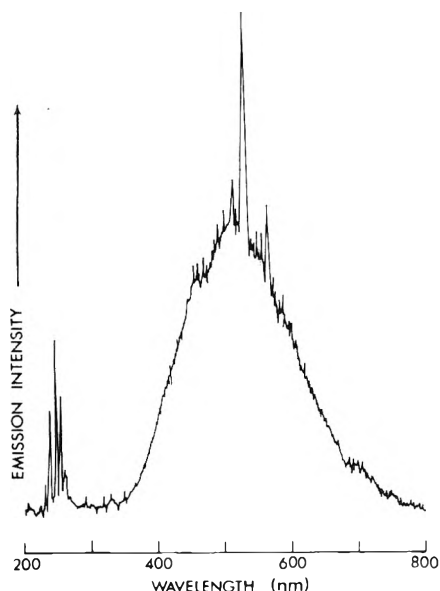


Figure 1. Chemiluminescence spectrum of the room temperature reaction, on contact with air, under atmospheric pressure, of P_4 vapor carried in a nitrogen stream saturated with water vapor. The spectrum was recorded with a 0.3-m McPherson Model 218 monochromator with an EMI 9558QB photomultiplier (VanZee and Khan).⁴

pressure system: (1) the PO γ system emission has disappeared, (2) the visible continuum onsets at a longer wavelength and has a smaller spectral bandwidth, and (3) the overall luminescence intensity is reduced. Emission from P_2 replaces the PO γ emission in the 250–300-nm region. In contrast, no obvious P_2 emission has been observed under atmospheric pressure of air in studies of phosphorus chemiluminescence. Figure 3 contains emission from the $C^1\Sigma_u^+ \rightarrow X^1\Sigma_g^+$ and $A^1\Pi_g \rightarrow X^1\Sigma_g^+$ transitions of P_2 . Table I is a comparison of literature values with a medium resolution phosphorus chemiluminescence spectrum under reduced pressure and oxygen deficient conditions. Figure 2 shows the relative energies of the electronically excited states of P_4 ,¹³ P_2 ,^{14–16} PO ,⁴ HPO ,⁴ and O_2 . Arrows indicate transitions identified to date in phosphorus chemiluminescence spectra under various conditions.

The continuum emission in Figure 3 starts at about 375 nm; whereas in the ambient chemiluminescence (Figure 1) the continuum emission starts at about 350 nm. There is thus a red shift of about 2000 cm^{-1} in the onset of the continuum in

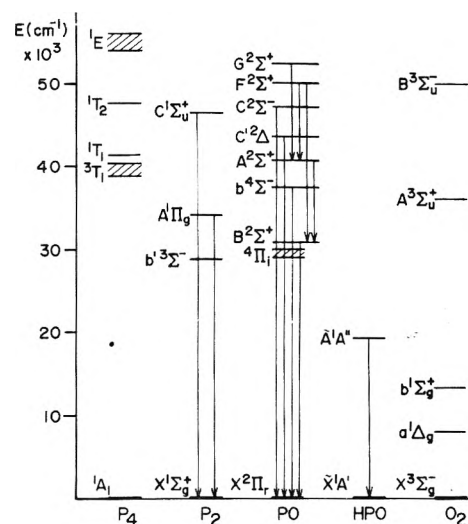


Figure 2. Relative energies of the electronically excited states of P_4 ,¹³ P_2 ,^{14–16} PO ,⁴ HPO ,⁴ and O_2 . Arrows indicate transitions identified to date in phosphorus chemiluminescence spectra under various conditions.

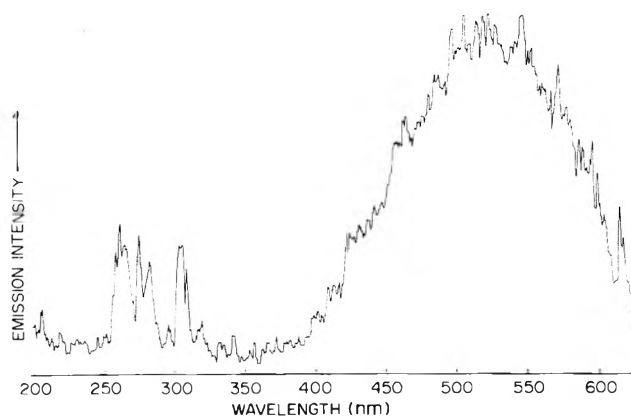


Figure 3. Chemiluminescence spectrum of the reaction at room temperature and 0.1 Torr total pressure of P_4 vapor on contact with air. Because of reduced intensity of the luminescence compared to Figure 1, the signal-to-noise ratio in this spectrum is lower. The spectrum was recorded with a 0.5-m Heath Model EU-700 monochromator with an RCA 1P28 photomultiplier.

going from ambient conditions to reduced pressure, oxygen deficient conditions. The emission maxima is not greatly affected, however. The bandwidth of the spectrum is narrower in Figure 3 when compared to the ambient chemiluminescence spectrum. There are two alternative interpretations to explain these observations: (i) emission from the $(\text{PO})_2^*$ excimer is modified by altering the vibrational distribution on going from atmospheric to reduced pressure conditions,¹⁷ or (ii) the species responsible is not the $(\text{PO})_2^*$ excimer but is an exciplex formed between P_2 and PO. The lowest metastable state of P_2 , the $^3\Sigma_{g^-}$ state (see Figure 2), is slightly lower in energy than the lowest metastable state of PO, the $^4\Pi$ state. Thus exciplex emission involving the $\text{P}_2(^3\Sigma_{g^-})$ and $\text{PO}(X^2\Pi)$ states would be red shifted with respect to the $(\text{PO})_2^*$ excimer where the complexing is between the $\text{PO}(^4\Pi)$ and $\text{PO}(X^2\Pi)$ states. This would be consistent with the observed experimental results. The absence of PO emission in the spectrum under reduced pressure conditions could be due to electronic energy transfer from PO^* to P_2 , accounting for at least a portion of the P_2 emission. There are also suggestions of weak HPO bands over the continuum in Figure 3, similar to the stronger HPO bands seen in Figure 1.

Discussion

From a kinetic study of the chemiluminescence of phosphorus oxidation, Semenov proposed a branch chain reaction mechanism, suggesting that oxygen atoms are the chain carriers of the branch chain reaction, and that they are inserted into the P_4 tetrahedron one by one.⁶ Dainton and Kimberley⁸ have expanded this model and suggested that the luminescent process in the reaction $\text{P}_{4(g)} + 5\text{O}_{2(g)} \rightarrow \text{P}_4\text{O}_{10(g)}$ ($\Delta H = -722.3 \text{ kcal mol}^{-1}$)⁹ is actually a side reaction of the oxidation process. However, the oxygen atom insertion mechanism is based upon monitoring the luminescence of the reaction. Moreover, now that the transient emitters have been identified as small di- and triatomic species, it is clear that the P_4 tetrahedron is dissociated in the reaction.¹⁸

The oxygen atom insertion mechanism also fails to explain the necessity of moisture in the reaction. Baker and Dixon observed that phosphorus and molecular oxygen, if previously dried for several months under very stringent conditions, do not undergo a luminescent reaction in the absence of water vapor, even when the temperature of the reaction chamber is raised to 290 °C.¹⁰ Furthermore, Verma and Broida have found that the reaction of atomic oxygen and molecular phosphorus requires a trace amount of water for activation.¹¹ Under atmospheric conditions there is also an increase in the total luminosity with increasing concentration of moisture.⁴

Chemiluminescence from the oxidation of P_4 by O_2 cannot be explained by considering the reaction of atomic phosphorus and atomic oxygen. In studies of the reaction of atomic phosphorus and atomic oxygen in a gas discharge, Walsh has found a precise cutoff in the PO emission at the nearly isoenergetic $\text{B}^2\Sigma^+$ ($v' = 10$) and $\text{A}^2\Sigma^+$ ($v' = 2$) states at $43\,500 \text{ cm}^{-1}$, reflecting the dissociation energy D_e of the ground state PO molecule.¹² The presence in the phosphorus flame at atmospheric pressure of vacuum ultraviolet and ultraviolet PO states of energies above D_e ^{4,5} eliminates the possibility that the chemiluminescence proceeds by stepwise combination of atomic phosphorus and atomic oxygen. For energetic reasons

it is likely that PO is initially generated in these high energy states, since the alternative means of exciting PO to these states would involve bimolecular energy summation processes. Further investigation is necessary to clarify the details of these processes under atmospheric conditions.

In summary, the essential features to be accounted for in the chemiluminescent mechanism are: (1) the presence of electronically excited PO in the reaction and the drastic change to P_2 emission in response to mild changes in experimental conditions, (2) the absolute requirement of water, and (3) the emission of high energy ultraviolet and vacuum ultraviolet photons from a cool flame.

References and Notes

- (1) (a) Presented at the Michael Kasha Symposium on Energy Transfer in Organic, Inorganic, and Biological Systems, held at Florida State University at Tallahassee, Tallahassee, Fla, Jan 8–10, 1976. (b) This paper is based on the thesis submitted by R.J.V. to the Graduate School of Michigan State University in partial fulfillment of the requirement for the degree of Doctor of Philosophy.
- (2) E. N. Harvey, "A History of Luminescence", The American Philosophical Society, Philadelphia, Pa., 1957.
- (3) (a) R. J. VanZee and A. U. Khan, *J. Am. Chem. Soc.*, **96**, 6805 (1974); (b) R. J. VanZee and A. U. Khan, *Chem. Phys. Lett.*, **36**, 123 (1975).
- (4) R. J. VanZee and A. U. Khan, *J. Chem. Phys.*, in press.
- (5) R. J. VanZee and A. U. Khan, *Chem. Phys. Lett.*, **41**, 180 (1976).
- (6) N. Semenov, *Z. Phys.*, **46**, 109 (1927); *Chem. Rev.*, **6**, 347 (1929).
- (7) W. E. Downey, *J. Chem. Soc.*, 347 (1924).
- (8) F. S. Dainton and H. M. Kimberley, *Trans. Faraday Soc.*, **46**, 629 (1950).
- (9) R. C. Weast and S. M. Selby, Ed., "Handbook of Chemistry and Physics", 47th ed, The Chemical Rubber Co., Cleveland, Ohio, 1966, p D25.
- (10) H. B. Baker, *J. Chem. Soc.*, **47**, 349 (1885); *Phil. Trans.*, **179A**, 571 (1888).
- (11) R. D. Verma and H. P. Broida, *Can. J. Phys.*, **48**, 2991 (1970).
- (12) A. D. Walsh in "The Threshold of Space", M. Zelkoff, Ed., Pergamon Press, London, 1957, p 165.
- (13) R. R. Hart, M. B. Robin, and N. A. Kuebler, *J. Chem. Phys.*, **42**, 3631 (1965), and references therein.
- (14) P. N. Skancke and J. E. Boggs, *Chem. Phys. Lett.*, **21**, 316 (1973).
- (15) R. D. Verma, *Can. J. Phys.*, **48**, 2391 (1970).
- (16) E. J. Marais, *Phys. Rev.*, **70**, 499 (1946).
- (17) We thank the referee (Dr. Brian Stevens) for drawing our attention to this possibility.
- (18) In the conference an exploding tetrahedron mechanism was proposed which is not included in the paper, since it is felt further exploration of the role of water is essential. The initiation step in the suggested model is a stable $[\text{P}_4 \cdots \text{O}_2]$ complex exploding on the approach of H_2O , generating diatomic and triatomic species in highly excited electronic states. In the propagation step a stable $[\text{P}_4 \cdots \text{O}_2]$ complex explodes by absorbing a high energy photon from the initiation step, again generating electronically excited species. The high energy photons act as the chain carriers.

Discussion

D. S. MCCLURE. Your exploding tetrahedron model breaks many bonds. This makes me wonder how there can be energy left over for the high degree of electronic excitation implied by your observations.

R. J. VANZEE. The total energy of reaction, 730 kcal/mol, is sufficient to produce, with unit efficiency, photons of wavelengths 400 Å. With this potential we need not worry about sufficiency of energy.

G. A. CROSBY. Has any one tried to isolate P_4 in a matrix and diffuse O_2 into the matrix? Any associative complex or new species could be monitored by infrared or Raman techniques.

R. J. VANZEE. I know of no such attempts.

H. SELIGER. I remember that many years ago a very strange kinetics was observed for this chemiluminescence. Is this the case in your experiments?

R. J. VANZEE. Not that we are aware of.

Luminescence Studies of Proton Transfer in the Excited Electronic States of Hydrogen Bonded Quinoline and Isoquinoline

William R. Moomaw* and Mary F. Anton

Department of Chemistry, Williams College, Williamstown, Massachusetts 01267 (Received February 27, 1976)

Publication costs assisted by The Camille and Henry Dreyfus Foundation

In the absence of a hydrogen bond, quinoline only exhibits phosphorescence in a 3-methylpentane glass at 77 K. Under these conditions isoquinoline both fluoresces and phosphoresces weakly. The addition of a weak hydrogen bond such as ethanol induces structured ultraviolet fluorescence originating from the lowest excited singlet state. More acidic alcohols such as trifluoroethanol and hexafluoro-2-propanol induce both the structured ultraviolet fluorescence, and a now broad, violet fluorescence. This new fluorescence resembles, but differs from, that of the corresponding protonated cation. An analysis of the excitation spectrum, which differs from the excitation spectrum of the structured fluorescence, leads to the conclusion that the proton has been displaced toward the nitrogen heterocycle in the excited state.

I. Introduction

Recently, we reported some detailed studies of the role of hydrogen bonding on the luminescence properties of quinoline and isoquinoline.^{1,2} In the case of quinoline we were able to show that in a 3-methylpentane glass at 77 K, phosphorescence occurs only from non-hydrogen bonded molecules, structured fluorescence from molecules hydrogen bonded in both the ground and excited states, and that a protonated-cationlike fluorescence occurs from molecules that are probably hydrogen bonded in the ground state, but which undergo at least a partial proton transfer in the excited state. An upper limit for the fluorescence to phosphorescence ratio of 20 ppm was established for non-hydrogen bonded quinoline, by utilizing an extensive purification method. It was not possible to obtain such rigorous limits for isoquinoline, although the findings of the same three types of luminescence leads us to the conclusion that the luminescence properties of isoquinoline are similar to those of quinoline.

It is the purpose of the present work to elucidate the luminescence mechanism of the protonated-cationlike fluorescence in quinoline and isoquinoline. The recently reported work of Taylor, El-Bayoumi, and Kasha³ on the excited state biprotonic tunneling in dimers of 7-azaindole has generated much interest in the hydrogen bonding and proton affinities of electronically excited states.

II. Experimental Section

Quinoline was obtained from Aldrich Chemical Co. as a yellowish brown liquid. Isoquinoline obtained from J. T. Baker was yellow. Vacuum distillation produces a colorless liquid in both cases which darkens upon standing, and which contains traces of the other isomer as an impurity. Both substances were purified as the picrate,⁴ by adding the base to picric acid dissolved in a minimum of 95% ethanol. The bright yellow crystals were washed with ethanol, air dried, and recrystallized from acetonitrile. The free base was regenerated by dissolving the picrate in dimethyl sulfoxide which had been dried over 4A molecular sieves. The bright yellow solution was passed down a basic alumina column to which the picric acid adsorbed, releasing the base. The effluent was extracted with spectral grade *n*-pentane and distilled under vacuum. Residual amounts of solvent could be readily removed by vapor

phase chromatography. Quinoline and isoquinoline prepared in this way remained colorless even after standing in air for periods in excess of 1 year.

3-Methylpentane was Phillips pure grade, which was shaken with three different aliquots of fuming sulfuric acid, washed with water, dried over anhydrous sodium sulfate, and refluxed for 12 h over metallic sodium. The 3-methylpentane was then distilled and passed through a neutral alumina column coated with silver nitrate.⁵ No detectable luminescence could be observed from solvent prepared in this way.

Hexafluoro-2-propanol was obtained from Pierce, and found to have an impurity which luminesced around 350 nm. Distillation from 2A molecular sieves followed by storage over fresh sieves at 0 °C proved to be an adequate remedy. Trifluoroethanol (TFE) was also obtained from Pierce, and was found to be suitable as received.

It was found that traces of chromic acid cleaning solution cling to ground glass joints and must be rigorously excluded to avoid forming the protonated quinolinium and isoquinolinium cations.

The concentration of quinoline or isoquinoline and the added hydrogen bonding alcohols were kept in the concentration range of 10^{-4} to 10^{-5} M to avoid solubility and alcohol aggregation problems.

The reported luminescence and excitation spectra are uncorrected for wavelength response of the measuring system. McPherson Model EU-700 monochrometers blazed at 500 nm for luminescence and 250 nm for excitation were used with an effective band pass of about 1.0 nm. A Hanovia 1000-W xenon lamp was used for excitation, and an EMI9789 QA photomultiplier connected to an SSR 1105 photon counter was used for detection. A Cary 14 double beam spectrophotometer was used for all absorption spectra. All measurements were carried out on samples immersed in liquid nitrogen at 77 K.

III. Results

As previously reported,^{1,2} quinoline in 3-methylpentane (3MP) at a temperature of 77 K only shows characteristic green phosphorescence starting at 457.2 nm ($21\,870\text{ cm}^{-1}$). The addition of ethanol ($pK_a = 17$) causes the appearance of structured naphthalene-like ultraviolet fluorescence beginning at 313.0 nm ($31\,950\text{ cm}^{-1}$). The addition of a more acidic

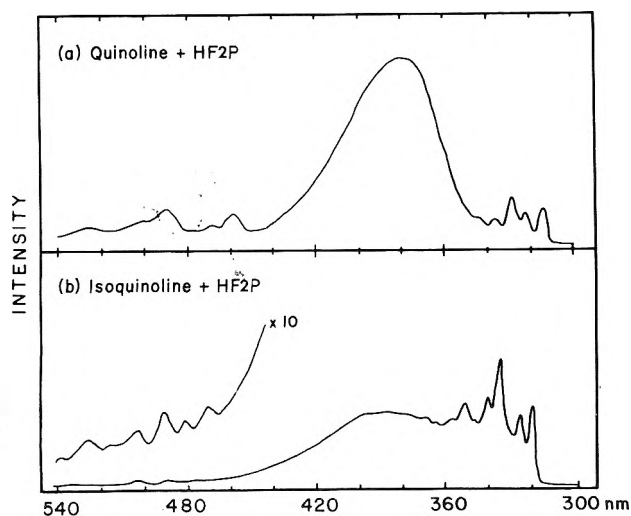


Figure 1. The total luminescence spectrum of a 1.6×10^{-4} M solution of quinoline in 3MP containing 3.7×10^{-4} M HF2P (a) and of a 1.0×10^{-4} M solution of isoquinoline in 3MP containing 0.55×10^{-4} M HF2P (b). Both spectra were measured at a temperature of 77 K. The cationlike fluorescence near 400 nm is between the structured fluorescence near 300 nm and the phosphorescence near 450 nm.

alcohol such as hexafluoro-2-propanol (HF2P, $pK_a = 9.3$) produces a dramatic change in the visible luminescence from green to violet. The reason for this change is readily apparent in the spectrum shown in Figure 1a. A strong broad band peaking at 384.0 nm ($26\,040\text{ cm}^{-1}$) is now present, and the phosphorescence and regular, structured fluorescence appear weakly on either side of it. The similarity of this new emission to that of the protonated cation may be seen in Figure 2, where the quinolinium fluorescence spectrum is shown. Quinolinium cation was prepared by bubbling gaseous hydrogen chloride into a quinoline solution in 3-methylpentane, allowing the cloudy solution to clear, and then freezing it to a clear glass in liquid nitrogen. It is to be noted that the maximum of the quinolinium cation fluorescence appears at 400.0 nm ($25\,000\text{ cm}^{-1}$). This is lower in energy than any of the spectra appearing in the HF2P containing solutions of quinoline.

The excitation spectrum of the broad cationlike fluorescence of quinoline is compared with the structured fluorescence excitation spectrum of the same solution in Figure 3. The two excitation spectra bear a superficial resemblance to each other in location and band structure (the 0,0 bands of both are at 313.2 nm or $31\,930\text{ cm}^{-1}$). While the structured fluorescence excitation spectrum and the absorption spectrum are essentially identical,² the cationlike fluorescence excitation spectrum is much broader. The rather sharp drop-off in excitation intensity below 290 nm is mostly due to the lower excitation lamp intensity in this region, but the 1L_a band at 275 nm is genuinely attenuated relative to the non-hydrogen bonded spectrum. Of equal importance is the comparison of the excitation spectra of the cationlike and genuine cation fluorescence. The cation excitation spectrum is broad like the fluorescence, and closely resembles the cation absorption spectra in other solvents published elsewhere.⁶ No quinolinium or isoquinolinium cation phosphorescence has ever been reported, and we were unable to detect any. A sizable Stokes shift can be seen for both the cationlike fluorescence (Figure 1a) and the cation fluorescence (Figure 2).

The luminescence properties of isoquinoline are very similar to those of quinoline. A major difference is that isoquinoline in 3-methylpentane both fluoresces and phosphoresces. There is evidence^{1,2} to suggest that some residual hydrogen bond

is responsible for the fluorescence. Like quinoline, however, the addition of hexafluoro-2-propanol in roughly equimolar amounts produces a broad cationlike violet fluorescence. The total luminescence is shown in Figure 1b, and the excitation spectra are shown in Figure 4. As is the case for quinoline, the cationlike fluorescence excitation spectrum is seen to be broad compared to the structured fluorescence excitation spectrum. In addition, the 0,0 band is shifted about 1.6 nm (160 cm^{-1}) to lower energy from the structured fluorescence excitation at 319.4 ± 0.3 nm ($31\,310\text{ cm}^{-1}$). The position of the isoquinoline spectrum is much more solvent dependent than is quinoline.

Another interesting feature of the isoquinoline cationlike fluorescence is the sensitivity of its shape to proton donor type and concentration. For an isoquinoline solution 1.0×10^{-4} M, for which the concentration of HF2P is half that amount, the cationlike fluorescence maximum appears at 390.0 ± 0.3 nm ($25\,640\text{ cm}^{-1}$). Increasing the concentration of HF2P eightfold causes a shift of the maximum to 396.6 nm. The 0,0 band of the excitation shifts by a smaller amount from 321.0 ± 0.3 nm ($31\,150\text{ cm}^{-1}$) to 321.8 ± 0.3 nm ($31\,090\text{ cm}^{-1}$). In an equimolar mixture of isoquinoline and trifluoroethanol (1.0×10^{-4} M) the broad fluorescence maximum is at 396.0 nm ($25\,250\text{ cm}^{-1}$). The 0,0 band of the excitation spectrum in this case lies at 321.0 nm.

IV. Discussion

There are three important cases to be considered in determining the nature of the fluorescence in these systems. The first is that of quinoline or isoquinoline hydrogen bonded to a weak proton donor such as ethanol. The second is that of the fully protonated quinolinium or isoquinolinium cation, and the third is the apparently intermediate case of these bases hydrogen bonded to a strong proton donor such as hexafluoro-2-propanol (HF2P) or trifluoroethanol (TFE).

Both quinoline and isoquinoline show well-structured absorption and fluorescence spectra when weakly hydrogen bonded in solution.^{1,2,7,8} Later reports of non-hydrogen bonded quinoline fluorescence^{9,10} have been shown to be in error.² The hydrogen bonded induced fluorescence appears to originate from a state of $\pi\pi^*$ character,⁶ although there is strong evidence of vibronic interaction and electronic state congestion^{11,12} in that region. It would appear reasonable, therefore, to assume a similar degree of hydrogen bonding in the ground and excited states.

The protonation of quinoline and isoquinoline by a strong acid such as HCl produces major changes in the absorption and luminescence spectra. Both the absorption and fluorescence spectra of the protonated cations are broad structureless, roughly symmetrical bands, possessing an approximate mirror image relationship to each other (Figure 2). For quinoline the mirror image relationship is not as clear as it might be because of the strong overlapping of the 1L_a and 1L_b bands in absorption.⁶ The small overlap of the absorption and fluorescence of the protonated cations, and the low transition probability in the region of the 0,0 transitions, suggest a large geometry difference between the ground and fluorescing states. Another possibility is that vibronic coupling not found in the unprotonated bases themselves may be playing a role. The basis for either of these explanations is not understood, nor is the lack of vibronic structure. Perhaps the broadness arises from the sensitivity of the proton normal modes to the large range of solvent environments.

The situation for quinoline and isoquinoline hydrogen bonded to strong hydrogen bonders such as HF2P or TFE is

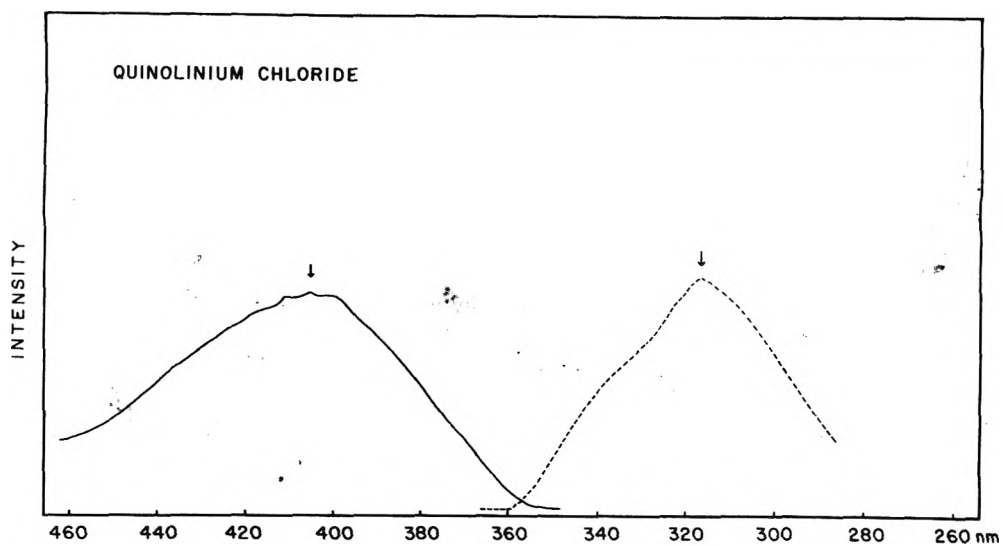


Figure 2. The fluorescence (solid line) and fluorescence excitation (dashes) spectra of a 10^{-3} M quinolinium chloride solution in 3MP at 77 K.

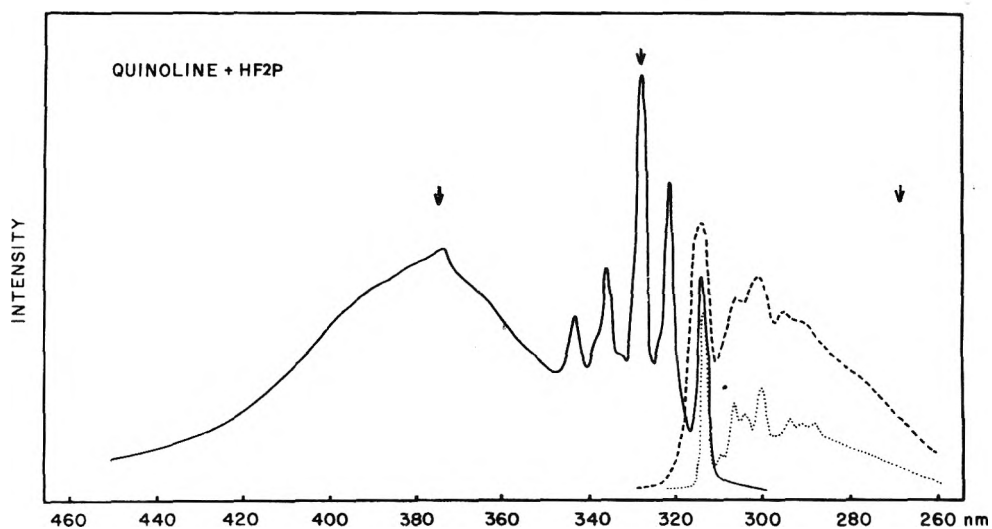


Figure 3. Quinoline fluorescence is shown by the solid line. The excitation spectrum of the structured fluorescence, which corresponds to the absorption spectrum, is shown by dots, while the excitation spectrum of the broad fluorescence is shown by dashes. Arrows denote either wavelengths monitored or excited.

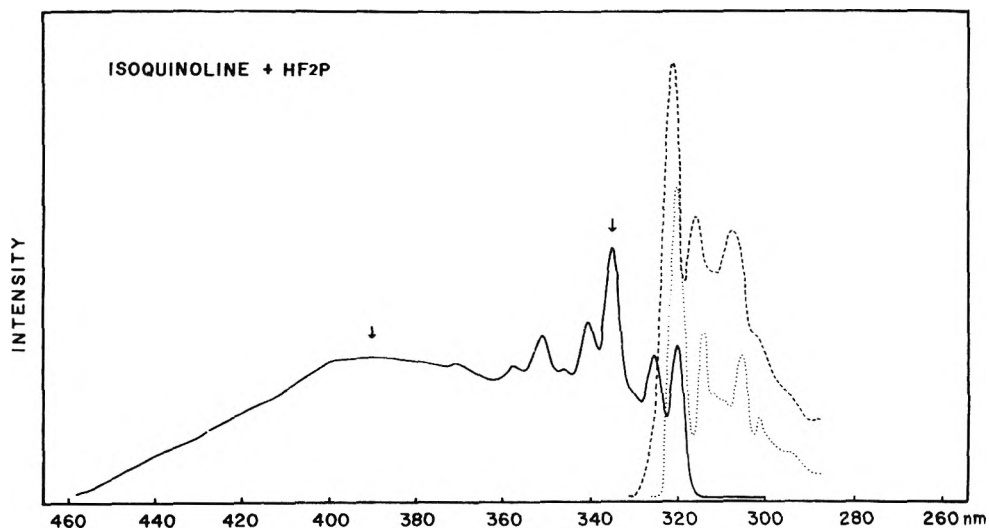


Figure 4. Isoquinoline fluorescence is shown by the solid line. The excitation spectrum of the structured fluorescence, which corresponds to the absorption spectrum, is shown by dots, while the excitation spectrum of the broad fluorescence is shown by dashes. Arrows denote either wavelengths monitored or excited.

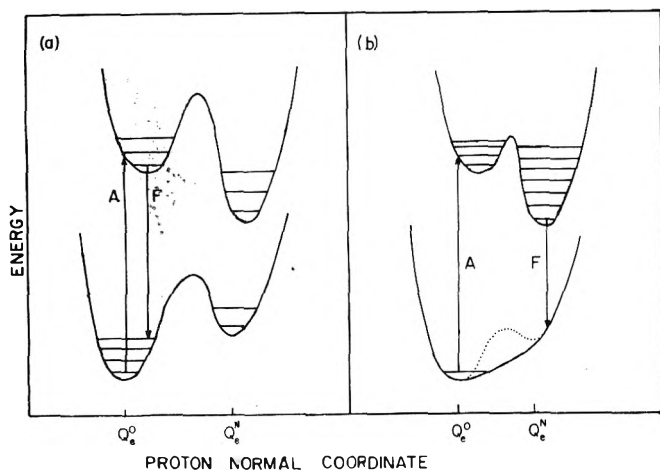


Figure 5. Possible potential energy surfaces for the ground and first excited electronic states plotted as a function of proton position between the oxygen of the alcohol and the nitrogen of the heterocycle. The minima of the oxygen and nitrogen wells are indicated by Q_e^O and Q_e^N . (a) Distant hydrogen bond gives rise to structured fluorescence. (b) Close hydrogen bond permits excited state proton tunneling, and broad cationlike fluorescence. Dotted curve represents possible low ground state barrier.

much more complicated than either of the situations so far described. The phosphorescence can be shown by the excitation spectrum to arise from non-hydrogen bonded molecules,² but the presence of both broad and sharp fluorescence requires a more elaborate explanation.

The excitation spectra of the structured fluorescence in the presence of HF2P or TFE are essentially the same as the absorption spectra for each molecule. The fluorescence itself is very similar to that induced by ethanol, although the position of the origin band in isoquinoline differs by as much as 1.0 nm from its value in the presence of ethanol. Since structured fluorescence is observed from the quinoline solution to which HF2P is added, hydrogen bonding must be responsible for this fluorescence just as it is for ethanol.

The appearance in these solutions of broad fluorescence, which resembles that of the protonated cation, is intriguing. One possibility is that some quinoline or isoquinoline is simply protonated in the ground state either by the fluoroalcohol or perhaps even by an acidic impurity. That this is not the case can be demonstrated both by the subtle ways in which this fluorescence differs from that of the true protonated cation, and by the fluorescence excitation spectrum. As previously noted, the excitation spectrum of the broad violet fluorescence resembles that of the structured fluorescence. It differs, however, in being broader, and having significant intensity on the red side of the origin band. In isoquinoline, the maximum of the 0,0 band in excitation is sensitive to the alcohol concentration, and actually lies from 1 to 3 nm below the 0,0 band in absorption (or structured fluorescence excitation).

This altered excitation spectrum clearly shows that the heterocycles are not protonated in the ground state, and that the broad and structured fluorescences originate from two different ensembles of molecules. The large Stokes shift or gap between the onset of the broad fluorescence and its excitation spectrum, and the lack of mirror symmetry of these spectral features imply that absorption and emission do not involve the same upper state potential surface. An attractive explanation of these observations can be had by postulating a double minimum potential for the proton in the excited state. See Figure 5. One potential minimum would be centered near the hydroxylic oxygen of the alcohol, and the second, lower

well, would be near the heterocyclic nitrogen. For any given molecule, the distance between these two wells, and the height and thickness of the barrier between them, is fixed by the rigid glass matrix.¹³

For both ensembles of fluorescing molecules, according to this scheme, absorption occurs from a hydrogen bonded ground state to a hydrogen bonded excited state, i.e., to the geometrical configuration in which the proton is located in the oxygen potential well. This would of course be required by the Franck-Condon principle for a conventional ground state hydrogen bond. In the case of "close" alcohol-heterocyclic complexes, the barrier is readily penetrated by the proton during the lifetime of the excited state, and a "semiprotonation" of the heterocycle takes place as the proton drops into the "nitrogen well". The broad, violet quinolinium- or isoquinolinium-like fluorescence then takes place as these molecules return to their ground state. In the ground state, the proton then relaxes back to its original position, closer to the oxygen atom. It is not necessary that the ground state possess a double minimum, but, it may, provided that the barrier is not too high to be readily penetrated.

The presence of the nearby hydroxylic oxygen and its effect on the shape of the "nitrogen well" region of the potential surface presumably accounts for the difference between the quinolinium-like and the true quinolinium fluorescence spectra. The greater breadth of the excitation spectrum of the broad quinolinium-like fluorescence relative to that of the structured naphthalene-like fluorescence may also be explained by the double minimum potential model. The vibrational levels within the oxygen potential well will be split by the presence of nearly degenerate levels in the nitrogen potential well leading to the observed broadening. This explanation also accounts for the subtle changes in the excitation spectra resulting from the use of different fluoroalcohols and concentrations. Another possible explanation of the broadening is the shortened lifetime of the upper state of the "oxygen well" resulting from proton tunneling. Additional measurements clearly need to be done to either confirm or deny these speculations.

The simultaneous appearance of the structured naphthalene-like fluorescence is also readily explained by this model. Alcohol-heterocycle complexes separated by large distances or possessing unfavorable geometries will have an upper state potential barrier between the oxygen and nitrogen potential wells which is too thick or high for the proton to penetrate during the lifetime of the excited states. For these systems the net result will be similar to that which occurs when the heterocycle is more weakly hydrogen bonded by ethanol. In this latter case, the barrier is presumably high because of the depth of the "oxygen-well" as evidenced by the low ethanol acidity and weaker hydrogen bonding capability in the ground state.

Previous work by three other research groups bears on the observations reported here. Ermolaev and Kotlyar¹⁴ report that the "violet-blue luminescence of the quinolinium ion" appears in petroleum ether solutions to which 0.5–2% of a variety of alcohols have been added. When these alcohols are added in lower concentration, 0.25–0.5%, or when isopropyl alcohol is used, only structured fluorescence is observed. They report similar effects when water or acetic acid are used. Unfortunately, they report no fluorescence or excitation spectra, and, we are unable to reproduce their results using ethanol in 3-methylpentane. We find that 1% ethanol added to a 10^{-4} M quinoline solution in 3-methylpentane produces a cracked glass, and only structured fluorescence. A similar solution

which had been saturated with water showed only phosphorescence. Perhaps the structure of the glass matrix permits closer approaches of the alcohol in petroleum ether than in 3MP. Whatever the source of the cationlike fluorescence in their experiments, Ermolaev and Kotlyar were the first to explain it as an excited state protonation. For some unknown reason, their observations appear to have been largely ignored, and few researchers today seem aware of their work.

O'Donnell and co-workers¹⁵ have studied the luminescence of a series of quinoline derivatives. Among them is 2-(2-hydroxyethyl)quinoline, which is a quinoline molecule to which an ethanol moiety has been attached in the β position, next to the nitrogen. This molecule shows broad cationlike fluorescence and a structured excitation spectrum in 3MP solvent "identical with that observed for quinoline".¹⁵ Since these authors were using fairly low resolution, and did not publish their excitation spectra, it is difficult to know whether their excitation spectra differed in the manner which we observed. They assign the luminescence to emission from the substituted quinolinium cation formed by intramolecular proton transfer from the hydroxy group during the lifetime of the excited state.

This result is particularly interesting since we fail to find any evidence that ethanol can effect an excited state protonation of quinoline in 3MP or in EPA (ether, pentane, ethyl alcohol). This suggests that the nitrogen-proton distance in the ground state hydrogen bond of 2-(2-hydroxyethyl)quinoline is much shorter than is the vast majority of ethanol-quinoline hydrogen bonds in the solutions we studied. This observation is consistent with our suggestion that excited state protonation occurs from closely hydrogen bonded HF2P-quinoline complexes. The very much lower acidity of the ethyl alcohol moiety on the substituted quinoline would require that the proton be much closer to the nitrogen than is the case for HF2P. On the other hand, it may be that the six-membered ring resulting from the intramolecular hydrogen bond of the substituted quinoline simply places the ethanolic proton near the plane of the quinoline ring where the nitrogen lone-pair density is the greatest.

Incidentally, O'Donnell and his co-workers erroneously assign the observed broad luminescence from both the quinolinium cation and from the substituted quinoline as phosphorescence. It is well known⁶ that the quinolinium luminescence is fluorescence. The long lifetime of 50 ms measured by these workers is probably a measuring artifact, as we find the broad luminescence lifetimes to be considerably less than 1 ms.

The general appearance of the broad fluorescence and its energy is also very reminiscent of excimer fluorescence. In fact, excimer fluorescence has recently been reported for quinoline at 160 K and for isoquinoline at 241 K in ethanol by Blaunstein and Gant.¹⁶ The excimer fluorescence maxima which they observe is near 400 nm in both cases, while we observe the maximum to be at 348 nm for quinoline and 390 nm for isoquinoline. These authors made their observations in fluid media at concentrations between 10^{-1} and 10^{-3} M. We observe no evidence of broad emission in a rigid EPA glass at 77 K, which has a high ethanol concentration, even at 10^{-3} M. Since our solutions were 10 to 100 times less concentrated in rigid 3MP at 77 K, it is difficult to see how the addition of HF2P under these conditions could produce excimers.

V. Conclusions

Both structured naphthalene-like fluorescence and broad structureless fluorescence resembling the protonated cations of quinoline and isoquinoline have been observed in 3MP glasses when hexafluoro-2-propanol or trifluoroethanol are used as hydrogen bonders. These observations can be explained by assuming a double minimum potential for the proton in the excited state. The proton in *close* alcohol-heterocycle complexes may undergo tunneling of the barrier between the oxygen and nitrogen potential wells. The broad fluorescence arises from these "semiprotonated" excited state species. The barrier between the wells for *distant* alcohol-heterocycle complexes is too large to be penetrated during the life of the excited state, and only structured naphthalene-like fluorescence is observed from such complexes. The glass matrix structure is important in determining the separation of the two potential wells and the shape of the barrier.

Acknowledgments. This research was made possible by funds from the Camille and Henry Dreyfus Foundation through their awarding of a grant to William R. Moomaw as a Dreyfus Teacher-Scholar. Our thinking about the role of the solvent matrix in shaping the upper state potential was greatly stimulated by conversations with Dr. H. B. Dellinger and Professor M. Kasha. We also gratefully acknowledge several helpful discussions with Professor E. C. Lim.

References and Notes

- (1) Preliminary results were presented at the 30th Symposium on Molecular Structure and Spectroscopy as paper RH8, Columbus, Ohio, June 19, 1975.
- (2) M. F. Anton and W. R. Moomaw, *J. Chem. Phys.*, in press.
- (3) C. A. Taylor, M. A. El-Bayoumi, and M. Kasha, *Proc. Natl. Acad. Sci. U.S.A.*, **63**, 253 (1969).
- (4) G. J. Brealey and M. Kasha, *J. Am. Chem. Soc.*, **77**, 4462 (1955).
- (5) E. C. Murray and R. N. Keller, *J. Org. Chem.*, **34**, 2234 (1969).
- (6) H. Zimmermann and N. Joop, *Z. Elektrochem.*, **65**, 61 (1961).
- (7) N. Mataga, Y. Kaifu, and M. Koizumi, *Bull. Chem. Soc. Jpn.*, **29**, 373 (1956).
- (8) M. A. El-Sayed and M. Kasha, *Spectrochim. Acta*, **15**, 758 (1959).
- (9) E. C. Lim and J. M. H. Yu, *J. Chem. Phys.*, **47**, 3270 (1967).
- (10) Y. H. Li and E. C. Lim, *Chem. Phys. Lett.*, **9**, 279 (1971).
- (11) G. Fisher, *J. Mol. Spectrosc.*, **49**, 201 (1974).
- (12) G. Fisher and R. Naaman, private communication.
- (13) H. B. Dellinger, Ph.D. Thesis, Florida State University, 1976.
- (14) V. L. Ermolaev and I. P. Kotlyar, *Opt. Spectrosc.*, **9**, 183 (1960).
- (15) C. M. O'Donnell, G. A. Knessel, T. S. Spencer, and F. R. Stermitz, *J. Phys. Chem.*, **74**, 3555 (1970).
- (16) R. P. Blaunstein and K. S. Gant, *Photochem. Photobiol.*, **18**, 347 (1973).

Discussion

M. A. EL-SAYED. Have you used deuterated alcohol?

W. R. MOOMAW. No, we have not, but we have plans to do so. The deuterated alcohols coupled with temperature dependent studies should tell us a great deal about the tunneling process.

J. W. LONGWORTH. Have you used a more acidic fluoroalcohol, in particular, I had in mind $\text{CF}_3\text{C}(\text{OH})_2\text{CF}_3$, hexafluoroacetone sesquihydrate?

W. R. MOOMAW. No, I have only used the less acidic trifluoroethanol which has a $\text{p}K_a$ of about 12 compared to a $\text{p}K_a$ of 17 for ethanol and 9 for hexafluoro-2-propanol.

Laser Intensity Measurements by Chemical Actinometry. A Photooxygenation Actinometer

J. N. Demas,* R. P. McBride, and E. W. Harris

Department of Chemistry, University of Virginia, Charlottesville, Virginia 22901 (Received January 26, 1976; Revised Manuscript Received June 25, 1976)

Publication costs assisted by the Petroleum Research Fund

A new chemical actinometer especially designed for intensity measurements on high power lasers in the uv to green region is described. The actinometer consists of a closed O₂-filled system containing methanolic tris(2,2'-bipyridine)ruthenium(II) chloride ([Ru(bpy)₃]Cl₂) and tetramethylethylene (TME). The highly colored Ru(bpy)₃²⁺ absorbs the laser radiation to form a long-lived charge-transfer excited state which is efficiently quenched by dissolved O₂ to form singlet oxygen (¹O₂). The ¹O₂ reacts efficiently with TME to give a nonvolatile hydroperoxide. The laser intensity is determined from the rate of O₂ consumption monitored on a gas buret. The system is easy to use, has a quantum flat response over the 280–560-nm region, and is particularly suited for the ionized Ar laser lines. Detailed characterization and use of the system are presented.

Introduction

Intensities of high power lasers are commonly measured with calibrated thermal detectors and silicon photodiodes.^{1–8} This procedure has a number of difficulties, however. Although home-made power meters of great accuracy can be constructed, they are expensive and difficult to use. Consequently, most workers use commercial meters with factory calibrations or one of the few commercial ones having their own internal heaters for calibration and restandardization. Clearly, most results are subject to the manufacturer's competence, but drift or detector degradation can destroy the best original calibration. Even most self-calibrating thermal detectors are subject to undetectable drift from target degradation.

Further, most detectors have small apertures and are unusable with the large beam of many photochemical and spectroscopy experiments. Scientech makes 1- and 4-in. diameter units, but the 4-in. unit in particular is quite expensive. Most manufacturers will recalibrate their power meters, but this is unsatisfactory when time, cost, and the need for frequent standardization are considerations.

Chemical actinometry overcomes many of these problems and supplies a complementary tool for power measurements. An actinometer is a chemical system which undergoes an irreversible photochemical reaction. Once the efficiency of the photoreaction is calibrated using an absolute method, the actinometer can be used as a secondary standard for measuring absolute light intensities from the rate of the light-induced reaction.

Actinometers can have the following advantages:

(a) They are inexpensive and once calibrated by an absolute method can be used for absolute calibration of all types of thermal or photoelectric detector. They are the only power meters which can be mailed on a postcard.

(b) Since the chemical reaction is always reproducible, actinometers are ideal for monitoring and correcting long term drift in other detectors.

(c) Results referenced either directly or indirectly to the actinometer can always be corrected if the absolute yield for the actinometer is ever revised, while results referenced to an improperly calibrated meter would rarely be recoverable.

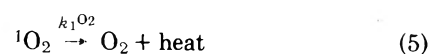
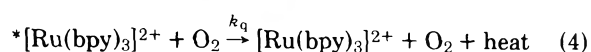
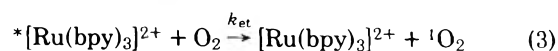
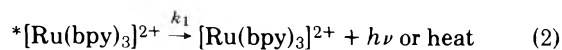
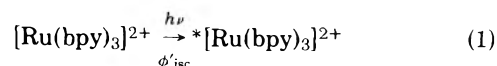
(d) Some actinometers will detect the quantum content of the beam, independent of its spectral distribution (quantum flat). To obtain the quantum content of a multiline laser with a thermal detector, the laser's spectral distribution must be accurately known and this is a frequently difficult task. Further, thermal measurements are notoriously sensitive to errors from infrared, while actinometers can be tailored to detect some wavelengths and discriminate against others, including infrared.

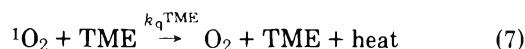
(e) Actinometers can be made easily in virtually any physical size and shape, including nearly completely surrounding a sample to intercept almost 4π steradians of radiation.

While no previously existing actinometer is completely satisfactory for high power lasers,⁹ we report a new singlet-oxygen actinometer which overcomes most of the previous shortcomings, gives exceedingly good reproducibility, uses commercially available chemicals, is easy to use, and requires no sophisticated equipment. It is also usable to wavelengths less than or equal to the 514.5-nm Ar line, to CW powers of ≥1.5 W, and is almost certainly quantum flat in response over the 280–560-nm region.

Actinometer

The basic system we have adopted is the tris(2,2'-bipyridine)ruthenium(II) chloride ([Ru(bpy)₃]Cl₂) sensitized photooxidation of tetramethylethylene (TME) in methanol. The physical and chemical processes are





where ${}^*\text{Ru}(\text{bpy})_3^{2+}$ is the complex in its long-lived excited state, ϕ'_{isc} is the efficiency of production of this state following optical excitation, O_2 is ground state oxygen, and ${}^1\text{O}_2$ is metastable excited singlet O_2 . The rate constant for each process is indicated over the arrow. Deactivation of ${}^*\text{Ru}(\text{bpy})_3^{2+}$ by TME has been omitted since it is an unimportant process.^{10,11}

This kinetic scheme gives the following instantaneous observed yield, ϕ_{obsd} , for disappearance of O_2 (mol of O_2 consumed/einstein of photons absorbed; 1 einstein = 6.023×10^{23} photons):

$$\phi_{\text{obsd}} = \phi_0 \left\{ \frac{[\text{TME}]}{\beta + [\text{TME}]} \right\} \left\{ \frac{K_{\text{sv}}[\text{O}_2]}{1 + K_{\text{sv}}[\text{O}_2]} \right\} \quad (8)$$

$$\phi_0 = \phi'_{\text{isc}} \phi_{\text{rx}} \phi_{\text{et}}$$

$$\phi_{\text{rx}} = k_{\text{rx}} / (k_{\text{rx}} + k_q^{\text{TME}}) \quad \phi_{\text{et}} = k_{\text{et}} / (k_{\text{et}} + k_q)$$

$$\beta = k_1 \text{O}_2 / k_{\text{rx}} \quad K_{\text{sv}} = (k_{\text{et}} + k_q) / k_1$$

where ϕ_{rx} and ϕ_{et} are the probabilities of reaction of ${}^1\text{O}_2$ with TME at infinite TME concentration and of energy transfer from ${}^*\text{Ru}(\text{bpy})_3^{2+}$ to O_2 at infinite O_2 concentration, respectively. $[\text{O}_2]$ and $[\text{TME}]$ denote molar concentrations of O_2 and TME, respectively. In practice ϕ_{obsd} can not be calculated directly from eq 8, because both $[\text{TME}]$ and $[\text{O}_2]$ change during photolysis. The procedure for obtaining ϕ_0 from measured quantities will be described in the Experimental Section.

$\text{Ru}(\text{bpy})_3^{2+}$ luminesces strongly in methanol, and K_{sv} is easily obtained from the variation of emission intensity, θ , with $[\text{O}_2]$ in the absence of TME from

$$(\theta_0/\theta - 1) = K_{\text{sv}}[\text{O}_2] \quad (9)$$

where the subscript 0 denotes the value in the absence of O_2 .¹²

β , while not readily obtained by our experiments, has been measured by the variation of ϕ_{obsd} with $[\text{TME}]$ at very low TME concentrations.¹³ In all calculations, we use Foote's value of 0.0027 M.¹³

The actinometer consists of a system with a gas buret filled with pure O_2 connected to the photolysis cell (Figure 1). A methanolic solution of $[\text{Ru}(\text{bpy})_3]^{2+}$ and TME forms the actinometer. The strongly orange-colored $[\text{Ru}(\text{bpy})_3]^{2+}$ absorbs the radiation, and the excited complex efficiently generates ${}^1\text{O}_2$ by collisional deactivation with O_2 . ${}^1\text{O}_2$ is then efficiently consumed by TME to yield a nonvolatile hydroperoxide.¹³ After irradiation and reequilibration, the degree of reaction (O_2 uptake) is read directly from the gas buret.

The quantum dose absorbed by the actinometer, I_{abs} (einstein), is given by

$$I_{\text{abs}} = n_{\text{O}_2} / \phi'_{\text{obsd}} = P_{\text{atm}} V_{\text{O}_2}(\infty) / RT \phi'_{\text{obsd}} \quad (10)$$

where n_{O_2} is the number of moles of O_2 absorbed, $V_{\text{O}_2}(\infty)$ is the total volume of pure O_2 consumed, P_{atm} is the atmospheric pressure, R is the gas constant, T (K) is the temperature of the apparatus, and ϕ'_{obsd} is the effective quantum yield for the reaction over a finite irradiation period (moles consumed/einstein). I_{abs} differs from the product of irradiation time and free air flux, I_0 (einstein)/s, because of the transmittance, T_w , of each actinometer cell window (reflection losses) and because a fraction of the beam, T_s , passes through the sample on a single pass without being absorbed. I_0 is given in terms of observables by

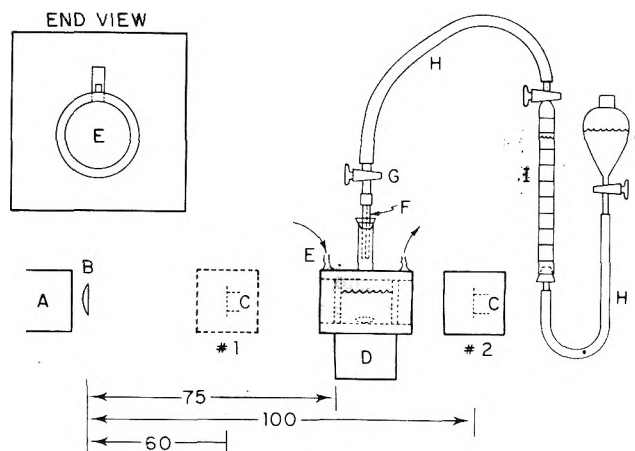


Figure 1. Photolysis apparatus: (A) Coherent Radiation Laboratories Model CR-5 laser; (B) 8-cm focal length Pyrex lens; (C) power meter detector head; (D) magnetic stirrer; (E) Pyrex photolysis cell (7.6 cm diameter windows and 5 cm pathlength) with Teflon stirring bar. End view shown in insert. The filling stem must be big enough to accept the stirring bar. Constant temperature water (0.1 °C) is circulated through the jacket; (F) capillary tube 8 cm \times 1 mm i.d. inserted in a rubber stopper; (G) Teflon stopcock; (H) Tygon tubing; (I) 100-ml inverted liquid buret; (J) 250-ml separatory funnel used as leveling bulb. The leveling fluid was ethylene glycol. All distances (cm) are approximate.

$$I_0 = \frac{I_{\text{abs}}(1 - rT_s)}{t_{\text{irr}}T_w(1 - T_s)} \quad r = 1 - T_w \quad (11)$$

where t_{irr} is the irradiation time, and r is the effective reflectance of the glass-air-solution interfaces to the beam.

To use the actinometer for measuring I_0 's, one must know T_w , T_s , and ϕ'_{obsd} . Since T_w and T_s are readily measured or calculated from Fresnel's laws, calibration of the actinometer consists of obtaining ϕ'_{obsd} by an absolute method. Since, as we shall show, ϕ'_{obsd} is easily calculated from observables and ϕ_0 , calibration consists of determining ϕ_0 .

Experimental Section

Materials. $[\text{Ru}(\text{bpy})_3]\text{Cl}_2 \cdot 6\text{H}_2\text{O}$ was obtained from G. Frederick Smith Chemical Co. and used without purification or after a single recrystallization from water. TME was either from Aldrich (99+% Gold Label) or an old bottle from Chemical Supply Co. (99%); both dissolved completely in methanol to give a clear solution and were used without further purification. Methanol was AR grade and was used without purification.

Spectrofluorimeter. The spectrofluorimeter described elsewhere^{10,14} was used for all measurements.

Absolute Power Meter. Absolute intensities were measured with a Jennings-West absolute bolometer.⁴ The ~ 38 -mm diameter solid aluminum target was equipped with a 60- Ω Manganin calibration heater and a four-junction copper-constantan thermopile. The target was blackened with Krylon 1602 flat black spray paint by applying several light coats. The thermopile readout was a Keithley Model 155 microvolt null detector.

Photolysis Apparatus. The complete photolysis setup and cell are shown in Figure 1. Such a cell is readily fabricated by a competent glass blower. Alternatively, an unjacketed cell could be mounted in a thermostated block. The stopcock and capillary tube minimized diffusion of methanol into the O_2 reservoir. All gas interconnections and stopcocks were lubricated with silicone vacuum grease to eliminate leakage.

The defocussing lens reduced power density on the actinometer and minimized reciprocity failure due to local hole

burning in the O₂ concentration.⁹

The use of solvent free O₂ in the gas line and the stopcock and capillary of Figure 1 is important. Considerable data were originally collected using methanol saturated O₂ in the cell and gas line, a very reproducible system. These results were, however, ~10% too low because of adsorption of methanol on the Tygon tubing. To show yields were independent of the gas composition, several methanol saturated O₂ runs were made with the Tygon replaced by glass tubing with only very short interconnections being made with Tygon; good agreement between the two procedures was then obtained (vide infra).

Procedures and Calculations

Determination of K_{sv}. Techniques described elsewhere were used.¹¹ Saturation O₂ concentrations, [O₂]_{sat}, were calculated from an Ostwald coefficient of 0.2471 at 21 °C.¹⁵ [O₂]_{sat} under our conditions is given by

$$[\text{O}_2]_{\text{sat}} = (0.010\ 22\ \text{M})P_{\text{O}_2}/760$$

$$P_{\text{O}_2} = P_{\text{atm}} - P_{\text{CH}_3\text{OH}} = P_{\text{atm}} - \exp[20.267 - 4609.0/T] \quad (12)$$

P_{O₂} is the partial pressure of O₂, P_{atm} is atmosphere pressure, and P_{CH₃OH} is the vapor pressure of methanol¹⁶ in the photolysis cell; all pressures are in Torr.

Power Meter Calibration. The electrical sensitivity, S_{elec} (microvolt output per watt of electrical heater power), determined by passing known currents through the Manganin heater, was slightly power dependent but stable during ~1 year, and all calibrations were combined. The function

$$S_{\text{elec}} = (286\ \mu\text{V}/\text{W}) - (0.012\ \text{W}^{-1})E \quad (13)$$

where E is the thermopile output voltage gave a good fit with an experimental scatter of ~1–2%. Optical sensitivity was ~1% less for a 25-mm diameter beam than for a 10 mm one.

The reflectance of the target's flat black paint, R', was determined by comparison with a freshly smoked magnesium oxide surface with the same orientation. MgO is an almost perfect diffuse reflector,¹⁷ and we have used unity for its reflectance in our calculations. Scattered radiation was monitored with a UDT PIN-10DP silicon photocell and a Keithley Model 160 microvoltmeter used in the current mode. The photocell was operated at ≤3 μA to ensure linear operation.

Absolute laser beam intensities were given by

$$I_0 = (8.359 \times 10^{-9})\lambda E/(1 - R')S_{\text{elec}} \quad (14)$$

where λ is the laser beam wavelength (nm).

Evaluation of r, T_w, and T_s. The reflection coefficient of the cell windows was obtained from the apparent solvent filled cell transmission. With the power meter at position no. 2 (Figure 1), we measured the bolometer output with the cell in place filled to its working volume with pure methanol, E_f, and with the cell removed, E_i. The apparent transmission is (E_f/E_i)_{solvent}.

The dose absorbed by the actinometer was obtained from the apparent actinometer transmission, (E_f/E_i)_{act}, which was measured similarly by placing the power meter head either before the photolysis cell (position no. 1) or following it (position no. 2) with the cell filled with actinometer solution. The laser beam in both cases underfilled the sensor surface.

By Fresnel's laws the transmittances of the entering and exiting windows at normal incidence are identical, and the transmittance per window, T_w, is

$$T_w = [(E_f/E_i)_{\text{solvent}}(1 - r^2)]^{1/2} \quad (15)$$

$$r \approx 1 - [(E_f/E_i)_{\text{solvent}}]^{1/2}$$

It is assumed that the combined air-glass and glass-methanol reflectances of a single window act like a single interface with a composite reflectance r, that there is no solvent or window absorption, and that all of the infinite interreflections exiting from the rear face strike the detector. Beam divergence makes the last assumption slightly incorrect; however, simpler equations result and the rapid attenuation of interreflected light makes the errors negligible (ca. ≤0.1%). The slight beam divergence should also minimize interference effects. T_s is given by

$$T_s \approx (E_f/E_i)_{\text{act}}/T_w^2 \quad (16)$$

The same assumptions are made in the derivation of T_s as for T_w.

Determination of φ₀. φ₀ can then be calculated from

$$\phi_0 = \phi'_{\text{obsd}}/\bar{K}_{\text{sv}}\bar{\beta}$$

$$\bar{K}_{\text{sv}} = \left\{ \frac{K_{\text{sv}}[\text{O}_2]}{1 + K_{\text{sv}}[\text{O}_2]} \right\} \quad \bar{\beta} = \left\{ \frac{[\text{TME}]}{\beta + [\text{TME}]} \right\} \quad (17)$$

where the bar over each term in braces indicates the function's average value during photolysis. For constant light intensity, [TME] decreases linearly with time, and β becomes

$$\bar{\beta} = \frac{[\text{TME}]}{\beta + [\text{TME}]} \quad (18a)$$

$$[\text{TME}]_f = [\text{TME}]_i - P_{\text{atm}}V_{\text{O}_2}(\infty)/RTV_{\text{irr}} \quad (18b)$$

$$\overline{[\text{TME}]} = ([\text{TME}]_i + [\text{TME}]_f)/2 \quad (18c)$$

where the subscripts i and f denote the initial and final concentrations, respectively, and V_{irr} is the volume of solution irradiated. Equation 18 is only approximate, but even for the extreme case of [TME]_f = [TME]_i/2 = 0.05 M, the difference between eq 18 and the exact solution is only ~0.2%.

The \bar{K}_{sv} correction arises because even though the solution is always under the same O₂ partial pressure, O₂ does not redissolve as rapidly as it is consumed. Thus, the average value of the \bar{K}_{sv} term will be smaller than if it were calculated using [O₂]_{sat}. Thus, [O₂] and φ'_{obsd} will decrease with time during a continuous irradiation. This error source, denoted the oxygen-debt error, varies with the rate and length of photolysis. Fortunately, because K_{sv} is large, it is usually simple to keep the variation of \bar{K}_{sv} within 1–2% of the value calculated using [O₂]_{sat}. \bar{K}_{sv} is given by

$$\bar{K}_{\text{sv}} = \frac{1}{t_{\text{irr}}} \int_0^{t_{\text{irr}}} \frac{K_{\text{sv}}[\text{O}_2]_t dt}{1 + K_{\text{sv}}[\text{O}_2]_t} \approx \frac{K_{\text{sv}}\overline{[\text{O}_2]}}{1 + K_{\text{sv}}\overline{[\text{O}_2]}} \quad (19)$$

where [O₂]_t is the time dependent O₂ concentration and $\overline{[\text{O}_2]}$ the average concentration during photolysis. The approximate form is typically accurate to better than 0.2%. For a photolysis broken up into several intervals with partial equilibration between intervals, t_{irr} is the total irradiation time and [O₂]_t becomes a discontinuous function. As will be shown, partial equilibration minimizes the oxygen-debt correction.

$\overline{[\text{O}_2]}$ is evaluated from the time dependence of the O₂ volumes consumed during irradiation and the total O₂ consumed. For simplicity data are taken at even time intervals. If the total irradiation is broken into J subirradiations of equal period with partial equilibration between intervals, [O₂] in eq 19 can be estimated from

$$[\text{O}_2] = [\text{O}_2]_{\text{sat}} + (P_{\text{atm}}/RTV_{\text{irr}}) \times \left\{ \frac{\sum_{k=1}^J \sum_{i=0}^N k V_{\text{O}_2}(t_i)}{(N+1)J} - \frac{V_{\text{O}_2}(\infty)}{2} \right\} \quad (20)$$

where $kV_{\text{O}_2}(t_i)$ is the total volume consumed from the beginning of the experiment until t_i of the k th subirradiation. $kV(t_i)$ is monitored at $N+1$ readings taken at even times for each subirradiation, including at the beginning ($t_0 = 0$) and the terminus ($t_N = t_{\text{irr}}/J$). The amount of O_2 reacted is assumed linear with photolysis time, an excellent assumption under our experimental conditions. For $J = 1$ eq 20 reduces to the case of a single irradiation period.

Procedure for Determining ϕ'_{obsd} . The experimental procedure was as follows: 150 ml of stock TME solution (~ 0.12 M) and the solid weighed $[\text{Ru}(\text{bpy})_3]\text{Cl}_2 \cdot 6\text{H}_2\text{O}$ were added to the cell. This solution was oxygenated by bubbling through ~ 0.5 – 1 l of solvent-saturated O_2 (two methanol bubblers) while magnetically stirring; the cell was immediately tightly stoppered.

After oxygenation of the actinometer solution, the bubblers were removed, and the gas buret filled and flushed several times with pure solvent free O_2 ; the O_2 connection was made at the cell side of the capillary. The buret was refilled with O_2 with the leveling-bulb level set near the bottom of the buret, and stopcock G was closed. The capillary and stopper were then quickly inserted into the photolysis cell. Stopcock G was opened to equalize pressure, the fluid level within the buret and leveling bulb was equalized, and the stopcock closed. A buret reading was then taken. The opening, leveling, closing, and reading procedure was repeated at 5-min intervals until the gas volume remained constant (≤ 0.05 ml) for at least two readings. Unless room temperature underwent large fluctuations, no more than 30 min was required.

Immediately before beginning irradiation, a bolometer reading was taken at position no. 1. The bolometer was then placed at position no. 2 to measure transmitted radiation, and the photolysis begun. Uptake was monitored at 1- or 2-min intervals during the photolysis by leveling the buret. Immediately after photolysis, the bolometer reading was repeated at position no. 1. I_{abs} (eq 11) was calculated using the readings at the beginning and at the end of the photolysis and the average value was used to calculate ϕ'_{obsd} in eq 11; the agreement between the initial and final I_{abs} was usually ≤ 1 – 2% .

Gas uptake was then monitored until equilibrium. As uptake slowed, stopcock G was closed between readings to minimize diffusion of methanol into the gas line. No more than 30 min was usually required for equilibration. $V_{\text{O}_2}(\infty)$ is then just the difference between the initial and final equilibrations.

The magnetic stirrer was left running at all times. The vortex did not dip into the laser beam. Several consecutive runs were usually made rather than several independent experiments, because the initial reading for the next irradiation is just the final reading for the previous run.

Results

The Stern–Volmer plot of $(\theta_0/\theta - 1)$ vs. $[\text{O}_2]$ was linear with $K_{\text{sv}} = 1400 \text{ M}^{-1}$, the value used in all calculations. This value is in good agreement with a previously obtained value.¹⁰

Using normal laser incidence, paint reflectances were measured for 10, 40, and 60° from normal. R' varied from 4.16

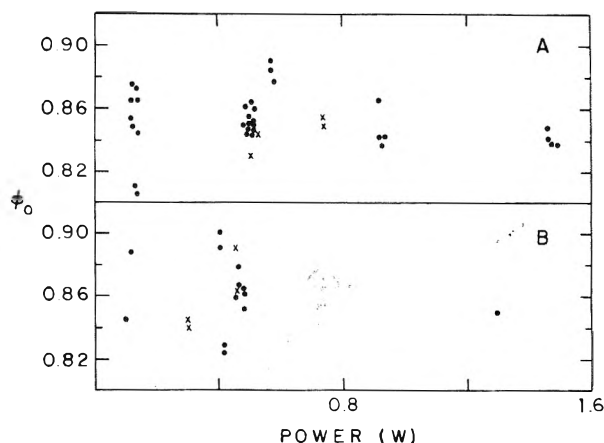


Figure 2. Variation of ϕ_0 with wavelength and power level: (A) 488 nm, ●'s used pure O_2 in the buret and the X's used methanol saturated O_2 ; (B) 457.9 nm (X) and 514.4 nm (●). Some points are displaced slightly on the power axis to improve viewing.

to 4.83% at 457.9 nm, from 4.16 to 4.64% at 488.0 nm, and from 3.81 to 5.09% at 514.5 nm. The average R' for each wavelength was within 0.03% of the average for all angles and wavelengths. The average R' of 4.3% was used in all calculations and is estimated accurate to $\pm 0.5\%$. This value is in good agreement with the 4% values reported for a similar flat-black spray paint⁴ and for benzene soot.¹⁸ Specular reflectance is ignored for two reasons: visual inspection of the scattered radiation showed no bright spot, and Ramsey has shown Krylon 1602 has $< 0.1\%$ specular reflectance in the 400–500-nm region.¹⁹

As a check for gross errors in our power meter, it was compared with a Coherent Radiation Laboratories Model 210 thermal power meter. Agreement was within experimental error (2–3%).

In the determination of the window reflectances by eq 15, $(E_t/E_i)_{\text{solvent}}$ was reproducible to ± 0.003 . r was 0.047 at 514 nm, 0.051 at 488 nm, and 0.054 at 457.9 nm.

ϕ'_{obsd} 's were calculated from eq 10 and 11 where I_0 was obtained from eq 14 and T_s from eq 16. ϕ'_{obsd} 's were then corrected to ϕ_0 's using eq 17 where $\bar{\beta}$ was obtained from eq 18 and \bar{K}_{sv} from eq 19 and 20.

We stress that the O_2 debt error was reproducible (0.1–0.5%) for a given set of operating conditions and can always be kept quite small (< 1 – 2%). For example, with 0.5 W at 488 nm and a single 10-min continuous irradiation, $V_{\text{O}_2}(\infty) = 24$ ml and $\{K_{\text{sv}}[\text{O}_2]_{\text{sat}}/[1 + K_{\text{sv}}[\text{O}_2]_{\text{sat}}]\}/\bar{K}_{\text{sv}}$ equals 1.011. With 1 W for 5 min, $V_{\text{O}_2}(\infty) = \sim 24$ ml and the ratio was 1.017.

For 1.5 W for 3 min with $V_{\text{O}_2}(\infty) = 19$ ml, the ratio was 1.019. To indicate how the ratio can be reduced, we repeated the 1.5-W irradiation using three 1-min subirradiations with partial equilibration between each (~ 5 – 10 min); the ratio was reduced to 1.007. Thus, even for these high power levels, the O_2 debt error can be reduced to a quite acceptable level and reliably corrected for.

Figure 2 summarizes numerous results with the 457.9-, 488.0-, and 514.5-nm Ar laser lines for powers ranging from 0.1 to 1.5 W. The average values of ϕ_0 are 0.851 ± 0.017 at 488 nm, 0.862 ± 0.023 at 514.4 nm, and 0.860 ± 0.023 at 457.9 nm. The average for all data is 0.855. Indicated errors are standard deviations. The values using methanol saturated O_2 were omitted in the averages because of their probable errors; the good agreement between the pure and solvent saturated O_2 runs, however, shows there was negligible loss of methanol vapor in the latter runs. Results were indistinguishable for two different samples of TME as well as for unpurified or recryst-

tallized $[\text{Ru}(\text{bpy})_3]\text{Cl}_2$; all data are combined. We also have one result using a 1-MW, 15-ns duration N_2 laser run at 15 Hz; the yield of 1.0 ($\pm 20\%$) was rather uncertain because of corrections for window absorption and the beams ir content. As can be seen there is no systematic variation of ϕ_0 with either wavelength or power levels; the 0.1-W values are somewhat less accurate because of bolometer noise.

The invariance of yield with wavelength is just as predicted. $[\text{Ru}(\text{bpy})_3]^{2+}$ in methanol has a wavelength invariant ($< 2\%$) ϕ'_{isc} over the 280–560-nm range.²⁰ The observed wavelength independence of ϕ_0 is merely a manifestation of this fact.

In addition to the insensitivity of the yield to the source of TME or $[\text{Ru}(\text{bpy})_3]^{2+}$, it is also noteworthy that a number of sequential runs made on a sample give the same value of ϕ_0 . We have made up to seven runs on a single sample, including letting it sit overnight between some runs; these results are indistinguishable from fresh samples.

We have not made an exhaustive temperature dependence study. Using a precise but inaccurate procedure, we have found no variation ($\pm 2\%$) or trend in ϕ_0 over the 19–24 °C range.

Finally, the measurements presented here were made by two nonoverlapping workers, and there were no discernible differences between their results. Thus, we believe that there are no hidden artifacts in the procedure.

Discussion

Errors. We estimate the accuracy of ϕ_0 and thus the actinometer to be better than 5%. Of course for monitoring only the stability of power meters, the accuracy should be better than 1–2%. The bolometer probably contributes the largest error due to the potential inequivalence of electrical and optical heating, variation of sensitivity across the bolometer face, and uncertainty in S_{elec} ; 2–3% uncertainty for these effects including the 0.5–1% uncertainty for the paint reflectance seems reasonable. Another 1–2% error arising from the window reflection correction seems realistic.

Temperature, pressure, and volumetric errors as well as vapor pressure corrections, and microvoltmeter reading errors and noise, and laser intensity fluctuations are insignificant or small and random. Oxygen-debt corrections are reproducible and should be an insignificant error source. All random errors are reduced to insignificance by the large number of readings. Microvolt meter accuracy does not enter into our considerations because S_{elec} was obtained using the same microvoltmeter.

The uncertainty of β is probably no greater than $\pm 20\%$ which produces negligible errors in ϕ_0 . Even if larger errors in β exist, however, the effect on the use of the actinometer would be insignificant as long as our recommended [TME] is used and all calculations used our assumed β .

One final point bears comment, the possible variation of ϕ_0 with the purity of the commercially available chemicals. We have carefully selected the current system to minimize the influence of any conceivable impurities, and we feel that impurity problems will not produce significant variation in the yield.

The TME from Aldrich is 99+% (verified by ir and gas chromatography). Any conceivable impurities are not likely to be good $^1\text{O}_2$ or $^*[\text{Ru}(\text{bpy})_3]^{2+}$ quenchers or better $^1\text{O}_2$ scavengers than TME. The absence of a detectable variation in ϕ_0 with either source of TME or storage for over 2 years further indicates impurity problems associated with the TME are insignificant.

The $[\text{Ru}(\text{bpy})_3]\text{Cl}_2$ from G. Frederick Smith likewise ap-

pears to be of exceptionally high quality. We have used material from this source over a period of ~ 7 years and find it to be spectroscopically uniform and identical with material prepared by us using several different methods. We attribute this high purity to its ease of recrystallization and to the cleanliness of the reactions yielding $[\text{Ru}(\text{bpy})_3]^{2+}$; it is difficult not to get this product even if one wishes to stop at an intermediate. Thus significant amounts of absorbing, or quenching, impurities are unlikely. The absence of impurity effects is supported by the invariance of ϕ_0 for two different batches of $[\text{Ru}(\text{bpy})_3]\text{Cl}_2$ as well as with one which had been recrystallized. A procedure for evaluating the purity of $[\text{Ru}(\text{bpy})_3]^{2+}$ and methods for purifying it if necessary are given in the supplementary material. (See paragraph at end of text regarding supplementary material.)

Summary. Our data show the $[\text{Ru}(\text{bpy})_3]^{2+}$ -TME system to be a precise, accurate, and quantum flat new actinometer for use with high power CW lasers ($\sim 330 \leq \lambda \leq \sim 520$). With the modifications outlined in the supplementary material, it should be quite simple and rapid to use. Further, different sensitizers should permit operation to beyond 700 nm.

Our preliminary N_2 -laser results and calculations suggest that the actinometer will be usable with high power pulsed N_2 lasers as long as the beam is spread out and the sensitizer's optical density is not so high as to concentrate the quantum dose into a small volume. Flash lamp pumped dye lasers can deliver much higher dose per flash, however, and the local O_2 concentration can be greatly depleted which causes O_2 debt errors regardless of the vigor of mixing. A detailed discussion of actinometer errors under pulsed conditions is given in ref 9.

Acknowledgments. We thank F. S. Richardson, H. Dewey, and R. A. Keller for the use of their lasers, R. B. Martin for the use of his spectrophotometer, F. A. Carey for use of the TME, A. W. Norvelle, Jr., for his skill in constructing the power meter, and E. D. West for a preprint and the kind gift of Manganin wire used in the power meter head.

We gratefully acknowledge support from the donors of the Petroleum Research Fund, administered by the American Chemical Society, the Research Corporation (Cottrell Research Grant), the National Science Foundation, and the Department of Chemistry.

Supplementary Material Available: A more detailed description of the use of the actinometer, methods of simplifying and improving the measurement in speed and wavelength range, and procedures for sensitizer purity evaluation and purification are given. Useful tables showing sensitizer extinction coefficients at important laser lines and the variation of ϕ_0 with O_2 partial pressure and [TME] are given. This material will be particularly useful for the nonchemist (8 pages). Ordering information is given on any current masthead page.

References and Notes

- (1) B. R. Clemsha, *J. Phys. E*, **5**, 859 (1972).
- (2) C. Davies and K. A. Hodgkinson, *J. Phys. E*, **5**, 544 (1972).
- (3) J. G. Edwards and R. Jefferies, *J. Phys. E*, **4**, 580 (1971).
- (4) D. A. Jennings and E. D. West, *Rev. Sci. Instrum.*, **41**, 565 (1970).
- (5) E. D. West, "Creation and Detection of the Excited State", Vol. IV, W. R. Ware, Ed., accepted for publication.
- (6) J. Geist, B. Steiner, R. Schaefer, E. Zalewski, and A. Corron, *Appl. Phys. Lett.*, **26**, 309 (1975).
- (7) E. D. West, W. E. Case, A. L. Rasmussen, and L. B. Schmidt, *J. Res. Natl. Bur. Stand., Sect. A*, **76**, 13 (1972).
- (8) S. R. Gunn, *J. Phys. E*, **6**, 105 (1973).
- (9) J. N. Demas in ref 5.

- (10) J. N. Demas, D. Diemente, and E. W. Harris, *J. Am. Chem. Soc.*, **95**, 6864 (1973).
- (11) J. N. Demas, E. W. Harris, and R. P. McBride, submitted for publication.
- (12) C. A. Parker, "Photoluminescence of Solutions", Elsevier, New York, N.Y., 1968.
- (13) C. S. Foote, *Acc. Chem. Res.*, **1**, 104 (1968).
- (14) J. N. Demas and J. W. Addington, *J. Am. Chem. Soc.*, accepted for publication.
- (15) C. B. Kretschmer, J. Nowakowska, and R. Wiebe, *Ind. Eng. Chem.*, **38**, 506 (1946).
- (16) "Handbook of Chemistry and Physics", 48th ed, Chemical Rubber Co., Cleveland, Ohio, 1968-1969, p D-140.
- (17) W. E. K. Middleton and C. L. Sanders, *J. Opt. Soc. Am.*, **41**, 419 (1951).
- (18) F. Kohlrash, "Praktische Physik", Vol. 1, B. G. Teubner Verlagsgesellschaft, Stuttgart, 1955, p 463.
- (19) W. Y. Ramsey, U.S. Department of Commerce Weather Bureau, Washington, D.C., Meteorological Satellite Report No. 31 (1964).
- (20) J. N. Demas and G. A. Crosby, *J. Am. Chem. Soc.*, **93**, 2841 (1971).
- (21) J. N. Demas, E. W. Harris, C. M. Flynn, Jr., and D. Diemente, *J. Am. Chem. Soc.*, **97**, 3838 (1975).
- (22) D. G. Taylor and J. N. Demas, work in progress.
- (23) D. G. Taylor, M.S. Thesis, University of Virginia, 1976.

Discussion

M. GOUTERMAN. What is the origin of the deviation of quantum counter efficiency from unity? Is it a breakdown of Kasha's law?

J. N. DEMAS. Organic dyes are terribly difficult to purify and keep clean. Also, at the concentrations used in quantum counting, they can dimerize and polymerize. Thus, we attribute the small variations in yield with wavelength to these factors rather than to a breakdown of Kasha's law.

High Resolution Zeeman Experiments on Singlet, Triplet, and Quartet States of Metalloporphines

G. W. Canters,* G. Jansen, M. Noort, and J. H. van der Waals†

Centre for the Study of the Excited States of Molecules, Gorlaeus Laboratories, Rijksuniversiteit, Leiden, The Netherlands (Received March 24, 1976)

Publication costs assisted by Gorlaeus Laboratories

A report is presented of the Zeeman effect measured at high resolution for the first excited singlet (S_1) states and the lowest phosphorescing states of various metalloporphines (MeP's). The degeneracy of the excited states appears to be lifted by the crystal field and a crystal field splitting δ is observed in the spectra which varies in magnitude from 10 to 100 cm^{-1} depending on the central metal in the MeP and the host. The Zeeman effect in the S_1 state of ZnP betrays the influence of vibronic coupling and the Jahn-Teller (JT) active mode is tentatively assigned to the 180- cm^{-1} vibration appearing in the spectrum. With this assignment one then arrives for the JT stabilization energy at a value of 30-40 cm^{-1} and for the JT distortion parameter α at a value of 1.2-1.4. Zero-field splittings between the spin components of the lowest triplet and quartet states of PdP and CuP, respectively, are found to be in the order of 0.5-1.0 cm^{-1} . The importance of the crystal field splitting and vibronic coupling for a proper understanding of the spectroscopic properties of the excited states of the MeP's is stressed.

1. Introduction

As well as having important biological implications porphines are an intriguing subject of spectroscopic investigation. From 1949 on many theoretical attempts have been made to understand the optical properties of these compounds.¹ Although the outcome of the calculations differed in many respects, all theories agreed that in an unsubstituted metalloporphine, the structure of which is shown in Figure 1, with its relatively high, fourfold symmetry, the first few excited states are doubly degenerate and bear the orbital symmetry label E_u in the point group D_{4h} . In addition it was predicted that the lowest of these states would carry a high orbital angular momentum. For instance, for a diamagnetic metalloporphine, such as zinc porphine (ZnP), Gouterman and co-workers calculated for the matrix element of the orbital angular momentum L_z about the z axis values of $4.3\hbar$ and $2.1\hbar$ for the first excited singlet state S_1 and the lowest triplet state T_0 , re-

spectively.^{2,3} For a spectroscopist these degenerate states are of great interest because they provide a sensitive probe for studying the effect of small perturbations, such as vibronic and spin-orbit coupling, a crystal field, or an external magnetic field (Zeeman effect).

A prerequisite to observe these effects spectroscopically is that the spectra are recorded under conditions where they are highly resolved. Optical spectroscopy of porphines has a history of almost 100 years but until recently only broad-banded spectra were obtained of the type exemplified by Figure 2a. A strong absorption called the Soret band, with an oscillator strength of about 1 is seen around $\lambda = 400$ nm while an approximately ten times weaker absorption called the Q-band occurs between 500 and 560 nm. Traditionally, the maximum to longer wavelengths of the latter band have been described as the origin of the $S_1 \leftarrow S_0$ transition and the second band in the given region has been described as a 1-0 transition built on this $\lambda \approx 550$ nm origin. The Q and Soret bands thus represent transitions to the first and second excited singlet state.¹

† Huygens Laboratory, Rijksuniversiteit, Leiden, The Netherlands.

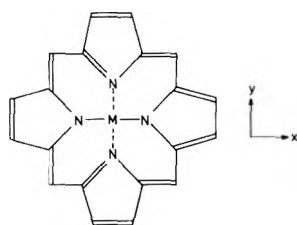


Figure 1. Structural formula of a metalloporphine. The metal atom is represented by M.

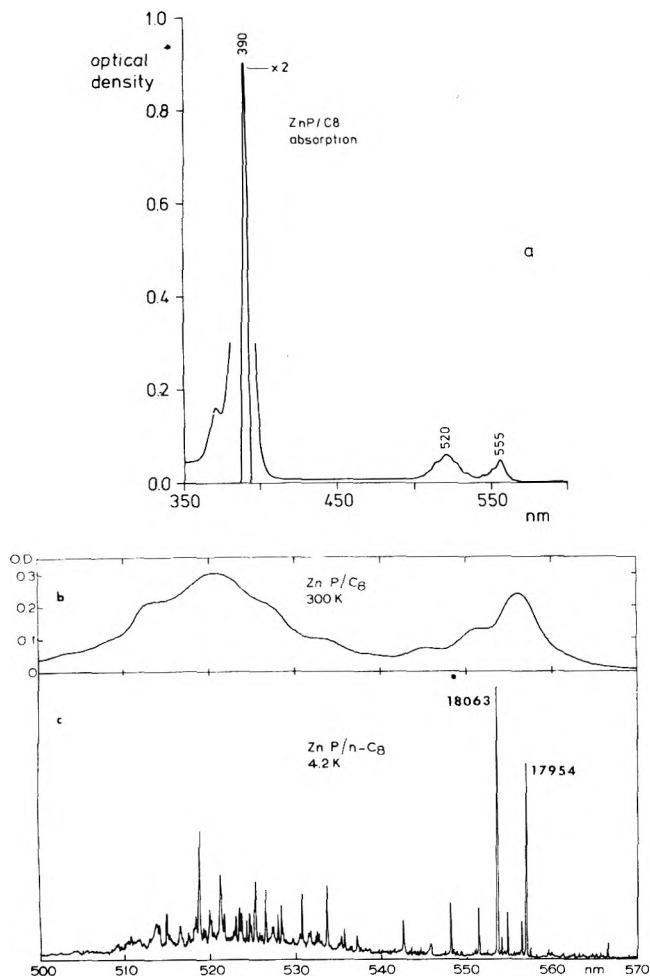


Figure 2. (a) Room temperature absorption spectrum of a saturated solution of ZnP in *n*-octane. Optical path length 1 cm. (b) Part of the same spectrum, path length 5 cm. (c) Absorption spectrum of a single crystal of the same solution as used in (a) and (b), recorded at 4.2 K. The spectrum was measured by means of the phosphorescence excitation method. The two strong bands at the long wavelength side of the spectrum occur at 17 954 and 18 063 cm^{-1} . (Peak positions previously reported for *n*-C₈⁷ were not calibrated and are off by approximately 7 cm^{-1} .)

The first report of high resolution spectra of MeP's appeared in 1961 when Russian investigators used Shpol'skii's method and incorporated the MeP's in polycrystalline masses of the *n*-alkanes.⁴ More extensive research was performed by Gradyushko et al. in 1969 who used the same method and reported the emission and absorption spectra of various MeP's at 77 K.⁵ Subsequent phosphorescence microwave double resonance (PMDR) experiments on ZnP in a *n*-alkane (*n*-C₈)⁶ indicated that the bands in the optical spectra may be sharpened even further by performing the measurements at 4.2 K on single crystals of an *n*-alkane containing the MeP as a

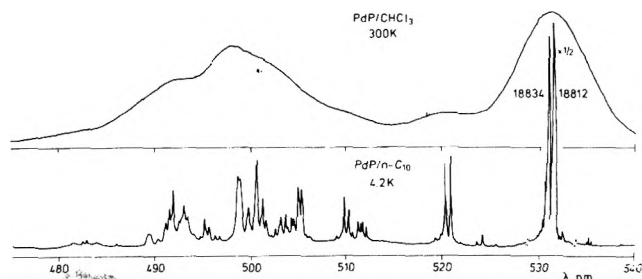


Figure 3. Absorption spectra of PdP (top) at room temperature in a solution of CHCl_3 , and (bottom) at 4.2 K in a single crystal of *n*-decane. The bottom spectrum was recorded by the phosphorescence excitation method. The upper spectrum was shifted 2.4 nm to the right on the wavelength scale in order to better demonstrate the similarity between top and bottom spectra. The positions of the two main peaks in the upper spectrum are indicated in cm^{-1} . Their actual intensity is twice as large as drawn in the figure.

very dilute solute. This expectation was borne out by experiment;⁷ an example of the resolution that can be obtained is shown in the Figures 2b and 2c where the room temperature absorption of a saturated solution of ZnP in *n*-C₈ in the region of the Q band is compared with the absorption spectrum at 4.2 K of a single crystal grown from the same solution. The spectra show that the two bands seen at room temperature actually are the envelopes of a rich vibronic structure.

In the present article we intend to show how high resolution spectroscopy in combination with Zeeman experiments can greatly increase our knowledge about the manner in which the perturbations previously mentioned affect the properties of the porphine molecule. More in particular the interplay between vibronic coupling on the one hand, and the effects of spin-orbit coupling, the crystal field, and a Zeeman field on the other has become clearer. As examples the Zeeman effect in the first excited singlet states of ZnP and PdP will be discussed. After that the Zeeman effect in the 0-0 transitions of the phosphorescence of PdP and CuP will be dealt with. Especially CuP, which is paramagnetic and has a doublet ground state presents an interesting case, because its phosphorescence has been predicted to arise from a quartet state.⁸

2. A Simple Case. The $S_1 \leftarrow S_0$ Transition of PdP in *n*-C₈ and *n*-C₁₀

An example of a Zeeman effect relatively easy to understand is provided by the $S_1 \leftarrow S_0$ transition of PdP. In Figure 3 the absorption spectrum of PdP in *n*-decane (*n*-C₁₀) at 4.2 K is shown. Comparison with the room temperature spectrum in CHCl_3 , reproduced in the same figure, again shows the tremendous gain in resolution obtained when a crystal of an *n*-alkane is used as a host.

The most prominent feature of the low temperature spectrum is the appearance of two strong bands at the long wavelength end. These bands have been shown to represent the 0-0 transitions to the two components of the E_u state⁹ (the minor peaks occurring in the same region have been ascribed to different sites in the crystal¹⁰). For a detailed understanding of this splitting one has to consider the interaction of the Jahn-Teller unstable state S_1 with the crystal field of the host, a problem to which we shall return in the next section. Here, however, it is sufficient to remark that while in an isolated molecule the two zero point levels of S_1 should be degenerate, because the system still retains its fourfold vibronic symmetry, this degeneracy must be destroyed when the molecule is incorporated in the triclinic *n*-alkane crystal. The two orbital

components ψ_ξ and ψ_η of S_1 , spanning the irreducible representation E_u of the group D_{4h} , have their nodal patterns at right angles and in the host the two charge distributions $|\psi_\xi|^2$ and $|\psi_\eta|^2$ will interact differently with the crystal field. As a result a crystal field splitting δ occurs in the absorption spectrum.

For PdP in $n\text{-C}_{10}$ (see Figure 3) δ amounts to 22 cm^{-1} , but it changes with the host, as one would expect if our interpretation is correct. So far we have investigated $n\text{-C}_8$, $n\text{-C}_9$, and $n\text{-C}_{10}$ as hosts and depending on the alkanes and on the particular site the PdP is in, δ varies from 10 to 30 cm^{-1} . The crystal field splitting should be visible not only at the origin but also throughout the rest of the absorption spectrum. This seems to be true for the region comprising the first few hundred wavenumbers of the spectrum¹⁰ but the unravelling of the vibrational structure becomes increasingly difficult at the point where absorption bands start to overlap, a problem that is presently being investigated further.

When considering the effect of intramolecular magnetic interactions, such as spin-orbit coupling, or the influence of an external magnetic field on the excited states of a porphine, one has to realize that these interactions are usually considerably weaker, or at most comparable to the crystal field splitting δ . Hence, to a first approximation one may describe the situation in a basis of the two components of S_1 split by the crystal field with the magnetic perturbations being reduced to second-order effects.

A good example is the Zeeman effect. Application of a magnetic field H_z along the z axis of the molecule provides for a perturbation $\mathcal{H}' = (\beta/\hbar)H_zL_z$ in which β is the Bohr magneton. Since L_z is a nontotally symmetric operator the diagonal matrix elements of L_z for the states ψ_ξ and ψ_η vanish, which means that there is no first-order effect of \mathcal{H}' . However, \mathcal{H}' couples ψ_ξ and ψ_η through the matrix element $\langle\psi_\xi|L_z|\psi_\eta\rangle \equiv i\Lambda\hbar$ and a simple variational treatment with ψ_ξ and ψ_η as a basis then yields for the energies of the two Zeeman components

$$E_{\xi,\eta} = E_0 \pm \left[\frac{\delta^2}{4} + \left(\frac{\beta}{hc} \right)^2 H_z^2 \Lambda^2 \right]^{1/2} \quad (1)$$

in which $E_0 \equiv (E_\xi + E_\eta)/2$. (All energies are expressed in wavenumbers.) When the Zeeman energy is small compared with δ , i.e.

$$\frac{\beta}{hc} H_z \Lambda \ll \delta \quad (2)$$

eq 1 reduces to

$$E_{\xi,\eta} \approx E_0 \pm \left[\frac{\delta}{2} + \frac{1}{\delta} \left(\frac{\beta}{hc} \right)^2 H_z^2 \Lambda^2 \right] \quad (3)$$

that is, one expects a quadratic Zeeman effect.

Experiments of this kind have been performed on PdP in $n\text{-C}_8$ and $n\text{-C}_{10}$ in which δ amounts to 30 and 22 cm^{-1} , respectively. The shifts of the two origins of the absorption spectrum in an external field have been plotted as a function of H_z^2 in Figure 4. For $n\text{-C}_8$ the quadratic dependence of the shift on the field is nicely borne out by experiment. For $n\text{-C}_{10}$ the quadratic dependence occurs at field strengths below $H_z \approx 55\text{ kG}$ but at higher fields the shifts become smaller than expected on the basis of the simple eq 3. The reason for this is that for PdP in $n\text{-C}_{10}$ δ only amounts to 22 cm^{-1} and condition 2 does not apply anymore for $H_z \geq 55\text{ kG}$. In fact for the other limiting case

$$\frac{\beta}{hc} H_z \Lambda \gg \delta \quad (4)$$

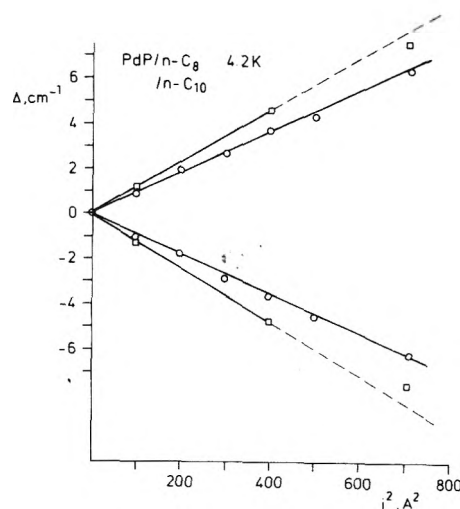


Figure 4. Shifts of the two main lines at the long wavelength side of the absorption spectra of PdP in $n\text{-C}_8$ and $n\text{-C}_{10}$ measured at 4.2 K as a function of the square of the external magnetic field. Squares indicate data measured in $n\text{-C}_{10}$ and circles data measured in $n\text{-C}_8$. On the horizontal scale the square of the current running through the magnet coil is indicated in (amps)². The relation between H_z in kG and i in A is $H_z = 2.52i$.

eq 1 reduces to

$$E_{\xi,\eta} \approx E_0 \pm \frac{\beta}{hc} H_z \Lambda \quad (5)$$

with the Zeeman shifts becoming linear in H_z .

In accordance with eq 3 we find that the slopes of the straight lines in Figure 4 for $n\text{-C}_8$ and $n\text{-C}_{10}$ are inversely proportional to δ . From the slopes we calculate $\Lambda = 4.3$, seemingly in agreement with the predictions of McHugh and Gouterman.² However, we shall see in the next section that the experimental value is to be considered a lower estimate since it still contains an unknown orbital reduction factor.

It is well known that the measurement of the magnetically induced circular dichroism (MCD) provides information about the presence of an orbital degeneracy in an electronic absorption band and yields the magnitude of the matrix element $\langle\psi_\xi|L_z|\psi_\eta\rangle$. Also, the sign of the MCD of a particular vibronic band may provide information about the symmetry of the vibrational state(s) involved in the transition. For a survey of the theory the reader is referred to recent review articles.¹¹

We thought it of interest to have a check on the data extracted from the Zeeman experiments through an independent method. The MCD spectra of a number of MeP's in EPA glasses were therefore measured by Kielman et al. and for the 0-0 transition to the Q band of PdP a value of $\Lambda = 4.0 \pm 0.4$ was found, in quite good agreement with the results from the Zeeman experiments. A detailed report and interpretation of the experiments will be given elsewhere.¹²

3. Effect of Vibronic Coupling

Until now vibronic coupling was not taken into consideration. It is of interest to see in what way Jahn-Teller (JT) coupling might reveal itself in our case. The best starting point is first to look at the free molecule in which the S_1 state is doubly degenerate. This state, of course, is susceptible to JT distortions and in order to keep matters simple we shall consider the case that only one normal coordinate of the proper symmetry (b_{1g} or b_{2g} in D_{4h}) exhibits vibronic coupling with the electronic motion. This case has been treated in detail by Hougén¹³ who showed that in this particular situation the JT

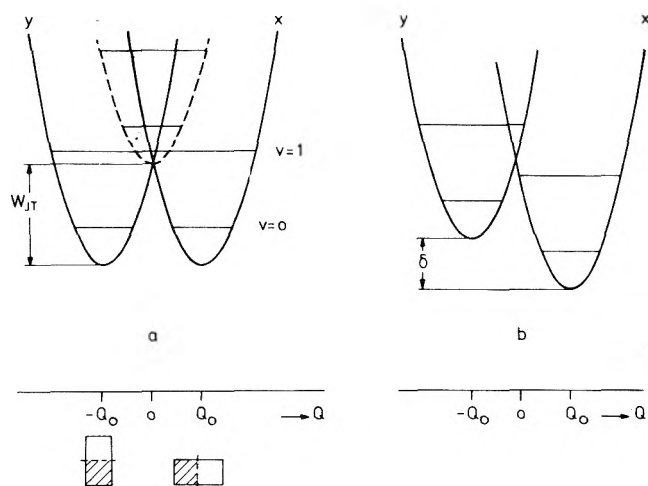


Figure 5. Nuclear potential energy as a function of the Jahn-Teller active normal coordinate Q . (a) Situation in the free molecule. The dashed curve represents the case when there is no vibronic coupling; the two potential wells coincide. Solid lines represent the case where there is vibronic coupling. The potential wells are stabilized by an energy W_{JT} and potential energy minima now occur at $+Q_0$ and $-Q_0$. (The fourfold symmetrical configuration corresponds to $Q = 0$.) Nuclear configurations at $Q = Q_0$ and $-Q_0$ are indicated below the horizontal axis together with the nodal plane of the corresponding electronic part of the wave function. The symmetry of the JT active vibration has been assumed to be b_{1g} . (b) Situation when the MeP molecule is embedded in a host. One configuration is now favored over the other by the crystal field and a splitting δ is induced. The configuration which is stabilized has been arbitrarily chosen to be the one corresponding to ψ_x .

distorted states can still be described by wave functions of the Born-Oppenheimer type. The two potential energy wells which correspond to these two wave functions, and which coincide in the absence of vibronic coupling, lower their energy by W_{JT} because of the vibronic coupling and no longer have their potential energy minima at $Q = 0$, but at $Q = -Q_0$ and $Q = Q_0$. This state of affairs is represented on the left-hand side of Figure 5.

In a molecule of symmetry D_{4h} the active vibrations are of symmetry b_{1g} , or b_{2g} ; in the former case the square, which symbolizes the molecule in its fourfold symmetrical configuration, is distorted into a rectangle and in the latter case into a diamond. In the construction of Figure 5 we have arbitrarily assumed that the dominant coupling occurs through a b_{1g} type mode. The Jahn-Teller distorted configurations have been symbolized in the drawing by two rectangles, and two of the nodal planes of the orbital parts of the wave functions ψ_ξ and ψ_η have been indicated in the rectangles by the shaded areas. It is important to realize, however, that even after the introduction of vibronic coupling the vibronic degeneracy remains for an isolated molecule. This changes when the molecule is incorporated in a crystalline host, as explained in the previous section. The crystal field lifts the degeneracy, one of the orbital components is favored in energy, and a crystal field splitting δ occurs. Of the two electronic wave functions, which we henceforth denote by $|x\rangle$ and $|y\rangle$, the potential well belonging to $|x\rangle$ is arbitrarily assumed to be the deeper of the two. (For a situation with fourfold symmetry, where the coupling is via a nondegenerate vibration, the vibronic coupling determines the position of the nodal planes in the molecule, at least as long as the vibronic coupling is large compared to the crystal field splitting, that is when $W_{JT} \gg \delta$. It is questionable, however, whether the latter inequality holds for the state S_1 of MeP's.¹⁴)

An important consequence of the occurrence of two po-

tential minima at different values of Q , first pointed out by Ham,^{15a} is that in each potential well the vibrational parts of the vibronic wave function are orthogonal but that the vibrational wave functions of one well no longer are orthogonal to those of the other one. An orbital operator, such as L_z , which couples the electronic factors $|x\rangle$ and $|y\rangle$ of the vibronic wave functions will therefore connect a given level $|x, v_x\rangle$ with all the levels $|y, v_y\rangle$ and vice versa. Here v_x and v_y denote the quantum numbers of the vibrational levels of the active mode in the $|x\rangle$ and the $|y\rangle$ manifolds.

In algebraic notation the expressions for the matrix elements of L_z become

$$\langle x, v_x | L_z | y, v_y \rangle = -i \Delta \hbar \langle v_x | v_y \rangle \quad (6)$$

in which $\langle v_x | v_y \rangle$ is now a vibrational overlap integral which acts as a so-called "orbital reduction factor" by which the matrix element $\langle x | L_z | y \rangle$ is reduced.

In the Zeeman effect the vibronic coupling may now manifest itself through an asymmetry in the shifts of the vibronic levels of the $|x\rangle$ and $|y\rangle$ manifolds as is shown by the following reasoning. When we look at the right-hand side of Figure 5 we see that the $|x, 0_x\rangle$ level is connected by the Zeeman perturbation with the whole set of levels $|y, v_y\rangle$, all of them higher in energy by an amount $\delta + v_y \bar{\nu}_{JT}$. Consequently the perturbation causes a downward shift of the $|x, 0_x\rangle$ level. On the other hand, the $|y, 0_y\rangle$ level is coupled to all the levels $|x, v_x\rangle$ whose energy with respect to the $|y, 0_y\rangle$ level is given by $-\delta + v_x \bar{\nu}_{JT}$. Some of these levels are lower in energy (in Figure 5 only the level with $v_x = 0$), others are higher. The net shift of the $|y, 0_y\rangle$ level thus is the sum of an upward and a downward shift of which the magnitude depends on Q_0 , δ , and $\bar{\nu}_{JT}$, $\bar{\nu}_{JT}$ being the frequency in cm^{-1} of the JT active mode.

By second-order perturbation theory the energies of the two $|x, 0_x\rangle$ and $|y, 0_y\rangle$ levels are found to be⁷

$$E_x(H) = E_0 - \frac{\delta}{2} - \left(\frac{\beta}{\hbar c}\right)^2 H_z^2 \Lambda^2 \sum_{v_x=0}^{\infty} \frac{|\langle 0_x | v_x \rangle|^2}{\delta + v_x \bar{\nu}_{JT}} \quad (7a)$$

$$E_y(H) = E_0 + \frac{\delta}{2} - \left(\frac{\beta}{\hbar c}\right)^2 H_z^2 \Lambda^2 \sum_{v_y=0}^{\infty} \frac{|\langle 0_y | v_y \rangle|^2}{-\delta + v_y \bar{\nu}_{JT}} \quad (7b)$$

The asymmetry in the shifts clearly comes about in the sign of δ in the energy denominator of the infinite sums. In case $\delta \gg \bar{\nu}_{JT}$ eq 7 reduce to eq 3 and the asymmetry is lost. This also happens when there is no Jahn-Teller distortion since then $\langle v_x | v_y \rangle = \delta_{v_x, v_y}$ and only the $v_x = 0$ and $v_y = 0$ level, respectively, contribute to the sums in eq 7a,b.

It is interesting to note that an asymmetry in the Zeeman shifts has been observed for ZnP. An example of a high resolution spectrum of ZnP was already given in Figure 2. Here also at the long wavelength end of the spectrum, two prominent bands are seen, namely, at 17 954 and 18 063 cm^{-1} . The Zeeman effect on these two bands is quadratic as in the case of PdP, but the effect is smaller. In a previous publication it was reported that the lower component shifts down in energy by only 2 cm^{-1} at the highest attainable value of H_z ($H_z = 68$ kG), while the upper component very slightly moves also to lower energies as the field is increased, the shift reaching a value of -0.8 cm^{-1} at the maximum field.⁷

A quantitative analysis of these shifts was based on the contention that the two bands correspond with transitions to the $|x, 0_x\rangle$ and $|y, 0_y\rangle$ levels of the ZnP molecule and that the distance of 109 cm^{-1} between the two peaks corresponds with a crystal field splitting of $\delta = 109 \text{ cm}^{-1}$. Simple inspection of eq 7a,b shows that the observed asymmetry in the Zeeman shifts can only occur if $\bar{\nu}_{JT}$ is of the order of or smaller than δ and if the distortion Q_0 of the molecule is at least of the order

of the amplitude of the zero point motion, ρ_0 , of the vibration. The latter conclusion means that the transition from the ground state to the $|x, 1_x\rangle$ and $|y, 1_y\rangle$ levels should carry a significant Franck–Condon intensity and ought to appear in the absorption spectrum. With $\delta = 109 \text{ cm}^{-1}$ $\bar{\nu}_{JT}$ should be a low frequency vibration. In Figure 6 the first part of the absorption and emission spectra of ZnP in *n*-C₁₀ are reproduced. Inspection of these spectra makes it clear that the only candidate fulfilling these requirements is the vibration with $\bar{\nu} = 180 \text{ cm}^{-1}$. On the assumption that this is the JT active vibration, eq 7a,b allow one to derive from the shifts of the two main bands in the ZnP spectrum the values of Λ and of the distortion parameter α defined by

$$\alpha \equiv \frac{2Q_0}{\rho_0} = 2 \left(\frac{2W_{JT}}{hc\bar{\nu}_{JT}} \right)^{1/2} \quad (8)$$

In terms of Goutermans parameter λ ,³ α is given by $\alpha = 2\lambda$. Since $|\langle 0_x | v_y \rangle|^2 = |\langle 0_y | v_x \rangle|^2 = (\alpha^2/2)^v (v!)^{-1} \exp(-\alpha^2/2)$,^{15b} it is possible to numerically evaluate expressions 7a,b once Λ and α have been chosen. By varying these parameters we have tried to establish the values of α and Λ which are best compatible with the experimental data. The results are $\alpha = 1.4 \pm 0.1$ and $\Lambda = 6.1 \pm 0.6$.⁷ (The uncertainties quoted are root-mean square deviations.) From the value of α we find $W_{JT} = 44 \pm 8 \text{ cm}^{-1}$ which points to the presence of a relatively weak JT coupling, in agreement with a prediction by Perrin, Gouterman, and Perrin.¹⁴ Recent experiments have established that the shifts of both the $|x, 0\rangle$ and the $|y, 0\rangle$ level are smaller than the shifts reported previously by about 0.5 cm^{-1} . With the new data one finds $\alpha = 1.2$, $\Lambda = 5.0$, and $W_{JT} = 33 \text{ cm}^{-1}$. Of course it may be that several JT active vibrations, possibly of different symmetry, contribute significantly to the instability. In that case analysis of the experimental data would become much more complicated. It is very gratifying therefore that recent MCD experiments on ZnP could be analyzed using the same assumption, namely, that only one vibration exhibits strong JT coupling. More important even, it could be shown that the 180-cm^{-1} vibration occurring in the absorption spectrum is the JT active vibration.¹²

Finally, as Gouterman has pointed out, support for the assignment of the JT active vibration comes from a consideration of the intensities of the vibronic bands in the high resolution absorption spectrum (Figure 2c). If we assume the ground state to have fourfold symmetry the Franck–Condon factors for the 0–0 and the 0–1 transition of the JT active vibration are given by^{15b} $\exp(\alpha^2/8)$ and $(\alpha^2/8) \exp(-\alpha^2/8)$, respectively. With $\alpha = 1.2$ one finds for the intensity of the 0–1 transition relative to the intensity of the 0–0 transition $\alpha^2/8 = 0.18$ which is close to the experimental ratio of 0.23.

An intriguing question, arising on the basis of recent experimental evidence, relates to the origin of the splitting of 109 cm^{-1} observed in the ZnP spectrum. In the foregoing this splitting was ascribed to the action of the crystal field on the JT instable S_1 state of the ZnP molecule and, therefore, was not considered as an intrinsic property of the molecule. It is remarkable, however, to see that the energy distance does not change whenever *n*-C₈, *n*-C₉, *n*-C₁₀, or *n*-C₁₂ is used as a host. We therefore studied the doublet structure in the ZnP spectra in somewhat more detail. First of all it was demonstrated by site selection experiments in *n*-C₉ and *n*-C₁₀ that the peaks separated by 109 cm^{-1} belong to one species. This is also apparent from a comparison of the absorption and emission spectra of ZnP reproduced in Figure 6: since at 4.2 K emission should occur only out of the lowest excited state one expects to see no splitting in the fluorescence spectrum of ZnP. In

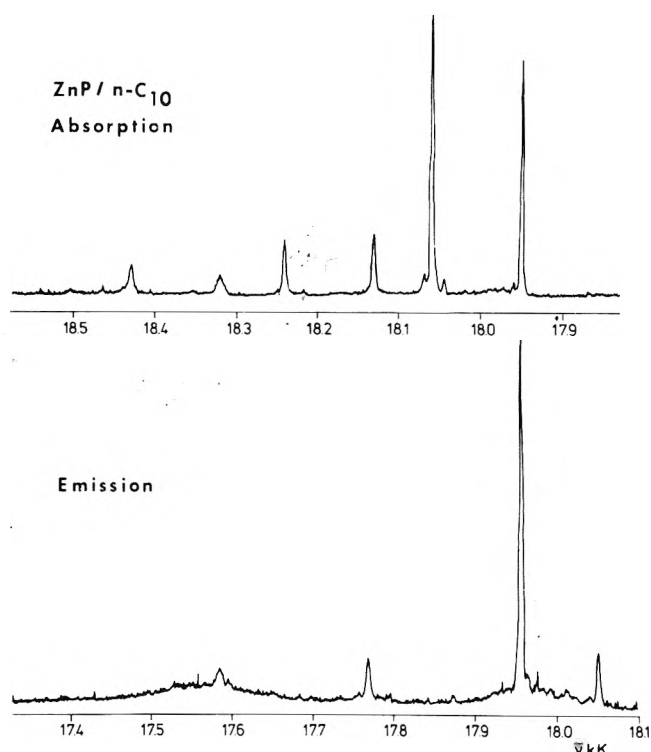


Figure 6. First part of the emission and absorption spectra of ZnP in *n*-C₁₀ at 4.2 K. Notice that wavenumber scales in the two spectra run in opposite directions. The peaks in the emission and absorption spectra at 18049 cm^{-1} are due to a different site.

Figure 6 it is seen that a splitting in the emission spectrum is absent, indeed. Apart from the 0–0 transition two vibronic bands at 180 and 365 cm^{-1} from the origin are seen. An exactly similar structure is seen in the absorption spectrum but here the whole pattern is repeated at an interval of 109 cm^{-1} . At the same time doublets of peaks of minor intensity with splittings ranging from 5 to 75 cm^{-1} are seen in the spectra of ZnP in various *n*-alkane hosts. The intensity of some of these depends on sample preparation as reported for PdP in polycrystalline *n*-alkanes.¹⁰ It could be established that the doublets each belong to a different species, possibly ZnP molecules at different sites in the crystal. The variety of splittings observed seems to preclude an intramolecular cause for their occurrence and the constancy of the splitting of 109 cm^{-1} is therefore very puzzling. On the basis of a recent solvation study^{15c} we had to rule out the possibility that the splitting is caused by a ligand attached to the central metal atom. Whether its lack of variation with the host crystal points to a similarity in the tensor of the crystal field around the ZnP molecule or to another, possibly intrinsic, cause is at present a subject of further research.

4. States with $S \neq 0$. PdP ($S = 1$) and CuP ($S = \frac{3}{2}$)

For metalloporphines the principal terms which have to be added to the molecular Hamiltonian when one goes from singlet states to states with $S > 0$ are the spin–orbit coupling (SOC) and the Zeeman energy of the spin angular momentum. The spin–spin interaction, although present, plays a less important role because of the smallness of its matrix elements. The effects of SOC are expected to be larger than in most planar π systems because of the near degeneracy (δ is small) between the $|x\rangle$ and $|y\rangle$ components of the E_u states involved, in combination with the fact that the d_{xz} and d_{yz} orbitals on the central metal are conjugated with the π -electron system

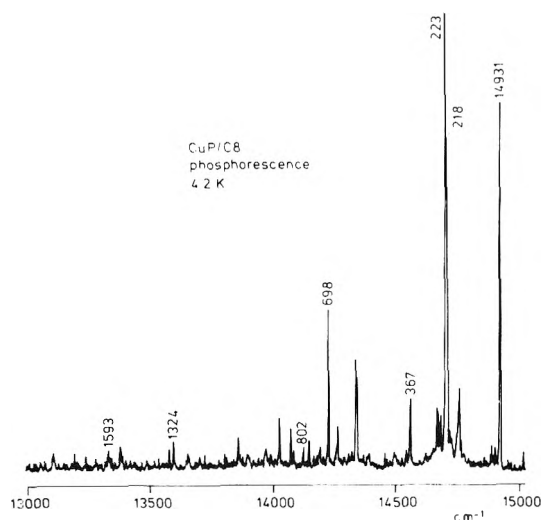


Figure 7. Phosphorescence spectrum of CuP in *n*-octane recorded at 4.2 K.

of the porphine nucleus. As a result a heavy central metal atom is expected to give a dominant contribution to the total SOC in an MeP.⁸ For the MeP's studied thus far, with metals as heavy as Pd, it has proved a useful starting point to describe the Zeeman energy levels in a scheme in which one takes the "pure" spin electronic components of the E_u state as a basis and then deals with the spin-dependent terms through a perturbation calculation or a variational treatment.

Both PdP and CuP provide nice cases to study the lowest metastable state since both give well-resolved phosphorescence spectra at 4.2 K when incorporated in a *n*-alkane host. As an example the phosphorescence spectrum of CuP in *n*-C₈ at 4.2 K is reproduced in Figure 7. The phosphorescent state of PdP is a triplet state but CuP is different. Cu has a d⁹ configuration and accordingly the ground state of CuP is a doublet with $S = 1/2$, while the phosphorescing state has been predicted to be a quartet state.⁸

The Zeeman effects of the 0–0 lines in the phosphorescence of PdP and CuP have been studied at 4.2 K in fields up to 75 kG. What is observed for instance in the case of CuP is a single line in zero field which splits into three lines shifted to lower energy¹⁶ by 14–15, 6–7, and about 0 cm⁻¹, respectively. A careful study of the small (1–2 cm⁻¹) anisotropies in the peak positions as a function of the orientation of the magnetic field with respect to the molecular framework has shown that we probably are observing emission out of the quartet sublevels with magnetic quantum numbers $m_s = -3/2$ and $-1/2$ to the magnetic sublevels of the ground state with $m_s = \pm 1/2$. Emission out of the other two quartet levels is strongly disfavored because of the Boltzmann factor. A theoretical treatment of the behavior of the magnetic sublevels in a magnetic field was developed by means of a variational calculation in which the eight spin-orbital wave functions of the lowest $|x\rangle$ and $|y\rangle$ states of the vibronic manifold were used as a basis.^{16,17} By comparing the experimentally determined anisotropy in the peak positions with those predicted on the basis of the theory a value of 0.7 cm⁻¹ was found for the zero-field splitting between the $m_s = \pm 1/2$ and $\pm 3/2$ sublevels of the lowest quartet state in zero field. The spin-orbital matrix element which is responsible for this splitting probably is at least an order of magnitude larger but its effect on the positions of the spin is again diminished by the presence of a crystal field splitting, the magnitude of which we have not yet determined, and possibly by the orbital reduction factor. Similar experiments

were performed on the 0–0 band of the phosphorescence of PdP.¹⁸ From the anisotropy in the peak positions a value of 0.5–1 cm⁻¹ was found for the zero-field splitting parameter.

5. Conclusion

The most conspicuous feature in the high resolution spectra of the MeP's is the presence of a crystal field splitting. Depending on host and central metal we found that this splitting may vary from 10 to 109 cm⁻¹. Undoubtedly splittings of this nature are also present in the spectra of liquid or glass solutions of MeP's where they will be hidden in the band widths as already shown in the work of Sutherland, Axelrod, and Klein.¹⁹ Their presence will be felt in experiments which are designed so as to make use of the mixing of the $|x\rangle$ and $|y\rangle$ wave functions under the influence of an external perturbation as in the case of an MCD experiment.¹⁹ Usually in cases like this the analysis of the experimental data relies on the approximation of rigidly shifting bands. The results reported here make it more probable that in a variety of environments as will occur in solution or in a glass, there will exist a distribution of crystal field splittings which could invalidate the rigid shift approximation.

Furthermore, it has become clear that vibronic coupling may complicate the interpretation of the experimental data. In the presence of JT coupling matrix elements of orbital operators are reduced by an orbital reduction factor which is a function of the strength of the JT coupling. The magnitude of the latter is difficult to establish experimentally unless the Jahn–Teller active mode(s) can be localized. In the case of the MeP's Zeeman and MCD experiments can be used to this purpose. An asymmetric quadratic Zeeman effect measured in a high resolution absorption spectrum, as was observed for ZnP, is a definite indication of a nonnegligible JT interaction with $\bar{\nu}_{JT}$ of the order of δ . The absence of asymmetry in the Zeeman effect, however, not necessarily means that the JT coupling is absent. If $\bar{\nu}_{JT} \gg \delta$ one expects a symmetric Zeeman effect even in the case of strong JT coupling. However, the orbital reduction factor then will deviate significantly from 1.

Finally, the experiments on the porphine compounds with heavy metals have shown that the matrix elements of the spin-orbit coupling operator, which connect the crystal field split $|x\rangle$ and $|y\rangle$ states, have a magnitude in the order of 10 cm⁻¹ or more. Nevertheless their influence on the spectral line positions is mitigated by the presence of a crystal field splitting and a possible Jahn–Teller distortion which causes the orbital reduction factor to be less than 1.

Acknowledgment. These investigations were supported by the Netherlands Foundation for Chemical Research (S.O.N.) with financial aid from the Netherlands Organization for the Advancement of Pure Research (Z.W.O.).

References and Notes

- (1) W. T. Simpson, *J. Chem. Phys.*, **17**, 1218 (1949); H. C. Longuet-Higgins, C. W. Rector, and J. R. Platt, *ibid.*, **18**, 1174 (1950); J. R. Platt in "Radiation Biology II", A. Hollaender, Ed., McGraw-Hill, New York, N.Y., 1956, Chapter 2, pp 71–123; M. Gouterman, *J. Chem. Phys.*, **30**, 1139 (1959).
- (2) A. J. McHugh, M. Gouterman, and C. Weiss, Jr., *Theor. Chim. Acta*, **24**, 346 (1972).
- (3) M. Gouterman, *Ann. N.Y. Acad. Sci.*, **206**, 70 (1973).
- (4) F. F. Litvin and R. I. Personov, *Dokl. Akad. Nauk SSSR*, **136**, 798 (1961).
- (5) A. T. Gradyushko, V. A. Mashenkov, and K. N. Solov'ev, *Biofizika*, **14**, 827 (1969).
- (6) I. Y. Chan, W. G. van Dorp, T. J. Schaafsma, and J. H. van der Waals, *Mol. Phys.*, **22**, 741, 753 (1971).

- (7) G. W. Canters, J. van Egmond, T. J. Schaafsma, and J. H. van der Waals, *Mol. Phys.*, **24**, 1203 (1972).
- (8) R. L. Ake and M. Gouterman, *Theor. Chim. Acta*, **15**, 20 (1969).
- (9) G. W. Canters, M. Noort, and J. H. van der Waals, *Chem. Phys. Lett.*, **30**, 1 (1975).
- (10) M. Noort, G. Jansen, G. W. Canters, and J. H. van der Waals, *Spectrochim. Acta, Part A*, **32**, 1371 (1976).
- (11) B. J. Stephens, *Annu. Rev. Phys. Chem.*, **25**, 201 (1974).
- (12) E. C. M. Kielman, H. P. J. M. Dekkers, and G. W. Canters, *Mol. Phys.*, in press.
- (13) J. T. Hougen, *Mol. Spectrosc.*, **13**, 149 (1964).
- (14) M. H. Perrin, M. Gouterman, and C. L. Perrin, *J. Chem. Phys.*, **50**, 4137 (1969).
- (15) (a) F. S. Ham, *Phys. Rev. A*, **138**, 1727 (1965); **166**, 307 (1968); (b) M. Wagner, *Z. Naturforsch. A*, **14**, 81 (1959); (c) G. Jansen and M. Noort, *Spectrochim. Acta, Part A*, **32**, 747 (1976).
- (16) W. G. van Dorp, G. W. Canters, and J. H. van der Waals, *Chem. Phys. Lett.*, **35**, 450 (1975).
- (17) M. Gouterman, B. S. Yamanashi, and A. L. Kwiram, *J. Chem. Phys.*, **56**, 4073 (1972); S. R. Langhoff, E. R. Davidson, M. Gouterman, W. R. Leenstra, and A. L. Kwiram, *ibid.*, **72**, 169 (1975).
- (18) G. W. Canters, M. Noort, G. Jansen, and J. H. van der Waals, Proceedings of the 12th European Congress on Molecular Spectroscopy, Elsevier, Amsterdam, 1976, p 445.
- (19) J. C. Sutherland, D. Axelrod, and M. P. Klein, *J. Chem. Phys.*, **54**, 2888 (1971).

Relaxation Processes in Excited Molecular Systems

M. Ashraf El-Bayoumi

Departments of Chemistry and Biophysics, Michigan State University, East Lansing, Michigan 48824 (Received March 29, 1976)

Publication costs assisted by Michigan State University

In addition to vibrational relaxation, an excited molecular system may undergo various relaxation processes that occur on the nanosecond time scale. Of these relaxation processes, we discuss intramolecular geometric relaxation, intramolecular excimer formation, solvent-cage relaxation, and proton transfer. An example will be given to demonstrate each phenomenon and to discuss photophysical and dynamical aspects using nanosecond time-resolved spectroscopy. The effects of polarity, temperature, and viscosity of the medium are examined.

Introduction

Following electronic excitation, molecules in a condensed phase undergo a rapid ($>10^{-12}$ s) vibrational relaxation leading to the emitting level of the excited state. In addition to vibrational relaxation, an excited molecular system may undergo various other relaxation processes that occur on the nanosecond time scale. These processes, which include intramolecular twisting relaxation, intramolecular excimer formation, solvent-cage relaxation, as well as proton transfer, are the subject of this paper. Dramatic changes in the luminescence properties often occur as a result of these relaxation processes, e.g., large Stokes shift, appearance of a new fluorescence band, significant fluorescence intensity changes, and/or fluorescence lifetimes different from those calculated from absorption intensities. In addition, unique medium and temperature effects as well as large viscosity effects on the fluorescence spectra may be observed. In this paper, I plan to discuss each relaxation process, give a specific example demonstrating its phenomenological manifestations, and examine important photophysical energetic and dynamic aspects. The latter is studied by nanosecond time-resolved spectroscopy.

In order to account for the fluorescence spectra observed in relaxing molecular systems it is necessary to draw potential energy surfaces along at least two coordinates. The vibrational coordinate, Q_v , represents a specific vibration which is coupled with the electronic transition; it is assumed for simplicity that only one vibrational mode is coupled. The relaxation coordinate, Q_r , may represent an angle of twist, the distance between a proton and a specific atom in the molecule, a coordinate

specifying the separation and orientation of two chromophores involved in excimer formation, or a generalized solute-solvent cage coordinate. Figure 1 shows how vertical excitation (process 1) of the equilibrium ground state configuration, $S^0_{r,v}$, leads to the Franck-Condon state, $S'_{r,v}$, in which both Q_v and Q_r did not change. This state undergoes rapid vibrational relaxation (process 2) leading to a state, $S'_{r,v'}$, where Q_r did not change but Q_v has the value of the equilibrium excited state configuration. Fluorescence may originate from $S'_{r,v'}$ where both Q_r and Q_v assume their values in the equilibrium excited configuration, from state $S'_{r,v}$, or from an intermediate configuration depending on the relative magnitudes of the rate constants of the relaxation process k_r and fluorescence k_f . Processes 6, 3, and 5 in Figure 1 represent those situations respectively. The vibrational spacing, usually of several hundred wavenumbers, which appears in the absorption and fluorescence spectra is illustrated by the potential energy cross section drawn along Q_v which represents the intramolecular vibrational mode coupled with the electronic transition. Relaxation along Q_r leads to a large Stokes shift, the magnitude of which depends on the difference between the values of Q_r in the equilibrium ground state and equilibrium excited state configurations. Energy levels that characterize potential energy cross sections along Q_r correspond to low frequency modes such as those associated with excimer libration, torsional motion, proton oscillations with respect to a proton acceptor, as well as solvent-solute oscillations. Coupling with these low frequency modes in addition to relaxation along Q_r in a fluid medium lead to an extensive broadening of each vibronic band and the disappearance of vibrational structure corresponding to Q_v . In a rigid medium, relaxation along Q_r

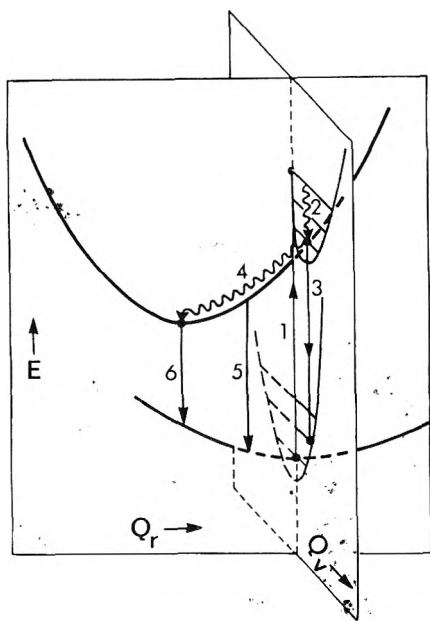


Figure 1. Potential energy cross sections drawn along two coordinates Q_v and Q_r for the ground and excited states. The diagram illustrates vertical excitation (1), vibrational relaxation (2), emission before relaxation along Q_v occurs (3), relaxation along Q_r (4), emission from an intermediate configuration (5), and emission from the equilibrium excited state configuration (6).

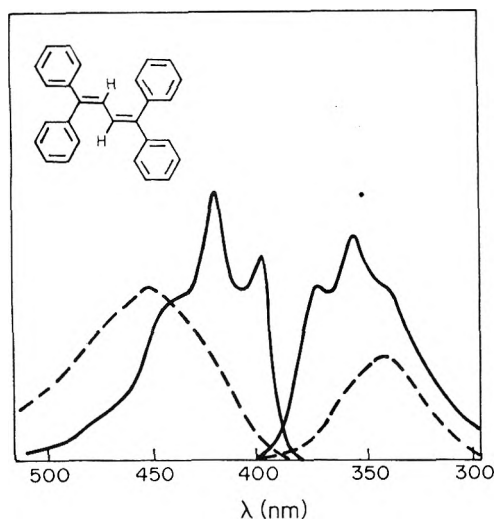


Figure 2. Absorption and emission spectra of TPB at 300 K (---) and at 77 K (—).

is prevented giving rise to an emission originating from $S'_{r,v}$; in addition, the low frequency modes will be frozen leading to a resolution of the vibrational structure corresponding to Q_v . Emission in rigid media occurs at higher energies relative to emission in fluid media.

Intramolecular Torsional Relaxation

In fluid media, molecules which have different geometric configurations in the equilibrium ground and excited states exhibit large Stokes shifts and their fluorescence spectra are diffuse. If such relaxation is prevented by a chemical bond or by rendering the medium rigid, the fluorescence maximum will shift to higher energies and the vibrational structure will be resolved. Absorption and fluorescence spectra of *trans*-1,1,4,4-tetraphenylbutadiene (TPB) in isopentane-methylcyclohexane solvent mixture at two different temperatures

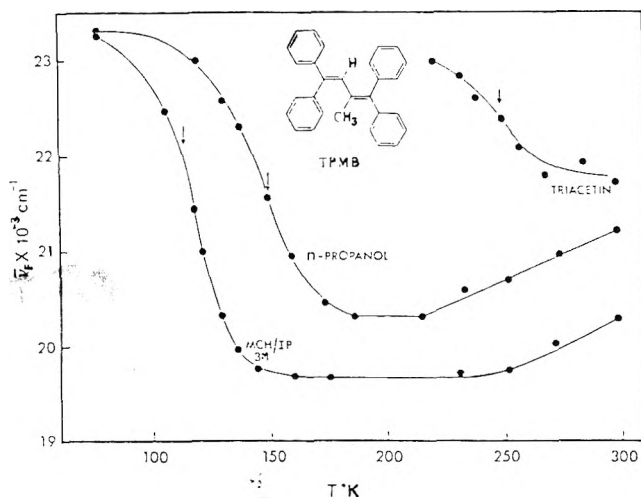


Figure 3. Effect of temperature on $\bar{\nu}_F$ the fluorescence energy maximum of TPMB in three different media. Arrows indicate the temperature at which the viscosity of the medium is 10^4 cP.

illustrate this phenomenon.¹ In Figure 2, a large blue shift of the fluorescence maximum is observed (1650 cm^{-1}) in going from a fluid medium at 300 K to a rigid glass at 77 K. Both the absorption and fluorescence spectra show a 1300-cm^{-1} vibrational structure at 77 K which disappears at room temperature. In Figure 1, Q_v may represent this 1300-cm^{-1} vibrational mode while Q_r represents θ , the angle of twist about an essential single C-C bond, probably that of butadiene. In a fluid medium, k_θ , the rate constant corresponding to intramolecular twisting relaxation (process 4 in Figure 1), is larger than k_f and fluorescence originates from the equilibrium configuration, $S'_{\theta,v}$, as represented by process 6. In a rigid medium k_θ is small compared to k_f and fluorescence originates from $S'_{\theta,v}$ as represented by process 3. It is obvious that in order to account for the observed blue shift one considers the potential energy cross section drawn along Q_r , while to account for the 1300-cm^{-1} vibrational structure one must consider the potential energy cross section drawn along that specific vibrational mode represented by Q_v .

The absorption band maximum of *trans*-1,1,4,4-tetraphenyl-2-methylbutadiene (TPMB) lies 2300 cm^{-1} at higher energies compared to TPB. This shift is due to the steric effect of the methyl group which leads the ground state configuration of TPMB to be less planar. In a fluid medium at room temperature TPMB exhibits a weak yellow emission in hydrocarbon solvent. A remarkable intensity enhancement (about 2 orders of magnitudes) and a large blue shift of 3700 cm^{-1} occurs as the sample forms a rigid glass at 77 K. To examine the dependence of fluorescence energy on viscosity and on temperature, the viscosity was varied at constant temperature using solvent mixtures and the temperature was changed for solvents that have different viscosity-temperature dependences. The results show clearly² that the fluorescence energy maximum $\bar{\nu}_F$ depends solely on the viscosity of the medium. Figure 3 shows the general increase of $\bar{\nu}_F$ upon lowering the temperature in three different solvents. The rapid increase of $\bar{\nu}_F$ occurs in a narrow temperature range which differs widely from one medium to the other. In contrast, these changes of $\bar{\nu}_F$ occur at nearly the same viscosity. The arrows in the figure mark a viscosity of 10^4 cP.

The apparent increase of $\bar{\nu}_F$ in the temperature range 220 K to room temperature in hydrocarbon solvent and in 1-propanol is not due to a viscosity change. The small viscosity change which occurs in this temperature range does not cause

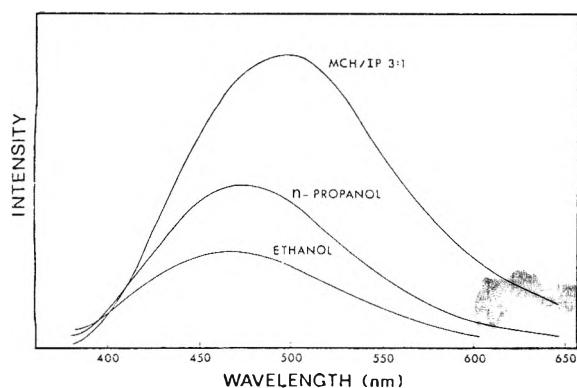


Figure 4. Emission spectra at 298 K in three solvents: MCH/IP (3:1), 1-propanol, and ethanol. The emission in MCH/IP is recorded at lower sensitivity ($\times 0.5$).

any change in $\bar{\nu}_F$ as shown by experiments where the viscosity is changed at room temperature. This effect has been interpreted² by us as a temperature-induced selective quenching where emission from the equilibrium configuration, $S'_{\theta, \nu'}$, is selectively quenched by populating the upper torsional modes which undergo more efficient internal conversion $S' \rightarrow S_0$. Emission originating from intermediate relaxed configurations occurs at shorter wavelength and will dominate the spectrum as the temperature is increased from 220 to 300 K, giving rise to the observed blue shift. Selective red quenching has been observed in other cases³ and may be common in relaxing molecular systems.

Selective red quenching may also be induced by the solvent, leading to a unique solvent effect on the fluorescence spectra of TPMB. The more polar solvent enhances internal conversion $S' \rightarrow S_0$ of completely relaxed molecules via a dipole-induced dipole solvent-solute interaction. Partially relaxed molecules are less affected, hence their shorter wavelength emission dominates. This effect is shown in Figure 4.

Fluorescence intensity in a viscosity range where $\bar{\nu}_F$ remains constant depends on both the temperature and viscosity of the medium. Lowering the temperature leads to a depopulation of molecules in the upper torsional levels of the excited state giving rise to an intensity enhancement effect with an activation energy of about 600 cm^{-1} . This corresponds to one or two quanta of torsional frequencies about a bond with a double-bond character. In addition to this, one identifies a genuine viscosity effect where the viscosity of the medium determines to some extent the effective shape of the potential energy surface. A large viscosity limits the maximum amplitude attainable by the molecule, leading to diminished overlap integrals and less efficient radiationless decay. This fluorescence enhancement effect has a solvent-dependent activation energy corresponding to those obtained from viscosity-temperature data.

Experimental results⁴ also show a large increase of the oscillator strength and a red shift of the TPMB first absorption band as the temperature is lowered as shown in Figure 5. We have interpreted these results in terms of depopulation of TPMB ground-state molecules which have several quanta of high amplitude-low frequency torsional modes and an electric-dipole transition moment that is dependent on θ , the angle of twist. This results in more planar configurations with larger conjugation, higher oscillator strengths, and smaller excitation energies at lower temperatures. The absorption intensity at a given temperature depends also on the viscosity of the medium as shown in Figure 6. This demonstrates a genuine viscosity effect on the absorption intensity of a flexible molecule

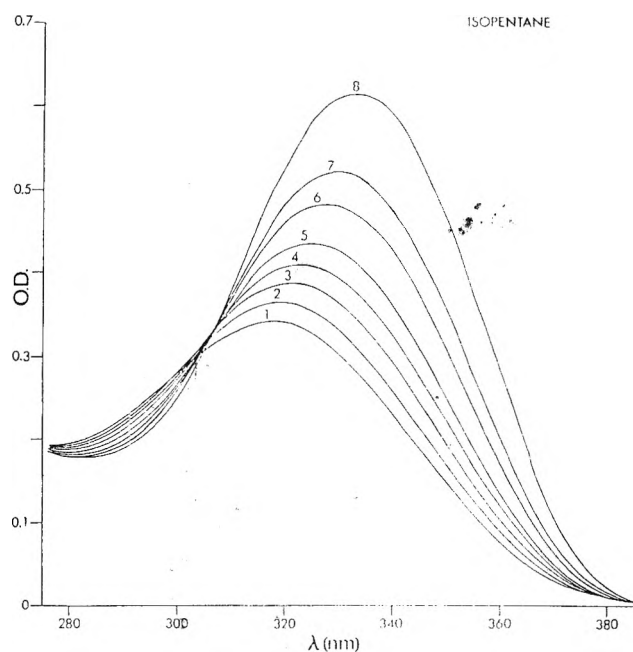


Figure 5. Effect of temperature on the absorption spectrum (uncorrected) of TPMB ($1.95 \times 10^{-5} \text{ M}$) in isopentane at (1) 297, (2) 272, (3) 248, (4) 223, (5) 200, (6) 166, (7) 146, and (8) 114 K.

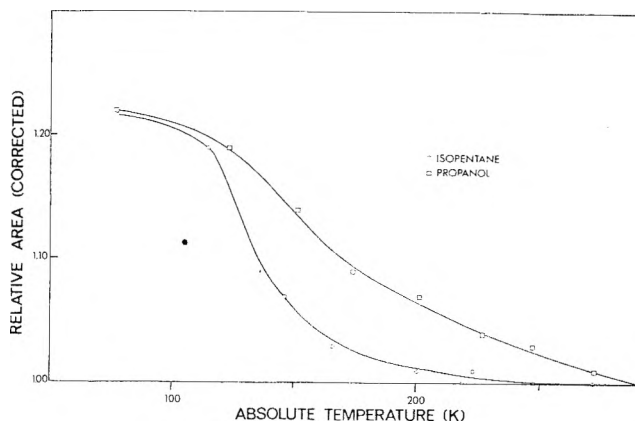


Figure 6. Corrected integrated absorption intensities at temperature T relative to that at room temperature are plotted as a function of temperature.

similar to that observed by Wald and co-workers⁵ for the spectra of visual pigments when measured in the quasicrystalline environment of the retina.

The TPMB system exhibits various effects as a result of geometric relaxation and the sensitivity of the transition moment to the viscosity and the temperature of the medium. To summarize:

- (i) The fluorescence energy maximum $\bar{\nu}_F$ undergoes a large blue shift that depends on the viscosity of the medium.
- (ii) Both a solute activation energy (which corresponds to a torsional frequency) and a solvent activation energy govern the dependence of fluorescence intensity on the temperature and viscosity of the medium in a range where $\bar{\nu}_F$ remains fixed.
- (iii) A selective red quenching effect induced by temperature and by medium polarity gives rise to an anomalous blue shift.
- (iv) Absorption intensities enhanced and red shifted as the temperature is lowered are caused by the depopulation of upper torsional levels of the ground state.

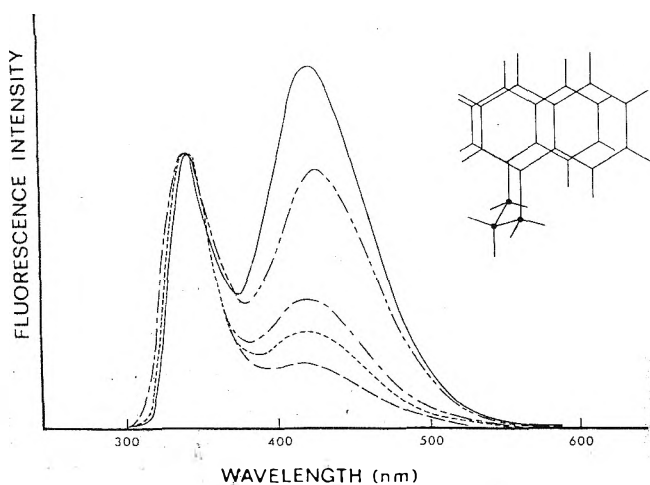


Figure 7. Effect of viscosity on the relative intensity of the monomer and excimer fluorescence bands in ethanol-glycerol mixtures. The percentage by volume of ethanol is indicated: (—) 100%, (---) 75%, (— · —) 50%, (- - -) 39%, (- -) 30%.

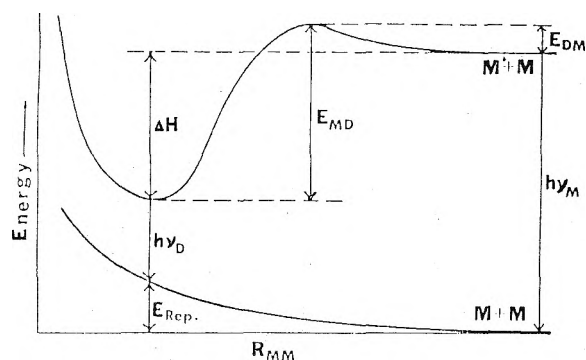


Figure 8. Qualitative potential energy curves representing excimer formation and excimer emission ν_D .

(v) Absorption intensities enhanced at higher viscosities. In a more viscous medium, the free volume is smaller and the torsional motions are more limited leading to less deformed configurations.

Intramolecular Excimer Interaction. Time-Resolved Study

Fluorescence spectra of 1,3-dinaphthylpropane in fluid solutions exhibit two bands; one band has a maximum of 340 nm and corresponds to the normal naphthalene fluorescence. The other band has a maximum at 420 nm and is attributed⁶ to an emission from an intramolecular excimer with the configuration shown in Figure 7.

The time-resolved fluorescence technique provides a powerful tool for the study of the dynamic processes involved in excimer interactions. A nanosecond pulse with an exciting band at 280 nm and with a half-width of about 4 ns was used to excite 10^{-4} M solutions of 1,3-DNP. The time development of the excimer fluorescence in the nanosecond range was obtained using a single-photon counting apparatus which consists mainly of a nanosecond pulser (Ortec 9352), time-to-amplitude converter (Ortec 457), multichannel analyzer (Nuclear Data 1100), and single-photon counting phototube (RCA 8850). Dissociation k_{MD} and association k_{DM} rate constants were derived from these data. The dissociation rate constants (10^3 – 10^4 s⁻¹) depend on the viscosity and are much lower than the ones found in intermolecular cases.⁷ Apparently this is due to the effect of the methylene chain that locks

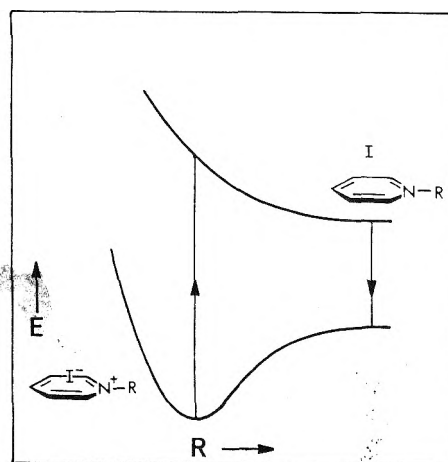


Figure 9. Potential energy curves illustrating excited-state dissociation of electron donor-acceptor ion pair.

the molecule in the excimer configuration. The activation energy (E_{DM}) for the association process (see Figure 8) was measured⁸ in ethanol to be 4.0 kcal/mol. This activation energy combines an activation required to overcome the rotational barriers of the methylene chain and activation connected with the solvent viscosity. Using this value and the rate constants obtained from time-resolved measurements one obtains an entropy activation of -10 cal mol⁻¹ deg⁻¹. This negative value is attributed to a loss of rotational degrees of freedom of both the naphthalene moieties and the methylene chain and is characteristic of thermal kinetic systems involving cyclic intermediates.

The radiative lifetime of the excimer state τ_{FD}^0 was determined by a combination of steady-state and time-dependent measurements, the value obtained was 720 ns. This result suggests that although the geometry of the excimer may be a centrosymmetric one, the excimer emission may be induced by the thermal excitation of torsional oscillation of the excimer components.⁹ There is an indication that the radiative lifetime τ_{FD}^0 increases with an increase of viscosity which supports the above mechanism of torsionally induced emission.

Excited State Dissociation of Electron Donor-Acceptor Ion Pairs

The transfer of an electron from the anion to the cation in an electron donor-acceptor ion pair may lead to excited state dissociation. In this case the fluorescence spectrum exhibits a large Stokes shift and the fluorescence lifetime is anomalously long by virtue of the much smaller transition probability from the equilibrium excited state configuration. An example of this is provided by methylpyridinium salts where a large Stokes shift ($10\,000$ – $20\,000$ cm⁻¹) and anomalously long fluorescence lifetimes (10^{-4} to 10^{-5} s) have been observed.¹⁰ In this case, the potential cross sections are drawn along R , the intermolecular separation between the anion and the cation. The ground state surface exhibits a deep minimum at small R while the excited state may exhibit a shallow minimum at larger R or may be dissociative as shown in Figure 9. This is the converse example of excimer formation. The Stokes shift decreases as the medium becomes rigid.

Solvent-Cage Relaxation

The permanent dipole moment of a molecule may change as a result of electronic excitation. This change may involve a change in the magnitude of the dipole moments, its direction, or both. Following excitation the ground state configu-

TABLE I: Fluorescence Lifetimes of 5-Dimethylaminonaphthalene-1-sulfonamide (DSA) at Room Temperature in Different Media

Solvent	Benzene	Ether	EPA	Methanol	H ₂ O	D ₂ O
τ_F , ns	13.5	12.8	17.8	14	3.5	6.2
ϕ_F	0.53	0.47	0.6	0.39	0.05	0.11
$10^{-7}k_F$, s ⁻¹	3.9	3.6	3.4	2.8	1.4	1.7
$10^{-7}k_{NR}$, s ⁻¹	3.4	4.0	2.3	4.2	26.6	13.7
$\Delta\bar{\nu}_{max}$, ^a cm ⁻¹	9 600	9 550	10 900	11 330	13 510	13 510

^a $\Delta\bar{\nu}_{max}$ is the frequency difference in cm⁻¹ of absorption and fluorescence maxima.

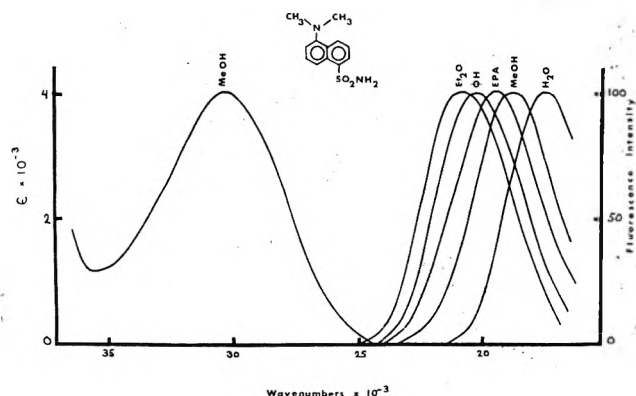


Figure 10. Room temperature absorption spectrum of DSA in methanol and fluorescence spectra in different media.

ration of the solvent cage may undergo relaxation to achieve the equilibrium excited state configuration. For a case where the dipole moment increases upon excitation a large red shift of the fluorescence energy maximum is observed proportional to the polarity of the medium. Moreover the fluorescence intensity decreases as the polarity increases. In polar media radiationless transitions leading to internal conversion $S^1 \rightarrow S^0$ are efficient, giving rise to weak emission. A solvent-deuterium isotope effect may be observed due to the importance of intramolecular solvent vibration in determining the radiationless rate constants of the solute-solvent cage complex.

A nice example demonstrating these effects is dansylsulfonamide (DSA). Room temperature absorption spectrum in methanol and fluorescence spectra in various solvents are shown in Figure 10. Fluorescence lifetimes and quantum yields were measured at room temperature in different media; these data are summarized in Table I. Both the radiative and nonradiative transition probabilities are observed to be strongly dependent on the medium. The observed fluorescence lifetime (Table I) in water is 3.5 ns, while in deuterium oxide the lifetime is about 6.2 ns.

The dansyl group acts as a convenient probe to study the local polarity of specific sites in enzymes. Dansylated lysozyme where the dansyl group is covalently attached through an amino group on the N-terminal lysine residue exhibits fluorescence spectra indicating a highly hydrophobic local environment. Polarization decay measurements¹¹ of dansylated lysozyme indicate that the fluorescence probe is rigidly locked giving rise to rotational relaxation constants of 22 and 42 ns at 27 and 22 °C, respectively. These values correspond to monomeric and dimeric enzyme molecules.

Currently we are engaged¹² in studying the fluorescence properties (spectra, lifetimes, intensities, and rotational relaxation constants) of another probe 1-anilino-8-naphthalenesulfonate, ANS, which forms a complex with α -chymotrypsin at a site different from the active site of the molecule.

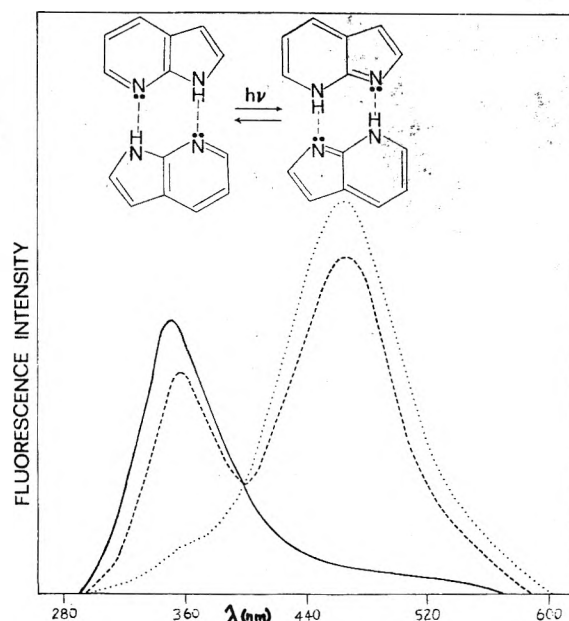


Figure 11. Time-resolved fluorescence spectra of N₁-D-7 azaindole in a 3MP matrix at 77°K: (—) 0–5 ns, (---) 10–15 ns, (···) 30–49 ns.

Nanosecond time-resolved fluorescence measurements were interpreted¹³ in terms of dipole reorientation of the solvent around the excited singlet state of the ANS molecule. The exact location of ANS in α -chymotrypsin is being examined using x-ray crystallographic techniques.

Excited State Proton Transfer. Time-Resolved Study

Solutions of 7-azaindole (7AI) in nonhydrogen bonding solvents exhibit two fluorescence bands.¹⁴ In addition to the normal violet fluorescence (F_1) in the region 320–360 nm there is a second green fluorescence (F_2) with a maximum near 480 nm. The relative intensity of F_1 and F_2 depends on concentration, excitation wavelength, and temperature. The second band F_2 was suggested¹⁴ to originate from a tautomer formed by a fast intermolecular double proton transfer reaction in the excited state of the doubly hydrogen bonded dimer as shown in Figure 11.

Since the excited state double proton transfer in 7AI dimers is too fast to follow at room temperature, the time-resolved study was performed at 77 K in 3MP solid matrix. Under these conditions virtually all 7AI molecules are present as dimers trapped in the matrix. To further slow down the photoreaction, a deuterated sample of 7AI was used where the indolic hydrogen (N_1 -H) was replaced by deuterium (N_1 -D). Time-resolved spectra of the system in the nanosecond time domain are shown in Figure 11. From the isotope effect on fluorescence spectra one calculates¹⁵ a value of 5×10^8 s⁻¹ for the rate constant for the forward double proton transfer reaction, k_{TP} .

Further analysis shows that at very low temperatures the proton transfer can take place by both thermally activated or tunneling mechanisms.

By studying the effect of temperature on the fluorescence spectra under conditions of continuous illumination a value of 500 cm^{-1} was obtained¹⁶ as the potential energy barrier for double proton transfer. It was found, however, that the relative integrated intensities of the tautomer and dimer fluorescence are the same at 77 and 4.2 K, i.e., $(k_{\text{TD}})_{77 \text{ K}} \approx (k_{\text{TD}})_{4.2 \text{ K}}$. Clearly these observations point strongly to quantum mechanical tunneling. At higher temperatures the proton transfer can take place by both thermally activated and tunneling mechanisms, while at very low temperatures tunneling may be the only reaction path.

The efficiency of proton tunneling in the 7AI dimers may be due to the coupling of the proton motions in the neighboring hydrogen bonds. The motion of the proton in one of the hydrogen bonds (single proton transfer) will create an electric field that will reduce the potential barrier for the second proton transfer. In this sense the motion of the two protons is expected to be correlated. Excited state single proton tunneling has been suggested as operating intramolecularly in the first excited state of salicylic ester.¹⁷

Acknowledgment. This work was supported by the Energy Research and Development Administration under Contract No. AT(11-1)2039.

References and Notes

- (1) M. Ashraf El-Bayoumi and F. M. Abdel Halim, *J. Chem. Phys.*, **48**, 2536 (1968).
- (2) J. Kordas and M. Ashraf El-Bayoumi, *J. Am. Chem. Soc.*, **96**, 3043 (1974).
- (3) H. Stegemeyer, *Ber. Bunsenges. Phys. Chem.*, **72**, 335 (1968).
- (4) J. Kordas, Ph. Avouris, and M. Ashraf El-Bayoumi, *J. Phys. Chem.*, **79**, 2420 (1975).
- (5) G. Wald and P. K. Brown, *Science*, **127**, 222 (1958).
- (6) Ph. Avouris, J. Kordas, and M. Ashraf El-Bayoumi, *Chem. Phys. Lett.*, **26**, 363 (1974).
- (7) J. B. Birks, *Prog. React. Kinet.*, **5**, 181 (1970).
- (8) E. A. Chandross and C. J. Dempster, *J. Am. Chem. Soc.*, **92**, 3586 (1969).
- (9) A. K. Chandra and E. Lim, *J. Chem. Phys.*, **48**, 2589 (1968).
- (10) G. Briegleb, J. Treucseni, and W. Herre, *Chem. Phys. Lett.*, **3**, 146 (1969).
- (11) D. Carr and M. Ashraf El-Bayoumi, M. Sc. Thesis, Michigan State University, 1975.
- (12) D. Johnson and M. Ashraf El-Bayoumi, to be submitted for publication.
- (13) S. K. Chakrabarti and W. R. Ware, *J. Chem. Phys.*, **55**, 5494 (1971).
- (14) C. A. Taylor, M. Ashraf El-Bayoumi, and M. Kasha, *Proc. Nat. Acad. Sci. U.S.A.*, **63**, 253 (1969).
- (15) M. Ashraf El-Bayoumi, Ph. Avouris, and W. R. Ware, *J. Chem. Phys.*, **62**, 2499 (1975).
- (16) K. C. Ingham and M. Ashraf El-Bayoumi, *J. Am. Chem. Soc.*, **96**, 1674 (1974).
- (17) H. Beens, K. H. Grellmann, M. Gurr, and A. H. Weller, *Discuss. Faraday Soc.*, **39**, 183 (1965).

Discussion

M. KASHA. It seems to me you may have some tools available to study the so-called Weber red edge effect.

A. EL-BAYOUMI. Yes, possibly so. Another thing I want to mention for a few seconds is the reverse phenomenon to an excimer formation, which is an excited-state dissociation. There are some charge-transfer complexes that become much weaker in the excited state so essentially they dissociate. This is the reverse of excimer formation; these really exhibit dramatic changes in fluorescence lifetime, because the molecules are basically different depending upon whether you trap them in the ground state configuration or you let them equilibrate in the excited state.

G. A. CROSBY. Are there any biological phenomena in the microsecond time range that are possibly susceptible to time-resolved spectroscopy? I ask this because some of the transition metal complexes we have studied luminesce in aqueous media at room temperature and might serve as probes for the microsecond domain.

A. EL-BAYOUMI. Yes, e.g., rotational relaxation of large biomolecules. The potential of using those complexes as probes in the microsecond domain is worth investigation.

P. R. CALLIS. Were you able to demonstrate a distribution of molecular environments for tetraphenylbutadiene for rigid media by excitation at different wavelengths near the absorption edge?

A. EL-BAYOUMI. Such experiments were not done.

G. KHALIL. Has the phosphorescence of azaindole (monomer and tautomer) been identified?

A. EL-BAYOUMI. The phosphorescence of the 7-azaindole monomer has been identified.

Visual Pigments. 4. Comprehensive Consideration of the Spectroscopy and Photochemistry of Model Visual Pigments

Ralph S. Becker,* Gordon Hug, P. K. Das, Arnold M. Schaffer, Takeshi Takemura, Naoto Yamamoto, and Walter Waddell

Department of Chemistry, University of Houston, Houston, Texas 77004 (Received February 17, 1976)

Publication costs assisted by the National Eye Institute

Consideration is given of the isomeric model visual pigments retinals, alkyl Schiff bases of retinals, and retinols. New room-temperature fluorescence quantum yield data are reported for some retinals and no fluorescence, $\leq 10^{-4}$, is seen in alkane solvents at temperatures down to 77 K. However, a large increase in fluorescence intensity occurs in hydroxylic solvents. The lowest singlet excited state of retinals in general in alkane solvents is believed to be principally of $^1(n,\pi^*)$ character. Both temperature- and solvent-dependent studies of retinals and Schiff bases indicate that the majority of the shifting of the long-wavelength band maxima on cooling, particularly for the Schiff bases, is environmentally not structurally caused—the 11-*cis* isomers require additional considerations. An analysis is made of the fate of the absorbed quanta in retinals and Schiff bases. New fluorescence lifetime data are presented for a Schiff base, approximately 3 ns at 77 K, and for retinal H-bonded complexes, 1.0–2.5 ns. For the Schiff bases, on the basis of quantum yield and lifetime data at 77 K, it is believed in general, that a π,π^* state with a dominantly forbidden character, 1A_g , lies below that corresponding to the strong long-wavelength absorption, 1B_u . On the basis of similar arguments and other spectral data, it is believed in general that a similar state order is valid for retinols at room temperature.

Introduction

Visual pigments are concentrated in the rods and cones of the retina. The rod pigment rhodopsin is principally responsible for vision under low light intensity (night) and is perceived by the brain in shades of gray. Color vision originates in the cone cells and they are responsible for vision under high light intensity (daylight). The rods dominate the cones by a factor of about 20. Rhodopsin extracted from rod segments is red-purple with an absorption maximum near 500 nm.

Wald and Hubbard¹ originally found rhodopsin to consist of the chromophore 11-*cis*-retinal covalently bonded to the apoprotein opsin. Although there has been considerable controversy concerning the binding site of the retinal in rhodopsin as for example ref 2 and 3, it now appears the matter is settled. The retinal is bound via a protonated Schiff base⁴ to the ϵ -amino group (terminal) of a lysine residue of opsin.³⁻⁵ The amino acid sequence of opsin is not known but the molecular weight of bovine opsin is in the vicinity of 26 000–29 000.⁶ The amino acid analysis has been determined although there is moderate variation depending upon the investigators.^{6,7} Two of the analyses show the presence of tryptophan while all show the presence of the other aromatic amino acids (plus 15 others).

The nature of the intermediates of the rhodopsin bleaching process has been discussed.⁸⁻¹⁰ The first observable intermediate at 77 K is prelumirhodopsin which has been presumed to be *all-trans*-rhodopsin.¹¹ It seems that prelumirhodopsin is a viable intermediate in the visual sequence since an absorption region present in prelumirhodopsin was observed in a 1-ps flash experiment.¹⁴ The rate of formation is $\sim 2 \times 10^{11} \text{ s}^{-1}$ (or faster) and the lifetime is about 30 ns. Primarily on the basis of the rate of formation, there is now some doubt whether prelumirhodopsin is *all-trans*-rhodopsin or

is at least formed as such in the excited state.¹⁴ Also, since only one wavelength was monitored in the picosecond experiments, any other species with an absorption at the same wavelength would be observed; *vide infra*. At liquid He temperatures, 4 K, hypsorhodopsin had been proposed as an intermediate possibly prior to prelumirhodopsin.¹² It has been suggested that this species is an unprotonated Schiff base twisted by some intermediate value around the C11–C12 double bond.¹³ This species could be an artifact relative to the visual sequence and exist only because of the temperature-viscosity conditions. The quantum yield of photobleaching of rhodopsin has been measured to be 0.67¹⁵ (presumably this is the equivalent of the total photoisomerization quantum yield).

The 11-*cis* isomer is not the only one which will bind with opsin to give a stable pigment. Both 9-*cis*- and 9,13-*cis,cis*-retinal will give isorhodopsin.¹⁶ These pigments upon irradiation ultimately give *all-trans*-retinal and opsin with a quantum efficiency of about 0.33¹⁶ (the final photoproducts from rhodopsin are the same).

The crystal structures of *all-trans*-¹⁷ and 11-*cis*-retinal¹⁸ have been determined. In *all-trans*-retinal, atoms C6 to oxygen lie in an approximate molecular plane with the C6–C7 single bond twisted about 62° from the *s-cis* conformation; see Figure 1. The 11-*cis* derivative differs by 180° around C11–C12 but also by rotation of $\sim 140^\circ$ around C12–C13 and $\sim 40^\circ$ instead of 62° around the C6–C7 single bond. Preliminary x-ray data indicate that, except for the C=O and C=N bond distances, the structures of the Schiff bases will be nearly identical with the aldehydes (C=N distance approximately 0.072 Å longer).¹⁹ The average C=C and C–C bond distances are 1.336 and 1.460 Å, respectively.^{17,18} Resonance-enhanced Raman studies show that the C=C and C–C stretching frequencies are essentially unchanged between *all-trans*-retinal and its aliphatic Schiff base.²⁰ In the protonated Schiff base, the C=C frequency is lowered.²⁰ We interpret this to

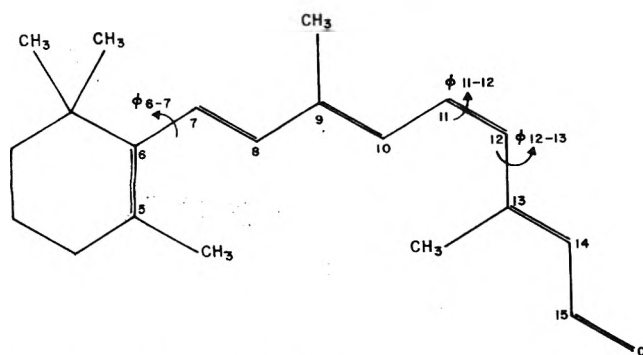


Figure 1. Structure of 11-*cis*-retinal.

indicate that there is less double-bond character and thereby a reduction in bond alternation compared with aldehyde and Schiff base.

We shall discuss the spectroscopic properties of the retinals, Schiff bases, and retinols later in appropriate sections. However, it is noted now that fluorescence has been observed from rod outer segments²¹ and several of the intermediates in the bleaching process of rhodopsin.²² Fluorescence has also been reported for rhodopsin²¹ although a later investigation designed to make such an observation was not successful.¹⁴

The remainder of the paper shall discuss separately the most currently available aspects of the retinals, Schiff bases, and retinols. Where it serves a useful purpose, interrelations among these will be developed. We shall present some new data on quantum yields of fluorescence at both 77 K and room temperature and on fluorescence lifetimes, as well as some new data on environmental effects on spectra as related to structural interpretations. A significant effort will be made to integrate published and unpublished spectral, photochemical, and theoretical data on these molecules to obtain the most up-to-date and reliable evaluation of the photophysical and chemical properties.

Experimental Section

all-trans- and 13-*cis*-retinal were obtained from Sigma Chemical Co. and 11-*cis*-retinal was a kind gift from Hoffman La Roche Co. These were used without further purification for the quantum yield studies. The 3-methylpentane (3MP) was purified by the same procedure as described previously.²³ A mixture of ether, isopentane, and ethanol (EPA) was obtained from Matheson Coleman and Bell and 2,2,2-trifluoroethanol was from Eastman Kodak Co. Concentration of all retinals for quantum yield studies was 5×10^{-5} M and the solutions were degassed by repeated freeze-pump-thaw cycles to a pressure of 10^{-5} Torr or less. Samples were prepared just prior to use under red light.

Absorption spectra were measured on a Cary Model 15 spectrophotometer. Emission spectra were done in optically flat-faced Suprasil quartz cells of 2-mm path length. Emission spectra at room temperature and some at 77 K were obtained using a single photon counting technique. An SSR Model 1110 photon counter and Model 1120 amplifier discriminator were used as well as a 0.35-M McPherson, Model EU 700, stepping motor driven grating monochromator (analyzing), a 0.25 M grating monochromator (exciting), and an EMI 9558B photomultiplier RF shielded and cooled to -75 °C, and a 1-kW Xe lamp. Slit widths were 0.75 mm (50-Å band-pass) for excitation and 1.0 mm (20-Å band-pass) for analyzing. The configuration was arranged for front-face excitation and detection.²³ The photomultiplier was calibrated with a standard tungsten lamp. Quantum yields were obtained using 9,10-

diphenylanthracene as a reference (assuming $\phi_F = 1$ at 77 K in 3MP) and the exciting lamp output was determined using a calibrated thermopile (Eppley) and an ethylene glycol solution of rhodamine B.²³

The measurement of excited-state lifetimes of the nonspecially dried principal isomeric retinals was done in 3MP at 77 K. We found that it was definitely necessary to purify the commercially available samples (Sigma) and this was done using high-pressure liquid chromatography techniques with 2% tetrahydrofuran (distilled once) in petroleum ether as a solvent.

The lifetimes of the retinals were determined using an Ortec fluorescence lifetime apparatus. The lifetimes reported in Table VI were obtained by exciting the samples with a broad band-pass (~ 25 nm) of radiation centered at 337 nm and the fluorescence was monitored at wavelengths greater than ~ 400 nm using a NaNO_2 chemical filter which eliminates the exciting light. Supplementary experiments were done on the 9-*cis* isomer by exciting at wavelengths of 340 and 380 nm and on the *all-trans* isomer by monitoring fluorescence using different filters to analyze lifetimes of different portions of the fluorescence spectrum. In both of these experiments, the variation in the conditions did not change the lifetimes of the appropriate isomer by more than 50%. Using our experimental arrangement, we found it was necessary to count for about 3 h to get adequate curves. This, of course, is potentially undesirable because photochemistry could occur. However, we examined some of the samples after 6 h of irradiation by our pulsing lamp with high-pressure liquid chromatography and found only minor amounts of other isomers present. The solutions were degassed using three or four freeze-thaw cycles with pressures down to 10^{-4} Torr.

All of the samples gave decay curves that fit well with a calculated curve that was obtained by convoluting the response of the system to the lamp with a single exponential decay constant. We should note here that *all-trans*-retinal did not give a decay curve characterized by a single decay rate constant before we purified it. There appeared to be two decays—one of about 3 or 4 ns and one of about 14 ns. It now appears that the short-lived component was due to the 13-*cis* isomer and the long-lived component was due to some unknown impurity. A very small amount of the long-lived impurity could still be seen in the purified sample, but it was so small that we were able to obtain a good fit to the experimental data even when we did not subtract the long-lived component. We also found that the 9-*cis* isomer contained an unusually large amount of the 13-*cis* isomer. In fact we found that before purification, the decay of 9-*cis* retinal was actually characteristic of 13-*cis* retinal.

Retinals

Considerable spectroscopic data are available on these molecules including (1) room- and low-temperature absorption spectra, (2) low-temperature (77 K) emission spectra and fluorescence quantum yields (ϕ_F), (3) intersystem crossing quantum yields (ϕ_{IS}) and triplet-triplet spectra at room temperature, (4) photoisomerization quantum yields (ϕ_{PI}) (primarily at room temperature but some to -60 °C), (5) lifetime of the triplet state, (6) carbon-13 and proton NMR spectra, and (7) theoretical calculations of transition energies and of potential energy curves as functions of angles of twist as well as the effect of the latter on transition energies and f number. We report here for the first time the fluorescence quantum yields of *all-trans*- and 11-*cis*-retinals at room temperature and 77 K using single-photon counting tech-

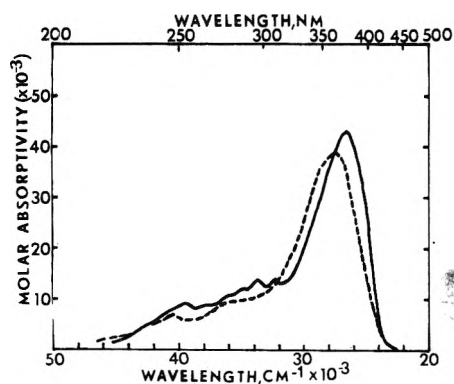


Figure 2. Absorption spectra of 9-*cis*-retinal at 298 K (---) and at 77 K (—).

niques. Also, we report the effect of solvent on the quantum yield as well as the fluorescence and absorption maxima—the similar effect of temperature is also discussed.

A typical absorption spectrum of 9-*cis*-retinal is given in Figure 2.²⁴ We have previously reported on the fact that the other retinals differ principally in the intensity of the long-wavelength band (~370 nm, 295 K) and the *cis* band (~250 nm); in addition, all of the long-wavelength band maxima are within 7 nm,^{24,25} Table I. Also, theoretical calculations of the SCF-MO-CI (single) type show good agreement exists between certain transition energies and relative intensities compared with those experimentally observed.²⁵ A complication exists regarding the existence of a potentially lower lying unobserved relatively forbidden state ($^1A_g^-$) which will be discussed later.

Although we shall discuss the Schiff bases more later, we can compare the energy of the lowest transition maximum, Table I. Theory correctly predicts the observed first transition should be blue shifted 10–15 nm compared to that for the retinals,²⁵ Table I.

In an earlier work, we noted relatively large shifts in the maximum of the long-wavelength transition of the retinals upon cooling from 295 to 77 K.²⁴ This amounted to about 1100 cm^{-1} for all except that for 11-*cis*-retinal which was larger, ~1500 cm^{-1} . In order to relate spectral changes with structures or events significant at physiological temperatures, it must be possible to discriminate between those spectral shifts caused by structural changes and those caused by environmental effects only. Although we realized that the index of refraction increased on cooling resulting from the increase in density, we anticipated this would not account for all or even perhaps most of the shift. Consequently, we have carried out an analysis to determine how much of the temperature-dependent spectral shift is caused by the environment as follows. For a polar solute in a nonpolar solvent the observed frequency shift, $\Delta\nu$, can be approximated by²⁶

$$\Delta\nu (\text{cm}^{-1}) = K \frac{n^2 - 1}{2n^2 + 1} \quad (1)$$

where K is a constant containing a sum of terms which depend only upon properties of the solute for a series of similar solvents and n is the index of refraction of the solvent. We determined the absorption spectra of *all-trans*-retinal and its *n*-butylamine Schiff base and 11-*cis*-retinal in 12 normal alkanes from *n*-pentane to *n*-hexadecane. Table II gives the results of these experiments and Figure 3 shows a plot of the band maxima of the compounds mentioned vs. $(n^2 - 1)/(2n^2 + 1)$ for 12 alkanes. From a least-squares analysis of the data, K can be determined. Assuming that the only effect of low-

TABLE I: Some Observed Experimental Band Maxima^d and Oscillator Strengths^a of Retinals and Butylamine Schiff Bases in 3MP²⁵ at 295 K

Compd	1 ^{a,c}	2 ^b (<i>cis</i> band)
<i>all-trans</i> -Retinal	369 (1.24)	247 (0.16) ^a
Schiff base	356 (1.28)	245 (.02)
9- <i>cis</i> -Retinal	362 (1.04)	247 (0.11)
Schiff base	351 (1.18)	250 (0.14)
11- <i>cis</i> -Retinal	365 (0.71)	255 (0.32)
Schiff base	350 (0.81)	250 (0.31)
13- <i>cis</i> -Retinal	364 (0.86)	251 (0.11)
Schiff base	352 (0.85)	250 (0.17)

^a Numbers in parentheses are oscillator strengths. ^b These are arbitrary designations of the transitions of reference; other transitions exist.²⁵ ^c This band red shifts 13–18 nm on cooling to 77 K for the retinals and 8–18 nm for the Schiff bases. ^d In nm.

TABLE II: First Observed Band Maxima (in nm) of *all-trans*-Retinal, 11-*cis*-Retinal, and *all-trans*-SB^a in a Variety of Solvents at Room Temperature

Solvent	n_D^b	D^b	<i>all-trans</i> -Retinal	11- <i>cis</i> -Retinal	<i>all-trans</i> -SB
<i>n</i> -Pentane	1.355	1.84	366	365	355
<i>n</i> -Hexane	1.372	1.89	368	366	356
<i>n</i> -Heptane	1.385	1.92	369	367	357
<i>n</i> -Octane	1.395	1.95	371	367	357
<i>n</i> -Nonane	1.403	1.97	372	368	358
<i>n</i> -Decane	1.410	1.99	371	370	358
<i>n</i> -Undecane	1.415	2.01	372	370	358
<i>n</i> -Dodecane	1.420	2.02	372	371	360
<i>n</i> -Tridecane	1.424	2.03	373	371	359
<i>n</i> -Tetradecane	1.427	2.04	374	372	360
<i>n</i> -Pentadecane	1.430	2.05	374	372	360
<i>n</i> -Hexadecane	1.433	2.06	374	373	360
Methanol	1.329	32.63	382		364
Acetonitrile	1.344	37.5	377		358
Ethyl ether	1.356	4.27	369		356
Acetone	1.358	20.70	375		358
Ethanol	1.359	24.30	382		364
Butanone	1.380	18.5	375		358
1,2-Dichloroethane	1.442	10.36	385		365
Chloroform	1.443	4.64	390		368
Carbon tetrachloride	1.457	2.02	380		364
Benzene	1.498	2.27	380		364
<i>o</i> -Dichlorobenzene	1.549	9.93	389		366

^a SB = Schiff base. ^b D is dielectric constant whereas D on n refers to the sodium D line.

ering temperature is to increase the index of refraction through the density change²⁷ and using the Lorentz-Lorenz equation to determine n , we can calculate from eq 1 the expected shift over a given temperature range. The results of this procedure are in the last column of Table III for the temperature change 295 to 77 K for 3MP and pentane.

These calculated environmental shifts must now be compared to the actual shifts observed for the given temperature change. Data that can be used for this comparison are given in Figures 4 and 5 and are listed in Table IV. Finally a comparison of the calculated and observed shifts are given in Table III. In view of the approximations made in the above procedure, the agreement is fairly close between the calculated environmental shift and the observed shift with temperature.

TABLE III: Comparison of Calculated and Experimental Shifts (in cm^{-1}) with Temperature^a

	Exptl	Calcd
<i>all-trans</i> -Retinal in 3MP	1160	785
<i>all-trans</i> -Retinal in <i>n</i> -pentane	870	585
<i>all-trans</i> -SB in 3MP	620	610
<i>all-trans</i> -SB in <i>n</i> -pentane	470	455
11- <i>cis</i> -Retinal in 3MP	1530	995

^a Temperature range is to 77 K for 3MP and 140 K for pentane.

TABLE IV: Experimental Red Shift (in cm^{-1}) of the First Band Maxima of Retinals and Schiff Bases upon Going from 295 to 77 K^a

	3MP ^b		EPA ^c Retinal	PMh ^{c,d} Retinal
	Retinal	SB		
All- <i>trans</i>	1160	620	880	1280
9- <i>Cis</i>	1310	1100	900	1570
11- <i>Cis</i>	1530	1360	1220	1880
13- <i>Cis</i>	1160	750	920	1340

^a In *n*-pentane *all-trans*-retinal and *all-trans*-SB are red shifted 870 and 470 cm^{-1} , respectively, upon going from 295 to 144 K. ^b Reference 25. ^c Reference 29. ^d PMh = 2-methylbutane-methylcyclohexane (5:1 v/v).

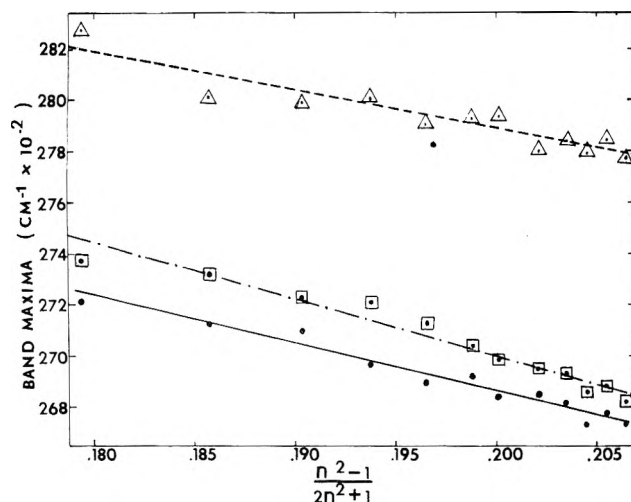


Figure 3. Plot of band maxima (ν_{\max}) of *all-trans*-retinal, *all-trans*-SB, and 11-*cis*-retinal vs. $(n^2 - 1)/(2n^2 + 1)$ for *n*-alkanes from *n*-pentane to *n*-hexadecane. See caption to Figure 4 for description of symbols.

This can be taken to mean that the temperature shift is largely due to environmental factors. However, there is enough deviation to leave open the possibility of conformational changes in the two retinals. We can look to other experimental results to resolve the question.

Another spectroscopic parameter that offers promise of being useful in determining conformational changes is the oscillator strength, f . The oscillator strengths of the 11-*cis* compounds show a definite increase with decreasing temperature.²⁵ This latter fact has been noted previously although the magnitude does seem to vary with the solvent.^{24,28,29} and two linear regions apparently exist in EPA.²⁸ On the basis of these results, we have calculated the expected changes in the

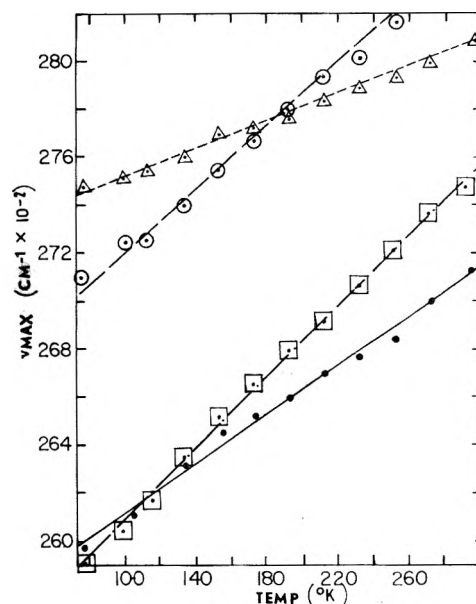


Figure 4. Plot of band maxima (ν_{\max}) vs. temperature for 3MP solutions of *all-trans*-retinal (●—), *all-trans*-SB (Δ--), 11-*cis*-retinal (□—·—), and 11-*cis*-SB (○—).

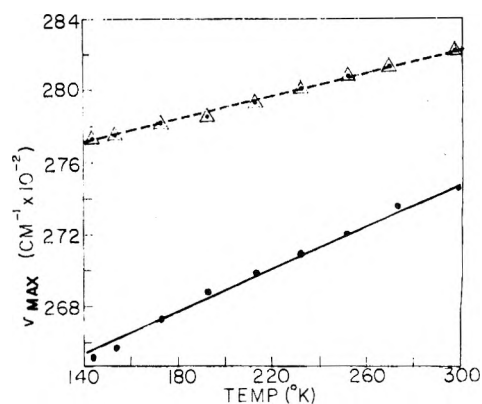


Figure 5. Plot of band maxima (ν_{\max}) vs. temperature for *n*-pentane solutions of *all-trans*-retinal (●—) and *all-trans*-SB (Δ--).

oscillator strengths (and band maxima) of two bands as a function of angle of twist around the C12-C13 single bond.²⁵

The calculation shows that the oscillator strength of the strong band of the *s-trans* conformer should be significantly greater than for the *s-cis* conformer (the intensity relation is reverse for the 250-nm *cis* band). This line of argument leads to the conclusion that the 11-*cis* isomers (retinal and Schiff base) contain an equilibrium mixture of distorted 12-*s-cis* ($\sim 130^\circ$) and 12-*s-trans* ($\sim 30^\circ$) conformers the latter of which predominate at low temperature (77 K).²⁵ In the case of the other isomers, the effects of any single-bond rotations are expected to be small.²⁵ This proposal was originally based on other arguments.^{30,31} Theoretical calculations^{30,31} as well as proton³¹ and carbon-13³² NMR studies are in agreement with this interpretation. Thus, although meaningful structural information can be obtained from temperature-dependent spectral data (with theory), care must be exercised to separate out solely environmental effects from structural ones—particularly when transitions of relatively high f number (~ 0.2) are involved.

In earlier work, fluorescence had been observed for *all-trans* and other retinals except 11-*cis* at 77 K^{23,33-36} and was re-

TABLE V: Fluorescence Spectra, Quantum Yields, and Lifetimes of Isomeric Retinals

Solute	Solvent	Temp, K	λ_{ex} , nm	$\lambda_F^{max, b}$ nm	ϕ_F^e	τ_F^f , ns
All-trans	3MP ^a	295	380		$\leq 10^{-5}$	
		77	380		$\leq 10^{-4}$	1.0
	EPA ^a	295	380	600 ^c	7×10^{-5}	
		77	380	540 ^c	8×10^{-3}	
11-Cis	CF ₃ CH ₂ OH	295	400 ^d	650 ^c	4×10^{-4}	
		295	380		5×10^{-5}	
13-Cis	3MP	77	380		$\leq 5 \times 10^{-4}$	2.0
		295	380		$\leq 10^{-4}$	
9-Cis	3MP	77	380		$\leq 10^{-4}$	2.5
		295	380		$\leq 5 \times 10^{-4}$	1.6
					$\leq 10^{-4}$	

^a 3MP and EPA are 3-methylpentane and a 5:5:2 mixture of ether-isopentane-alcohol, respectively. ^b The values are correct for the photomultiplier tube and monitoring monochromator response. ^c Error ± 10 nm at 77 K, ± 25 nm at 295 K; H bonded with water the maximum is 520 nm. ^d The absorption maximum is at 402 nm, whereas in the other solutions the value ranges from 364 to 385 nm depending upon the geometric isomer. ^e The error is estimated to be $\pm 60\%$ near 10^{-5} and $\pm 30\%$ near 10^{-3} . These are likely upper limits since emission contains some stray light. Excitation wavelength dependence of ϕ_F exists. ^f Error ± 0.2 – 0.4 ns. These are measured lifetimes of H₂O-retinal complexes (see text); see Experimental Section for procedure.

TABLE VI: Quantum Yields of Various Processes for Some Retinals Near 295 K

Compd	ϕ_F	ϕ_{IS}	ϕ_{PI}	ϕ_{PI}^a
All-trans	$\leq 10^{-5}$	HC, 0.7, ^a 0.6, ^b 0.5, ^c 0.4 ^{d,i}	HC, 0.1, ^a 0.04, ^e 0.06–0.2 ^f	HC, < 0.002 , ^a 0.17, ^g < 0.003 ^e
	EPA, 7×10^{-5}	MeOH, 0.08, ^c 0.06 ⁱ	MeOH, 0.006 ^e EtOH, 0.1 ^h	
11-Cis	HC, $\leq 5 \times 10^{-5}$	HC, 0.6, ^a 0.5 ^{d,i}	HC, 0.2, ^f 0.24, ^e 0.10 ^a	HC, 0.16 ^a 0.75, ^g 0.17 ^e
		MeOH, 0.055 ⁱ	EtOH, < 0.2 ^h MeOH, 0.04 ^e	

^a Reference 50; ϕ_{PI}^a is the triplet sensitized photoisomerization quantum yield. ^b Reference 51. ^c Reference 46. ^d Reference 52. ^e Reference 49; ϕ_{PI} data in acetonitrile. ^f Reference 48; ϕ_{PI} of *all-trans*-retinal is 0.002–0.005 at -65 °C. The ϕ_{PI} at -65 °C for *11-cis*-retinal apparently increases to 0.6 while decreasing for other *cis* isomers. ^g Reference 53. ^h Said to be similar to that in hexane for *all-trans*-retinal but less than that in hexane for *11-cis*-retinal; see ref 48. ⁱ Reference 47; excitation at 353 nm; decrease for other *cis* isomers from HC to MeOH is 4–7-fold.

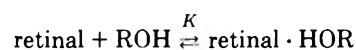
ported for *all-trans*-retinal at 295 K³⁷ (also see ref 23, footnote 21). The fluorescence at 77 K was strongest near the onset and ϕ_F showed a marked dependence upon the wavelength of excitation.^{23,33,35} It has been proposed that the $^1A_g(\pi, \pi^*)$ state is lowest in polyenes in general including the retinals.^{35,38–41} Other workers have suggested a $^1(n, \pi^*)$ state is lowest^{42–44} or degenerate with a lowest $^1(\pi, \pi^*)$.⁴⁴ However, the fluorescence emission properties did not seem compatible with a $^1(n, \pi^*)$ as the lowest state.

Very recently, absorption and emission spectral studies have been carried out on *all-trans*- and *13-cis*-retinals, *all-trans*-retinone, and two homologues of retinal.⁴⁵ These studies provide strong evidence that the $^1(n, \pi^*)$ state is the lowest excited singlet state for the two dry retinals in dry alkane solvents.⁴⁵

Fluorescence of *all-trans*- and *13-cis*-retinals is observed in ethanol (243 K), methanol (243 K), EPA (77 K), trifluoroethanol (270 K), and alkane or non-H-bonding polar solvents containing phenol. The intensity of fluorescence, the apparent ϕ_F , is dependent upon the wavelength of excitation. However, fluorescence does not occur, $\phi_F \leq 10^{-4}$, for the *dry* retinals in dry 3MP down to 77 K or in dry non-H-bonding polar solvents such as dichloromethane (to 183 K) and acetonitrile (to 238 K). Any fluorescence, $\phi_F \leq 10^{-4}$, seen thus far seems to originate only from H-bonded retinal species for which we believe a $^1(\pi, \pi^*)$ state is the lowest singlet state.⁴⁵

The degree of presence of a dependence of the apparent ϕ_F upon the exciting wavelength then has its primary origin in the presence of varying concentration of H-bonded retinal in

the presence of nonemitting non-H-bonded retinal



as in EPA, ethanol, methanol, and 3MP containing water H-bonded species.⁴⁵

In Table V, we present some new data on quantum yields and lifetimes of fluorescence. Chronologically, these data were obtained prior to the discovery of the effect of H bonding on fluorescence of the two retinals discussed above. Consequently, we must surmise that the fluorescence lifetimes are to be associated with fluorescence emissions of H-bonded H₂O-retinal species. Single-photon counting was used to determine some of the limits of ϕ_F (as for *all-trans*- and *11-cis*-retinals in 3MP) and to determine ϕ_F data in EPA and trifluoroethanol. The wavelength of excitation, λ_{ex} , was chosen to be near the absorption band maximum.

As just discussed above, there is a substantial dependence of the apparent quantum yield of fluorescence upon the H-bonding ability of the solvent. Moreover, this occurs because of changes in the excited-state order where a nonemitting principally $^1(n, \pi^*)$ state is lowest in non-H-bonding environments while an emitting principally $^1(\pi, \pi^*)$ is the lowest in H-bonding environments.⁴⁵ This change in state order could also have a consequence on the intersystem crossing quantum yield (ϕ_{IS}). The large increase in the apparent ϕ_F going from an alkane to an alcohol solvent correlates with a six- to sevenfold decrease in the apparent ϕ_{IS} for *all-trans*-

TABLE VII: Quantum Yields of Various Processes for Some Schiff Bases and Protonated Schiff Bases

Compd	Abs-Ex-F (max), ^h nm	ϕ_F^a	ϕ_{IS}	ϕ_{PI}	ϕ_{PI}^T
All-trans 77 K	364–360–500	HC, 0.05 ^b			
295 K	356–356–538	HC, <0.001 ^b	~0.008 ^c	0.002 ^d	0.02–0.05 ^d
11-Cis 77 K	368–365–560	HC, obsd			
295 K	350–350	HC, <0.001 ^b	<0.01 ^d	0.004 ^d	0.45 ^d
All-trans-H ⁺ 77 K	460–475–680	HC, 0.005 ^e			
295 K		HC, <0.001 ^e	<0.001 ^c		<0.05 ^g
11-Cis-H ⁺ 295 K	450–450	HC, <0.001 ^b	<0.01 ^f	~0.05 ^{g,i}	1 ^g

^a $\pm 30\%$, the solvent is 3MP. ^b Reference 23 and/or this work. ^c Reference 46. ^d Reference 56; value of <0.01 for ϕ_{IS} is based on lack of T-T transient absorption. ^e Reference 23 for species with $\lambda_{max} \sim 460$ nm; species with $\lambda_{max} 542$ nm has a value of 0.03. ^f The estimate for ϕ_{IS} is ours based on a limit of accuracy of detection of 0.01 noted in ref 56. ^g Reference 57, in acidified ethanol. ^h Absorption-excitation-fluorescence maxima. ⁱ Excitation wavelength dependent, ref 57.

TABLE VIII: Spectroscopic Data for Retinol in 3-MP

Compd	Abs-Ex-F (max), nm	ϕ_F^a	ϕ_{IS}^a	$\tau_{obsd},^a$ ns
All-trans 77 K	325–325–480	0.25 ^b		5 ^d (1.0) ^{a,f}
295 K	333–333–500	0.02 ^b ($\leq 10^{-5}$) ^a	0.017 ^c (~ 0.5) ^a	1.3 ^d

^a Data in parentheses are for corresponding retinal. ^b Preliminary data from ref 60; ref 61 gives the same numbers at 295 K and notes that an approximate 20-fold increase in ϕ_F occurs at 77 K for *all-trans*-retinol (ϕ_F relative to *all-trans* derivative in ref 61). ^c T. G. Truscott, private communication 1974; $\pm 25\%$. ^d Reference 60; 4.4 and ~ 16.5 ns at 295 and 77 K, respectively, ref 62 for *all-trans*-retinol in 3MP.

retinal when going from an alkane to methanol as a solvent, Tables V and VI. The term "apparent" must now be used since the ϕ_{IS} of dry retinal in a dry alkane solvent may be different from those reported, Table VI. In fact, some of the variation that exists in ϕ_{IS} data, Table VI, may be the result of differences in dryness of the combined retinal-solvent system. Despite this fact, the substantial relative increase in the apparent ϕ_F going from an alkane to alcohol solvent, Table V, is clearly not complementary in absolute magnitude even to the apparent decrease in ϕ_{IS} of ≤ 0.4 unit upon going from an alkane to methanol,^{46,47} Table VI. More concerning the effect of alcohol solvents upon ϕ data will be given shortly.

The triplet-state lifetime for all retinals is close to 10^{-5} s at 298 K.^{46,54} Phosphorescence (P) of retinals has not been observed despite efforts²³ ($\phi_P \leq 10^{-3}$). We are now in a position to consider the fate of the absorbed quanta, insofar as possible. We shall be limited in certain respects since we cannot know if ϕ_{IS} , ϕ_{PI} (photoisomerization), and ϕ_{PI}^T would be the same for dry retinals in dry alkane solvents as compared to those determined thus far, Table VI. Also, for *all-trans*-retinal some thermally reversible photochemistry (PC) has been seen at 77 K.³³ At 77 K for *all-trans*-retinal in alkane solvent with excitation at ~ 380 nm, $\phi_F \approx 0$, $\phi_{PI} \approx 0$, and $\phi_P \approx 0$, and assuming $\phi_{PC} \leq 0.05$, then 0.95 or greater of the quanta are lost via radiationless transitions. At room temperature for *all-trans*-retinal in alkane solvents with excitation at ~ 380 nm, similar results are obtained.

In the case of 11-*cis*-retinal in alkane solvent at 77 K, $\phi_F \approx 0$, $\phi_P \approx 0$, but ϕ_{PI} is really undetermined. Although ϕ_{PI} presumably increases from 298 to 208 K, at 77 K the low temperature and high viscosity very likely lower ϕ_{PI} to ~ 0.1 or less. In such a case again the major fraction, ~ 0.9 , of the absorbed quanta are radiationlessly lost. At room temperature for 11-*cis*-retinal, $\phi_F \approx 0$ and $\phi_P = 0$, and if $\phi_{PI} \approx 0.2$, Table VI, then 0.8 of the absorbed quanta are radiationlessly lost.

In hydroxylic solvents at room temperature, the apparent ϕ_{PI} and ϕ_{IS} of *all-trans*-retinal undergo large decreases, Table VI. However, again we cannot accurately analyze for the fate of the absorbed quanta since the true quantum yields are

unknown. That is, there is a mixture of H-bonded and non-H-bonded retinal in the hydroxylic solvents, and, therefore, the quantum yield data determined thus far reflect the resultant of this equilibrium mixture. For example, it has been shown that for *all-trans*-retinal in hexane, the intersystem crossing is completely quenched in the presence of 3×10^{-1} M phenol, utilizing laser flash spectroscopy and $T_1 \rightarrow T_n$ data.⁵⁵ On the basis of the foregoing result involving phenol and upon consideration of the large decrease in the observed ϕ_{IS} in methanol, it may be presumed that the ϕ_{IS} for H-bonded *all-trans*-retinal is essentially zero. More on the effect of solvent and H-bonding properties will appear elsewhere.⁵⁵ Nonetheless, since ϕ_F and ϕ_{PI} are already nearly zero and no phosphorescence exists, any further change will have only a very small absolute effect. Thus, nearly 100% of the absorbed quanta are radiationlessly lost.

In the case of 11-*cis*-retinal in methanol at 295 K, radiationless losses increase to ~ 0.95 from ~ 0.8 in an alkane solvent. The apparent ϕ_{IS} is dramatically decreased to 0.055, Table VI, in methanol.

In the case of the other *cis* isomers in an alkane solvent at 295 K, $\phi_F \approx 0$, Table V, $\phi_P = 0$, and $\phi_{PI} \approx 0.2$,⁴⁹ so the general results are very similar to 11-*cis*-retinal. In hydroxylic solvents, on the basis of ϕ_{PI} data⁴⁹ and ϕ_F values comparable to the *all-trans*- and 11-*cis*-retinals, Tables V and VI, there again will be a significant increase in the radiationless losses compared to those of a hydrocarbon solvent.

Schiff Bases

Table I compares some transitions for some alkylamine Schiff bases with retinals—again note that blue shift which is in agreement with theoretical predictions.²⁵ Table VII gives some spectroscopic data for Schiff bases and protonated Schiff bases. The fluorescence maxima are blue shifted 50–100 nm compared with those of the H-bonded retinals. No photochemistry has been observed.

For the *all-trans* Schiff base at room temperature, $\phi_F \approx 0$ and $\phi_{PI} \approx 0$, Table VII, and phosphorescence has not been observed; however, on the basis of the value of ϕ_{IS} , $\phi_P \approx 0$. The

protonated Schiff base has similar properties. In both of the foregoing compounds, it is presumed that ϕ_F is essentially not wavelength dependent as verified (to 300 nm) in general at 77 K ($\pm 30\%$).²³

New measurements on the fluorescence lifetimes of the 9-cis *n*-butylamine Schiff base give approximately 3 ns (in 3MP) at 77 K. From $\phi_F = 0.015$,²³ the natural lifetime is 200 ns. The natural lifetime calculated from the integrated absorption of the long-wavelength intense transition ($\lambda_{\max} \sim 364$ nm) is ~ 3 ns. It appears that the state corresponding to the strongly allowed transition, 1B_u , is not the state from which emission occurs. A more weakly allowed state of principally 1A_g character could be the emitting state.

In view of the fact that protonated Schiff bases should be good models for rhodopsin, we have considered several aspects related to them. The pK_a values of the ground and excited states of the all-trans protonated Schiff base are 7 and ~ 16 , respectively.¹³ On the basis of calculations of the nitrogen charge density, the corresponding 11-cis derivative is expected to be similar. Calculations of the nitrogen charge density as a function of angle of twist around C11–C12 show that the nitrogen charge density in the excited 1B_u and ${}^1A_g^-$ states becomes less than that of the ground state near 80 and 120°.¹³ This suggests the possibility that the proton could come off during isomerization and go onto the protein. When reprotonation occurs, it would be most significant if the proton came from a different site of the protein. In such a case, this could act as the trigger for unfolding of the protein.

We have previously noted the existence of a new protonated species in addition to that with a λ_{\max} of ~ 450 nm—the λ_{\max} is ~ 540 nm.^{23,58,59} This can be observed with both all-trans^{23,58} and 11-cis Schiff bases⁵⁹ and with HBr⁵⁹ as well as HCl.^{23,58,59} Based upon the experimental conditions^{23,58,59} and theoretical calculations,⁵⁹ the new species is believed to be a protonated Schiff base where the HCl or HBr molecules are interacting (via the relatively negative halide ends) with the relatively positive carbons of the polyene chain.⁵⁹ The energy of the lowest observed transition is sensitive to the distance and intensity of the negative charge (relative to the polyene carbons) as well as the particular polyene carbon(s) chosen. This has implications regarding the geometry of a model for rhodopsin where negative charges of the protein are positioned near the polyene.

Retinols

The retinols are alcohols and have one double bond less than the retinals and Schiff bases. Because of the foregoing, the long-wavelength absorption maxima are blue shifted to about ~ 325 nm (~ 365 nm for retinals). Table VIII summarizes some of the spectroscopic data for some retinols. The fluorescence quantum yields^{60,61} are very much greater at 77 K than for the H-bonded retinals while, at room temperature, the difference is still even greater. The ϕ_F values of the retinols do decrease 20–35-fold from 77 to 295 K.

For the retinols, ϕ_F has no dependence on the wavelength of excitation at 295 or 77 K⁶⁰ (in marked contrast to the retinals). The ϕ_{IS} appears to be very low, ~ 0.02 , Table VIII, and no ϕ_{PI} values appear to be available. Particularly because the latter data are absent, no really accurate analysis of the fate of absorbed quanta can be made. Nonetheless, unless all-trans-retinol is very different from other all-trans compounds, ϕ_{PI} can be expected to be quite small, perhaps ~ 0.05 .

It has been noted that at 295 K there is a considerable discrepancy between τ_0 (natural radiative lifetime) obtained using observed lifetimes and ϕ_F data and that obtained from

the integrated absorption of the strong long-wavelength absorption band.⁶² Actually at 77 K, the τ_0 values calculated in these ways are less different. One explanation for the difference appears to rely on changes in geometry within various vibrational sublevels and the relative absorption–emission oscillator strengths of these levels.⁶² It is also possible that if a forbidden state principally of ${}^1A_g^-$ character is lowest, then the τ_0 calculated from the integrated absorption would not be appropriate to the emitting state; indeed, the τ_0 would be predicted to be considerably shorter than measured. We⁶³ have attempted to determine the state ordering by investigating the effect of the index of refraction on the location of the maxima of both the strong long-wavelength absorption band and the fluorescence. If the change in the dipole moment is small upon excitation, then the shift in the maximum can be expressed as

$$\Delta\nu_{A,F} (\text{cm}^{-1}) = K'L \frac{n^2 - 1}{2n^2 + 1} \quad (2)$$

where K' is a constant associated with the solute and contains the oscillator strength of the transition, $\Delta\nu_{A,F}$ is the shift of the absorption (A) and fluorescence maxima (F), and L is the weighted mean wavelength of the solvent.²⁶ A plot of $(n^2 - 1)/(2n^2 + 1)$ vs. $\Delta\nu_{A,F}$ for all-trans-retinol over a broad range of n indicates that the oscillator strengths of the emitting and strongly absorbing state, 1B_u , are different.⁶³ This result indicates that it is possible that a relatively forbidden state, principally of ${}^1A_g^-$ character, is below the lowest allowed state, 1B_u . This plus the lifetime considerations, vide supra, strongly suggests that an ${}^1A_g^-$ state is the lowest excited state in the retinols, at least for the all-trans isomer at 295 K.

It is worth noting that we have strong indication that all-trans-retinol forms thermally reversible polymers (dimers) upon cooling from 295 and 77 K in alkane hydrocarbons.⁶⁰ This occurs to concentrations as low as 2×10^{-6} M. This would warn us to be precautious regarding interpretation of the significance of lifetime and quantum yield data at 77 K in such solvents.

Perspective

The foregoing considerations even though not complete, clearly demonstrate that considerable spectroscopic knowledge is now at hand for certain model visual pigments. In many respects these results lead more to the understanding of vision regarding what it is not rather than what it is. The nature of the primary photoproduct of rhodopsin is obscure because of the time scale. On the picosecond scale, it appears as if the C11–C12 double bond is not completely isomerized.¹⁴ The product was called preluorhodopsin,¹⁴ nominally meaning C11–C12 double bond isomerization, but only one absorption wavelength was monitored. Regardless, the real identity of the “first” photoproduct on any time scale is obscure, if known at all.

In the case of retinols, Schiff bases and protonated ones, there are still some questions on state ordering regarding low-lying π, π^* states. It seems quite certain that for retinols in general, a ${}^1(n, \pi^*)$ state is lowest in dry alkanes. The low-lying π, π^* ones may be highly mixed. It appears likely that a ${}^1(\pi, \pi^*)$ with a dominant 1A_g character is generally lowest in Schiff bases of retinals, protonated Schiff bases, and the retinols at 295 K. This does not mean exceptions are not possible particularly for the 11-cis isomer because of s-cis,s-trans conformers but will be true in general. The predominant character of the lowest excited singlet or triplet state may be important regarding isomerization since the bonding char-

acter, single-double, might be of significant difference for A_g , B_u , and $(n\pi^*)$. However, it must be kept in mind that state crossing could occur while twisting at relatively small angles so that the lowest excited singlet state observed spectroscopically may not be the most important one from the point of view of the photoisomerization. Certainly also the findings of s-cis,s-trans conformers in the 11-cis isomers (retinal and Schiff base at least) and a new species absorbing at wavelengths comparable to those of rhodopsin (and prelumirhodopsin) are meaningful steps toward understanding the visual process. Nonetheless, it is clear from all of the evidence that new model systems will have to be developed before definite ideas on the photochemistry and mechanism of the reaction sequence in vision are understood.

NOTE ADDED IN PROOF: In the case of the retinals, it has been found that (1) a state of principally $^1(n, \pi^*)$ character is lowest in alkanes, (2) a state of principally $^1(\pi, \pi^*)$ is lowest in H-bonded retinals, and (3) that an equilibrium mixture of non-H-bonded and H-bonded retinal exists in the presence of hydroxylic solvents, *vide supra* and ref 45. This causes the answers to questions in the Discussion regarding the reasons for the excitation wavelength dependence of the fluorescence quantum yield to be largely modified with the basis being that as described in the section on Retinals, *vide supra*. Although there is still the possibility of some dependence arising from photochemical effects, it will make only a very minor contribution.

Acknowledgment. We wish to acknowledge the additional contribution of Tsuguo Yamaoka to the understanding of this problem. This work was supported to a considerable extent by Grant R01-EY-00875 of the National Institutes of Health and, in addition, by a grant from the Robert A. Welch Foundation.

References and Notes

- Hubbard and G. Wald, *J. Gen. Physiol.*, **36**, 269 (1952).
- R. P. Poincelot, P. G. Millar, R. L. Kimbel, and E. W. Abrahamson, *Biochemistry*, **9**, 1809 (1970), and references therein.
- W. J. De Grip, S. L. Bonting, and F. M. Daemen, *Biochem. Biophys. Acta*, **303**, 189 (1973), and references therein.
- A. R. Oseroff and R. H. Callender, *Biochemistry*, **13**, 4243 (1974).
- D. Bownds, *Nature (London)*, **216**, 1178 (1967).
- H. J. A. Dartnall, Ed., *Handb. Sens. Physiol.*, **7**, Part 1, 122-145 (1972).
- J. E. Shields, E. C. Dinovo, R. A. Henriksen, R. L. Kimbel, and P. G. Millar, *Biochem. Biophys. Acta*, **147**, 238, (1967); J. Heller, *Biochemistry*, **7**, 2906 (1968); H. Shichi, M. S. Lewis, F. Irreverre, and A. L. Stone, *J. Biol. Chem.*, **244**, 529 (1969); M. Azuma and Y. Kito, *Annu. Rep. Biol. Works, Fac. Sci., Osaka Univ.*, **15**, 59 (1967).
- T. Yoshizawa and G. Wald, *Nature (London)*, **197**, 1279 (1963).
- R. G. Matthews, R. S. Hubbard, P. K. Brown, and G. Wald, *J. Gen. Physiol.*, **47**, 215 (1963).
- E. W. Abrahamson and S. E. Ostroy, *Prog. Biophys. Mol. Biol.*, **17**, 179 (1967).
- T. Yoshizawa and G. Wald, *Nature (London)*, **197**, 1279 (1963).
- T. Yoshizawa, *Handb. Sens. Physiol.*, **7**, Part 1, 146-179 (1972).
- A. N. Schaffer, T. Yamaoka, and R. S. Becker, *Photochem. Photobiol.*, **21**, 297 (1975).
- G. E. Busch, M. L. Applebury, A. A. Lamola, P. M. Rentzepis, *Proc. Natl. Acad. Sci. U.S.A.*, **69**, 2802 (1972).
- H. J. A. Dartnall, *Vision Res.*, **8**, 339 (1968).
- R. Crouch, V. Purvin, K. Nakanishi, and T. Ebrely, *Proc. Natl. Acad. Sci. U.S.A.*, **72**, 1538 (1975).
- T. Hamanaka, T. Mitsui, T. Ashida, and M. Kakudo, *Acta Crystallogr., Sect. B*, **28**, 214 (1972).
- R. D. Gilardi, I. L. Karle, and J. Karle, *Acta Crystallogr., Sect. B*, **28**, 2605 (1972).
- T. Hamanaka, private communication, 1974.
- M. E. Heyde, D. Gill, R. G. Kilponen, and L. Rimai, *J. Am. Chem. Soc.*, **93**, 6776 (1971).
- A. V. Guzzo and G. L. Pool, *Science*, **159**, 312 (1968).
- A. V. Guzzo and G. L. Pool, *Photochem. Photobiol.*, **9**, 565 (1969).
- W. H. Waddell, A. M. Schaffer, and R. S. Becker, *J. Am. Chem. Soc.*, **95**, 8223 (1973).
- R. S. Becker, K. Inuzuka, and D. E. Balke, *J. Am. Chem. Soc.*, **93**, 38 (1971).
- A. M. Schaffer, W. H. Waddell, and R. S. Becker, *J. Am. Chem. Soc.*, **96**, 2063 (1974).
- E. G. McRae, *J. Phys. Chem.*, **61**, 562 (1957).
- The density of the solvent as a function of temperature is calculated from an empirical equation given by R. R. Dreisbach, "Physical Properties of Chemical Substances", Dow Chemical Co., Midland, Mich., 954.
- L. Jurkowitz, J. N. Loeb, P. K. Brown, and G. Wald, *Nature (London)*, **184**, 614 (1959).
- W. Sperling, "Biochemistry and Physiology of Visual Pigments" H. Langer, Ed., Springer-Verlag, New York, N.Y., 1973, p 19.
- B. Honig and M. Karplus, *Nature (London)*, **229**, 558 (1971).
- R. Rowan, A. Warshel, B. D. Sykes, and M. Karpus, *Biochemistry*, **13**, 970 (1974).
- R. S. Becker, S. Berger, D. K. Dalling, D. M. Grant, and R. J. Pugmire, *J. Am. Chem. Soc.*, **96**, 7008 (1974).
- R. S. Becker, K. Inuzuka, J. King, and D. E. Balke, *J. Am. Chem. Soc.*, **93**, 43 (1971).
- D. E. Balke and R. S. Becker, *J. Am. Chem. Soc.*, **89**, 5061 (1967).
- R. L. Christensen and B. E. Kohler, *Photochem. Photobiol.*, **19**, 401 (1974).
- P. S. Song, Q. Chae, M. Fujita, and H. Baba, *J. Am. Chem. Soc.*, **98**, 819 (1976).
- E. W. Abrahamson and S. M. Japar, *Handb. Sens. Physiol.*, **7**, Part 1, 31 (1972).
- K. Schulten and M. Karplus, *Chem. Phys. Lett.*, **14**, 305 (1972); B. S. Hudson and B. E. Kohler, *ibid.*, **14**, 299 (1972).
- R. L. Christensen and B. Kohler, *J. Chem. Phys.*, **63**, 1837 (1975).
- R. L. Christensen and B. E. Kohler, *Photochem. Photobiol.*, **18**, 293 (1973).
- M. Karplus, R. M. Gavin, and S. A. Rice, *J. Chem. Phys.*, **63**, 5507 (1975).
- L. J. Weimann, G. M. Maggiora, and P. E. Blatz, *Int. J. Quantum Chem., Quantum Biol. Symp.*, **No. 2**, 9-24 (1975).
- W. A. Dawson and E. W. Abrahamson, *J. Phys. Chem.*, **66**, 2542 (1962); J. R. Weisenfeld and E. W. Abrahamson, *Photochem. Photobiol.*, **8**, 487 (1968).
- K. Inuzuka and R. S. Becker, *Bull. Chem. Soc. Jpn.*, **45**, 1557 (1972).
- T. Takemura, P. K. Das, G. Hug, and R. S. Becker, *J. Am. Chem. Soc.*, in press.
- M. M. Fischer and K. Weiss, *Photochem. Photobiol.*, **20**, 423 (1974).
- R. V. Bensasson and E. J. Land, private communication, 1976.
- A. Kropf and R. Hubbard, *Photochem. Photobiol.*, **12**, 249 (1970).
- Other work [W. H. Waddell, R. Crouch, K. Nakanishi, and N. J. Turro, *J. Am. Chem. Soc.*, **98**, 4189 (1976)] indicates a large decrease in ϕ_{PI} going from HC to MeOH, Table VI. This indicates an even increased dominance of radiationless processes to the ground state although the specific excited state is not identifiable.
- T. A. Rosenfeld, A. Alchalel, and M. Ottolenghi, *J. Phys. Chem.*, **78**, 336 (1974).
- R. Bensasson, E. J. Land, and T. G. Truscott, *Photochem. Photobiol.*, **17**, 53 (1973).
- R. Bensasson, E. J. Land, and T. G. Truscott, *Photochem. Photobiol.*, **21**, 419 (1975).
- R. A. Raubach and A. V. Guzzo, *J. Phys. Chem.*, **77**, 889 (1973).
- A. Azerad, R. Bensasson, M. B. Cooper, E. A. Wainne, and E. J. Land, "Excited States of Biological Molecules", J. B. Birks, Ed., Wiley, London, in press.
- R. S. Becker and R. Bensasson, submitted for publication.
- T. Rosenfeld, A. Alchalel, and M. Ottolenghi, *Photochem. Photobiol.*, **20**, 121 (1974).
- A. Alchalel, B. Honig, M. Ottolenghi, and T. Rosenfeld, *J. Am. Chem. Soc.*, **97**, 2161 (1975).
- W. Waddell and R. S. Becker, *J. Am. Chem. Soc.*, **93**, 3788 (1971).
- W. Waddell, A. Schaffer, and R. S. Becker, in preparation.
- R. S. Becker, T. Yamaoka, N. Yamamoto, and T. Takemura, in preparation.
- A. J. Thomson, *J. Chem. Phys.*, **51**, 4106 (1969).
- J. P. Dalle and B. Rosenberg, *Photochem. Photobiol.*, **12**, 151 (1970).
- R. S. Becker, A. Schaffer, T. Yamaoka, and T. Takemura, in preparation.

Discussion

R. M. HOCHSTRASSER. I have a short question and a comment. What is your interpretation of the wavelength dependence of the fluorescence quantum yield for *all-trans*-retinal?

Recently Drs. David Narva and A. Nelson in my laboratory have studied the spectra of transients produced immediately following excitation of retinal with a 353-nm, 6-ps pulse. The excited singlet state absorption decays away in tens of picoseconds, being replaced by the well-known triplet-triplet absorption. These are experiments at 300 K in a hydrocarbon solvent. The identification of the fast transient as excited singlet is assumptive. Are these observations consistent with your quantum yield measurements?

R. S. BECKER. Yes. You mentioned that yesterday; I think that is consistent with our data. At low temperature we have a lifetime (measured) of about 1 ns. If we changed the quantum yield and went back up (we would have to estimate it), it would be about 10 ps. I think you said you found 10–30 ps. I think it's very comparable.

We have proposed before and we still propose that the wavelength dependence is photochemical in nature, that the aldehyde is unique in that respect. The product, for example, could be a photocyclization, which is known to occur in the β -ionone series, for example. That would not happen in the nitrogen ones; it would not happen in the alcohols; it would not happen in the protonated Schiff bases. Retinal is very unique from that point of view. It is a photochemical phenomenon that is competing with internal conversion among the vibrational levels of the first excited singlet. We have seen this before in other molecules where the rate constants for photochemistry can be as fast as internal conversion; they can be up around 10^{12} .

R. L. CHRISTENSEN: You mentioned that in the photochemistry associated with vision it doesn't matter which electronic state (1A_g or 1B_u) is involved. On the other hand, you have shown us several pictures of potential energy diagrams and have made arguments based on these for various details of polyene excited states such as the movement of the proton on and off the protonated Schiff base models.

I would think that these details would be very sensitive to which electronic state is involved. How do you reconcile this?

R. S. BECKER. We get the same potential energy diagrams for both 1A_g and 1B_u . The calculations have been optimized for both the ground and excited states.

R. L. CHRISTENSEN. You have ascribed retinal's wavelength dependent quantum yield to photochemistry from vibronic excited states. There seems to be no evidence, however, for photochemical changes which have yields approaching the fluorescence quantum yield "lost" on the high energy side of the absorption. I think that intersystem crossing between $n\pi$ and $\pi\pi$ singlets and triplets provides a better explanation for the observations.

R. S. BECKER. The photochemical product may thermally relax and thus not be detected. We also have detected small changes in the fluorescence of irradiated samples. At low temperature one can actually see a new fluorescence arise as irradiation continues. If you warm it up and then cool it back down, that all disappears. I'm afraid what may be happening at room temperature is that it may be photochemically going forward and thermally going backward so fast you don't even see it. But you can see the photoproducts at low temperatures.

Model Systems for Photosynthetic Energy Conversion

Gordon Tollin

Department of Chemistry, University of Arizona, Tucson, Arizona 85721 (Received February 4, 1976)

Energy conversion in photosynthesis is known to proceed via light-induced one-electron-transfer reactions involving chlorophyll and electron donors and acceptors. Although the chemical identities of all of the components have not as yet been elucidated, considerable evidence has been accumulated which points to quinones (Q) as primary electron acceptors in both green plants and bacterial photosynthesis. Furthermore, it has been established that the initial photoprocess leads to the formation of a chlorophyll cation radical (C^+). The research described in this paper has as its goal the elucidation of the molecular-electronic mechanism of chlorophyll participation in photosynthesis. The approach used is to investigate model photoreactions in solution (mainly in alcohols) which lead to quinone reduction and chlorophyll oxidation. Electron spin resonance spectroscopy and laser flash photolysis have been the major techniques utilized in these studies. The following reactions have been observed. (a) The first is photoproduction of C^+ in solution in the absence of added electron acceptors. This is a low quantum yield reaction which proceeds via the lowest excited singlet state. Bacteriochlorophyll also undergoes this reaction, whereas pheophytin does not. (b) The second reaction observed is one-electron phototransfer between the chlorophyll lowest triplet state and quinones to yield a radical pair (C^+Q^-). This may either recombine or separate. The C^+ formed upon separation is unstable and either undergoes reverse electron transfer with Q^- or reacts with hydroxylic compounds to regenerate chlorophyll. The excess Q^- species disproportionates. Both bacteriochlorophyll and pheophytin are also able to react with quinones in this manner. The quenching of the chlorophyll lowest singlet state by quinones does not, however, lead to detectable radical formation. These reactions seem to provide acceptable models for certain aspects of photosynthetic energy conversion, and thus elucidation of their detailed mechanisms should lead to useful insights into the nature of the biological process.

Introduction

The essence of photosynthesis is a light-driven transfer of electrons against an electrochemical gradient which results in the conversion of electromagnetic energy into chemical energy. The transduction element in this system is, of course, chlorophyll. The bulk of the chlorophyll in plants serves a light-gathering function, with the subsequent nonradiative transfer of the absorbed energy to specialized chlorophyll molecules located within a so-called reaction center. Upon arrival of this energy, a one-electron-transfer process occurs leading to the oxidation of an electron donor and the reduction of an electron acceptor.

Two reaction centers are known to participate in green plant photosynthesis. One of these is located on the water oxidation (oxygen evolution) side of the electron-transport system (photosystem II; PSII) and the other on the pyridine nucleotide reduction side (photosystem I; PSI). The reaction center chlorophyll of PSII is usually designated as P_{680} , and that of PSI as P_{700} , based upon the wavelengths at which spectral changes can be observed which correlate with the functioning of these species. The immediate electron donor to P_{680} is unknown; the acceptor is probably plastoquinone, a *p*-benzoquinone derivative.^{1,2} The donor to P_{700} is probably plastocyanin (a copper protein), or possibly cytochrome *f* (a heme protein). The electron acceptor is uncertain, although it is probably a nonheme iron protein.³

The situation in the photosynthetic bacteria is somewhat simpler than in green plants. Here only a single photosystem is most likely operative which resembles PSI in its properties. The reaction center bacteriochlorophyll has been designated as P_{870} . The electron donor to P_{870} is a cytochrome; the electron acceptor is either ubiquinone (another *p*-benzoquinone analogue) or a nonheme iron protein, or perhaps a complex containing both of these species.^{4,5}

A great deal of evidence has been accumulated⁶ which demonstrates that the light reaction of PSI and its bacterial counterpart involves the intermediate formation of a chlorophyll cation radical (C^+) as a consequence of a one-electron transfer to the primary acceptor. This is rapidly followed by the reduction of C^+ by the primary donor. The situation in PSII is not quite as clear, but a similar mechanism is believed to be operative.⁷ An excellent source of information concerning the primary photochemistry of photosynthesis can be found in ref 8.

It is clear from the above that the basic phenomenon underlying energy conversion in photosynthesis is the coupling of photon absorption to one-electron transfer. Thus the critical question is: What are the molecular-electronic mechanisms by which this coupling is achieved in the two photosystems? The approach to this question which is utilized in this laboratory has been to study model systems involving the interaction of chlorophyll with electron donors and acceptors in solution. Much of the work which we have done thus far has used quinones and hydroquinones as donor and acceptor species. Implicit in such an approach is the assumption that one can in fact devise models which are relevant to chlorophyll function in the biological environment. As will be demonstrated below, we feel that this requirement has been reasonably met. It is also important to point out that, in our current state of relative ignorance concerning the ultrastructure of the photosynthetic apparatus, no simple model can hope to duplicate all of the *in vivo* properties of chlorophyll. The best that can one can do is to formulate general principles concerning chlorophyll photophysical and photochemical properties and to utilize these to interpret and explain the results obtained from *in vivo* studies. As chemists, we have held the view that the means by which chlorophyll functions in the primary energy conversion steps of photosynthesis must be mirrored in the molecular-electronic

properties of the isolated molecule. This is, in fact, a common occurrence in biology, as is amply demonstrated by substances such as flavin, pyridine nucleotide, thiamine, heme, and pyridoxal which function as coenzymes or prosthetic groups in a variety of enzyme systems and whose properties when free in solution show many analogies to their biological roles. It is well-known that, in these cases, binding to specific proteins serves to enhance these inherent properties and to direct them toward specific biochemical goals. It is not unreasonable to expect a similar situation to exist in photosynthesis.

Experimental Section

Techniques of sample preparation,⁹ ESR spectroscopy,¹⁰ NMR spectroscopy,¹¹ and picosecond laser photolysis¹² have been described previously. Laser photolysis in the nanosecond time domain utilized a Avco Everett (Model C950) pulsed nitrogen laser to pump a conventional untuned dye laser which consisted of a 10^{-4} M benzene solution of 2,5-bis(2-(5-*tert*-butylbenzoxazolyl)thiophene)) (BBOT). Stimulated emission by BBOT provided a 10-ns pulse (at 436 nm) of maximum energy approximately 0.1 mJ. The sample solutions were accommodated in rectangular 1-cm Pyrex cells (with degassing side arms). Appropriate cutoff filters were used to protect the samples against decomposition by the analyzing beam (75-W xenon arc lamp). Both the excitation and analyzing beam were focused on the sample cell through a 0.2-mm aperture. A Jarrel-Ash (Model 82410) monochromator was used for dispersion of the analyzing beam. An RCA 1P28 photomultiplier tube (wired for fast signal response) was used as a detector. The signal obtained from the photomultiplier was coupled to a Tektronix 7904 scope through a Tektronix 7A19 plug-in. Horizontal sweep was provided by a Tektronix 7B92 time base plug-in.

Results and Discussion

Upon steady-state illumination of deoxygenated alcohol solutions of chlorophyll and various quinones at room temperature in an ESR spectrometer, resonance spectra are obtained¹⁰ which are clearly due to the formation of the corresponding semiquinone anion radicals ($Q^{\cdot-}$). The wavelength dependence of signal formation demonstrates that chlorophyll absorption is involved.¹⁰ Under these conditions, no ESR signal due to $C^{\cdot+}$ formation can be observed. The $Q^{\cdot-}$ signal decays completely when the light is extinguished and kinetic measurements show that disproportionation is the decay mechanism.⁹ No permanent optical spectral changes occur in the chlorophyll absorption bands even after prolonged illumination. Quenching experiments utilizing oxygen and β -carotene demonstrate that $Q^{\cdot-}$ formation proceeds via the lowest triplet state of chlorophyll.¹³

At temperatures below about -50 °C, an ESR signal due to $C^{\cdot+}$ begins to become detectable.¹⁴ The formation of this species occurs simultaneously with and independently of $Q^{\cdot-}$ formation. Quenching studies indicate that the chlorophyll-excited-singlet state is the intermediate in this process. $C^{\cdot+}$ production will proceed in the absence of quinone as well and is thus probably due to direct electron photoejection, although we have not observed the solvated electron in this system.

Pheophytin (chlorophyll minus the central magnesium atom) behaves similarly to chlorophyll except that no steady-state photoproduction of $Phe^{\cdot+}$ can be seen. Bacteriochlorophyll will also sensitize quinone photoreduction as well as generate $BChl^{\cdot+}$ upon illumination. With this latter pigment we have observed an interesting spin polarization effect in dry acetone at low temperatures.¹⁵ As one increases

the temperature above -140 °C, the $Q^{\cdot-}$ ESR signal begins to diminish in intensity until at about -120 °C it becomes undetectable. Above this temperature, the signal reappears, this time as a microwave emission rather than as an absorption. The mechanism of this effect is probably a spin-conserved transfer from a polarized triplet state (i.e., one in which the electron spin states are unequally populated) to the upper spin state of the quinone radical. The observation of microwave emission would then depend upon the competition between spin-lattice relaxation and chemical relaxation. At low temperatures, chemical decay is retarded and spin relaxation occurs giving rise to a normal ESR signal. At higher temperatures, chemical decay proceeds faster than spin relaxation and thus an emissive signal results. The large background ESR signal due to direct formation of $BChl^{\cdot+}$ precludes the observation of an emissive signal from this species.

The lack of appearance at high temperatures of a steady-state ESR signal due to $C^{\cdot+}$ which can be associated with $Q^{\cdot-}$ is quite interesting in view of flash photolysis results. Thus, several groups¹⁶⁻¹⁸ as well as ourselves (see below) have observed $C^{\cdot+}$ formation in the presence of quinone at room temperature. The lifetime of this species is rather short (~ 100 μ s) however, and thus it would not be expected to build up to any appreciable extent in a steady-state experiment. These results, coupled with the fact that an ESR signal for $Q^{\cdot-}$ can be observed at room temperature, lead to the conclusion that not all of the $C^{\cdot+}$ can decay by recombination with $Q^{\cdot-}$. This point will be further elaborated below.

Further insight into the dynamics of radical formation in these systems has been obtained from NMR studies¹¹ involving measurement of the resonance spectrum while the photochemical reaction is proceeding in a steady state. If radical pairs are involved in the mechanism, it is possible to obtain nuclear spin polarization as a consequence of electron spin-nuclear spin interactions. This phenomenon is known as CIDNP (chemically induced dynamic nuclear polarization). We have observed such effects in the NMR spectrum of an illuminated mixture of chlorophyll and 2,6-dimethylbenzoquinone in methanol. The aromatic protons appear in emission whereas the methyl protons appear in enhanced absorption. The CIDNP effects are quenched by both oxygen and β -carotene, indicating that the chlorophyll triplet state is involved as a precursor. This conclusion is also reached on the basis of the signs of the polarizations and the magnetic properties of $C^{\cdot+}$ and $Q^{\cdot-}$. One can also deduce that a $C^{\cdot+}$ - $Q^{\cdot-}$ ion pair must exist which partly recombines and partly separates.

From a study of the quinone concentration dependence of both the CIDNP effects and the ESR spectra, we can conclude that quinone quenching of the chlorophyll lowest excited singlet state does not give rise to separated $C^{\cdot+}$ and $Q^{\cdot-}$ species. This could be a consequence of either of two possibilities: (a) no electron transfer occurs at all during singlet-state quenching (which seems a priori unlikely); (b) the radical ions do not escape during the quenching encounter; i.e., recombination is fast compared to separation.

If a $C^{\cdot+}$ - $Q^{\cdot-}$ radical pair is indeed formed during singlet quenching and if it has an appreciable lifetime prior to recombination, it should be detectable by laser photolysis on the picosecond time scale. Such experiments have been performed¹² and the results are as follows. With chlorophyll alone, bleaching of the main absorption at 665 nm occurs within the time resolution of the instrument (i.e., ~ 10 ps). Similarly, new absorptions appear in the 460-550- and 800-830-nm regions, also within 10 ps. These changes persist for times longer than 500 ps and are probably due to excitation

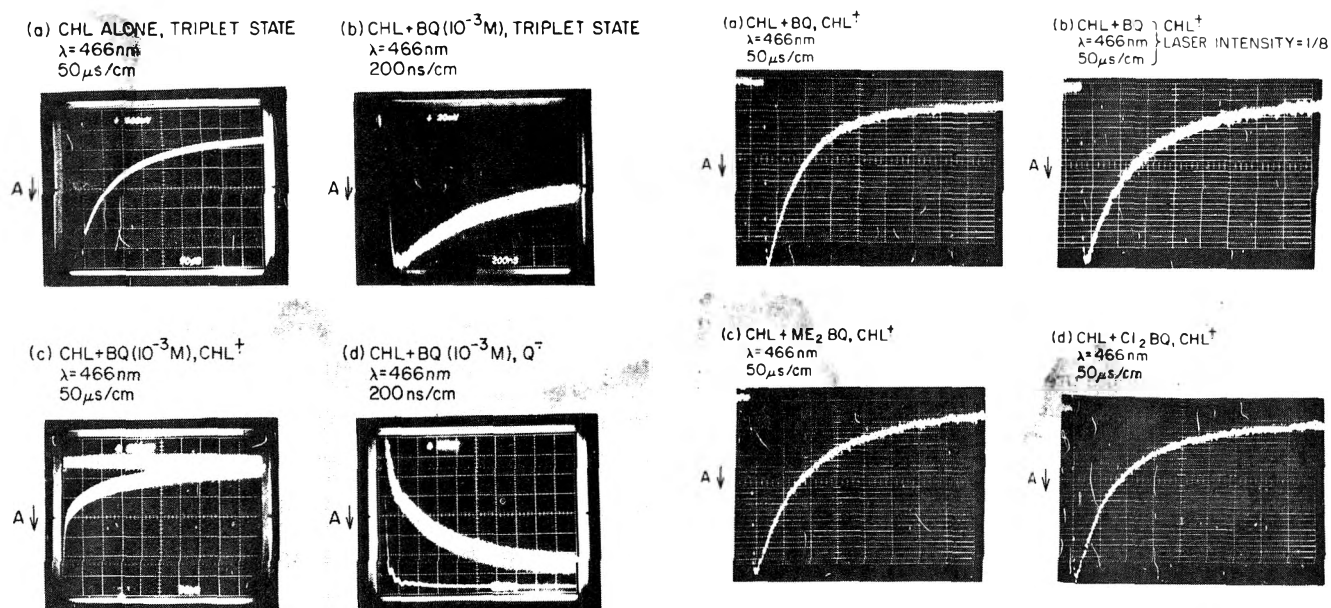


Figure 1. Absorbance change transients obtained upon laser photolysis of chlorophyll solutions (10^{-5} M) in ethanol with and without benzoquinone.

of chlorophyll to its lowest excited singlet state. Addition of 2,6-dimethylbenzoquinone causes quenching of these absorbance changes. No indication of $C^{\cdot+}$ formation is obtained. Thus, if $C^{\cdot+}-Q^{\cdot-}$ is formed, its lifetime must be less than 10 ps. It should be emphasized that a $(C^{\cdot+}-Q^{\cdot-})$ radical pair can exist in both singlet and triplet states and that these states may differ in their relative rates of dissociation and recombination. In particular, recombination must occur via a singlet state if products are the neutral ground-state species, as is indicated by the present experiments. Thus, since singlet quenching necessarily produces a singlet radical pair, one can account for the lack of dissociation by assuming that internal conversion (via reverse electron transfer) is more rapid than intersystem crossing to the radical pair triplet state. In the case of triplet quenching, the radical pair is formed as a triplet and it is not unreasonable to suppose that dissociation can effectively compete with intersystem crossing.

The failure of singlet quenching to generate stable radical species has interesting implications for the photosynthetic mechanism of radical production and stabilization if singlet states are involved *in vivo*, as is generally believed.⁶ It is significant that similar results have been obtained with quinone quenching of bacteriopheophytin singlet states (M. Windsor and W. W. Parson, personal communication, 1976). Thus, this may turn out to be a general phenomenon of quinone-chlorophyll photochemistry. If so, one can ask how the biological systems overcome this obstacle. The answer to this is as yet unknown.

Still further insights into the triplet-state pathway has been obtained by laser photolysis in the nanosecond and microsecond time regions.¹⁹ Some of the results of these studies are shown in Figure 1. In curve a, obtained with chlorophyll alone, the normal triplet-state transient is seen. When benzoquinone is added (curves b and c), the triplet decay rate is increased and a new transient due to $C^{\cdot+}$ is observed. It is also possible to see the growing in of the $Q^{\cdot-}$ species (curve d). The rate of formation of $Q^{\cdot-}$ closely parallels the triplet decay, thus providing direct confirmation of the precursor role of the triplet.

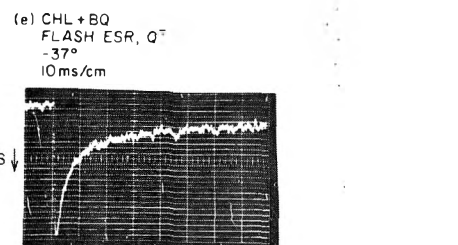


Figure 2. Absorbance change and ESR transients obtained upon laser photolysis of chlorophyll solutions in ethanol in the presence of various quinones.

The decay kinetics of $C^{\cdot+}$ (Figure 2) are observed to be approximately second order, with a rate constant of $1.7 \pm 0.2 \times 10^{10} \text{ M}^{-1} \text{ s}^{-1}$, independent of quinone structure (we have examined a series of quinones ranging from tetramethyl-*p*-benzoquinone to tetrachloro-*p*-benzoquinone; these span a redox potential range of approximately 1 V). This value of the decay constant is close to the diffusion-controlled limit. Assuming this, and using the Debye equation,²⁰ one can calculate that electron transfer occurs when the $C^{\cdot+}$ and $Q^{\cdot-}$ species are within 5 Å of one another. Thus, the picture that emerges from these data is that the decay of $C^{\cdot+}$ occurs predominantly via a diffusion-limited recombination reaction with $Q^{\cdot-}$ when these two species are essentially within contact distance of one another. There are no indications that radical ion recombination leads to triplet state formation, as has been observed in other systems, e.g., pyrene-diethylaniline.²¹

We have also utilized the flash technique to follow the decay of $Q^{\cdot-}$ in ESR (Figure 2e). Inasmuch as the time resolution of this method is much poorer than that of laser photolysis ($\sim 10^{-4}$ s), we are unable to see the rapidly decaying $Q^{\cdot-}$ signal or the $C^{\cdot+}$ signal at room temperature. We can, however, observe the disproportionation. At lower temperatures we do see biphasic decay kinetics (Figure 2e) and we are presently engaged in a detailed comparison of the temperature dependence of the laser photolysis and flash ESR signals. This study should allow us to obtain a complete picture of the decay reaction.

Experiments utilizing pheophytin in place of chlorophyll show that $Phe^{\cdot+}$ decay is much faster than $C^{\cdot+}$ decay, under identical conditions (compare Figure 2a with Figure 3b). Thus, changing the electron donor does change the cation radical

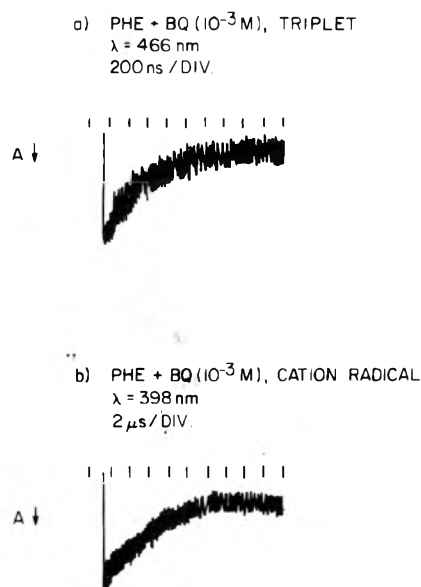
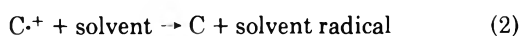
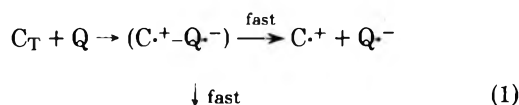


Figure 3. Absorbance change transients obtained upon laser photolysis of alcohol solutions of pheophytin and benzoquinone:

decay rate, in contrast to the results obtained with the various quinones.

All of the results which we have obtained thus far are consistent with the mechanism



Evidence for the formation of solvent radicals in these systems (reaction 2) has been previously obtained by low temperature ESR spectroscopy.¹⁴ Inclusion of this reaction provides a rationale for the fact that some of the C^+ must decay by a pathway other than recombination so as to allow a portion of the Q^- species to disproportionate (reaction 4). It is this latter population which is observed in the room temperature ESR spectra.

The reactions described in this paper clearly show analogies to the processes known to occur in the photosynthetic system, namely, C^+ production, acceptor (quinone) reduction, and donor (solvent) oxidation. Thus, they provide acceptable models for the biological energy conversion mechanism. The insights gained by studying these systems should have application to our understanding of the role of chlorophyll in photosynthesis.

Acknowledgment. This work was supported in part by the U.S. Energy Research and Development Administration, Contract E(11-1)908.

References and Notes

- (1) H. J. Van Gorkom, *Biochim. Biophys. Acta*, **347**, 439 (1974).
- (2) M. P. J. Pulles, P. L. M. Kerkhof, and J. Amesz, *FEBS Lett.*, **47**, 143 (1974).
- (3) R. Malkin and A. J. Bearden, *Proc. Natl. Acad. Sci. U.S.A.*, **68**, 16 (1971).

- (4) G. Feher, M. Y. Okamura, and J. D. McElroy, *Biochim. Biophys. Acta*, **267**, 222 (1972).
- (5) J. R. Bolton and K. Cost, *Photochem. Photobiol.*, **18**, 417 (1973).
- (6) See W. W. Parson and R. J. Cogdell, *Biochim. Biophys. Acta*, **416**, 105 (1975), for review.
- (7) W. L. Butler, *Acc. Chem. Res.*, **6**, 177 (1973).
- (8) Govindjee and R. Govindjee, "Bioenergetics of Photosynthesis", Academic Press, New York, N.Y., 1975.
- (9) D. C. Mukherjee, D. H. Cho, and G. Tollin, *Photochem. Photobiol.*, **9**, 273 (1969).
- (10) G. Tollin and G. Green, *Biochim. Biophys. Acta*, **60**, 524 (1962).
- (11) A. A. Lamola, M. L. Manion, H. D. Roth, and G. Tollin, *Proc. Natl. Acad. Sci. U.S.A.*, **72**, 3265 (1975).
- (12) D. Huppert, P. M. Rentzepis, and G. Tollin, *Biochim. Biophys. Acta*, in press.
- (13) R. A. White and G. Tollin, *J. Am. Chem. Soc.*, **89**, 1253 (1967).
- (14) J. R. Harbour and G. Tollin, *Photochem. Photobiol.*, **19**, 147 (1974).
- (15) J. R. Harbour and G. Tollin, *Photochem. Photobiol.*, **19**, 163 (1974).
- (16) A. K. Chibisov, *Photochem. Photobiol.*, **10**, 331 (1969).
- (17) J. M. Kelley and G. Porter, *Proc. R. Soc. London, Ser. A.*, **319**, 319 (1970).
- (18) K. Seifert and H. T. Witt, *Naturwissenschaften*, **55**, 222 (1968).
- (19) F. Rizzuto, F. R. Castelli, and G. Tollin, unpublished results.
- (20) P. Debye, *Trans. Electrochem. Soc.*, **82**, 265 (1942).
- (21) H. Schomburg, H. Staerk, and A. Weller, *Chem. Phys. Lett.*, **21**, 433 (1973).

Discussion

M. W. WINDSOR. We (Gouterman, Holten, Rockley, and myself) have studied the quenching of molecular solutions of bacteriopheophytin (BPh) by benzoquinone (Q) using picosecond techniques. The quinone quenches the S_1 state of BPh without producing the cation, BPh^+ . When we add excess methyl iodide to enhance the formation of the triplet state of BPh, then quenching by Q does lead to the production of the pheophytin cation. These results agree with your results for chlorophyll. Our tentative explanation is that the singlet state of the charge-transfer pair suffers very rapid internal conversion to the ground state, whereas the triplet state of the pair survives long enough for completion of the charge separation to occur. [See above authors, *Photochem. Photobiol.*, in press.]

V. KOESTER. Is there any evidence for photoionization in the lowest triplet state of monomeric chlorophyll?

G. TOLLIN. In the experiments that we have done we were not able to look at the chlorophyll NMR spectrum. The chlorophyll concentration needs to be rather low in order to get sufficient light into the system to carry out the photochemistry. The instrument that we were using was simply not sensitive enough to observe the chlorophyll NMR spectrum.

H. A. FRANK. Could not one explain the redox reaction by having chlorophyll cation react with hydroquinone? The resulting Q^- reacts with the photoformed Q^- in the observed second-order reaction. The hydroquinone could be formed by reaction of quinone with solvent ethanol.

G. TOLLIN. Hydroquinone formation is too slow to account for this; hydroquinone formation must occur via disproportionation. If we add hydroquinone, we see only a small effect on decay rates.

R. S. BECKER. Are any of the processes biphotonic?

G. TOLLIN. Not as far as we have been able to tell. The light intensity dependence is always linear.

R. S. BECKER. Why is recombination so much faster in singlet than in triplet?

G. TOLLIN. If you start with a radical pair, which is either singlet or triplet, one has to go through the singlet state of this radical pair in order to get back to the starting materials. So one possible way of looking at this is that if one generates the radical pair in a triplet state, as one would do from the quenching of the triplet of chlorophyll by quinone, in order for recombination to occur this has to go back through a singlet state. Whereas, if one generates the radical pair in a singlet state, as one does from the quenching of the chlorophyll singlet by quinone, one already has a state which is set for recombination, and it may be that the kinetics here are such that the triplet radical pair can, at least partly, separate before going back through the singlet.

H. A. FRANK. Have you measured the triplet state decay time of bacteriochlorophyll?

G. TOLLIN. We haven't, but it has been measured. I think it's somewhat faster than chlorophyll.

Picosecond Flash Photolysis Studies of Dyes, Inorganic Complexes, Biological Pigments, and Photosynthetic Systems^{1,2}

Maurice W. Windsor

Department of Chemistry, Washington State University, Pullman, Washington 99163 (Received March 15, 1976)

Publication costs assisted by the National Science Foundation

We have developed a picosecond flash photolysis apparatus, capable of photographic recording of the spectra of transient intermediates for exploratory studies, coupled with provisions for subsequent detailed kinetic studies at any wavelength in the range 400 to 950 nm using a vidicon detector coupled to an optical multichannel analyzer.³ The sample is excited with a single optical pulse of 5–8 ps duration at a wavelength of 530, 694, or 1060 nm and monitored by a time-delayed continuum pulse, also of picosecond duration. Time resolution of about ± 4 ps is obtainable over the range from a few picoseconds to a few nanoseconds.

We have used this apparatus to study the short-time photophysics and photochemistry of a variety of dyes, inorganic complexes, and other large molecules, including biological pigments and photosynthetic systems. Measurements of both ground-state repopulation (GSR) and excited-state absorption (ESA) are used to obtain kinetic data. In the molecule crystal violet, we observe a pronounced effect of viscosity on the excited state relaxation that appears to be connected with solvent-hindered rotation of the phenyl rings.⁴ The molecule bis(4-dimethylaminodithiobenzil)nickel(II) (BDN) exhibits a large and interesting dependence of internal conversion rate on solvent. The extreme values of the excited state lifetime are 9 ns in benzene and 220 ps in iodoethane.⁵ We have discussed the significance of these data for laser mode-locking.⁶

We have also studied inorganic complexes of chromium, manganese, iron, and ruthenium.⁷ Picosecond techniques are especially valuable for studying transition metal complexes, because few such complexes luminesce with intensity sufficient for emission spectroscopic studies, especially at room temperature where most photochemical studies are carried out. In fact, the very weakness of the luminescence points to very short lifetimes for the excited states involved. Our observations on chromium complexes show that the rise time of the ESA of the Reineckate ion, *trans*-[Cr(NH₃)₂(NCS)₄]⁻, cannot be distinguished from that of the 5-ps pump pulse.⁷ Also, our spectrum of the ESA matches that of the ²E state obtained at -196 °C by Ohno and Kato.⁸ Unless the ESA spectra of the ⁴T₂ and the ²E states are fortuitously the same, we are obliged to conclude that the ⁴T₂ state, initially populated by the 530-nm pump pulse, undergoes very rapid intersystem crossing, $k_{isc} \gtrsim 10^{11}$ s⁻¹ to the doublet manifold. We observed a similarly rapid rise of ESA in the acetylacetonate, [Cr(acac)₃], and in [Cr(NCS)₆]³⁻.

Picosecond spectroscopy also makes possible a novel and very direct approach to the problem of measuring quantum yields of internal conversion and intersystem crossing. The basic problem in measuring quantum yields is to count the number of excited states produced in a given volume and compare this value with the number of photons absorbed in that same volume, both in a given time. Experimental difficulties are often encountered, because indirect techniques

employing standard solutions of assumed unit effective fluorescence yield must be used to measure the number of photons absorbed under conditions of photostationary equilibrium. In principle, these difficulties can be circumvented by measuring the initial depletion of the ground state, following pulse excitation, since the number of molecules removed from the ground state is the most reliable indicator of the number of photons absorbed. However, for a fluorescence lifetime of 2 ns, knowledge of the initial depletion to an accuracy of 5% requires a time resolution of 100 ps. This is well beyond the scope of even nanosecond flash photolysis instrumentation. With the advent of picosecond flash photolysis techniques, this most direct of all methods can now be implemented.

We have demonstrated the feasibility of this technique by applying it to the dye, rose bengal, a halogenated analogue of the important laser dye, rhodamine 6G.⁹ The initial bleaching of the ground state absorption, following absorption of the 530-nm picosecond pump pulse, measures the number of photons absorbed by the sample. Subsequently the ground state absorption recovers in two stages. Some of the molecules in the excited singlet state, S₁, return rapidly via singlet channels, i.e., fluorescence emission or internal conversion. Concurrently, the balance of the S₁ molecules undergo intersystem crossing to the triplet manifold. Eventually, but much later (tens of nanoseconds) these molecules also return to the ground state. Thus, when observed as a function of time, the bleaching shows an initial fast decrease to an intermediate value and then a much slower decay to zero as the triplet molecules return. The intermediate bleaching level measures the number of molecules held up in the triplet state. The difference between the initial bleaching and the intermediate bleaching measures the number of molecules that return via singlet channels. The ratio of these two figures gives a value for $\Phi_{ISC}/(\Phi_F + \Phi_{IC})$, where Φ_{ISC} , Φ_F , and Φ_{IC} are the quantum yields for, respectively, intersystem crossing, fluorescence emission, and internal conversion. For rose bengal in ethanol solution our results give a value of 3.1 ± 0.5 for the above ratio. Since $(\Phi_F + \Phi_{IC} + \Phi_{ISC}) = 1.0$, we obtain $\Phi_{ISC} = 0.76 \pm 0.03$ and $(\Phi_F + \Phi_{IC}) = 0.24 \pm 0.03$. From integrated absorption studies, Berlman¹⁰ has reported a value of 1.7×10^8 s⁻¹ for the radiative rate constant, k_F . By combining this with our value for the fluorescence lifetime (1.35 ns) we obtain a value of 0.23 for Φ_F . Thus we arrive at a value of $\Phi_{IC} = 0.01 (+0.03, -0.01)$ for the quantum yield of internal conversion. Gollnick and Schenck^{11,12} have reported values of Φ_{ISC} for rose bengal of 0.76 in methanol and 0.75 in ethanol solution. Their measurements were based on the quantum yield of the photosensitized oxygen transfer reaction. The closeness of agreement between our value and theirs is undoubtedly fortuitous, but does perhaps offer some reassurance regarding the validity of our technique. Given appropriate excitation wavelengths, this approach should be capable of extension to a wide range of compounds. A more comprehensive account of this work

is in preparation by Rockley and the author.⁹

In the area of photobiology we have determined the absorption spectra of both the first excited singlet S_1 and the lowest triplet T_1 of several porphyrins, together with extinction coefficients and kinetic and quantum yield data.¹³ Picosecond flash photolysis is especially useful for studying systems such as these that have very low fluorescence yields (<1% for octaethylporphyrin- SnCl_2) and would therefore be very difficult to study by other techniques. More recently, we have studied the quenching of bacteriopheophytin (BPh) via electron transfer to *p*-benzoquinone to produce the π -cation radical, BPh^+ . It appears that electron transfer to the acceptor goes predominantly via the triplet state of the donor. The results are discussed in terms of the spin selectivity of the reverse electron transfer process within the intermediate charge transfer complexes and contribute some insights into the primary charge separation process in bacterial photosynthesis.¹⁴

Finally, we have made a picosecond study of the spectroscopy and kinetics of the intermediates in the photochemical reaction of bacterial photosynthesis itself.^{15,16} Reaction centers of *Rhodospseudomonas sphaeroides* exhibit a transient spectroscopic state that decays with an exponential lifetime of 246 ± 16 ps to produce the known spectrum of the radical cation of the bacteriochlorophyll complex. This indicates that the transient state is a direct intermediate in the photooxidation of the bacteriochlorophyll. The absorption spectrum of the transient state shows the state to be identical with a state (P^F) which has been detected previously in reaction centers that are prevented from completing the photooxidation, because of chemical reduction of the electron acceptor.¹⁷ Analysis of this spectrum suggests either that P^F is to be identified with the cation-anion biradical, $\text{BChl}^+-\text{BChl}^-$ or that the formation of P^F involves electron transfer from the dimeric P870 bacteriochlorophyll reaction center complex over to a neighboring molecule of bacteriopheophytin,¹⁸ to give the structure $(\text{BChl}-\text{BChl})^+-\text{BPh}^-$. Whichever it turns out to be, there seems little doubt that P^F represents a crucial intermediate stage between the initial locally excited singlet, BChl^* , and the final state of complete photooxidation, $\text{BChl}^+ \cdots \text{X}^-$ in which the electron has been completely transferred over to the primary acceptor. The initial absorbance changes following flash excitation also include a bleaching of an absorption band at 800 nm. The bleaching decays with $\tau \sim 30$ ps and may be connected with the excited singlet state of the reaction center complex that precedes the formation of P^F . It is significant that picosecond flash photolysis provides for the first time the time resolution necessary to study the primary events in photosynthesis under physiological conditions, where the photochemical events can proceed unimpeded, rather than in systems in which photochemistry is artificially blocked by chemical reduction of the acceptor.

References and Notes

- (1) Plenary invited address presented at The Michael Kasha Symposium on Energy Transfer in Organic, Inorganic, and Biological Systems, Florida State

- University, Tallahassee, Fla., Jan. 8-10, 1976.
- (2) This research was supported in part by the Office of Naval Research.
- (3) D. Magde and M. W. Windsor, *Chem. Phys. Lett.*, **27**, 31 (1974).
- (4) M. D. Magde and M. W. Windsor, *Chem. Phys. Lett.*, **24**, 144 (1974).
- (5) D. Magde, B. A. Bushaw, and M. W. Windsor, *Chem. Phys. Lett.*, **28**, 263 (1974).
- (6) D. Magde, B. A. Bushaw, and M. W. Windsor, *IEEE J. Quant. Electron.*, **QE10**, 394 (1974).
- (7) A. D. Kirk, P. E. Hoggard, G. B. Porter, M. G. Rockley, and M. W. Windsor, *Chem. Phys. Lett.*, **37**, 199 (1976).
- (8) T. Ohno and S. Kato, *Bull. Chem. Soc. Jpn.*, **43**, 8 (1970).
- (9) M. G. Rockley and M. W. Windsor, to be submitted for publication.
- (10) I. B. Berlman, "Handbook of Fluorescence Spectra of Aromatic Molecules", 2d ed., Academic Press, New York, N.Y., 1971, p. 415.
- (11) K. Gollnick and G. O. Schenck, *Pure Appl. Chem.*, **9**, 507 (1964).
- (12) K. Gollnick, *Adv. Photochem.*, **8**, 1-122 (1968), see especially pp. 17, 18, and 20 (Table II).
- (13) D. Magde, M. W. Windsor, D. Holten, and M. Gouterman, *Chem. Phys. Lett.*, **29**, 183-188 (1974).
- (14) D. Holten, M. Gouterman, W. W. Parson, M. W. Windsor, and M. G. Rockley, *Photochem. Photobiol.*, **23**, 415 (1976).
- (15) M. G. Rockley, M. W. Windsor, R. J. Cogdell, and W. W. Parson, *Proc. Natl. Acad. Sci.*, **72**, 2251-2255 (1975).
- (16) M. W. Windsor, M. G. Rockley, R. J. Cogdell, and W. W. Parson, "Lasers in Physical Chemistry and Biophysics", J. Jousot-Dubien, Ed., Elsevier, New York, N.Y., 1975, p. 369.
- (17) W. W. Parson, R. K. Clayton, and R. J. Cogdell, *Biochim. Biophys. Acta*, **387**, 265 (1975).
- (18) J. Fajer, D. C. Brune, M. S. Davis, A. Forman, and L. D. Spaulding, *Proc. Nat. Acad. Sci., U.S.A.*, **72**, 4956-4960 (1975).

Discussion

R. M. HOCHSTRASSER. Do you know the spectral widths of the various pulses arriving at the sample, namely the 530-nm pulse and the continuum? Secondly, how could you distinguish, in the rose bengal experiments, between an induced vs. a spontaneous recovery of the ground state?

M. W. WINDSOR. The spectral width of the 530-nm pulse is about 20 Å. The continuum, of course, extends over several thousand angstroms. With regard to your second question, I believe that, at the levels of intensity that we have in the continuum, stimulated return will be insignificant. Induced emission, if present, would change the quantum yields, increasing Φ_F at the expense of Φ_{IC} and Φ_{ISC} .

E. C. LIM. I am sure you have worried about this, but in order for your technique to work the triplet-triplet absorption spectrum should not overlap the ground state absorption. Do you know whether this is the case with your system?

M. W. WINDSOR. We have a manuscript just about ready to send in on this; I will suggest you as a referee. When we were writing the paper we were very concerned about that. We know enough about the triplet absorption to conclude that the triplet absorption will affect minimally the ground state bleaching measurements.

M. A. EL-SAYED. Your method as described could not work if there is photochemistry. You need additional data.

M. W. WINDSOR. In the case of rose bengal, I am ignoring photochemistry. I think it is justified, because the ground state absorption recovers more or less completely.

Excitons, Energy Transfer, and Charge Resonance in Excited Dinucleotides and Polynucleotides. A Photoselection Study

Robert W. Wilson[†] and Patrik R. Callis*

Department of Chemistry, Montana State University, Bozeman, Montana 59715 (Received March 5, 1976)

Absorption, fluorescence, and fluorescence polarization measurements as a function of excitation and fluorescence wavelengths (λ_e and λ_f) covering the spectral region 240–450 nm are reported for the nucleic acid constituents 5'CMP, (3' → 5')CpC, poly(rC), 5'-TMP, (3' → 5')dpTpT, 5'-GMP, (3' → 5')GpG, 5'-AMP, (3' → 5')ApA, and poly(rA) at ca. 10^{-4} M solution in neutral ethylene glycol–water glasses at temperatures near -120 °C. AMP exhibits considerable mixed polarization in contrast to the free base adenine. CpC and ApA show evidence of stacking in their spectra, and their polarizations are dramatically different than for the monomers. The spectra of dpTpT and GpG are not detectably different from the monomers but evidence of interaction is seen in the polarizations. In all cases, the dinucleotide fluorescence showed very little depolarization when λ_e and λ_f were near the origin, in marked contrast to both vibronic exciton theory and Förster theory. In general, the polarization ratios decrease steeply as both λ_e and λ_f are varied away from the origin. For CpC and ApA the variation of polarization vs. λ_f is apparently due to a transition moment directed perpendicular to the molecular planes indicating charge resonance character in the excited dimer state. Polarized fluorescence spectra calculated from vibronic exciton theory are shown. The poor agreement leads to the conclusion that, for these systems, the usual assumptions employed in stationary exciton and energy transfer theories regarding the states initially reached upon excitation are not valid. The spectra of poly A and poly C show only partial depolarization relative to the respective dinucleotides.

Introduction

The source of free energy which drives much of the chemistry on the earth may be traced to molecules which have been electronically excited by the sun.

Interaction of the initially excited molecule with one or more ground state molecules is usually involved in the process by which the energy is ultimately stored or produces a mutation, etc. The interaction is of two main types: (1) exciton interaction involving excitation resonances which is effective at distances of tens of angstroms and (2) electron exchange interaction involving charge resonance which essentially requires orbital overlap. This paper is primarily concerned with dimers in which one of the two monomers is excited. Such systems have played an important role in the development of understanding of excited state interactions.

Exciton theory has been successfully employed in time dependent form by Förster to explain long-range energy transfer such as occurs in the first steps of photosynthesis.¹ In stationary state form, exciton theory has proven successful in qualitatively describing the spectra and phosphorescence enhancement of certain aggregates characterized by moderately strong interactions and whose intermolecular distance does not appreciably change upon excitation.² It is not generally clear whether the lack of relaxation is because of lattice restrictions or because the force to do so is small. At any rate another class of dimers is distinguished by essentially monomer-like absorption spectra (because of weak or absent ground state interaction) and by greatly red-shifted fluorescence due to intermolecular relaxation in response to both excitation and electron exchange interaction. Such excited dimers with repulsive ground state potentials are known as excimers.³

Photoselection studies⁴ have played an important role in elucidating the symmetry of excited electronic state wave

functions in monomeric systems but very few such studies on dimer systems have emerged.^{2g,5-8} One reason is that a homogeneous ensemble of dimers (free of monomers, trimers, etc.) is difficult to prepare. Furthermore, the first-mentioned class of dimers generally fluoresces very weakly whereas excimers require high concentrations in fluid media, i.e., conditions which lead to complete loss of polarization information.

We present here results of a photoselection study on the fluorescence from dinucleotides which have been shown to exhibit intramolecular excimer-type fluorescence in dilute rigid solution.⁹ The purpose of this study has been dual from the beginning: (1) to test the predictions of theories of dimers, excimers, and energy transfer, (2) to help elucidate the primary steps leading to uv photodamage in nucleic acids. Of particular interest is the relation of this work to that for rhodamine B dimers^{2g} which conform well to stationary-state vibronic exciton theory^{2d,e} and the very weakly coupled dimers studied by Weber and Shinitsky⁵ which were discussed entirely from the time-dependent or energy transfer point of view. It will be seen that neither point of view seems appropriate here and that these experiments are a probe of the little-understood transition region, discussed by Kasha,^{2c} between conventional exciton theory and Förster's very weak coupling theory.^{1a}

This paper is restricted to results for the four basic nucleotides of DNA, the four "homodinucleotides", and two homopolymers. The nucleotides are cytidine 5'-monophosphate (CMP), thymidine 5'-monophosphate (TMP), adenosine 5'-monophosphate (AMP), and guanosine 5'-monophosphate (GMP). The homodinucleotides are: cytidyl(3' → 5')cytidine (CpC), 5'-O-deoxyphosphorylthymidyl(3' → 5')thymidine (dpTpT), adenylyl(3' → 5')adenine (ApA), and guanylyl(3' → 5')guanine (GpG). The two polymers are poly(rC) and poly(rA) high molecular weight extensions of CpC and ApA.

A preliminary account of the CMP and CpC results has

[†] Present Address: Institute of Molecular Biology, University of Oregon, Eugene, Ore. 97403.

appeared previously.⁷ We intend to publish similar findings for a number of heterodinucleotides in the near future.

Experimental Section

Materials. The nucleic acid components used in this work were purchased from commercial sources as follows: GMP, CMP, CpC, poly C, and polyA were from Sigma; TMP was from Calbiochem; dpTpT from Collaborative Research; GpG from P. L. Biochemicals. ApA and AMP were obtained from both Sigma and Calbiochem. The compounds were used without further purification in this study. Fluorescence spectra in all cases did not shift more than ± 2 nm as a function of excitation wavelength. The fluorescence excitation spectrum for ApA was coincident with its absorption spectrum but deviated significantly for the other compounds. This behavior, which we believe to be intrinsic, has been the subject of a recent paper.¹⁰

Ethylene glycol from Eastman or Matheson Coleman and Bell was treated with activated charcoal to remove fluorescent impurities. Water was once distilled. Both solvents had background fluorescence levels about ten times less than their respective prominent O-H stretch Raman lines when excited at 260 nm with a spectral half-width of 6 nm. In general the solvent fluorescence was about 30 times less than that of the molecules under study except for AMP.

Optical Measurements. All measurements reported here were for dilute (ca. 10^{-4} M) solutions in mixtures of ethylene glycol and water ranging in respective proportions from 50:50 to 70:30 by volume. The temperature ranged from -110 to -130 °C and was known and controlled to ca. ± 2 °C. In this range the mixtures are clear glasses, loosely described as rigid to brittle at the extremes. The glasses tended to fracture at lower temperatures thereby destroying polarization information. The solutions were adjusted to near pH 7 with sodium or potassium phosphate buffer. The results reported here were virtually independent of the temperature and solvent variations.

The room temperature and low temperature absorption spectra were obtained with a Cary 14 recording spectrophotometer. For low temperature measurements a stainless steel dewar fitted with fused silica windows was placed in the sample compartment of the Cary 14. Within this dewar was placed a fused silica rectangular fluorescence cell containing the sample. Cooling to the desired temperature was accomplished by bathing the cell in nitrogen gas which had been percolated through liquid nitrogen. The temperature at the cell was monitored with a thermocouple and was adjusted by varying the flow rate of the nitrogen gas.

The apparatus used for the fluorescence measurements is a collection of separate components arranged to monitor emission at 90° to the direction of the incident light propagation. The excitation source was an Osram XBO 150W/1 high-pressure xenon lamp, the light from which was passed through a 500-mm Bausch and Lomb grating monochromator. The emitted light was passed through a second monochromator, identical to the first, and detected by an EMI 9558QC phototube. The photocurrent was measured with a Pacific Photometric Laboratory Model II photometer. When the samples exhibited both fluorescence and phosphorescence, the phosphorescence was removed by chopping the incident light and monitoring the ac component of the photocurrent at the chopping frequency using a PAR Model 122 lock-in amplifier. Plots of the photocurrent vs. wavelength were made by a Hewlett Packard Model 7030A x-y recorder. The sample cell, dewar, and cooling methods used for fluorescence mea-

surements are identical with those used for the absorption measurements.

The fluorescence spectra were not corrected for phototube response because the corrections were not large in the region of interest. Normalized to unity at 310 nm, the detector system response increased gradually from 0.9 at 300 nm to 1.15 at 375 nm, from which it fell almost linearly to 0.4 at 500 nm.

The photoselection experiments were carried out by polarizing the excitation source with a Polacoat PL40 polarizing filter and analyzing the emitted light with a deplasticized polaroid sheet mounted in quartz. Since monochromators tend to be quite anisotropic, large corrections for this are usually necessary. To reduce the magnitude of the corrections we have inserted crystal quartz wedge depolarizers at the exit slit and entrance slit of the excitation and fluorescence monochromators, respectively.

Photoselection experiments may be carried out in two equivalent ways. The first (and most common) is to keep the excitation polarizer fixed and rotate the emission polarizer. In the second the reverse is done. We found both to give the same result but with the latter no corrections (within experimental error) were necessary and so was the method usually employed.

In the case of AMP only, the measurements were made using unpolarized light, that is, with $p = 0.5$ (vide infra, eq 1). The results given for AMP have been transposed with the use of eq 1 to what they would have been if $p = 1$, as it was for all other measurements.

The zero correction was ascertained in two ways: (1) when the emission polarizer was oriented so as to pass horizontally polarized light (i.e., the electric vector parallel to the incident light propagation direction) the fluorescence intensity was not significantly dependent on the orientation of the excitation polarizer. (2) The fluorescence from benzene showed no measurable polarization in hexane at 25 °C.

Polarization ratios were determined manually point by point with resolutions of 3–6 nm. The points in the figures are averages of points obtained from 3 to 7 separate samples.

Photoselection Theory

The following analysis refers to experiments in which the exciting light and emitted light propagate at right angles to one another in the horizontal plane. Let p represent the fraction of the exciting light which is vertically polarized (E-field in vertical direction) and I_v , I_h represent the fluorescence intensities measured when the fluorescence polarizer is oriented to pass vertically and horizontally polarized light, respectively. The combined formalism of Albrecht^{4a} and Liptay^{4b} leads to

$$R = I_v/I_h = \frac{p(2S + 1) + (1 - p)(2 - S)}{2 - S} \quad (1)$$

where

$$S = \frac{\sum_k \sum_l m_k^2 m_l^2 (\vec{k} \cdot \vec{l})^2}{\sum_k \sum_l m_k^2 m_l^2} = \frac{\sum_k \sum_l (\vec{m}_k \cdot \vec{m}_l)^2}{\sum_k \sum_l (\vec{m}_k \cdot \vec{m}_k)(\vec{m}_l \cdot \vec{m}_l)} = \sum_k \sum_l r_k q_l (\vec{k} \cdot \vec{l})^2 \quad (2)$$

and where m_k and \vec{k} are the magnitude and unit vector of the electric dipole transition moment, \vec{m}_k , effecting the k th

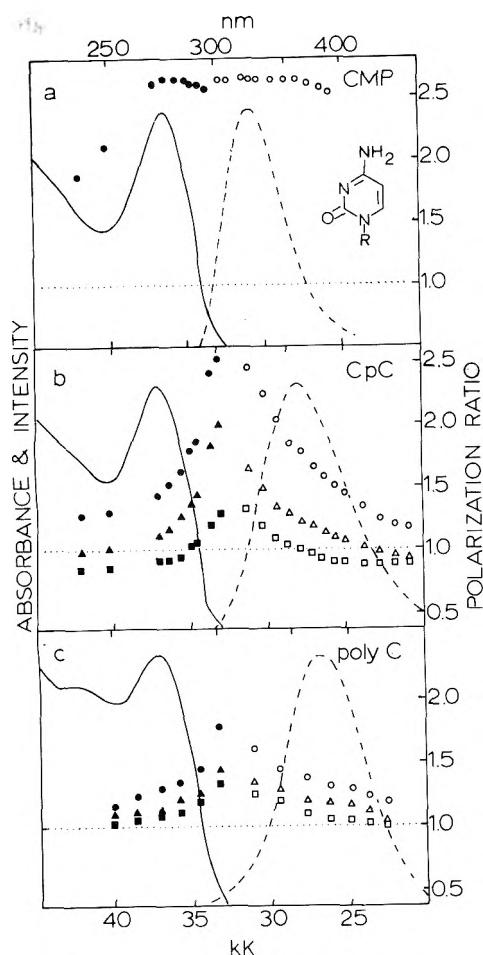


Figure 1. Absorption (—), fluorescence (---), and fluorescence polarization ratios for ca. 10^{-4} M solutions of cytosine derivatives in neutral ethylene glycol-H₂O (6:4) glasses at ca. -110°C . (a) 5'-CMP (—R represents ribose phosphate): (●) $\lambda_f = 325$ nm; (○) $\lambda_e = 280$ nm. (b) CpC: (●) $\lambda_f = 320$ nm; (▲) $\lambda_f = 360$ nm; (■) $\lambda_f = 450$ nm; (○) $\lambda_e = 300$ nm; (△) $\lambda_e = 280$ nm; (□) $\lambda_e = 250$ nm. (c) Poly C: (●) $\lambda_f = 325$ nm; (▲) $\lambda_f = 375$ nm; (■) $\lambda_f = 425$ nm; (○) $\lambda_e = 295$ nm; (△) $\lambda_e = 280$ nm; (□) $\lambda_e = 250$ nm. (λ_e = excitation wavelength, λ_f = fluorescence wavelength.)

transition in the absorption spectrum, m_l and \bar{l} are the corresponding quantities for \bar{m}_l which governs the l th transition contributing to the emission spectrum and r_k and q_l are the fraction of the light absorbed due to \bar{m}_k and the fraction emitted due to \bar{m}_l , respectively. The equations in this form are valid only for the usual case corresponding to Kasha's rule, i.e., that the emission process is independent of the absorption process. Thus, fluorescence polarization experiments are seen to yield a quantity, S , which is the average of the square of the cosine of the angle between the absorbing and emitting transition moments for a photon.

For the purposes of discussion here we shall assume the symmetrical molecule case in which all transition moments must lie along three mutually perpendicular directions x , y , and z . This leads to the form of S seen in Albrecht's equations.

$$S(\lambda_e, \lambda_f) = r_x(\lambda_e)q_x(\lambda_f) + r_y(\lambda_e)q_y(\lambda_f) + r_z(\lambda_e)q_z(\lambda_f) \quad (3)$$

where λ_e and λ_f are the wavelengths for excitation and fluorescence. In this case S reduces to the probability that a photon will be emitted by a moment parallel to the moment through which it was absorbed. Clearly when this probability is unity, $R = 3$ for $p = 1$. When the emission polarization is

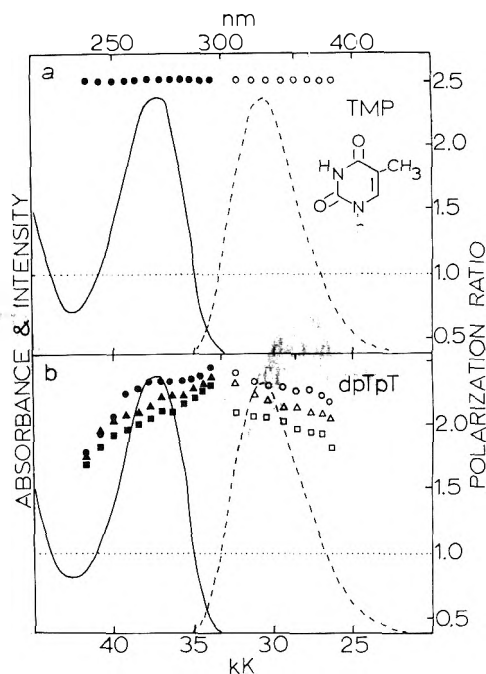


Figure 2. Absorption (—), fluorescence (---), and polarization ratios of ca. 10^{-4} M solutions of thymine derivatives in neutral ethylene glycol-H₂O glasses at ca. -120°C . (a) 5'-TMP (—r represents 2'-deoxyribose phosphate): (●) $\lambda_f = 330$ nm; (○) $\lambda_e = 270$ nm. (b) dpTpT: (●) $\lambda_f = 305$ nm; (▲) $\lambda_f = 330$ nm; (■) $\lambda_f = 370$ nm; (○) $\lambda_e = 290$ nm; (△) $\lambda_e = 270$ nm; (□) $\lambda_e = 250$ nm. (λ_e = excitation wavelength, λ_f = fluorescence wavelength.)

equally probable for all three directions, $S = 1/3$ and $R = 1$. When the emitting moment is perpendicular to the absorbing moment, $S = 0$, and $R = 0.5$. For reasons not fully understood, few if any molecules exhibit the extreme values of 3 and 0.5 but these intrinsic depolarizations have been found to behave as if¹¹ the molecules all rotate randomly by an angle ϕ after absorption but before emission. This introduces a randomization factor,^{4a} $\epsilon = 3/2 \sin^2 \phi$, into the equations such that

$$R = \frac{p[2S + 1 - 2\epsilon(S - 1/3)] + (1 - p)[2 - S + \epsilon(S - 1/3)]}{(2 - S) + \epsilon(S - 1/3)} \quad (4)$$

Results

The experimental results are summarized in Figures 1–4. Each figure is dedicated to one of the four basic chromophores found in DNA: cytosine, thymine, adenine, and guanine. Part a of each figure is for the monomeric nucleotide whereas part b is for the dinucleotide. For adenine and cytosine, results for the corresponding polymers are shown in part c.

In each figure the solid curve is the low-temperature absorbance in arbitrary units. The dashed line is the fluorescence spectrum obtained with unpolarized light. The solid symbols give the polarization ratios ($R = I_v/I_h$) as a function of λ_e . The shape of the symbols indicates λ_f . Circles mean λ_f is a fixed value near the 0–0 region, triangles mean λ_f is near the fluorescence maximum, and boxes indicate λ_f is in the long-wavelength tail. The actual wavelengths are given in the captions. The open circles give R as a function of λ_f and now the shape gives an indication of the particular λ_e . Circles mean λ_e is in the 0–0 region, triangles mean λ_e is near the absorption maximum, while boxes mean λ_e is at shorter wavelengths yet. Again, the actual values of λ_e are in the captions.

We now make some general observations. (1) The polarization ratio when both λ_e and λ_f are near the 0–0 region is

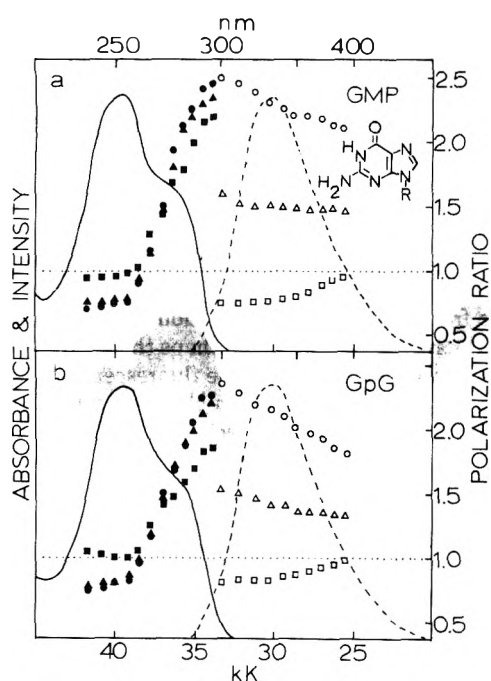


Figure 3. Absorption (—), fluorescence (---), and polarization ratios for ca. 10^{-4} M solutions of guanine derivatives in neutral ethylene glycol–water glasses at ca. -120 °C. (a) 5'-GMP (—R represents ribose phosphate): (●) $\lambda_f = 310$ nm; (▲) $\lambda_f = 330$ nm; (■) $\lambda_f = 390$ nm; (○) $\lambda_e = 290$ nm; (△) $\lambda_e = 270$ nm; (□) $\lambda_e = 250$ nm. (b) GpG: (●) $\lambda_f = 310$ nm; (▲) $\lambda_f = 330$ nm; (■) $\lambda_f = 390$ nm; (○) $\lambda_e = 290$ nm; (△) $\lambda_e = 270$ nm; (□) $\lambda_e = 250$ nm. (λ_e = excitation wavelength, λ_f = fluorescence wavelength.)

always greater than 2 except for the polymers, and usually approaches a value which one commonly attributes to $S = 1$, i.e., only one transition moment involved, common to both absorption and emission. (2) The polarization ratios for the pyrimidine monomers (CMP and TMP) show virtually no dependence on λ_e and λ_f for wavelengths greater than 260 nm in contrast to the purine monomers. (3) The purine monomer polarization ratios show marked dependences on λ_e and λ_f . (4) The differences between nucleotide and dinucleotide polarization patterns seem to be correlated somewhat with the corresponding differences in absorption and fluorescence spectra and are in the order $C > A > T = G$. The difference is quite striking for the pyrimidines, and, although significant for the purines, it is not so striking because the presence of two overlapping transitions and/or vibronic borrowing partly obscures the effect. (5) In the dinucleotides exhibiting large polarization differences relative to the monomer the variation of R with wavelength tends to fall off "exponentially", i.e., with positive curvature as the wavelength is changed away from the origin whereas for the monomers R changes characteristically in "sigmoidal" fashion, i.e., initially with negative curvature, often followed by an inflection. The latter behavior is very commonly observed in photoselection experiments where there are overlapping transitions and vibronic intensity borrowing.^{4d} (6) The polarization patterns of the polymers retain the essential features of their respective dimers but show significant randomization. That is, the polarization ratios have moved toward unity.

Finally, we point out a more subtle (but very important) feature present in the dimer and polymer spectra of C and A. The feature is the more or less parallel nature of the polarization curves, i.e., no matter how low a curve starts near the origin it always decreases as the wavelength varies away from the origin. This will be seen later to imply that the transition

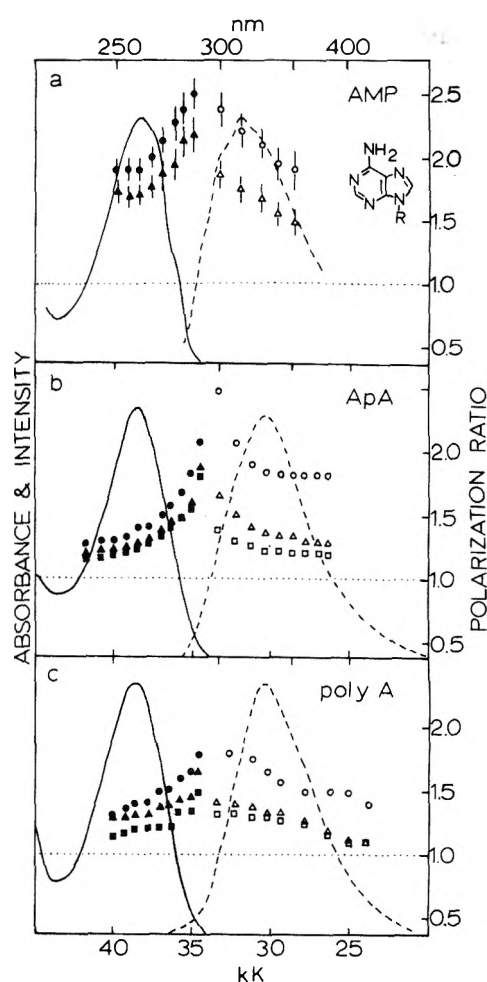


Figure 4. Absorption (—), fluorescence (---), and fluorescence polarization for dilute solutions of adenine derivatives in neutral ethylene glycol–water glasses at ca. -120 °C. (a) ca. 10^{-3} M 5'-AMP (—R represents ribose phosphate): (●) $\lambda_f = 300$ nm; (▲) $\lambda_f = 325$ nm; (○) $\lambda_e = 280$ nm; (△) $\lambda_e = 260$ nm. (b) ca. 10^{-4} M ApA: (●) $\lambda_f = 310$ nm; (▲) $\lambda_f = 330$ nm; (■) $\lambda_f = 360$ nm; (○) $\lambda_e = 290$ nm; (△) $\lambda_e = 270$ nm; (□) $\lambda_e = 250$ nm. (c) poly A, ca. 10^{-4} M in nucleotide units: (●) $\lambda_f = 310$ nm; (▲) $\lambda_f = 330$ nm; (■) $\lambda_f = 380$ nm; (○) $\lambda_e = 290$ nm; (△) $\lambda_e = 260$ nm; (□) $\lambda_e = 250$ nm. (λ_e = excitation wavelength, λ_f = fluorescence wavelength.)

moments involved must span a three-dimensional space, thus implicating charge resonance character in the excited state.

Discussion

Monomers. The polarization of the pyrimidine nucleotides shown in Figures 1a and 2a is high and constant throughout the first absorption band and also throughout the fluorescence. The results agree well in both cases with previous work on the free bases, 5-methylcytosine¹² and thymine.¹³ The high constant values allow for the reasonable assumption that $S = 1$ thereby establishing an R of 2.55 ± 0.05 as signifying $S = 1$, i.e., that the randomization factor, $\epsilon = 0.15 \pm 0.015$. We will assume this value to hold for the other systems studied here.

The results for GMP shown in Figure 3a are in close agreement with those previously reported¹⁴ for guanine and 9-ethylguanine in ethylene glycol–water (7:3) at -78 °C. The polarization drops rapidly as λ_e is decreased so as to excite into the second (more intense) band at 252 nm. As was pointed out in the previous fluorescence work and verified by subsequent polarized single-crystal reflection experiments,^{15,16} this is clear

evidence that there are two electronic transitions comprising the composite band from 300 to 230 nm whose transition moments are nearly perpendicular. Using $\epsilon = 0.15$ and the lowest value of R (0.70 ± 0.02), the value of S from eq 4 is 0.12 ± 0.02 . Assuming excitation is only to the higher state yields $S = \cos^2 \theta$ where θ is the angle between the two moments. One thus calculates $\theta = 69 \pm 2^\circ$, a value consistent with that reported by Clark¹⁶ for 9-ethylguanine of $71 \pm 6^\circ$.

A new feature reported here is the dependence of the polarization upon λ_f which is taken to be evidence of vibronic mixing in the fluorescent state. There are numerous examples of similar behavior in other molecules with nearby states.⁴ The two transitions under consideration have been assumed to be $\pi \rightarrow \pi^*$ because of their high intensity, and this has been born out by the crystal work.^{15,16} Let us define the transition moment direction for the 270-nm band as x and that for the 250-nm band as close to y and in-plane. The open circles show the polarization decreasing vs. λ_f when the absorbing moment is essentially pure x . The decrease could be either due to y or z intensity. Excitation into the y band yields the open boxes which are seen to indicate increasing polarization as λ_f increases. This means the y component of the fluorescence intensity is increasing with λ_f . Had it been z , the values given by the open boxes would not have increased but would have remained nearly constant with λ_f . Thus the borrowed intensity cannot be attributed to an out-of-plane transition. (This result is in marked contrast to that found for the dinucleotides ApA and CpC.) Of course, the weakness of low-lying z -polarized transitions, e.g., $n \rightarrow \pi^*$ is such that vibronic mixing with such states would not likely result in observable depolarization.

The appearance of mixed polarization in the fluorescence now warns us to be cautious in accepting at face value our predicted angle of 69° between the two moments since it is possible that vibronic mixing is partly responsible for the value $R = 0.70$ and that the actual angle is larger (a value of $R = 0.56$ would correspond to $S = 0$). The assumption that $\theta = 90^\circ$ leads to a predicted $R(\lambda_e, \lambda_f) = R(250, 390)$ of 0.85 whereas if $\theta = 69^\circ$, $R(250, 390)$ is predicted to be 0.92 in better agreement with the experimental value of 0.95. At this time we shall simply say that an angle near 70° is more likely than near 90° .

The polarized fluorescence for the other purine monomer, AMP, is shown in Figure 4a. The absorption band at 260 nm (as with the free base adenine and other alkyl or sugar substituted derivatives) shows no hint of being composite in nature, yet several experimental^{14,17-19} and theoretical²⁰ investigations have concluded that the band is composed to two $\pi \rightarrow \pi^*$ transitions. At least one $n \rightarrow \pi^*$ transition is also expected²¹ in this region since the lowest excited singlet in purine is definitely (n, π^*).²²

In contrast to the other bases there are marked differences in the photophysical properties of the free base, adenine (A), and the nucleotide, AMP. The fluorescence efficiency for AMP is on the order of ten times less than for A at a variety of temperatures and whereas A shows little or no mixed polarization when excited with $\lambda_e > 260 \text{ nm}$ ¹⁴ one sees considerable polarization dependence on λ_e and λ_f for AMP, even near the origin. It turns out that the fluorescence properties of A are, as predicted by Eastman,²³ dominated by a minor but highly fluorescent tautomer protonated at the 7 position as opposed to the 9 position. Drefus et al.²⁴ have recently shown from the temperature dependence of the uv spectrum of adenine in H₂O compared to 9-methyladenine and 7-methyladenine (7MA) that the tautomerization constant $K_T = [7\text{HA}]/[9\text{HA}]$ is 0.28 at 20 °C. We have recently found¹⁰ the

fluorescence efficiency (ϕ_f) of 7MA to be 0.20 at -110°C whereas that for AMP is only ca. 0.002. Furthermore we have found the fluorescence spectrum, excitation spectrum, and polarized fluorescence of 7MA to be very close to those of adenine. Thus there is little doubt that the difference between the fluorescence characteristics of A and AMP should be thought of more properly as, say, the difference between 7MA and AMP.

The fluorescence lifetime of AMP at 77 K in ethylene glycol-water has been reported to be ~ 100 times longer than expected from the integrated absorption and ϕ_f .^{9b} Eisinger and Lamola^{9a} have suggested that perhaps the wrong integrated absorption was used, i.e., that the fluorescence is actually a forbidden transition obscured in absorption by the nearby intense transition. This hypothesis was somewhat in discord with the polarized fluorescence work on adenine.¹⁴ However, it is now clear the results for adenine are not pertinent and the mixed polarization seen for AMP is consistent with the notion that the fluorescence is forbidden. We cannot say at this time whether the mixture involves out-of-plane intensity (as expected from $n \rightarrow \pi^*$ fluorescence) but we expect to clarify this point with experiments over an extended spectral range. The possibility also remains¹⁰ that ϕ_f intrinsically varies with λ_e and that the fluorescence lifetime predicted from measurements when $\lambda_e = \lambda_{\text{max}}$ was too short.

Dinucleotides. We first point out that the perturbation of "connecting" identical nucleotide moieties into a dinucleotide results in two distinct classes of response for the four systems studied here. For CpC and ApA there are small but significant blue shifts in the absorption and somewhat larger red shifts in the fluorescence relative to the monomers. In both cases the ϕ_f 's are larger, by a factor of ~ 2 and ~ 10 for CpC and ApA respectively and truly large effects are seen in the polarization. In contrast, the spectra and ϕ_f 's for dpTpT and GpG are virtually identical with those of their monomeric forms. However, considerable differences exist in their polarizations demonstrating the great sensitivity of this technique for detecting excited state interactions. In the discussion that follows we shall concentrate on CpC and dpTpT as the prototypes because of the apparent simplicity of their monomer polarization spectra.

In general, two superficially different points of view have been utilized in the study of excited state interactions between pairs of identical molecules which are not exchanging electrons. In the stationary exciton approach stationary states are constructed and the system treated as if it were a single molecule, i.e., absorption and emission spectra and intensities are deduced from the dimer energy eigenvalues and eigenfunctions. This approach has arisen and had its early successes²⁵ in application to systems characterized by intermediate to strong coupling, that is, when the intermolecular interaction is similar to or larger than the width of the vibronic envelope. The exciton formalism has also been used successfully to predict absorption properties of systems characterized by weak coupling, i.e., when the spectra are only slightly perturbed by the interaction.²⁶

In the other view, the energy transfer approach, the system is supposed to have been prepared with all the excitation localized on one of the monomers. Because of the intermolecular interaction this is not a dimer stationary state and the probability of finding excitation on the other monomer increases with time. This approach has had its origin and successes primarily in application to the kinetics of long range energy transfer¹ where the coupling is indeed very weak, i.e., no perceptible perturbation on the spectra. However the for-

malism of this approach has been extended to the strong coupling region.^{1b} Simpson and Peterson^{2b} have summarized the basic aspects of these two approaches in the two limits.

The two models obey the same Schrodinger equation and only differ in their initial time "boundary condition". However this "boundary condition" would seem to play a critical role in the understanding of polarized fluorescence measurements because one is presumably determining the average angle between the absorbing and emitting transition moments. Indeed, depending upon one's background or prejudice with regard to the two approaches, entirely different results would be predicted from "intuition" for the type of systems we are concerned with in this paper. The authors' initial approach was the stationary exciton model. Assuming that the monomer transition moments make an angle of ca. 36°, that the planes are stacked approximately face-to-face,²⁷ and that the dipole-dipole term dominates the interaction, the strong-coupling limit gives rise to two states with the higher-energy one connected to the ground state by transition moment $\tilde{m}_+ = 2^{-1/2} (\tilde{m}_A + \tilde{m}_B)$ and the lower by $\tilde{m}_- = 2^{-1/2} (\tilde{m}_A - \tilde{m}_B)$ where \tilde{m}_A and \tilde{m}_B are the monomer transition moments.^{2b} One then envisions the electronic structure of the dimer as not unlike that of GMP, i.e., two nearby perpendicularly polarized transitions with the higher one carrying the bulk of the oscillator strength. According to Kasha's rule²⁸ the fluorescence would always be from the lowest excited singlet, i.e., controlled by \tilde{m}_- . Thus the polarization picture was anticipated to be similar to that seen for GMP, namely, that when excitation is at short wavelengths the polarization ratio would be <1 because the absorption would be primarily by \tilde{m}_+ but emission by \tilde{m}_- . In contrast the energy transfer picture assumes that absorption is either by \tilde{m}_A or \tilde{m}_B and that emission is also by either \tilde{m}_A or \tilde{m}_B . If transfer is rapid there is a 50% probability that either \tilde{m}_A or \tilde{m}_B will emit when \tilde{m}_A absorbs, leading to a predicted *S* value of $\frac{1}{2}(1 + \cos^2 36^\circ) = 0.83$ or *R* = 2, independent of λ_e . The two pictures are grossly different and clearly our experimental results do not fit either picture at all well.

We shall return to this line of discussion later but now will describe our attempt to understand the experimental results from the stationary exciton approach. The picture outlined above was somewhat crude in that the molecular vibrations were not considered. Because the interaction is so weak in the dinucleotides the "+" and "-" bands are very overlapped. Fulton and Goutermann,^{2e,29} in developing the Moffitt-Witkowski³⁰ dimer model, have shown the formal equivalence between the vibronic dimer problem and the vibronic coupling between two electronic states of a single molecule (e.g., the coupling of the B_{2u} and E_{1u} states of benzene by e_{2g} vibrations from which the 260-nm transition derives its intensity). We have used the same model³¹ and performed many calculations in search of parameters which would predict spectra and polarizations similar to our observations. The model assumes two identical monomers topologically related by a symmetry operation. The dimer excited states in question are assumed to be well described by a basis consisting only of monomer Born-Oppenheimer wave functions in the harmonic approximation derived from a single monomer excited electronic state and in which only one monomer is excited. That is, monomer vibronic coupling and second order electronic effects of the type which lead to hypochromism, for example, are not considered. It is further assumed that the monomer spectrum shows a progression in only one vibrational normal mode, i.e., only one mode (the optical mode) changes its equilibrium position upon excitation. Its frequency does not change,

however.³² Other vibrations do not enter into the picture in the harmonic approximation and the relative intermolecular geometry is assumed fixed. The intermolecular interaction Hamiltonian, *H*_{AB}, is assumed independent of the monomer vibrations.

In practice we found the most transparent method of visualizing the problem and solving it was as a linear variation calculation in a representation for which the Hamiltonian matrix is diagonal in the strong coupling limit:³³

$$|\pm, q\rangle |a, Q_-\rangle |s, Q_+\rangle$$

$$|\pm, q\rangle = 2^{-1/2} [\psi_1(q_A)\psi_0(q_B) \pm \psi_0(q_A)\psi_1(q_B)]$$

$\psi_i(q_A)$ and $\psi_0(q_B)$ are the electronic wave functions for monomer A excited and monomer B in the ground state, respectively.

$|s, Q_+\rangle$ represents a displaced harmonic oscillator energy eigenstate with energy $(s + \frac{1}{2}) h\nu$ where ν is the frequency of the optical mode.

$$Q_+ = 2^{-1/2} [(Q_A - L/2) + (Q_B - L/2)] = Q_+ - L/2$$

where *Q*_A and *Q*_B are the monomer optical mode coordinates relative to the ground state equilibrium position and *L* is the equilibrium position in the excited monomer. Some insight into why this representation yields a diagonal Hamiltonian in the strong coupling limit is obtained by noticing $|\pm, q\rangle$ are the usual stationary exciton electronic functions and that, by definition, the excitation hopping is very fast relative to vibrational motion. Therefore the nuclei feel a force field which is the average of that for an excited and an unexcited molecule. *Q*_A and *Q*_B are thus displaced by only *L*/2 so that *Q*₊ is displaced by *L*/√2. This is a good time to note that such a displacement actually occurs in the strong coupling limit and requires an amount of energy $2 \times \frac{1}{2} k(L/2)^2 = k/4(L^2)$ where *k* is the force constant. Thus the center of gravity of the dimer exciton bands is shifted to higher energies by an amount equal to half the classical Franck-Condon band width. This is not a small term but has often been overlooked in attempts to estimate the magnitude of exciton interactions from shifts in absorption and fluorescence spectra.

Q₋ is $2^{-1/2} (Q_B - Q_A)$, the out-of-phase combination of the monomer optical modes. It acts as a promoting mode in the dimer to mix $|+\rangle$ and $|-\rangle$. This can be understood qualitatively by realizing that when *Q*₋ ≠ 0 *Q*_A ≠ *Q*_B and the two monomers are instantaneously nonidentical, i.e., the resonance is momentarily destroyed.

In this basis the Hamiltonian matrix is

$$H_{\pm, a, s; \pm a', s'} = [W + kL^2/4 \pm \beta + (a + \frac{1}{2})h\nu + (s + \frac{1}{2})h\nu] \delta_{aa'} \delta_{ss'}$$

$$H_{\pm, a, s; \mp a', s'} = 2^{1/2} kL(Q_-)_{aa'} \delta_{ss'} \delta_{a, a' \pm 1}$$

where *W* is a constant representing the energy of one excited and one ground state molecule in the absence of resonance interaction.

$$\beta = \langle \psi_1(q_A)\psi_0(q_B) | H_{AB}(q_A, q_B) | \psi_0(q_A)\psi_1(q_B) \rangle$$

the exciton interaction parameter, and $(Q_-)_{aa'}$ the position operator matrix for a harmonic oscillator. Thus we see this particular representation reduces the Hamiltonian into blocks identified by the quantum number *s* and the parity with respect to the symmetry operation. It is necessary only to diagonalize the two *s* = 0 blocks as the eigenvectors are independent of *s* and eigenvalues differ only by the constant *sh* ν . The solutions can be arbitrarily close to exact, depending on

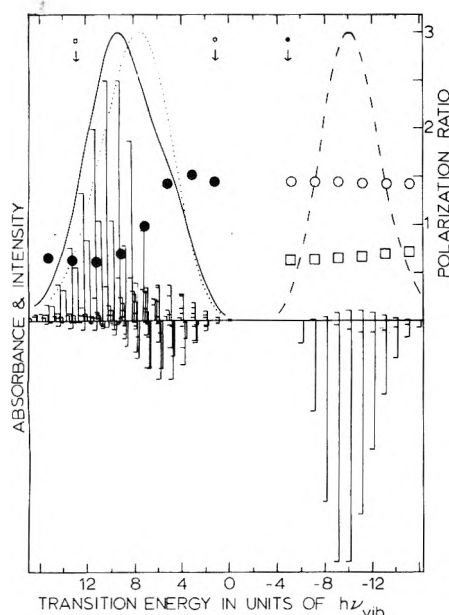


Figure 5. Theoretical absorption, fluorescence, and polarization spectra of a symmetrical dimer with sandwich geometry whose monomer transition moments make an angle of 60° . The monomer optical mode displacement upon excitation, L , is such that $\frac{1}{2} kL^2/h\nu_{\text{vib}} = 8$. Lines were broadened with Gaussians with half-widths of $2 h\nu_{\text{vib}}$ and $3.5 h\nu_{\text{vib}}$ in absorption and fluorescence respectively. (—) is the absorption when the exciton coupling constant, β , is $1.4 h\nu_{\text{vib}}$. (---) is the fluorescence when $\beta = 10 h\nu_{\text{vib}}$. \uparrow and \downarrow are the individual vibronic intensities due to \tilde{m}_+ and \tilde{m}_- , respectively. The fluorescence polarization ratios predicted from these parameters are indicated by the symbols. \bullet are for the fluorescence near the origin as shown by the arrow. \circ indicates excitation near the origin and \square near the high energy tail. Doubling $h\nu_{\text{vib}}$ relative to the bandwidth had very little effect on the polarization pattern. To illustrate the effect of interaction on the spectra, the monomer absorption envelope is also shown (....). The monomer 0-0 transition defines zero on the energy scale. Note that the fluorescence is shifted by only 6 units although $\beta_F = 10$ units.

the size of the Q_- basis chosen and the coupling strength. For the purpose of computing spectra and polarizations we found convergence, even in the weak-coupling limit ($\beta = 0$), for the case where $\frac{1}{2}kL^2 = 8h\nu$ using a basis of only 30 ($a = 0 - 29$).

Chambers et al.^{2g} have recently determined the polarized fluorescence of rhodamine B dimers in $\text{LiCl-H}_2\text{O}$ at 77 K and have shown that the perturbation limit of the approach described above provides a satisfactory qualitative explanation of their results. We have carried out exact calculations which indeed fit their published data quite well, although not perfectly. Chandross, Ferguson, and McRae^{2f} have also used this model to account successfully for the spectra of a stable dimer of anthracene. Thus, despite severe restrictions, the model is apparently useful for understanding the essential features of dimer spectra in some instances. The above cases are characterized by monomers which have a dominant optical mode and coupling of intermediate strength.

In attempting to apply this theory to DNA bases, which exhibit almost no vibrational structure, we have assumed the lack of structure to be the result of inhomogeneous broadening. This was accomplished by broadening the computed lines with a Gaussian of half-width = $h\nu$. Another problem is that, in general, considerable relaxation of the intermolecular distance is possible after excitation and before emission, as is deduced from the large fluorescence shifts relative to those of the absorption. This is often referred to as intramolecular excimer formation. For CpC the fluorescence shift is ca. 3000

cm^{-1} to longer wavelengths whereas the absorption peak is only shifted ca. 500 cm^{-1} to the blue. We have incorporated this relaxation into the theory by fitting the absorption curve with one value of $\beta = \beta_A$ and the fluorescence curve with a larger value of $\beta = \beta_F$. It is difficult to know a reasonable value to use for β_F since much of the fluorescence shift likely originates from charge resonance and the raising of the ground state. We have proceeded arbitrarily to use a value which produces the entire shift after determining that the predictions were not greatly effected by the actual value once the intermediate coupling region was reached.

Absorption and fluorescence spectra were computed by the usual³⁴ procedure in which the critical assumption is that only the pure transition moments \tilde{m}_+ and \tilde{m}_- are involved and that rapid vibrational relaxation and internal conversion occurs. Thus the fluorescence was assumed to originate entirely from the lowest level when $\beta = \beta_F$. This level was always well isolated relative to kT at the temperature of our experiments. Equations 3 and 4 were used to compute polarization ratios with the identification “-” $\leftrightarrow x$ and “+” $\leftrightarrow y$. We have assumed that excited state relaxation does not significantly change the direction of \tilde{m}_+ and \tilde{m}_- so that this theory cannot account for z polarization.

Figure 5 shows calculated spectra and polarizations for parameter values which gave a qualitative fit for the spectra of CpC. The calculated polarizations, however, cannot be said to represent the experimental results even qualitatively. No better fit could be found by varying β , L , ν , and θ_{AB} , the angle between \tilde{m}_A and \tilde{m}_B .

The nature of the failure of the theory for polarizations as a function of λ_e is that for reasonable value of β_A and θ_{AB} the vibronic coupling always introduces considerable “+” intensity into the absorption near the origin which leads to low polarization, independent of β_F . Experimentally there is always very high polarization at the origin. According to the theory, excitation at shorter wavelengths is almost entirely via \tilde{m}_+ and for reasonable values of θ_{AB} and β_F the fluorescence is mostly by \tilde{m}_- , leading to polarization less than unity. Experimentally the polarization does not drop below 1.2 when λ_f is near the origin. Probably the most important point is that the theory predicts an “S”-shaped transition from the higher to lower polarization values whereas the experimental results for CpC and ApA show an “exponential” type of variation. For dpTpT the polarizations could be matched by assuming negative values for β , as if \tilde{m}_A and \tilde{m}_B were head-to-tail instead of side-by-side. The required magnitudes of β however lead to significant spectral shifts whereas experimentally there are none.

Turning now to the variation in polarization with λ_f we see that the large changes seen for CpC are not in any way predicted by the theory. It was pointed out in some detail in a preliminary account⁷ of the CpC results that the transition moment responsible for the long-wavelength fluorescence is directed perpendicular to the plane of the two moments responsible for absorption. The basis for this assignment lies in the observation that if one assumes the depolarization when $\lambda_e = 250 \text{ nm}$ and $\lambda_f = 310 \text{ nm}$ is the consequence of light being absorbed $\sim 50\%$ along x and $\sim 50\%$ along y and likewise when $\lambda_e = 300 \text{ nm}$ and $\lambda_f = 460 \text{ nm}$, then, when $\lambda_e = 250 \text{ nm}$ and $\lambda_f = 460 \text{ nm}$ one still expects the probability of the photon being emitted by a moment parallel to its absorbing moment to be $\sim 50\%$, i.e., $S = 0.5$ or $R \sim 1.28$. Instead, $R(250,460) = 0.9$ corresponding to $S = 0.27$. Only a mixture of x and z intensity at 460 nm is consistent with this value. If the dimer is of the sandwich type, this means z is perpendicular to the molecular

planes. This apparently large out-of-plane component is also seen in Figures 1 and 4 for ApA, poly C, and poly A. It is furthermore present in the other dinucleotides ApC, ApU, GpA, ApG,³⁵ dpApA, and dpCpC.³⁶ Such behavior may indeed be even more general because it is strikingly apparent in the recently reported polarized fluorescence of the anthracene sandwich dimer.⁸ Furthermore Chaudhuri and Ganguly³⁷ have concluded that excimer fluorescence from pyrene crystals has an out-of-plane component of 38%.³⁸

A number of theoretical treatments have concluded that charge resonance is probably as important as excitation resonance in the excited dimers of hydrocarbons.³⁹ Such a conclusion is consistent with the idea that the molecular planes relax to such a close distance that fluorescence is to a steeply rising part of the ground state intermolecular potential curve.⁴⁰ The broadness and diffuseness of excimer fluorescence has been shown derivable from such a model.^{40b} For sandwich dimers exhibiting fairly high symmetry, charge resonance is expected to contribute only in-plane intensity of a weaker nature than that from the exciton part of the wave function.^{39b} This was our justification for expecting the purely excitonic theory described above to be qualitatively correct. However the actual geometry of excited dimers is generally uncertain even when the ground state geometry is known and it has been shown that charge resonance leads to out-of-plane intensity when the monomers are not perfectly superimposed or if they are noncoplanar.⁴¹ We have pointed out previously⁷ that the wavelength dependence of the polarization could be a manifestation of the strong dependence of charge resonance character upon intermolecular distance coupled with the large displacement of equilibrium separation in the ground and excited states. However we should like to point out that the fluorescence polarization experiments do not definitely prove out-of-plane polarization since a number of assumptions have been made along the way which we shall see may be somewhat questionable. Furthermore, uncertainty about actual geometries has discouraged theoretical investigations of sufficient rigor to say with confidence that out-of-plane intensity is the source of the effects observed. Experiments with oriented samples would be very helpful in this regard.

This note of caution with respect to charge resonance is prompted, in part, by the observation that the stationary exciton model apparently fails to properly describe the absorption process where charge resonance is not expected to be important. Thus whatever we are leaving out of the theory may eventually explain the fluorescence behavior without recourse to charge resonance.

An observation which emphasizes the last point and also serves to swing the focus back to the energy transfer picture is that the polarization ratio for dpTpT is considerably dependent on λ_f although there is no experimentally significant shift in the absorption or fluorescence relative to the monomer. Unfortunately, the changes are not quite sufficient within the present experimental precision to distinguish whether the source of the variation is as for CpC and ApA or not. The same may be said for GpG. From the energy transfer point of view one may say that our experiments fall into the general pattern noted by Weber and Shinitzky.⁵ They have found that a large number of aromatic systems fail to exhibit energy transfer (depolarization) between identical molecules when excited at the long wavelength edge. Considerable effort was made to find the source of the apparent breakdown of the Förster theory which has been very well obeyed for transfer between nonidentical molecules, but none was found. However the particularly intriguing observation was made by them that

when λ_e was away from the origin, the polarization of the fluorescence was time dependent but not so when λ_e was at the origin. Translated into stationary exciton language the observation would say that the rate of internal conversion between the "+" and "-" dimer electronic states depends on the amount of vibrational excitation. Such a concept is very commonplace in present investigations of radiationless transitions⁴² (of which energy transfer is certainly an example). To emphasize this we note that energy transfer from one excitation-localized state to the other spans exactly the same space as internal conversion from $|+\rangle$ to $|-\rangle$. Within the context of the vibronic stationary exciton theory which we have described, internal conversion between "+" and "-" states is technically not possible for the isolated dimer because they are eigenfunctions of the full Hamiltonian of the model. The reason for expecting the internal conversion is simply through analogy with the behavior of single molecules which was seen to be sufficient for the rhodamine B dimer. This dimer seems to conform to the model discussed here fairly well in that only one optical mode is obvious, the first transition is well isolated and the intramolecular geometry is apparently quite rigid. On the other hand the dinucleotides may well have several optical modes, the first transition is not so well isolated, and the intramolecular geometry is clearly free to relax in many cases. However we feel the more significant difference is the much weaker coupling in the case of the dinucleotides.

Clearly, stationary exciton theory has to break down in the extreme limit of weak coupling because this is also the monomer limit, i.e., where the monomers behave independently. A proper theory must make a smooth transition from the intermediate coupling example of rhodamine B (where the assumption that excitation leaves the system in a statistical mixture of dimer stationary states) to the monomer limit (where excitation produces a statistical mixture of excited monomers). We suggest that the systems under consideration here fall in the transition region which, as usual, is not characterized by simple rules. Rhodes⁴³ and Simpson⁴⁴ have recently presented treatments of the interaction of radiation and matter which may be useful here.

Polymers. The polarization of fluorescence in poly A and poly C relative to that for the respective dinucleotides is of interest with regard to the question of long range energy transfer in polynucleotides. The current understanding has been summarized by Eisinger and Lamola.^{9a} The similarity of polymer spectra to dinucleotide spectra has been the basis for assuming the excited states of the polymers to be excimer-like. Gueron et al. have predicted from the Förster theory that considerable transfer is possible for poly A and poly C before vibrational relaxation but very little after relaxation. If energy was indeed transferred over many monomer units before being trapped as an excimer, the polymer fluorescence should be greatly depolarized relative to that of the monomer. Such an effect has apparently been searched for with negative result but no details have been published.^{9a}

For the case of poly A there is seen to be little difference relative to ApA when λ_e and λ_f are at the respective maxima. However since I_v/I_h is ca. 1.25 ($S \sim 0.5$) considerable transfer could go undetected providing the transition moments were essentially perpendicular to the direction of transfer. Looking at all the wavelengths shows significant differences but the essential features characteristic of the dinucleotide are retained. The polarization is sufficiently high near the origin as to preclude transfer by more than one or two units. Much the same may be said of poly C.

Clearly little more which is meaningful may be said regarding the polymers until an acceptable understanding of the dinucleotides is reached. All the questions regarding the stationary vs. energy transfer picture are applicable to larger aggregates.

Acknowledgment. This work was supported in part by a grant from the Research Corporation.

References and Notes

- (1) For example: (a) Th. Förster, *Discuss. Faraday Soc.*, **27**, 7 (1959); (b) Th. Förster in "Modern Quantum Chemistry III", O. Sinanoglu, Ed., Academic Press, New York, N.Y., 1965, pp 93-137; (c) I. B. Berlman, "Energy Transfer Parameters of Aromatic Compounds", Academic Press, New York, N.Y., 1973.
- (2) For example: (a) W. T. Simpson and D. L. Peterson, *J. Chem. Phys.*, **26**, 588 (1957); (b) G. S. Levinson, W. T. Simpson, and W. Curtis, *J. Am. Chem. Soc.*, **79**, 4314 (1957); (c) M. Kasha, *Radiat. Res.*, **20**, 55 (1963); (d) E. G. McRae, *Aust. J. Chem.*, **14**, 344 (1961); (e) R. L. Fulton and M. Gouterman, *J. Chem. Phys.*, **41**, 2280 (1964); (f) E. A. Chandross, J. Ferguson, and E. G. McRae, *ibid.*, **45**, 3546 (1966); (g) R. W. Chambers, T. Kajiwara, and D. R. Kearns, *J. Phys. Chem.*, **78**, 380 (1974).
- (3) Two comprehensive review articles on excimers are: (a) Th. Förster, *Angew. Chem., Int. Edit. Engl.*, **8**, 33 (1969); (b) J. B. Birks, *Nature (London)*, **214**, 1187 (1967).
- (4) (a) A. C. Albrecht, *J. Mol. Spectrosc.*, **6**, 84 (1961); (b) W. Liptay in "Modern Quantum Chemistry III", O. Sinanoglu, Ed., Academic Press, New York, N.Y., p. 81; (c) F. Dörr in "Creation and Detection of the Excited State", Vol. 1A, A. Lamola, Ed., Marcel Dekker, New York, N.Y., 1971, p 53; (d) A. H. Kalantar and A. C. Albrecht, *Ber. Bunsenges. Phys. Chem.*, **68**, 361 (1964).
- (5) G. Weber and M. Shinitzky, *Proc. Natl. Acad. Sci. U.S.A.*, **65**, 823 (1970).
- (6) H. Beens, H. Mohwald, D. Rehm, E. Sackman, and A. Weller, *Chem. Phys. Lett.*, **8**, 341 (1971).
- (7) P. R. Callis, *Chem. Phys. Lett.*, **19**, 551 (1973).
- (8) P. C. Subudhi, N. Kanamaru, and E. C. Lim, *Chem. Phys. Lett.*, **32**, 503 (1975).
- (9) (a) J. Eisinger and A. A. Lamola in "Excited States of Proteins and Nucleic Acids", R. F. Steiner and I. Weinryb, Ed., Plenum Press, New York, N.Y., 1971, Chapter 3; (b) J. Eisinger, *Photochem. Photobiol.*, **7**, 597 (1968).
- (10) R. W. Wilson, J. P. Morgan, and P. R. Callis, *Chem. Phys. Lett.*, **36**, 618 (1975).
- (11) We wish to emphasize that ϕ can in no way be related to actual rotary Brownian motion since the randomization is independent of temperature, viscosity, and molecular size in the limit where the rotational relaxation time \gg fluorescence lifetime.
- (12) P. R. Callis and W. T. Simpson, *J. Am. Chem. Soc.*, **92**, 3593 (1970).
- (13) P. R. Callis, Ph.D. Thesis, University of Washington, 1965, p 39.
- (14) P. R. Callis, E. J. Rosa, and W. T. Simpson, *J. Am. Chem. Soc.*, **86**, 2292 (1964).
- (15) P. R. Callis, B. Fanconi, and W. T. Simpson, *J. Am. Chem. Soc.*, **93**, 6679 (1971).
- (16) L. B. Clark, personal communication.
- (17) R. F. Stewart and N. Davidson, *J. Chem. Phys.*, **39**, 255 (1963).
- (18) H. H. Chen and L. B. Clark, *J. Chem. Phys.*, **58**, 2593 (1973).
- (19) L. B. Clark and I. Tinoco, Jr., *J. Am. Chem. Soc.*, **87**, 11 (1965).
- (20) W. Hug and I. Tinoco, Jr., *J. Am. Chem. Soc.*, **95**, 2803 (1973).
- (21) W. Hug and I. Tinoco, Jr., *J. Am. Chem. Soc.*, **96**, 665 (1974), and references therein.
- (22) B. J. Cohen and L. Goodman, *J. Am. Chem. Soc.*, **87**, 548 (1965).
- (23) J. W. Eastman, *Ber. Bunsenges. Phys. Chem.*, **73**, 407 (1969).
- (24) M. Drefus, G. Dodin, O. Bensaude, and J. E. Dubois, *J. Am. Chem. Soc.*, **97**, 2369 (1975).
- (25) For examples see ref 2b, 2c, 2d, 2f, and 2g.
- (26) See, for example, H. DeVoe, *J. Chem. Phys.*, **37**, 1534 (1962), and references therein.
- (27) (a) W. C. Johnson, Jr., and I. Tinoco, Jr., *Biopolymers*, **8**, 715 (1969); (b) B. W. Bangerter and S. I. Chan, *J. Am. Chem. Soc.*, **91**, 3910 (1969), and references therein; (c) M. J. Lowe and J. A. Schellman, *J. Mol. Biol.*, **65**, 91 (1972); (d) R. O. Day, N. C. Seeman, J. M. Rosenberg, and A. Rich, *Proc. Natl. Acad. Sci. U.S.A.*, **70**, 849 (1973), and references therein; (e) ref 9a, p 127.
- (28) M. Kasha, *Discuss. Farad. Soc.*, **9**, 14 (1950).
- (29) R. F. Fulton and M. Gouterman, *J. Chem. Phys.*, **35**, 1059 (1961).
- (30) A. Witkowski and W. Moffitt, *J. Chem. Phys.*, **33**, 879 (1960).
- (31) A number of interesting discussions within the framework of this model have appeared. For example: (a) R. Lefebvre and M. Garcia Sucre, *Int. J. Quantum Chem.*, **1S**, 339 (1967); (b) A. Witkowski in "Modern Quantum Chemistry III", O. Sinanoglu, Ed., Academic Press, New York, N.Y., 1965, pp 161-175; (c) R. E. Merrifield, *Radiat. Res.*, **20**, 154 (1963); (d) A. Bierman, *J. Chem. Phys.*, **45**, 647 (1966); (e) J. H. Young, *ibid.*, **49**, 2566 (1968).
- (32) The theory has been extended to include the force constant change by M. Garcia Sucre, *Int. J. Quantum Chem. III*, 327 (1969).
- (33) This representation is, of course, suggested by the finding of Merrifield^{31c} and of Fulton and Gouterman.²⁹ The Hamiltonian is also diagonal in the representation used by McRae^{2d} in the strong coupling limit. We have found that the transformation between the two representations only mixes functions with same total number of vibrational quanta in accordance with the preceding sentence.
- (34) References 2c-2g, 32, and 31a provide examples.
- (35) R. W. Wilson, Ph.D. Thesis, Montana State University, 1974.
- (36) R. W. Wilson and P. R. Callis, unpublished results.
- (37) M. K. Chaudhuri and S. C. Ganguly, *J. Phys. C*, **3**, 1791 (1970).
- (38) However, in a similar study [R. Hochstrasser and A. Malliaris, *J. Chem. Phys.*, **42**, 2243 (1965)] reported no evidence of out-of-plane intensity although their experimental results were nearly identical. In fact, the short axis and out-of-plane axis have very similar projections in the faces studied and it is probably not possible to make a definitive statement regarding the amount of out-of-plane intensity.
- (39) (a) T. Azumi, A. T. Armstrong, and S. P. McGlynn, *J. Chem. Phys.*, **41**, 3839 (1964); (b) T. Azumi and S. P. McGlynn, *ibid.*, **41**, 3131 (1964); (c) M. T. Vala, Jr., I. H. Hillier, S. A. Rice, and J. Jortner, *ibid.*, **44**, 23 (1966); (d) J. N. Murrell and J. Tanaka, *Mol. Phys.*, **7**, 363 (1964).
- (40) (a) J. B. Birks and A. A. Kazzaz, *Proc. R. Soc. London, Ser. A.*, **304**, 291 (1968); (b) L. Glass, I. H. Hillier, and S. A. Rice, *J. Chem. Phys.*, **45**, 3886 (1966).
- (41) (a) T. Azumi and S. P. McGlynn, *J. Chem. Phys.*, **42**, 1675 (1965); (b) B. N. Srinivasan, J. V. Russell, and S. P. McGlynn, *ibid.*, **48**, 1931 (1968).
- (42) C. S. Huang and E. C. Lim, *J. Chem. Phys.*, **62**, 3826 (1975), and references therein.
- (43) W. Rhodes, *Chem. Phys.*, **4**, 259 (1974).
- (44) W. T. Simpson, *Theor. Chim. Acta*, **23**, 295 (1972).
- (45) M. Gueron, J. Eisinger, and R. G. Shulman, *J. Chem. Phys.*, **47**, 4077 (1967).

Discussion

J. W. LONGWORTH. What was the temperature used when the fluorescence anisotropy spectra were measured?

R. W. WILSON. We probably know it to within 2 or 3° of 150 K, the glass transition temperature. These glasses crack at temperatures just slightly below this.

In Vitro Energy Transfer in *Renilla* Bioluminescence

William W. Ward* and Milton J. Cormier

Bioluminescence Laboratory, Department of Biochemistry, University of Georgia, Athens, Georgia 30602

(Received February 17, 1976)

Publication costs assisted by the U.S. Energy Research and Development Administration

The *in vitro* bioluminescent oxidation of *Renilla* (sea pansy) luciferin by luciferase produces a broad, structureless emission, peaking in the blue at 490 nm. In contrast, the live animal produces a structured emission peaking in the green at 509 nm. This difference in emission characteristics is due to the presence, in *Renilla*, of a green fluorescent protein (GFP). Addition of GFP *in vitro* sensitizes the oxyluciferin product excited state, resulting in the narrow, structured green emission characteristic of GFP fluorescence (λ_{\max} 509 nm). Under conditions of efficient *in vitro* energy transfer (2.7×10^{-6} M GFP) the radiative quantum yield (with respect to luciferin) increases 5.7-fold from 5.3% (blue pathway) to 30% (green pathway). The fluorescence quantum yield of the *Renilla* GFP has been measured as 30%; thus, within the precision of our measurements (15% coefficient of variation) the *in vitro* energy transfer efficiency is a surprising 100%. We submit this report as the first quantitative study of *in vitro* energy transfer in a natural biological system.

Introduction

Most bioluminescent marine coelenterates are known to produce green light with a characteristically narrow and structured emission spectrum.¹⁻⁴ Their soluble extracts, however, generate broad unstructured emissions peaking in the blue.⁴⁻⁷ A green fluorescent protein (GFP), containing an unidentified chromophore whose fluorescence emission matches the *in vivo* bioluminescence, has been isolated from several of these coelenterates.^{3-6,8} This protein has been thought to function as a sensitizer or energy-transfer acceptor in the *in vivo* reaction,^{2,4,5} but previous demonstrations of bioluminescence energy transfer *in vitro* have been inconclusive due to impure components, the high concentrations of proteins required, and questionable quantum yield data.^{4,5} Those obstacles have been overcome and we now report the first quantitative evidence that energy transfer to the green fluorescent protein does occur in a soluble *in vitro* system at low protein concentrations with a substantial increase in radiative quantum yield.

Reaction Scheme

The requirements for bioluminescence in the sea pansy *Renilla reniformis* are known and each component has been purified to homogeneity and physically characterized.⁸⁻¹² These components include the enzyme luciferase, the substrate luciferin (either free or bound to a specific protein—the luciferin binding protein), and the green fluorescent protein (GFP). Luciferase catalyzes the oxidative decarboxylation of luciferin to yield enzyme-bound oxyluciferin monoanion in the excited state.¹¹ In the absence of GFP, oxyluciferin decays to the ground state with the emission of blue light (λ_{\max} 490 nm). In the presence of the green fluorescent protein, the *in vitro* light emission changes from blue to green (λ_{\max} 509 nm). A scheme representing the *Renilla* bioluminescence system appears in Figure 1.

In Vitro Assay

In vitro energy transfer to the *Renilla* green fluorescent protein was quantitatively assayed by measuring the green to blue photon emission ratio with a dual-phototube photometer. Collimated light from the bioluminescent sample was

split into two perpendicular beams by a prismatic beam splitter. Before reaching the phototubes, the two beams were filtered through narrow-band-pass interference filters (Ditric Optics) with transmission maxima at 510 nm (green) and 480 nm (blue), respectively. The ratio (R) of corrected¹³ phototube outputs is represented in eq 1 where G and B are the numbers of photons emitted at specified wavelengths, via the green (GFP) pathway and the blue (oxyluciferin monoanion) pathway, respectively.

$$R_{510/480} = \frac{G_{510} + B_{510}}{G_{480} + B_{480}} \quad (1)$$

The blue pathway produces virtually equal (1.02:1.00) photon intensities at 510 and 480 nm.¹⁴ The green-pathway emission at 480 nm is negligible (<1%) in comparison to its emission at 510 nm. Thus eq 1 can be simplified as

$$R = \frac{G_{510} + B_{510}}{B_{510}} \quad (2)$$

$$R = \frac{G_{510}}{B_{510}} + 1 \quad (3)$$

$$R - 1 = \frac{G_{510}}{B_{510}} \quad (4)$$

The percentage of luciferin molecules which emit via the green pathway (G_{path}), as opposed to the blue pathway (B_{path}), is expressed by

$$\% G_{\text{path}} = \frac{G_{\text{path}}}{G_{\text{path}} + B_{\text{path}}} \times 100 \quad (5)$$

Algebraic manipulations of (5) yield

$$\% G_{\text{path}} = \frac{G_{510} \frac{G_{\text{tot}}}{\phi_G G_{510}}}{G_{510} \frac{G_{\text{tot}}}{\phi_G G_{510}} + B_{510} \frac{B_{\text{tot}}}{\phi_B B_{510}}} \times 100 \quad (6)$$

$$= \frac{G_{510} X}{G_{510} X + B_{510} Y} \times 100 \quad (7)$$

$$= \frac{G_{510}/B_{510}}{G_{510}/B_{510} + Y/X} \times 100 \quad (8)$$

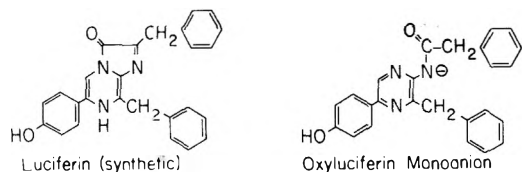
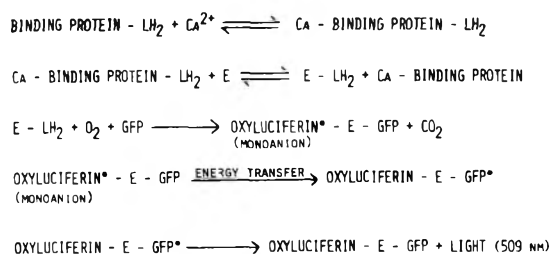


Figure 1. *Renilla* bioluminescence reaction scheme. Luciferase and green fluorescent protein are abbreviated with the letters E and GFP, respectively. The structures for a fully active synthetic analogue of luciferin (LH₂) and its oxidation product are also shown.

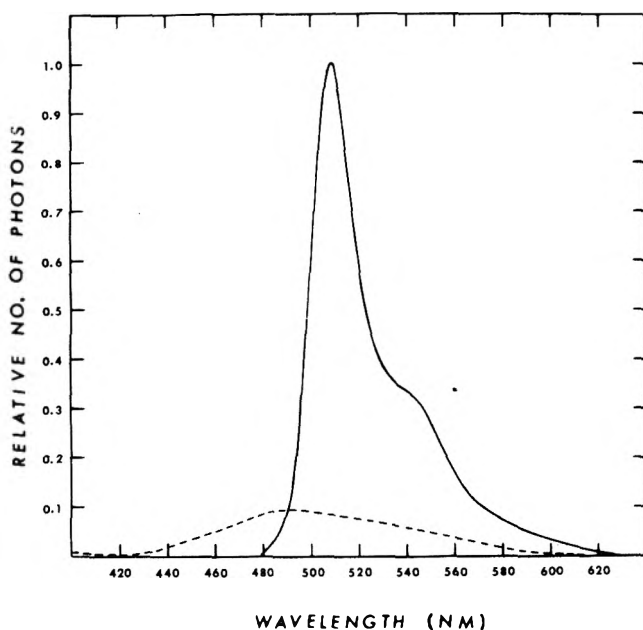


Figure 2. The *Renilla* green emission spectrum (solid line) and blue emission spectrum (dash line). These spectra are plotted in the green to blue total photon ratio ϕ^2 5.7. (Spectral data were taken from Wampler et al.⁴ and Cormier et al.¹⁴.)

where the subscript "tot" refers to the total number of photons over the entire emission spectrum and ϕ refers to the bioluminescence quantum yield relative to luciferin.

Substitution of (4) into (8) yields

$$\% G_{\text{path}} = \frac{R - 1}{R - 1 + Y/X} \times 100 \quad (9)$$

A value of 12.2 has been calculated for the term Y/X .

Routine energy-transfer assays were performed at room temperature in standard 10×75 mm test tubes containing a final volume of 200 μl . A listing of the requirements for efficient in vitro energy transfer appears in Table I.

Energy-Transfer Efficiency

The efficiency (E) of energy transfer from the excited-state oxyluciferin monoanion to the green fluorescent protein is defined

TABLE I: Requirements for in Vitro Energy Transfer in *Renilla* Bioluminescence (pH 6-9)

Component	Final concn, M
GFP	10^{-7} - 10^{-5}
Luciferase	10^{-9} - 10^{-4}
Luciferin or binding protein	10^{-8} - 10^{-5}
Tris-HCl or Phosphate ^a	10^{-3}

^a Other buffer systems have not been tested. Low ionic strength and presence of dissolved oxygen are both required for energy-transfer assays.

TABLE II: Experimental Determinations for Terms of Eq 11

Term	Value	Std dev
ϕ_B	0.0532 einstein/mol of LH ₂	$\pm 0.0015^a$
ϕ_G/ϕ_B	5.71 ^b	± 0.66
ϕ_{F1}	0.30 ^c	

^a Calculation of this standard deviation incorporates the major source of error—assay variability (four determinations). Confidence limits for the phototube calibration (reported by Lee et al.¹⁵ to be $\pm 7\%$) and the luciferin extinction coefficient determination have not been established. ^b The seven determinations of the green-pathway quantum yield, from which this number is calculated, were performed at a final GFP concentration of 2.7×10^{-6} M. Under these conditions the percentage of luciferin molecules emitting via the green pathway approaches 90%. Thus 5.71 must be considered a minimum estimate. ^c Data from Wampler et al.⁴ reported relative to quinine sulfate.

$$E = \phi_G \frac{1}{\phi_{F1}} \quad (10)$$

where ϕ_G is the quantum yield of green-pathway bioluminescence with respect to luciferin and ϕ_{F1} is the fluorescence quantum yield of the GFP. The photometer used for absolute quantum yield determinations had been calibrated against the luminol standard of Lee et al.¹⁵ for the blue-pathway *Renilla* emission. Thus it is convenient to modify eq 10 as follows

$$E = \phi_B \left(\frac{\phi_G}{\phi_B} \right) \frac{1}{\phi_{F1}} \quad (11)$$

Experimental determinations for the three terms in eq 11 are listed in Table II. A numerical solution to eq 11 which incorporates these determinations is shown by

$$E = 0.0532 \times 5.71 \times \frac{1}{0.30} = 1.01 \pm 0.15 \quad (12)$$

Discussion

The addition of micromolar quantities of *Renilla* green fluorescent protein (GFP) to a *Renilla* bioluminescence reaction mixture markedly affects the wavelength distribution and quantum yield of the in vitro emission. The bioluminescence emission spectrum shifts from the broad, unstructured blue emission of the oxyluciferin monoanion (λ_{max} 490 nm) to the narrow, structured green emission characteristic of the fluorescence of the GFP. Concomitant with this spectral shift is a 5.7-fold increase in the bioluminescence quantum yield. These spectral changes are illustrated in Figure 2. Within the limitations of our measurements, the bioluminescence quantum yield in the presence of 2.7×10^{-6} M GFP is iden-

tical with the fluorescence quantum yield of GFP. Thus, the calculated efficiency of energy transfer is 100%.

Radiationless energy transfer has been proposed as a mechanism to account for the green emission in coelenterates.² However, sensitized fluorescence of the green fluorescent protein cannot be explained by Förster-type energy transfer in homogeneous solution;¹⁶ the concentration of GFP required for efficient energy transfer is several orders of magnitude too low. Therefore we must propose an association of the green fluorescent protein with luciferase. Our present studies and the earlier work of Wampler et al.^{4,8} lend support for that proposal. The green emission is highly dependent on GFP concentration and ionic strength implying that complex formation between luciferase and GFP is necessary prior to the emission of green luminescence. Such an association could result in radiationless energy transfer from the electronic excited state of enzyme-bound oxyluciferin monoanion to the chromophore on GFP. We have recently shown, by the chromatographic method of Hummel and Dreyer,¹⁷ that luciferase does associate with GFP in dilute aqueous solution at low ionic strength. A preliminary report of these findings has been presented.¹⁸ Details of this protein-protein association, currently under investigation in our laboratory, will be communicated at a later date.

Our reports on the *Renilla* bioluminescence system represent the first quantitative study of in vitro energy transfer in a natural biological system. Through further study on the mechanism of energy transfer in *Renilla* we hope to establish this as a model system for the study of biological energy transfer and protein-protein interaction.^{19,20}

References and Notes

- (1) F. H. Johnson, O. Shimomura, Y. Saiga, L. C. Gershman, G. T. Reynolds, and J. R. Waters, *J. Cell. Comp. Physiol.*, **60**, 85 (1962).
- (2) J. G. Morin and J. W. Hastings, *J. Cell. Physiol.*, **77**, 313 (1971).
- (3) J. E. Wampler, Y. D. Karkhanis, J. G. Morin, and M. J. Cormier, *Biochim. Biophys. Acta*, **314**, 104 (1973).
- (4) J. E. Wampler, K. Hori, J. W. Lee, and M. J. Cormier, *Biochemistry*, **10**, 2903 (1971).
- (5) H. Morise, O. Shimomura, F. H. Johnson, and J. Winant, *Biochemistry*, **13**, 2656 (1974).
- (6) M. J. Cormier, K. Hori, and J. M. Anderson, *Biochim. Biophys. Acta*, **346**, 137 (1974).
- (7) J. G. Morin and J. W. Hastings, *J. Cell. Physiol.*, **77**, 305 (1971).
- (8) J. E. Wampler, Y. D. Karkhanis, K. Hori, and M. J. Cormier, *Fed. Proc., Fed. Am. Soc. Exp. Biol.*, **31**, 419 (1972).
- (9) J. C. Matthews, K. Hori, and M. J. Cormier, Abstracts, American Society for Photobiology Meeting, Louisville, Ky., 1975, p. 42.
- (10) K. Hori and M. J. Cormier, *Proc. Natl. Acad. Sci. U.S.A.*, **70**, 120 (1973).
- (11) K. Hori, J. E. Wampler, J. C. Matthews, and M. J. Cormier, *Biochemistry*, **12**, 4463 (1973).
- (12) J. M. Anderson, H. Charbonneau, and M. J. Cormier, *Biochemistry*, **13**, 1195 (1974).
- (13) The absolute photon ratio (510 nm:480 nm) for the *Renilla* blue emission is 1.02. Thus a correction factor is determined by dividing 1.02 by the instrumental photon ratio for the blue emission.
- (14) M. J. Cormier, K. Hori, Y. D. Karkhanis, J. M. Anderson, J. E. Wampler, J. G. Morin, and J. W. Hastings, *J. Cell. Physiol.*, **81**, 291 (1973).
- (15) J. Lee, A. A. Wesley, J. F. Ferguson, and H. H. Seliger in "Bioluminescence in Progress", F. H. Johnson and Y. Haneda, Ed., Princeton University Press, Princeton, N.J., 1966, p. 35.
- (16) T. Förster, *Z. Naturforsch., A*, **4**, 321 (1949).
- (17) J. P. Hummel and W. J. Dreyer, *Biochim. Biophys. Acta*, **63**, 530 (1962).
- (18) W. W. Ward and M. J. Cormier, Abstracts, American Society for Photobiology Meeting, Denver, Col., 1976, p. 121.
- (19) The research was supported in part by an NIH postdoctoral fellowship (1 F32 EY 05104-01) to W. W. Ward and grants from the NSF (BMS 74-06914) and the ERDA (AT 38-1-635) to M. J. C. This paper is contribution No. 312 from the University of Georgia Marine Institute, Sapelo Island, Ga.
- (20) The authors wish to thank Dr. K. Hori, who supplied synthetic benzyl luciferin, and Mr. J. C. Matthews, who prepared pure luciferase for these experiments.

Excited State Interactions of α -Tocopherol and Molecular Oxygen

Dale E. Brabham* and John Lee

Department of Biochemistry, University of Georgia, Athens, Georgia 30602 (Received February 17, 1976)

Publication costs assisted by the National Institutes of Health

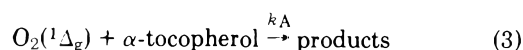
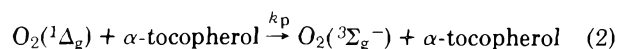
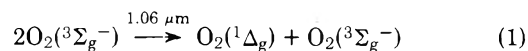
One function suggested for α -tocopherol in biological systems is for protection of cellular components against attack by singlet oxygen ($^1\Delta_g$). We wish to report the total quenching constant, k_Q , and chemical reaction rate constant, k_A , for directly generated (laser) singlet oxygen by α -tocopherol in freon 113. By its rate of competition with the chemical reaction of singlet oxygen with bilirubin, the sum of k_P and k_A (i.e., k_Q) is measured to be $3.1 \pm 1.2 \times 10^7 \text{ M}^{-1} \text{ s}^{-1}$, and by following the loss of α -tocopherol, k_A is found to be $1.9 \pm 0.5 \times 10^6 \text{ M}^{-1} \text{ s}^{-1}$. The ratio k_A/k_Q is similar to that found in studies of indirectly generated (sensitized) singlet oxygen but the absolute value of k_Q is lower. Comparison of the indirect measurements reveals that whereas k_A is unaffected by polarity in non-hydroxylic solvents, in methanol it is increased about ten times, and this, as well as the reactivity differences among substituted tocopherols, suggests a mechanism of electrophilic attack by the singlet oxygen. A novel result is the oxygen enhancement of absorption of the long-wavelength side of the first excited singlet absorption of α -tocopherol in freon 113. This enhancement depends linearly on oxygen concentration which, based on a similar observation of naphthalene by Evans, can be taken as evidence for a contact charge-transfer interaction; however, comparison of the relevant matrix elements illustrates only a potential role for this charge-transfer interaction in the quenching of singlet oxygen.

Tocopherols are naturally occurring phenols that have a long chain aliphatic tail. Of these α -tocopherol (vitamin E) has the highest degree of methyl substitution on the phenolic ring and the greatest sensitivity to dye-sensitized photooxidation. The chemical and physical interactions of molecular oxygen with α -tocopherol are not only of biochemical importance, but also stimulate and point to the necessity for more systematic studies of phenols and aromatics.

The electronic state dynamics of a collision complex of α -tocopherol and molecular oxygen can be examined both by chemical kinetics and by optical spectroscopy. One significant aspect is the quenching of the oxygen $^1\Delta_g$ state by tocopherol,¹⁻⁴ for the quenching process is primarily physical in nature. Because of this a protective function has been proposed for tocopherols in mammalian systems^{1,2} that is analogous to the proposed role for β -carotene in green plants.⁵ Singlet oxygen can be produced by light in red blood cells containing porphyrin breakdown products of heme. The presence of tocopherols in membranes might serve to inhibit oxidative reactions of this singlet oxygen.

The mechanism suggested for the efficient quenching of singlet oxygen by β -carotene is an energy transfer process that produces a triplet state carotene.⁵ This postulated triplet must be lower in energy than the singlet state of oxygen. Although this is conceivable for β -carotene, it is not possible for tocopherol since the lowest triplet state is located in the ultraviolet.⁶ Instead a mechanism has been proposed where quenching of the singlet oxygen is a result of a charge-transfer interaction between tocopherol (electron donor) and oxygen (electron acceptor).² The basis of this proposal is from quenching studies of electron donors (amines) where the physical quenching constant correlates inversely with the amine ionization potential.⁷⁻¹⁰

Experiments were undertaken to directly measure k_P and k_A the rate constants for processes 2 and 3 by generating ($^1\Delta_g$) oxygen in solution with the 1.06- μm output of a Nd-YAG laser (1). These values indicate the degree to which tocopherol physically quenches singlet oxygen in an inert solvent.



Higher state interactions of the oxygen-tocopherol collision complex were investigated by optical absorption. The extent to which the interaction Hamiltonian of the complex mixes higher states of the complex can be partially determined from these spectra.

Experimental Section

CP grade α -*dl*-tocopherol was obtained from Nutritional Biochemical Co.; Sigma grade bilirubin from Sigma Chemical Co., and technical grade freon 113 from Matheson Gas Products. All were used as supplied.

A Holobeam Nd-YAG laser was operated continuous wave in an apparatus previously described.¹¹ The high-pressure cell was constructed of stainless steel and quartz windows. Spectra were measured on a Cary 14 spectrophotometer.

Results and Discussion

All experiments were performed in the high-pressure cell under varying pressures of oxygen up to 1500 psi (4.2 M O₂). Expected difficulties from reaction of tocopherol with ground state oxygen at this high concentration were avoided by designing experiments of short duration and by maintaining pressurized solutions in the dark prior to use. Determination of tocopherol by optical absorbance was found unsatisfactory for samples treated with singlet oxygen¹² and the method of Emmerie-Engel (Analytical Methods Committee¹³) was adopted. Samples were transferred quantitatively from the high-pressure cell to a vacuum system, where the freon could quickly be removed leaving a residue to be assayed.

Loss of α -tocopherol is shown in Figure 1. The k_A is calculated from

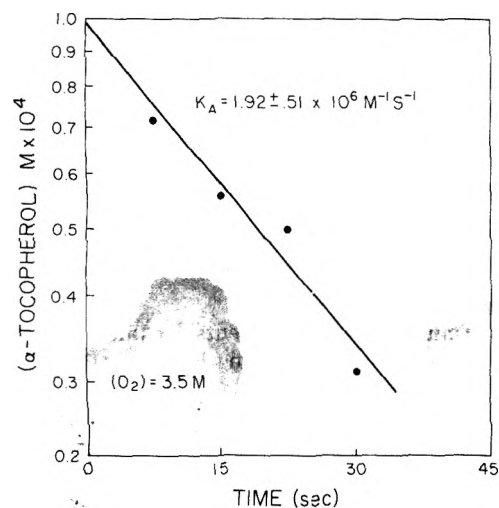


Figure 1. Loss of α -tocopherol in freon in presence of laser generated singlet oxygen. Output of Nd-YAG laser was 3.0 W continuous wave. The concentration of tocopherol was determined by chemical assay.

TABLE I: Extinction Coefficient of the Induced Absorption of the α -Tocopherol-Molecular Oxygen Collision Complex

λ , nm	ϵ , $M^{-2} \text{ cm}^{-1}$	λ , nm	ϵ , $M^{-2} \text{ cm}^{-1}$
450	0	380	4.6
440	0.5	370	5.6
430	0.8	360	6.9
420	1.2	350	8.3
410	1.7	340	10.2
400	2.3	330	13.1
390	3.3	320	17.5

$$k_A = \frac{kk_{O_2}}{\frac{\sigma}{a}E[O_2]} \quad (4)$$

where k is the slope of the line in Figure 1, k_{O_2} is the singlet oxygen quenching constant for molecular oxygen ($k_{O_2} = 2.7 \times 10^3 \text{ M}^{-1} \text{ s}^{-1}$),¹¹ σ/a is the oxygen absorption cross section divided by the cell cross-sectional area ($\sigma/a = 0.505$), E is the output of the laser reaching the sample ($E = 3.0 \times 10^{-5} \text{ einstein s}^{-1}$), and $[O_2]$ is 3.5 M. By a least-squares analysis k_A is $1.9 \pm 0.5 \times 10^6 \text{ M}^{-1} \text{ s}^{-1}$. This is a reasonable precision for this technique; however, the systematic error may be substantially larger, even as high as 50% due primarily to uncertainty of k_{O_2} .¹⁴

The total quenching k_Q ($k_Q = k_p + k_A$) was determined by a previously described competition method¹⁵ where the reaction of the singlet oxygen acceptor, bilirubin, is determined in the presence of various concentrations of tocopherol. From

$$k_Q = \frac{k_{O_2}[O_2]}{[T]} \left(\frac{k}{k'} - 1 \right) \quad (5)$$

k_Q can be determined; $[T]$ is the tocopherol concentration and k/k' is the ratio of the rate of bilirubin loss in the absence (k) and presence (k') of tocopherol. The results of experiments using an oxygen concentration of 3.0 M are shown in Figure 2 and, from a least-squares analysis that constrains the intercept to unity, k_Q is $3.1 \pm 1.2 \times 10^7 \text{ M}^{-1} \text{ s}^{-1}$. Again the precision is as expected, but the systematic error is larger (50%) due to uncertainty of k_{O_2} .¹⁴

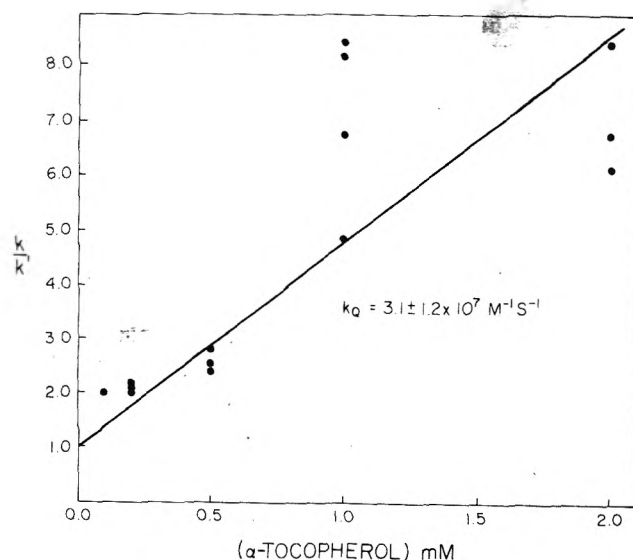


Figure 2. Ratio of the loss rate of bilirubin (in presence of laser generated singlet oxygen) in the absence of α -tocopherol (k) to the loss rate in the presence of tocopherol (k') vs. the concentration of tocopherol. The oxygen concentration was 3.0 M.

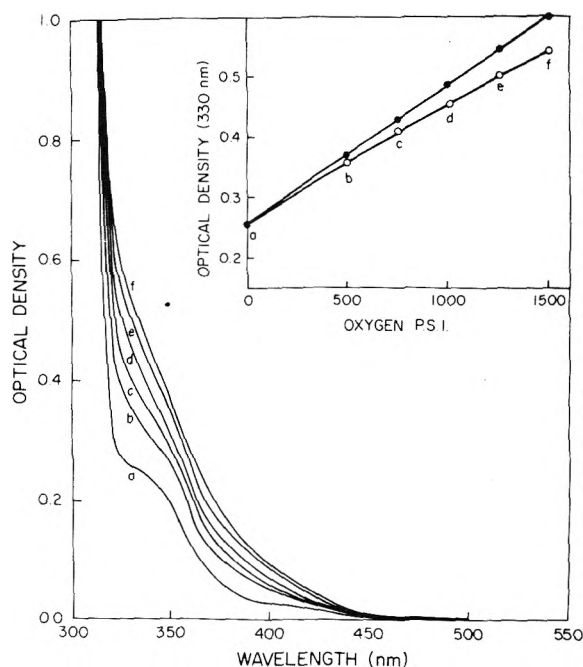
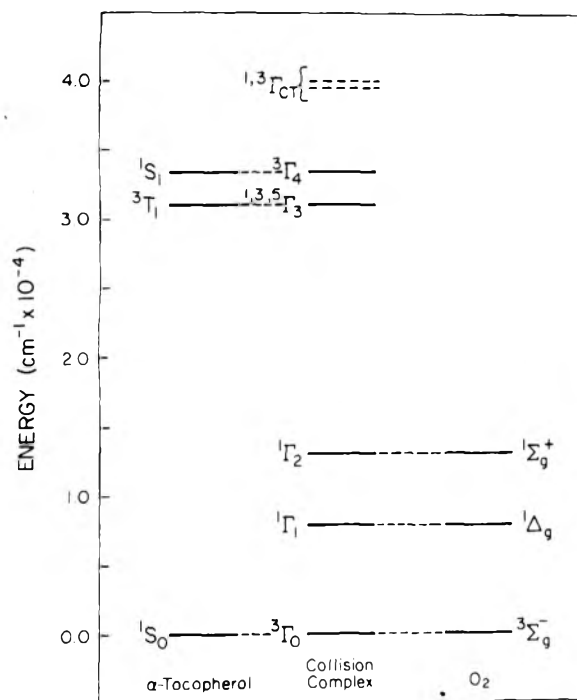


Figure 3. The absorption spectra of 3.4 mM α -tocopherol in freon at various oxygen pressures: (a) atmospheric O_2 ; (b) 500 psi; (c) 750 psi; (d) 1000 psi; (e) 1250 psi; (f) 1500 psi. The open circles of the insert are directly from the spectra and the filled circles are corrected for dilution of the freon by oxygen.¹⁷

The oxygen enhancement of the tocopherol absorption shown in Figure 3 is exactly as might be expected from Evans' work on aromatics.¹⁶ A correction for dilution of the solution by oxygen must be applied, and the correction factor is independently determined by absorption changes of tetracyclone (tetracyclone) as a function of oxygen pressure.¹⁷ This correction leads to an induced absorption that is linear in oxygen concentration (Figure 3 insert). From Figure 3 and similar experiments the extinction coefficient could be calculated at different wavelengths and is tabulated in Table I. The induced band appears to have remarkable asymmetry, but this is undoubtedly due to the presence of the

TABLE II: Chemical and Total Quenching Rate Constants for the Quenching of Singlet Oxygen by α -Tocopherol

Ref	Solvent	$10^7 k_Q, M^{-1} s^{-1}$	$10^5 k_A, M^{-1} s^{-1}$	k_A/k_Q
This work	Freon	3.1 ± 1.2	19 ± 5.1	0.061 ± 0.024
2	Isooctane	12		
4	Cyclohexane	9	10	0.011
4	Benzene	17		
2	Pyridine	25	20	0.008
3	Methanol	67	460	0.067
1,2	Methanol	70		

Figure 4. Energy levels of α -tocopherol and molecular oxygen electronic states.

strong $\pi^* \leftarrow \pi$ absorption of tocopherol at 294 nm. This allowed transition of the tocopherol seems to lose some intensity in the presence of oxygen and this would be expected if the induced absorption were borrowing intensity from the allowed $\pi^* \leftarrow \pi$ transition. This conclusion is not sound, however, because the decrease in extinction coefficient at 294 nm is of the same magnitude as the error in the determination of the correction factor for dilution by oxygen. Investigation of enhanced absorption at any higher energy was prevented by the strong absorption of oxygen at wavelengths lower than 260 nm. In this study no charge-transfer state could be identified.

A concentrated tocopherol solution (≈ 1 M) under 1500 psi of oxygen was scanned in the near-infrared to determine if the electric-dipole-forbidden transition ${}^1\Delta_g \leftarrow {}^3\Sigma_g^-$ could be induced by tocopherol. The absorptions observed were identical with absorptions found in either tocopherol or oxygen alone. The absence of enhanced absorption at 1270 nm in this experiment supports the conclusion that tocopherol does not perturb the ${}^1\Delta_g \leftarrow {}^3\Sigma_g^-$ electric dipole transition of oxygen. Also, tocopherol has negligible absorption at 1270 and 1590 nm.

The Quenching of Singlet Oxygen by α -Tocopherol. In Table II the values of k_A and k_Q , as well as the ratio k_A/k_Q , can be compared to literature values measured by dye photosensitization methods. The ratio of k_A/k_Q is the fraction of quenching collisions that are chemical in nature and is of the order of 1–10%. The k_A measured in freon 113 agrees with

those determined in other solvents by photosensitization except for the case of methanol, in which the k_A is an order of magnitude larger. This agreement on k_A by the two techniques is surprising because of contrasting measurements of the k_A of diphenylisobenzofuran (DPBF) in freon by the two techniques.^{11,18} The techniques agree on the total quenching measurements for DPBF; but the laser work¹¹ claims this quenching is largely a physical interaction, and the dye-sensitization study¹⁸ attributes this quenching entirely to chemical reaction. The reason for that discrepancy is not known, but it may not be important here because the k_Q for tocopherol in freon agrees somewhat with the trend of the other k_Q measurements in Table II.

The products of the reaction are not known but the initial product is probably a 1,4 addition to the ring to form an endoperoxide. The products of the dye photosensitization of phenols have been analyzed, but confusion arises because the mechanism is often a hydrogen abstraction rather than a singlet oxygen mechanism.¹⁹ This supposed endoperoxide intermediate is likely to be unstable and decompose to products, and it is possible that the endoperoxide could revert back to α -tocopherol and molecular oxygen in an inert solvent. If, in the latter case, the oxygen is in the ground state, then neither our experiments nor the photosensitization results could distinguish between this possibility and a purely physical quenching mechanism.

An endoperoxide intermediate may explain the high k_A in methanol, where a solvent molecule could add across the peroxide bond to form an unstable hydroperoxide–methyl ether derivative. Note that the k_A in methanol is (within error) not greater than the k_Q in any solvent. Perhaps the breakdown of the endoperoxide into products is maximized in methanol where the solvent adds to the intermediate, but in freon where the peroxide might form at the same rate the final products appear more slowly (than in methanol) because of the inert solvent. A physical mechanism is still required to explain the high k_Q in the other solvents.

We would like to note that the reaction can be considered as an electrophilic addition to an aromatic ring. Grams and Eskins¹ showed a correlation between the methyl substitution of a series of tocopherols with reactivity toward singlet oxygen. They claimed a correlation of singlet oxygen reactivity of tocopherols with biological activity of tocopherols, but it is more likely that the two activities correlate to the susceptibility of the tocopherols to electrophilic attack rather than to each other.

Excited State Interactions of the Collision Complex. The electronic states of the collision complex of α -tocopherol and molecular oxygen are presented with their nominal energetic level in Figure 4. The quenching of singlet oxygen by tocopherol is represented by a radiationless transition from ${}^1\Gamma_1$ to ${}^3\Gamma_0$ and is governed by the rate equation²³

$$W_{1\Gamma_1 \rightarrow 3\Gamma_0} = \frac{2\pi}{\hbar} \langle 1\Gamma_1 | \mathcal{H} | 3\Gamma_0 \rangle^2 \rho_E \quad (6)$$

where W is the rate of the transition, ρ_E is the density of final states per unit of energy, and \mathcal{H} is the Hamiltonian. The term $\langle {}^1\Gamma_1 | \mathcal{H} | {}^3\Gamma_0 \rangle$ vanishes to first order unless \mathcal{H} contains a spin-orbit term. The second-order term is

$$\frac{\langle {}^1\Gamma_1 | \mathcal{H} | {}^{1,3}\Gamma_{CT} \rangle \langle {}^{1,3}\Gamma_{CT} | \mathcal{H} | {}^3\Gamma_0 \rangle}{E_{CT} - E_1} \quad (7)$$

where E_i is the energy of the Γ_i state. In (7) the intermediate virtual state is a charge transfer state, but could easily be some other "real" state such as the singlet and triplet components of the ${}^{1,3,5}\Gamma_3$ state.

The rate equation applies only when the initial and final state have nearly the same energy. This requires the transition to occur to a vibrationally excited state of ${}^3\Gamma_0$. If the states, Γ_i , can be separated into electronic, ψ_i , and vibrational, χ_i , functions, then eq 6 with second-order terms (7) is

$$W_{1\Gamma_1 \rightarrow 3\Gamma_0} = \frac{2\pi}{\hbar} \left| \frac{\langle \psi_1 | \mathcal{H} | {}^{1,3}\psi_{CT} \rangle \langle {}^{1,3}\psi_{CT} | \mathcal{H} | {}^3\psi_0 \rangle}{E_{CT} - E_1} \right|^2 \times \rho_E \sum_n |\langle \chi_1^0 | \chi_0^n \rangle|^2 \quad (8)$$

In (8), the superscript of χ is the vibrational quanta and the subscript of χ is the associated electronic state. The Franck-Condon terms, $|\langle \chi_1^0 | \chi_0^n \rangle|^2$ are summed over the possible vibrational quanta, n , of the final state. The explicit dependence of the rate on the Franck-Condon terms has been used as an argument for correlating vibrational overtone frequencies of quenchers with quenching rate constants.^{20,21} The electronic energy of the singlet oxygen becomes vibrational energy of the quencher. Comparisons of different quenchers in different solvents, however, give only qualitative trends because both electronic and Franck-Condon terms contribute to the decay rate. Merkel and Kearns²¹ extended this idea to solvent quenching of singlet oxygen and correlate the optical extinction of the solvent at 1270 and 1590 nm with quenching rates. This argument should apply also to the case of tocopherol physical quenching; however, neither tocopherol nor freon 113 have detectable absorption at these wavelengths. This poses a dilemma in that there is no place in the system for the energy flow in this electronic-to-vibrational energy transfer process. The only choice is to suppose that lattice vibrations of the solvent can incorporate a significant amount of energy. It is possible that our value for k_Q is lower than other values because there is less solvent vibrational interaction in freon than in the other solvents.

More direct evidence of the role of higher states (such as ${}^{1,3}\Gamma_{CT}$) in the quenching process might come from spectral analysis. Enhancement of singlet-triplet absorption of aromatics by oxygen has been proposed to arise from either

$$\frac{\langle {}^{1,3,5}\Gamma_3 | \mathcal{H} | {}^{1,3}\Gamma_{CT} \rangle \cdot \langle {}^{1,3}\Gamma_{CT} | \mathbf{R} | {}^3\Gamma_0 \rangle}{E_{CT} - E_3} \quad (9)$$

or

$$\frac{\langle {}^{1,3,5}\Gamma_3 | \mathcal{H} | {}^3\Gamma_4 \rangle \cdot \langle {}^3\Gamma_4 | \mathbf{R} | {}^3\Gamma_0 \rangle}{E_4 - E_3} \quad (10)$$

where \mathbf{R} is the electric dipole operator. In (9) the intensity is borrowed from the dipole allowed charge-transfer transition,²² and in (10) the intensity is borrowed from the ${}^3\Gamma_4 \leftarrow {}^3\Gamma_0$ transition, which is nominally an allowed absorption of the aromatic system.²³ The energy of the ${}^{1,3}\Gamma_{CT}$ states varies directly with the ionization potential of the aromatic donor; and term (9) should be sensitive to substitution on the ring system of electron-withdrawing and releasing groups. We have found

in our phenolic system an induced transition that is two orders of magnitude larger than the oxygen-induced absorption found by Evans¹⁶ for benzene (cf. Table I to his extinction coefficient of ≈ 0.06). The magnitude of the transition is consistent with a charge-transfer interaction as in (9), but Robinson²³ demonstrated theoretically that a charge-transfer interaction is unnecessary to explain oxygen-induced singlet-triplet absorptions in aromatics. Although the exact nature of the interaction remains unresolved, the perturbed transition that we observe for tocopherol is certainly not different from the transitions that Evans found in numerous aromatic systems.¹⁶

Whatever this higher state interaction is, it does not perturb the ${}^1\Delta_g \leftarrow {}^3\Sigma_g^-$ absorption in oxygen. Our failure to observe a tocopherol-induced absorption in oxygen at 1270 nm means that charge-transfer state terms such as in

$$\frac{\langle {}^1\Gamma_1 | \mathcal{H} | {}^{1,3}\Gamma_{CT} \rangle \cdot \langle {}^{1,3}\Gamma_{CT} | \mathbf{R} | {}^3\Gamma_0 \rangle}{E_{CT} - E_1} \quad (11)$$

are negligible. Apparently, interactions that relieve the spin forbiddenness of the radiationless transition fail to induce an absorption ${}^1\Delta_g \leftarrow {}^3\Sigma_g^-$ in oxygen. This may be because the real forbiddenness in the radiative transition is the angular momentum change of two ($\Delta\Lambda = 2$). It is interesting that molecular oxygen itself perturbs the absorption as in (1), but is a poor quencher of singlet oxygen ($k_{O_2} = 2.7 \times 10^3$).¹¹

A detailed theoretical investigation of the interactions of oxygen with aromatic ring systems is needed. Further the mechanism of physical quenching of singlet oxygen by tocopherol may be clarified by a complete study of substituted phenols, in which the phenolic ionization potential can be compared to the physical quenching constant for the phenols. It would be interesting to know also the intermediates and products of the reaction of tocopherol and singlet oxygen.

Acknowledgment. We hereby acknowledge support by grants of NIH (HD 07714-02), NSF (GP-38218X1), and Public Health Service Research Grant No. CA 00503 (to D.E.B.) from the National Cancer Institute (DHEW).

References and Notes

- (1) G. W. Grams and K. Eskins, *Biochemistry*, **11**, 606 (1972).
- (2) S. R. Fahrenholtz, F. H. Doleiden, A. M. Trozzolo, and A. A. Lamola, *Photochem. Photobiol.*, **20**, 505 (1974).
- (3) C. S. Foote, Ta-Yen Ching, and G. G. Geller, *Photochem. Photobiol.*, **20**, 511 (1974).
- (4) B. Stevens, R. D. Small, Jr., and S. R. Perez, *Photochem. Photobiol.*, **20**, 515 (1974).
- (5) C. S. Foote and R. W. Denny, *J. Am. Chem. Soc.*, **90**, 6233 (1968).
- (6) This is predicted by comparison of the electronic structure of α -tocopherol to benzene and phenol and is confirmed in this paper by the assignment of the oxygen-induced absorption of tocopherol at 320 nm to an enhanced singlet-triplet transition.
- (7) I. B. C. Matheson and J. Lee, *J. Am. Chem. Soc.*, **94**, 3310 (1972).
- (8) C. Ouannès and T. Wilson, *J. Am. Chem. Soc.*, **90**, 6527 (1968).
- (9) E. A. Ogryzlo and C. W. Tang, *J. Am. Chem. Soc.*, **92**, 5034 (1970).
- (10) K. Furukawa and E. A. Ogryzlo, *Chem. Phys. Lett.*, **12**, 370 (1971).
- (11) I. B. C. Matheson, J. Lee, B. S. Yamanashi, and M. L. Wolbarscht, *J. Am. Chem. Soc.*, **96**, 3343 (1974).
- (12) This is probably due to interfering absorptions of products. The absorption method seemed unreasonably nonreproducible.
- (13) Analytical Methods Committee, *Analyst*, **84**, 356 (1959).
- (14) I. B. C. Matheson, J. Lee, B. S. Yamanashi, and M. L. Wolbarscht, *Chem. Phys. Lett.*, **27**, 355 (1974).
- (15) I. B. C. Matheson, R. D. Etheridge, N. R. Kratowich, and J. Lee, *Photochem. Photobiol.*, **21**, 165 (1975).
- (16) D. F. Evans, *J. Chem. Soc.*, 1351 (1957).
- (17) Although tetracyclone reacts with singlet oxygen, it was used because it is unreactive toward ground state oxygen. The factor arises because oxygen dilutes the solution and corrects the absorption to a constant tocopherol concentration. The corrected absorption is the measured absorption times $(1 + 10^{-4}P)$ where P is the oxygen pressure in psi.
- (18) J. A. Ors, Ph.D. Dissertation, University of South Florida, 1974.
- (19) T. Matsuura, H. Matsushima, S. Kato, and I. Saito, *Tetrahedron*, **28**, 5119 (1972).

- (20) J. A. Davidson and E. A. Ogryzlo in "Chemiluminescence and Bioluminescence", M. J. Cormier, D. M. Hercules, and J. Lee, Ed., Plenum Press, New York, N.Y., 1973, p 111.
- (21) P. B. Merkel and D. R. Kearns, *J. Am. Chem. Soc.*, **94**, 7244 (1972).
- (22) H. Tsubomura and R. S. Mulliken, *J. Am. Chem. Soc.*, **82**, 5966 (1960).
- (23) G. W. Robinson, *J. Chem. Phys.*, **46**, 572 (1967).

Discussion

B. STEVENS. I think one must expect a dependence of k_Q on solvent if this involves reversible electron transfer, but estimates of k_A for

various $O_2(^1\Delta)$ acceptors in different solvents indicate that k_A is solvent independent within a factor of 2. To this extent your results agree with those obtained for the photosensitized reaction.

D. E. BRABHAM. There is a definite trend. Unfortunately we don't have a slide comparing all those results. Your value was 1×10^6 and this was 2×10^6 and Foote's value was very high, an order of magnitude higher, but he worked in methanol. If there is an endo peroxide intermediate, there may be some kind of enhancement, because the solvent may play a role in the reaction itself.

Chemical Production of Excited States. Chemiluminescence of Carcinogenic Hydrocarbons Accompanying Their Metabolic Hydroxylation and a Proposal for Common Active Site Geometries for Hydroxylation

H. H. Seliger* and J. P. Hamman

McCollum-Pratt Institute and Department of Biology, The Johns Hopkins University, Baltimore, Maryland 21218 (Received March 8, 1976)

Publication costs assisted by the U.S. Energy Research and Development Administration

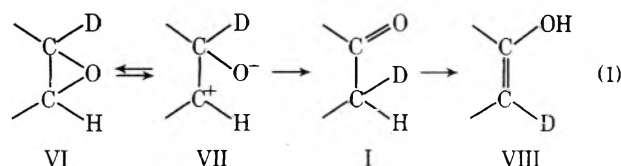
A mechanism is proposed whereby metabolically produced epoxides of polycyclic aromatic hydrocarbons may be subject to an adventitious oxygenation, resulting in ring-opened carbonyl residues in excited electronic states. These carbonyl excited states may be assayed by light emission despite their low quantum yields of fluorescence. The intensities of chemiluminescence of the carcinogens benzo[*a*]pyrene, dibenz[*a,h*]anthracene, and 3-methylcholanthrene, incubated with rat liver microsomes in the presence of cofactors, are correlated with the initial rates of hydroxylation of these parent compounds by the induced cytochrome P-448 system. The chemiluminescence intensity may be a tracer for the concentration of reactive epoxides formed during the metabolism of aromatic carcinogens. It is proposed that the preponderant fraction of the excited state carbonyl products that do not deexcite by light emission can add covalently to cellular macromolecules; a dark chemical analogue of the photochemical reactions of carbonyls. It is proposed that the metabolic products of all polycyclic aromatic hydrocarbons can be produced through three active site geometries. Carcinogens can be characterized by two of these three geometries. This common geometry mechanism and the predictions of chemiluminescence are consistent with the reported carcinogenicities of the fluoranthenes and can be extended to include the activating effects of methyl and amino substituents to noncarcinogenic or weakly carcinogenic parent polycyclic aromatic hydrocarbons. In particular, it can be applied to explain the carcinogenicity of 7,8-epoxybenzo[*a*]pyrene and the lack of carcinogenicity of the 9,10-oxide.

Introduction

The various substrate molecules of different genera of bioluminescent organisms have a common active site configuration¹ (structure I of Figure 1) for the enzymatic oxygenation reaction leading to excited state products. These same excited state product molecules are produced in nonenzymatic chemiluminescence under conditions where oxygen may be reduced to its superoxide radical form, although this in no way requires that the enzymatic pathway involve free radicals.

The enzymatic hydroxylation of aromatic hydrocarbons involves the formation of an intermediate arene oxide (epoxide)²⁻⁵ which subsequently undergoes spontaneous transition to the phenol through steps shown in eq 1. The deuterium label has been included to illustrate the NIH shift.^{4,6,7} The retention of the deuterium (up to 85% for hydroxylations of toluene⁸ and 70% in the case of naphthalene⁹) requires the intermediate keto tautomer I.

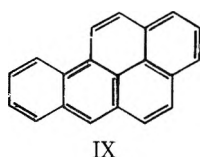
The carbonium ion, VII, tautomeric with the epoxide, VI, is subject to nucleophilic attack by a variety of nucleophiles, and for this reason has been proposed as the ultimate carcinogenic molecular species of the parent carcinogenic polycyclic aromatic hydrocarbons (PAH). This same electrophilic reactant should also be accessible to attack by molecular oxygen, forming the identical intermediates, II, implicated in the bond-splitting reactions leading to the keto excited states, V. The product of the oxygenation of arene oxides at the carbonium carbon would be a ring-opened carbonyl residue. The free energy release is sufficient to leave the product in an excited electronic state, for carbonyls the $\eta\pi^*$ excited state. The reactivity of the carbonium ion, VII, which determines the mutagenicity and presumably the carcinogenicity of the epoxide, may also be correlated with the production of carbonyl excited states as the result of nucleophilic attack by molecular oxygen. The keto intermediate, I, on the pathway to spontaneous rearrangement to the phenol, VIII, is also



subject to adventitious oxygenation leading to the same carbonyl excited states.

In the lower aldehydes the $\eta\pi^*$ state is the lowest energy singlet state and no fluorescence can be observed. An increase in the number of π electrons will lower the energies of the $\pi\pi^*$ states. This resonance effect, together with the additional lowering of $\pi\pi^*$ energy levels due to solvation in polar solvents, can result in observable fluorescence of aromatic aldehydes.

Carcinogenic PAH's should produce more reactive epoxides, VI, than noncarcinogens. Since some of these may react with molecular oxygen to produce carbonyl excited states, we looked for the chemiluminescence (CL) of the carcinogenic PAH benzo[*a*]pyrene¹⁰ (IX; 3,4-benzopyrene) in liver mi-



croosomal extracts of rats in which the aryl hydrocarbon hydroxylase (AHH) system was induced by 3-methylcholanthrene. We have verified the prediction of chemiluminescence associated with metabolism of carcinogenic PAH's.¹¹ We found that (a) benzo[*a*]pyrene can be used as a chemiluminescent substrate for the assay of AHH activity; (b) liver microsomes from noninduced rats hydroxylated benzo[*a*]pyrene at reduced rates and exhibited a lower chemiluminescence; (c) the kinetics of the CL were consistent with the production of an epoxide intermediate; and (d) the fraction of the parent carcinogen reacting via the CL pathway was ca. $10^{-8}/\phi$, where ϕ is the fluorescence quantum yield of the proposed carbonyl excited state. There appears to be evidence for at least two forms of the AHH enzyme system.¹² In the present paper we have extended the CL studies to include a number of inducers of rat liver microsomal hydroxylases: 3-methylcholanthrene, dibenz[*a,h*]anthracene, anthracene, phenobarbital, and corn oil as a control, and have used benzo[*a*]pyrene, 3-methylcholanthrene, dibenz[*a,h*]anthracene, and anthracene as chemiluminescent substrates.

A very old concept of the detailed steps in the metabolism of PAH's involves a site for binding to the hydroxylase and a separate chemical site for oxygenation.¹³⁻¹⁵ In an effort to generalize from the observations that carcinogens induce AHH systems in liver microsomes which can metabolize a variety of parent carcinogenic PAH's we looked for common active site geometrical configurations among all of the PAH's.¹⁶ Using the known distributions of metabolites of naphthalene, benz[*a*]anthracene, and benzo[*a*]pyrene it can be shown that all PAH's can be characterized by only three active site geometries. All known unsubstituted carcinogenic PAH's can be represented by two of these active site geometries, each of which consists of an electron-dense region for binding and a pair of carbon atoms on an external ring at which an epoxide can be formed. These arguments are extended to include the methyl-substituted PAH's, the fluoranthenes, the most recently synthesized epoxides of benzo[*a*]pyrene, and the arylamines. In all of these cases the

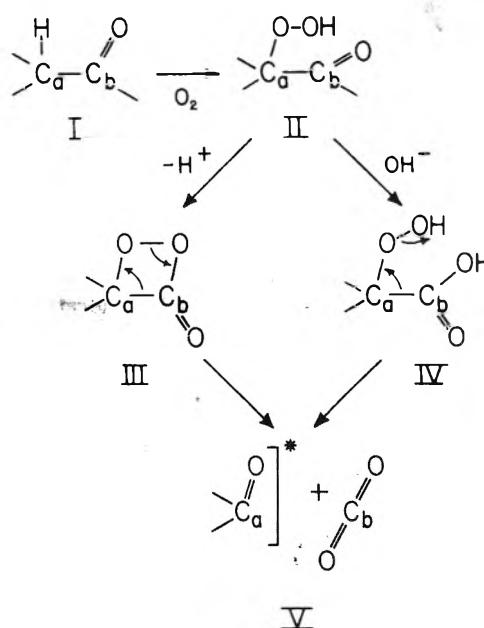


Figure 1. The common active structure (I) for bioluminescent substrates, showing pathways of oxygenation (dioxetane formation (III) or hydroxyl attack (IV) leading to the rupture of the C_a-C_b bond and the keto product molecule in an electronically excited state.

empirical common geometry mechanism predicts the sites of epoxide formation and the correlation of CL with reactivity.

Experimental Section

Liver microsomes were isolated¹⁷ from Long-Evans rats (Charles River Animal Farms) injected 24 h previously with 3-methylcholanthrene, dibenz[*a,h*]anthracene, anthracene (25 mg/kg ip in 0.5 ml of corn oil), or corn oil (0.5 ml) alone. Phenobarbital-induced animals were injected daily with 80 mg/kg of phenobarbital¹⁸ in saline for 3 days prior to sacrifice. Protein was determined by a modified Lowry procedure.¹⁹ AHH activity was determined by adding benzo[*a*]pyrene and the cofactor NADPH and measuring the rate of increase of fluorescence of an alkaline extract of the reaction mixture.²⁰ Chemiluminescence intensities were measured in a modified light collecting system similar to that used for liquid scintillation counting, using a specially selected low-noise phototube in a single photon counting mode. The photon detection system was calibrated absolutely with the Luminol chemiluminescent reaction.²¹ For CL and fluorescence assays the reaction mix contained 50 μmol of Tris-HCl, pH 7.5, 3 μmol of MgCl_2 , 0-1.4 mg of microsomal protein, 75 nmol of the polycyclic aromatic hydrocarbon substrate, and 0.5 μmol NADPH per milliliter. Reactions were run at room temperature 22 °C and initiated by the addition of the NADPH.

Results and Discussion

The kinetics of the chemiluminescence observed upon the addition of several polycyclic aromatic hydrocarbons and NADPH to rat liver microsomes prepared from 3-methylcholanthrene treated rats are shown in Figure 2. The fluorescence intensity of the hydroxylated benzo[*a*]pyrene is included to show that the rate of formation of fluorescent alkali soluble product is a maximum initially and approaches zero as NADPH becomes limiting. The CL intensity increases to a maximum value at a finite time (ca. 10 min) and then decreases. The kinetics are consistent with the formation of an

TABLE I: Rate of Hydroxylation of Three Carcinogenic Hydrocarbons by Microsomal Aryl Hydrocarbon Hydroxylase (from 3-Methylcholanthrene-Induced Rat Livers)^a

Substrate	Chemiluminescence, photons s ⁻¹ mg ⁻¹ × 10 ⁻⁴	Rate of alkali soluble product formation, arbitrary fluorescence units mg ⁻¹	Chemiluminescence rate of hydroxylation
Benzo[a]pyrene	8	130	620
3-Methylcholanthrene	2	(47)	430
Dibenz[a,h]anthracene	1.3	(16)	810

^a Assayed by chemiluminescence and by the rate of formation of alkali extractable products. Data in parentheses were taken from Nebert and Gelboin²⁰ and normalized to the rate of hydroxylation of benzo[a]pyrene that we measured. The units in column 1 are maximum chemiluminescence intensity in photons per second per milligram of protein in the microsomal preparation for initial concentrations of carcinogen substrate of 75 μM and NADPH of 500 μM.

TABLE II: Maximum Intensities of CL^a

Inducer	Substrate	Maximum chemiluminescence intensity, (hν s ⁻¹ mg ⁻¹ × 10 ⁻⁴)			
		Benz[a]-pyrene	Anthracene	Dibenz[a,h]-anthracene	3-Methylcholanthrene
3-Methylcholanthrene		8	0.6	1.3	2
Dibenz[a,h]anthracene		7	1.5	1.6	
Anthracene		2	0.5		
Corn oil		0.9			
Phenobarbital		0.6			
Saline		0.4			

^a These are proportional to the rates of hydroxylation of the hydrocarbon substrates by the microsomal aryl hydrocarbon hydroxylase system extracted from the livers of rats that had been induced with the hydrocarbons shown in the inducer column.

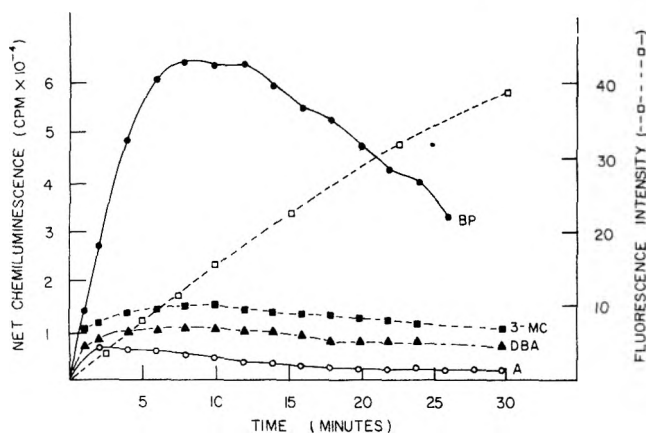


Figure 2. Kinetics of microsomal aryl hydrocarbon hydroxylase activity; chemiluminescence assay and fluorescence assay. The chemiluminescence intensity was monitored continuously. Benzo[a]pyrene, 3-methylcholanthrene, dibenz[a,h]anthracene, and anthracene were used as substrates for the chemiluminescence assay. The amount of hydroxylated benzo[a]pyrene was assayed by measuring the intensity of fluorescence of the 3-hydroxy product. The reaction was stopped at the indicated time with 1 ml of cold acetone. The reaction mix was extracted with hexane and the hydroxylated products were then extracted from the hexane fraction into 1 N NaOH. The intensity of fluorescence was measured at 520 nm (excitation at 390 nm).

intermediate which is responsible for the CL observed. This is further supported by the observation that after the aryl hydrocarbon hydroxylase is denatured (the reaction stopped) by the addition of acetone, the CL continues for many minutes. This CL is dependent on the concentration of molecular oxygen, determined by bubbling N₂ and O₂ respectively through the denatured system. For the hydroxylation of benzo[a]pyrene by rat liver microsomes the maximum CL intensity is directly proportional to the initial rate of hydroxylation (as assayed by the amount of alkali soluble product formed in 10 min). All factors that increased the ini-

tial rate of hydroxylation (oxygenated buffer, increased incubation temperature, increased NADPH and/or microsomal protein concentration) increased the maximal intensity of CL. Conversely, 7,8-benzoflavone, a competitive inhibitor of microsomal aryl hydrocarbon hydroxylase,²² decreased the initial rate of hydroxylation and the maximum CL intensity.

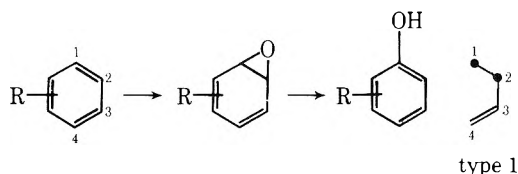
Table I compares the maximum CL intensities and the initial rates of hydroxylated product formation for three different carcinogenic substrates. Although the specific maximum CL intensity [photons s⁻¹ mg of protein⁻¹] for equimolar additions of the three carcinogens varies over a factor of 6 the ratio of CL to the rate of hydroxylation is within a factor of 2. This factor of 2 may approach 1 if we could account for (a) differences in fluorescence quantum yields of the excited state products formed, (b) differences in susceptibilities of the carbonium form, VII, to oxygen attack, or (c) the fact that a portion of the CL observed is from an epoxide, i.e., the 9,10-epoxide of benzo[a]pyrene, different from the 2,3-epoxide which rearranges to the 3-phenol and whose fluorescence is assayed for the rate of hydroxylation.

The maximum CL intensities observed in a matrix experiment in which various hydrocarbons were used as inducers of the AHH system and as substrates for the AHH system are given in Table II.

The substrate specificity of liver microsomal oxygenase resides in the cytochrome protein.²³ 3-Methylcholanthrene induces a cytochrome (P-448) which is specific for the hydroxylation of PAH's while phenobarbital induces primarily cytochrome P-450.^{24,25} This is consistent with column 1 where 3-methylcholanthrene-induced microsomes produced 13× higher CL of the benzo[a]pyrene substrates than phenobarbital-induced microsomes. Anthracene-induced microsomes also produced a higher CL of the benzo[a]pyrene substrate than the corn oil control. This is additional evidence that the CL assay using benzo[a]pyrene as a substrate is a sensitive assay for the AHH system. The CL of dibenz[a,h]anthracene

and 3-methylcholanthrene, although lower than that of an equal concentration of benzo[*a*]pyrene, can be seen from column 3 of Table I to be attributable to their lower rates of hydroxylation. The intensities of CL of the anthracene substrates in column 2 are low except for a slightly higher value for dibenz[*a,h*]anthracene-induced microsomes. The comparison of the CL of benzo[*a*]pyrene with that of anthracene for 3-methylcholanthrene and anthracene-induced microsomes respectively implies that there are at least two different species of hydroxylase induced by these PAH's.

Anderson¹³ was among the first to suggest that the Pullman's K region, the bond of greatest electron density,²⁶⁻²⁸ was the binding site of a carcinogenic PAH to the hydroxylase (enzyme). Boyland^{14,15} proposed a separate site for perhydroxylation. Only recently have any quantitative studies been made of the distributions of metabolic products of hydroxylations.^{29,30} Benzene, naphthalene, and anthracene are hydroxylated to the 1-phenol through arene oxide intermediates. In all cases the active site geometry located on a single ring is proposed as type 1. The double bond 3,4 represents the



binding site of the substrate molecule to the hydroxylase and the solid dots represent the carbon atoms across which the epoxide is formed.

If, as in the case of naphthalene and anthracene, the bond of greatest electron density is the 3,4 bond, the geometry is a K-1 geometry. In the schematic representation it is made solid black. Otherwise it is left as an open double bond as shown. In the strict sense the Pullmans used the term K region to define only the angular phenanthrenic double bond. We do not feel the original intent to be subverted if the definition of the K region is broadened to include the double bond(s) of highest bond order independent of the presence of the phenanthrenic angular region. In this way the analogy can be carried to the mechanism of reactivity when methyl and amino substitutions are made to noncarcinogens such as anthracene and naphthalene, respectively (see below).

The metabolites which have been identified for the carcinogenic PAH's benzo[*a*]pyrene (IX) and benz[*a*]anthracene (X; 1,2-benzanthracene) are listed in Table III together with the proposed active site geometry for the initial formation of the epoxide from which the metabolite is produced. Only in the cases of the major metabolites observed, the 3-hydroxybenzo[*a*]pyrene and the 3-hydroxy- and 4-hydroxybenz[*a*]anthracene produced through the 2,3-oxide of benzo[*a*]pyrene and the 3,4-oxide of benz[*a*]anthracene, respectively, are K-2, rather than type 2 geometries applicable. Thus a minor prediction of the common geometry mechanism, that K-region binding is most probable and therefore rate determining in the hydroxylase reactions, is seen to hold. The binding constant for bonds other than the K-region bond and thus the rates of production of oxides other than through K-type geometries should be lower than for K-region reactions. A restricted form of the K-2 geometry which we designate as K-2R and which cannot lead to epoxide intermediates is invoked to explain the presence of mesoanthracenic quinones among the metabolites. The type 3 geometry might appear to be superfluous in explaining the origin of the 9-hydroxy and the 9,10-dihydrodiol of benzo[*a*]pyrene; these could just as

TABLE III: Metabolites of the Microsomal Metabolism of Benzo[*a*]pyrene and Benz[*a*]anthracene and the Proposed Molecular Geometries Involved in Enzyme Binding and Hydroxylation^a

	BENZO[<i>a</i>]PYRENE ^{29,30}	BENZ[<i>a</i>]ANTHRACENE ³¹
GEOMETRY		
TYPE 1)	 	
TYPE 2)	 	
TYPE 3)		

^a The metabolites of benzo[*a*]pyrene were separated and identified on a high pressure liquid chromatograph by Selkirk et al.^{29,30} The thin layer chromatographic separation of the metabolites of benz[*a*]anthracene and their identification was reported by Boyland et al.³¹

well have been produced by virtue of the type 1 geometry. In addition the type 3 geometry for benzo[*a*]pyrene does not include the K region, although the 11,12 bond is almost as electron dense as the 4,5 bond. However, as we shall see in Table IV, the type 3 geometry is necessary for consistency in the carcinogenicities of dibenzo[*a,h*]pyrene (XIX; 4,5:9,10-dibenzopyrene; 3,4:8,9-dibenzopyrene), dibenzo[*a,i*]pyrene (XX; 3,4:9,10-dibenzopyrene; 4,5:8,9-dibenzopyrene), and tribenzo[*b,h,l*]pyrene (XXI; 1,2:4,5:8,9-tribenzopyrene; 3,4:6,7:9,10-tribenzopyrene).

In Table IV we have presented the structures and the proposed active site geometries for 16 nonsubstituted, carcinogenic PAH's. Thirteen of these have K-2 geometry and three structures (XIX, XX, and XXI) exhibit type 3 geometry. Thus, *all nonsubstituted carcinogenic PAH's can be reduced to two active site geometries, types 2 and 3.*

The noncarcinogenic PAH's naphthalene (XXV), phenanthrene (XXVI), pyrene (XXVII), and anthranthrene

TABLE IV: Structures and Proposed Active Site Geometries for Carcinogenic Unsubstituted Polycyclic Hydrocarbons^a

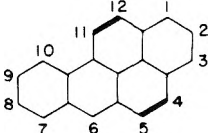
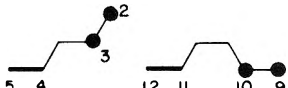
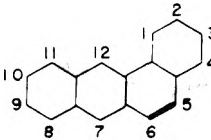

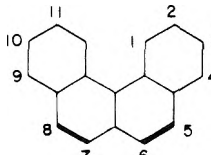
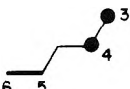
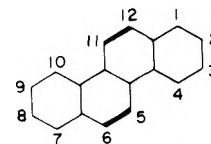
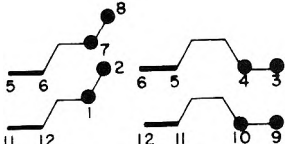
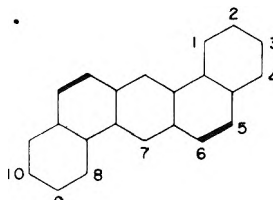

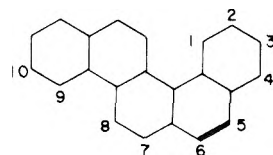
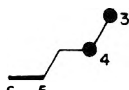
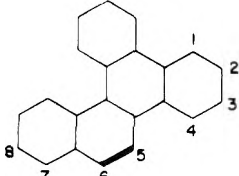
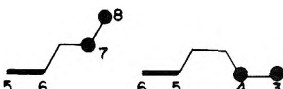
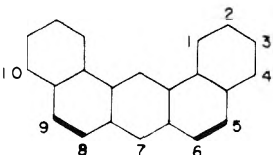
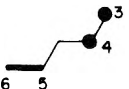
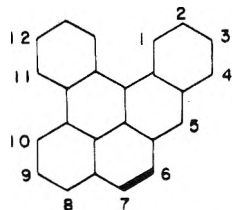
Benzo [a] pyrene (3,4-benzo pyrene) dibenzo [a, m:n] anthracene			IX	
Benz [a] anthracene (1,2-benz anthracene)			X	
Benzo [a] phenanthrene (3,4-benzo phenanthrene)		K-2 	K-3	XI
Benzo [c] phenanthrene chrysene (1,2-benzo phenanthrene)			XII	
Dibenz [a,h] anthracene (1,2:5,6 dibenz anthracene)			XIII	
Benzo [c] chrysene (1,2:5,6 dibenzo phenanthrene)			XIV	
Benzo [g] chrysene (1,2:3,4 dibenzo phenanthrene) (11,12 benzo chrysene) (5,6 benzo chrysene)			XV	
Dibenz [a,j] anthracene (1,2:7,8 dibenz anthracene)			XVI	

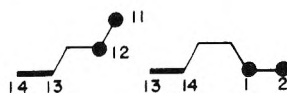
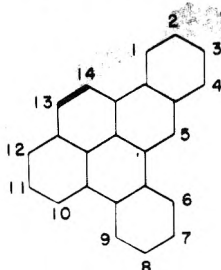
TABLE IV (Continued)

Dibenzo [a, l] pyrene
(1,2 : 9,10 dibenzo pyrene)
(6,7 : 8,9 dibenzopyrene)



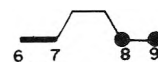
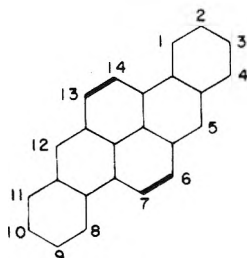
XVII

Dibenzo [a, e] pyrene
(6,7 : 9,10 dibenzo pyrene)
(1,2 : 8,9 dibenzopyrene)

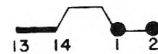


XVIII

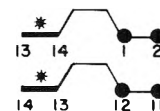
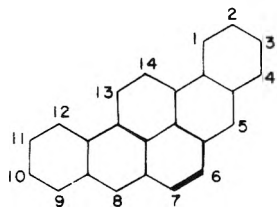
Dibenzo [a, h] pyrene
(4,5 : 9,10 dibenzo pyrene)
(3,4 : 8,9 dibenzopyrene)



XIX

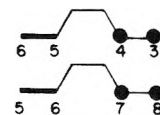
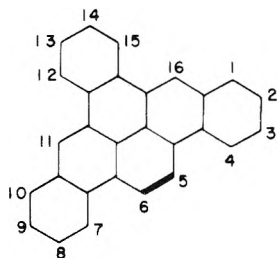


Dibenzo [a, i] pyrene
(3,4 : 9,10 dibenzo pyrene)
(4,5 : 8,9 dibenzopyrene)



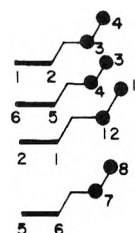
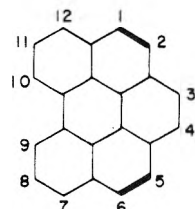
XX

Tribenzo [b, h, l] pyrene
(1,2 : 4,5 : 8,9 tribenzopyrene)
(3,4 : 6,7 : 9,10 tribenzopyrene)



XXI

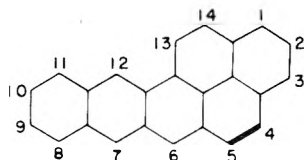
Dibenzo [c : d, e] pyrene
(1,12 benzoperylene)



XXII

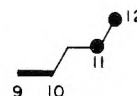
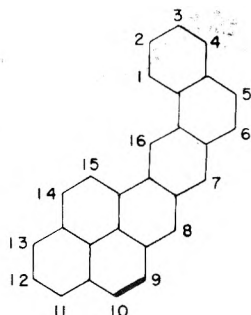
TABLE IV (Continued)

Naphtho [b] pyrene
[(naphtho - 2', 3') - 3,4 - pyrene]



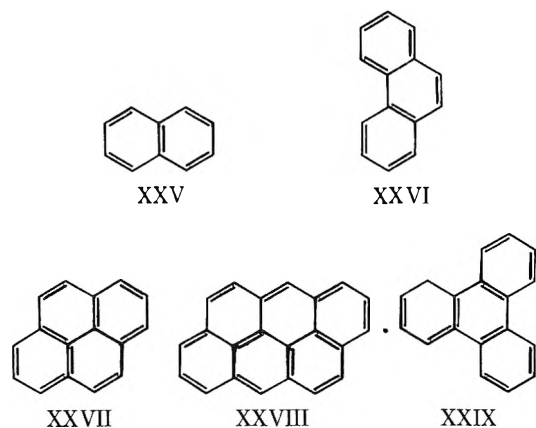
XXIII

Phenanthra [a] pyrene
[(phenanthra - 2', 3') - 3,4 - pyrene]



XXIV

^a In this table the thick line indicates the binding site for the hydroxylase enzyme. Sites other than the K region are indicated by a star above the line.

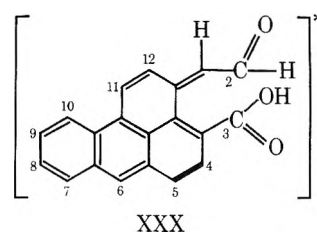


(XXVIII) have K-2 geometries. Triphenylene (XXIX) has six equivalent K-3 geometries. In all of these cases, the molecules have planes and axes of symmetry which allow for the π electron orbitals to be uniformly distributed. Naphthalene has four equivalent K-2 geometries. Phenanthrene has four equivalent K-2 geometries and two equivalent K-3 geometries. Pyrene has four equivalent K-2 geometries and four additional type 2 geometries. Anthanthrene has two equivalent K-2 geometries, two type 2 geometries, and two K-2R geometries. The redundancy in K-region geometries means a more uniform distribution of π electrons and a decreased bond order for each K region. In these cases the epoxide intermediates will not be readily induced to the carbonium ion and enzymic hydration or rapid rearrangement to the phenol will occur. In the case of anthanthrene, XXVIII, a new feature is introduced, competition through K-2R to produce the presumably non-carcinogenic meso-anthracenic quinones. It is known that the methylation of anthanthrene in the 6 or the 6,12 positions makes the substituted molecule a carcinogen.^{32,33} The assumption made is that methylation eliminates the K-2R pathway competing with epoxide formation.

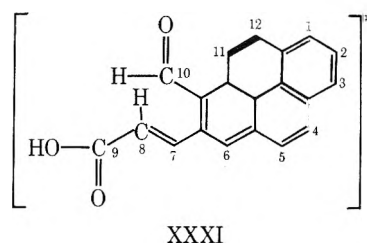
The most intriguing prediction of the common geometry scheme is that of a common mechanism for CL. The CL intensity is determined by the rate of formation of the epoxide and the rate of subsequent oxygenation.

In the cases of the 2,3 oxide of benzo[c]pyrene and the

9,10-oxide, ring cleavage as the result of the low probability chemiluminescence oxygenation should yield, respectively, an anthracene-like excited state (XXX) and a pyrene-like excited state (XXXI). For each product the bond involved in

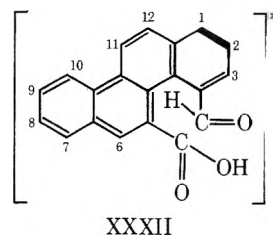


XXX



XXXI

enzyme binding is shown as the thick black line. Chemiluminescent oxidation at the K-region oxide (4,5-oxide) should result in a chrysene-like excited state. In structures XXX, XXXI, and XXXII the original numbering system of the parent benzo[a]pyrene has been retained to show the origin of the ring splitting. The excited state products XXX, XXXI, and XXXII would more properly be named benz[*mn*]an-



XXXII

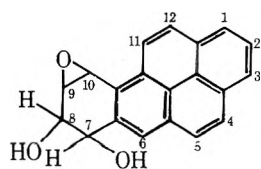
thracene-2-acetaldehyde-3-carboxylic acid; pyrene-7-propenoic acid 8-aldehyde, and chrysene-4-aldehyde-5-carboxylic acid, respectively.

It should be possible to differentiate among the three epoxide intermediates leading to the excited state carbonyls from an analysis of the spectral intensity distribution of the microsomal chemiluminescent emission and a comparison with the fluorescence spectrum of these product molecules prepared synthetically. It is important to point out that the very low yields of CL may make detection of these products by ordinary analytical chemical techniques virtually impossible (see also ref 34, 35). Therefore for the present only by their quanta can they be traced and identified.

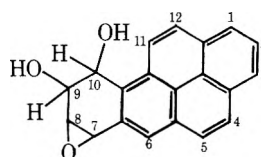
Since this mechanism was initially reported¹⁶ a number of extremely potent epoxides of benzo[*a*]pyrene have been synthesized.^{36,37} The common geometry mechanism remains consistent with the observed mutagenicity, carcinogenicity, or the lack of these properties in all of the epoxides tested.

A chemical reaction proposed to explain the cytotoxicity of epoxides is a nucleophilic attack on the carbonium ion (form VII) by cellular macromolecules. The carbonium ion formation and the subsequent rearrangement to the phenol are dependent on the ease of intramolecular donation of π electrons to the ring containing the epoxide. Thus epoxides of molecules containing electron-donating substituents should result in phenol products, VIII. Conversely electron-withdrawing substituents displace the epoxide-carbonium ion equilibrium to the epoxide, VI, increasing the probability of subsequent enzymatic formation of diols and glutathione conjugates. Proximity of the epoxide to cellular macromolecules with loosely bound electrons may induce the opening of the oxirane ring to the carbonium ion. For low activation energy reactions intermolecular electron transfer from the macromolecule can occur, resulting in covalent binding of the epoxide. However, the induced carbonium electrophile may react with molecular oxygen, resulting in the extremely reactive, ring-opened, excited state carbonyl products. These excited states, analogous to the photochemical reactions of carbonyls, can readily form Schiff base or oxetane additions with the inducing macromolecule. Thus there may be an excited state mechanism for cytotoxicity of carcinogenic PAH's, separate from ground state carbonium ion reactions. It should be possible to test for this class of carbonyl reactions by incubating synthesized epoxides with mutagen test systems³⁸⁻⁴² or by measuring binding to DNA⁴³⁻⁴⁷ in the presence and absence of oxygen. Carbonium ion reactions should be independent of oxygen while the production of excited state carbonyls requires oxygen.

7,8-Dihydroxy-7,8,9,10-tetrahydrobenzo[*a*]pyrene 9,10-oxide (XXXIII) has been reported to be mutagenic in the absence of microsomal activation³⁹⁻⁴² and to bind covalently

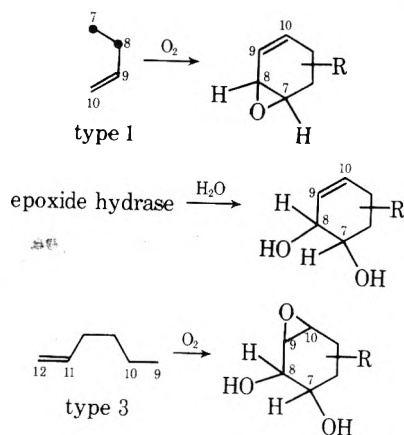


XXXIII



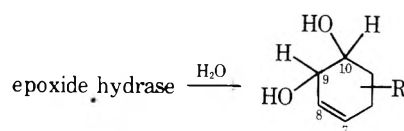
XXXIV

to DNA.⁴³⁻⁴⁶ The metabolic formation of this epoxide can proceed through the following reactions:

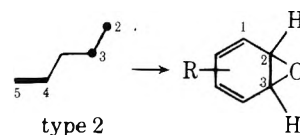


Therefore it is possible, by incubating the 7,8-diol of benzo[*a*]pyrene with microsomes, to produce the mutagenic 9,10-oxide-7,8-diol (XXXIII) through a type 3 geometry.^{39,42} Thus the 7,8-diol of benzo[*a*]pyrene plus microsomes will bind to DNA^{43,47} and, significantly, the 7,8-epoxybenzo[*a*]pyrene has been shown to be carcinogenic on mouse skin.⁴⁸

However, although the synthetically formed 9,10-dihydroxy-7,8,9,10-tetrahydrobenzo[*a*]pyrene 7,8-oxide (XXXIV) will bind to DNA,⁴⁴ 9,10-epoxybenzo[*a*]pyrene is not carcinogenic to mouse skin.⁴⁸ From the common geometry mechanism it can be seen that, starting from 9,10-epoxybenzo[*a*]pyrene in the presence of the AHH system we can produce the 9,10-diol through epoxide hydrase:



However, it should no longer be possible to form the 7,8-oxide metabolically since this cannot be arrived at through any of the three possible geometries. There may still be some minor reactivity due to epoxides produced through type 2 geometries and this may be the explanation of the slight residual muta-



type 2

genicity⁴² and low DNA binding⁴⁷ found for 9,10-dihydroxybenzo[*a*]pyrene incubated with microsomes.

When the adventitious oxygenation of one of the epoxide tautomers was originally proposed we were concerned because there was a sequence of two successive oxygenations required; one to produce the oxide and the second to open the ring. However this does not appear too improbable now in comparison with the three successive enzymatic steps required to produce the mutagenic 7,8-diol-9,10-oxide of benzo[*a*]pyrene.

An analogous argument for K-2 and K-3 active site geometries may be made for the carcinogenicity of the nonalternant hydrocarbons 3,4-benzofluoranthene (K-3); 10,11-benzofluoranthene (K-2, K-3); 11,12-benzofluoranthene (K-2); ace[*de*]benz[*a*]anthracene (K-3); ace[*fg*]benz[*a*]anthracene (cholanthrene) (K-2, K-3); ace[*kl*]benz[*a*]anthracene (K-2, K-3); ace[4',5'-*b*]benz[*a*]anthracene (K-2); ace[*fg*]dibenz[*a,kl*]anthracene (K-2, K-3); diace[*fg,kl*]-

benz[a]anthracene (K-2, type 3); and cyclopentano[h]-benz[a]anthracene (K-2). It is also possible that during the metabolism of steroids, intermediates which possess type 2 or type 3 geometries can occur.

Amino substituents to PAH's such as naphthylamine and anthramine convert these originally noncarcinogenic PAH's to potent carcinogens, in several aspects resembling the carcinogenic PAH's.⁴⁹ It is therefore possible that the metabolism of these arylamines to *N*-hydroxy and nitroso intermediates and the subsequent epoxidation of these same compounds at the opposite end of the molecule (through type 1 geometry) may result in extremely reactive carbonium ions. Under these conditions the carcinogenicity and the chemiluminescence due to adventitious oxygenation should be directly correlated. The common geometry-chemiluminescence mechanism predicts therefore that the metabolism of arylamines in microsomal systems should produce chemiluminescence. In the case of *N*-hydroxy-2-aminoanthracene, further metabolism to the 8,9-oxide through type 1 geometry may accelerate the production of the ring-opened excited state naphthalene-2-hydroxylamine-6-propenoic acid 7-carbonyl.

There are a number of older observations relating to the carcinogenicity of methyl-substituted benzo[a]pyrene which can be explained through the common geometry mechanism. For example, 6-methylbenzo[a]pyrene and 2-methylbenzo[a]pyrene are both highly active carcinogens and 7-methylbenzo[a]pyrene is less active than the unsubstituted PAH.⁵⁰ Until now these, by comparison with analogous substitutions in benz[a]anthracene, have been considered to be contradictions. However, as can be seen 6-methyl eliminates the competing K-2R reactions leading to quinones.

The 2-methyl substitution eliminates the K-2 geometry leading to the major 3-hydroxybenzo[a]pyrene metabolite. The remaining reactions are type 1 to form the 7,8-oxide; epoxide hydase to form the 7,8-diol; and type 3 to form the 9,10-oxide. Since these will be produced with higher probability 2-methylbenzo[a]pyrene should be a potent carcinogen.

Methylation at the 7 position interferes with the formation of the 7,8-diol. Although the 9,10-oxide can still be produced through type 3 geometry the reactivity of the 9,10-oxide alone will not be as great as that of the 7,8-diol-9,10-oxide and 7-methylbenzo[a]pyrene should be less carcinogenic than benzo[a]pyrene alone. As a consequence of this mechanism it is possible to predict that 8,9-dimethylbenzo[a]pyrene and 7,11,12-trimethylbenzo[a]pyrene should be noncarcinogenic; 9-methylbenzo[a]pyrene and 11,12-dimethylbenzo[a]pyrene should be weakly carcinogenic.

Similar arguments can be made with methyl substituents of benz[a]anthracene. From the distribution of the metabolites of benz[a]anthracene it is possible that the reactive intermediate is the 1,2-diol-3,4-oxide. This can be formed through type 1 geometry to produce the 1,2-epoxide; epoxide hydase to produce the 1,2-diol and K-2 geometry to produce the 3,4-epoxide. This would remove a long-standing problem in explaining the fact that methyl substitutions in the benzo ring of benz[a]anthracene abolish carcinogenicity in the substituted molecule and even of the initially active 7-methylbenz[a]anthracene. Since the 8,9-diol is a metabolic product any methyl substitution interfering with the type 1 geometry



should increase the carcinogenicity of the substituent molecule. This would be true for the 8,9,10,11 monomethyl substituents of benz[a]anthracene. The mechanism is not sufficiently precise to decide between 5-methylbenz[a]anthracene and 6-methylbenz[a]anthracene. The fact that 6-methylbenz[a]anthracene is a strong carcinogen compared with 5-methylbenz[a]anthracene would implicate the 5-carbon as the major charge localization site for binding to the cytochrome system.

Summary

The common geometry mechanism is an empirical theory which was constructed to fit the observed distributions of metabolites of PAH's with only two initial criteria: (a) metabolic oxygenation of the parent carcinogen must occur and therefore the binding site of the substrate to the enzyme must be different from the site for attack by molecular oxygen; (b) the large number of pyrolytically formed PAH's have no biological function and came upon the scene late in evolution. Therefore the first step in detoxification, the oxygenation step, should be the same as that already evolved for biological aromatic hydrocarbons. The optimum efficiency would be achieved if, due to the structures of the PAH's, they exhibited common geometrical relationships between the most probable binding site and the site of oxygenation. This would permit a degree of nonspecificity for the detoxifying enzymes.

With this major simplification it was possible to correlate carcinogenicity with K-2 or K-3 geometries. It also appears that meso-anthracenic reactions are not appreciably carcinogenic. Elimination of meso-anthracenic reactions in 7-methyl- or 7,12-dimethylbenz[a]anthracene or even in 5,10-dimethylanthracene increases the probability of epoxide-forming reactions and therefore the carcinogenicities of the substituted molecules.

There is nothing inherent in the common geometry scheme that predicts the carcinogenicity of benzo[a]pyrene. However by correlation it requires that dibenzo[a,h]pyrene and other PAH's possessing K-2 or K-3 geometries also be carcinogens. Since the 7,8-dihydroxybenzo[a]pyrene 9,10-oxide is a potent mutagen the mechanism can predict that 11,12-dimethylbenzo[a]pyrene should be a weak carcinogen. In this case the type 3 geometry which is assumed to produce the 9,10-oxide will be inhibited. In addition the 7,8-oxide of benzo[a]pyrene must be formed by type 1 geometry prior to the formation of the 9,10-oxide through type 3 geometry. Otherwise the type 1 geometry leading to the 7,8-diol would be inhibited. Therefore 9,10-epoxybenzo[a]pyrene should be a weak or a noncarcinogen. This confirms the recent finding that 9,10-epoxybenzo[a]pyrene is indeed noncarcinogenic.⁴⁸

The utility of this mechanistic approach to PAH carcinogenicity is that it can be extrapolated to the characterization of carcinogenicity in the PAH's containing five-membered rings, the fluoranthenes. In addition, by virtue of prescribing the active site geometries the mechanism eliminates previous apparent contradictions between the observed and expected carcinogenicities of methyl substituents of benzo[a]pyrene and benz[a]anthracene. It also suggests that the arylamines may be carcinogenic through the same carbonium ion reactions as the PAH's; the observed metabolism at the N position may serve to make any epoxides formed more reactive.

The correlation of chemiluminescence with the metabolic hydroxylation of the PAH carcinogens came about initially by analogy with the observed chemiluminescence of the luciferin substrates of bioluminescent systems. However the substrate giving rise to the excited state product in biolumi-

nescence evolved for efficient fluorescence to provide visual signals. The introduction of the carcinogenic PAH into biological systems is fortuitous. The projected excited state products are carbonyls which are extremely reactive. Two corollaries arise. The first is that despite their low quantum yield of fluorescence the production of these excited state carbonyls can be measured by the intensity of light emission. This provides a simple experimental method for following the kinetics of the hydroxylation reactions of PAH carcinogens by the AHH system. The second is that the carbonyl excited states might be a source of cytotoxicity at the site where the parent PAH may have already intercalated. They might participate in a class of electrophilic attack not easily accessible to ground state carbonium ions.

We have already verified that the intermediates produced in benzo[a]pyrene-AHH systems are chemiluminescent in the enzyme denatured system and require oxygen for chemiluminescence. We are in the process of testing the spontaneous CL of the newly synthesized epoxides of benzo[a]pyrene and of testing their mutagenicity in bacterial revertant systems in the presence and absence of oxygen.³⁸

Acknowledgments. Research supported under U.S. ERDA Contract No. AT(11-1)3277. Contribution No. 867 of the McCollum-Pratt Institute.

The authors wish to thank Mr. W. H. Biggley, Dr. M. E. Loftus, and Dr. E. N. Moudrianakis for discussions and many helpful suggestions.

References and Notes

- H. H. Seliger, *Photochem. Photobiol.*, **21**, 355 (1975).
- D. M. Jerina, J. W. Daly, B. Witkop, P. Zaltman-Niremberg, and S. Udenfriend, *Biochemistry*, **9**, 147 (1970).
- D. M. Jerina and J. W. Daly, *Science*, **185**, 573 (1974).
- J. W. Daly, D. M. Jerina, and B. Witkop, *Experientia*, **28**, 1129 (1972).
- G. J. Kasperek and T. C. Bruice, *J. Chem. Soc., Chem. Commun.*, 784 (1972).
- G. Guroff, J. W. Daly, D. M. Jerina, D. M. Renson, B. Witkop, and S. Udenfriend, *Science*, **158**, 1524 (1967).
- J. W. Daly, G. Guroff, D. M. Jerina, S. Udenfriend, and B. Witkop, *Adv. Chem., Ser.*, No. 77, 77, 279 (1968).
- D. M. Jerina, J. W. Daly, and B. Witkop, *J. Am. Chem. Soc.*, **90**, 6523 (1968).
- D. R. Boyd, J. W. Daly, and D. M. Jerina, *Biochemistry*, **11**, 1961 (1972).
- There are a number of different nomenclatures used for labeling the structures of aromatic hydrocarbons [J. C. Arcos and M. F. Argus, "Chemical Induction of Cancer", Vol. IIA, Academic Press, New York, N.Y., 1974]. The following labeling and naming system will be used: the new molecule will be numbered according to the IUPAC rules. The name used will reflect the ring fusions to the largest possible trivial-named segment, using numbers to denote the bonds of the fused addition and Italic letters to denote the bonds of the trivial-named segments to which the rings are fused. In addition the old name of the compound (Richter nomenclature) will be included in parentheses in order to preserve continuity from the earlier literature.
- J. P. Hamman and H. H. Seliger, *Biochem. Biophys. Res. Commun.*, **70**, 675 (1976).
- N. Kinoshita and H. V. Gelboin, *Proc. Natl. Acad. Sci. U.S.A.*, **69**, 824 (1972).
- W. Anderson, *Nature (London)*, **160**, 892 (1947).
- E. Boyland, *Yale J. Biol. Med.*, **20**, 321 (1948).
- E. Boyland, *Annu. Rev. Biochem.*, **18**, 217 (1949).
- H. H. Seliger, *Fed. Proc.*, **34**, 623 (1975).
- L. Ernster, *J. Cell Biol.*, **15**, 541 (1962).
- H. Remmer, H. Greim, J. B. Schenkman, and R. W. Estabrook, "Methods in Enzymology", Vol. X, R. W. Estabrook and M. E. Pullman, Ed., Academic Press, New York, N.Y., 1967, p 703.
- E. W. Sutherland, C. F. Cori, R. Haynes, and W. S. Olsen, *J. Biol. Chem.*, **180**, 825 (1949).
- D. W. Nebert and H. V. Gelboin, *J. Biol. Chem.*, **243**, 6242 (1968).
- J. Lee and H. H. Seliger, *Photochem. Photobiol.*, **15**, 227 (1972).
- L. Diamond and H. V. Gelboin, *Science*, **166**, 1023 (1969).
- A. Y. H. Lu, R. Kuntzman, S. West, and A. H. Conney, *Biochem. Biophys. Res. Commun.*, **42**, 1200 (1971).
- A. Y. H. Lu, R. Kuntzman, S. West, M. Jacobson, and A. H. Conney, *J. Biol. Chem.*, **247**, 1727 (1972).
- A. Y. H. Lu, W. Levin, S. West, M. Jacobson, D. Ryan, R. Huntzman, and A. H. Conney, *J. Biol. Chem.*, **248**, 456 (1973).
- A. Pullman and B. Pullman, *Adv. Cancer Res.*, **3**, 117 (1955).
- B. Pullman, *J. Cell Comp. Physiol.*, **64**, Suppl. 1, 91 (1964).
- A. Pullman and B. Pullman, "The Jerusalem Symposia on Quantum Chemistry and Biochemistry", Vol. I, E. D. Bergmann and B. Pullman, Ed., Academic Press, New York, N.Y., 1969, p 9.
- J. K. Selkirk, R. G. Croy, and H. V. Gelboin, *Arch. Biochem. Biophys.*, **168**, 322 (1975).
- J. K. Selkirk, R. G. Croy, and H. V. Gelboin, *Science*, **184**, 169 (1974).
- E. Boyland, M. Kimura, and P. Sims, *Biochem. J.*, **92**, 631 (1964).
- N. P. Buu-Hoi, *Cancer Res.*, **24**, 1511 (1964).
- A. Lacassagne, N. P. Buu-Hoi, and F. Zajdela, *C. R. Acad. Sci. Paris*, **246**, 1477 (1958).
- J. C. Arcos and M. F. Argus, "Chemical Induction of Cancer", Vol. IIA, Academic Press, New York, N.Y., 1974, p 137.
- S. Beck, A. H. M. Kirby, and P. R. Peacock, *Cancer Res.*, **5**, 135 (1945).
- H. Yagi, and D. M. Jerina, *J. Am. Chem. Soc.*, **97**, 3185 (1975).
- H. Yagi, O. Hernandez, and D. M. Jerina, *J. Am. Chem. Soc.*, **97**, 6881 (1975).
- B. N. Ames, J. McCann, and E. Yamasaki, *Mutation Res.*, **31**, 347 (1975).
- C. Malaveille, H. Bartsch, P. L. Grover, and P. Sims, *Biochem. Biophys. Res. Commun.*, **66**, 693 (1975).
- R. F. Newbold and P. Brookes, *Nature (London)*, **261**, 54 (1976).
- P. G. Wistocki, A. W. Wood, R. L. Chang, W. Levin, H. Yagi, O. Hernandez, D. M. Jerina, and A. H. Conney, *Biochem. Biophys. Res. Commun.*, **68**, 1006 (1976).
- E. Heiberger, L. Sachs, S. K. Yang, and H. V. Gelboin, *Proc. Nat. Acad. Sci. U.S.A.*, **73**, 607 (1976).
- P. Sims, P. L. Grover, A. Swaisland, K. Pal, and A. Hewer, *Nature (London)*, **252**, 326 (1974).
- P. Daudel, M. Duquesne, P. Vigny, P. L. Grover, and P. Sims, *FEBS Lett.*, **57**, 250 (1975).
- M. R. Osborne, M. H. Thompson, E. M. Tarmy, F. A. Beland, R. G. Harvey, and P. Brookes, *Chem.-Biol. Interact.*, **13**, 343 (1976).
- H. W. S. King, M. H. Thompson, E. M. Tarmy, P. Brookes, and R. G. Harvey, *Chem.-Biol. Interact.*, **13**, 349 (1976).
- A. Borgen, H. Darvey, N. Castagnoli, T. T. Crocker, R. E. Rasmussen, and I. Y. Wang, *J. Med. Chem.*, **16**, 502 (1973).
- W. Levin, A. W. Wood, H. Yagi, P. M. Dansette, D. M. Jerina, and A. H. Conney, *Proc. Nat. Acad. Sci. U.S.A.*, **73**, 243 (1972).
- Reference 34, Vol. IIB, Section 5 12.
- Reference 34, Vol. IIA, p 34.
- Reference 34, Vol. IIA, Table IV, p 31; p 213.

Discussion

A. KHAN. Is there any experimental data on the bond cleavage of the cyclic structure resulting in the generation of electronically excited carbonyl from the hydroperoxide species?

H. SELIGER. Yes, the work of DeLuca et al. (M. DeLuca and M. E. Dempsey in "Chemiluminescence and Bioluminescence", M. J. Carmies, D. M. Hercules, and J. Lee, Ed., Plenum Press, New York, N.Y., 1973, p 345) on mechanism of firefly bioluminescence.

S. FRED. How does this mechanism apply to what would be considered marginal carcinogens?

H. SELIGER. The reactions and the active site geometries comprising this mechanism apply as well to compounds that are normally considered to be noncarcinogens. It is proposed that anthracene or naphthalene can be modified to become carcinogenic if the rates of formation of specific epoxide intermediates as well as the reactivities of these epoxides can be enhanced. For example, the carcinogenicity of 5,10-dimethylanthracene is proposed in part to be due to the elimination of competing K-2R reactions that lead to mesoanthracenic quinones. The inference here is that the 1,2-epoxide may be the precursor leading to the carcinogenic event. There are also a number of hydroxylase enzymes in crude liver extracts. As we have indicated in the paper these can be induced to different degrees by ingestion of different inducers. There is a derivative of herbicide, 2,3,7,8-tetrachlorodibenzoparadioxin, TCDD which induces long-lasting aryl hydrocarbon hydroxylase activity in rats, at concentrations between 10^{-4} and 10^{-6} below those at which the potent carcinogen 3-methylcholanthrene is an effective inducer. It is possible that the induction of a hydroxylase that can operate on type 3 geometries may have a synergistic effect with other hydroxylases that operate on type 1 geometries. This could result in a greater probability for the fortuitous formation of the reactive 7,8-dihydroxybenzo[a]pyrene 9,10-oxide than in the noninduced case where type 3 geometry enzymes are unavailable. This increased rate of production of the reactive epoxide should also be correlated with an increase in chemiluminescence in-

tensity. In this specific case the chemiluminescence intensity is proposed to be proportional to the concentration of potentially reactive epoxides. These are nonexclusive alternatives leading from this hypothesis. The epoxide or the carbonium ion may react with molecular oxygen producing a highly reactive excited state which can add covalently to nucleophiles analogous to the photochemistry of carbonyls. Some of these excited states can decay by fluorescence and this is the chemiluminescence we observe. The ground state epoxide may react directly with cellular nucleophiles. The binding of (\pm)-7 β ,8 α -dihydroxy-9 α ,10 α -epoxy-7,8,9,10-tetrahydrobenzo[a]pyrene to the 2-amino group of guanine through C-10 of the diol epoxide has recently been reported (I. B. Weinstein, A. M. Jeffrey, K. W. Jernette, S. H. Blobstein, R. G. Harvey, C. Harris, H. Autrup, H. Kasai, and K. Nakanishi, *Science*, **193**, 592 (1976)). Inhibition of the epoxide hydase associated with the type 3 geometry epoxidase could inhibit formation of the noncytotoxic 9,10-diol from the reactive 7,8-diol-9,10-epoxide. Thus there are a number of ways in which the rate of formation of specific reactive epoxides may be enhanced. The only assumption made in the common geometry chemiluminescence mechanism is that the reactivity of the epoxide which leads to the initial carcinogenic reaction may also be related to the rate at which the epoxide may react with dissolved molecular oxygen to produce a ring-opened excited state product molecule. If the chemilumines-

cence intensity is observed to increase it is assumed that the rate of damage is also increased. This then taxes the rest of the system, the repair mechanism and the immune mechanism. In this manner there is a complete spectrum of potential carcinogenicity and a distinction is not made in quality, i.e., the types of reactions between a weak carcinogen and a strong carcinogen. Any modification along the steps of the entire protective system, the induction of the hydroxylases, the inhibition of certain of the epoxide hydases, of the nucleic acid repair system, of nonhistone chromosomal protein synthesis, of the immune system, may increase the probability of the transformation of a normal cell to a cancer cell. A possible corollary of the mechanism is that upon accidental ingestion of a strong carcinogen such as benzo[a]pyrene the purposeful ingestion of a linear noncarcinogen with a strong K region such as anthracene or tetracene may inhibit the type 1 geometry leading to 7,8-dihydroxybenzo[a]pyrene in preference to the K-2 geometry leading to 3-hydroxybenzo[a]pyrene and thus permit the excretion of the carcinogen with a minimum of damage.

S. FREED. Have you examined cancerous liver microsomes for the hydroxylation reactions?

H. SELIGER. Not yet.

Fluorescence and Multiple Excitation in Photosynthetic Systems

D. Mauzerall

The Rockefeller University, New York, New York 10021 (Received January 26, 1976)

Publication costs assisted by Rockefeller University

Changes in the quantum yield of fluorescence in *Chlorella* both during and following 7-ns pulses of light has been measured as a function of pulse intensity. The increase in yield has a 35-ns risetime for singly hit units and a 4- μ s risetime for doubly hit units. The short time constant is thought to reflect a change in coupling between antenna and trap chlorophylls and the long time constant the lifetime of a carotenoid triplet state which quenches the fluorescence of chlorophyll singlets. The gradual decrease in yield of the dark adapted state during the 7-ns pulse as a function of increasing number of hits is explained by a multitrapped photosynthetic unit. The sharp decrease in yield of the high fluorescence yield state following a saturating flash is fit to a single hit Poisson saturation, and the striking difference in response of these two states is related to the finite risetime of this high yield state.

Much of what we know about the mechanisms of photosynthesis has been learned by experiments using single-turnover flashes.¹ These experiments are possible because a flash of saturating intensity, operationally defined, can be given in a time short compared to the turnover time, 10^{-4} s. To the first approximation hits on the photosynthetic units will follow the Poisson distribution. For example, at an average hit of one photon per unit, the specific hits will be: 37% none, 37% one, and 26% two or greater. Of necessity, therefore, saturating flashes must result in multiple hits to the operational photosynthetic unit, and the effects of these multiple hits are of inherent interest. It has always been tacitly assumed that such multiple excitations produce the same effect as a single excitation. Measurements of fluorescence yield changes in the short time range show that this assumption is incorrect. These measurements also give direct information on the pathways of excitation transfer in photosynthetic systems.

Experimental Section

The actinic light is supplied by a 7-ns (full-width at half-maximum intensity) pulse of 337-nm light from a nitrogen laser. A similar but usually far less intense pulse following a variable delay allows measurement of the change of the quantum yield of fluorescence as a function of time.² A gated detection system is used, with a small photomultiplier switched on and off with 3-ns rise and fall times.³ Single photoelectrons can be detected in a 10-ns time slot. A representation of the measurement is given in Figure 1. Linearity is enhanced by using the detector in a near-null mode: the fluorescence emission is attenuated corresponding to the excitation intensity. Faster time resolution is obtained with a nanosecond photomultiplier and a sampling system. The algae are in a flow system such that each individual measurement is made on a fresh batch of dark adapted algae. Typically 30 to 100 pulses are integrated in a determination. A complete

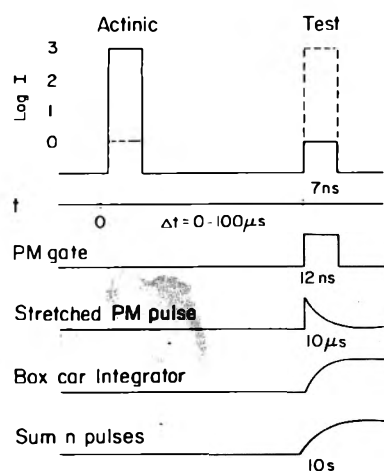


Figure 1. Time sequence of events in a typical experiment. A nitrogen laser supplies a strong (variable) intensity actinic pulse at $t = 0$. At various times later (Δt) an optical delay line (0–100 ns) or a second nitrogen laser (30 ns–1 s) supplies a weak (variable) intensity test flash. The photomultiplier (PM) is gated on exclusively during the test pulse, which can include the actinic pulse at $t = 0$. The PM pulse is stretched to $\sim 10 \mu\text{s}$ and integrated by a box car integrator which also averages n pulses either exponentially for scanning or linearly for maximum signal-to-noise ratio.

description of the apparatus and of the technique of data analysis is being published.⁴ The observed quantum yield of fluorescence is defined as the ratio of fluorescence quanta emitted in the delayed or test pulse, F , to the average quanta absorbed, x :

$$\phi = \frac{F}{x} = \frac{a \int \mathcal{F} dt}{\sigma \int I dt} \quad (1)$$

In eq 1, a is an instrumental constant, \mathcal{F} is the instantaneous fluorescence intensity, σ is the optical cross section of a unit, I is the exciting light intensity, and the integrals are over the pulse length. Since the light and photomultiplier gate pulses (~ 10 ns) are longer than the longest fluorescence lifetimes (≤ 2 ns), the latter can be ignored at the present level of analysis. The quantum yield as a function of average hits is given in general by $\phi = \sum_1^\infty \phi_n P_n$ where ϕ_n is the fluorescence yield for a unit hit n times and P_n is the n th Poisson distribution: $P_n = x^n e^{-x} / n!$. All of the fluorescence yields are normalized to the limiting yield, ϕ_0 , of dark adapted algae as $x \rightarrow 0$. This yield has been shown⁴ to be constant from one hit per 10^3 to one hit per 5×10^4 chlorophyll molecules.

Results

I will first summarize what is known about the changes in fluorescence yield of algae on the short time scale. It has been previously hypothesized that the quantum yield of fluorescence in dark adapted photosynthetic systems was low because the primary acceptor, Q, quenched the fluorescence. On being reduced to Q^- , the fluorescence yield increased and remained high until Q^- was reoxidized. However, measurements in the short time range showed that the changes in fluorescence yield following a saturating light pulse to *Chlorella* are highly dynamic.² In Figure 2 these kinetics of the changes in fluorescence yield are presented ranging over eight orders of magnitude on the time scale. For clarity they have been decomposed into the yields of units specifically hit once, twice, and many times. This is done by kinetic and Poisson analysis⁴ of data where x is varied from $1/4$ to 15. The scale for the average number of hits, x , was obtained by fitting the cumulative one-hit Poisson distribution to the pulse in-

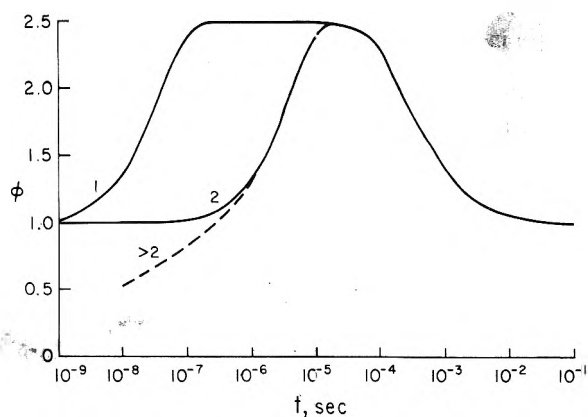


Figure 2. The kinetics of the changes of fluorescence yield in *Chlorella* as a function of the specific number of hits per unit, obtained by analysis of data.⁴ The numbers 1, 2, and >2 refer to the specific number of hits per unit.

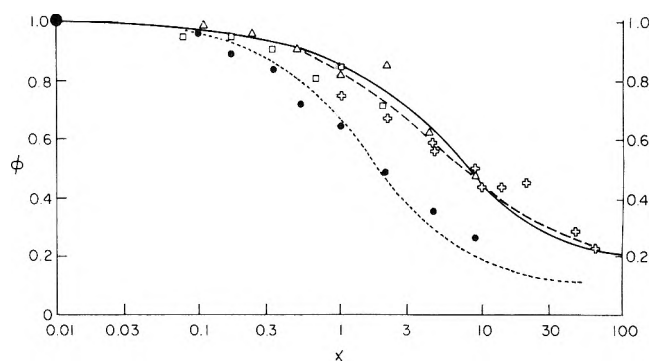


Figure 3. The relative quantum yield of fluorescence, ϕ , as a function of the average number of excitations, x , during a flash for both the dark adapted state (open symbols) and for the high fluorescence yield state (closed circles) $30 \mu\text{s}$ following a saturating flash. The solid line is eq 2 with $1/k = 1.4$ ns; the dashed line is eq 3 with $t = 3$, both covering a change of 80% in ϕ . The dotted curve is eq 5 with no adjustable parameters, covering a change of 90% in ϕ .

tensity saturation curve of the fluorescence yield increase which is complete $30 \mu\text{s}$ after the actinic pulse. The optical cross section, σ , so determined corresponds to about 10^2 chlorophyll molecules. The increase in fluorescence yield in the singly hit units has a risetime of 35 ns. This finite risetime is interpreted as a change of the coupling between the antenna and trap molecules, and may be related to an early electron transfer process.² In contrast, the doubly hit units show a risetime of $4 \mu\text{s}$. This is related to a carotenoid triplet state⁴⁻⁷ formed on the second hit with quantum yield equal to that of the first photochemical hit. The latter fact is a result of the Poisson-kinetic analysis.⁴ This carotenoid triplet state acts as an efficient quencher of the singlet excitation. Multiply hit units ($x \gg 2$) show a quantum yield of fluorescence lower than that of the dark adapted state. The yield decreases with increasing number of hits and is attributed to quenching by other triplet states. These triplets annihilate themselves in the 100-ns time range⁴ where the fluorescence yield increases, always joining the $4\text{-}\mu\text{s}$ rise as a limit. Irrespective of the number of hits, by about $30 \mu\text{s}$ the system is in the high fluorescent yield state. This state decays with complex kinetics shown to have an intimate correspondance in their dependence on time and temperature to that of the turnover kinetics of the oxygen producing system.²

These results aroused interest in what was happening near $t = 0$ i.e., during the ~ 10 -ns actinic flash. As shown in Figure 3 (open symbols), fluorescence yield of the integrated pulse

decreases in the multiple excitation region.⁸ The extended region of decrease, broader than that of Poisson distributions, suggests that a second random process in addition to the rain of photons is involved. This second process can occur either in the time or in the spatial domain. In the former case, the data can be fit with a lifetime of 1.4 or 2.3 ns of a quenching state,⁸ depending on details of the annihilation. Such a calculation implies that the sum of the rate constants for the decay of this state, k , competes with the mean frequency of excitations in the unit, $f = x/T$ where x is the average number of hits and T is the equivalent square wave time period of the pulse of light. The saturation function will be of the form:

$$\phi = \phi_0 \frac{k + fe^{-(k+f)T}}{k + f} \quad (2)$$

In ref 8 a similar equation is derived, but using the discrete hit Poisson distribution. However, this fit to eq 2 is obtained using the quantum yield of the dark adapted state, and *not* with the fivefold larger yield expected from the increase of lifetime from ~ 0.3 to ~ 1.5 ns. The observation of a similar broad function of yield vs. intensity in an experiment by Campillo et al.⁹ using 20-ps pulses also indicates that kinetic competition is not the primary cause of the decrease in yield of fluorescence. The 300-fold decrease in T should have caused a collapse of the fluorescence into the relatively sharp Poisson single hit distribution, i.e., $\phi = \phi_0 \exp(-x)$. These two facts strongly suggest that the second random process is in the spatial domain. Although the data could possibly be fit by a suitable distribution of optical cross sections and quantum yields of fluorescence, a simple model suggests itself.⁸ Assume there are t traps per unit and the following rule applies: an excitation on collision with an open trap fills it and fluorescence is emitted with yield ϕ_0 where $1 - \phi_0 \sim 1$; with equal probability an excitation collides with a filled trap and is annihilated.

The observed fluorescence yield as a function of average hits, x , will be⁸

$$\phi = \frac{\phi_0}{x} \sum_1^{\infty} t P_n \left[1 - \left(\frac{t-1}{t} \right)^n \right] \quad (3)$$

where P_n is the n th Poisson distribution and t is the number of traps per unit. The data are fit with $t = 3 \pm 1$ and allowing that 80% of the original yield (ϕ_0) is so decreased (Figure 3). This hypothesis implies that losses occur during the short flash by the annihilation of excitations. The effective hits can be calculated, and account for deviations from the cumulative one hit Poisson distribution observed in data on the increase in fluorescence yield at high intensities⁸ of the actinic pulse.

The above data and discussion refer to the dark adapted state. The question naturally arises: does the high fluorescence yield state formed following a saturating flash show the same behavior? The change in fluorescence yield is measured by the ratio of fluorescence yields with and without the previous actinic flash:

$$\phi = \frac{\phi_x^t}{\phi_x^0} = \frac{\phi_0^t J(x)}{\phi_0^0 K(x)} \quad (4)$$

where the superscripts refer to the delay time of the test pulse (0 meaning no preactinic pulse) and J and K are saturation parameters, decreasing functions of x such as eq 3. If $J = K$, then ϕ would be independent of x , the intensity of the test flash. This is not found to be so. The change in yield decreases with increasing hits, indicating that the high yield state is more sensitive to inhibition by multiple excitations than is the dark

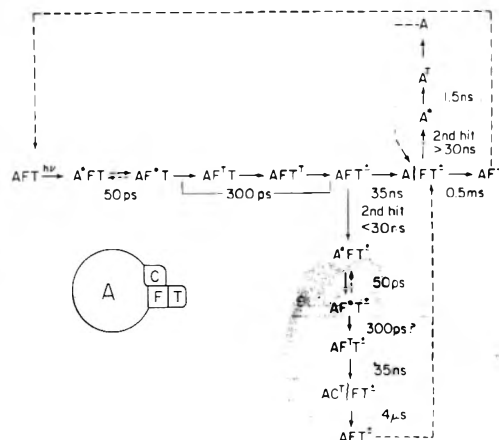


Figure 4. Model for the flow of excitation energy in a photosynthetic unit. Chlorophyll occurs in tightly coupled domains of half a dozen molecules. The antenna, A, contains two to three dozen of these domains. The funnel, F, contains one or two domains and serves as a bridge and buffer between A and T. The trap, T, is composed of a specialized domain containing the stabilized charge transfer components. The energy in a singly or first hit unit travels along the horizontal sequence. Fluorescence is emitted from both A and F, with a lifetime limited by the formation of triplet chlorophyll, F^1 , and the charge transfer state, T^\pm . The effect of further hits depends on when they occur. If the second hit occurs before the uncoupling of A and FT^\pm then F^1 forms the carotenoid triplet which quenches the fluorescence of A. The formation of further triplets in F may account for the multitraping if the effect is restricted to fluorescence. If the second hit occurs in the high yield state, $A|FT^\pm$, uncoupled A has a rather long life, but forms A' which efficiently quenches any further excitation in A.

adapted state. Knowing $K(x)$ one can calculate $J(x)$. The data (Figure 3, filled circles) can be fit with an equation completely free of adjustable parameters, if 90% of the high quantum yield is allowed to change. I call this curve the Poisson saturation, and it is given by eq 3 with $t = 1$, i.e.

$$\phi = \phi_1 \frac{(1 - e^{-x})}{x} \quad (5)$$

It represents the case where the first hit has a quantum yield of fluorescence of ϕ_1 and the second and all succeeding hits have a yield of zero.

Conclusions

The quantum yield of fluorescence of *Chlorella* following a saturating light pulse increases in the time range of 50 ns to 10 μ s. The detailed kinetics of this increase depend on the number of hits received by the photosynthetic units during the light pulse (Figure 2). In contrast, the integrated fluorescence yield over a short (10 ps–10 ns) pulse of light is a continually decreasing function of average number of hits (Figure 3). As described above, the decrease in yield is more consistently ascribed to events in the spatial domain than it is the time domain. The data are fit by a unit composed of an antenna and three traps. The statistical treatment implies that the trapping time is rapid compared to the shortest mean interhit time of our experiments, ~ 0.3 ns. Following this interpretation the results with picosecond pulses^{9–12} suggest that the antenna-trap equilibration time is about 50 ps. It is possible that the decrease in yield of fluorescence with intense picosecond pulses⁹ may also have a contribution from the time domain, i.e., direct exciton annihilation in the antenna. The short trapping time is reasonable if the antenna chlorophyll occurs in domains of half a dozen molecules. The closeness and orientation of these molecules in a domain could ensure a very rapid energy delocalization. The far fewer steps required to

transfer energy between antenna domains to the trap domain results in a rapid trapping time. The domain connecting the antenna to the trap(s) is called the funnel. There is evidence for such packaging of chlorophyll in both the antenna-funnel protein-bacteriochlorophyll complex¹³ and in the trap or reaction center from photosynthetic bacteria.¹⁴ The phycobiliproteins which compose the phycobilisome of the blue-green algae are another example of this organization.¹⁵ The outstanding problem raised by this model is the relation of these fluorescence traps to those producing photochemistry and yielding oxygen. The fluorescence traps could be sites of triplet chlorophyll formation, but with or without ensuing useful charge transfer. It should be noted that the multitrapped model can also be interpreted as a limiting case of the general problem of randomly located traps in an extensive antenna. Both σ and t would then be statistically defined averages.

The quenching of the excitation by a filled trap is expected to occur whether the filled trap is an excited state or a charge transfer state and whether it is in the singlet or triplet configuration. Either energy transfer and rapid thermalization of the doubly excited state, or rapid and reversible electron transfer can account for the quenching. The multitrapped model implies that the lifetime of the filled trap is considerably greater than 7 ns. Since the fluorescence lifetime of the dark adapted state is ~ 0.3 ns, we conclude that this singlet lifetime represents the intersystem crossing to the triplet state or the electron transfer to the charge transfer state, both of which have a lifetime ≥ 30 ns.

The unique quenching of fluorescence in the high yield state is consistent with the interpretation of the 35-ns risetime of this state as a decrease in the coupling between antenna and the trap.² The first hit produces fluorescence with a yield ϕ_1 (~ 0.05) and forms a triplet state with yield $1 - \phi_1$. This state then quenches further excitations. The fraction of quenching acts that occur by photoionization could lead to the variety of delayed luminescences which have been observed.¹ The lifetime of the high yield state is about 1.5 ns. If the fluorescence emission were homogeneous, the increase in lifetime from ~ 0.3 to ~ 1.5 ns should lead to at least a fivefold increase of quantum yield of fluorescence instead of the two-threefold increase observed. This smaller increase is however quite consistent with the model proposed here. The long lived high yield fluorescence comes principally from uncoupled antenna which when coupled to the trap has a lifetime of ~ 50 ps and a correspondingly low fluorescence yield. The decreasing yield in the multiply excited region will be accompanied by shorter average lifetimes. The assumption that one excitation is retained in the multitrapped model means that mixed lifetimes will be observed. This view, that the fluorescence of photosynthetic systems is heterogeneous, has been championed by

Borisov and Il'ina.¹⁶ The model proposed here furnishes a mechanism for this heterogeneity and is diagrammed in Figure 4.

The fact that the residual fluorescence yield at extreme hits is 20% of ϕ_0 and 10% of ϕ_1 argues that its absolute quantum yield is a constant, since ϕ_1 is about twice ϕ_0 . This yield could be a constant amount of extraneous fluorescence, but its origins from the multiple-excited states cannot be completely ruled out.

It is clear that an analysis of the effect of multiple excitations in the photosynthetic system leads to considerable information on energy transfer and its transformations. By these experiments we may arrive at some of the topological constraints which operate in this amazing product of one billion years of evolution.

Acknowledgments. It is a pleasure to recognize the assistance of a National Science Foundation Grant No. BMS 74-11747.

References and Notes

- (1) Govindjee, Ed., "Bioenergetics of Photosynthesis", Academic Press, New York, N.Y., 1975.
- (2) D. Mauzerall, *Proc. Natl. Acad. Sci. USA*, **69**, 1358 (1972).
- (3) M. Rossetto and D. Mauzerall, *Rev. Sci. Instrum.*, **43**, 1244 (1972).
- (4) D. Mauzerall, *Adv. Biol. Med. Phys.*, submitted for publication.
- (5) P. Mathis and J. M. Galmiche, *C. R. Acad. Sci. Paris, Ser. D*, **264**, 1903 (1967).
- (6) H. T. Witt, *Q. Rev. Biophys.*, **4**, 365 (1971).
- (7) L. V. M. Duysens, G. A. den Haan, and J. A. von Best in "Proceedings of the Third International Congress on Photosynthesis", M. Avron, Ed., Elsevier, Amsterdam, 1974, pp 1-12.
- (8) D. Mauzerall, *Biophys. J.*, **16**, 87 (1976).
- (9) A. J. Campillo, S. L. Shaprio, V. H. Kollmon, K. R. Winn, and R. C. Hyer, *Biophys. J.*, **16**, 93 (1976).
- (10) W. Yu, P. P. Ho, R. R. Alfano, and M. Seibert, *Biochim. Biophys. Acta*, **387**, 159 (1975).
- (11) V. Z. Paschenko, S. P. Protosov, A. B. Rubin, K. N. Timofeev, L. M. Zamazova, and L. B. Rubin, *Biochim. Biophys. Acta*, **408**, 143 (1975).
- (12) G. S. Beddard, G. Porter, C. J. Tredwell, and J. Barber, *Nature (London)*, **258**, 166 (1975).
- (13) R. E. Fenna and B. W. Matthews, *Nature (London)*, **258**, 573 (1975).
- (14) S. C. Straley, W. W. Parson, D. Mauzerall, and R. K. Clayton, *Biochim. Biophys. Acta*, **305**, 597 (1973).
- (15) B. H. Gray and E. Gantt, *Photochem. Photobiol.*, **21**, 121 (1975).
- (16) A. Yu Borisov and M. D. Il'ina, *Biochim. Biophys. Acta*, **305**, 364 (1973).

Discussion

H. SELIGER. Are the intensities of light in your experimental calculations in any way related to natural sunlight intensities?

D. MAUZERALL. Absolutely not, by some six orders of magnitude. There is no question about these things happening in nature. However, in nature one can saturate the 100- μ s turnover time. That, of course, is what the saturation curve of photosynthesis in nature is all about. The present work concerns events on a time scale about a millionfold shorter.

Exciton Interactions in the Symmetrical Dimeric Aggregate of Chlorophyll a Monohydrate¹

Vaughn J. Koester[†] and Francis K. Fong*

Department of Chemistry, Purdue University, West Lafayette, Indiana 47907 (Received February 17, 1976)

Publication costs assisted by the National Science Foundation

In this paper we present a theoretical expression for exciton interactions in C_2 symmetrical Chl a dimers with special emphasis on the theoretical analysis of the red absorption band of the in vitro A700 (700-nm absorbing) dimeric aggregate of chlorophyll a monohydrate. The treatment is based on the point dipole approximation in first-order perturbation theory. The comparison between theory and experiment is based on established molecular parameters relevant to the unique C_2 symmetrical (Chl a-H₂O)₂ aggregate structure.

Introduction

The hydrated aggregates of Chl a have been the subject of several recent studies from this laboratory.² These studies have been motivated by a number of recent developments that have led to the conclusion that the most probable primary molecular adduct in the photosystem (PS) I reaction center photoactive aggregate P700³ is a C_2 symmetrical dimer of Chl a monohydrate.^{4,5} Recent experiments on the photogalvanic effects of Chl a and quinhydrone half-cell reactions have shown that the onset of photoactivity in Chl a is probably the photoactivation of a charge transfer state in Chl a-H₂O aggregates.⁶ The purpose of the present paper is to characterize the optical properties in the proposed P700 dimer (Chl a-H₂O)₂ using the point dipole approximation in exciton theory. Exciton calculations for biological model systems have been concerned with a variety of possible aggregate interactions and consequent energy transfer processes.⁷⁻⁹ Possible exciton effects for unsymmetrical dimeric chlorophyll models have been considered in an earlier study.¹⁰

It has been concluded^{2a} from the observed experimental effects of water titration and temperature on the optical and redox properties of Chl a-H₂O aggregates that the in vitro 700-nm (A700) absorbing adduct (Chl a-H₂O)₂ is probably the in vivo P700 PSI aggregate. The computer deconvolution of the red absorption band of A700 into spectral components appears to be interpretable in terms of the expected exciton interactions.^{2a} Earlier treatment of exciton interactions in the C_2 symmetrical dimer (Chl a-H₂O)₂ did not include the effects arising from the relatively minor horizontal displacement between the Mg atoms of the two chlorin planes.^{4a} We present in this work a theoretical expression for exciton interactions in C_2 symmetric Chl a dimers that properly account for the effects arising from the parallel Mg displacements of the chlorin planes. The treatment is applicable not only to the symmetrical hydrated dimer (Chl a-H₂O)₂ but also to the anhydrous dimer Chl a₂ that is also believed to assume^{4b} a C_2 symmetrical aggregate configuration. Deconvolutions of optical data along with experimentally determined molecular structural data and the unique geometrical restrictions of the C_2 symmetric dimer configurations make possible a satisfactory comparison between theory and experiment.

[†] Present address: Graduate School of Biomedical Sciences, University of Texas Health Science Center, Dallas, Tex. 75235.

Exciton Interactions in C_2 Symmetric Chlorophyll Dimers

It has been shown in the original treatment of exciton interactions in the C_2 symmetric dimer (Chl a-H₂O)₂ that the symmetric ¹Ψ₁(A) and antisymmetric ¹Ψ₁(B) singlet exciton components are separated in energy by two times the dipole-dipole (dd) coupling parameter^{4a,5}

$$\xi = \frac{e^2\mu^2}{R_{12}^3} \cos \theta \quad (1)$$

where the Chl a-H₂O subunit singlet-singlet ($S_0 \rightarrow S_1$) transition moments $e\mu$ subtend angles of $\pm\theta/2$ with respect to the C_2 z axis, R_{12} is the distance between the two parallel chlorin planes, and A and B are respectively the symmetric and antisymmetric representations in the C_2 point group. Also derived was the ³Ψ₁(A) and ³Ψ₁(B) triplet exciton splitting attributable to the dd interaction^{4a,5}

$$\kappa = 0.4\xi(\delta/\Delta)^2 \quad (2)$$

where the factor δ/Δ is determined within each subunit by the spin-orbit coupling interaction and the energy separation between S_1 and the lowest triplet T_1 . In (1) and (2), effects arising from the horizontal displacement of the Chl a chlorin planes have been neglected for the sake of simplicity. From (1) and (2) the antisymmetric exciton components ¹Ψ₁(B) and ³Ψ₁(B) will be lower in energy than the corresponding symmetric components ¹Ψ₁(A) and ³Ψ₁(A) for $\theta < \pi/2$ and positive ξ .

Taking into consideration the relative displacements between the two Chl a molecules in the C_2 symmetrical structure of (Chl a-H₂O)₂ (see Figure 1), it is easy to show from the standard theory¹¹ for dd exciton interaction that the coupling energy is given by

$$\xi = \frac{e^2\mu^2}{R_{12}^3} \left[1 - (3\rho^2 - 1) \sin^2 \frac{\theta}{2} \right] \quad (3)$$

where

$$0 \leq \rho = \frac{R_{\perp}}{R_{12}} \leq 1 \quad (4)$$

and R_{12} and R_{\perp} are the center-center and perpendicular interplanar distances, respectively. The indices 1 and 2 are dummy indices for the two partner Chl a molecules. Solutions to (3) represent all possible exciton splittings resulting from parallel translations of the molecular planes in the C_2 sym-

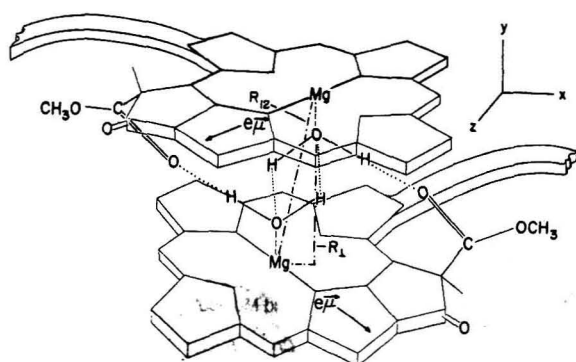


Figure 1. Scaled model representation of the C_2 symmetrical A700 dimer ($\text{Chl a}\cdot\text{H}_2\text{O}$)₂ displaying the reciprocal ester $\text{CO}\cdots\text{H}(\text{H})\text{O}\cdots\text{Mg}$ linkages. R_{12} and R_{\perp} are the center-center and perpendicular distances (---), respectively. The subunit transition moment $e\vec{\mu}$ is oriented according to the polarization of the 661-nm transition in monomeric chlorophyll a in ether (see text).

metric dimer. The ordering of exciton components is determined by the geometric factor

$$G = \left[1 - (3\rho^2 - 1) \sin^2 \frac{\theta}{2} \right] \quad (5)$$

which is plotted in Figure 2 for $0 \leq \theta \leq \pi$ and values of ρ in the range $0 \leq \rho \leq 1$.

The $S_0 \rightarrow S_1$ transition dipole strengths for the two exciton components¹¹

$$D_{\pm} = \frac{e^2}{2} (\vec{\mu}_1 \pm \vec{\mu}_2)^2 \quad (6)$$

where the plus and minus signs refer to the symmetric and antisymmetric components, respectively, are related to the angle θ subtended by the subunit transition moments according to the expression

$$D_{\pm} = e^2 \mu^2 (1 \pm \cos \theta) \quad (7)$$

Equation 7 may be recast in the form of a ratio

$$\frac{D_+}{D_-} = \cot^2 \frac{\theta}{2} \quad (8)$$

which will become convenient in later applications. The above results are exact in first-order perturbation theory for point dipole interactions.¹¹ The validity of this treatment will be examined in the following by applying (3)–(8) to a correlative interpretation of the experimental behavior of the in vitro ($\text{Chl a}\cdot\text{H}_2\text{O}$)₂ dimeric species.

Exciton Interactions in the C_2 Symmetric Dimer ($\text{Chl a}\cdot\text{H}_2\text{O}$)₂

We have accounted for the computer deconvoluted ($\text{Chl a}\cdot\text{H}_2\text{O}$)₂ A700 absorption band components at 699 and 713 nm in terms of exciton interactions.^{2a} Using the experimentally observed^{2a} ratio 3.03 ± 0.15 for the integrated 699 nm/713 nm band intensity ratio in (8), we obtain $\theta \approx 60^\circ$. The observed^{2a} energy difference of 280 cm^{-1} between the deconvoluted components corresponds to $\xi = 140 \text{ cm}^{-1}$.

The interplanar distances R_{\perp} and R_{12} in Figure 1 can be estimated from interatomic distances determined from x-ray diffraction studies¹² of the polymeric ethyl chlorophyllide a dihydrate aggregate. The similarities between the $\text{Chl a}\cdot\text{H}_2\text{O}$ interactions in ($\text{Chl a}\cdot\text{H}_2\text{O}$)₂ and ($\text{Chl a}\cdot 2\text{H}_2\text{O}$)_n have been described earlier.^{4c,5} In Figure 1, we observe that the Mg atoms and H_2O oxygens lie in a plane perpendicular to the $C_2(z)$ axis with the $(\text{H})\text{HO}\cdots\text{Mg}$ bonds directed perpendicular to the

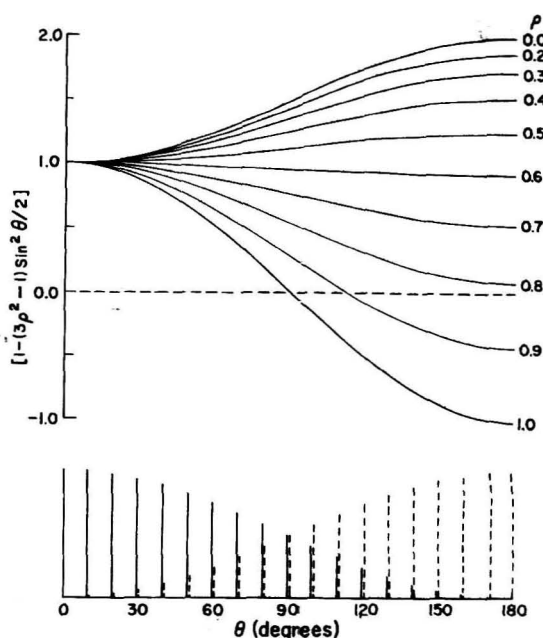


Figure 2. The relationship between exciton splitting and geometrical configuration for C_2 symmetric chlorophyll dimers. Regions above and below the zero line correspond to positive and negative values of ξ , respectively. Relative transition dipole strengths for the symmetric (—) and antisymmetric (---) exciton components are represented in the bottom portion of the figure. The angle $\theta = 60^\circ$ with the corresponding intensity ratio 3:1 is obtained for the hydrated dimer ($\text{Chl a}\cdot\text{H}_2\text{O}$)₂.

chlorin planes. The bonding interactions within ($\text{Chl a}\cdot\text{H}_2\text{O}$)₂ may be envisaged to be equivalent to a symmetrical addition of a Chl a molecule to a monomeric unit of $\text{Chl a}\cdot 2\text{H}_2\text{O}$.^{4c} These interactions are accordingly seen to be equivalent^{4c} to the subunit interactions in the ethyl chlorophyllide $\text{a}\cdot 2\text{H}_2\text{O}$ polymeric aggregate,¹² in which the two water oxygens are respectively ~ 2.4 and $\sim 3.6 \text{ \AA}$ from the chlorin plane and are separated by $\sim 2.8 \text{ \AA}$. The 2.4-\AA value corresponds to the water molecule bonded to the Mg atom. For the unique C_2 symmetrical ($\text{Chl a}\cdot\text{H}_2\text{O}$)₂ structure given in Figure 1, we obtain $R_{\perp} = 6.0 \text{ \AA}$, $R_{12} = 6.5 \text{ \AA}$, and $\rho = 0.92$. Using these molecular parameters, we arrive at $G = 0.62$ and $e^2 \mu^2 = 12 D^2$ from (5) and (3), respectively. The subunit transition dipole strength $e^2 \mu^2$, $12 D^2$ corresponds to a transition dipole length of $\mu = 0.73 \text{ \AA}$, with which we compute the subunit oscillator strength¹³

$$f = \left(\frac{8\pi^2 mc}{3h} \right) \nu \mu^2 = 0.09 \quad (9)$$

where h is Planck's constant, m is the electron mass, c is the speed of light, and $c\nu$ is the transition frequency. In the numerical computation of (9), we have used the chlorophyll monomer absorption $\nu = 1.51 \times 10^{-4} \text{ cm}^{-1}$.

Discussion

The subunit transition dipole strength $e^2 \mu^2 = 12 D^2$ and dipole length $\mu = 0.73 \text{ \AA}$ calculated for ($\text{Chl a}\cdot\text{H}_2\text{O}$)₂ are on the order of the corresponding experimental values $21.7 D^2$ and 0.96 \AA for monomeric chlorophyll a in ether.¹⁴ There are two factors that may contribute to the apparent discrepancy: (1) The subunit oscillator strength $f = 0.09$ of ($\text{Chl a}\cdot\text{H}_2\text{O}$)₂ may be expected to differ somewhat from that (0.155) of monomeric Chl a in ether.¹⁴ (2) The inherent difficulties encountered in applying the point-dipole exciton theory for finite intersubunit distances R_{12} . In the present case, the calculated

subunit dipole length $\mu = 0.73 \text{ \AA}$ corresponds to $R_{12} = 6.5 \text{ \AA}$.

Attempts to explain the origin of spectral red shifts in Chl a aggregates relative to the 661-nm absorption in monomeric Chl a have not been successful.¹² The exciton splitting centered at 706 nm suggests that the red shift in the hydrated dimer may be due to Coulombic or exchange effects.

The sign of the exciton splitting parameter from Figure 1 is positive in the region $\theta < 90^\circ$. Consequently the symmetric component which has the greater transition dipole intensity for $\theta < 90^\circ$ is on the short wavelength side of the antisymmetric component. For $\theta > 90^\circ$, the transition dipole intensity for the antisymmetric component is larger and the latter can lie on either side of the symmetric component depending on the magnitude of ρ . The agreement between theory and experiment is consistent with the previous determination that the hydrated dimer symmetric exciton component $^1\Psi_1(A)$ lies at a higher energy than the antisymmetric component $^1\Psi_1(B)$.

An alternative solution to (8) obtained from the observed^{2a} intensity ratio of the exciton components yields $\theta \approx 120^\circ$. This solution appears to be less reasonable for physical reasons. CPK molecular models show that the reciprocal ester $C=O \cdots H(H)O \cdots Mg$ linkages in $(Chl a \cdot H_2O)_2$ are favored in configurations in which $\theta \approx 60^\circ$.¹⁵ An upper limit $\theta = 80^\circ$ is calculated in the dimer configuration where the carbomethoxy oxygens, H_2O oxygens, and Mg atoms lie in the same plane, using the orientation of the transition moment $e\vec{\mu}$ (see Figure 1) in monomeric chlorophyll a^{14,16} and interatomic distances for ethyl chlorophyllide a.¹²

References and Notes

- (1) This research was supported by NSF Grant No. BMS7411919.
- (2) (a) F. K. Fong and V. J. Koester, *Biochim. Biophys. Acta*, **423**, 52 (1976); (b) N. Winograd, A. Shepard, D. H. Karweik, V. J. Koester, and F. K. Fong, *J. Am. Chem. Soc.*, **98**, 2369 (1976); (c) V. J. Koester, L. Galloway, and F. K. Fong, *Naturwissenschaften*, **62**, 530 (1975); (d) V. J. Koester, J. S. Polles, J. G. Koren, L. Galloway, R. A. Andrews and F. K. Fong, *J. Lumin.*, **12**, 718 (1976).
- (3) B. Kok, *Biochim. Biophys. Acta*, **48**, 527 (1961).
- (4) (a) F. K. Fong, *J. Theor. Biol.*, **46**, 407 (1974); *Proc. Natl. Acad. Sci. USA*, **71**, 3692 (1974); *Appl. Phys.*, **6**(2), 151 (1975); (b) F. K. Fong and V. J. Koester, *J. Am. Chem. Soc.*, **97**, 6888 (1975); (c) F. K. Fong, *ibid.*, **97**, 6890 (1975).
- (5) For a review of recent developments, see, F. K. Fong, "Theory of Molecular Relaxation: Applications in Chemistry and Biology", Wiley-Interscience, New York, N.Y., 1975, Chapter 9.
- (6) F. K. Fong and N. Winograd, *J. Am. Chem. Soc.*, **98**, 2287 (1976).
- (7) E. G. McRae and M. Kasha, *J. Chem. Phys.*, **28**, 721 (1958).
- (8) R. M. Hochstrasser and M. Kasha, *Photochem. Photobiol.*, **3**, 317 (1964).
- (9) R. S. Knox in "Bioenergetics of Photosynthesis", Govindjee, Ed., Academic Press, New York, N.Y., 1975, Chapter 4.
- (10) J. C. Chang, Ph.D. Thesis, University of Rochester, Rochester, N.Y., 1972.
- (11) (a) A. S. Davydov, "Theory of Molecular Excitons", McGraw-Hill, New York, N.Y., 1962; (b) I. Tinoco, Jr., *Radiat. Res.*, **20**, 33 (1963).
- (12) H.-C. Chow, R. Serlin, and C. E. Strouse, *J. Am. Chem. Soc.*, **97**, 7230 (1975).
- (13) G. Herzberg, "Molecular Spectra and Molecular Structure", Vol. 1, Van Nostrand, New York, N.Y., 1950.
- (14) C. Houssier and K. Sauer, *J. Am. Chem. Soc.*, **92**, 779 (1970).
- (15) Reference 5, p 282.
- (16) M. Gouterman and L. Stryer, *J. Chem. Phys.*, **37**, 2260 (1962).

Discussion

S. FREED. Would you elaborate on your deconvolution experiment?

V. KOESTER. It was a computer deconvolution of the experimentally obtained absorption spectrum.

M. GOUTERMAN. Are the 680-nm band in one dimer (the anhydrous) and the 700-nm band in the other, the upper exciton bands?

V. KOESTER. In the hydrated dimer A700 that is correct; for the anhydrous dimer theory predicts the upper exciton component to be weaker than the lower exciton band.

M. GOUTERMAN. What is the mechanism for the red shift in the dimer? Isn't such a red shift for an upper exciton band without precedent?

V. KOESTER. That is an excellent question. I can only speculate at this point by a comparison with the spectrum of the 743-nm absorbing species. The crystal structure of ethyl chlorophyllide-2H₂O has been done, and it's a polymeric species that absorbs at 743 nm. The 700-nm absorbing species also contains hydrogen bonded water, and the anhydrous species does not. If one plays with resonance structure models, one can, for hydrated chlorophyll, make resonance forms that allow ring 5 to resonate with the entire π system of the chlorin ring, that is, if one invokes an admixture of the enol form.

**New concepts
new techniques
new interpretations**

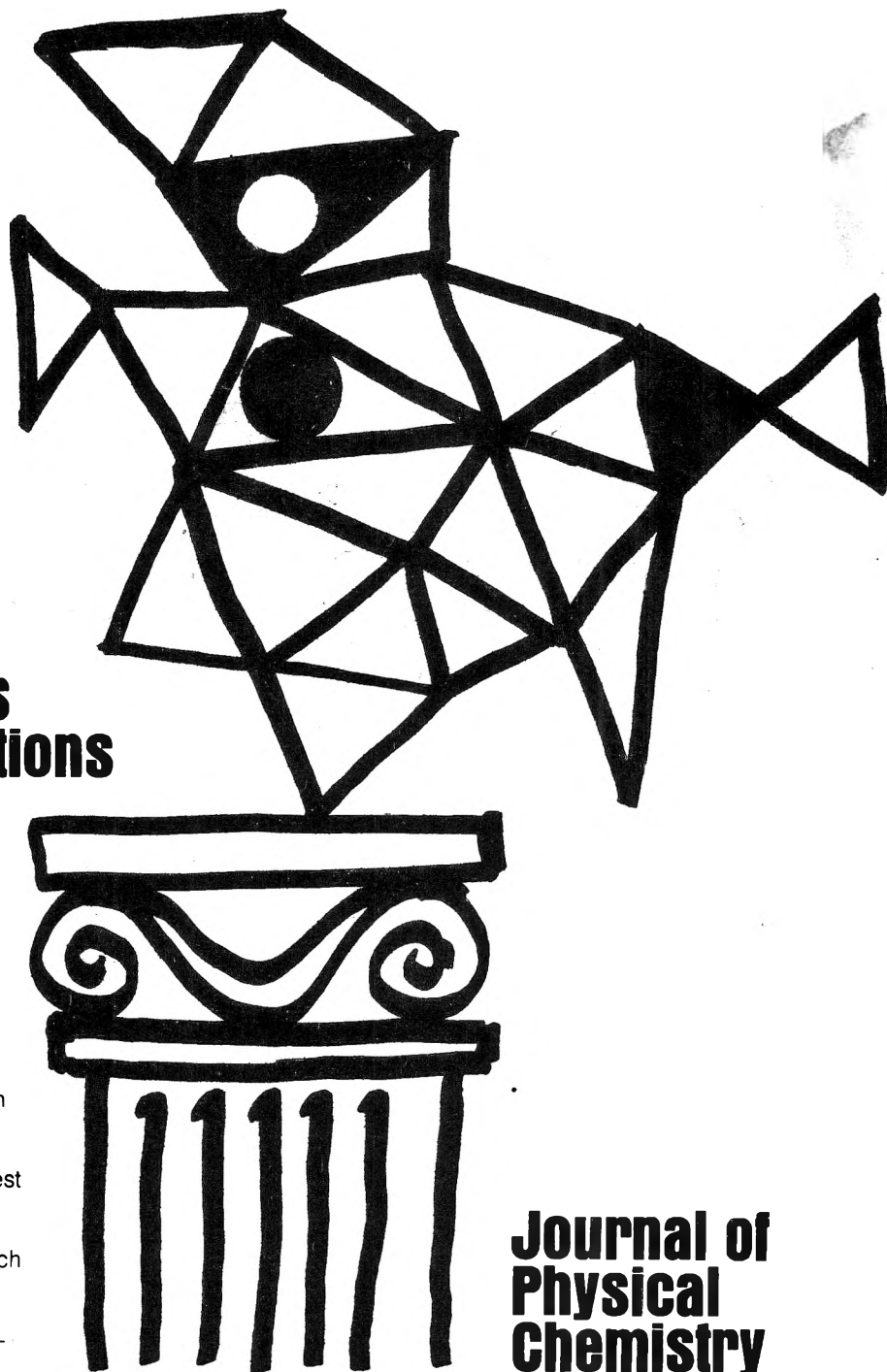
**... together
with valuable reports
on classical areas**

They are all waiting for you between the covers of our well-balanced JOURNAL OF PHYSICAL CHEMISTRY. Whatever your particular interest in physical chemistry, you'll find the JOURNAL's broad range of experimental and theoretical research reports are relevant and beneficial to your work. Each biweekly issue brings you an average of 30 authoritative, comprehensive reports on fundamental aspects of atomic and molecular phenomena, as well as timely notes, communications and reports plus the proceedings of selected symposia.

Join your fellow physical chemists who rely on JPC as an excellent biweekly source of data in both new and classical areas. Just complete and return the form to start your own subscription.



... another ACS service



Journal of Physical Chemistry

**The Journal of Physical Chemistry
American Chemical Society**

1155 Sixteenth Street, N.W.
Washington, D.C. 20036

1976

Yes, I would like to receive the JOURNAL OF PHYSICAL CHEMISTRY at the one-year rate checked below:

	U.S.	Canada**	Latin America**	Other Nations**
ACS Member One-Year Rate*	<input type="checkbox"/> \$24.00	<input type="checkbox"/> \$30.25	<input type="checkbox"/> \$29.75	<input type="checkbox"/> \$30.25
Nonmember	<input type="checkbox"/> \$96.00	<input type="checkbox"/> \$102.25	<input type="checkbox"/> \$101.75	<input type="checkbox"/> \$102.25
Bill me <input type="checkbox"/>	Bill company <input type="checkbox"/>	Payment enclosed <input type="checkbox"/>		

Air freight rates available on request.

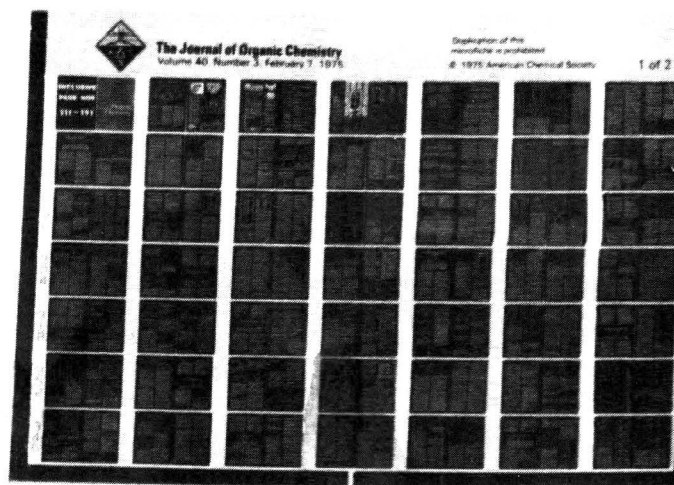
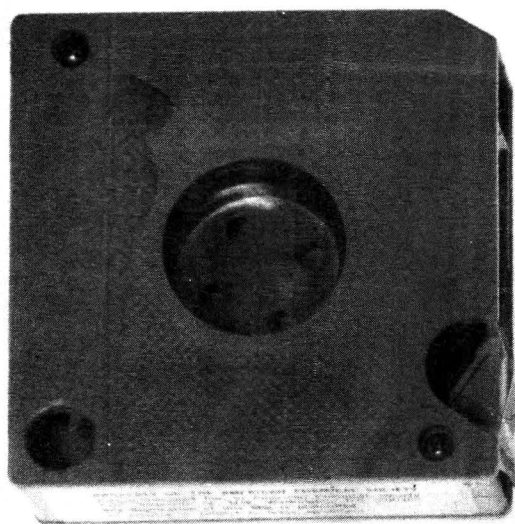
Name _____

Street _____ Home
Business

City _____ State _____ Zip _____

Journal subscriptions start January '76

*NOTE: Subscriptions at ACS member rates are for personal use only. **Payment must be made in U.S. currency, by international money order, UNESCO coupons, U.S. bank draft, or order through your book dealer.



MICROFORMS

American Chemical Society publications in microform

MICROFILM OR MICROFICHE?

With the ACS microform program you can receive either, or both

Microfilm

All periodical publications back to volume one

Copying privileges included with current subscriptions

All non-print supplementary materials provided free on microfilm

Archival quality silver halide film supplied as you request; positive or negative; 16 or 35mm; cartridge, reel, or cassette.

Microfiche

Current issues of primary journals, beginning with January 1975

Individual issues or full volumes available

Supplementary materials also available on microfiche

Fiche supplied are archival quality silver halide, negative, 105 x 148mm (4" x 6"); 24x, with eye legible headers, start and end targets, and page numbers

For information about our microfilm/microfiche write:

Microform Program

Special Issues Sales
American Chemical Society
1155 16th Street, N.W.
Washington, D.C. 20036
(202) 872-4363

Tape Cassettes From The American Chemical Society Famous Scientists

ENERGY

- Energy & Industry**
A Waterland
Energy & Environment
Dr. S. Manahan
 - Energy on the Shelf**
H₂ and You
Dr. D. Gregory
 - Green-Thumb Energy**
Dr. D. Klass
 - Methane from Coalbeets**
Dr. R. Stefanko
 - The Promise of Hydrogen**
Optical Communications
Jack Russell
 - Energy in the Future**
Solar Homes for the Future
Dr. Paul Donovan
 - Coal's New Face**
More Power, Less Pollution
Dr. Daniel Bienstock
 - Cleaning A Dirty Fuel**
From Wastes to Energy
H. Feldman
 - Energy: A Critique**
Puzzles of Air Pollution
Arthur Levy
 - Fusion: Prospects & Pitfalls—I**
Fusion: Prospects & Pitfalls—II
Dr. H. Furth & Dr. H. Forsen
 - Antidote to the Energy Crisis**
George Long
 - Fusion and Fission: An Appraisal**
The Prospects for Energy
Dr. M. King Hubert
- ## ENVIRONMENT
- The Spray Can Threat**
The Invisible Enemy
Dr. R. Stewart
 - Cities & Weather—I**
Cities & Weather—II
Dr. R. Braham
 - Putting Potatoes in Plastics**
Lead Poisoning in Children
Dan Darow
 - New Look in Phosphorus Removal**
Dr. Gilbert Levin
 - A Solution for Metals**
Thomas Chapman
 - Turning Insects Against Themselves**
Updating Aluminum
Dr. Allen Russell
 - Energy and Environmental Thrift**
Tracing the Skeleton's Image
Er. T. Raby
 - Seafood From Waste**
Underwater World of Communications
Dr. J. Atema
 - Water Supply of The Future**
The Secrets of Salmon
Dr. A. Hasler
 - Cleaner Water Through Chemistry**
Bromine Chloride: A Better Disinfectant
Dr. J. Mills
 - The Damaged Air—I**
The Damaged Air—II
 - How Smells Shape Up**
Urban Auto Design
 - Tough Filaments of Fragile Liquid**
Electricity from Rooftops
Dr. Charles Backus
 - The Struggle for Clean Water—I**
The Struggle for Clean Water—II
 - The Oil Mystery**
Harold Bernard
 - The Language of Odors**
Dr. Stanley Freeman
 - The Lonely Atom**
How Green The Revolution
Lester Brown
 - Mercury: Another Look—Part I**
Mercury: Another Look—Part II
Dr. John Wood & D. G. Langley
 - The Troubles with Water**
Pure Oxygen for Polluted Water
Dr. Jack McWhirter

- Bubble Machines & Pollution Finders**
The Steam Engine: A Modern Approach
Dr. W. Doerner & Dr. M. Bechtold
- New Weapons Against Insects**
Moths, Drugs, & Pheromones
Dr. Wendell Roelofs
- The Lead Issue**
Smog: An Environmental Dilemma
Dr. James Pitts
- Monitoring High Risk Pregnancies**
Progress in Enzyme Replacement
Therapy
Dr. Roscoe Brady
- Safety for Premature Infants**
Help for the Critically Ill
Dr. Joseph Moylan
- Pinningpoint Hepatitis Viruses**
New Key to Heart Disease
Dr. Antonio Gorto
- Nature's Own Toxicants in Foods**
Added, Not Intended
Dr. H. Kraybill
- Seventy-Two Per Minute—I**
Seventy-Two Per Minute—II
Dr. N. Razor
- Two Drugs, More or Less**
Filling the Molar Gap
Dr. J. Cassel
- A Titt at Genetic Ills**
Binding the Catalysts of Life
Dr. H. Garfinkel
- Early Prenatal Diagnosis of Genetic Disease**
From Mother to Child
Dr. M. Horning & Dr. R. Hill
- Insulin & Diabetes—I**
Insulin & Diabetes—II
Dr. George Cahill
- Stalking the Molecules of Memory**
Immunotherapy
Dr. Kenneth Bagshawe
- Engineering Enzymes**
On Drugs, Plasticizers, & Mass Spec
Dr. G. W. A. Milne
- Birth Control: Problems & Prospects**
Hormones, Terpenes, & the German Air Force
Dr. Carl Djerassi
- Prospects for Implants**
New Dimensions for Polymers
Dr. Alan Michaels
- Fabricating Life**
New Ways to Better Food
Dr. R. W. F. Hardy
- Chemistry of the Mind: Schizophrenia**
Chemistry of the Mind: Depression
Dr. Joel Elkes
- The Molecules of Memory**
The Matter with Memory
Dr. W. L. Byrne & Dr. A. M. Golub

- Why We Grow Old**
Dr. Howard Curtis
- New Materials for Spare Parts**
Against Individuality
Dr. R. Reisfeld & Dr. B. Kahan
- A Richness of Lipids**
Life: Origins to Quality
Dr. Stanley Miller
- The Nitrogen Fixer**
Prostaglandins: A Potent Future
Dr. E. J. Corey & Dr. S. Bergstrom
- Chemical Evolution**
An Evolving Engine
Dr. R. E. Dickerson

- Cosmic Ray Astronomy**
The Reactor Never Lies
T. Raby
- Wine From Native American Grapes—I**
Wine From Native American Grapes—II
Dr. A. Rice
- Community Needs: New Emphasis in Research**
Aspirin vs. Prostaglandins
Dr. John Vane
- A Breakdown in Plastics—I**
A Breakdown in Plastics—II
Dr. J. Guillet & G. Scott
- Protein: The Next Big Production?**
Clean Energy: A One-Way Dream
Dr. J. R. Eaton
- Nitrosamines: A Reappraisal**
The Emperor of Ice Cream
Dr. Wendell Arbutuckle
- Ethics and Genetics**
The American Diet: A Critique
Dr. Arnold Schaefer
- Probing Creation**
New Directions in U.S. Science
Dr. William McElroy
- Aspirins, Enzymes, & Fragrant Redheads**
Vitamin D: A New Dimension
Dr. Hector DeLuca
- Engineering Microbes**
Liquid Crystals: A Bright Promise
Dr. George Heilmeyer
- Lively Xenon**
The Repressor Hunt
Dr. Mark Prasine

NOBEL PRIZE WINNERS

- Dr. Linus Pauling**
The Committed Scientist
Science and Man
- Dr. Glenn Seaborg**
The Atomic World of Glenn Seaborg
- Dr. George Wald**
Vision, Night Blindness, & Professor Wald
- Dr. Melvin Calvin**
The Search for Significance—Parts I & II

SCIENCE

- Tapping the Oceans**
Davy Jones' Treasure
Dr. S. Gerard
- The Need for Nitrogen**
Modifying Milk for Millions
A Rand & J. Hourigan
- The Seas in Motion**
Rumbles in the Earth
Dr. Wallace Broecker
- Stalking the Molecules of Memory**
Immunotherapy
Dr. Kenneth Bagshawe
- Engineering Enzymes**
On Drugs, Plasticizers, & Mass Spec
Dr. G. W. A. Milne
- Birth Control: Problems & Prospects**
Hormones, Terpenes, & the German Air Force
Dr. Carl Djerassi
- Prospects for Implants**
New Dimensions for Polymers
Dr. Alan Michaels
- Fabricating Life**
New Ways to Better Food
Dr. R. W. F. Hardy
- Chemistry of the Mind: Schizophrenia**
Chemistry of the Mind: Depression
Dr. Joel Elkes
- The Molecules of Memory**
The Matter with Memory
Dr. W. L. Byrne & Dr. A. M. Golub

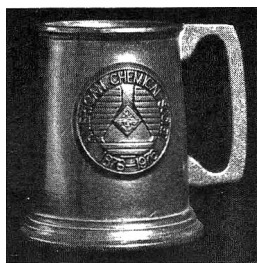
BIO-MEDICAL

- Fighting Fat**
Tackling Tooth Decay
Dr. J. J. Marshall
- Progress Against Diabetes**
The Sickle Cell Problem
Dr. R. Jackson
- A New Look at Stroke**
Chemical Look at Mental Illness
Dr. S. Kety
- Nutrition & the Brain**
The Forgotten Nutrient
Dr. J. Scala
- Remodeling the Body**
Nuclear Medicine
Dr. W. Wolf
- Seafood From Waste**
Underwater World of Communications
Dr. J. Atema
- Water Supply of The Future**
The Secrets of Salmon
Dr. A. Hasler
- Cleaner Water Through Chemistry**
Bromine Chloride: A Better Disinfectant
Dr. J. Mills
- The Damaged Air—I**
The Damaged Air—II
- How Smells Shape Up**
Urban Auto Design
- Tough Filaments of Fragile Liquid**
Electricity from Rooftops
Dr. Charles Backus
- The Struggle for Clean Water—I**
The Struggle for Clean Water—II
- The Oil Mystery**
Harold Bernard
- The Language of Odors**
Dr. Stanley Freeman
- The Lonely Atom**
How Green The Revolution
Lester Brown
- Mercury: Another Look—Part I**
Mercury: Another Look—Part II
Dr. John Wood & D. G. Langley
- The Troubles with Water**
Pure Oxygen for Polluted Water
Dr. Jack McWhirter

ACS Members \$5.95
Nonmembers \$6.95
Single cassette \$4.95/cassette
Any Eight cassettes \$4.95/cassette \$5.95/cassette
 Any 20 or more cassettes to one address \$4.00/cassette
10% Discount if payment accompanies order

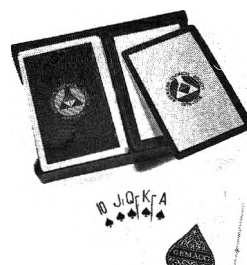
Name _____ State _____ Zip _____
 Address _____
 City _____
 Order from: American Chemical Society, Dept. SH
 1155 16th St., N.W., Wash., D.C. 20036
 Allow 4 to 6 weeks for delivery

ACS CENTENNIAL MEMENTOS



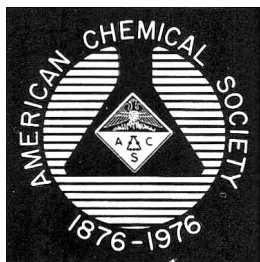
ACS Centennial Mug

The perfect accessory for office, den, or bar—4 3/4 inch high pewter-colored noggin with ACS Centennial seal made of Armetale® to keep beer or ale ice cold. **\$8.50**



ACS Playing Cards

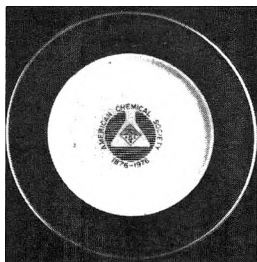
Blue and gold bridge set with ACS Centennial seal design. Case included. **\$5.00**



ACS Centennial Seals

1 1/2 inch blue and gold ACS Centennial seal. Ideal for business correspondence or greeting cards.

Roll of 2,000 for **\$10.00**
200 for **1.00**



ACS Centennial Plate

10 3/4 inch blue and white plate with gold rim featuring ACS Centennial seal. Made of top-quality Pickard china. **\$20.00**



ACS Centennial Tie

Necktie with ACS Centennial date and emblem pattern. Specify blue or red background. **\$6.50**



ACS Centennial Medallion

1 1/2 inch Franklin Mint proof-quality circular medallion with ACS Centennial seal front, and chemical symbols reverse. Housed in protective plastic holder. Limited Edition.

gold on sterling silver **\$20.00**
sterling silver **15.00**
bronze **7.00**
presentation case **3.00**



ACS Centennial Emblem

Blue, white, and gold diamond-shaped emblem commemorating the Centennial is available with pin back for women members, or as a lapel pin for men. **\$2.00**



A Century of Chemistry

An illuminating portrait of the growth and activities of the ACS in the context of a century that saw two World Wars, the Great Depression, the Cold War, the Space Race, and the environmental movement. Includes a compact 100-year record of ACS people and events. 468 pages (1976) clothbound **\$15.00**

Taking Things Apart and Putting Things Together

An absorbing narrative of what chemistry is all about; case histories tell the fascinating stories of cyclamates, DDT, insulin, anesthetics, penicillin, polio vaccine, and more. Profusely illustrated with four-color designs and photographs from the ACS Centennial Exhibit.

128 pages (1976) paperback **\$1.75**

Books Dept./American Chemical Society
1155 16th St., N.W., Washington, D.C. 20036

- | | | |
|--|---|--|
| <input type="checkbox"/> ACS Mug (\$8.50 each) | <input type="checkbox"/> ACS Tie (\$6.50 each) | <input type="checkbox"/> ACS Cards (\$5.00 set) |
| <input type="checkbox"/> ACS Plate (\$20.00 each) | _____ blue tie | <input type="checkbox"/> A Century of Chemistry |
| <input type="checkbox"/> ACS Seals | _____ red tie | (clothbound \$15.00) |
| _____ roll of 2,000 (\$10.00) | <input type="checkbox"/> ACS Medallion | <input type="checkbox"/> Taking Things Apart |
| _____ 200 for \$1.00 | _____ gold or silver (\$20.00) | (paperback \$1.75) |
| <input type="checkbox"/> ACS Emblem (\$2.00 each) | _____ sterling silver (\$15.00) | |
| _____ women's pin | _____ bronze (\$7.00) | |
| _____ men's lapel pin | _____ case (\$3.00) | |

Check enclosed for \$ _____ . All orders postpaid in U.S. and Canada.

Name _____
Address _____
City _____
State _____ Zip _____